The art of perfection : on the self-assembly of discrete block co-oligomers

The Art of Perfection

On the Self-Assembly of Discrete Block Co-Oligomers

PROEFSCHRIFT

ter verkrijging van de graad van doctor aan de Technische Universiteit Eindhoven, op gezag van de rector magnificus prof. dr. ir. F.P.T. Baaijens, voor een commissie aangewezen door het College voor Promoties, in het openbaar te verdedigen op dinsdag 6 maart 2018 om 16:00 uur

door

Bas van Genabeek

geboren te ’s-Hertogenbosch

Dit proefschrift is goedgekeurd door de promotoren, en de samenstelling van de promotiecommissie is als volgt:

voorzitter:	prof. dr. ir. R. Tuinier
promotor:	prof. dr. E.W. Meijer
copromotor:	dr. ir. A.R.A. Palmans
leden:	prof. dr. C.J. Hawker (University of California, Santa Barbara)
	prof. dr. ir. R.A.J. Janssen
	prof. dr. D.J. Broer
	prof. dr. R.P. Sijbesma
adviseur:	dr. ir. J.P.A. Heuts

Het onderzoek of ontwerp dat in dit proefschrift wordt beschreven is uitgevoerd in overeenstemming met de TU/e Gedragscode Wetenschapsbeoefening.

Voor Berend

Cover design: Bas van Genabeek

Printed by: Gildeprint Drukkerijen – The Netherlands

A catalogue record is available from the Eindhoven University of Technology Library

ISBN: 978-90-386-4455-4

This work has been financially supported by the Koninklijke Nederlandse Akademie van Wetenschappen (KNAW).

♦ Table of Contents ♦

♦ Chapter 1 ♦

Macro-Organic Chemistry: Precision Fabrication of Small and Smaller

Abstract: The current state of polymer synthesis permits the production of a large number of polymer architectures in which the variation between the molecular structures of the individual chains is under better control than ever before. Still, if ultimate perfection is required, stepwise synthesis remains the best option. In this chapter, we provide a literature overview of the most appealing examples in uniform polymer synthesis. Additionally, we discuss the development of block copolymer microphase separation as a well-established method to generate organized, nanoscopic features and provide examples indicating that an unexplored, gray area between polymer and low-MW materials slowly starts to unveil its secrets. The desire for a better molecular understanding of the self-assembly of polymer-like molecules serves as an inspiration to create and explore the properties of perfectly defined, low-MW block co-oligomers.

"Every adventure requires a first step. Trite, but true, even here."
—Charles Lutwidge Dodgson (Lewis Carroll), in *Alice's Adventures in Wonderland*, 1865.

1.1 Introduction

Unmistakably, polymer chemistry faced a difficult time in the years prior to its acceptance as a research field with huge potential. In retrospect, it is hard to imagine that less than a century ago, the existence of high-molecular-weight (high-MW) entities was largely dismissed as nonsense.[1] Particularly when considering the ease with which macromolecules, incorporating nearly any desired combination of functionalities and properties, are generated at the present time. Primarily, the development of sophisticated polymerization techniques, commonly designated as 'living polymerizations', enabled chemists to generate polymers of which the endgroups and variation in molecular weight are under near-perfect control.[2] Moreover, it facilitated the process of synthesizing block copolymers (BCPs); molecules comprising two or more chemically distinct polymeric segments, linked together by one or more covalent connections. In general, precision polymer synthesis has been recognized as a very promising strategy to fabricate materials with unprecedented complexity and functionalities.[3–6]

Unfortunately, even the most sophisticated living polymerization reactions are not perfect. Nonetheless, we often notice the (ab)use of the term 'monodisperse' in literature for many materials that are generated *via* these techniques. Formally, all are low-dispersity ($Đ > 1$) polymers, and the term 'monodisperse' is often erroneously employed to highlight the contrast with more disperse samples. Because of the deeply rooted improper usage of the term monodisperse in literature, we will avoid this term as much as possible throughout this thesis, and use 'uniform' or 'discrete-length' instead to indicate materials that are composed of molecules of only one particular mass and constitution ($Đ = 1$).[7]

This chapter consists of three main parts. In the first, we will concentrate on methods for the precision synthesis of polymers, approaching the limit $Đ = 1$. The concept of precision polymer synthesis is largely the basis for all the work presented in the remainder of this thesis. This is followed by a brief introduction to the concept of block copolymer self-assembly. Finally, the aim and outline of this thesis will be presented.

1.2 Creating uniform polymers

In general, synthesis of uniform macromolecules is a well-established field, providing a plethora of high-MW materials of excellent purity. For example, great synthetic effort

resulted in many examples of dendritic molecules of uniform MW.[8–10] However, in the work presented here, we focus on polymeric compounds of the linear type, for which the number of discrete-length materials is much more limited. Here, the main difficulty of creating polymers with a discrete length is directly hidden in the definition of a (synthetic) polymer, which—according to the standard IUPAC nomenclature—is a molecule of relatively high molecular mass, consisting of multiple repeating molecular fragments of low relative molecular mass, such that the addition or removal of one or a few of the units has a negligible effect on the molecular properties.[7] Consequently, differentiating between two polymer molecules comprising n and n+1 repeat units on a preparative scale is extremely difficult.

In the following overview, we discuss the different methodologies for obtaining uniform, linear polymers. We choose to exclude many of the (mainly) biological structures made by solid-phase synthesis, since the amounts of pure material that can be isolated are often very small. Famous examples that utilize this strategy include the Merrifield solid-phase synthesis[11] and peptoid syntheses of Zuckermann and coworkers.[12–17] Still, solution-phase synthesis allows more thorough intermediate purification steps and more convenient up-scaling, thus resulting in larger quantities and a higher purity of the final oligomers.

1.2.1 Removing dispersity by purification

Despite the difficulties to distinguish between polymers of similar MW, obtaining extremely low dispersity polymers by purification of less discrete materials is possible. Chang *et al.* have shown that low dispersity polystyrene-*block*-polyisoprene (PS-*b*-PI)[18,19] and polystyrene-*block*-poly(methyl methacrylate) (PS-*b*-PMMA)[20] with relatively high average MW (20–80 kDa) can be fractionated into samples with dramatically reduced dispersities ($Đ$ > 1.01) using preparative high-performance liquid chromatography (HPLC). Furthermore, a lower MW (2.4 kDa) disperse polymer was fully separated into its discrete-length components.[19]

In practice, obtaining uniform polymers by fractionation of a disperse starting material is very much restricted to low molecular weights and small amounts. For example, milligram quantities of oligo(pyrrole-2,5-diyl)s up to the 20-mer with purities >90% have been obtained by preparative HPLC of a disperse mixture.[21] In 2016, Hawker and co-workers published a versatile strategy for obtaining larger amounts discrete-length oligomers of three commonly used classes of compounds: oligoacrylates, oligostyrenics, and oligodimethylsiloxanes.[22] In a follow-up paper, the protocols were extended for conjugated oligomers.[23] Discrete-length components could be isolated after purification of a disperse mixture (either a commercially

available material or prepared *via* standard controlled polymerization reactions). This was achieved by automated column chromatography with a Biotage system using normal-phase silica gel or reversed-phase C_{18} columns (Figure 1–1A). Here, the major advantage was the larger scale (2 to >10 grams) on which the separation could be conducted. Although the maximum length of oligomers that could be isolated as 100% pure compounds was limited to approximately 15 repeat units (depending on the type of oligomer, Figure 1–1B), the process is straightforward and applicable to oligomers that are not easily synthesized in a stepwise manner (*vide infra*).

A neat example of a preparation of relatively high MW conjugated materials is given by Otsubo.[24] By preparing uniform octithiophenes, decorated with one or two acetylene endgroups and subsequently performing an oxidative coupling reaction, a mixture of oligo(octithienylene–diethynylene)s was obtained. Because of the considerable MW differences between the different oligomers, compounds consisting of 1 to 11 repeat units (with a maximum MW of 13.8 kDa and up to 96 thiophene repeat units, see Figure 1–2) could be separated by preparative size exclusion chromatography and isolated in pure form. A similar approach already lead to the formation of oligothiophenes up to the 48-mer.[25] Also notable is the development of routes toward a conjugated thiophene 96-mer in the same group.[26]

Instead of utilizing a single polymerization step, followed by separation of the different formed oligomers, an iterative protocol has been developed in the group of Junkers.[27] An alternation of so-called single or multiple unit monomer insertions and automated column

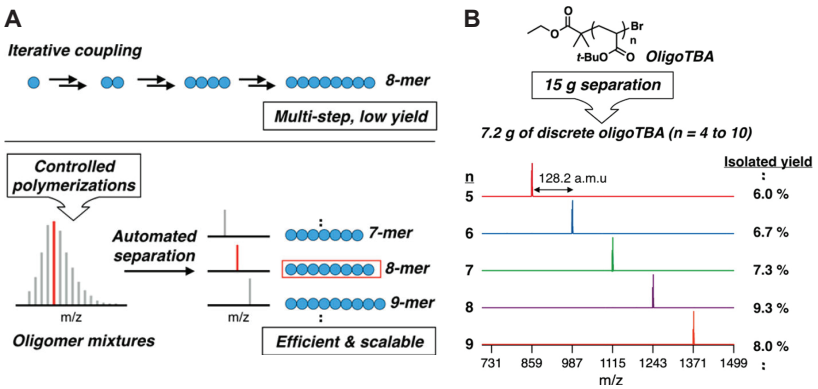

Figure 1–1. (**A**) Flowchart for obtaining discrete-length oligomers from a disperse starting material by automated column chromatography; (**B**) MALDI-TOF MS spectra of discrete-length oligo(*tert*-butyl acrylate) with 5 to 9 repeat units, which were isolated on gram scale after chromatographic separation of a disperse mixture. The isolated yields are given for each oligomer. Images are adapted from ref. [22].

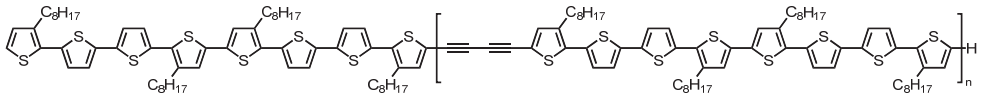

Figure 1–2. Molecular structures of a series of conjugated oligo(octithienylene–diethynylene)s (n = 1–11).[24]

purification steps resulted in sequence controlled oligomers. However, also here the maximum polymer length is limited to 10 repeat units (20 units after dimerization of the decamer).

1.2.2 Stepwise synthesis of long, linear molecules

If substantial quantities of uniform oligomers or polymers with a higher number of repeat units are required, then often the last remaining alternative is direct synthesis of the desired molecules. Numerous examples describing the synthesis of low-MW oligomers (under 20 repeat units) are reported, and excellent reviews have been published.[6,28–31]

Practically all syntheses of discrete-length, high-MW materials utilize stepwise, iterative synthesis strategies, most of which can be categorized into two distinct growth modes: exponential and linear. The exponential growth strategy (also frequently named divergent/convergent approach)[i] is the most efficient process for making discrete-length oligomers of high MW in the smallest number of steps (Figure 1–3A). The core of this approach is the use of a bifunctional molecule (often the monomer), of which both functionalities (*X* and *Y*) can react with each other and form a new covalent bond, leading to a dimer. To prevent uncontrolled continuation of this dimerization process—which essentially is a polycondensation reaction, leading to a very broad MW distribution ($Đ \rightarrow 2$)[32]—the use of protective groups or other means to mask the reactivity of the endgroups is mandatory. Consequently, a second prerequisite is the possibility to selectively deprotected or activate each of the two endgroups (the divergent part). Subsequent ligation of these two mono-activated components (the convergent part) leads to a materials that closely represents the dimerized starting material, containing two, non-reactive endgroups. With this higher-MW material, the divergent/convergent process can be repeated until the desired MW is reached.

A major drawback of the exponential growth approach is the reduced flexibility for inserting molecularly different monomer residues and the need for the orthogonal reactions to activate the endgroups. A solution is provided in Figure 1–3B and C. Here, the two most common linear growth approaches are depicted, which result in a mono- or bidirectional growth, respectively. For this, a hetero or homotelechelic starting compound—bearing one

[i] Not to be confused with divergent and convergent approaches in dendrimer synthesis.[130]

or two equivalent, reactive endgroup(s) *X*—is reacted with a single building block. This building block can either be a single monomeric unit or a premade small oligomer, as long as it includes a matching reactive group *Y* (to create the covalent link with *X*) and also a masked version of the reactive endgroup *X*. After ligation of the building block, the masked endgroup is transformed into the reactive group, and the process is repeated. Obviously, this strategy requires more synthesis steps to obtain an arbitrary oligomer length than needed with the exponential growth strategy, particularly for the monodirectional growth. However, it permits the controlled insertion of many slightly differently substituted monomers in the growing chain, and thus full control over the position of every monomeric residue. The following two subsections provide a number of examples that illustrate how the above explained synthesis protocols can be utilized to obtain oligomers with >20 repeat units. We focus mainly on solution-phase synthesis.

1.2.3 Long oligomers by exponential growth

An early and often cited example of discrete-length polymer synthesis is the work of Whiting on long, linear (and later also branched) alkanes.[33–42] Interestingly, often overlooked

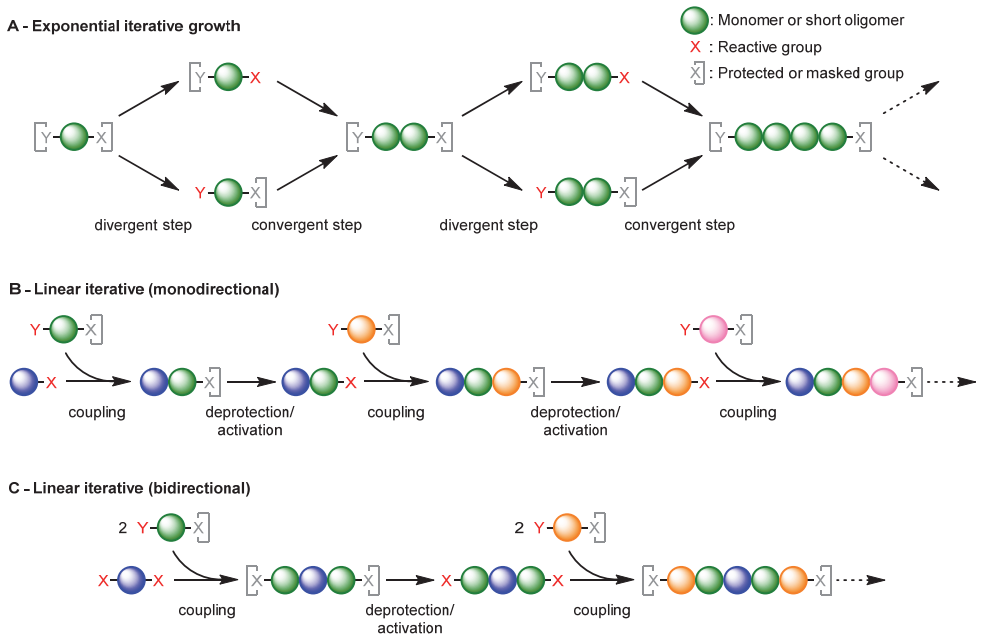

Figure 1–3. (**A**) Exponential growth strategy or divergent/convergent approach based on the selective activation or deprotection of bifunctional molecules; (**B–C**) Linear growth strategy based on sequential coupling of building blocks at one (**B**) or both sides (**C**) of the growing chain, and activation or deprotection to restore the reactive endgroup.

is much of the preceding work by others,[43–46] under which the synthesis of tetranonacontane ($C_{94}H_{190}$) by Dixon on an (in modern view) astonishing 100 g scale.[47] Nonetheless, the very systematic process developed by Whiting and coworkers allowed the fabrication of many different alkane lengths (up to nonacontatrictane, $C_{390}H_{782}$) and even polydeuterated compounds[37] in very high purity. We will further elaborate on the synthesis of mono- and bifunctional long alkanes in Chapter 5.

Polyesters embody a second class of compounds that are ideal candidates for iterative exponential growth synthesis. An appealing example is the work of Seebach *et al.*,[48] describing a feasible route toward oligomers of (*R*)-3-hydroxybutyric acid from the dimer up to the 128-mer. Their strategy was based on the use of two protective groups for the hydroxyl and carboxyl termini of the mono- and oligomers: a *tert*-butyldiphenylsilyl ether and a benzyl ester, respectively (see Scheme 1–1). Selective removal of these groups, either by Pd/C catalyzed hydrogenolysis, or treatment with HF·pyridine complex, gave two equally long oligomers with a free carboxylic acid (**2**) or alcohol (**3**) functionality. Transformation of the acid into the acid chloride with oxalyl chloride and ligation with the hydroxy-terminated oligomer resulted in twofold protected product **4**, which effectively is the dimer of **1**. This resulted in oligomers with 2, 4, 8, 16, 32, 64, or 128 repeat units. However, the authors noticed that the ligation and subsequent purification of the reaction mixture became increasingly difficult for longer oligomer lengths. In total, 25 mg of the 128-mer was obtained, which contained approximately 10% of the 64-mer.

Also most noteworthy is the synthesis and full characterization of oligomers with up to 64 butylene glutarate residues in the group of Chapman,[49] as well as 64-mers of caprolactone

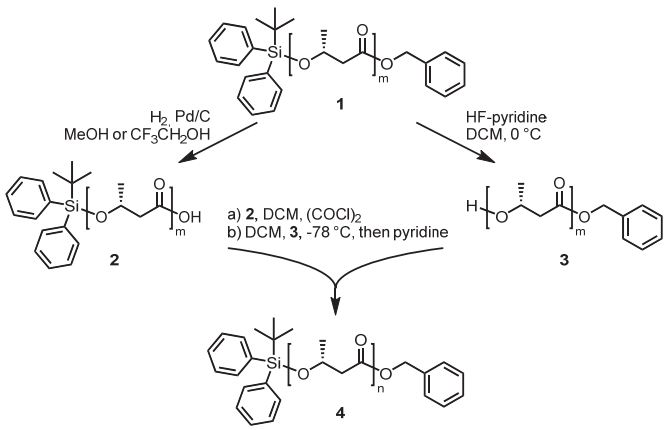

Scheme 1–1. Exponential growth strategy for oligo((*R*)-3-hydroxybutyric acid) up to the 128-mer according to ref. [48].

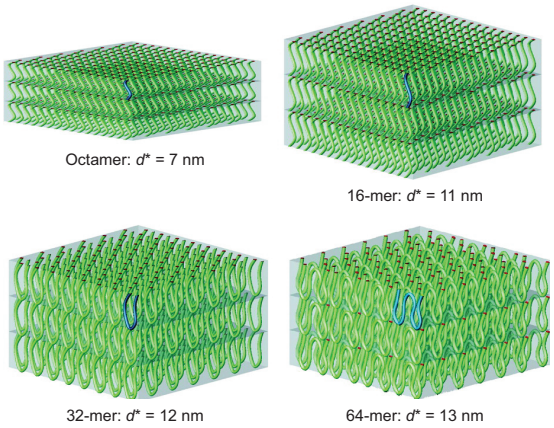

Figure 1–4. Schematic representation of the chain packing and variation of lamellar domain spacing (*D*) for crystalline oligocaprolactone with 8 to 64 repeat units. Figure adapted from ref. [50].

(formally, the ring-opened monomer 6-hydroxycaproic acid) and lactic acid by the Hawker group in two separate publications.[50,51] Although each type of backbone residues required a specific preparation of the two-fold protected starting materials, a similar strategy was employed as for the oligomers of (*R*)-3-hydroxybutyric acid. This work nicely illustrated the added value of uniform oligomers as a tool to determine the exact length-dependency of various physical properties of the oligomers, and its relation to disperse analogues (*e.g.*, the lamellar domain spacing of oligocaprolactone; see Figure 1–4).

For polyamides, a straightforward solution-phase protocol toward nylon-6 mimics in the form of uniform 6-aminohexanoic acid 32-mers was presented by Whiting and coworkers,[52,53] adding to the impressive number of reactions that already were available for the preparation of sequence controlled polyamides by solid-phase synthesis (usually in the form of peptide sequences).[54]

The research on discrete-length polyethers is centralized around polyethylene glycol (PEG), because of the widespread use of this material in biological and biochemical context.[55] Early attempts to generate PEG of uniform length by Hibbert *et al.* resulted in the 42-mer of ethylene glycol.[56] Almost 70 years later, a longer oligomer, comprising 44 repeat units was synthesized by Tanaka,[57] and the preparation of multigram quantities of lower-MW compounds was demonstrated in the group of Hill.[58] In 2009, a publication by Davis even showcases PEG_{48}, albeit that the maximum purity for that compound was no more than 98%.[59] Additionally, uniform, aromatic polyethers with a maximum of 31 repeat units were prepared by Hawker.[60]

A very elegant route to uniform (block) copolymers with side-group modification was reported by the group of Johnson.[61,62] Their work was based on copper catalyzed azide–alkyne click-chemistry and gave access to uniform oligomers consisting of 2 different monomer residues and up to 32 repeat units. The basic strategy is depicted in Figure 1–5A, showing the synthesis of azide and alkyne functionalized monomers **5-N$_3$** and **5-alkyne** from a common precursor. Also visible are the masked endgroups: 1) a bromide acting as a precursor for the azide and 2) a triisopropyl (TIPS) protected alkyne. As a result, both monomers were selectively dimerized *via* the CuAAC catalyzed azide-alkyne click-reaction, resulting in the 'inert' triazole dimer, containing both of the abovementioned masked endgroups. Selective

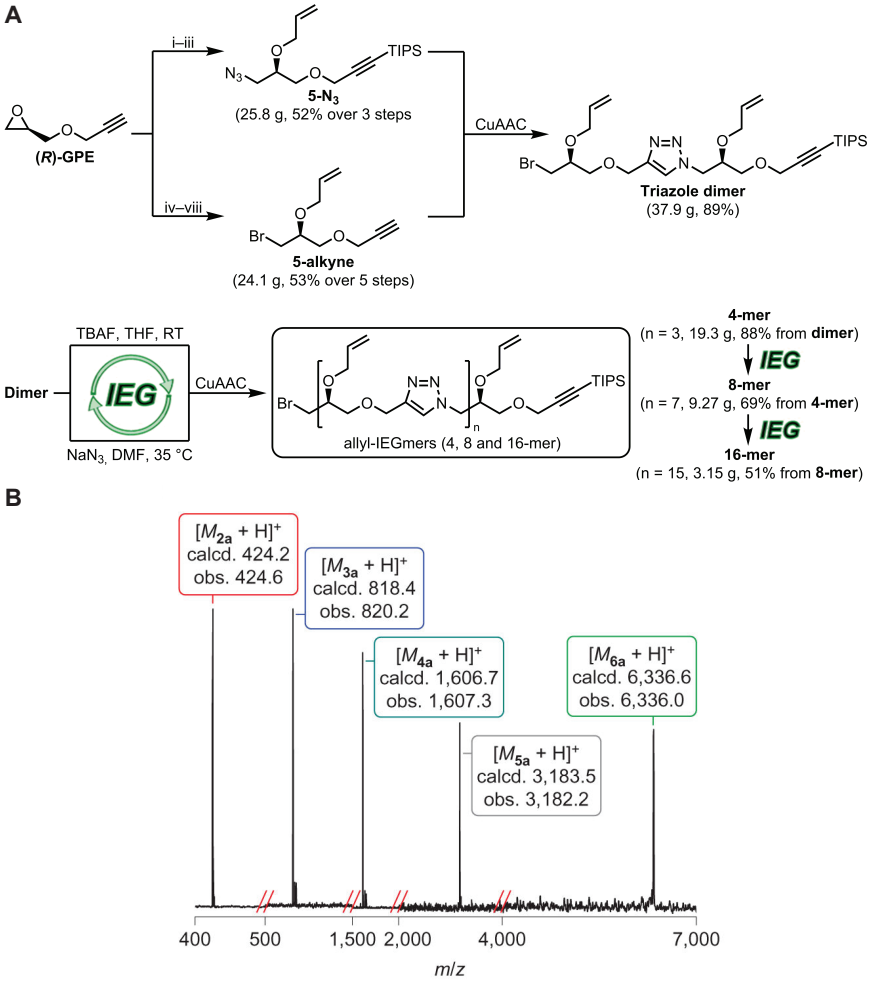

Figure 1–5. (**A**) Fabrication of uniform oligomers up to 16 repeat units with azide-alkyne click chemistry; (**B**) High-resolution MS data for a number of the discrete-MW materials. Images are adapted from refs. [61–62].

transformation of these endgroups into the azide or free alkyne by treatment with sodium azide and tetrabutylammonium fluoride, respectively, followed by another click reaction gave access to the tetramer. Iteration of this process resulted higher-MW compounds with very uniform lengths, as evidenced by the high-resolution mass spectra (Figure 1–5B).

A combination of thiol–maleimide Michael coupling reactions and orthogonal chain-end deprotections based on a retro-Diels–Alder reaction were employed by Zhu to generate discrete-MW materials up to the 128-mer, albeit that the reported purity of the longest oligomer was no more than 95%.[63]

Remarkable results have also been achieved in the synthesis of discrete-length conjugated polymers.[31] Most often, high-MW conjugated polymers are obtained by the ligation of pre-made oligomeric blocks, as already discussed before with the work of Otsubo.[24,25] Although direct synthesis of oligomers with 20 or more repeat units are rarely reported, we find notable exceptions from the group of Osuka.[64–66] As a most extreme example, they prepared linear polyporphyrins with up to 1024 repeat units ($C_{65536}H_{83970}N_{4096}O_{4096}Zn_{1024}$) by iterative homodimerization and recycling GPC purification steps.[65] However, mass spectra confirming the discrete length of the materials were only available up to the 128-mer.

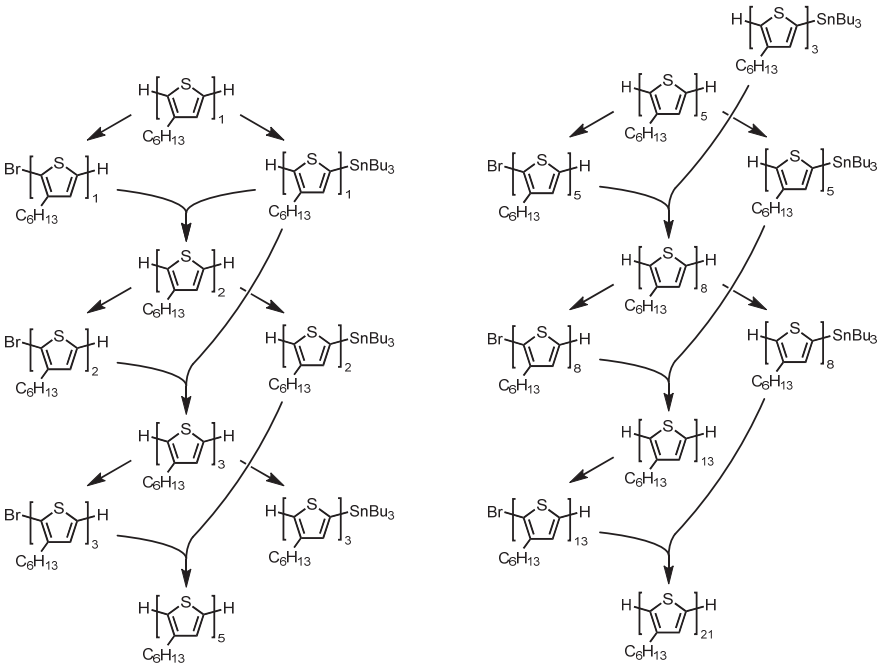

Scheme 1–2. Synthesis of discrete-length oligothiophenes up to the 21-mer. Scheme adapted from ref. [67].

Heeney and coworkers displayed a more systematic strategy for obtaining regioregular oligothiophenes that was less reliant on state-of-the-art recycling GPC equipment.[67,68] The route they developed was based on the selective bromination and stannylation reactions at the 2 and 5'-positions of the oligothiophene termini (Scheme 1–2). Subsequently, the desymmetrized materials were coupled by means of a Stille reaction. By following the Fibonacci sequence when selecting two monofunctional blocks for ligation, purification was facilitated, and lengths up to the 36-mer became available.

1.2.4 Long oligomers by linear growth

The number of reported long linear molecules prepared by solution-phase synthesis *via* a linear strategy is much more limited. Likely, this is directly related to the significantly increased number of steps that is required to obtain a decent number of repeat units (*e.g.*, 20 or more).

A number of examples exist that relate to the synthesis of PEG. The work of Springer is based on benzyl protected and tosylated oligoethylene glycol (*o*EG) building blocks.[69] Ligation of these blocks ultimately lead to PEG 29-mers, which were functionalized with small peptide sequences afterward. Also, a very efficient route was demonstrated by Jiang and coworkers.[70,71] Here, the formation of a large amounts (>100 g) of macrocyclic oligoethylene glycol sulfate **7** from small linear oligomethylene glycol **6** was described (Figure 1–3). Subsequently, this building block was reacted with a broad selection of nucleophiles to give

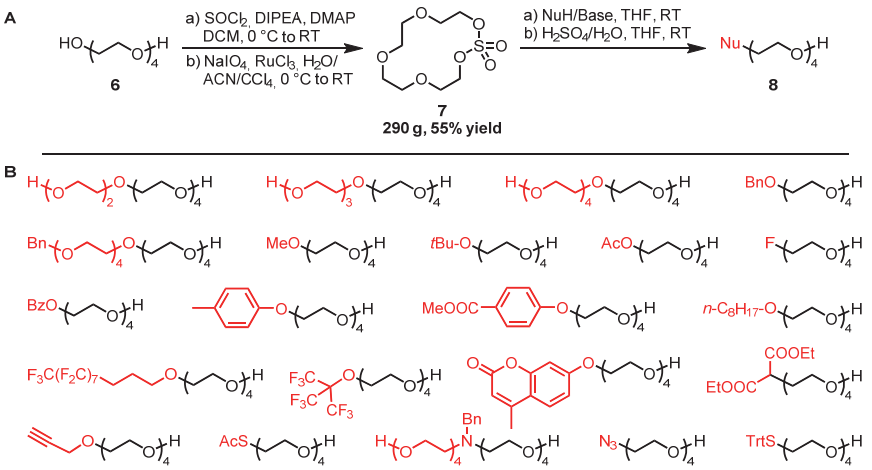

Scheme 1–3. (**A**) Formation of a macrocyclic oligomethylene glycol sulfate **7** and subsequent ring-opening. (**B**) Accessible products **8** after ring-opening with a nucleophile or base (the nucleophile residue is indicated in red). Scheme adapted from ref. [71].

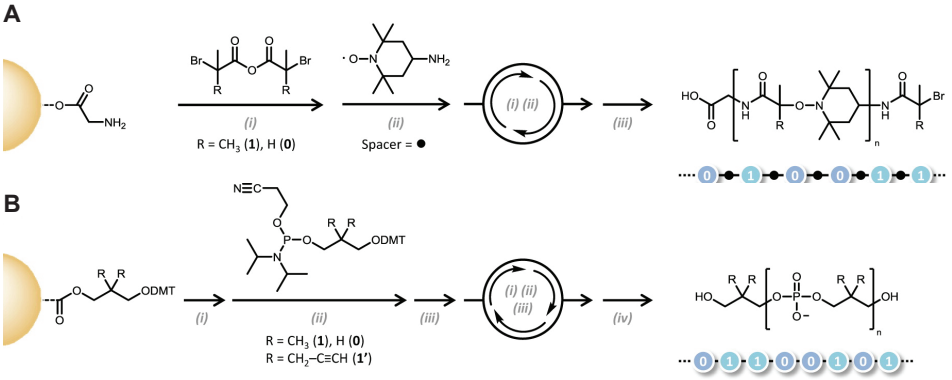

Scheme 1–4. Strategies for obtaining sequence encoded oligomers by iterative solid-phase chemistry, using: (**A**) phosphoramidite chemistry; (**B**) successive anhydride–amine and nitroxide radical coupling steps. Figure adapted from ref. [72].

ring-opened products **8**. Repetitive macrocyclyzation and ring-opening with a small *o*EG diol allowed the fabrication of longer oligomers, containing up to 36 repeat units.

Finally, we provide two examples from Lutz and coworkers in which automated solid-phase synthesis is used to generate oligomers of notable length.[72] The synthesis of oligo(alkoxamine amide)s gave sequence encoded molecules containing up to 24 repeat units (Figure 1–4A).[73] A second strategy employed phosphoramidite chemistry to create oligomers with a maximum of 104 repeat units (Figure 1–4B).[74,75] It should be noted that large excesses of monomers (10 eq) were required to attain sufficiently high coupling yields. Ultimately, 2.3 mg of the 104-mer was obtained.

To conclude this section, discrete polymer synthesis requires both high yielding transformations and, preferably, efficient methods to purify intermediate (and final) compounds. Depending on the anticipated final MW and complexity of the materials, different strategies are available, each having their own pros and cons. Nevertheless, if uniform materials, comprising only one type of monomer residue, are required, then exponential growth strategy generally provides the best growth rate. Although, stepwise precision polymer synthesis (even if automated) clearly is very inefficient in the light of modern—or old—polymerization techniques, normally inaccessible properties and insights into polymer behavior might be unveiled by the resulting uniform materials.

1.3 A brief introduction to block copolymer self-assembly

The term block co-polymer (BCP) generally describes all polymers in which at least two chemically distinct (homo)polymeric blocks are linked by means of covalent—or, in special cases, non-covalent—links. Obviously, this category holds a wide variety of compounds with vastly different block connection topologies, including linear, cyclic, branched and brush-type structures (Figure 1–6).[76] As such, a myriad of different, mostly unstudied molecular designs with unique behavior and application possibilities is within reach.[77] As a result of their relative simplicity—and thus good accessibility—by far the most studied BCP designs (theoretically and experimentally) are of the linear, diblock type. In these systems, a block of polymerized 'A' (*e.g.*, a 'red' block) is linked at one chain-end to a second linear polymer containing 'B' monomer residues (the 'blue' block). Here, we define N as the total number of A and B monomer segments,[ii] and f_A and $f_B = 1 - f_A$ as the volume fractions of A and B (*i.e.*, ratio of the volume occupied by each block to the total polymer volume). In the following subsections, we primarily focus on the behavior of such AB-type diblock copolymers (di-BCPs).

1.3.1 The evolution of microphase separation theory

As a bulk material, most diblock copolymers are designed to microphase segregate into two phases, both of which are ideally composed of either one of the two linked blocks. The underlying thermodynamic driving forces that dictate the microphase segregation process are closely related to those regulating macrophase segregation in homopolymer blends, and result from the total sum of unfavorable enthalpic interactions between dislike monomer residues. However, the strong link between the disparate blocks prevents macrophase separation and, consequently, only allows microphase separation on length scales that are in

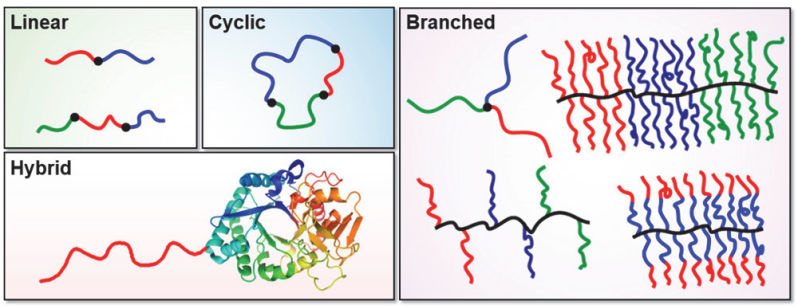

Figure 1–6. Overview of different block connection types in BCPs. Figure adapted from ref. [76].

[ii] Normalized to a common segmental reference volume v.

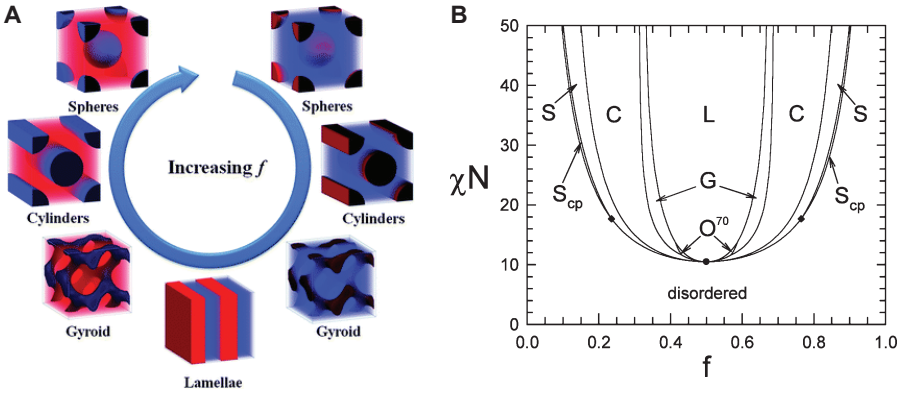

Figure 1–7. (**A**) A graphical representation of various BCP microstructures that can be accessed by altering the volume fraction. The *f* indicates the volume fraction of the red block. Less frequently observed structures (see text) are not shown here; (**B**) Theoretical phase diagram for an AB-type di-BCP (calculated using SCFT). Stable morphologies are indicated: lamellar (L), cylindrical (C), bcc spherical (S), hcp spherical (S_{cp}), gyroid (G), and *Fddd* (O^{70}). The lower dot marks a mean-field critical point at $\chi N = 10.495$. The images are adapted from refs. [78] and [92].

the order of that of the individual polymer chain. In most cases, at least one of the phases is discontinuous, resulting in many, equally shaped domains. The type of microphase-segregated structure is predominantly determined by the volume ratio of both blocks. As pictured in Figure 1–7A, thermodynamically stable domain structures typically consist of simple geometrical shapes of the minor component surrounded by a matrix of the major component. This results in lamellae (LAM), hexagonally packed cylinders (CYL) or bcc-packed spheres (SPH).[78] Also known is the more complex, bicontinous gyroid structure.[79,80] Even more exotic and less frequently found morphologies such as hexagonally modulated layer (HML) and hexagonally perforated layer (HPL) morphologies are predicted, and very stable structures are observed.[81] Yet, simultaneously, their (meta)stability is still under debate.[82] Additionally, the hexagonally close-packed spherical (S_{cp}),[83] orthorhombic *Fddd* (O^{70}),[84] and Frank-Kasper σ-phase[85–87] can be observed in very narrow composition windows.

A pioneering work by Leibler offers an important theoretical basis describing BCP self-assembly.[88] Here, copolymer composition (*f*), length (*N*) and the effective Flory-Huggins interaction parameter (χ) are linked to the equilibrium state of the system. The parameter χ quantifies the overall repulsion between single A and B components that form the BCP molecules, and rarely exceeds 0.2 (*e.g.*, $\chi_{PS\text{-}b\text{-}PMMA} = 0.05$; $\chi_{PS\text{-}b\text{-}PLA} = 0.217$ at 298 K).[iii,89] Self-consistent or mean field theory (SCFT or, equivalently, MFT), introduced by Helfand,[90] could

[iii] PS: polystyrene; PMMA: poly(methyl methacrylate); PLA: polylactic acid.

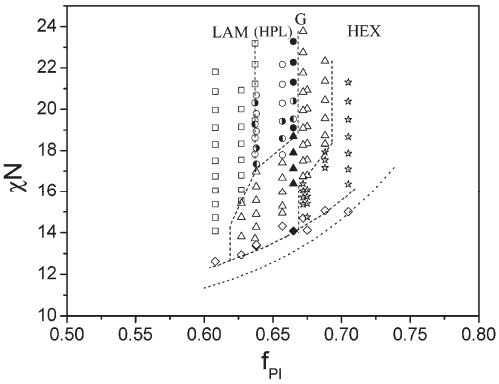

Figure 1–8. Microphase diagram of PS-*b*-PI constructed with fractionated PS-*b*-PI BCPs. Different symbols stand for the different morphologies as shown in the figure. Filled symbols represent the unfractionated PS-*b*-PI. The dotted line is the ODT calculated according to SCFT. Rhombuses are the measured ODT. The dashed line is the phase boundary drawn for visual aid. Half-filled circles represent the data points to test the stability of HPL phase. More details and the original figure can be found in ref. [18].

be used to predict the location of various BCP morphologies as a function of f and the product χN.[91] This gave access to BCP phase diagrams, of which a recently calculated version is given in Figure 1–7B.[92] At low values of χN, the overall repulsion between the A and B fragments of the BCP will be small. Consequently, entropy with dominate and the system will be in a disordered state in which both blocks are practically homogeneously mixed. Only at length scales close to that of the unperturbed (Gaussian) chain a so-called correlation hole is found, which is the indirect result of the remaining covalent connection between the two blocks.[93] For a symmetrical BCP ($f_A = f_B = 0.5$), an order–disorder transition (ODT) is predicted for $(\chi N)_{ODT} = 10.495$.[88] However, this prediction is only valid for BCPs in the limit $N \rightarrow \infty$. Later, a correction for lower N was provided by Helfand:[94] $(\chi N)_{ODT} = 10.495 + 41.022\ \overline{N}^{-\frac{1}{3}}$.[iv] Still, this approximation remains valid only for $N > 10{,}000$. Recently, more sophisticated models, such as the renormalized one-loop (ROL) calculations, have been developed to accurately predict $(\chi N)_{ODT} = 10.495 + 41.0\overline{N}^{-\frac{1}{3}} + 123.0\overline{N}^{-0.56}$ for low-MW BCPs.[95] More qualitatively: according to theory, $(\chi N)_{ODT}$ will significantly increase for very low N (*e.g.*, $N < 100$).

Although the experimental phase diagram of fractionated, low-dispersity PS-*b*-PI BCPs, provided by Park *et al.*, [18] elegantly shows the qualitative agreement with theory (Figure 1–8), two major assumptions that are often employed to simplify the mathematical description of BCP microphase behavior still require attention. In most literature, conformational

[iv] $\overline{N} = a^6 v^{-2} N$ is the invariant polymerization index; a is the statistical segment length, and v is the segment volume.

symmetry of the A and B segments (*i.e.*, having equal statistical segment lengths) and monodispersity ($Đ = 1$) are assumed. However, for most synthetic polymers it is questionable if these assumptions are valid. For example, it was shown that conformational asymmetry causes significant shifts in both experimental and SCFT predicted phase diagrams.[96,97] This shift was explained as a new zero curvature point of the domain interface in the microphase-segregated polymer at $f \neq 0.5$, resulting from counteracting—and balancing—effects of compositional and conformational asymmetry. Secondly, chain-length and compositional dispersity has a strong influence on BCP self-assembly.[98] Most of the theoretical and experimental work on this topic has been nicely summarized by Lynd, Meuler and Hillmyer a decade ago.[99] From the conclusions drawn in this review paper and the articles cited within, it follows that dispersity has a tremendous impact on BCP self-assembly, affecting the average domain sizes, interfacial thickness, location of phase transitions and the value of $(\chi N)_{ODT}$. Many of these behavioral changes were explained as entropy reduction in microphase-segregated domains with increased dispersity. But, importantly, not all of the underlying physical principles were understood at that point. And some still are not, despite advances with lattice-based Monte Carlo simulations that bypass most of the shortcomings of the aforementioned SCFT.[100–102]

1.3.2 High χ–low N BCPs

Block copolymer self-assembly provides a very versatile approach to small and well-organized two- and three-dimensional structures, with a broad variety of applications.[103,104] These systems primarily owe their popularity to the broad choice of polymer backbones and block architectures, as well as the nearly continuous control over the block lengths. Consequently, not only the type of morphology is under synthetic control by adjusting the block volume ratios, but also feature sizes by changing the overall BCP length. If we restrict ourselves to compositionally symmetrical BCPs ($f = 0.5$), SCFT calculations provide us with scaling laws for the domain spacing L_0.[v] However, we have to discriminate between different regions in the phase diagram along the vertical line at $f = 0.5$. Typically, two regions are considered: the strong segregation limit (SSL), where $\chi N \gg 10.5$, and the weak segregation limit (WSL), where $\chi N \approx 10.5$. For these two regions, L_0 depends on N and χ as follows:[78]

SSL: $L_0 \sim N^{2/3}\chi^{1/6}$
WSL: $L_0 \sim N^{1/2}\chi^{1/3}$

[v] For alternating A and B lamellae, the domain spacing is the combined thickness of the A and B domains. In many cases, the domain spacing is denoted as d^*.

As an example, domain sizes of more than 100 nm have been attained with very high MW BCPs ($N > 1000$) for their use in photonic materials.[105–107] On the other end of the spectrum, a large collection of low-MW materials is found that come close to the (SCFT) microphase segregation limit of $\chi N = 10.5$.[vi] Such designer materials often try to achieve lower MW limits, and thus feature sizes, whilst maintaining decent microphase segregation by utilizing block combinations that offer a very high mutual incompatibility.[vii] Collectively, these materials are known as high χ–low N BCPs[108] and are anticipated to fulfill a star role in the fabrication of next-generation nanotechnology.[76,109–111]

A benchmark for small BCP feature sizes was set by Russell in 2009.[112] Herein, the self-assembly of various, cylinder forming polystyrene-*block*-poly(ethylene oxide) (PS-*b*-PEO), polystyrene-*block*-poly(2-vinylpyridine) (PS-*b*-P2VP), and polystyrene-*block*-poly(4-vinylpyridine) (PS-*b*-P4VP) BCPs on sapphire wafers was studied. By exploiting gold complexation to prevent dewetting, microphase separation of low-MW PS-*b*-PEO (M_n = 7.0 kDa) into cylindrical features with domain spacings of 6.9 nm was observed (Figure 1–9). In terms of information storage—image each cylinder as representing one single bit—this corresponds to 10 terabit per square inch (~1.25 TB in^{-2}).

A major downside of incorporating metal salts into BCPs is the incompatibility of those metals with many of the subsequent processing steps and device applications.[108] Consequently, tremendous synthetic effort has been put in finding new block combinations that show high χ values, and thus allow self-assembly of the pristine materials even for very

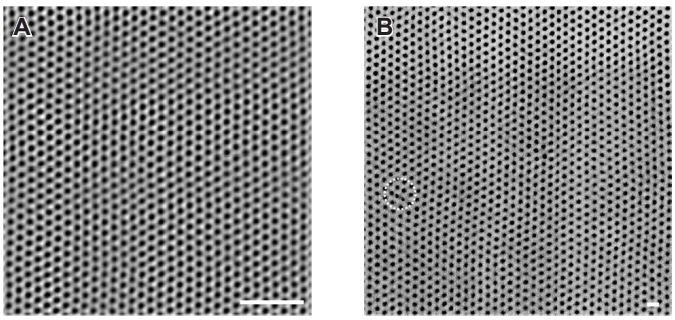

Figure 1–9. AFM images of highly ordered 7kDa (**A**) and 26.5 kDa (**B**) PS-*b*-PEO thin films annealed in solvent vapor. The dotted, white circle marks a defect in the hexagonal packing. Scale bars are 50 nm. Figure adapted from ref. [112].

[vi] In most literature, the non-infinite-N corrections provided by Helfand and ROL calculations are ignored, and the 'classical' value of $\chi N_{ODT} \approx 10.5$ is used.

[vii] Changing N is more convenient that changing χ, and also has a bigger impact on L_0 according to the scaling laws.

low *N*. An overview of BCPs that resulted in self-assembled structures with under-10-nm domain spacings is provided in Table 1–1 (for comparison, the aforementioned PS-*b*-PEO/Au blend is included in entry 4). Remarkably, all of the materials in this overview are published in the last 5 years, revealing the tremendous interest and recent developments in this field.

No single block type dominates in this list, but some blocks occur more than once. Silicon containing blocks such as polydimethylsiloxane (PDMS, entries 5, 7 and 10) or poly(*p*-trimethylsilylstryrene) (PTMSS, entry 8) have been used successfully and provide a high incompatibility with almost all organic materials. For example, the block combination PDMS and polylactic acid (PLA) has an estimated χ parameter close to one at 150 °C.[113] Additionally, a silicon-rich block is beneficial for post-processing steps such as selective etching of one of the blocks because of its high etch-resistivity.[114]

We noticed that the BCPs in entries 1–3, featuring the smallest domain sizes, were all comprised of an apolar block in conjunction with a counterblock that contained a large number of hydroxyl functionalities. For example, Sita developed a conjugate of cellobiose (CB, a disaccharide) and atactic polypropylene (*at*-PP),[viii] which resulted in lamellar domain sizes of 6.5 nm.[115] In the groups of Kim[116] and Russell,[117] polystyrene was employed as

Table 1–1. Overview of the smallest feature sizes for pristine BCPs.[a]

Entry	Polymer type (A-*b*-B)	M_n [kDa]	f_A[b]	Morphology	d^* [nm]	Reference
1	PGM-*b*-PS	2.2	0.52	LAM	5.4	Russell *et al.*, **2017**[117]
2	PDHS-*b*-PS	2.15	0.50	LAM	5.9	Kim *et al.*, **2017**[116]
3	CB-*b*-*at*-PP	n.a.	n.a.	LAM	6.5	Sita *et al.*, **2017**[115]
4	PS-*b*-PEO/Au	7.0	n.a.	CYL	6.9	Russell *et al.*, **2009**[112]
5	PDMS-*b*-PMMA	3.0	0.51	LAM	7.1	Hawker *et al.*, **2017**[125]
6	Post-functionalized PS-*b*-PVDMA	3.5[c]	0.59[c]	LAM	7.6	Mahanthappa *et al.*, **2016**[131]
7	PLA-*b*-PDMS	3.2	0.63	LAM	8.1	Hawker *et al.*, **2016**[129]
8	PTMSS-*b*-cyclodextrin	~3.6	n.a.	CYL	8.3	Ellison *et al.*, **2012**[132]
9	PLA-*b*-PI	2.8	0.51	LAM	8.5	Bates *et al.*, **2013**[85]
10	PDMS-*b*-PMMA	3.9	0.49	LAM	8.7	Hawker *et al.*, **2015**[133]
11	PCHE-*b*-PMMA	4.9	0.46	LAM	9.0	Hillmyer *et al.*, **2014**[134]
12	PTBS-*b*-P2VP	4.5	0.52	LAM	9.6	Gopalan *et al.*, **2014**[135]

[a] Excluding the materials described in this thesis; [b] Volume fraction of the A block; [c] MW and f_A before post-functionalization; n.a. = not directly mentioned in the paper or supporting information. LAM: lamellar, CYL: hexagonally packed cylinders.

[viii] We find it arguable if materials with such short 'oligomeric' blocks should be still be named a BCP.

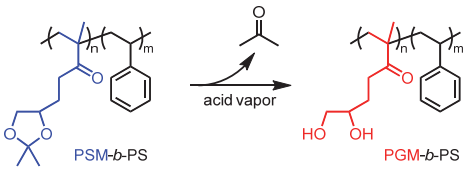

Scheme 1–5. Acid-catalyzed conversion of PSM-*b*-PS to PGM-*b*-PS. Acetone is released during the transformation. Scheme adapted from ref. [117].

hydrophobic block. As second block, Kim used poly(3,4-dihydroxystyrene) (PDHS), achieving 5.9 nm lamellar domains. Current record holder is a poly(glycerol monomethacrylate)-*block*-polystyrene (PGM-*b*-PS) BCP of 2.2 kDa, showing 5.4 nm structures. Interestingly, in this work, not only the MW is tuned to achieve microphase segregation but also χ is increased by transforming a PSM-*b*-PS pre-BCP into PGM-*b*-PS (see Scheme 1–5). In contrast to PGM-*b*-PS, microphase segregation of PSM-*b*-PS was only observed for MW > 14.5 kDa.

Clearly, the ongoing exploration of BCP self-assembly limits has pushed molecular designs far beyond the common definition of polymer. For example, the smallest PGM-*b*-PS BCO that formed a microphase-segregated structure only contained 6 PGM and 9.6 PS repeat units on average. On the contrary, a number of molecules has been developed that received the exclusive label 'liquid crystals' (LCs)[118–121] or 'block molecules' (BMs),[122–124] but resembled BCO-like molecular structures and MWs. Apparently, the synthetic strategy with which the materials were obtained seems to have a significant impact on the final compound classification (BCO or LC/BM), despite similar self-assembly characteristics. Arguably, the crossover point between high-MW BCPs and low-MW LCs (or comparable self-assembling materials) does not exist. That is, the molecule does not care if we categorize it as one or the other.

Nevertheless, we can recognize one major difference between the materials labeled either as polymers or as (small) molecules: molecular uniformity. It was already pointed out that practically all polymers exhibit a molar mass distribution, quantified by a dispersity value. Conversely, small molecules are primarily studied as pure compounds. Although a number of discrete-length polymers have been generated (*vide supra*), only very limited examples of discrete BCPs exist to date, particularly in the low-MW regime.[13,15,125]

1.4 Aim and outline of this thesis

The work of which the highlights are described in this thesis is based on a very simple question: what is the effect of molecular uniformity on block co-polymer self-assembly? As described in this chapter, a major trend in BCP research is the development of smaller feature sizes and/or achieving perfect control over the exact size, shape and location of these features. Since microphase-segregated domains in BCPs are in essence a self-contained ensemble of alike molecular fragments, it seems intuitively logical that allowing less fragments to take part in one of such domains (*i.e.*, by making the domains smaller and smaller), ultimately results in a much larger dependence of the characteristics of such domain—and, consequently, the complete organized network of a myriad of such domains—on the *exact* molecular make-up of its constituents. Importantly, this is not equivalent to postulating that all molecules have to be exactly the same for achieving the most perfectly microphase-segregated BCP. As already pointed out before, an ample number of imperfect, disperse BCPs is known that allow the fabrication of (very) well organized, very small structures. Nonetheless, the intriguing question remains: what will happen to the behavior of such materials *if* we put that 'extra bit of effort' in the synthetic part of the process to make all molecules equal?[108] And, additionally, will it help to better understand the phase behavior of systems with less molecular perfection?

As became clear from the limited number of synthetic protocols for discrete-length polymers above DP = 20, the 'extra bit of effort' tends to roughly increase exponentially with the molecular length. Consequently, we restricted ourselves to relatively low MW materials (20 < DP < 100), which we will often refer to as block co-oligomers or BCOs. A major portion of this thesis discusses BCOs that are comprised of two highly incompatible blocks: oligodimethylsiloxane (*o*DMS) and oligolactic acid (*o*LA). The disperse, higher-MW variants of these molecules have previously been described by Hillmyer and coworkers[113] and Meijer and coworkers[126–129] for triblock, diblock and branched topologies, and form structures that mostly are marginally larger than those listed in Table 1–1 (albeit that for the diblock a domain spacing $d^* = 8.1$ nm is reported).[129]

Chapter 2 contains an in-depth discussion of a modified iterative synthesis protocols for oligolactic acid and a novel protocol for the synthesis of oligodimethylsiloxane on a multigram scale. In addition, we demonstrate the covalent linkage of both blocks, resulting in a unique library of discrete-length diblock co-oligomers. To ensure that microphase separation occurs, we aim for BCOs that have an MW of up to 6.9 kDa. Additionally, the use of different *o*LA volume fractions allows the exploration of a large region of the traditional BCP phase diagram.

The molecules synthesized can be divided into two main categories; *i.e.*, fully amorphous and semicrystalline. In **Chapter 3**, we study the microphase behavior of the BCOs of the first category. With differential scanning calorimetry (DSC), small-angle X-ray scattering (SAXS), and atomic force microscopy (AFM) experiments, we explore the limits of (amorphous) BCO self-assembly in the uniform BCOs. Furthermore, an extra set of low-disperse BCOs will be generated, and the self-assembly assessed. Accordingly, a direct comparison of discrete and disperse in this BCO system is possible.

Next, **Chapter 4** will elaborate on the intriguing role of crystallinity in the microphase segregation behavior of *o*DMS and *o*LA based BCOs. For this, we used isotactic *o*LA, of which the synthesis is already described in Chapter 2. We wondered whether the crystalline properties of isotactic *o*LA remain extant after ligation with a fully amorphous *o*DMS block, and how the discrete nature of the material influences its crystallization behavior. Again, the materials are investigated with DSC and SAXS. Moreover, we also probe the consequences of small amounts of dispersity in such systems. With those results, we postulate a basic model that describes the organization of the semicrystalline BCOs at a molecular level.

Finally, we turn to a different BCO type in **Chapter 5**. We discuss the synthesis and characterization of materials that consist of an *o*DMS block linked to a uniform alkane block (oligomethylene, *o*M) of intermediate length (up to 2.7 kDa). The molecular design of *o*DMS–*o*M is such that it permits the investigation of self-assembly characteristics of molecules in a largely unexplored MW domain that can be pictured as a cross-over region between conventional, high-MW BCPs at one side and low-MW liquid crystals at the other. By carefully studying the self-assembly behavior, our goal is to link the molecular structure of these materials with the type and size of self-assembled structures, as well as the precise molecular orientation within those assemblies. With that, we try to achieve a better understanding of the relation between sub-nanometer molecular design and the self-assembly properties of (uniform) oligomeric materials at the nanometer or even micrometer length scales.

1.5 References

(1) Mülhaupt, R. *Angew. Chemie Int. Ed.* **2004**, *43*, 1054.
(2) Grubbs, R. B.; Grubbs, R. H. *Macromolecules* **2017**, *50*, 6979.
(3) Hawker, C. J. *Science* **2005**, *309*, 1200.
(4) Badi, N.; Chan-Seng, D.; Lutz, J.-F. *Macromol. Chem. Phys.* **2013**, *214*, 135.
(5) Lutz, J.-F. J.-F. *Polym. Chem.* **2010**, *1*, 55.
(6) Lutz, J.-F.; Ouchi, M.; Liu, D. R.; Sawamoto, M. *Science* **2013**, *341*, 1238149.

(7) IUPAC. Compendium of Chemical Terminology, 2nd ed. (the "Gold Book"). Compiled by A. D. McNaught and A. Wilkinson. Blackwell Scientific Publications, Oxford (1997). XML on-line corrected version: http://goldbook.iupac.org (2006).
(8) Zeng, F.; Zimmerman, S. C. *Chem. Rev.* **1997**, *97*, 1681.
(9) Grayson, S. M.; Fréchet, J. M. J. *Chem. Rev.* **2001**, *101*, 3819.
(10) Carlmark, A.; Hawker, C.; Hult, A.; Malkoch, M. *Chem. Soc. Rev.* **2009**, *38*, 352.
(11) Merrifield, R. B. *J. Am. Chem. Soc.* **1963**, *85*, 2149.
(12) Rosales, A. M.; Segalman, R. A.; Zuckermann, R. N. *Soft Matter* **2013**, *9*, 8400.
(13) Sun, J.; Teran, A. A.; Liao, X.; Balsara, N. P.; Zuckermann, R. N. *J. Am. Chem. Soc.* **2014**, *136*, 2070.
(14) Sun, J.; Zuckermann, R. N. *ACS Nano* **2013**, *7*, 4715.
(15) Sun, J.; Teran, A. A.; Liao, X.; Balsara, N. P.; Zuckermann, R. N. *J. Am. Chem. Soc.* **2013**, *135*, 14119.
(16) Murnen, H. K.; Khokhlov, A. R.; Khalatur, P. G.; Segalman, R. A.; Zuckermann, R. N. *Macromolecules* **2012**, *45*, 5229.
(17) Zuckermann, R. N.; Kerr, J. M.; Kent, S. B. H.; Moos, W. H. *J. Am. Chem. Soc.* **1992**, *114*, 10646.
(18) Park, S.; Kwon, K.; Cho, D.; Lee, B.; Ree, M.; Chang, T. *Macromolecules* **2003**, *36*, 4662.
(19) Park, S.; Cho, D.; Ryu, J.; Kwon, K.; Lee, W.; Chang, T. *Macromolecules* **2002**, *35*, 5974.
(20) Chung, B.; Park, S.; Chang, T. *Macromolecules* **2005**, *38*, 6122.
(21) Groenendaal, L.; Peerlings, H. W. I.; Van Dongen, J. L. J.; Havinga, E. E.; Vekemans, J. A. J. M.; Meijer, E. W. *Macromolecules* **1995**, *28*, 116.
(22) Lawrence, J.; Lee, S.-H.; Abdilla, A.; Nothling, M. D.; Ren, J. M.; Knight, A. S.; Fleischmann, C.; Li, Y.; Abrams, A. S.; Schmidt, B. V. K. J.; Hawker, M. C.; Connal, L. A.; McGrath, A. J.; Clark, P. G.; Gutekunst, W. R.; Hawker, C. J. *J. Am. Chem. Soc.* **2016**.
(23) Lawrence, J.; Goto, E.; Ren, J. M.; McDearmon, B.; Kim, D. S.; Ochiai, Y.; Clark, P. G.; Laitar, D.; Higashihara, T.; Hawker, C. J. *J. Am. Chem. Soc.* **2017**, *139*, 13735.
(24) Inouchi, K.; Kobashi, S.; Takimiya, K.; Aso, Y.; Otsubo, T. *Org. Lett.* **2002**, *4*, 2533.
(25) Sumi, N.; Nakanishi, H.; Ueno, S.; Takimiya, K.; Aso, Y.; Otsubo, T. *Bull. Chem. Soc. Jpn.* **2001**, *74*, 979.
(26) Izumi, T.; Kobashi, S.; Takimiya, K.; Aso, Y.; Otsubo, T. *J. Am. Chem. Soc.* **2003**, *125*, 5286.
(27) Haven, J. J.; De Neve, J. A.; Junkers, T. *ACS Macro Lett.* **2017**, *6*, 743.
(28) Binauld, S.; Damiron, D.; Connal, L. A.; Hawker, C. J.; Drockenmuller, E. *Macromol. Rapid Commun.* **2011**, *32*, 147.
(29) Martens, S.; Holloway, J. O.; Du Prez, F. E. *Macromol. Rapid Commun.* **2017**, 1700469.
(30) Solleder, S. C.; Schneider, R. V.; Wetzel, K. S.; Boukis, A. C.; Meier, M. A. R. *Macromol. Rapid Commun.* **2017**, *38*, 1600711.
(31) Martin, R. E.; Diederich, F. *Angew. Chemie Int. Ed.* **1999**, *38*, 1350.
(32) Carothers, W. H. *Trans. Faraday Soc.* **1936**, *32*, 39.
(33) Ungar, G.; Stejny, J.; Keller, A.; Bidd, I.; Whiting, M. C. *Science* **1985**, *229*, 386.
(34) Paynter, O. I.; Simmonds, D. J.; Whiting, M. C. *J. Chem. Soc. Chem. Commun.* **1982**, 1165.
(35) Brooke, G. M.; Burnett, S.; Mohammed, S.; Proctor, D.; Whiting, M. C. *J. Chem. Soc. Perkin Trans. 1* **1996**, 1635.
(36) Bidd, I.; Whiting, M. C. *J. Chem. Soc. Chem. Commun.* **1985**, 543.
(37) Brooke, G. M.; Farren, C.; Harden, A.; Whiting, M. C. *Polymer* **2001**, *42*, 2777.
(38) Bidd, I.; Holdup, D. W.; Whiting, M. C. *J. Chem. Soc. Perkin Trans. 1* **1987**, 2455.
(39) Igner, E.; Paynter, O. I.; Simmonds, D. J.; Whiting, M. C. *J. Chem. Soc. Perkin Trans. 1* **1987**, 2447.

(40) Adegoke, E. A.; Ephraim-Bassey, H.; Kelly, D. J.; Whiting, M. C. *J. Chem. Soc. Perkin Trans. 1* **1987**, 2465.
(41) Bidd, I.; Whiting, M. C. *J. Chem. Soc. Chem. Commun.* **1985**, 543.
(42) Bidd, I.; Kelly, D. J.; Ottley, P. M.; Paynter, O. I.; Simmonds, D. J.; Whiting, M. C. *J. Chem. Soc. Perkin Trans. 1* **1983**, 1369.
(43) Ställberg, G.; Ställberg-Stenhagen, S.; Stenhagen, E.; Finsnes, E.; Sörensen, J. S.; Sörensen, N. A. *Acta Chem. Scand.* **1952**, *6*, 313.
(44) Carothers, W. H.; Hill, J. W.; Kirby, J. E.; Jacobson, R. A. *J. Am. Chem. Soc.* **1930**, *52*, 5279.
(45) Lee, K. S.; Wegner, G. *Die Makromol. Chemie, Rapid Commun.* **1985**, *6*, 203.
(46) Doolittle, A. K.; Peterson, R. H. *J. Am. Chem. Soc.* **1951**, *73*, 2145.
(47) Reinhard, R. R.; Dixon, J. A. *J. Org. Chem.* **1965**, *30*, 1450.
(48) Lengweiler, U. D.; Fritz, M. G.; Seebach, D. *Helv. Chim. Acta* **1996**, *79*, 670.
(49) Williams, J. B.; Chapman, T. M.; Hercules, D. M. *Macromolecules* **2003**, *36*, 3898.
(50) Takizawa, K.; Tang, C.; Hawker, C. J. *J. Am. Chem. Soc.* **2008**, *130*, 1718.
(51) Takizawa, K.; Nulwala, H.; Hu, J.; Yoshinaga, K.; Hawker, C. J. *J. Polym. Sci. Part A Polym. Chem.* **2008**, *46*, 5977.
(52) Brooke, G. M.; Mohammed, S.; Whiting, M. C. *J. Chem. Soc. Perkin Trans. 1* **1997**, 3371.
(53) Brooke, G. .; Hugh MacBride, J. .; Mohammed, S.; Whiting, M. . *Polymer* **2000**, *41*, 6457.
(54) Hermkens, P. H. H.; Ottenheijm, H. C. J.; Rees, D. *Tetrahedron* **1996**, *52*, 4527.
(55) Haag, R.; Kratz, F. *Angew. Chemie Int. Ed.* **2006**, *45*, 1198.
(56) Fordyce, R.; Lovell, E. L.; Hibbert, H. *J. Am. Chem. Soc.* **1939**, *61*, 1905.
(57) Ahmed, S. A.; Tanaka, M. *J. Org. Chem.* **2006**, *71*, 9884.
(58) Loiseau, F. A.; Hii, K. K.; Hill, A. M. *J. Org. Chem.* **2004**, *69*, 639.
(59) French, A. C.; Thompson, A. L.; Davis, B. G. *Angew. Chemie Int. Ed.* **2009**, *48*, 1248.
(60) Hawker, C. J.; Malmström, E. E.; Frank, C. W.; Kampf, J. P. *J. Am. Chem. Soc.* **1997**, *119*, 9903.
(61) Barnes, J. C.; Ehrlich, D. J. C.; Gao, A. X.; Leibfarth, F. A.; Jiang, Y.; Zhou, E.; Jamison, T. F.; Johnson, J. A. *Nat. Chem.* **2015**, *7*, 810.
(62) Jiang, Y.; Golder, M. R.; Nguyen, H. V.-T.; Wang, Y.; Zhong, M.; Barnes, J. C.; Ehrlich, D. J. C.; Johnson, J. A. *J. Am. Chem. Soc.* **2016**, *138*, 9369.
(63) Huang, Z.; Zhao, J.; Wang, Z.; Meng, F.; Ding, K.; Pan, X.; Zhou, N.; Li, X.; Zhang, Z.; Zhu, X. *Angew. Chemie Int. Ed.* **2017**, *56*, 13612.
(64) Aratani, N.; Osuka, A.; Kim, Y. H.; Jeong, D. H.; Kim, D. *Angew. Chemie Int. Ed.* **2000**, *39*, 1458.
(65) Aratani, N.; Takagi, A.; Yanagawa, Y.; Matsumoto, T.; Kawai, T.; Yoon, Z. S.; Kim, D.; Osuka, A. *Chem. – A Eur. J.* **2005**, *11*, 3389.
(66) Aratani, N.; Osuka, A. *Bull. Chem. Soc. Jpn.* **2015**, *88*, 1.
(67) Koch, F. P. V; Smith, P.; Heeney, M. *J. Am. Chem. Soc.* **2013**, *135*, 13695.
(68) Koch, F. P. V.; Heeney, M.; Smith, P. *J. Am. Chem. Soc.* **2013**, *135*, 13699.
(69) Niculescu-Duvaz, D.; Getaz, J.; Springer, C. J. *Bioconjugate Chem.* **2008**, *19*, 973.
(70) Zhang, H.; Li, X.; Shi, Q.; Li, Y.; Xia, G.; Chen, L.; Yang, Z.; Jiang, Z.-X. *Angew. Chem. Int. Ed. Engl.* **2015**, *54*, 3763.
(71) Li, Y.; Qiu, X.; Jiang, Z.-X. *Org. Process Res. Dev.* **2015**, *19*, 800.
(72) Lutz, J.-F. *Macromolecules* **2015**, *48*, 4759.
(73) Roy, R. K.; Meszynska, A.; Laure, C.; Charles, L.; Verchin, C.; Lutz, J.-F. *Nat. Commun.* **2015**, *6*, 7237.
(74) Al Ouahabi, A.; Charles, L.; Lutz, J.-F. *J. Am. Chem. Soc.* **2015**, *137*, 5629.

(75) Ouahabi, A. Al; Kotera, M.; Charles, L.; Lutz, J.-F. *ACS Macro Lett.* **2015**, *4*, 1077.
(76) Bates, C. M.; Bates, F. S. *Macromolecules* **2017**, *50*, 3.
(77) Bates, F. S.; Hillmyer, M. A.; Lodge, T. P.; Bates, C. M.; Delaney, K. T.; Fredrickson, G. H. *Science* **2012**, *336*, 434.
(78) Koo, K.; Ahn, H.; Kim, S.-W.; Ryu, D. Y.; Russell, T. P. *Soft Matter* **2013**, *9*, 9059.
(79) Matsen, M. W.; Schick, M. *Phys. Rev. Lett.* **1994**, *72*, 2660.
(80) Fredrickson, G. H.; Bates, F. S. *Annu. Rev. Mater. Sci.* **1996**, *26*, 501.
(81) Loo, Y.-L.; Register, R. A.; Adamson, D. H.; Ryan, A. J. *Macromolecules* **2005**, *38*, 4947.
(82) Hajduk, D. A.; Takenouchi, H.; Hillmyer, M. A.; Bates, F. S.; Vigild, M. E.; Almdal, K. *Macromolecules* **1997**, *30*, 3788.
(83) Matsen, M. W.; Bates, F. S. *Macromolecules* **1996**, *29*, 1091.
(84) Tyler, C. A.; Morse, D. C. *Phys. Rev. Lett.* **2005**, *94*, 208302.
(85) Lee, S.; Gillard, T. M.; Bates, F. S. *AIChE J.* **2013**, *59*, 3502.
(86) Lee, S.; Leighton, C.; Bates, F. S. *Proc. Natl. Acad. Sci. U. S. A.* **2014**, *111*, 17723.
(87) Arora, A.; Qin, J.; Morse, D. C.; Delaney, K. T.; Fredrickson, G. H.; Bates, F. S.; Dorfman, K. D. *Macromolecules* **2016**, *49*, 4675.
(88) Leibler, L. *Macromolecules* **1980**, *13*, 1602.
(89) Keen, I.; Cheng, H.-H.; Yu, A.; Jack, K. S.; Younkin, T. R.; Leeson, M. J.; Whittaker, A. K.; Blakey, I. *Macromolecules* **2014**, *47*, 276.
(90) Helfand, E. *Macromolecules* **1975**, *8*, 552.
(91) Bates, F. S.; Fredrickson, G. H. *Annu. Rev. Phys. Chem.* **1990**, *41*, 525.
(92) Matsen, M. W. *Macromolecules* **2012**, *45*, 2161.
(93) Bates, F. S. *Macromolecules* **1985**, *18*, 525.
(94) Fredrickson, G. H.; Helfand, E. *J. Chem. Phys.* **1987**, *87*, 697.
(95) Beardsley, T. M.; Matsen, M. W. *Phys. Rev. Lett.* **2016**, *117*, 217801.
(96) Bates, F. S.; Schulz, M. F.; Khandpur, A. K.; Förster, S.; Rosedale, J. H.; Almdal, K.; Mortensen, K. *Faraday Discuss.* **1994**, *98*, 7.
(97) Matsen, M. W.; Bates, F. S. *J. Polym. Sci. Part B Polym. Phys.* **1997**, *35*, 945.
(98) Register, R. A. *Nature* **2012**, *483*, 167.
(99) Lynd, N. A.; Meuler, A. J.; Hillmyer, M. A. *Prog. Polym. Sci.* **2008**, *33*, 875.
(100) Beardsley, T. M.; Matsen, M. W. *Eur. Phys. J. E* **2008**, *27*, 323.
(101) Beardsley, T. M.; Matsen, M. W. **2010**, *32*, 255.
(102) Beardsley, T. M.; Matsen, M. W. *Macromolecules* **2011**, *44*, 6209.
(103) Schacher, F. H.; Rupar, P. a; Manners, I. *Angew. Chemie Int. Ed.* **2012**, *51*, 7898.
(104) Bates, F. S.; Fredrickson, G. H. *Phys. Today* **1999**, *52*, 32.
(105) Xia, Y.; Olsen, B. D.; Kornfield, J. A.; Grubbs, R. H. *J. Am. Chem. Soc.* **2009**, *131*, 18525.
(106) Urbas, A.; Sharp, R.; Fink, Y.; Thomas, E. L.; Xenidou, M.; Fetters, L. J. *Adv. Mater.* **2000**, *12*, 812.
(107) Urbas, A. M.; Maldovan, M.; DeRege, P.; Thomas, E. L. *Adv. Mater.* **2002**, *14*, 1850.
(108) Sinturel, C.; Bates, F. S.; Hillmyer, M. A. *ACS Macro Lett.* **2015**, *4*, 1044.
(109) Hawker, C. J.; Russell, T. P. *MRS Bull.* **2005**, *30*, 952.
(110) Hu, H.; Gopinadhan, M.; Osuji, C. O. *Soft Matter* **2014**, *10*, 3867.
(111) Durand, W. J.; Blachut, G.; Maher, M. J.; Sirard, S.; Tein, S.; Carlson, M. C.; Asano, Y.; Zhou, S. X.; Lane, A. P.; Bates, C. M.; Ellison, C. J.; Willson, C. G. *J. Polym. Sci. Part A Polym. Chem.* **2015**, *53*, 344.

(112) Park, S.; Lee, D. H.; Xu, J.; Kim, B.; Hong, S. W.; Jeong, U.; Xu, T.; Russell, T. P. *Science* **2009**, *323*, 1030.

(113) Rodwogin, M. D.; Spanjers, C. S.; Leighton, C.; Hillmyer, M. A. *ACS Nano* **2010**, *4*, 725.

(114) Nunns, A.; Gwyther, J.; Manners, I. *Polymer* **2013**, *54*, 1269.

(115) Nowak, S. R.; Hwang, W.; Sita, L. R. *J. Am. Chem. Soc.* **2017**, *139*, 5281.

(116) Kwak, J.; Mishra, A. K.; Lee, J.; Lee, K. S.; Choi, C.; Maiti, S.; Kim, M.; Kim, J. K. *Macromolecules* **2017**, *50*, 6813.

(117) Jeong, G.; Yu, D. M.; Mapas, J. K. D.; Sun, Z.; Rzayev, J.; Russell, T. P. *Macromolecules* **2017**, *50*, 7148.

(118) Goodby, J. W.; Davis, E. J.; Mandle, R. J.; Cowling, S. J.; Goodby, J. W.; Davis, E. J.; Mandle, R. J.; Cowling, S. J. In *Handbook of Liquid Crystals*; Wiley-VCH Verlag GmbH & Co. KGaA: Weinheim, Germany, 2014; pp. 1–30.

(119) Tschierske, C. *J. Mater. Chem.* **1998**, *8*, 1485.

(120) Kato, T. *Science* **2002**, *295*, 2414.

(121) Nickmans, K.; Murphy, J. N.; de Waal, B.; Leclère, P.; Doise, J.; Gronheid, R.; Broer, D. J.; Schenning, A. P. H. J. *Adv. Mater.* **2016**, *28*, 10068.

(122) Zha, R. H.; de Waal, B. F. M.; Lutz, M.; Teunissen, A. J. P.; Meijer, E. W. *J. Am. Chem. Soc.* **2016**, *138*, 5693.

(123) Berrocal, J. A.; Zha, R. H.; de Waal, B. F. M.; Lugger, J. A. M.; Lutz, M.; Meijer, E. W. *ACS Nano* **2017**, *11*, 3733.

(124) Kim, H.-J.; Kim, T.; Lee, M. *Acc. Chem. Res.* **2011**, *44*, 72.

(125) Oschmann, B.; Lawrence, J.; Schulze, M. W.; Ren, J. M.; Anastasaki, A.; Luo, Y.; Nothling, M. D.; Pester, C. W.; Delaney, K. T.; Connal, L. A.; McGrath, A. J.; Clark, P. G.; Bates, C. M.; Hawker, C. J. *ACS Macro Lett.* **2017**, *6*, 668.

(126) Pitet, L. M.; Wuister, S. F.; Peeters, E.; Kramer, E. J.; Hawker, C. J.; Meijer, E. W. *Macromolecules* **2013**, *46*, 8289.

(127) Pitet, L. M.; van Loon, A. H. M.; Kramer, E. J.; Hawker, C. J.; Meijer, E. W. *ACS Macro Lett.* **2013**, *2*, 1006.

(128) Pitet, L. M.; Alexander-Moonen, E.; Peeters, E.; Druzhinina, T. S.; Wuister, S. F.; Lynd, N. A.; Meijer, E. W. *ACS Nano* **2015**, *9*, 9594.

(129) Minehara, H.; Pitet, L. M.; Kim, S.; Zha, R. H.; Meijer, E. W.; Hawker, C. J. *Macromolecules* **2016**, *49*, 2318.

(130) Hawker, C. J.; Frechet, J. M. J. *J. Am. Chem. Soc.* **1990**, *112*, 7638.

(131) Carter, M. C. D.; Jennings, J.; Speetjens, F. W.; Lynn, D. M.; Mahanthappa, M. K. *Macromolecules* **2016**, *49*, 6268.

(132) Cushen, J. D.; Otsuka, I.; Bates, C. M.; Halila, S.; Fort, S.; Rochas, C.; Easley, J. A.; Rausch, E. L.; Thio, A.; Borsali, R.; Willson, C. G.; Ellison, C. J. *ACS Nano* **2012**, *6*, 3424.

(133) Luo, Y.; Montarnal, D.; Kim, S.; Shi, W.; Barteau, K. P.; Pester, C. W.; Hustad, P. D.; Christianson, M. D.; Fredrickson, G. H.; Kramer, E. J.; Hawker, C. J. *Macromolecules* **2015**, *48*, 3422.

(134) Kennemur, J. G.; Yao, L.; Bates, F. S.; Hillmyer, M. A. *Macromolecules* **2014**, *47*, 1411.

(135) Sweat, D. P.; Kim, M.; Larson, S. R.; Choi, J. W.; Choo, Y.; Osuji, C. O.; Gopalan, P. *Macromolecules* **2014**, *47*, 6687.

♦ Chapter 2 ♦

A Convenient Route to Synthesize Uniform, Dimethylsiloxane and Lactic Acid Based Diblock Co-Oligomers

Abstract: By utilizing iterative synthetic protocols, diblock co-oligomers consisting of oligodimethylsiloxane (*o*DMS) and oligolactic acid (*o*LA) with molar masses up to 6.9 kDa and ultra-low molar mass dispersities ($Đ \leq 1.00002$) were synthesized and characterized. This required the development of a new, divergent strategy for *o*DMS structures by which both bi- and monofunctional *o*DMS derivatives containing up to 59 siloxane repeat units became available. Furthermore, we obtained *o*LA blocks up to the 64-mer, which comprised different types of tacticity in the oligomer backbone. The incompatibility of the *o*DMS and *o*LA blocks made the final coupling more demanding as the block length increases. The optimized synthetic procedures allowed access to multi-gram quantities of most of the block co-oligomers, permitting to study the lower limits of block copolymer phase segregation in detail.

This work was performed in close collaboration with Bas de Waal and Brigitte Lamers.

Part of this work has been published:
van Genabeek, B.; de Waal, B. F. M.; Gosens, M. M. J.; Pitet, L. M.; Palmans, A. R. A.; Meijer, E. W. *J. Am. Chem. Soc.* **2016**, *138*, 4210.
van Genabeek, B.; Lamers, B. A. G.; de Waal, B. F. M.; van Son, M. H. C.; Palmans, A. R. A.; Meijer, E. W. *J. Am. Chem. Soc.* **2017**, *139*, 14869.

"Dear Colleague, leave the concept of large molecules well alone; organic molecules with a molecular weight above 5000 do not exist. Purify your products, such as rubber, then they will crystallize and prove to be lower molecular substances. Organic molecules with more than 40 atoms do not exist. Molecules cannot be larger than the crystallographic unit cell, so there can be no such thing as a macromolecule."

—Heinrich Otto Wieland, Advice to Hermann Staudinger, 1920.[1]

2.1 Introduction

As discussed in Chapter 1, we are interested in the evolution of BCP phase behavior as a function of the chain length and composition dispersity. Of particular interest is the behavior of a system of which the dispersity is unity, *i.e.*, of which the molecular weight distribution has coalesced into a single molecular weight, identical for every polymer chain. However, attaining (substantial) amounts of discrete-length polymers is far from straightforward. In some cases, separation techniques such as recycling GPC were successful to minimize—but not remove—the dispersities in diblock copolymers.[2] Remarkably, to our knowledge, there is only a limited number of examples of uniform synthetic block copolymers reported to date.[3,4] In fact, whereas great synthetic effort resulted in many examples of dendrimers of uniform MW,[5] the list of reported uniform, linear homopolymers and oligomers with more than 20 repeat units—excluding the biological structures made by solid-phase synthesis—is remarkably short, covering (un)branched olefins,[6–9] oligoethylene glycols,[10–16] polyethers,[17,18] polyesters,[19–22] and conjugated oligomeric systems.[23–27] Every oligomer/polymer required its own synthetic approach, typically divided into either a divergent or a convergent approach, similar to the synthesis of dendrimers.

The purpose of this chapter is to provide a robust and scalable route toward discrete-length 'block co-oligomers' (BCOs), consisting of oligodimethylsiloxane (*o*DMS) and oligolactic acid (*o*LA) blocks (Scheme 2–1). Since the *o*DMS and *o*LA blocks have such disparate chemical compatibilities and functionalities, we chose to synthesize the two uniform blocks separately. Here we aimed for a maximum length of 59 and 64 repeat units for the *o*DMS and *o*LA blocks, respectively. Finally, two different coupling strategies were optimized to combine the discrete homo-oligomers to furnish a library of uniform block co-oligomers, with the longest one having a combined total of 92 siloxane and lactic acid repeat units: *i.e.*, a dononacontamer.

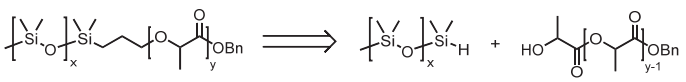

Scheme 2–1. Molecular design of the *o*DMS–*o*LA BCO and the required building blocks *o*DMS and *o*LA.

2.2 Synthesis of discrete-length oligomeric blocks

Two different synthetic methodologies were employed for the synthesis of linear oligodimethylsiloxanes and oligolactic acid molecules. Despite using a similar strategy of iterative condensation and endgroup deprotection/activation, the methods differ both by the type of reactions involved, as well as the growth rate (linear and exponential, respectively) of the resulting oligomers.

2.2.1 Homotelechelic and heterotelechelic oligodimethylsiloxane blocks

In this work, oligodimethylsiloxanes are divided into two categories: homotelechelic or heterotelechelic, as pictured in Figure 2–1. Homotelechelic *o*DMS contains two identical and functionalizable endgroups—usually in the form of a hydride or hydroxyl group—whereas the heterotelechelic oDMS only contains one single functionalizable endgroup and is endcapped with a methyl group at the other chain-end. For clarity, throughout this and subsequent chapters, the following abbreviations will be used for the *o*DMS blocks aside from the conventional numbering of molecules: **A-Si$_x$-B**, where **A** and **B** represent the oligomer endgroups (*e.g.*, Me, H, OH or Cl) and **Si$_x$** represents the number of silicon atoms in the block.[i]

Literature examples that describe the synthesis, modification or purification of oligomers based on the dimethylsiloxane building block are scarce and limited to eight repeat units.[53–55] Consequently, a novel synthetic protocol to produce the discrete-length *o*DMS blocks was developed in our group by Bas de Waal. Because of the commercial unavailability of siloxane building blocks with more than 4 repeat units, a large number of sequential steps is required to obtain *o*DMS blocks with a desired number of up to 59 repeat units. Thus, in order to obtain practical amounts of *o*DMS, very high yielding reactions are essential. Those reactions have to be chemically orthogonal so they can be employed in an iterative manner. This further limits the already small number of chemical transformations available for organo-silicon chemistry.

HO-Si$_8$-OH **Me-Si$_{15}$-H**

Figure 2–1. Examples of a homotelechelic *o*DMS (HO-Si$_8$-OH, left) and a heterotelechelic *o*DMS (Me-Si$_{15}$-H, right).

[i] Although not strictly equivalent (the number of oxygen atoms connecting two silicon atoms will always be one less than the number of silicon atoms itself), we will often refer to '**Si$_x$**' or 'the number of silicon atoms' with the near-identical quantity 'the number of siloxane repeat units'. Formally, by the way we defined our abbreviations, all siloxanes have a non-integer number of siloxane repeat units, *e.g.*, 6.5 for Me-Si$_7$-H

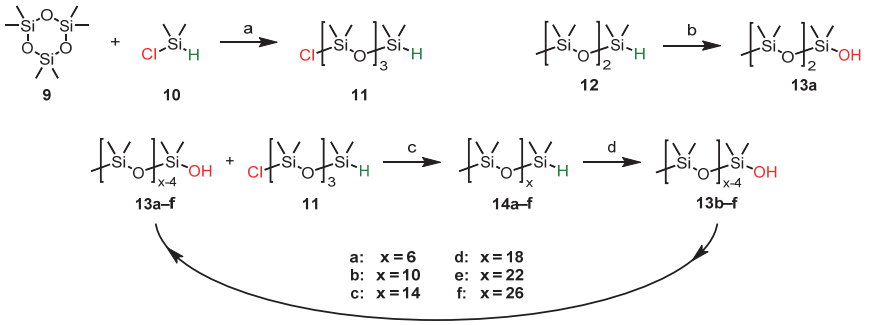

Scheme 2–2. Linear route toward siloxane monohydrides **14a–f**. Dormant and reactive endgroups are depicted in green and red, respectively. Reagents and conditions: (a) ACN, DMF (cat.), RT, 70 h (65%); (b and d) Pd/C, dioxane, 1 M phosphate buffer (pH = 7), RT, 20 h (91–99%); (c) pyridine, toluene, RT, 3 h (66–99%).

The first generation of heterotelechelic *o*DMS, comprising under 30 repeat units, was obtained via the protocol that is depicted in Scheme 2–2. Here, the iterative (*i.e.*, chain-growth) process consists of two main reactions: 1) the base-catalyzed condensation of a silanol (R_3Si-OH) and a silyl chloride (R'_3Si-Cl) (reaction *c*), resulting in the silicon equivalent of a C-O-C ether bond (commonly known as a siloxane, R_3Si-O-SiR'_3), and 2) the selective conversion of a silyl hydride (R_3Si-H) into the corresponding silanol (R_3Si-OH) (reactions *b* and *d*). Notably, silyl hydrides do not react with silyl chlorides under the conditions employed here, and as such both reactions can be considered orthogonal and thus suitable for our synthesis.

First, the tetrasiloxane building block Cl-Si_4-H **11** was generated by the ring-opening of the cyclic hexamethylcyclotrisiloxane **9** with chlorodimethylsilane **10**. Here, a small amount of DMF acted as a catalyst, facilitating the insertion of the chlorosilane in the ring and formation of the bifunctional linear species containing a chloro and hydride endgroup. Because of the good commercial availability and low cost of the starting materials, the building block could be generated on large scale (~150 g, 65% yield). The product was purified by vacuum distillation, which removed byproducts such as the heptasiloxane H-Si_7-Cl. These materials were formed in minor quantities as a result of subsequent ring-opening reactions initiated by the product. A high purity of the building block was required to prevent any amplification of the fraction of siloxanes with a disparate number of repeat units after every subsequent elongation step in the *o*DMS synthesis (*vide infra*).

Next, commercially available, heterotelechelic trisiloxane hydride **12** was converted into the corresponding silanol **13a** by stirring in a phosphate buffer/dioxane mixture in the presence of Pd/C catalyst. This very mild reaction, followed by a simple work-up, resulted in

an almost quantitative isolation (96%) of the silanol without any byproducts. Subsequently, chlorosilane **11** was reacted with silanol Me-Si_3-OH **13a** in toluene. Pyridine was added to capture the HCl that was released during the reaction, driving the reaction to completion. The silyl hydride product Me-Si_7-H **14a** did not react further with additional chlorosilane. To ensure high purity of the product, the material was subjected to vacuum distillation, resulting in a slightly diminished yield of 66%. Repetition of these last 2 steps resulted in the stepwise extension of the *o*DMS molecule with 4 siloxane units in every cycle. Purification steps primarily involved automated column chromatography after the reaction with chlorosilane **11**. Alternatively, *o*DMS blocks with more than 11 siloxane repeat units could be purified easily by washing the neat compounds with acetonitrile because of the insolubility of the longer siloxanes in this solvent. Finally, *o*DMS hydrides with 11, 15, 19, 23, and 27 repeat units (**14b–f**) were all obtained in multi-gram quantities and overall yields of 57, 50, 45, 38, and 27%, respectively.

The method described above is very effective for the synthesis of relatively short siloxanes (less than 30 repeat units). However, accessing longer *o*DMS blocks, containing up to 59 repeat units, necessitated an alternative, more efficient route involving homotelechelic siloxane disilanols **17g–k**. As a result of their symmetry, reacting the siloxane diols with two equivalents of chlorosilane **11** gives a direct elongation by eight siloxane repeat units instead of four in each consecutive cycle. Later, the homotelechelic siloxane can be transformed into a heterotelechelic silanol **13l** by a statistical reaction with a methyl endcapped siloxane chloride containing 15 siloxane repeat units. Consequently, the required number of steps to reach 59 repeat units is significantly reduced (Scheme 2–3).

First, dihydride H-Si_8-H **16** was prepared in two steps. Hydrolysis of building block Cl-Si_4-H **11** with $NaHCO_3$ in a water/diethyl ether mixture gave HO-Si_4-H **15**. Subsequent coupling with another equivalent of Cl-Si_4-H gave the desired material in 80% overall yield. The dihydride was converted into the disilanol HO-Si_8-OH **17g** in 94% yield using the palladium-catalyzed insertion of water, in analogy to the reactions with the heterotelechelic siloxanes. Next, disilanol **17g** was reacted with 2 equivalents of chlorosilane building block **11**, resulting in elongated dihydride H-Si_{16}-H **18g**. In a similar way as described above, dihydride **18g** was converted to the corresponding disilanol **17h**. Threefold repetition of these 2 steps eventually lead to the formation of more than 3 grams of disilanol HO-Si_{40}-OH **17k**. After each elongation step, residual chlorosilane **11** and byproducts resulting from incomplete conversion of both silanol groups were removed either by washing with acetonitrile or using column chromatography. Here, we exploited the unexpectedly strong

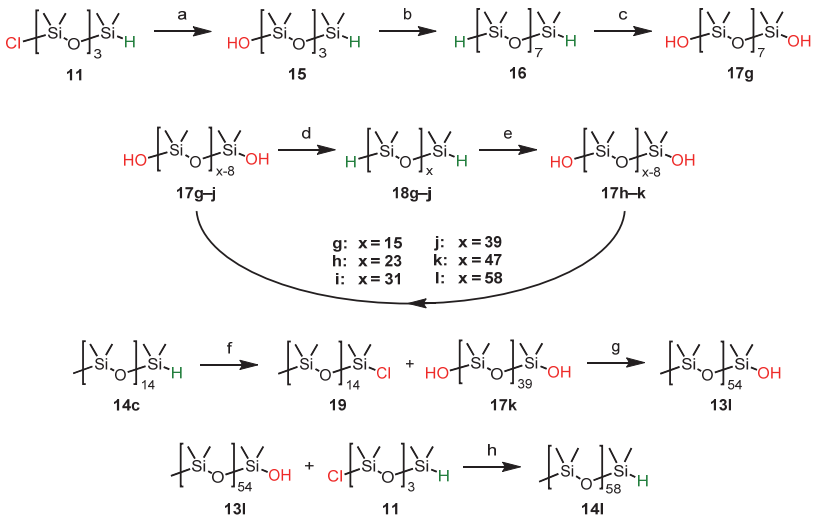

Scheme 2–3. Synthesis of longer siloxane monohydride **14l**. Dormant and reactive endgroups are depicted in green and red, respectively. Reagents and conditions: (a) $NaHCO_3$, diethyl ether, water, 0–20 °C , 4 h (99%); (b and d) **11**, pyridine, toluene, 0–20 °C, 3–5 h (47–94%); (c and e) Pd/C, dioxane, 1 M phosphate buffer (pH = 7), 0–20 °C, 3–24 h (82–100%); (f) $PdCl_2$, CCl_4, RT, 16 h (92%); (g) pyridine, toluene, RT, 22 h (27%); (h) pyridine, toluene, RT, 3 h (65%).

influence of the endgroup combination (2 × hydride, 2 × silanol or hydride–silanol) on the affinity of the product with the column material. The transformation of the homotelechelic siloxane into the heterotelechelic silanol Me-Si_{55}-OH **13l** required a statistical reaction with siloxane chloride Me-Si_{15}-Cl **19**. This material was obtained by the reaction of Me-Si_{15}-H **14c** with tetrachloromethane in the presence of $PdCl_2$ catalyst. Finally, condensation of the silanol **13l** with chlorosilane **11** resulted in 340 mg of discrete-length siloxane hydride Me-Si_{59}-H **14l**. All siloxane hydrides were fully characterized with ^{1}H NMR, ^{13}C NMR, size exclusion chromatography (SEC) and matrix assisted laser desorption/ionization time-of-flight (MALDI-TOF) mass spectrometry. It was noticed that detecting the oligodimethylsiloxanes by MALDI-TOF is hard, especially for the highest MW oligomers. Nevertheless, no evidence was found for the presence of oligomers with differing numbers of siloxane repeat units.

2.2.2 Discrete-length atactic and isotactic oligolactic acid blocks

Because of the chiral nature of the lactic acid repeat unit, all oligolactic acid molecules considered in this work are divided in two related groups: atactic and isotactic (Figure 2–2). From a molecular viewpoint, the sole difference between these groups is the relative absolute configuration of all methine carbons throughout the oligomer backbone. The atactic *o*LA (*at*-*o*LA) can be considered as a mixture of molecules that includes all possible permutations

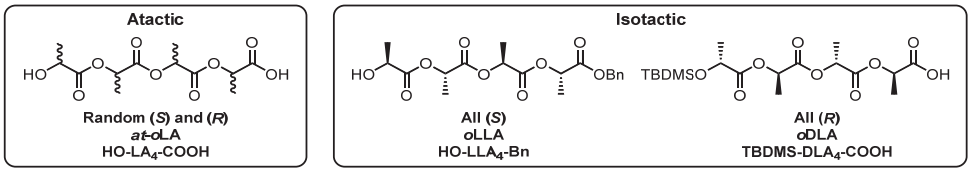

Figure 2–2. Two main groups of *o*LA used in this work: atactic (*at*-*o*LA) and isotactic (*o*LLA and *o*DLA).

for the arrangement of absolute configurations—(*S*) or (*R*)—for all lactic acid residues. In other words: all possible stereoisomers that exist for a particular *o*LA length.[ii] In contrast, the methine carbons of isotactic *o*LA (*i*-*o*LA) have either all (*S*)-configuration or all (*R*)-configuration. Both enantiomers of the related lactic acid monomer are often denoted as L-lactic acid (LLA, (*S*)-configuration) or D-lactic acid (DLA, (*R*)-configuration), and the associated polylactic acid as PLLA or PDLA, respectively. Here, this nomenclature is extended with *o*LLA and *o*DLA, referring to isotactic all (*S*)- and all (*R*)-oligomers, respectively. Furthermore, a more specific notation will be used that includes both lactic acid endgroups, the tacticity, and the number of lactic acid repeat units. Atactic *o*LA blocks are abbreviated as **C-LA$_y$-D**, where **C** and **D** represent the oligomer endgroups (*e.g.*, OH, COOH, TBDMS or Bn)[iii] and **LA$_y$** represents the number of lactic acid repeat units (note: the designation *atactic* is not explicitly used). Isotactic *o*LLA and *o*DLA are abbreviated as **C-LLA$_y$-D** and **C-DLA$_y$-D**, respectively.

At first, our aim was to obtain monodisperse, atactic lactic acid oligomers with 8 to 32 repeating lactic acid units. For this, we modified a route first described by Hawker and coworkers for the synthesis of isotactic L-lactic acid oligomers.[22] In this route, the use of orthogonal protective group chemistry enabled sequential deprotection and coupling steps, resulting in discrete-length oligolactic acid blocks (Scheme 2–4). Because of the limited stability of ester bonds, mild reaction conditions were chosen for each consecutive step. Benzyl (Bn) ester and *tert*-butyldimethylsilyl (TBDMS) ether protective groups were used at the carboxylic acid and hydroxy termini of the lactic acid oligomers, respectively, owing to nearly quantitative and orthogonal deprotection possibilities. Carbodiimide coupling chemistry was subsequently utilized for the efficient and controlled ligation of hydroxy and carboxylic acid terminated *at*-*o*LA.

[ii] Strictly, as a result of the synthesis protocol we envisioned, *at*-*o*LA used in this work always consists of pairs of two neighboring lactic acid residues with equal absolute configuration.

[iii] TBDMS = *tert*-butyldimethylsilyl; Bn = benzyl.

Initially, the benzyl protected dimeric building block HO-LA$_2$-Bn *rac*-**22m** was obtained in a two-step process from the readily available DL-lactide *rac*-**20** (*i.e.*, a racemate of (*R,R*)-lactide and (*S,S*)-lactide without the meso form). First, ring-opening of the lactide with water at elevated temperatures gave the linear lactic acid dimer HO-LA$_2$-COOH *rac*-**21**. After reaching 80–90% conversion of the lactide, the reaction was stopped to prevent over-hydrolysis of the remaining ester functionality in the product. Still, significant quantities (up to 10%) of the monomeric lactic acid was formed. Next, the carboxylic acid could be protected as the benzyl ester by the reaction with benzyl bromide in the presence of *N,N*-diisopropylethylamine in DCM. The material was purified by column chromatography, giving pure benzyl ester *rac*-**22m** without monomeric byproducts in yields up to 60%. However, the outcome of the ring-opening reaction was relatively unpredictable and difficult to control, particularly upon up-scaling. Partly, this is due to the fact that the reaction is heterogeneous (the solubility of DL-lactide is water is very low). Also, the ring-opening is acid-catalyzed, making the conversion autocatalytic—the product is a relatively strong organic acid itself—and also strongly dependent on the initial concentrations of traces of acid

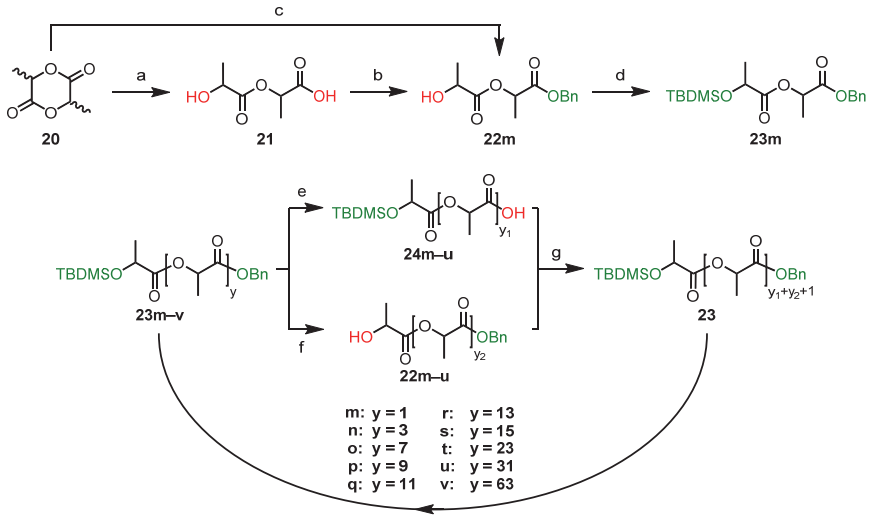

Scheme 2–4. General synthesis scheme for lactic acid oligomers **23m–v**. Dormant and reactive endgroups are depicted in green and red, respectively. *rac*-Lactide was used to generate *at*-oLA, whereas L- and D-lactide afforded the corresponding isotactic *o*LLA and *o*DLA. For clarity, the absolute configurations of the methine carbons (indicated by the wavy bonds in the lactide structure) are omitted in the remainder of this scheme. Reagents and conditions: (a) H_2O, 40 °C, 7h (84%); (b) BnBr, *N,N*-diisopropylethylamine, DCM, room temperature, 18 h (69%); (c) BnOH, CSA, toluene, 80 °C, 8 h (64–77%); (d) TBDMSCl, imidazole, DMF, RT, O/N (59–90%); (e) H_2, Pd/C, EtOAc, RT, 2 h (86-100%); (f) $BF_3{\cdot}Et_2O$, DCM, RT, 4 h (76–96%); (g) EDC·HCl, DPTS, DCM, RT, 3 h (47–94%). CSA = D-camphorsulfonic acid, EDC·HCl = *N*-(3-dimethylaminopropyl)-*N'*-ethylcarbodiimide hydrochloride, DPTS = 4-(dimethylamino)pyridinium 4-toluenesulfonate.

resulting from starting material that was hydrolyzed during storage. Therefore, an alternative route was followed, in which lactide *rac*-**20** was directly converted into benzyl ester *rac*-**22m** via a ring-opening reaction initiated by benzyl alcohol in the presence of catalytic amounts of D-camphorsulfonic acid. Although this reaction could be better controlled, still a side-reaction was observed between the remaining ester functionality in the dimeric product and additional benzyl alcohol, resulting in undesired monomeric *rac*-HO-LA_1-Bn. We found that the use of an equimolar ratio of lactide and benzyl alcohol and stopping the reaction after consumption of approximately 80% of the alcohol suppressed the formation of monomer. Afterward, complete removal the monomer in the crude product was necessary to prevent cross-coupling at later stages, resulting in inseparable mixtures. Albeit laborious, the dimer and monomer could be separated using automated column chromatography. Repurification of all mixed fractions finally resulted an acceptable yield (73%) of pure dimer HO-LA_2-Bn *rac*-**22m**.

To minimize waste, a part of the less pure fractions were reacted with *tert*-butyldimethylsilyl chloride (TBDMS-Cl) and then purified by column chromatography to give monomer-free double protected dimer TBDMS-LA_2-Bn *rac*-**23m** on >30 g scale in high yield (90%). A major portion of the material was treated with Pd/C under a hydrogen atmosphere to remove the benzyl ester and liberate the carboxylic acid *rac*-**24m** in quantitative yield. The remainder was converted back to alcohol *rac*-**22m**. The removal of the TBDMS protective group was first attempted with tetrabutylammonium fluoride (TBAF) solution in THF. However, the amphiphilic character of this reagent and the significant water solubility of the hydroxy dimer *rac*-**22m** lead to difficulties during the aqueous workup of the reaction and a rather low yield of 55%. In addition, the formation of substantial amounts of monomeric hydrolysis products was observed. Luckily, BF_3 etherate could be used to selectively cleave the TBDMS ether in a large scale reaction without the formation of any hydrolysis byproducts.[28] After purification by column chromatography, hydroxy dimer *rac*-**22m** was obtained in 88% yield.

Formation of the doubly protected tetramer TBDMS-LA_4-Bn *at*-**23n** was conducted by ligation of the dimeric free acid *rac*-**24m** and the hydroxy dimer *rac*-**22m** under standard carbodiimide coupling conditions. After purification, the tetramer was obtained in excellent yield (94%). By repeating the deprotection and coupling steps, combined with purification by column chromatography after each reaction, a range of hydroxy-terminated lactic acid oligomers *at*-**22o–u**, containing 8, 10, 12, 14, 16, 24, and 32 repeat units, were obtained (22% overall yield for the longest oligomer). All materials remained very viscous to nearly glassy,

depending on the oligomer length. The high purity and discrete length of these oligomers were confirmed by ^{1}H NMR, ^{13}C NMR, and MALDI-TOF MS. In all cases, only minor quantities (<0.5 mol%) of chains containing ±1 repeat unit were observed, translating to dispersity values $Đ < 1.00001$.

Both isotactic oligo-L-lactic acid (*o*LLA) and oligo-D-lactic acid (*o*DLA) were obtained in close analogy to the atactic compounds by starting from the corresponding optically pure L- and D-lactide (L-**20** and D-**20**). To further decrease the formation of undesired block lengths at later stages of the synthesis, we very carefully selected only the purest fractions that resulted from purification by column chromatography of the compounds at the dimeric stage (*i.e.*, compounds L-**22m**, D-**22m**, L-**23m**, and D-**23m**). For this, all fractions were analyzed by gas chromatography-mass spectrometry (GC-MS), using an acceptation threshold of <0.05% monomer byproduct. Continuation of the synthetic route as described above led to the formation of *o*LLA and *o*DLA with up to 64 repeat units. In contrast to the atactic analogues, most of the isotactic compounds were crystalline solids at room temperature. Again, the purity of the compounds was checked with NMR spectroscopy and MALDI-TOF MS.

Two representative *o*LA ^{1}H NMR spectra (of TBDMS-LA$_{16}$-Bn *at*-**23s** and TBDMS-LLA$_{16}$-Bn L-**23s**) are provided in Figure 2–3A. Most of the signals that originate from the molecule endgroups appear as nearly identical for both types of *o*LA, whereas two regions of overlapping peaks, corresponding to the backbone methine and methyl protons—around 5.2 ppm and 1.5 ppm—reveal clear differences between the two (see insets). This discrepancy is caused by differences in tacticity. The large number of possible configurations of linked

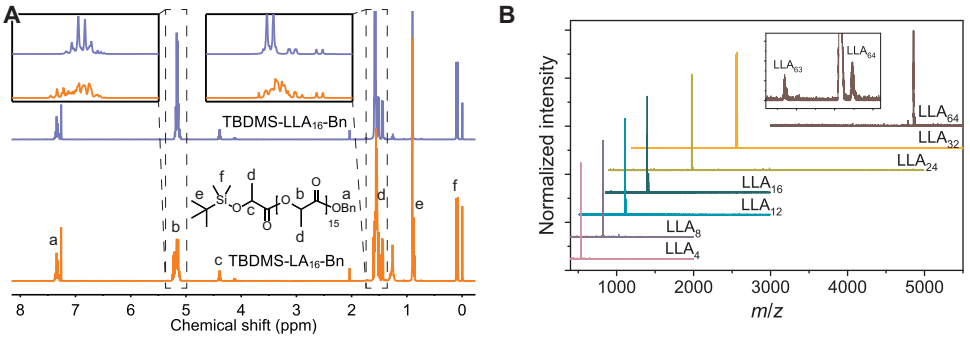

Figure 2–3. (**A**) ^{1}H NMR spectra ($CDCl_3$) of TBDMS-LA$_{16}$-Bn (*at*-**23s**, orange curve) and TBDMS-LLA$_{16}$-Bn (L-**23s**, purple curve). The insets show magnified regions around 5.2 ppm and 1.5 ppm, respectively. Peaks around 4.12, 2.02, 1.26 and 0.88 ppm resulted from residual solvents (heptane and ethyl acetate); (**B**) MALDI-TOF mass spectra (DCTB matrix) for *o*LLA with 4 to 64 repeat units. LLA$_y$ is a shorthand notation for TBDMS-LLA$_y$-Bn. The data are shifted vertically for clarity. The inset shows the magnified region around m/z = 4900.

L- and D-lactide units in *at*-*o*LA is reflected by a large number of signals, each with a slight offset in the chemical shift. In contrast, the chemical shifts of most methine or methyl protons in isotactic *o*LLA (or *o*DLA) are nearly identical, resulting in quartet- and doublet-resembling multiplets. A selection of MALDI-TOF mass spectra of *o*LLA (Figure 2–3B) demonstrates the extremely low dispersity of all isotactic *o*LA blocks. In particular, the absence of peaks indicative for undesired *o*LLA lengths translates to dispersity values $Đ \ll 1.0000005$. We owe the extremely low dispersities to the more strict purity analyses performed at the dimeric stage of the isotactic *o*LA syntheses, compared to the *at*-*o*LA formation. Only the highest MW materials, TBDMS-LLA_{64}-Bn (L-**23v**) and TBDMS-DLA_{64}-Bn (D-**23v**), contain approximately 2–5% material that has a single repeat unit less. TBDMS-DLA_{64}-Bn also contained traces of remaining HO-DLA_{32}-Bn D-**22u**.

2.3 Synthesis of discrete-length *o*DMS–*o*LA block co-oligomers

For the ligation of the *o*DMS blocks to atactic *o*LA, we selected the efficient and selective Karstedt hydrosilylation reaction between a siloxane hydride and a terminal alkene as a key reaction step.[29] As depicted in the top section of Scheme 2–5, the optically pure allyl derivative L-**26** was selected as the appropriate alkene, since it resulted in the smallest possible length of the molecular link between the *o*DMS block and *at*-*o*LA block. Also, the carboxylic acid residue provided a direct anchor to couple any desired hydroxy terminated *at*-*o*LA block. Although a racemic mixture of both enantiomers of compound **25** seemed a more reasonable choice in conjunction with an atactic *o*LA block, we justified our choice for the (*S*)-enantiomer with two reasons: 1) better commercial availability of the starting compound; 2) dual applicability of resulting functionalized siloxane in the syntheses of both *at*-*o*LA and *o*LLA containing BCOs (*vide infra*).

The allyl ether derivative of benzyl (*S*)-lactate was obtained moderate yield (60%) by a silver(I) oxide mediated etherification. Subsequently, the lactate was coupled to the *o*DMS block using the Karstedt hydrosilylation reaction. Removal of the benzyl ester by Pd/C catalyzed hydrogenolysis, followed by purification with column chromatography, afforded pure and monodisperse L-lactic acid functionalized *o*DMS Me-Si_x-LLA_1-COOH L-**28c**, **e**, **f** and **l**, having either 15, 23, 27, or 59 siloxane repeat units, respectively. During purification,

care was taken to remove all undesired siloxane-rich compounds (*e.g.*, remaining hydride). The troublesome purification of siloxane 59-mer L-**28l** was the main reason for the low yield (6%) of this product. Subsequent carbodiimide-facilitated ligation of these blocks with hydroxy-terminated *at*-*o*LA *at*-**22** of various lengths resulted in the formation of a series of

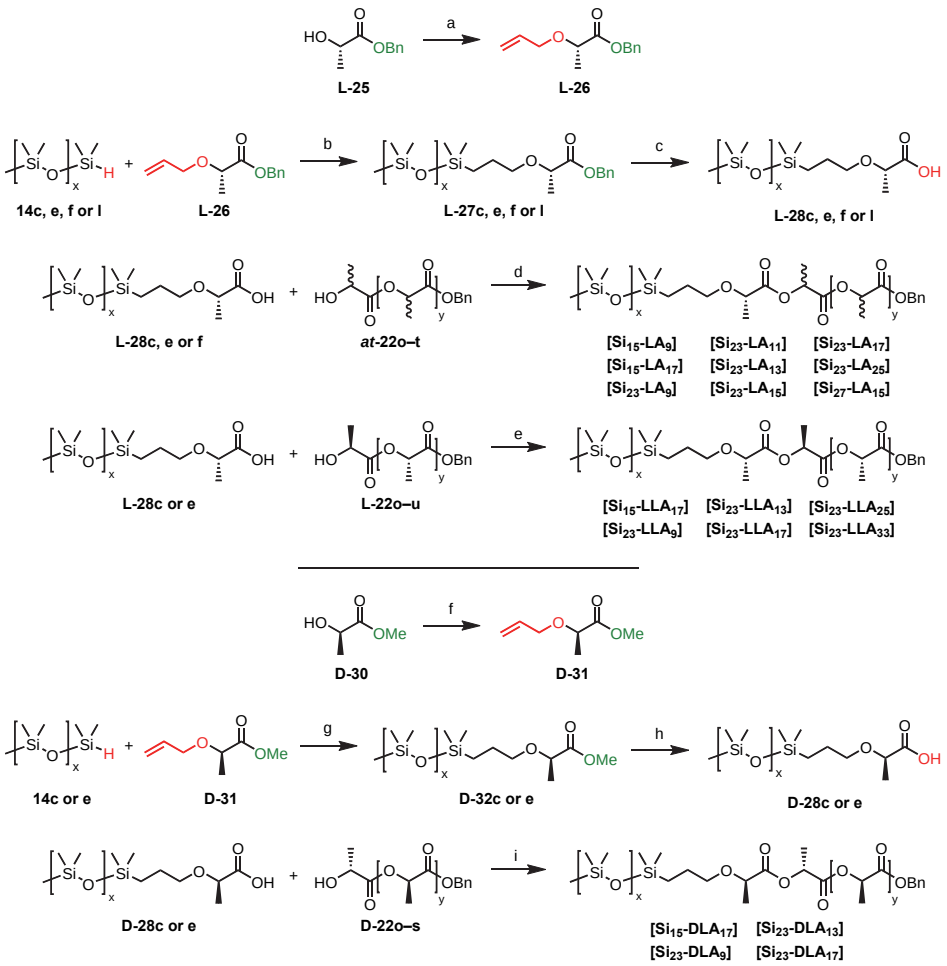

Scheme 2–5. Synthesis of *o*DMS–*o*LA block co-oligomers. Dormant and reactive endgroups are depicted in green and red, respectively. Reagents and conditions: (a and f) allyl bromide, silver(I) oxide, Et_2O, reflux, O/N (60–68%); (b and g) Karstedt catalyst, toluene, 60 °C, 3h (63–97%); (c) Pd/C, EtOAc, RT, 2 h (6–85%); (d, e and i) EDC·HCl, DPTS, DCM, RT, O/N (16–96%); (h); $SnMe_3OH$, DCE, 70 °C, 3 d (48–74%). DCE = dichloroethane, EDC·HCl = *N*-(3-dimethylaminopropyl)-*N*'-ethylcarbodiimide hydrochloride, DPTS = 4-(dimethylamino)pyridinium 4-toluenesulfonate.

block co-oligomers, denoted [$\mathbf{Si_x\text{-}LA_y}$][iv] (*e.g.*, [$\mathbf{Si_{23}\text{-}LA_{25}}$] for the BCO containing 23 siloxane and 25 lactic acid repeat units). During the final coupling reaction, it was found that a high concentration of the reactant was crucial for obtaining high yields. Therefore, all reactions were carried out close to the solubility limit of the reactants. Interestingly, the BCO is less soluble in DCM than the separate blocks, as evidenced by the formation of an emulsified reaction mixture, visually confirming the formation of product. After work-up and purification by column chromatography, the [$\mathbf{Si_x\text{-}LA_y}$] BCOs were obtained as waxy solids.

The reaction of the longest siloxane block (Me-Si_{59}-LLA_1-COOH L-**28l**) with the longest *at*-*o*LA block (HO-LA_{32}-Bn *at*-**22u**) under similar carbodiimide coupling conditions did not give significant amounts of BCO. Instead, most of the unreacted lactic acid block was recovered. In addition, a siloxane derivative was isolated which most probably is the *N*-acylurea EDC adduct. Presumably, this rearrangement byproduct was formed as result of the slow reaction of the reactive *O*-acylurea EDC adduct with the *at*-*o*LA block, which is turn was caused by high endgroup dilution and intrinsic tendency of both blocks to remain unmixed. Therefore, an alternative strategy was employed to obtain BCOs [$\mathbf{Si_{27}\text{-}LA_{25}}$] and [$\mathbf{Si_{59}\text{-}LA_{33}}$] (Scheme 2–6). Acid functionalized *o*DMS L-**28f** or **l** was transformed into the corresponding acid chloride with Ghosez's reagent.[30] Reaction of the crude acid chloride with hydroxy-terminated *at*-*o*LA *at*-**22t** or **u** gave the desired BCOs, albeit in low to moderate yields of 48 and 18%, respectively, after purification.

As mentioned above, the homochiral L-lactic acid unit in functionalized siloxanes L-**28** allowed a repetition of the final ligation step using isotactic *o*LLA blocks (see Scheme 2–5). This directly afforded the corresponding BCOs [$\mathbf{Si_x\text{-}LLA_y}$]. On the other hand, the chirality mismatch between siloxanes L-**28** and *o*DLA D-**22** necessitated the formation of a siloxane

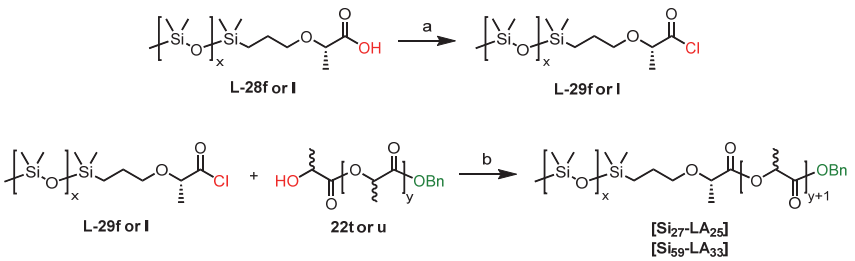

Scheme 2–6. Alternative coupling of the blocks. Dormant and reactive endgroups are depicted in green and red, respectively. Reagents and conditions: (a) Ghosez's reagent (1-chloro-*N*,*N*,2-trimethyl-1-propenylamine), DCM, RT, O/N (no purification); (b) dry pyridine, DCM, RT, 5 h (18–48% over two steps).

[iv] In line with the introduced terminology for the *o*LA blocks, the designation *atactic* is not explicitly used in the abbreviated BCO names.

derivatized with a D-lactic acid residue (bottom section of Scheme 2–5). For this, we started from the commercially available methyl ester of D-lactic acid D-**30**, which was transformed into allyl ether D-**31** in 68% yield. Next, the material was reacted with oDMS hydride **14c** or **e**, giving siloxane derivatives D-**32c** or **e** with 15 or 23 siloxane repeat units in good yield (79%). The methyl esters of both materials were hydrolyzed under mild conditions with trimethyltin hydroxide to give free carboxylic acid D-**28c** and **e**. Finally, ligation of these compounds with *o*DLA of various lengths completed the third series of BCOs: [**Si$_x$-DLA$_y$**]. In line with the isotactic *o*LLA and *o*DLA blocks and in contrast to the atactic BCOs, most of the BCOs based on isotatic *o*LA block formed crystalline solids at room temperature.

In Table 2–1, an overview is presented of the most relevant *o*DMS and *o*LA block lengths, stereo configurations and associated BCOs that were generated using the methods described above, and of which properties will be studied throughout this thesis. To keep the overview concise, *o*DMS and *o*LA blocks that were synthesized, but never incorporated into an *o*DMS–

Table 2–1. Overview of most relevant *o*DMS and *o*LA blocks and associated BCOs.

*o*LA \ *o*DMS	Me-Si$_{15}$-H	Me-Si$_{23}$-H	Me-Si$_{27}$-H	Me-Si$_{59}$-H
HO-LA$_8$-Bn	**[Si$_{15}$-LA$_9$]**	**[Si$_{23}$-LA$_9$]**		
HO-LLA$_8$-Bn		**[Si$_{23}$-LLA$_9$]**		
HO-DLA$_8$-Bn		**[Si$_{23}$-DLA$_9$]**		
HO-LA$_{10}$-Bn		**[Si$_{23}$-LA$_{11}$]**		
HO-LA$_{12}$-Bn		**[Si$_{23}$-LA$_{13}$]**		
HO-LLA$_{12}$-Bn		**[Si$_{23}$-LLA$_{13}$]**		
HO-DLA$_{12}$-Bn		**[Si$_{23}$-DLA$_{13}$]**		
HO-LA$_{14}$-Bn		**[Si$_{23}$-LA$_{15}$]**	**[Si$_{27}$-LA$_{15}$]**	
HO-LA$_{16}$-Bn	**[Si$_{15}$-LA$_{17}$]**	**[Si$_{23}$-LA$_{17}$]**		
HO-LLA$_{16}$-Bn	**[Si$_{15}$-LLA$_{17}$]**	**[Si$_{23}$-LLA$_{17}$]**		
HO-DLA$_{16}$-Bn	**[Si$_{15}$-DLA$_{17}$]**	**[Si$_{23}$-DLA$_{17}$]**		
HO-LA$_{24}$-Bn		**[Si$_{23}$-LA$_{25}$]**	**[Si$_{27}$-LA$_{25}$]**	
HO-LLA$_{24}$-Bn		**[Si$_{23}$-LLA$_{25}$]**		
HO-LA$_{32}$-Bn				**[Si$_{59}$-LA$_{33}$]**
HO-LLA$_{32}$-Bn		**[Si$_{23}$-LLA$_{33}$]**		

*o*LA BCO are omitted. Those blocks will be discussed individually in the remainder of this and subsequent chapters.

2.4 Molecular characterization of monodisperse BCOs

Conventional size exclusion chromatography (SEC) is insufficiently sensitive for determining accurate values of co-oligomer molar mass dispersity, since all BCOs show dispersities that are far below the typical lower detection limit of this technique ($Đ \approx 1.01$). However, a striking difference was observed between the discrete-length BCO **[Si$_{15}$-LA$_{17}$]** (M_n = 2486 Da) and a reference PDMS–PLA BCP [**2.5k-Ref**] (M_n = 2.5 kDa, $Đ$ = 1.15) that was synthesized following known procedures[31] (Figure 2–4A). More accurate results were obtained by MALDI-TOF MS, showing that co-oligomers with the expected mass were present in each sample (a selection of mass spectra is depicted in Figure 2–4B). Only co-oligomers **[Si$_{23}$-LA$_{17}$]**, **[Si$_{23}$-LA$_{25}$]** and **[Si$_{59}$-LA$_{33}$]** contained traces (~1%) of material that differed from the correct co-oligomer length by one lactic acid repeat unit. For those BCOs, the molar mass dispersity was estimated from the MALDI-TOF data by assuming that the

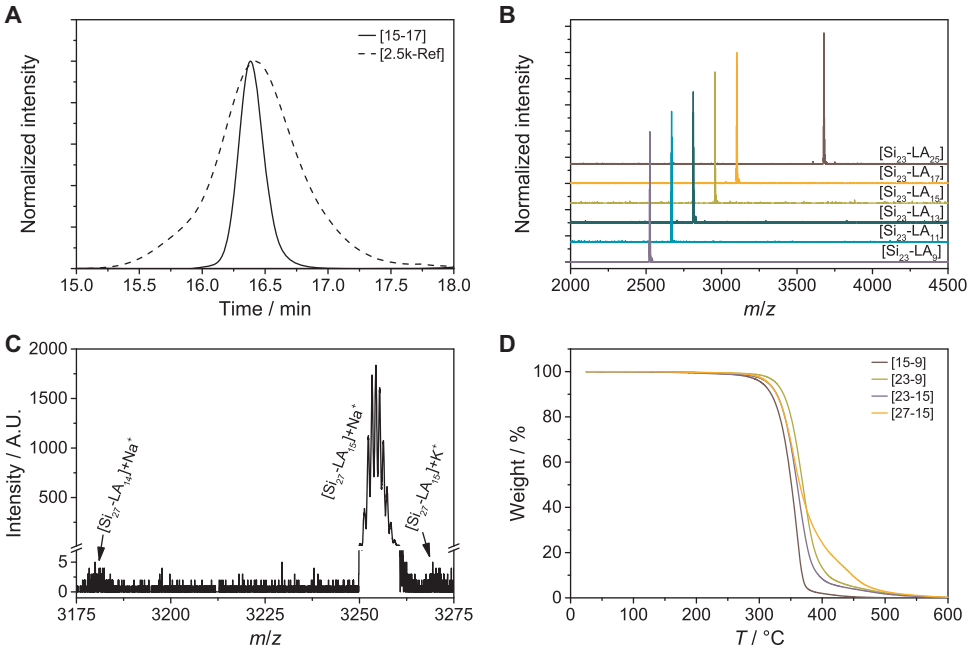

Figure 2–4. (**A**) Normalized SEC traces (RI detector) for compounds **[Si$_{15}$-LA$_{17}$]** and **[2.5k-Ref]**; (**B**) MALDI-TOF mass spectra (DCTB matrix) for the [**Si$_{23}$-LA$_y$**] BCO series; (**C**) MALDI-TOF mass spectrum (DCTB matrix) of [**Si$_{27}$-LA$_{15}$**]. A smaller tick spacing is used for the low-intensity region to amplify weak signals; (**D**) TGA plots for a selection of [**Si$_x$-LA$_y$**] BCOs. Samples were heated with 10 °C min^{-1} in a nitrogen atmosphere.

relative peak intensities corresponding to the desired and undesired oligomer lengths directly represent the molar ratios of these BCOs. For all other co-oligomers with either an atactic or isotactic *o*LA block, only an upper limit of for the dispersities could be estimated, resulting in values (significantly) lower than $Đ = 1.00001$; isotope distributions not taken into account. An example is provided in Figure 2–4C, showing the mass spectrum of BCO [**Si$_{27}$-LA$_{15}$**]. Here a dominant peak reflects the isotope distribution pattern of the sodium ion adduct of [**Si$_{27}$-LA$_{15}$**]. Only under high magnification, two anomalies could be detected in the noise of the baseline, which most likely can be identified as the potassium ion adduct of [**Si$_{27}$-LA$_{15}$**] and the sodium ion adduct of [**Si$_{27}$-LA$_{14}$**].

The monodisperse BCOs are chemically stable, even after long storage in ambient conditions. MALDI-TOF MS analysis of samples that were stored in air for 6 months at room temperature did not show any degradation products. Furthermore, the thermal stability of the [**Si$_x$-LA$_y$**] BCOs was investigated with thermogravimetric analysis (TGA).[v] The start of the degradation onset at temperatures close to 300 °C highlighted the remarkable stability for a polyester containing material (see Figure 2–4D for a selection of TGA traces).

2.5 Conclusions

We have demonstrated that an iterative synthesis process with orthogonal protection/deprotection and coupling strategies can be successfully employed to obtain discrete-length oligomers of dimethylsiloxane and lactic acid. A very strict selection of only the purest reaction intermediates were key for obtaining final compounds with ultra–low dispersities ($Đ < 1.00001$). Additionally, we could tune the tacticity in the *o*LA block by selecting either racemic or optically pure starting material. Subsequently, two different methods to ligate the uniform blocks afforded three sets of *o*DMS–*o*LA diblock co-oligomers: [**Si$_x$-LA$_y$**], [**Si$_x$-LLA$_y$**], [**Si$_x$-DLA$_y$**], in which we have full control over the number of siloxane and lactic acid repeat units, x and y. The robustness of the synthetic procedures that were developed, permitted the production of BCOs with molecular weights up to 6.9 kDa, or a total degree of polymerization of 92. As a result of the mild reaction conditions that were used during the carbodiimide facilitated ligation and acid chloride formation, practically no degradation of the oligomers took place, resulting in extremely low molar mass dispersities of the final BCOs ($Đ \leq 1.00002$). In principle, this synthesis strategy could be extended to generate even longer BCOs, BCOs composed of a different type of polyester block or BCOs

[v] Isotactic BCOs [**Si$_x$-LLA$_y$**] and [**Si$_x$-DLA$_y$**] were not studied with TGA, but we expect a similar stability.

containing moieties that provide additional stabilizing interactions. However, when interested in multigram quantities, the synthesis of the dononacontamer is at present time the limit from the siloxane point of view. Additionally, for the specific case of *o*DMS or *o*LA, there is a practical length limit for the individual blocks around 100–150 repeat units due to decreasing reaction rates as a result of endgroup dilution and increased purification difficulties. Moreover, ligation of two highly incompatible blocks becomes extremely inefficient at individual oligomer lengths of 50 repeat units and higher.

2.6 Experimental

2.6.1 Materials and methods

All chemicals were purchased from commercial sources and used without further purification. Dry solvents were obtained with an MBRAUN Solvent Purification System (MB-SPS). Toluene was dried over 4Å molecular sieves before use. Oven-dried glassware (120 °C) was used for all reactions carried out under argon atmosphere. Reactions were followed by thin-layer chromatography (TLC) using 60-F254 silica gel plates from Merck and visualized by UV light at 254 nm and/or cerium molybdate (CeMo) staining. Automated column chromatography was conducted on a Grace Reveleris X2 Flash Chromatography System using Reveleris Silica Flash Cartridges. Elution gradients are specified in column volumes (CVs).

NMR spectra were recorded on Varian Mercury Vx 400 MHz, Varian 400MR 400 MHz, Bruker 400 MHz Ultrashield (400 MHz for ^{1}H NMR), and/or Varian Inova 500 MHz (500 MHz for ^{1}H NMR) spectrometers. Deuterated solvents used are indicated in each case. Chemical shifts (δ) are expressed in ppm and are referred to the residual peak of the solvent. Peak multiplicity is abbreviated as s: singlet; d: doublet; t: triplet; dt: doublet of triplets; ddt: doublet of doublets of triplets; td: triplet of doublets; tt: triplet of triplets; q: quartet; ABq: AB quartet; qd: quartet of doublets; sept: septet; m: multiplet; bs: broad singlet. **Matrix assisted laser desorption/ionization time-of-flight** (MALDI-TOF) mass spectra were obtained on a PerSeptive Biosystems Voyager DE-PRO spectrometer using α-cyano-4-hydroxycinnamic acid (CHCA) or *trans*-2-[3-(4-*tert*-butylphenyl)-2-methyl-2-propenylidene]-malononitrile (DCTB) as matrix. **FT-IR** measurements were performed on a Perkin Elmer FT-IR Spectrum Two apparatus in ATR mode. **Gas chromatography-mass spectrometry** (GC-MS) measurements were conducted on a Shimadzu GC-17A gas chromatograph with a Shimadzu AOC-20i auto injector, Shimadzu GCMS-QP5000 gas chromatograph mass spectrometer and Phenomenex Zebron ZB-35 column (l = 30 meters, ID = 0.25 mm, film thickness = 0.25 μm). **Size exclusion chromatography** (SEC) measurements were conducted on a Shimadzu Prominence-i LC-2030C 3D with a Shimadzu RID-20A Refractive index detector, using an eluent flow of 1 mL min^{-1} (THF or $CHCl_3$). The molecular weight is determined based on narrow dispersity polystyrene standards purchased from Polymer Source Inc. **Thermogravimetric analysis** (TGA) was conducted on a TGA Q500 from TA instruments. The samples were heated from 25 °C to 600 °C at a rate of 10 °C min^{-1} in a nitrogen flow (60 mL min^{-1}).

2.6.2 Synthetic procedures

Synthesis of Cl-Si$_4$-H (**11**).

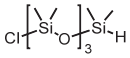

Hexamethylcyclotrisiloxane **9** (D3, 156.6 g, 0.704 mol) was put in a 1 L round-bottom flask under an argon atmosphere. Chlorodimethylsilane **10** (66.62 g, 0.704 mol, 1 eq) and acetonitrile (35 mL) was added, followed by

DMF (1.8 mL). This mixture was stirred at room temperature (initially the round bottomed flask became cold). After 70 h, completion of the reaction was confirmed by ^{1}H NMR. The reaction mixture was directly purified by vacuum distillation, collecting the fraction 39–41 °C at 1.1 mbar as a colorless oil (145 g, 65%).^{1}H NMR (400 MHz, $CDCl_3$): δ = 4.70 (sept, 1H, H-Si, ^3J = 2.8 Hz), 0.45 (s, 6H, Cl-Si-(CH_3)$_2$), 0.20 (d, 6H, H-Si-(CH_3)$_2$), ^3J = 2.8 Hz), 0.13 (s, 6H, CH_3), 0.09 ppm (s, 6H, CH_3); ^{13}C NMR (100 MHz, $CDCl_3$): δ = 4.02, 0.85, 0.77, 0.64 ppm. GC-MS (EI, oven 50–300 °C): t = 3.09 min; *m/z* calcd for $C_7H_{22}ClO_3Si_4$: 301.03 [M-CH_3]; found 301.

*General method **A** for synthesis of silanols Me-Si$_x$-OH* (**13**).

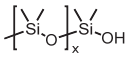

Pd/C (10 w% Pd, 0.02 eq of Pd) was suspended in a mixture of 1 M phosphate buffer (25 mL, pH = 7) and dioxane (120 mL) in a 500 mL round-bottom flask under an argon atmosphere and cooled to 0 °C with an ice bath. Then a solution of silyl hydride **12** or **14** (*e.g.*, 75.5 mmol) in dioxane (60 mL) was added dropwise over a period of 20 min. After stirring for 2 h, the ice bath was removed and stirring was continued at room temperature for another 2 h. The Pd/C was removed by filtration and toluene (300 mL) was added to the filtrate. The aqueous layer was separated and extracted with toluene (100 mL). The combined organic phases were then washed with water (3 × 200 mL) and dried with $MgSO_4$. Removal of the solvents *in vacuo* gave the corresponding silanol **13** in good purity.

Synthesis of Me-Si$_3$-OH (**13a**).

Starting from silyl hydride **12** (18.0 g, 75.5 mmol), pure silanol **13a** was obtained as a colorless oil (18.47 g, 96%) using general method **A**. ^{1}H NMR (400 MHz, $CDCl_3$): δ = 2.05 (s, 1H, OH), 0.14 (s, 6H, HO-Si-(CH_3)$_2$), 0.10 (s, 9H, (CH_3)$_3$-Si), 0.07 ppm (s, 6H, CH_3). ^{13}C NMR (100 MHz, $CDCl_3$): δ = 1.77, 1.12, 0.32 ppm; GC-MS (EI, oven 50–300 °C): t = 2.40 min; *m/z* calcd for $C_6H_{19}O_3Si_3$: 223.06 [M-CH_3]; found 223.

Synthesis of Me-Si$_7$-OH (**13b**).

Starting from silyl hydride **14a** (18.0 g, 75.5 mmol), pure silanol **13b** was obtained as a colorless oil (25.90 g, 91%) using general method **A**. ^{1}H NMR (400 MHz, $CDCl_3$): δ = 2.27 (s, 1H, OH), 0.14 (s, 6H, (CH_3)$_2$-Si-OH), 0.10–0.06 (m, 33H, CH_3), 0.05 ppm (s, 6H, CH_3); ^{13}C NMR (100 MHz, $CDCl_3$): δ = 1.78, 1.14, 1.05, 0.99, 0.31 ppm; MS (MALDI-TOF): *m/z* calcd for $C_{15}H_{46}O_7Si_7$+Na^+: 557.15 [M+Na]$^+$; found: 557.17.

Synthesis of Me-Si$_{11}$-OH (**13c**).

Starting from silyl hydride **14b** (37.5 g, 45.97 mmol), pure silanol **13c** was obtained as a colorless oil (38.7 g, 99%) using general method **A**. ^{1}H NMR (400 MHz, $CDCl_3$): δ = 2.23 (s, 1H, OH), 0.14 (s, 6H, HO-Si-(CH_3)$_2$), 0.10–0.07 (m, 54H, CH_3), 0.05 ppm (s, 6H, CH_3); ^{13}C NMR (100 MHz, $CDCl_3$): δ = 1.77, 1.31, 1.04, 0.98, 0.30 ppm; MS (MALDI-TOF): *m/z* calcd for $C_{23}H_{70}O_{11}Si_{11}$+$Na^+$: 853.23 [M+Na]$^+$; found 853.21.

Synthesis of Me-Si$_{15}$-OH (**13d**).

Starting from silyl hydride **14c** (5.00 g, 4.49 mmol), pure silanol **13d** was obtained as a colorless oil (4.89 g, 96%) using general method **A**. ^{1}H NMR (400 MHz, $CDCl_3$): δ = 2.22 (s, 1H, OH), 0.14 (s, 6H, HO-Si-(CH_3)$_2$), 0.10–0.07 (m, 81H, CH_3), 0.04 ppm (s, 6H, CH_3; ^{13}C NMR (100 MHz, $CDCl_3$): δ = 1.78, 1.14, 1.05, 0.99, 0.31 ppm; MS (MALDI-TOF): *m/z* calcd for $C_{31}H_{94}O_{15}Si_{15}$+$Na^+$: 1149.30 [M+Na]$^+$; found 1149.33; *m/z* calcd for $C_{31}H_{94}O_{15}Si_{15}$+$K^+$: 1165.28 [M+K]$^+$; found 1165.31.

Synthesis of Me-Si$_{19}$-OH (**13e**).

Starting from silyl hydride **14d** (5.70 g, 4.00 mmol), pure silanol **13e** was obtained as a colorless oil (5.33 g, 92%) using general method **A**. ^{1}H NMR (400 MHz, $CDCl_3$): δ = 2.22 (s, 1H, OH), 0.14 (s, 6H, CH_3), 0.09 –0.05 (m, 105H, CH_3), 0.04 (s, 6H, CH_3) ppm; ^{13}C NMR (100 MHz, $CDCl_3$): δ = 1.78, 1.14, 1.04, 0.98, 0.67, 0.31 ppm; MS (MALDI-TOF): *m/z* calcd for $C_{39}H_{118}O_{19}Si_{19}$+$Na^+$: 1445.38 [M+Na]$^+$; found 1445.38.

Synthesis of Me-Si$_{23}$-OH (**13f**).

Starting from silyl hydride **14e** (1.20 g, 0.68 mmol) pure silanol **13f** was obtained as a colorless oil (1.18 g, 97%) using general method **A**. ^{1}H NMR (400 MHz, $CDCl_3$): δ = 0.14 (s, 6H, C$\underline{H}_3$), 0.09 –0.05 (m, 129H, C$\underline{H}_3$), 0.04 (s, 6H, C$\underline{H}_3$) ppm; ^{13}C NMR (100 MHz, $CDCl_3$): δ = 1.76, 1.39, 1.12, 1.02, 0.97, 0.55, 0.29 ppm; MS (MALDI-TOF): *m/z* calcd for $C_{47}H_{142}O_{23}Si_{23}+Na^+$: 1741.45 $[M+Na]^+$; found 1741.47.

Synthesis of Me-Si$_{55}$-OH (**13l**).

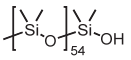

Pyridine (98 mg, 100 µl, 1.24 mmol, 2.8 eq) and **HO-Si$_{40}$-OH 17k** (1.344 g, 0.45 mmol) were dissolved in toluene (5 mL). The mixture was cooled down to 0 °C in ice water and **Me-Si$_{15}$-Cl 19** (0.54 mL, 0.45 mmol, 1 eq) was added dropwise over a period of 7 min. After stirring for 22 h at room temperature, toluene (70 mL) was added and the mixture washed with water (2 × 40 mL). The organic layer was dried with $MgSO_4$ and the solvent was removed in *vacuo*, giving the crude product as a colorless oil (2.84 g). Further purification was done by automated column chromatography using heptane/chloroform (gradient 100/0 to 30/70) as eluent, yielding the pure product **13l** as a colorless oil (490 mg, 27%). ^{1}H NMR (400 MHz, $CDCl_3$): δ = 2.04 (s, 1H, $\underline{H}$O-Si-$(CH_3)_2$), 0.10–0.04 ppm (m, 333H, C$\underline{H}_3$); ^{13}C NMR (50 MHz, $CDCl_3$): δ = 1.77, 1.13, 1.00, 0.67, 0.30 ppm; MS (MALDI-TOF): *m/z* calcd for $C_{111}H_{334}O_{55}Si_{55}+Na^+$ = 4110.05 $[M+Na]^+$; found: 4114.08 (5th isotope peak).

*General method **B** for synthesis of silyl hydride Me-Si$_x$-H* (**14**).

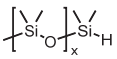

Chlorosilane **11** (*e.g.*, 0.114 mol) was dissolved in dry toluene (100 mL, 1 M) in a 500 mL round-bottom flask under an argon atmosphere and cooled in an ice bath. Next pyridine (12 mL, 0.15 mol) was added over the period of 1 min, followed by the dropwise addition of a solution of silanol **5** (0.114 mol, 1 eq) in dry toluene (100 mL) over the period of 30 min. Afterward, the ice bath was removed and the mixture was stirred for another 2 h at room temperature. Then water (100 mL) and toluene (100 mL) were added, and the aqueous layer was removed. The organic layer was washed with water (2 × 100 mL) and dried with $MgSO_4$. The solvent was then removed in *vacuo*, giving the crude silyl hydride **6** as a colorless to slightly yellow oil.

Synthesis of Me-Si$_7$-H (**14a**).

Starting from silanol **13a** (27.1 g, 0.114 mmol) and chlorosilane **3** (36.1 g, 0.114 mol, 1 eq), crude silyl hydride **14a** was obtained as a slightly yellow oil using general method **B**. The material was purified fractional vacuum distillation, collecting the fraction 92–94 °C at 0.28 mbar as a colorless oil (39.15 g, 66%). ^{1}H NMR (400 MHz, $CDCl_3$): δ = 4.70 (sept, ^3J = 2.8 Hz, 1H, $\underline{H}$-Si-$(CH_3)_2$), 0.19 (d, ^3J = 2.8 Hz, 6H, H-Si-(C$\underline{H}_3)_2$), 0.09 (s, 9H, (C$\underline{H}_3)_3$-Si), 0.09–0.07 (m, 24H, C$\underline{H}_3$), 0.05 ppm (s, 6H, C$\underline{H}_3$). ^{13}C- NMR (400 MHz, $CDCl_3$): δ = 1.79, 1.15, 1.05, 1.03, 0.85, 0.69 ppm; MS (MALDI-TOF): *m/z* calcd for $C_{15}H_{46}O_6Si_7+Na^+$: 541.16 $[M+Na^+]$; found: 541.16.

Synthesis of Me-Si$_{11}$-H (**14b**).

Starting from silanol **13b** (22.82 g, 42.62 mmol) and chlorosilane **3** (13.51 g, 42.62 mmol, 1 eq), crude silyl hydride **14b** was obtained as a colorless oil using general method **B**. The product was put under high vacuum (0.7 mbar) in a waterbath at 80 °C to remove all volatile byproducts, giving the pure hydride (34.37 g, 99%). ^{1}H NMR (400 MHz, $CDCl_3$): δ = 4.70 (sept, ^3J = 2.8 Hz, 1H, $\underline{H}$-Si-$(CH_3)_2$), 0.19 (d, ^3J = 2.8 Hz, 6H, H-Si-(C$\underline{H}_3)_2$), 0.10–0.00 ppm (m, 63H, C$\underline{H}_3$); ^{13}C NMR (100 MHz, $CDCl_3$): δ = 1.78, 1.14, 1.05, 1.02, 0.85, 0.69 ppm; MS (MALDI-TOF): *m/z* calcd for $C_{23}H_{70}O_{10}Si_{11}+Na^+$: 837.23 $[M+Na^+]$; found: 837.23.

Synthesis of Me-Si$_{15}$-H (**14c**).

Starting from silanol **13c** (37.26 g, 44.80 mmol) and chlorosilane **3** (14.21 g, 44.80 mmol, 1 eq), crude silyl hydride **14c** was obtained as a colorless oil using general method **B**. The product was put under high vacuum (0.06 mbar) in a waterbath at 70 °C to remove all volatile byproducts. Further purification was done by automated column chromatography using heptane/chloroform (gradient 100/0 to 70/30) as eluent. The title compound was obtained as a colorless oil (43.86 g, 88%). ^{1}H NMR (400 MHz, $CDCl_3$): δ = 4.70 (sept, ^3J = 2.4 Hz, 1H, H-Si-$(CH_3)_2$), 0.19 (d, ^3J = 2.4 Hz, 6H, H-Si-$(CH_3)_2$), 0.10–0.03 ppm (m, 87H, CH_3); ^{13}C NMR (100 MHz, $CDCl_3$): δ = 1.78, 1.14, 1.05, 1.02, 0.85, 0.69 ppm; MS (MALDI-TOF): *m/z* calcd for $C_{31}H_{94}O_{14}Si_{15}+Na^+$: 1133.31 [M+Na$^+$]; found: 1133.31.

Synthesis of Me-Si$_{19}$-H (**14d**).

Starting from silanol **13d** (4.85 g, 4.30 mmol) and chlorosilane **3** (1.36 g, 4.30 mmol, 1 eq), crude silyl hydride **14d** was obtained as a colorless oil using general method **B**. Lower molecular weight impurities were removed by washing with acetonitrile (2 × 15 mL), giving the pure silyl hydride as a colorless oil (5.70 g, 94%). ^{1}H NMR (400 MHz, $CDCl_3$): δ = 4.70 (sept, ^3J = 2.8 Hz, 1H, H-Si-$(CH_3)_2$), 0.19 (d, ^3J = 2.8 Hz, 6H, H-Si-$(CH_3)_2$), 0.10–0.04 ppm (m, 111H, CH_3); ^{13}C NMR (100 MHz, $CDCl_3$): δ = 1.76, 1.39, 1.11, 1.02, 0.99, 0.82, 0.66 ppm; MS (MALDI-TOF): *m/z* calcd for $C_{39}H_{118}O_{18}Si_{19}+Na^+$: 1429.38 [M+Na$^+$]; found: 1429.43.

Synthesis of Me-Si$_{23}$-H (**14e**).

Starting from silanol **13e** (5.32 g, 3.73 mmol) and chlorosilane **3** (1.18 g, 3.73 mmol, 1 eq), crude silyl hydride **14e** was obtained as a colorless oil using general method **B**. Lower molecular weight impurities were removed by washing with acetonitrile (2 × 15 mL), giving the pure silyl hydride as a colorless oil (5.93 g, 93%). ^{1}H NMR (400 MHz, $CDCl_3$): δ = 4.70 (sept, ^3J = 2.8 Hz, 1H, H-Si-$(CH_3)_2$), 0.19 (d, ^3J = 2.8 Hz, 6H, H-Si-$(CH_3)_2$), 0.10–0.04 ppm (m, 135H, CH_3); ^{13}C NMR (100 MHz, $CDCl_3$): δ = 1.78, 1.41, 1.14, 1.04, 0.84, 0.68 ppm; MS (MALDI-TOF): *m/z* calcd for $C_{47}H_{142}O_{22}Si_{23}+Na^+$: 1725.46 [M+Na$^+$]; found: 1725.46.

Synthesis of Me-Si$_{27}$-H (**14f**).

Starting from silanol **13f** (1.24 g, 0.720 mmol) and chlorosilane **3** (0.40 g, 1.26 mmol, 1.75 eq), crude silyl hydride **14f** was obtained as a colorless oil using general method **B**. Lower molecular weight impurities were removed by washing with acetonitrile (2 × 10 mL). Further purification was done by automated column chromatography using heptane/chloroform (gradient 100/0 to 65/35) as eluent. The title compound was obtained as a colorless oil (1.05 g, 73%). ^{1}H NMR (400 MHz, $CDCl_3$): δ = 4.70 (sept, ^3J = 2.8 Hz, 1H, H-Si-$(CH_3)_2$), 0.19 (d, ^3J = 2.8 Hz, 6H, H-Si-$(CH_3)_2$), 0.10–0.05 (m, 153H, CH_3), 0.04 ppm (s, 6H, CH_3); ^{13}C NMR (50 MHz, $CDCl_3$): δ = 1.77, 1.13, 1.04, 0.84, 0.68 ppm; MS (MALDI-TOF): *m/z* calcd for $C_{55}H_{166}O_{26}Si_{27}+Na^+$: 2021.55 [M+Na$^+$]; found: 2021.53.

Synthesis of Me-Si$_{59}$-H (**14l**).

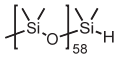

A solution of **Me-Si$_{55}$-OH 13l** (490 mg, 0.478 mmol) in toluene (5 mL) was cooled down to 0 °C in ice water. After the addition of pyridine (78 mg, 80 µl, 0.989 mmol, 2.1 eq), **Cl-Si$_4$-H 11** (170 µl, 0.50 mmol, 1.05 eq) was dropwise added over a period of 1 min. After stirring for 22 h at room temperature, toluene (5 mL) and second portion of **Cl-Si$_4$-H 11** (50 µl, 0.15 mmol, 0.3 eq) was added. After 1 h, the reaction mixture was diluted with toluene (70 mL) and washed with water (3 × 20 mL). The organic layer was dried with $MgSO_4$ and concentrated in *vacuo*. The remaining material was washed with acetonitrile (5 × 20 mL) to give crude product as a colorless oil. Further purification was done by automated column chromatography using heptane/chloroform (gradient 100/0 to 60/40) as eluent, giving the pure product **14l** as a colorless oil (338 mg, 65%). ^{1}H NMR (400 MHz, $CDCl_3$): δ = 4.70 (sept, ^3J = 2.8 Hz, 1H, H-Si-$(CH_3)_2$), 0.19 (d, ^3J = 2.8 Hz, 6H, H-Si-$(CH_3)_2$), 0.13–0.04 ppm (m, 351H, CH_3); ^{13}C NMR (50

MHz, $CDCl_3$): δ = 1.78, 1.03, 0.28 ppm; MS (MALDI-TOF): *m/z* calcd for $C_{119}H_{358}O_{58}Si_{59}+Na^+$: 4390.14 $[M+Na]^+$; found: 4397.36 (8th isotope peak).

Synthesis of HO-Si$_4$-H (**15**).

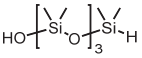

A solution of sodium bicarbonate (4.40 g, 52.37 mmol, 1.1 eq) in water (80 mL) and diethylether (300 mL) was cooled down to 0 °C in ice water. A solution of **Cl-Si$_4$-H 11** (15.09 g, 16 mL, 47.74 mmol) in diethylether (200 mL) was added dropwise over a period of 90 min. After another 45 min stirring at 0 °C, the icebath was removed and stirring was continued at room temperature for 1.5 h. The mixture was washed with water (200 mL) and brine (200 mL). The organic layer was concentrated in *vacuo* and the residue subjected to co-evaporation with toluene (50 mL). Pure hydroxysilane **7** was obtained as a colorless oil (14.11 g, 99 %). ^{1}H NMR (400 MHz, $CDCl_3$): δ = 4.71 (sept, ^3J = 2.8 Hz, 2H, H-Si-$(CH_3)_2$), 2.10 (s, 1H, HO-Si-$(CH_3)_2$), 0.20 (s, 6H, HO-Si-$(CH_3)_2$)), 0.15 (s, 6H, CH_3), 0.10 (s, 6H, CH_3), 0.08 ppm (s, 6H, CH_3); ^{13}C NMR (100 MHz, $CDCl_3$): δ = 0.97, 0.84, 0.65, 0.31 ppm; FT-IR (neat): 2979, 2921, 1608, 1488, 1445, 1378, 950 cm^{-1}; GC-MS (EI, oven 50–300 °C): t = 3.19 min; *m/z* calcd for $C_8H_{25}O_3Si_4$: 281.09 [M-OH]; found 281.

Synthesis of H-Si$_8$-H (**16**).

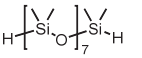

A solution of **Cl-Si$_4$-H 11** (15.6 mL, 46.4 mmol, 1.02 eq) in toluene (50 mL) was cooled down to 0 °C in ice water. Pyridine (4.18 g, 4.27 mL, 52.8 mmol, 1.2 eq) was added dropwise over the period of 5 min. Next, a solution of **HO-Si$_4$-H 15** (13.64 g, 45.7 mmol) in toluene (50 mL) was added dropwise over a period of 40 min. After 2.5 h the ice bath was removed and stirring was continued for 1 h at room temperature. The turbid, white reaction mixture was diluted with toluene (150 mL) and the mixture was washed with water (3 × 150 mL). The organic layer was dried with $MgSO_4$ and the solvent was removed *in vacuo*. The remaining material was co-evaporated with toluene (2 × 30 mL). Low molecular weight siloxane impurities were removed by in high vacuum (0.30 Torr) at 70 °C. The pure product **16** was obtained as a colorless oil (21.80 g, 81%). ^{1}H NMR (400 MHz, $CDCl_3$): δ = 4.70 (sept, ^3J = 2.8 Hz, 2H, H-Si-$(CH_3)_2$), 0.20 (d, ^3J = 2.8 Hz, 12H, H-Si-$(CH_3)_2$), 0.10–0.08 ppm (m, 36H, CH_3); ^{13}C NMR (100 MHz, $CDCl_3$): δ = 1.04, 1.02, 0.85, 0.69 ppm; FT-IR (neat): 2963, 2905, 2127, 1413, 1258, 1017, 907, 788 cm^{-1}; MS (MALDI-TOF): *m/z* calcd for $C_{16}H_{50}O_7Si_8+Na^+$: 601.16 $[M+Na]^+$; found: 601.22; GC-MS (EI, oven 50–300 °C): t = 5.45 min.

Synthesis of HO-Si$_8$-OH (**17g**).

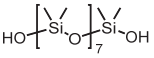

A mixture of dioxane (65 mL) and 1 M phosphate buffer (34 mL, pH = 7) was purged with argon and cooled down to 0 °C in ice water. Pd/C (10 w% Pd, 480 mg) was added, followed by the dropwise addition of **H-Si$_8$-H 16** (11.23 g, 19.4 mmol) in dioxane (10 mL) over a period of 10 min. After 3.5 h stirring at 0 °C, stirring was continued at room temperature. After stirring 1 additional hour, toluene (400 mL) was added and the reaction mixture was filtered to remove all Pd/C. The filtrate was washed with water (3 × 300 mL) and dried with $MgSO_4$. The solvent was removed in *vacuo*, followed by co-evaporation with toluene (2 × 10 mL), giving the pure product **17g** as a colorless, viscous oil (11.14 g, 94%). ^{1}H NMR (400 MHz, $CDCl_3$): δ = 2.30 (s, 2H, HO-Si-$(CH_3)_2$), 0.14 (s, 12H, HO-Si-$(CH_3)_2$), 0.12–0.05 ppm (m, 36H, CH_3); ^{13}C NMR (100 MHz, $CDCl_3$): δ = 1.06, 1.00, 0.31 ppm; FT-IR (neat): 3304, 2963, 2906, 1412, 1258, 1017, 891, 858, 787 cm^{-1}; MS (MALDI-TOF): *m/z* calcd for $C_{16}H_{50}O_9Si_8+Na^+$: 633.15 $[M+Na]^+$; found: 633.24.

Synthesis of HO-Si$_{16}$-OH (**17h**).

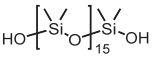

A mixture of dioxane (100 mL) and 1 M phosphate buffer (31 mL, pH = 7) was purged with argon and cooled down to 0 °C in ice water. Pd/C (10 w% Pd, 340 mg) was added, followed by the dropwise addition of **H-Si$_{16}$-H 18g** (8.05 g, 6.87 mmol) in dioxane (10 mL) over a period of 10 min. After 15 min stirring at 0 °C, stirring was continued at room temperature. After stirring 23 additional hours, toluene (250 mL) was added and the reaction mixture was filtered to remove all Pd/C. The filtrate was washed with water (2 × 200 mL) and dried with $MgSO_4$. The solvent was removed in *vacuo*, followed by co-evaporation with toluene (2 × 20 mL), giving the pure product **17h** as a colorless oil (6.74 g, 82%). ^{1}H NMR (400 MHz, $CDCl_3$): δ = 2.27 (s, 1H, HO-Si-(CH$_3$)$_2$), 0.14 (s, 12H, HO-Si-(CH$_3$)$_2$), 0.10–0.06 ppm (m, 84H, CH$_3$); ^{13}C NMR (100 MHz, $CDCl_3$): δ = 1.02, 0.97, 0.29 ppm; FT-IR (neat): 3305, 2963, 2906, 1412, 1258, 1017, 891, 787 cm^{-1}; MS (MALDI-TOF): *m/z* calcd for $C_{32}H_{98}O_{17}Si_{16}$+Na$^+$: 1225.30 [M+Na]$^+$; found:1225.44.

Synthesis of HO-Si$_{24}$-OH (**17i**).

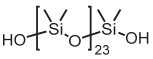

A mixture of dioxane (60 mL) and 1 M phosphate buffer (32 mL, pH = 7) was purged with argon and cooled down to 0 °C in ice water. Pd/C (10 w% Pd, 198 mg) was added, followed by the dropwise addition of **H-Si$_{24}$-H 18h** (3.14 g, 1.78 mmol) in dioxane (15 mL) over a period of 10 min. After 20 min stirring at 0 °C, stirring was continued at room temperature. After stirring 3 additional hours, toluene (200 mL) was added and the reaction mixture was filtered to remove all Pd/C. The filtrate was washed with water (3 × 200 mL) and dried with $MgSO_4$. The solvent was removed in *vacuo*, followed by co-evaporation with toluene (2 × 20 mL), giving the pure product **17i** as a colorless oil (3.20 g, quant.). ^{1}H NMR (400 MHz, $CDCl_3$): δ = 0.14 (s, 12H, CH$_3$), 0.09–0.05 ppm (m, 132H, CH$_3$); ^{13}C NMR (100 MHz, $CDCl_3$): δ = 1.40, 1.03, 0.98, 0.66, 0.30 ppm; MS (MALDI-TOF): *m/z* calcd for $C_{48}H_{146}O_{25}Si_{24}$+Na$^+$: 1817.45 [M+Na]$^+$; found: 1817.50.

Synthesis of HO-Si$_{32}$-OH (**17j**).

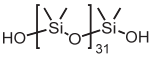

A mixture of dioxane (130 mL) and 1 M phosphate buffer (50 mL, pH = 7) was purged with argon and cooled down to 0 °C in ice water. Pd/C (10 w% Pd, 250 mg) was added, followed by the dropwise addition of **H-Si$_{32}$-H 18i** (5.0 g, 2.12 mmol) in dioxane (20 mL). After 30 min stirring at 0 °C, stirring was continued at room temperature. After stirring 18 additional hours, toluene (300 mL) was added and the reaction mixture was filtered to remove all Pd/C. The filtrate was washed with water (4 × 200 mL) and dried with $MgSO_4$. The solvent was removed in *vacuo*, giving the pure product **17j** as a colorless oil (4.80 g, 95%). ^{1}H NMR (400 MHz, $CDCl_3$): δ = 0.14 (s, 12H, CH$_3$), 0.09–0.06 ppm (m, 180H, CH$_3$); ^{13}C NMR (100 MHz, $CDCl_3$): δ = 1.03, 0.98, 0.30 ppm; MS (MALDI-TOF): *m/z* calcd for $C_{64}H_{194}O_{33}Si_{32}$+Na$^+$: 2409.60 [M+Na]$^+$; found: 2409.62.

Synthesis of HO-Si$_{40}$-OH (**17k**).

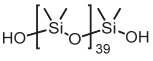

A solution of **H-Si$_{40}$-H 18j** (1.50 g, 0.51 mmol) in 14 mL dioxane and 1 M phosphate buffer (0.50 mL, pH = 7) was cooled down to 0 °C in ice water. The solution was purged with argon and Pd/C (10 w% Pd, 120 mg) was added. After stirring for 15 min, stirring was continued at room temperature for 23 h. Then toluene (60 mL) was added and the reaction mixture was filtered to remove all Pd/C. The filtrate was washed with water (3 × 50 mL) and dried with $MgSO_4$. The solvent was removed in *vacuo*, giving the pure product **17k** as a colorless oil (1.35 g, 89%).^{1}H NMR (400

MHz, $CDCl_3$): δ = 0.14 (s, 12H, C<u>H</u>$_3$), 0.09–0.06 ppm (m, 228H, C<u>H</u>$_3$); ^{13}C NMR (100 MHz, $CDCl_3$): δ = 1.03, 0.98, 0.30 ppm; MS (MALDI-TOF): *m/z* calcd for $C_{80}H_{242}O_{41}Si_{40}$+$Na^+$: 3001.75 $[M+Na]^+$; found: 3003.82 (3rd isotope peak).

Synthesis of H-Si$_{16}$-H (**18g**).

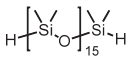

A solution of **Cl-Si$_4$-H 11** (14.0 mL, 41.6 mmol, 2.3 eq) in toluene (50 mL) was cooled down to 0 °C in ice water. Pyridine (3.96 g, 3.95 mL, 48.8 mmol, 2.7 eq) was added dropwise over the period of 1 min. Next, a solution of **HO-Si$_8$-OH 17g** (11.03 g, 18.0 mmol) in toluene (15 mL) was added dropwise over a period of 10 min. After 1.5 h, the ice bath was removed and stirring was continued for 1.5 h at room temperature. Then, toluene (200 mL) was added and the mixture was washed with water (3 × 200 mL). The organic layer was dried with $MgSO_4$ and the solvent was removed *in vacuo*. The remaining material washed with acetonitrile (4 × 40 mL). The crude material (18.72 g) was purified by automated column chromatography using heptane/chloroform (gradient 100/0 to 88/12) as eluent, yielding the pure product **18g** as a colorless oil (9.85 g, 47%). ^{1}H NMR (400 MHz, $CDCl_3$): δ = 4.70 (sept, ^3J = 2.8 Hz, 2H, <u>H</u>-Si-$(CH_3)_2$), 0.19 (d, ^3J = 2.8 Hz, 12H, H-Si-$(C\underline{H}_3)_2$), 0.08–0.06 ppm (m, 36H, C<u>H</u>$_3$); ^{13}C NMR (100 MHz, $CDCl_3$): δ = 1.06, 1.05, 1.04, 1.02, 0.85, 0.69 ppm; FT-IR (neat): 2963, 2906, 2127, 1413, 1258, 1013, 910, 788 cm^{-1}; MS (MALDI-TOF): *m/z* calcd for $C_{32}H_{98}O_{15}Si_{16}$+$Na^+$: 1193.31 $[M+Na]^+$; found: 1193.35.

Synthesis of H-Si$_{24}$-H (**18h**).

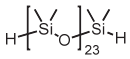

A solution of **Cl-Si$_4$-H 11** (4.6 mL, 13.8 mmol, 2.5 eq) in toluene (30 mL) was cooled down to 0 °C in ice water. Pyridine (1.43 g, 1.46 mL, 18.04 mmol, 3.3 eq) was added dropwise over the period of 1 min. Next, a solution of **HO-Si$_{16}$-OH 17h** (6.62 g, 5.48 mmol) in toluene (10 mL) was added dropwise over a period of 10 min. A white, turbid mixture was directly formed. After 2 h, the ice bath was removed and stirring was continued for 2 h at room temperature. Then, toluene (150 mL) was added and the mixture was washed with water (3 × 150 mL). The organic layer was dried with $MgSO_4$ and the solvent was removed *in vacuo*. The remaining material was co-evaporated with toluene (2 × 20 mL) and then washed with acetonitrile (4 × 30 mL). The pure product **18h** was obtained as a colorless oil (9.15 g, 94%). ^{1}H NMR (400 MHz, $CDCl_3$): δ = 4.70 (sept, ^3J = 2.8 Hz, 2H, <u>H</u>-Si-$(CH_3)_2$), 0.19 (d, ^3J = 2.8 Hz, 12H, H-Si-$(C\underline{H}_3)_2$), 0.08–0.06 ppm (m, 132H, C<u>H</u>$_3$); ^{13}C NMR (100 MHz, $CDCl_3$): δ = 1.40, 1.03, 0.84, 0.68 ppm; FT-IR (neat): 2963, 2906, 2127, 1403, 1258, 1013, 910, 788 cm^{-1}; MS (MALDI-TOF): *m/z* calcd for $C_{48}H_{146}O_{23}Si_{24}$+$Na^+$: 1785.46 $[M+Na]^+$; found: 1785.46.

Synthesis of H-Si$_{32}$-H (**18i**).

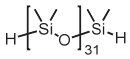

A solution of **Cl-Si$_4$-H 11** (2.20 mL, 6.49 mmol, 2.9 eq) in toluene (15 mL) was cooled down to 0 °C in ice water. Pyridine (0.63 g, 0.64 mL, 7.96 mmol, 3.6 eq) was added dropwise over the period of 1 min. Next, a solution of **HO-Si$_{24}$-OH 17i** (4.21 g, 2.24 mmol) in toluene (15 mL) was added dropwise over a period of 5 min. A turbid white reaction mixture was formed. After 2 h the ice bath was removed and stirring was continued for 2 h at room temperature. Then toluene (100 mL) was added and the mixture was washed with water (3 × 100 mL). The organic layer was dried with $MgSO_4$ and the solvent was removed *in vacuo*. The remaining material was co-evaporated with toluene (30 mL) and subsequently washed with acetonitrile (4 × 30 mL). The pure product **18i** was obtained as a colorless oil (5.14 g, 93%). ^{1}H NMR (400 MHz, $CDCl_3$): δ = 4.70 (sept, ^3J = 2.8 Hz, 2H, <u>H</u>-Si-$(CH_3)_2$), 0.19 (d, ^3J = 2.8

Hz, 12H, H-Si-(C<u>H</u>$_3$)$_2$)), 0.08–0.06 ppm (m, 180H, C<u>H</u>$_3$); ^{13}C NMR (100 MHz, $CDCl_3$): δ = 1.02, 0.83, 0.67 ppm; MS (MALDI-TOF): *m/z* calcd for $C_{64}H_{194}O_{31}Si_{32}+Na^+$: 2377.61 $[M+Na]^+$; found: 2377.58.

Synthesis of H-Si$_{40}$-H (**18j**).

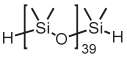

A solution of **Cl-Si$_4$-H 11** (1.65 mL, 4.87 mmol, 2.5 eq) in toluene (15 mL) was cooled down to 0 °C in ice water. Pyridine (0.52 g, 0.53 mL, 6.55 mmol, 3.4 eq) was added dropwise over the period of 1 min. Next, a solution of **HO-Si$_{32}$-OH 17j** (4.64 g, 1.94 mmol) in toluene (15 mL) was added dropwise over a period of 10 min. A turbid white reaction mixture was formed. After 2 h the ice bath was removed and stirring was continued for 3 h at room temperature. Then toluene (300 mL) was added and the mixture was washed with water (3 × 100 mL). The organic layer was dried with $MgSO_4$ and the solvent was removed *in vacuo*. The remaining material was washed with acetonitrile (5 × 40 mL). Further purification was done by automated column chromatography using heptane/chloroform (gradient 100/0 to 70/30) as eluent, yielding the pure product **18j** as a colorless oil (5.00 g, 87%). ^{1}H NMR (400 MHz, $CDCl_3$): δ = 4.70 (sept, ^3J = 2.8 Hz, 2H, <u>H</u>-Si-(CH$_3$)$_2$), 0.19 (d, ^3J = 2.8 Hz, 12H, H-Si-(C<u>H</u>$_3$)$_2$), 0.08–0.06 ppm (m, 228H, C<u>H</u>$_3$); ^{13}C NMR (100 MHz, $CDCl_3$): δ = 1.40, 1.03, 0.84, 0.68, 0.66 ppm; MS (MALDI-TOF): *m/z* calcd for $C_{80}H_{242}O_{39}Si_{40}+Na^+$: 2969.76 $[M+Na]^+$; found: 2971.56 (3rd isotope peak).

Synthesis of Me-Si$_{15}$-Cl (**19**).

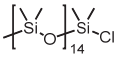

A solution of **Me-Si$_{15}$-H 14c** (1.27 g, 1.14 mmol) in tetrachloromethane (4 mL) was cooled down to 0 °C in ice water. $PdCl_2$ (11.4 mg) was added and the resulting suspension stirred at room temperature for 16 h. The reaction mixture was filtered through a 0.22 micrometer PTFE filter. The filtrate was concentrated *in vacuo*, giving the title compound **19** as a colorless oil (1.21 g, 92%). ^{1}H NMR (400 MHz, $CDCl_3$): δ = 0.45 (s, 6H, Cl-Si-(C<u>H</u>$_3$)$_2$), 0.13 (s, 6H, C<u>H</u>$_3$), 0.10–0.05 (m, 75H, C<u>H</u>$_3$), 0.04 ppm (s, 6H, C<u>H</u>$_3$); ^{13}C NMR (100 MHz, $CDCl_3$): δ = 4.06, 1.79, 1.42, 1.16, 1.06, 1.00, 0.91, 0.68 ppm.

Synthesis of HO-LA$_2$-Bn (*at*-**22m**).

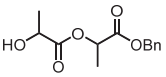

A mixture of (*S,S*)- and (*R,R*)-lactide *rac*-**20** (33.35 g, 0.231 mol), dry benzyl alcohol (24.1 mL, 0.231 mol, 1 eq) and D-camphorsulfonic acid (2.69 g, 11.6 mmol, 0.05 eq) was suspended in toluene (170 mL) in a 500 mL round-bottom flask under an argon atmosphere. The mixture was stirred for 8 h at 80 °C and allowed to cool down to room temperature afterward. Next, extra toluene (100 mL) was added and the solution washed with 0.2 M $NaHCO_3$ (2 × 200 mL). The combined aqueous layers were back-extracted with EtOAc (100 mL) and the combined organic layers washed with brine (150 mL) and dried with $MgSO_4$. Removal of the solvent *in vacuo* gave the crude product as a colorless oil (62.02 g). The crude material was purified by automated column chromatography in three separate batches of 10–11 grams, each using heptane/EtOAc (gradient 70/30 to 50/50) as eluent. The pure product *at*-**22m** (with traces of lactide and monomeric byproduct) was obtained as a colorless oil (47.32 g, 77%). ^{1}H NMR (400 MHz, $CDCl_3$): δ = 7.40–7.30 (m, 5H, Ar-<u>H</u>), 5.23 (q, ^3J = 7.1 Hz, 1H, O-C<u>H</u>(CH$_3$)-CO), 5.21 (d, ^2J = 12.2 Hz, 1H, Ar-C<u>H</u>$_2$-O), 5.15 (d, ^2J = 12.2 Hz, 1H, Ar-C<u>H</u>$_2$-O), 4.34 (qd, ^3J = 6.9 Hz, ^3J = 5.9 Hz, 1H, HO-C<u>H</u>(CH$_3$)-CO), 2.67 (d, ^3J = 5.8 Hz, 1H, <u>H</u>O-CH, 1.54 (d, J = 7.1 Hz, 3H, O-CH(C<u>H</u>$_3$)-CO), 1.44 ppm (d, J = 6.9 Hz, 3H, HO-CH(C<u>H</u>$_3$)-CO); ^{13}C NMR (100 MHz, $CDCl_3$): δ = 175.25, 170.11, 135.19, 128.77, 128.68, 128.38, 69.53, 20.58, 16.97 ppm; GC-MS (EI, oven 50–300 °C): Dimer: t = 6.02 min; *m/z* calcd for $C_{10}H_{12}O_3$: 180.08 $[M-C_3H_4O_2]$; found 180.6; Monomer: t = 4.34 min; *m/z* calcd for $C_{10}H_{12}O_3$: 180.08 [M]; found 180.6.

Synthesis of TBDMS-LA$_2$-Bn (*at*-**23m**).

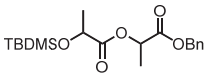

Alcohol *at*-**22m** (11.50 g, 45.6 mmol) was dissolved in dry DMF (80 mL) in a 250 mL 3-necked round-bottom flask under an argon atmosphere. Imidazole (12.82 g, 188 mmol, 4.13 eq) and *tert*-butyldimethylsilyl chloride (TBDMSCl, 14.64 g, 97 mmol, 2.13 eq) were added as solids and the resulting light yellow solution was stirred overnight at room temperature. Full conversion of the alcohol was confirmed by TLC analysis (hept/EtOAc 50:50; UV and CeMo stain; $R_{f,prod}$ = 0.87). The mixture was poured into sat. $NaHCO_3$ (150 mL) and extracted with hexane (3 × 150 mL). The combined organic layers were dried over $MgSO_4$ and the solvent was removed *in vacuo*, giving the crude product as a colorless oil (20.76 g). The crude material was purified by automated column chromatography in two separate batches of 10–11 grams each using heptane/EtOAc (gradient 100/0 to 95/5) as eluent. Completely pure material *at*-**23m** (without any lactide or monomeric by-product) was obtained as a colorless oil (15.02 g, 90%). ^{1}H NMR (400 MHz, $CDCl_3$): δ = 7.39–7.29 (m, 5H, Ar-H), 5.20–5.12 (m, 3H, O-CH(CH$_3$)-CO and Ar-CH$_2$-O), 5.15 (4.38 (q, ^2J = 6.8 Hz, 1H, TBDMSO-CH(CH$_3$)-CO), 1.51 (d, ^3J = 7.1 Hz, 1H, O-CH(CH$_3$)-CO), 1.41 (d, ^3J = 6.8 Hz, 1H, TBDMSO-CH(CH$_3$)-CO), 0.90 (s, 9H, (CH$_3$)$_3$C-Si(CH$_3$)$_2$), 0.10 (s, 3H, (CH$_3$)$_3$C-Si(CH$_3$)$_2$), 0.08 ppm (s, 3H, (CH$_3$)$_3$C-Si(CH$_3$)$_2$); ^{13}C NMR (100 MHz, $CDCl_3$): δ = 178.61, 170.49, 135.40, 128.73, 128.56, 128.36, 68.96, 68.21, 67.18, 25.84, 21.33, 18.43, 17.04, −4.78, −5.16 ppm; GC-MS (EI, oven 50–300 °C): Dimer: t = 7.08 min; *m*/*z* calcd for $C_{15}H_{21}O_5Si$: 309.12 [M-*t*-Bu]; found 309.4; Monomer: t = 5.68 min; *m*/*z* calcd for $C_{12}H_{17}O_3Si$: 237,10 [M-*t*-Bu]; found 237.4; MS (MALDI-TOF): *m*/*z* calcd for $C_{19}H_{30}O_5Si+Na^+$: 389.18 [M+Na$^+$]; found: 389.23.

Synthesis of HO-LLA$_2$-Bn (L-**22m**).

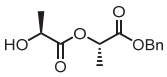

Optically pure L-lactide L-**20** (25.43g, 0.176 mol, 1 eq), dry benzyl alcohol (20 mL, 0.176 mol, 1 eq) and D-camphorsulfonic acid (2.05 g, 8.8 mmol, 0.05 eq) were dissolved in toluene (90 mL) in a 250 mL round-bottom flask under an argon atmosphere. The mixture was stirred for 2 hours at 80 °C and cooled down afterward. Subsequently, extra toluene (100 mL) was added and the solution washed with 0.2 M aq. $NaHCO_3$ soln. (2 × 100 mL). The combined aqueous layers were extracted with EtOAc (100 mL) and the combined organic layers were washed with brine (60 mL) and dried with $MgSO_4$. The solvent was removed in *vacuo* giving the crude product as a colorless oil (49.12 g). The crude material was purified by automated column chromatography in five separate portions of 10 grams each using heptane/EtOAc (gradient 75/25 to 50/50) as eluent. The product L-**22m** (with traces of lactide and monomeric by-product) was obtained as a colorless oil (28.4 g, 64%). ^{1}H NMR (400 MHz, $CDCl_3$): δ = 7.46–7.28 (m, 5H, Ar-H), 5.31–5.08 (m, 3H, O-CH(CH$_3$)-CO and O-CH$_2$-Ar), 4.42–4.23 (m, 1H, HO-CH(CH$_3$)-CO), 2.67–2.65 (d, ^3J = 6.1 Hz, 1H, HO-CH(CH$_3$)), 1.53 (d, ^3J = 7.1 Hz, 3H, O-CH(CH$_3$)-CO), 1.43 ppm (d, ^3J = 6.9 Hz, 3H, HO-CH(CH$_3$)-CO); ^{13}C NMR (100 MHz, $CDCl_3$): δ = 175.07, 169.99, 135.05, 128.61, 128.52, 128.22, 69.35, 67.23, 66.69, 20.41, 16.82 ppm.

Synthesis of HO-DLA$_2$-Bn (D-**22m**).

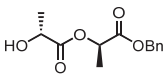

Optically pure D-lactide D-**20** (17.65 g, 0.12 mol, 1 eq), dry benzyl alcohol (12.5 mL, 0.12 mol, 1 eq) and D-camphorsulfonic acid (1.42 g, 6.12 mmol, 0.05 eq) were dissolved in toluene (80 mL) in a 250 mL round-bottomed flask under an argon atmosphere. The mixture was stirred for 3 hours at 80 °C and cooled down afterward. Subsequently, extra toluene (75 mL) was added and the solution washed with 0.2 M aq. $NaHCO_3$ soln. (2 × 125 mL).

The combined aqueous layers were extracted with EtOAc (80 mL) and the combined organic layers were washed with brine (50 mL) and dried with $MgSO_4$. The solvent was removed in *vacuo* giving the crude product as a colorless oil. The crude material was purified by automated column chromatography in three separate portions using heptane/EtOAc (gradient 75/25 to 50/50) as eluent. The product D-**22m** (with traces of lactide and monomeric by-product) was obtained as a colorless oil (22.5 g, 73%). ^{1}H NMR (400 MHz, $CDCl_3$): δ = 7.39–7.31 (m, 5H, Ar-H), 5.25–5.13 (m, 3H, O-CH(CH$_3$)-CO and Ar-CH$_2$-O), 4.33–4.37 (m, 1H, HO-CH(CH$_3$)-CO), 2.85 (d, ^3J = 5.8 Hz, 1H, HO-CH(CH$_3$)-CO), 1.54 (d, ^3J = 7.2 Hz, 3H, O-CH(CH$_3$)-CO), 1.42 ppm (d, ^3J = 7.0 Hz, 3H, O-CH(CH$_3$)-CO); ^{13}C NMR (100 MHz, $CDCl_3$) δ = 175.21, 170.15, 135.14, 128.74, 128.65, 128.36, 69.48, 67.37, 66.81, 62.47, 20.54, 16.96 ppm.

General method ***C*** *for removal of the TBDMS protective group giving HO-LA$_y$-Bn* (*at*-**22**), *HO-LLA$_y$-Bn* (L-**22**) or *HO-DLA$_y$-Bn* (D-**22**).

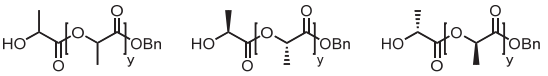

The TBDMS protected oligomer **23** (*e.g.*, 18 mmol) was dissolved in dry DCM (300 mL, 0.06 M) in a 1000 mL round-bottom flask under an argon atmosphere. The solution was cooled down to 0 °C in ice water. Next, BF_3-etherate (*e.g.*, 90 mmol, 5 eq) was added slowly and the mixture was allowed to warm to room temperature. The reaction mixture became light yellow. Stirring was continued at room temperature for 1–4 h (until TLC analysis of the reaction mixture (hept/EtOAc 50:50, CeMo stain) showed full conversion of the starting material). Afterward, the solution was poured into a mixture of sat. $NaHCO_3$ (75 mL) and brine (25 mL). The resulting colorless organic layer was separated, washed with another portion of brine (10 mL) and dried with $MgSO_4$. The solvent was then removed in *vacuo*, giving the crude product as a colorless to light yellow oil. Purification by column chromatography (see below for details) gave the pure material **22**.

Synthesis of HO-LA$_2$-Bn (*at*-**22m**).

Starting with TBDMS protected dimer *at*-**23m** (10.53 g, 28.7 mmol) and BF_3-etherate (14.63 g, 13.06 mL, 3.6 eq), crude deprotected dimer *at*-**22m** was obtained as a colorless oil (7.70 g) using general method **C**. The material was purified by automated column chromatography using heptane/EtOAc (gradient 80/20 to 50/50) as eluent, giving the pure material (no traces of residual lactide or monomeric byproduct) as a colorless oil (6.40 g, 88%). ^{1}H NMR (400 MHz, $CDCl_3$): δ = 7.40–7.30 (m, 5H, Ar-H), 5.23 (q, ^3J = 7.0 Hz, 1H, O-CH(CH$_3$)-COOBn), 5.20 (d, ^2J = 12.2 Hz, 1H, Ar-CH$_2$-O), 5.15 (d, ^2J = 12.2 Hz, 1H, Ar-CH$_2$-O), 4.34 (qd, ^3J = 6.9 Hz, ^3J = 5.9 Hz, 1H, HO-CH(CH$_3$)-CO), 2.80 (d, ^3J = 5.8 Hz, 1H, HO-CH(CH$_3$)-CO), 1.53 (d, ^3J = 7.1 Hz, 3H, O-CH(CH$_3$)-COOBn), 1.43 ppm (d, ^3J = 6.9 Hz, 3H, HO-CH(CH$_3$)-CO).

Synthesis of HO-LA$_4$-Bn (*at*-**22n**).

Starting with TBDMS protected tetramer *at*-**23n** (9.34 g, 18.29 mmol) and BF_3-etherate (12.98 g, 11.59 mL, 5 eq), crude deprotected tetramer *at*-**22n** was obtained as a light yellow oil (7.46 g) using general method **C**. The material was purified by automated column chromatography using heptane/EtOAc (gradient 70/30 to 50/50) as eluent, giving the pure material as a colorless oil (6.62 g, 91%). ^{1}H NMR (400 MHz, $CDCl_3$): δ = 7.40–7.29 (m, 5H, Ar-H), 5.29–5.10 (m, 5H, O-CH(CH$_3$)-CO and Ar-CH$_2$-O), 4.34 (qd, ^3J = 7.0 Hz, ^3J = 6.0 Hz, 1H, HO-CH(CH$_3$)-CO), 2.73 and 2.70 (d, ^3J = 5.9 Hz, 1H, HO-CH(CH$_3$)-CO), 1.65–1.44 ppm (m, 12H, O-CH(CH$_3$)-CO); ^{13}C NMR (100 MHz, $CDCl_3$): δ = 175.10, 174.97, 169.90, 169.63, 169.51, 169.40, 169.29, 135.06, 128.60–128.23, 69.31–69.07, 67.20, 66.69–66.64, 20.49, 16.75, 16.59 ppm; MS (MALDI-TOF): *m/z* calcd for $C_{19}H_{24}O_9$+Na$^+$: 419.13 [M+Na]$^+$; found 419.19; *m/z* calcd for $C_{19}H_{24}O_9$+K$^+$: 435.24 [M+K$^+$]; found 435.16.

Synthesis of HO-LLA$_4$-Bn (L-**22n**).

Starting from TBDMS protected tetramer L-**23n** (3.37 g, 6.6 mmol) and BF_3-etherate (2.88 g, 2.5 mL, 3 eq), crude deprotected tetramer L-**22n** was obtained (2.74 g) using general method **C**. The material was purified by automated column chromatography using heptane/EtOAc (gradient 70/30 to 50/50) as eluent, giving the pure material as a colorless oil (2.07 g, 79%). ^{1}H NMR (400 MHz, $CDCl_3$): δ = 7.45–7.27 (m, 5H, Ar-H), 5.26–5.08 (m, 5H, O-CH(CH$_3$)-CO and O-CH$_2$-Ar), 4.34 (m, 1H, HO-CH(CH$_3$)-CO), 2.84 (s, 1H, HO-CH(CH$_3$)-CO), 1.59 (d, ^3J = 7.1 Hz, 3H, HO-CH(CH$_3$)-CO), 1.55–1.45 ppm (m, 9H, O-CH(CH$_3$)-CO); ^{13}C NMR (100 MHz, $CDCl_3$): δ = 175.27, 170.13, 169.95, 169.77, 135.30, 128.88, 128.86, 128.84, 128.77, 128.74, 128.73, 128.47, 69.53, 69.33, 69.27, 69.23, 67.44, 66.93, 20.69, 16.97, 16.95, 16.81 ppm; MS (MALDI-TOF): *m/z* calcd for $C_{19}H_{24}O_9$+Na$^+$: 419.13 [M+Na]$^+$; found 419.17 Da; *m/z* calcd for $C_{19}H_{24}O_9$+K$^+$: 435.11 [M+K]$^+$; found 435.13 Da.

Synthesis of HO-DLA$_4$-Bn (D-**22n**).

Starting from TBDMS protected tetramer D-**23n** (7.03 g, 13.77 mmol) and BF_3-etherate (7.19 g, 6.25 mL, 3.6 eq), crude deprotected tetramer D-**22n** was obtained using general method **C**. The material was purified by automated column chromatography using heptane/EtOAc (gradient 70/30 to 50/50) as eluent, giving the pure material as a colorless oil (4.95 g, 91%). ^{1}H NMR (400 MHz, $CDCl_3$) δ = 7.38–7.30 (m, 5H, Ar-H), 5.23–5.11 (m, 5H, O-CH(CH$_3$)-CO and Ar-CH$_2$-O), 4.36–4.33 (m, 1H, HO-CH(CH$_3$)-CO), 2.81 (d, ^3J = 4.5 Hz, 1H, HO-CH(CH$_3$)-CO), 1.62–1.48 ppm (m, 12H, O-CH(CH$_3$)-CO); ^{13}C NMR (50 MHz, $CDCl_3$) δ = 175.22, 170.02, 169.80, 169.65, 135.14, 128.72, 128.63, 128.36, 69.39, 69.16, 67.34, 66.80, 20.61, 16.85, 16.70 ppm; MS (MALDI-TOF): *m/z* calcd for $C_{19}H_{24}O_9$+Na$^+$: 419.13 [M+Na]$^+$; found 419.14; *m/z* calcd for $C_{19}H_{24}O_9$+K$^+$: 435.24 [M+K$^+$]; found 435.08.

Synthesis of HO-LA$_8$-Bn (*at*-**22o**).

Starting with TBDMS protected octamer *at*-**23o** (6.38 g, 7.99 mmol) and BF_3-etherate (5.67 g, 5.06 mL, 5 eq), crude deprotected octamer *at*-**22o** was obtained as a light yellow oil (5.53 g) using general method **C**. The material was purified by automated column chromatography using heptane/EtOAc (gradient 60/40 to 35/65) as eluent, giving the pure material as a colorless oil (5.265 g, 96%). ^{1}H NMR (400 MHz, $CDCl_3$): δ = 7.39–7.28 (m, 5H, Ar-H), 5.28–5.09 (m, 9H, O-CH(CH$_3$)-CO and Ar-CH$_2$-O), 4.33 (m, 1H, HO-CH(CH$_3$)-CO), 2.76 (m, 1H, HO-CH(CH$_3$)-CO), 1.62–1.43 ppm (m, 24H, O-CH(CH$_3$)-CO); ^{13}C NMR (100 MHz, $CDCl_3$): δ = 175.08, 174.94, 169.90–169.11, 135.07, 128.59–128.21, 69.29–68.95, 67.19–67.17, 66.67–66.62, 53.42, 20.49, 16.70–16.58 ppm; MS (MALDI-TOF): *m/z* calcd for $C_{31}H_{40}O_{17}$+Na$^+$: 707.22 [M+Na]$^+$; found 707.23; *m/z* calcd for $C_{31}H_{40}O_{17}$+K$^+$: 723.19 [M+K$^+$]; found 723.20.

Synthesis of HO-LLA$_8$-Bn (L-**22o**).

Starting from TBDMS protected octamer L-**23o** (3.13 g, 9.92 mmol) and BF_3-etherate (1.67 g, 1.5 mL, 3 eq), crude deprotected octamer L-**22o** was obtained (2.90 g) using general method **C**. The reaction was complete in 3 hours, and the material was purified by automated column chromatography using heptane/EtOAc (gradient 60/40 to 35/65) as eluent, giving the pure material as a colorless oil (2.30 g, 89%). ^{1}H NMR (400 MHz, $CDCl_3$): δ = 7.37–7.30 (m, 5H, Ar-H), 5.27–5.06 (m, 9H, O-CH(CH$_3$)-CO and O-CH$_2$-Ar), 4.34 (m, 1H, HO-CH(CH$_3$)-CO), 2.75 (s, 1H, HO-CH(CH$_3$)-CO), 1.58 (m, 15H, O-CH(CH$_3$)-CO), 1.51 (m, 6H, O-CH(CH$_3$)-CO), 1.48 ppm (d, ^3J = 6.9 Hz, 3H, HO-CH(CH$_3$)-CO); ^{13}C NMR (100 MHz, $CDCl_3$): δ = 175.41, 170.20, 169.97, 169.89, 169.88, 169.83, 135.38, 128.92, 128.83, 128.55, 69.59, 69.37, 69.35, 69.33, 67.52, 67.01, 20.82, 17.05, 16.98, 16.95, 16.88 ppm; MS (MALDI-TOF): *m/z* calcd for $C_{31}H_{40}O_{17}$+Na$^+$: 707.22 [M+Na]$^+$; found 707.25; *m/z* calcd for $C_{31}H_{40}O_{17}$+K$^+$: 723.19 [M+K$^+$]; found 723.21.

Synthesis of HO-DLA$_8$-Bn (D-**22o**).

Starting from TBDMS protected octamer D-**23o** (2.184 g, 2.73 mmol) and BF_3-etherate (1.2 g, 1.04 mL, 3 eq), crude deprotected octamer D-**22o** was obtained using general method **C**. The material was purified by automated

column chromatography using heptane/EtOAc (gradient 60/40 to 35/65) as eluent, giving the pure material as a colorless oil (1.74 g, 93%). ^{1}H NMR (400 MHz, $CDCl_3$) δ = 7.38–7.3 (m, 5H, Ar-H), 5.24–5.11 (m, 9H, O-CH(CH_3)-CO and Ar-CH_2-O), 4.36–4.34 (m, 1H, HO-CH(CH_3)-CO), 2.71 (d, ^3J = 5.7 Hz, 1H, HO-CH(CH_3)-CO), 1.66–1.48 ppm (m, 24H, O-CH(CH_3)-CO); ^{13}C NMR (100 MHz, $CDCl_3$) δ = 175.24, 170.02–169.65, 135.19, 128.74–128.37, 69.41–69.15, 67.35, 66.83, 20.64, 16.87, 16.84, 16.77, 16.70 ppm; MS (MALDI-TOF): *m/z* calcd for $C_{31}H_{40}O_{17}$+Na^+: 707.22 [M+Na]$^+$; found 707.24; *m/z* calcd for $C_{31}H_{40}O_{17}$+K^+: 723.19 [M+K$^+$]; found 723.22.

Synthesis of HO-LA$_{10}$-Bn (*at*-**22p**).

Starting with TBDMS protected decamer *at*-**23p** (0.884 g, 0.891 mmol) and BF_3-etherate (0.690 g, 0.600 mL, 5.5 eq), crude deprotected decamer at-**22p** was obtained as a colorless oil (0.77 g) using general method **C**. The material was purified by automated column chromatography using heptane/EtOAc (gradient 60/40 to 35/65) as eluent, giving the pure material as a thick, colorless oil (0.630 g, 85%). ^{1}H NMR (400 MHz, $CDCl_3$): δ = 7.40–7.29 (m, 5H, Ar-H), 5.29–5.09 (m, 11H, O-CH(CH_3)-CO and Ar-CH_2-O), 4.35 (q, ^3J = 6.9 Hz, 1H, HO-CH(CH_3)-CO), 2.16 (bs, 1H, HO-CH(CH_3)-CO), 1.62–1.45 ppm (m, 30H, O-CH(CH_3)-CO); ^{13}C NMR (100 MHz, $CDCl_3$): δ = 175.04, 174.92, 169.92–169.15, 135.17, 128.63, 128.54–128.51, 128.24, 69.32, 69.22, 69.07, 69.04, 69.00, 67.20, 66.72, 66.67, 20.49, 16.80–16.59 ppm; MS (MALDI-TOF): *m/z* calcd for $C_{37}H_{48}O_{21}$+Na^+: 851.26 [M+Na]$^+$; found 851.25; *m/z* calcd for $C_{37}H_{48}O_{21}$+K^+: 867.23 [M+K$^+$]; found 867.22.

Synthesis of HO-LA$_{12}$-Bn (*at*-**22q**).

Starting with TBDMS protected 12-mer *at*-**23q** (0.401 g, 0.369 mmol) and BF_3-etherate (0.262 g, 0.228 mL, 5 eq), crude deprotected 12-mer *at*-**22q** was obtained as a colorless oil (0.351 g) using general method **C**. The material was purified by automated column chromatography using heptane/EtOAc (gradient 60/40 to 35/65) as eluent, giving the pure material as a thick, colorless oil (0.334 g, 93%). ^{1}H NMR (400 MHz, $CDCl_3$): δ = 7.36–7.25 (m, 5H, Ar-H), 5.23–5.03 (m, 13H, O-CH(CH_3)-CO and Ar-CH_2-O), 4.29 (q, ^3J = 6.9 Hz, 1H, HO-CH(CH_3)-CO), 3.15 (bs, 1H, HO-CH(CH_3)-CO), 1.64–1.36 ppm (m, 36H, O-CH(CH_3)-CO); ^{13}C NMR (100 MHz, $CDCl_3$): δ = 175.11, 175.00, 174.98, 169.96, 169.94, 169.72–169.19, 135.20, 135.17, 128.68, 128.58–128.56, 128.28, 69.36–69.03, 67.26–67.24, 66.76–66.71, 20.55, 16.85–16.63 ppm; MS (MALDI-TOF): *m/z* calcd for $C_{43}H_{56}O_{25}$+Na^+: 995.30 [M+Na]$^+$; found 995.30; *m/z* calcd for $C_{43}H_{56}O_{25}$+K^+: 1011.27 [M+K$^+$]; found 1011.27.

Synthesis of HO-LLA$_{12}$-Bn (L-**22q**).

Starting from TBDMS protected 12-mer L-**23q** (0.16 mg, 0.15 mmol) and BF_3-etherate (0.06 g, 0.06 mL, 3 eq), crude deprotected 12-mer L-**22q** was obtained (0.14 g) using general method **C**. The material was purified by automated column chromatography using heptane/EtOAc (gradient 60/40 to 30/70) as eluent, giving the pure material as a white solid (0.12 g, 80%). ^{1}H NMR (400 MHz, $CDCl_3$): δ = 7.43–7.27 (m, 5H, Ar-H), 5.39–5.07 (m, 13H, O-CH(CH_3)-CO and O-CH_2-Ar), 4.33 (p, ^3J = 6.4 Hz, 1H, HO-CH(CH_3)-CO), 2.72 (d, ^3J = 5.9 Hz, 1H, HO-CH(CH_3)-CO), 1.62–1.53 (m, 27H, O-CH(CH_3)-CO), 1.51 (d, ^3J = 7.1 Hz, 6H, O-CH(CH_3)-CO), 1.48 ppm (d, ^3J = 6.9 Hz, 3H, HO-CH(CH_3)-CO); ^{13}C NMR (100 MHz, $CDCl_3$): δ = 175.47, 170.23, 169.99, 169.93, 169.86, 135.36, 128.95, 128.86, 128.57, 69.60, 69.47, 69.41, 69.37, 69.34, 67.55, 67.02, 20.86, 17.08, 17.01, 16.97, 16.90 ppm; MS (MALDI-TOF): *m/z* calcd for $C_{43}H_{56}O_{25}$+Na^+: 995.30 [M+Na]$^+$; found: 995.31; *m/z* calcd for $C_{43}H_{56}O_{25}$+K^+: 1011.27 [M+K]$^+$; found 1011.29.

Synthesis of HO-DLA$_{12}$-Bn (D-**22q**).

Starting from TBDMS protected 12-mer D-**23q** (0.27 mg, 0.29 mmol) and BF_3-etherate (0.12 g, 0.1 mL, 3 eq), crude deprotected 12-mer D-**22q** was obtained (0.26 g) using general method **C**. The material was purified by automated column chromatography using heptane/EtOAc (gradient 60/40 to 30/70) as eluent, giving the pure material as a white solid (0.23 g, 87%). ^{1}H NMR (400 MHz, $CDCl_3$): δ = 7.43–7.27 (m, 5H, Ar-H), 5.27–5.07 (m,

13H, O-C<u>H</u>(CH$_3$)-CO and O-C<u>H</u>$_2$-Ar), 4.33 (q, ^3J = 6.8 Hz, 1H, HO-C<u>H</u>(CH$_3$)-CO), 2.75 (d, ^3J = 4.3 Hz, 1H, <u>H</u>O-CH(CH$_3$)-CO), 1.67–1.54 (m, 27H, O-CH(C<u>H</u>$_3$)-CO), 1.5 (d, ^3J = 7.1 Hz, 6H, O-CH(C<u>H</u>$_3$)-CO), 1.47 ppm (d, ^3J = 6.9 Hz, 3H, HO-CH(C<u>H</u>$_3$)-CO); ^{13}C NMR (100 MHz, CDCl$_3$): δ = 175.34, 170.15, 169.94, 169.85, 169.78, 135.34, 128.88, 128.79, 128.50, 77.68, 69.55, 69.29, 69.28, 67.47, 66.95, 20.76, 17.01, 16.94, 16.91, 16.83 ppm; MS (MALDI-TOF): *m/z* calcd for $C_{43}H_{56}O_{25}$+Na$^+$: 995.30 [M+Na]$^+$; found: 995.30; *m/z* calcd for $C_{43}H_{56}O_{25}$+K$^+$: 1011.27 [M+K]$^+$; found: 1011.27.

Synthesis of HO-LA$_{14}$-Bn (*at*-**22r**).

Starting with TBDMS protected 14-mer *at*-**23r** (0.350 g, 0.284 mmol) and BF$_3$-etherate (0.202 g, 0.175 mL, 5 eq), crude deprotected 14-mer *at*-**22r** was obtained as a colorless oil (0.365 g) using general method **C**. The material was purified by automated column chromatography using heptane/EtOAc (gradient 55/45 to 30/70) as eluent, giving the pure material as a thick, colorless oil (0.245 g, 77%). ^{1}H NMR (400 MHz, CDCl$_3$): δ = 7.36–7.22 (m, 5H, Ar-<u>H</u>), 5.22–5.03 (m, 15H, O-C<u>H</u>(CH$_3$)-CO and Ar-C<u>H</u>$_2$-O), 4.29 (q, ^3J = 6.7 Hz, 1H, HO-C<u>H</u>(CH$_3$)-CO), 2.97 (bs, 1H, <u>H</u>O-CH(CH$_3$)-CO), 1.59–1.38 ppm (m, 42H, O-CH(C<u>H</u>$_3$)-CO); ^{13}C NMR (100 MHz, CDCl$_3$): δ = 174.90, 174.87, 174.78, 169.81–169.06, 135.13, 135.10, 128.55, 128.44–128.42, 128.15, 69.24, 69.13, 68.99–68.90, 67.09, 66.61, 66.56, 20.39, 17.01–16.51 ppm; MS (MALDI-TOF): *m/z* calcd for $C_{49}H_{64}O_{29}$+Na$^+$: 1139.34 [M+Na]$^+$; found 1139.33; *m/z* calcd for $C_{49}H_{64}O_{29}$+K$^+$: 1155.32 [M+K$^+$]; found 1155.30.

Synthesis of HO-LA$_{16}$-Bn (*at*-**22s**).

Starting with TBDMS protected 16-mer *at*-**23s** (1.47 g, 1.069 mmol) and BF$_3$-etherate (0.758 g, 0.677 mL, 5 eq), crude deprotected 16-mer *at*-**22s** was obtained as a colorless oil (1.36 g) using general method **C**. The material was purified by automated column chromatography using heptane/EtOAc (gradient 50/50 to 20/80) as eluent, giving the pure material as a sticky, colorless solid (1.15 g, 85%). ^{1}H NMR (400 MHz, CDCl$_3$): δ = 7.39–7.28 (m, 5H, Ar-<u>H</u>), 5.27–5.08 (m, 17H, O-C<u>H</u>(CH$_3$)-CO and Ar-C<u>H</u>$_2$-O), 4.34 (q, ^3J = 6.9 Hz, 1H, HO-C<u>H</u>(CH$_3$)-CO), 2.79–2.70 (m, 1H, <u>H</u>O-CH(CH$_3$)-CO), 1.62–1.43 ppm (m, 48H, O-CH(C<u>H</u>$_3$)-CO); ^{13}C NMR (100 MHz, CDCl$_3$): δ = 175.19, 175.05, 170.01–169.22, 135.20, 128.71–128.33, 69.42–69.05, 67.31, 67.29, 66.79, 66.74, 20.60, 16.84–16.75 ppm; MS (MALDI-TOF): *m/z* calcd for $C_{55}H_{72}O_{33}$+Na$^+$: 1283.39 [M+Na]$^+$; found 1283.38; *m/z* calcd for $C_{55}H_{72}O_{33}$+K$^+$: 1299.36 [M+K$^+$]; found 1299.35; T_g = 19.1 °C (DSC; 2nd heating run; 10 °C/min).

Synthesis of HO-LLA$_{16}$-Bn (L-**22s**).

Starting from TBDMS protected 16-mer L-**23s** (0.78 g, 0.564 mmol) and BF$_3$-etherate (0.28 g, 0.25 mL, 4 eq), crude deprotected 16-mer L-**22s** was obtained (0.71 g) using general method **C**. The material was purified by automated column chromatography using heptane/EtOAc (gradient 50/50 to 20/80) as eluent, giving the pure material as a white solid (0.66 g, 92%). ^{1}H NMR (400 MHz, CDCl$_3$): δ = 7.43–7.28 (m, 5H, Ar-<u>H</u>), 5.28–5.09 (m, 17H, O-C<u>H</u>(CH$_3$)-CO and O-C<u>H</u>$_2$-Ar), 4.34 (qd, ^3J = 6.8 Hz, ^3J = 6.0 Hz, 1H, HO-C<u>H</u>(CH$_3$)-CO), 2.66 (d, ^3J = 6.0 Hz, 1H, <u>H</u>O-CH(CH$_3$)-CO), 1.58 (m, 39H, O-CH(C<u>H</u>$_3$)-CO), 0.52 (m, 6H, O-CH(C<u>H</u>$_3$)-CO), 1.49 ppm (d, ^3J = 7 Hz, 3H, HO-CH(C<u>H</u>$_3$)-CO); ^{13}C NMR (100 MHz, CDCl$_3$): δ = 175.48, 170.23, 169.98, 169.93, 169.86, 135.40, 128.96, 128.87, 128.58, 69.62, 69.45, 69.39, 69.35, 67.56, 67.05, 20.87, 17.09, 17.02, 16.99, 16.92 ppm; MS (MALDI-TOF): *m/z* calcd for $C_{55}H_{72}O_{33}$+Na$^+$: 1283.39 [M+Na]$^+$; found 1283.39; *m/z* calcd for $C_{55}H_{72}O_{33}$+K$^+$: 1299.36 [M+K$^+$]; found 1299.37.

Synthesis of HO-DLA$_{16}$-Bn (D-**22s**).

Starting from TBDMS protected 16-mer D-**23s** (1.135 g, 0.825 mmol) and BF$_3$-etherate (0.50 g, 0.43 mL, 4.1 eq), crude deprotected 16-mer D-**22s** was obtained using general method **C**. The material was purified by automated column chromatography using heptane/EtOAc (gradient 50/50 to 20/80) as eluent, giving the pure material as a white solid (0.96 g, 93%). ^{1}H NMR (400 MHz, CDCl$_3$) δ = 7.38–7.3 (m, 5H, Ar-<u>H</u>), 5.24–5.11 (m, 17H, O-C<u>H</u>(CH$_3$)-CO and Ar-C<u>H</u>$_2$-O), 4.36–4.34 (m, 1H, HO-C<u>H</u>(CH$_3$)-CO), 2.70 (d, ^3J = 6.0 Hz, 1H, <u>H</u>O-CH(CH$_3$)-CO), 1.66–1.48

ppm (m, 48H, O-CH(C<u>H</u>$_3$)-CO); ^{13}C NMR (100 MHz, $CDCl_3$) δ = 175.24, 170.01–169.64, 135.19, 128.74–128.37, 69.41–69.13, 67.34, 66.82, 20.65, 16.87, 16.81, 16.74, 16.69 ppm; *m/z* calcd for $C_{55}H_{72}O_{33}$+Na^+: 1283.39 [M+Na]$^+$; found 1283.42; *m/z* calcd for $C_{55}H_{72}O_{33}$+K^+: 1299.36 [M+K$^+$]; found 1299.40.

Synthesis of HO-LA$_{24}$-Bn (*at*-**22t**).

Starting with TBDMS protected 24-mer *at*-**23t** (0.808 g, 0.414 mmol) and BF_3-etherate (0.411 g, 0.367 mL, 7 eq), crude deprotected 24-mer *at*-**22t** was obtained as a colorless oil (0.745 g) using general method **C**. The material was purified by automated column chromatography using DCM/EtOAc (gradient 85/15 to 70/30) as eluent, giving the pure material as a sticky, colorless solid (0.733 g, 96%). ^{1}H NMR (400 MHz, $CDCl_3$): δ = 7.37–7.27 (m, 5H, Ar-<u>H</u>), 5.26–5.07 (m, 25H, O-C<u>H</u>(CH_3)-CO and Ar-C<u>H</u>$_2$-O), 4.32 (q, ^3J = 6.9 Hz, 1H, HO-C<u>H</u>(CH_3)-CO), 2.79 (bs, 1H, <u>H</u>O-CH(CH_3)-CO), 1.60–1.43 ppm (m, 72H, O-CH(C<u>H</u>$_3$)-CO); ^{13}C NMR (100 MHz, $CDCl_3$): δ = 175.14, 175.00, 169.97–169.20, 135.17, 135.14, 128.68–128.30, 69.32–69.04, 67.26, 66.76–66.70, 60.45, 20.57, 16.81–16.73 ppm; MS (MALDI-TOF): *m/z* calcd for $C_{79}H_{104}O_{49}$+Na^+: 1859.55 [M+Na]$^+$; found 1859.58; *m/z* calcd for $C_{79}H_{104}O_{49}$+K^+: 1875.53 [M+K$^+$]; found 1875.56; T_g = 28.9 °C (DSC; 2nd heating run; 10 °C/min).

Synthesis of HO-LLA$_{24}$-Bn (L-**22t**).

Starting from TBDMS protected 24-mer L-**23t** (0.15 g, 0.08 mmol) and BF_3-etherate (0.04 g, 0.04 mL, 3 eq), crude deprotected 24-mer L-**22t** was obtained (0.11 g) using general method **C**. The material was purified by automated column chromatography using DCM/EtOAc (gradient 90/10 to 70/30) as eluent, giving the pure material as a white solid (0.10 g, 86%). ^{1}H NMR (400 MHz, $CDCl_3$): δ = 7.43–7.27 (m, 5H, Ar-<u>H</u>), 5.25–5.07 (m, 25H, O-C<u>H</u>(CH_3)-CO and O-C<u>H</u>$_2$-Ar), 4.34 (q, ^3J = 6.9 Hz, 1H, HO-C<u>H</u>(CH_3)-CO), 2.71 (d, ^3J = 6 Hz, 1H, <u>H</u>O-CH(CH_3)-CO), 1.62–1.53 (m, 63H, O-CH(C<u>H</u>$_3$)-CO), 1.5 (d, ^3J = 7.1 Hz, 6H, O-CH(C<u>H</u>$_3$)-CO), 1.47 ppm (d, ^3J = 6.9 Hz, 3H, HO-CH(C<u>H</u>$_3$)-CO); ^{13}C NMR (100 MHz, $CDCl_3$): δ = 175.04, 169.83, 169.59, 169.52, 169.45, 135.01, 128.56, 128.47, 128.18, 69.23, 69.01, 68.95, 67.15, 66.63, 20.56, 16.69, 16.62, 16.59, 16.51 ppm; MS (MALDI-TOF): *m/z* calcd for $C_{79}H_{104}O_{49}$+Na^+: 1859.55 [M+Na]$^+$; found: 1859.57; *m/z* calcd for $C_{79}H_{104}O_{49}$+K^+: 1875.53 [M+K]$^+$; found 1875.54.

Synthesis of HO-LA$_{32}$-Bn (*at*-**22u**).

Starting with TBDMS protected 32-mer *at*-**23u** (0.404 g, 0.160 mmol) and BF_3-etherate (0.181 g, 0.162 mL, 1.278 mmol, 8 eq), crude deprotected 32-mer *at*-**22u** was obtained as a colorless oil using general method **C**. The material was purified by automated column chromatography using DCM/EtOAc (gradient 90/10 to 70/30) as eluent, giving the pure material as a sticky, colorless solid (0.367 g, 95%). ^{1}H NMR (400 MHz, $CDCl_3$): δ = 7.37–7.27 (m, 5H, Ar-<u>H</u>), 5.25–5.08 (m, 33H, O-C<u>H</u>(CH_3)-CO and Ar-C<u>H</u>$_2$-O), 4.32 (q, ^3J = 6.9 Hz, 1H, HO-C<u>H</u>(CH_3)-CO), 2.82 (bs, 1H, <u>H</u>O-CH(CH_3)-CO), 1.61–1.42 ppm (m, 96H, O-CH(C<u>H</u>$_3$)-CO); ^{13}C NMR (100 MHz, $CDCl_3$): δ = 175.05, 174.92, 169.91–169.15, 135.13, 128.63, 128.52, 128.24, 69.23–68.95, 67.20, 66.68–66.63, 60.38, 20.50, 16.81–16.62 ppm; MS (MALDI-TOF): *m/z* calcd for $C_{103}H_{136}O_{65}$+Na^+: 243c5.72 [M+Na]$^+$; found 2435.75; *m/z* calcd for $C_{103}H_{136}O_{65}$+K^+: 2451.70 [M+K$^+$]; found 2451.74.

Synthesis of HO-LLA$_{32}$-Bn (L-**22u**).

Starting from TBDMS protected 32-mer L-**23u** (0.17 g, 0.07 mmol) and BF_3-etherate (0.08 g, 0.07 mL, 8 eq), crude deprotected 32-mer L-**22u** was obtained (0.16 g) using general method **C**. The material was purified by automated column chromatography using DCM/EtOAc (gradient 90/10 to 70/30) as eluent, giving the pure material as a white solid (0.13 g, 77%). ^{1}H NMR (400 MHz, $CDCl_3$): δ = 7.36–7.3 (m, 5H, Ar-<u>H</u>), 5.24–5.13 (m, 33H, O-C<u>H</u>(CH_3)-CO and O-C<u>H</u>$_2$-Ar), 4.35 (p, ^3J = 6.8 Hz, 1H, HO-C<u>H</u>(CH_3)-CO), 2.67 (d, ^3J = 6 Hz, 1H, <u>H</u>O-CH(CH_3)-CO), 1.57 (d, ^3J = 7.1 Hz, 87H, O-CH(C<u>H</u>$_3$)-CO), 1.51 (d, ^3J = 7.1 Hz, 9H, O-CH(C<u>H</u>$_3$)-CO), 1.48 ppm (d, ^3J = 6.9 Hz, 3H, HO-CH(C<u>H</u>$_3$)-CO); ^{13}C NMR (100 MHz, $CDCl_3$): δ = 175.09, 169.87, 169.64, 169.57, 169.51, 135.06, 128.61,

128.52, 128.23,69.28, 69.06, 69.00, 67.20, 66.68, 20.52, 16.74, 16.64, 16.57 ppm; MS (MALDI-TOF): *m/z* calcd for $C_{103}H_{136}O_{65}$+Na^+: 2435.72 [M+Na]$^+$; found: 2435.78; *m/z* calcd for $C_{103}H_{136}O_{65}$+K^+: 2451.70 [M+K]$^+$; found: 2451.77.

Synthesis of HO-DLA$_{32}$-Bn (D-**22u**).

Starting from TBDMS protected 32-mer D-**23u** (0.31 g, 0.121 mmol) and BF_3-etherate (92 mg, 0.08 mL, 4.65 eq), crude deprotected 32-mer D-**22u** was obtained using general method **C**. The material was purified by automated column chromatography using chloroform/EtOAc (gradient 90/10 to 70/30) as eluent, giving the pure material as a white solid (0.22 g, 76%). ^{1}H NMR (400 MHz, $CDCl_3$) δ = 7.37–7.27 (m, 5H, Ar-H), 5.22–5.10 (m, 33H, O-CH(CH$_3$)-CO and Ar-CH$_2$-O), 4.33 (p, ^3J = 6.8 Hz, 1H, HO-CH(CH$_3$)-CO), 2.71 (d, ^3J = 5.9 Hz, 1H, HO-CH(CH$_3$)-CO), 1.68–1.46 ppm (m, 96H, O-CH(CH$_3$)-CO); ^{13}C NMR (100 MHz, $CDCl_3$) δ = 175.21, 169.99–169.62, 135.17, 128.72, 128.52 128.35, 69.39, 69.37, 69.11, 67.32, 66.80, 20.62, 16.85, 16.72, 16.68 ppm; MS (MALDI-TOF): *m/z* calcd for $C_{103}H_{136}O_{65}$+Na^+: 2435.72 [M+Na]$^+$; found 2435.73; *m/z* calcd for $C_{103}H_{136}O_{65}$+K^+: 2451.70 [M+K$^+$]; found 2451.71.

Synthesis of TBDMS-LA$_2$-Bn (*at*-**23m**).

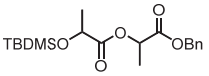

Alcohol *at*-**22m** (11.50 g, 45.6 mmol) was dissolved in dry DMF (80 mL) in a 250 mL 3-necked round-bottom flask under an argon atmosphere. Imidazole (12.82 g, 188 mmol, 4.13 eq) and *tert*-butyldimethylsilyl chloride (TBDMSCl, 14.64 g, 97 mmol, 2.13 eq) were added as solids and the resulting light yellow solution was stirred overnight at room temperature. Full conversion of the alcohol was confirmed by TLC analysis (hept/EtOAc 50:50; UV and CeMo stain; $R_{f,prod}$ = 0.87). The mixture was poured into sat. $NaHCO_3$ (150 mL) and extracted with hexane (3 × 150 mL). The combined organic layers were dried over $MgSO_4$ and the solvent was removed *in vacuo*, giving the crude product as a colorless oil (20.76 g). The crude material was purified by automated column chromatography in two separate batches of 10–11 grams each using heptane/EtOAc (gradient 100/0 to 95/5) as eluent. Completely pure material *at*-**23m** (without any lactide or monomeric by-product) was obtained as a colorless oil (15.02 g, 90%). ^{1}H NMR (400 MHz, $CDCl_3$): δ = 7.39–7.29 (m, 5H, Ar-H), 5.20–5.12 (m, 3H, O-CH(CH$_3$)-CO and Ar-CH$_2$-O), 5.15 (4.38 (q, ^2J = 6.8 Hz, 1H, TBDMSO-CH(CH$_3$)-CO), 1.51 (d, ^3J = 7.1 Hz, 1H, O-CH(CH$_3$)-CO), 1.41 (d, ^3J = 6.8 Hz, 1H, TBDMSO-CH(CH$_3$)-CO), 0.90 (s, 9H, (CH$_3$)$_3$C-Si(CH$_3$)$_2$), 0.10 (s, 3H, (CH$_3$)$_3$C-Si(CH$_3$)$_2$), 0.08 ppm (s, 3H, (CH$_3$)$_3$C-Si(CH$_3$)$_2$); ^{13}C NMR (100 MHz, $CDCl_3$): δ = 178.61, 170.49, 135.40, 128.73, 128.56, 128.36, 68.96, 68.21, 67.18, 25.84, 21.33, 18.43, 17.04, −4.78, −5.16 ppm; GC-MS (EI, oven 50–300 °C): Dimer: t = 7.08 min; *m/z* calcd for $C_{15}H_{21}O_5Si$: 309.12 [M-*t*-Bu]; found 309.4; Monomer: t = 5.68 min; *m/z* calcd for $C_{12}H_{17}O_3Si$: 237,10 [M-*t*-Bu]; found 237.4; MS (MALDI-TOF): *m/z* calcd for $C_{19}H_{30}O_5Si$+Na^+: 389.18 [M+Na$^+$]; found: 389.23.

Synthesis of TBDMS-LLA$_2$-Bn (L-**23m**)**.**

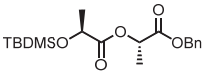

Alcohol L-**22m** (15.30 g, 60.7 mmol) was dissolved in dry DMF (90 mL) in 250 mL round-bottom flask under an argon atmosphere. Imidazole (10.28 g, 152 mmol, 2.5 eq) and *tert*-butyldimethylsilyl chloride (TBDMS-Cl, 10.97 g, 72.8 mmol, 1.2 eq) were added as solids and the resulting yellow solution was stirred overnight at room temperature. Full conversion of the alcohol was confirmed by TLC analysis (hept/EtOAc 50/50; CeMo stain; $R_{f,prod}$ = 0.85). The mixture was poured into sat. aq. $NaHCO_3$ soln. (200 mL) and extracted with pentane (4 × 100 mL). The combined organic layers were dried with $MgSO_4$ and the solvent was removed in *vacuo,* giving in the crude product as a colorless oil (23.02 g). The crude material was purified by automated column chromatography in two separate portions of 11–12 grams each using heptane/EtOAc (gradient 100/0 to 85/15) as eluent. Pure L-**23m** (without any residual lactide or monomeric by-product) was obtained as a colorless oil (13.35 g, 60%). ^{1}H NMR (400 MHz,

$CDCl_3$): δ = 7.41–7.27 (m, 5H, Ar-H), 5.24–5.08 (m, 3H, O-CH(CH_3)-CO and O-CH_2-Ar), 4.38 (q, ^3J = 6.8 Hz, 1H, Si-O-CH(CH_3)-CO), 1.51 (d, ^3J = 7 Hz, 3H, O-CH(CH_3)-CO), 1.41 (d, ^3J = 6.8 Hz, 3H, Si-O-CH(CH_3)-CO), 0.90 (s, 9H, (CH_3)$_3$C-Si(CH_3)$_2$), 0.10 (s, 3H, (CH_3)$_3$C-Si(CH_3)$_2$), 0.07 ppm (s, 3H, (CH_3)$_3$C-Si(CH_3)$_2$); ^{13}C NMR (100 MHz, $CDCl_3$): δ = 173.44, 170.32, 135.23, 128.56, 128.39, 128.19, 68.97, 68.05, 67.01, 25.68, 21.17, 18.27, 16.87, 5.32, 4.94 ppm.

Synthesis of TBDMS-DLA$_2$-Bn (D-**23m**).

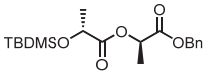

Alcohol D-**22m** (22.5 g, 89.0 mmol) was dissolved in dry DMF (100 mL) in a 250 mL round-bottomed flask under an argon atmosphere. Imidazole (22.61 g, 332 mmol, 3.7 eq) and *tert*-butyldimethylsilyl chloride (TBDMS-Cl, 28.47 g, 189 mmol, 2 eq) were added as solids and the resulting yellow solution was stirred overnight at room temperature. Full conversion of the alcohol was confirmed by TLC analysis (hept/EtOAc 50:50; CeMo stain; $R_{f,prod}$ = 0.85). The mixture was poured into sat. aq. $NaHCO_3$ soln. (250 mL) and extracted with pentane (4 × 100 mL). The combined organic layers were dried with $MgSO_4$ and the solvent was removed in *vacuo,* giving in the crude product as a colorless oil. The crude material was purified by automated column chromatography in two separate portions using heptane/EtOAc (gradient 100/0 to 90/10) as eluent. Completely pure D-**23m** (without any lactide or monomeric by-product) was obtained as a colorless oil (19.32 g, 59%). ^{1}H NMR (200 MHz, $CDCl_3$): δ = 7.39–7.30 (m, 5H, Ar-H), 5.16 (q, ^3J = 7.1 Hz, 1H, O-CH(CH_3)-CO), 5.16 (s, 2H, Ar-CH_2-O)), 4.38 (q, ^3J = 6.8 Hz, 1H, Si-O-CH(CH_3)-CO), 1.51 (d, ^3J = 7.1 Hz, 1H, O-CH(CH_3)-CO), 1.41 (d, ^3J = 6.6 Hz, 1H, Si-O-CH(CH_3)-CO), 0.89 (s, 9H, (CH_3)$_3$C-Si(CH_3)$_2$), 0.10 (s, 3H, (CH_3)$_3$C-Si(CH_3)$_2$), 0.08 ppm (s, 3H, (CH_3)$_3$C-Si(CH_3)$_2$).

*General method **D** for the oLA coupling reactions giving TBDMS-LA$_y$-Bn* (*at*-**23**), *TBDMS-LLA$_y$-Bn* (L-**23**) or *TBDMS-DLA$_y$-Bn* (D-**23**).

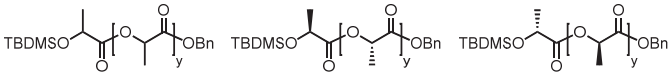

TBDMS protected oligomer **24** (*e.g.*, 40.9 mmol, 1.06 eq) and 4-(dimethylamino)pyridinium 4-toluenesulfonate (DPTS, *e.g.*, 7.71 mmol, 0.2 eq) were dissolved in dry DCM (70 mL, 0.55 M) in a 3-necked round-bottom flask under an argon atmosphere. The solution was cooled to 0 °C in ice water and *N*-(3-dimethylaminopropyl)-*N*'-ethylcarbodiimide hydrochloride (EDC·HCl, *e.g.*, 50.1 mmol, 1.3 eq) was added. The mixture was stirred for 10 min at 0 °C, followed by the addition of a solution of benzyl protected oligomer **22** (*e.g.*, 38.6 mmol, 1.0 eq) in 15 mL of DCM. The resulting solution was stirred 2–12 h at room temperature (until all starting material 13 was consumed, visualized by TLC analysis (hept/EtOAc 50:50; UV and CeMo stain)). The reaction mixture was then poured into a separation funnel containing water (70 mL). The two layers were separated and the organic layer washed with brine (40 mL), and dried with $MgSO_4$. The solvent was removed in *vacuo*, giving the crude product **23** as a colorless to light yellow oil. Purification by column chromatography (see below for details) gave the pure material.

Synthesis of TBDMS-LA$_4$-Bn (*at*-**23n**).

Starting with TBDMS protected dimer *at*-**24m** (7.43 g, 26.9 mmol, 1.06 eq), benzyl protected dimer *at*-**22m** (6.40 g, 25.4 mmol, 1.0 eq), DPTS (1.49 g, 5.07 mmol, 0.2 eq) and EDC·HCl (6.32 g, 33.0 mmol, 1.3 eq), crude double protected tetramer *at*-**23n** was obtained as a light yellow oil (13.93 g) using general method **D**. The material was purified by automated column chromatography using hept/EtOAc (gradient 100/0 to 75/25) as eluent, giving the pure material as a colorless oil (12.16 g, 94%). ^{1}H NMR (400 MHz, $CDCl_3$): δ = 7.41–7.28 (m, 5H, Ar-H), 5.26–5.06 (m, 5H, O-CH(CH_3)-CO and Ar-CH_2-O), 4.40 (q, ^3J = 6.7 Hz, 1H, TBDMSO-CH(CH_3)-CO), 1.62–1.40 (m, 12H, O-CH(CH_3)-CO), 0.90 (s, 9H, (CH_3)$_3$C-Si(CH_3)$_2$), 0.10 (s, 3H, (CH_3)$_3$C-Si(CH_3)$_2$), 0.08 ppm (s, 3H, (CH_3)$_3$C-Si(CH_3)$_2$);

^{13}C NMR (100 MHz, $CDCl_3$): δ = 173.64, 173.46, 170.09, 169.91, 169.78, 169.52, 135.24–135.22, 128.73, 128.61, 128.36, 69.40, 69.31, 69.08, 68.98, 68.86, 68.10, 67.31–67.29, 25.83, 21.39, 18.42, 16.98–16.71, −4.77, −5.16 ppm; MS (MALDI-TOF): *m/z* calcd for $C_{25}H_{38}O_9Si+Na^+$: 533.22 $[M+Na]^+$; found 533.25.

Synthesis of TBDMS-LLA$_4$-Bn (L-**23n**).

Starting with TBDMS protected dimer L-**24m** (4.66 g, 16.85 mmol, 1.06 eq), benzyl protected dimer L-**22m** (4.01 g, 15.9 mmol, 1 eq), DPTS (0.94 g, 3.18 mmol, 0.2 eq) and EDC·HCl (3.96 g, 20.66 mmol, 1.3 eq), crude double protected tetramer L-**23n** was obtained as a light yellow oil (8.78 g) using general method **D**. The material was purified by automated column chromatography using hept/EtOAc (gradient 100/0 to 75/25) as eluent, giving the pure material as a white solid (6.74 g, 84%).

^{1}H NMR (400 MHz, $CDCl_3$): δ = 7.46–7.28 (m, 5H, Ar-H), 5.26–5.05 (m, 5H, O-CH(CH_3)-CO and O-CH_2-Ar), 4.40 (q, ^3J = 6.7 Hz, 1H, Si-O-CH(CH_3)-CO), 1.57 (d, ^3J = 7.1 Hz, 3H, O-CH(CH_3)-CO), 1.52 (m, 6H, O-CH(CH_3)-CO), 1.45 (d, ^3J = 6.7 Hz, 3H, Si-O-CH(CH_3)-CO), 0.90 (s, 9H, (CH_3)$_3$C-Si(CH_3)$_2$), 0.11 (s, 3H, (CH_3)$_3$C-Si(CH_3)$_2$), 0.09 ppm (s, 3H, (CH_3)$_3$C-Si(CH_3)$_2$); ^{13}C NMR (100 MHz, $CDCl_3$): δ = 173.85, 170.30, 170.27, 169.98, 135.42, 128.94, 128.83, 128.57, 128.56, 69.57, 69.16, 68.87, 68.33, 67.52, 26.03, 21.55, 18.61, 17.09, 17.07, 16.93, −4.57, −4.96 ppm; MS (MALDI-TOF): *m/z* calcd for $C_{25}H_{38}O_9Si+Na^+$: 533.22 $[M+Na]^+$; found 533.25; *m/z* calcd for $C_{25}H_{38}O_9Si+K^+$: 549.19 $[M+K]^+$; found 549.20.

Synthesis of TBDMS-DLA$_4$-Bn (D-**23n**).

Starting with TBDMS protected dimer D-**24m** (9.87 g, 35.7 mmol, 1.06 eq), benzyl protected dimer D-**22m** (8.5 g, 33.7 mmol, 1 eq), DPTS (2.0 g, 6.79 mmol, 0.2 eq) and EDC·HCl (9.0 g, 47.2 mmol, 1.4 eq), crude double protected tetramer D-**23n** was obtained as a light yellow oil using general method **D**. The material was purified by automated column chromatography using heptane/EtOAc (gradient 100/0 to 75/25) as eluent, giving the pure material as a colorless oil (14.38 g, 87%).

^{1}H NMR (400 MHz, $CDCl_3$): δ = 7.39–7.30 (m, 5H, Ar-H), 5.22–5.09 (m, 5H, O-CH(CH_3)-CO and Ar-CH_2-O), 4.40 (q, ^3J = 6.8 Hz, 1H, Si-O-CH(CH_3)-CO), 1.57 (d, ^3J = 7.1 Hz, 3H, O-CH(CH_3)-CO), 1.52 (d, ^3J = 7.2 Hz, 6H, O-CH(CH_3)-CO), 1.45 (d, ^3J = 6.8 Hz, 3H, Si-O-CH(CH_3)-CO), 0.91 (s, 9H, (CH_3)$_3$C-Si(CH_3)$_2$), 0.11 (s, 3H, (CH_3)$_3$C-Si(CH_3)$_2$), 0.08 ppm (s, 3H, (CH_3)$_3$C-Si(CH_3)$_2$); ^{13}C NMR (100 MHz, $CDCl_3$): δ = 173.69, 170.10, 169.80, 135.19, 128.74, 128.65, 128.38, 110.52, 69.36, 68.95, 68.67, 68.11, 67.33, 25.82, 25.38, 21.37, 18.42, 16.89, 16.74, −4.78, −5.17 ppm; MS (MALDI-TOF): *m/z* calcd for $C_{25}H_{38}O_9Si+Na^+$: 533.22 $[M+Na]^+$; found 533.23.

Synthesis of TBDMS-LA$_8$-Bn (*at*-**23o**).

Starting with TBDMS protected tetramer *at*-**24n** (2.45 g, 5.83 mmol, 1.06 eq), benzyl protected tetramer *at*-**22n** (2.18 g, 5.50 mmol, 1.0 eq), DPTS (0.324 g, 1.10 mmol, 0.2 eq) and EDC·HCl (1.37 g, 7.14 mmol, 1.3 eq), crude double protected octamer *at*-**23o** was obtained as a light yellow oil (5.54 g) using general method **D**. The material was purified by automated column chromatography using hept/EtOAc (gradient 90/10 to 60/40) as eluent, giving the pure material as a colorless oil (3.99 g, 91%).

^{1}H NMR (400 MHz, $CDCl_3$): δ = 7.40–7.29 (m, 5H, Ar-H), 5.26–5.08 (m, 9H, O-CH(CH_3)-CO and Ar-CH_2-O), 4.39 (q, ^3J = 6.8 Hz, 1H, TBDMSO-CH(CH_3)-CO), 1.60–1.48 (m, 21H, O-CH(CH_3)-CO), 1.44 (d, ^3J = 6.7 Hz, 3H, TBDMSO-CH(CH_3)-CO), 0.90 (s, 9H, (CH_3)$_3$C-Si(CH_3)$_2$), 0.10 (s, 3H, (CH_3)$_3$C-Si(CH_3)$_2$), 0.08 ppm (s, 3H, (CH_3)$_3$C-Si(CH_3)$_2$); ^{13}C NMR (100 MHz, $CDCl_3$): δ = 173.62, 173.43, 170.03–169.37, 169.24, 135.20–135.17, 128.71, 128.61, 128.33, 69.41–68.60, 68.07, 67.36, 67.28, 25.80, 21.38–21.35, 18.37, 16.97–16.73, −4.80, −5.19 ppm; MS (MALDI-TOF): *m/z* calcd for $C_{37}H_{54}O_{17}Si+Na^+$: 821.30 $[M+Na]^+$; found 821.31; *m/z* calcd for $C_{37}H_{54}O_{17}Si+K^+$: 837.41 $[M+K^+]$; found 837.28.

Synthesis of TBDMS-LLA$_8$-Bn (L-**23o**).

Starting with TBDMS protected tetramer L-**24n** (2.33 g, 5.54 mmol, 1.06 eq), benzyl protected tetramer L-**22n** (2.07g, 5.22 mmol, 1 eq), DPTS (0.31 g, 1.04 mmol, 0.2 eq) and EDC·HCl (1.30 g, 6.79 mmol, 1.3 eq), crude double protected octamer L-**23o** was obtained as a light yellow oil (9.5 g) using general method **D**. The material was purified by automated column chromatography using hept/EtOAc (gradient 90/10 to 50/50) as eluent, giving the pure material as a colorless oil (3.74 g, 90%).

^{1}H NMR (400 MHz, $CDCl_3$): δ = 7.38–7.3 (m, 5H, Ar-H), 5.32–5.04 (m, 9H, O-CH(CH_3)-CO and O-CH_2-Ar), 4.39 (q, ^3J = 6.7 Hz, 1H, Si-O-CH(CH_3)-CO), 1.57 (m, 15H, O-CH(CH_3)-CO), 1.51 (m, 6H, O-CH(CH_3)-CO), 1.44 (d, ^3J = 6.8 Hz, 3H, Si-O-CH(CH_3)-CO), 0.90 (s, 9H, (CH_3)$_3$C-Si(CH_3)$_2$), 0.10 (s, 3H, (CH_3)$_3$C-Si(CH_3)$_2$), 0.07 ppm (s, 3H, (CH_3)$_3$C-Si(CH_3)$_2$); ^{13}C NMR (100 MHz, $CDCl_3$): δ = 173.80, 171.37, 170.27, 170.17, 170.00, 169.92, 169.89, 169.87, 169.81, 135.37, 128.91, 128.82, 128.54, 69.57, 69.31, 69.28, 69.25, 69.11, 68.83, 68.29, 67.50, 26.00, 21.52, 21.33, 18.57, 17.05, 16.97, 16.94, 16.87, −4.61, −5.00 ppm; MS (MALDI-TOF): *m/z* calcd for $C_{37}H_{54}O_{17}Si+Na^+$: 821.30 $[M+Na]^+$; found 821.30.

Synthesis of TBDMS-DLA$_8$-Bn (D-**23o**).

Starting with TBDMS protected tetramer D-**24n** (5.2 g, 12.4 mmol, 1.06 eq), benzyl protected tetramer D-**22n** (4.7 g, 11.7 mmol, 1 eq), DPTS (0.67 g, 2.31 mmol, 0.2 eq) and EDC·HCl (3.0 g, 15.4 mmol, 1.2 eq), crude double protected octamer D-**23o** was obtained as a light yellow oil using general method **D**. The material was purified by automated column chromatography using heptane/EtOAc (gradient 90/10 to 50/50) as eluent, giving the pure material as a colorless oil (8.75 g, 88%). ^{1}H NMR (400 MHz, $CDCl_3$): δ = 7.38–7.27 (m, 5H, Ar-H), 5.20–5.09 (m, 9H, O-CH(CH_3)-CO and Ar-CH_2-O), 4.39 (q, ^3J = 6.7 Hz, 1H, TBDMSO-CH(CH_3)-CO), 1.61–1.50 (m, 21H, O-CH(CH_3)-CO), 1.44 (d, ^3J = 6.8 Hz, 3H, Si-O-CH(CH_3)-CO), 0.90 (s, 9H, (CH_3)$_3$C-Si(CH_3)$_2$), 0.10 (s, 3H, (CH_3)$_3$C-Si(CH_3)$_2$), 0.08 ppm (s, 3H, (CH_3)$_3$C-Si(CH_3)$_2$); ^{13}C NMR (100 MHz, $CDCl_3$): δ = 173.65, 170.12–169.66, 135.20, 128.75, 128.66, 128.38, 128.37, 69.41, 69.14, 69.12, 69.10, 68.94, 68.67, 68.13, 67.35, 25.83, 21.35, 18.42, 16.89, 16.81, 16.79, 16.70, −4.77, −5.16 ppm; MS (MALDI-TOF): *m/z* calcd for $C_{37}H_{54}O_{17}Si+Na^+$: 821.30 $[M+Na]^+$; found 821.31.

Synthesis of TBDMS-LA$_{10}$-Bn (*at*-**23p**).

Starting with TBDMS protected octamer *at*-**24o** (2.74 g, 3.87 mmol, 1.05 eq), benzyl protected dimer *at*-**22m** (0.962 g, 3.67 mmol, 1.0 eq), DPTS (0.216 g, 0.734 mmol, 0.2 eq) and EDC·HCl (0.915 g, 4.77 mmol, 1.3 eq), crude double protected decamer D-**23p** was obtained as a light yellow oil (3.64 g) using general method **D**. The material was purified by automated column chromatography using hept/EtOAc (gradient 90/10 to 60/40) as eluent, giving the pure material as a colorless oil (2.434 g, 70%).

^{1}H NMR (400 MHz, $CDCl_3$): δ = 7.37–7.27 (m, 5H, Ar-H), 5.24–5.06 (m, 11H, O-CH(CH_3)-CO and Ar-CH_2-O), 4.37 (q, ^3J = 6.7 Hz, 1H, TBDMSO-CH(CH_3)-CO), 1.58–1.46 (m, 27H, O-CH(CH_3)-CO), 1.42 (d, ^3J = 6.7 Hz, 3H, TBDMSO-CH(CH_3)-CO), 0.88 (s, 9H, (CH_3)$_3$C-Si(CH_3)$_2$), 0.08 (s, 3H, (CH_3)$_3$C-Si(CH_3)$_2$), 0.06 ppm (s, 3H, (CH_3)$_3$C-Si(CH_3)$_2$); ^{13}C NMR (100 MHz, $CDCl_3$): δ = 173.59–173.58, 173.41, 171.04–169.34, 169.21, 169.20, 135.15, 135.12, 128.68, 128.59, 128.57, 128.31–128.29, 69.40–68.83, 68.59, 68.04–68.02, 67.26, 67.24, 25.76, 21.34, 21.28, 18.35–18.34, 16.94, 16.81–16.63, −4.84, −5.24 ppm; MS (MALDI-TOF): *m/z* calcd for $C_{43}H_{62}O_{21}Si+Na^+$: 965.35 $[M+Na]^+$; found 965.34; *m/z* calcd for $C_{43}H_{62}O_{21}Si+K^+$: 981.32 $[M+K^+]$; found 981.38.

Synthesis of TBDMS-LA$_{12}$-Bn (D-**23q**).

Starting with TBDMS protected decamer D-**24p** (0.818 g, 0.911 mmol, 0.92 eq), benzyl protected dimer D-**22m** (0.251 g, 0.995 mmol, 1.0 eq), DPTS (0.059 g, 0.199 mmol, 0.2 eq) and EDC·HCl (0.248 g, 1.293 mmol, 1.3 eq), crude double protected 12-mer D-**23q** was obtained as a light yellow oil (1.02 g) using general method **D**. The material was

purified by automated column chromatography using hept/EtOAc (gradient 83/17 to 45/55) as eluent, giving the pure material as a colorless oil (0.591 g, 55%).

^{1}H NMR (400 MHz, $CDCl_3$): δ = 7.40–7.29 (m, 5H, Ar-H), 5.27–5.09 (m, 13H, O-CH(CH_3)-CO and Ar-CH_2-O), 4.39 (q, ^3J = 6.8 Hz, 1H, TBDMSO-CH(CH_3)-CO), 1.61–1.47 (m, 33H, O-CH(CH_3)-CO), 1.44 (d, ^3J = 6.8 Hz, 3H, TBDMSO-CH(CH_3)-CO), 0.90 (s, 9H, (CH_3)$_3$C-Si(CH_3)$_2$), 0.10 (s, 3H, (CH_3)$_3$C-Si(CH_3)$_2$), 0.08 ppm (s, 3H, (CH_3)$_3$C-Si(CH_3)$_2$); ^{13}C NMR (100 MHz, $CDCl_3$): δ = 173.65, 173.46, 170.07–169.25, 135.26, 135.23, 128.75, 128.66–128.64, 128.37, 69.43–68.93, 68.68, 68.13, 67.35–67.33, 25.84, 21.40, 21.35, 18.42, 17.02, 16.88–16.71, −4.76, −5.14 ppm; MS (MALDI-TOF): *m/z* calcd for $C_{49}H_{70}O_{25}Si+Na^+$: 1109.39 $[M+Na]^+$; found 1109.42; *m/z* calcd for $C_{49}H_{70}O_{25}Si+K^+$: 1125.36 $[M+K^+]$; found 1125.38.

Synthesis of TBDMS-LLA$_{12}$-Bn (L-**23q**).

Starting with TBDMS protected tetramer L-**24n** (0.17 g, 0.40 mmol, 1.06 eq), benzyl protected octamer L-**22o** (0.261 g, 0.381 mmol, 1 eq), DPTS (0.02 g, 0.08 mmol, 0.2 eq) and EDC·HCl (0.10 g, 0.50 mmol, 1.3 eq), crude double protected 12-mer L-**23q** was obtained as a light yellow oil (0.40 g) using general method **D**. The material was purified by automated column chromatography using hept/EtOAc (gradient 85/15 to 45/55) as eluent, giving the pure material as a white solid (0.19 g, 47%). ^{1}H NMR (400 MHz, $CDCl_3$): δ = 7.42–7.27 (m, 5H, Ar-H), 5.23–5.05 (m, 13H, O-CH(CH_3)-CO and O-CH_2-Ar), 4.39 (q, ^3J = 6.8 Hz, 1H, Si-O-CH(CH_3)-CO), 1.57 (d, ^3J = 7.1 Hz, 27H, O-CH(CH_3)-CO), 1.51 (d, ^3J = 7.1 Hz, 6H, O-CH(CH_3)-CO), 1.44 (d, ^3J = 6.7 Hz, 3H, Si-O-CH(CH_3)-CO), 0.89 (s, 9H, (CH_3)$_3$C-Si(CH_3)$_2$), 0.10 (s, 3H, (CH_3)$_3$C-Si(CH_3)$_2$), 0.08 ppm (s, 3H, (CH_3)$_3$C-Si(CH_3)$_2$); ^{13}C NMR (100 MHz, $CDCl_3$): δ = 173.87, 170.33, 170.23, 170.06, 169.98, 169.95, 169.93, 169.92, 169.86, 135.37, 128.95, 128.86, 128.58, 69.61, 69.34, 69.33, 69.31, 69.28, 69.14, 68.86, 68.32, 67.55, 26.02, 21.56, 18.61, 17.08, 17.01, 16.98, 16.90, −4.58, −4.98 ppm; MS (MALDI-TOF): *m/z* calcd for $C_{49}H_{70}O_{25}Si+Na^+$: 1109.39 $[M+Na]^+$; found: 1109.38; *m/z* calcd for $C_{49}H_{70}O_{25}Si+K^+$: 1125.36 $[M+K]^+$; found: 1125.36.

Synthesis of TBDMS-DLA$_{12}$-Bn (D-**23q**).

Starting with TBDMS protected octamer D-**24o** (0.33 g, 0.47 mmol, 1.06 eq), benzyl protected tetramer D-**22n** (0.20 g, 0.50 mmol, 1 eq), DPTS (0.03 g, 0.09 mmol, 0.2 eq) and EDC·HCl (0.12 g, 0.61 mmol, 1.3 eq), crude double protected 12-mer D-**23q** was obtained as a light yellow oil (0.39 g) using general method **D**. The material was purified by automated column chromatography using hept/EtOAc (gradient 85/15 to 45/55) as eluent, giving the pure material as a white solid (0.32 g, 63%). ^{1}H NMR (400 MHz, $CDCl_3$): δ = 7.43–7.27 (m, 5H, Ar-H), 5.24–5.06 (m, 13H, O-CH(CH_3)-CO and O-CH_2-Ar), 4.39 (q, ^3J = 6.7 Hz, 1H, Si-O-CH(CH_3)-CO), 1.58 (d, ^3J = 7.1 Hz, 27H, O-CH(CH_3)-CO), 1.51 (d, ^3J = 7.1 Hz, 6H, O-CH(CH_3)-CO), 1.44 (d, ^3J = 6.7 Hz, 3H, Si-O-CH(CH_3)-CO), 0.9 (s, 9H, (CH_3)$_3$C-Si(CH_3)$_2$), 0.10 (s, 3H, (CH_3)$_3$C-Si(CH_3)$_2$), 0.08 ppm (s, 3H, (CH_3)$_3$C-Si(CH_3)$_2$); ^{13}C NMR (100 MHz, $CDCl_3$): δ = 173.83, 170.30, 170.20, 170.03, 169.95, 169.90, 169.89, 169.83, 135.39, 128.93, 128.84, 128.56, 69.60, 69.33, 69.32, 69.27, 69.13, 68.85, 68.31, 67.53, 26.02, 21.54, 18.59, 17.07, 16.99, 16.96, 16.89, −4.59, −4.98 ppm; MS (MALDI-TOF): *m/z* calcd for $C_{49}H_{70}O_{25}Si+Na^+$: 1109.39 $[M+Na]^+$; found: 1109.41; *m/z* calcd for $C_{49}H_{70}O_{25}Si+K^+$: 1125.36 $[M+K]^+$; found: 1125.38.

Synthesis of TBDMS-LA$_{14}$-Bn (*at*-**23r**).

Starting with TBDMS protected tetramer *at*-**24n** (0.240 g, 0.571 mmol, 1.11 eq), benzyl protected decamer *at*-**22p** (0.434 g, 0.514 mmol, 1.0 eq), DPTS (0.030 g, 0.103 mmol, 0.2 eq) and EDC·HCl (0.128 g, 0.668 mmol, 1.3 eq), crude double protected 14-mer *at*-**23r** was obtained as a light yellow oil (0.645 g) using general method **D**. The material was purified by automated column chromatography using hept/EtOAc (gradient 90/10 to 45/55) as eluent, giving the pure material as a colorless, thick oil (0.425 g, 67%). ^{1}H NMR (400 MHz, $CDCl_3$): δ = 7.39–7.27 (m, 5H, Ar-H), 5.25–5.07 (m, 15H, O-CH(CH_3)-CO and Ar-CH_2-O), 4.37 (q, ^3J = 6.8 Hz, 1H, TBDMSO-CH(CH_3)-CO), 1.61–1.45 (m, 39H, O-CH(CH_3)-CO), 6.7 (d, 3H, TBDMSO-CH(CH_3)-CO), 0.89 (s, 9H, (CH_3)$_3$C-Si(CH_3)$_2$), 0.09 (s,

3H, $(CH_3)_3C$-Si($C\underline{H}_3)_2$), 0.07 ppm (s, 3H, $(CH_3)_3C$-Si($C\underline{H}_3)_2$); ^{13}C NMR (100 MHz, $CDCl_3$): δ = 173.55, 173.37, 170.02–169.32, 169.21–169.18, 135.21, 135.18, 128.68, 128.59–128.57, 128.29, 69.36, 69.25, 69.11–69.04, 68.95, 68.89–68.86, 68.61, 68.07, 67.27–67.25, 25.78, 21.34, 21.28, 18.34, 16.95–16.65, −4.82, −5.21 ppm; MS (MALDI-TOF): *m/z* calcd for $C_{55}H_{78}O_{29}Si+Na^+$: 1253.43 $[M+Na]^+$; found 1253.43; *m/z* calcd for $C_{55}H_{78}O_{29}Si+K^+$: 1269.40 $[M+K^+]$; found 1269.39.

Synthesis of TBDMS-LA$_{16}$-Bn (*at-**23s**).

Starting with TBDMS protected octamer *at*-**24o** (3.04 g, 4.29 mmol, 1.06 eq), benzyl protected octamer *at*-**22o** (2.77 g, 4.05 mmol, 1.0 eq), DPTS (0.238 g, 0.809 mmol, 0.2 eq) and EDC·HCl (1.008 g, 5.26 mmol, 1.3 eq), crude double protected 16-mer *at*-**23s** was obtained as a colorless, thick oil (5.689 g) using general method **D**. The material was purified by automated column chromatography using hept/EtOAc (gradient 80/20 to 45/55) as eluent, giving the pure material as a colorless, thick oil (4.22 g, 76%). ^1H NMR (400 MHz, $CDCl_3$): δ = 7.37–7.27 (m, 5H, Ar-$\underline{H}$), 5.23–5.06 (m, 17H, O-C$\underline{H}(CH_3)$-CO and Ar-C$\underline{H}_2$-O), 4.36 (q, ^3J = 6.7 Hz, 1H, TBDMSO-C$\underline{H}(CH_3)$-CO), 1.58–1.44 (m, 45H, O-CH(C$\underline{H}_3$)-CO), 1.41 (d, ^3J = 6.7 Hz, 3H, TBDMSO-CH(C$\underline{H}_3$)-CO), 0.87 (s, 9H, $(C\underline{H}_3)_3C$-Si$(CH_3)_2$), 0.08 (s, 3H, $(CH_3)_3C$-Si($C\underline{H}_3)_2$), 0.06 ppm (s, 3H, $(CH_3)_3C$-Si($C\underline{H}_3)_2$); ^{13}C NMR (100 MHz, $CDCl_3$): δ = 173.52, 173.34, 169.99–169.28, 169.17–169.15, 135.15, 135.12, 128.64, 128.53, 128.25, 69.34–68.52, 68.00, 67.27–67.13, 25.73, 21.29, 21.05, 18.31, 16.90–16.63, −4.87, −5.26 ppm; MS (MALDI-TOF): *m/z* calcd for $C_{61}H_{86}O_{33}Si+Na^+$: 1397.47 $[M+Na]^+$; found 1397.46; *m/z* calcd for $C_{61}H_{86}O_{33}Si+K^+$: 1413.45 $[M+K^+]$; found 1413.45.

Synthesis of TBDMS-LLA$_{16}$-Bn (L-***23s***).

Starting with TBDMS protected octamer L-**24o** (2.05 g, 2.89 mmol, 1.06 eq), benzyl protected octamer L-**22o** (1.87 g, 2.73 mmol, 1 eq), DPTS (0.16 g, 0.546 mmol, 0.2 eq) and EDC·HCl (0.68 g, 3.55 mmol, 1.3 eq), crude double protected 16-mer L-**23s** was obtained as a light yellow solid (3.98 g) using general method **D**. The material was purified by automated column chromatography using hept/EtOAc (gradient 75/25 to 40/60) as eluent, giving the pure material as a white solid (2.70 g, 72%). ^1H NMR (400 MHz, $CDCl_3$): δ = 7.43–7.27 (m, 5H, Ar-$\underline{H}$), 5.27–5.06 (m, 17H, O-C$\underline{H}(CH_3)$-CO and O-C$\underline{H}_2$-Ar), 4.39 (q, ^3J = 6.8 Hz, 1H, Si-O-C$\underline{H}(CH_3)$-CO), 1.57–1.55 (m, 39H, O-CH(C$\underline{H}_3$)-CO), 1.51 (m, 6H, O-CH(C$\underline{H}_3$)-CO), 1.44 (d, ^3J = 6.8 Hz, 3H, Si-O-CH(C$\underline{H}_3$)-CO), 0.89 (s, 9H, $(C\underline{H}_3)_3C$-Si$(CH_3)_2$), 0.10 (s, 3H, $(CH_3)_3C$-Si($C\underline{H}_3)_2$), 0.07 ppm (s, 3H, $(CH_3)_3C$-Si($C\underline{H}_3)_2$); ^{13}C NMR (100 MHz, $CDCl_3$): δ = 173.82, 170.29, 170.19, 170.02, 169.94, 169.89, 169.88, 169.82, 135.38, 128.93, 128.84, 128.55, 69.59, 69.31, 69.27, 69.12, 68.84, 68.31, 67.52, 26.01, 21.53, 18.59, 17.06, 16.99, 16.96, 16.88, −4.59, −4.99 ppm; MS (MALDI-TOF): *m/z* calcd for $C_{61}H_{86}O_{33}Si+Na^+$: 1397.47 $[M+Na]^+$; found 1397.48; *m/z* calcd for $C_{61}H_{86}O_{33}Si+K^+$: 1413.45 $[M+K^+]$; found 1413.45.

Synthesis of TBDMS-DLA$_{16}$-Bn (D-***23s***).

Starting with TBDMS protected octamer D-**24o** (1.93 g, 2.73 mmol, 1.06 eq), benzyl protected octamer D-**22o** (1.76 g, 2.57 mmol, 1 eq), DPTS (0.15 g, 0.51 mmol, 0.2 eq) and EDC·HCl (0.80 g, 4.15 mmol, 1.6 eq), crude double protected 16-mer D-**23s** was obtained as a light yellow solid using general method **D**. The material was purified by automated column chromatography using hept/EtOAc (gradient 75/25 to 40/60) as eluent, giving the pure material as a white solid (2.7 g, 76%). ^1H NMR (400 MHz, $CDCl_3$): δ = 7.37–7.29 (m, 5H, Ar-$\underline{H}$),), 5.19–5.09 (m, 17H, O-C$\underline{H}(CH_3)$-CO and Ar-C$\underline{H}_2$-O), 4.38 (q, ^3J = 6.8 Hz, 1H, Si-O-C$\underline{H}(CH_3)$-CO), 1.58–1.50 (m, 45H, O-CH(C$\underline{H}_3$)-CO), 1.43 (d, ^3J = 6.7 Hz, 3H, Si-O-CH(C$\underline{H}_3$)-CO), 0.89 (s, 9H, $(C\underline{H}_3)_3C$-Si$(CH_3)_2$), 0.10 (s, 3H, $(CH_3)_3C$-Si($C\underline{H}_3)_2$), 0.07 ppm (s, 3H, $(CH_3)_3C$-Si($C\underline{H}_3)_2$); ^{13}C NMR (100 MHz, $CDCl_3$): δ = 173.63, 170.10–169.63, 135.18, 128.73, 128.64, 128.35, 69.40, 69.12, 69.08, 68.93, 68.65, 68.11, 67.33, 25.81, 21.33, 18.39, 16.87, 16.79, 16.76, 16.69, −4.79, −5.18 ppm;

MS (MALDI-TOF): *m/z* calcd for $C_{61}H_{86}O_{33}Si+Na^+$: 1397.47 $[M+Na]^+$; found 1397.47; *m/z* calcd for $C_{61}H_{86}O_{33}Si+K^+$: 1413.45 $[M+K^+]$; found 1413.45.

Synthesis of TBDMS-LA$_{24}$-Bn (*at*-**23t**).

Starting with TBDMS protected 16-mer *at*-**24s** (1.67 g, 1.273 mmol, 1.06 eq), benzyl protected octamer *at*-**22o** (0.822 g, 1.201 mmol, 1.0 eq), DPTS (0.071 g, 0.240 mmol, 0.2 eq) and EDC·HCl (0.299 g, 1.562 mmol, 1.3 eq), crude double protected 24-mer *at*-**23t** was obtained as a colorless, thick oil (2.410 g) using general method **D**. The material was purified by automated column chromatography using DCM/EtOAc (gradient 100/0 to 80/20) as eluent, giving the pure material as a white, fluffy powder (2.008 g, 86%). ^{1}H NMR (400 MHz, $CDCl_3$): δ = 7.37–7.26 (m, 5H, Ar-H), 5.22–5.07 (m, 25H, O-CH(CH$_3$)-CO and Ar-CH$_2$-O), 4.36 (q, ^3J = 6.7 Hz, 1H, TBDMSO-CH(CH$_3$)-CO), 1.57–1.40 (m, 69H, O-CH(CH$_3$)-CO), 1.41 (d, ^3J = 6.8 Hz, 3H, TBDMSO-CH(CH$_3$)-CO), 0.85 (s, 9H, (CH$_3$)$_3$C-Si(CH$_3$)$_2$), 0.07 (s, 3H, (CH$_3$)$_3$C-Si(CH$_3$)$_2$), 0.05 ppm (s, 3H, (CH$_3$)$_3$C-Si(CH$_3$)$_2$); ^{13}C NMR (100 MHz, $CDCl_3$): δ = 173.43, 173.26, 169.88–169.24, 169.09, 135.11, 135.08, 128.58, 128.47, 128.19, 69.28–68.93, 67.94, 67.12, 25.67, 21.24–21.18, 20.96, 18.24, 16.83–16.56, −4.93, −5.32 ppm; MS (MALDI-TOF): *m/z* calcd for $C_{85}H_{118}O_{49}Si+Na^+$: 1973.64 $[M+Na]^+$; found 1973.60; *m/z* calcd for $C_{85}H_{118}O_{49}Si+K^+$: 1989.61 $[M+K^+]$; found 1989.58.

Synthesis of TBDMS-LLA$_{24}$-Bn (L-**23t**).

Starting with TBDMS protected octamer L-**24o** (0.25 g, 0.35 mmol, 1.06 eq), benzyl protected 16-mer L-**22s** (0.41 g, 0.33 mmol, 1 eq), DPTS (0.02 g, 0.07 mmol, 0.2 eq) and EDC·HCl (0.08 g, 0.43 mmol, 1.3 eq), crude double protected 24-mer L-**23t** was obtained as a light yellow solid (3.98 g) using general method **D**. The material was purified by automated column chromatography using DCM/EtOAc (gradient 100/0 to 80/20) as eluent, giving the pure material as a white solid (0.44 g, 67%). ^{1}H NMR (400 MHz, $CDCl_3$): δ = 7.44–7.28 (m, 5H, Ar-H), 5.25–5.06 (m, 25H, O-CH(CH$_3$)-CO and O-CH$_2$-Ar), 4.39 (q, ^3J = 6.7 Hz, 1H, Si-O-CH(CH$_3$)-CO), 1.57 (d, ^3J = 7.1 Hz, 63H, O-CH(CH$_3$)-CO), 1.52 (d, ^3J = 7.1 Hz, 6H, O-CH(CH$_3$)-CO), 1.44 (d, ^3J = 6.7 Hz, 3H, Si-O-CH(CH$_3$)-CO), 0.9 (s, 9H, (CH$_3$)$_3$C-Si(CH$_3$)$_2$), 0.1 (s, 3H, (CH$_3$)$_3$C-Si(CH$_3$)$_2$), 0.08 ppm (s, 3H, (CH$_3$)$_3$C-Si(CH$_3$)$_2$); ^{13}C NMR (100 MHz, $CDCl_3$) δ = 173.84, 170.30, 170.20, 170.04, 169.95, 169.90, 169.83, 135.36, 128.93, 128.84, 128.55, 69.59, 69.31, 69.26, 69.11, 68.84, 68.29, 67.53, 26.00, 21.53, 18.59, 17.06, 16.95, 16.88, −4.60, −4.99 ppm; MS (MALDI-TOF): *m/z* calcd for $C_{85}H_{118}O_{49}Si+Na^+$: 1973.64 $[M+Na]^+$; found: 1973.64; *m/z* calcd for $C_{85}H_{118}O_{49}Si+K^+$: 1089.61 $[M+K]^+$; found: 1989.63.

Synthesis of TBDMS-LA$_{32}$-Bn (*at*-**23u**).

Starting with TBDMS protected 16-mer *at*-**24s** (0.55 g, 0.419 mmol, 1.06 eq), benzyl protected 16-mer *at*-**22s** (0.499 g, 0.396 mmol, 1.0 eq), DPTS (0.023 g, 0.079 mmol, 0.2 eq) and EDC·HCl (0.099 g, 0.514 mmol, 1.3 eq), crude double protected 32-mer *at*-**23u** was obtained as a white, fluffy solid (1.124 g) using general method **D**. The material was purified by automated column chromatography using DCM/EtOAc (gradient 100/0 to 80/20) as eluent, giving the pure material as a white, fluffy powder (0.806 g, 81%). ^{1}H NMR (400 MHz, $CDCl_3$): δ = 7.36–7.26 (m, 5H, Ar-H), 5.22–5.07 (m, 33H, O-CH(CH$_3$)-CO and Ar-CH$_2$-O), 4.36 (q, ^3J = 6.7 Hz, 1H, TBDMSO-CH(CH$_3$)-CO), 1.57–1.40 (m, 93H, O-CH(CH$_3$)-CO), 1.41 (d, ^3J = 6.8 Hz, 3H, TBDMSO-CH(CH$_3$)-CO), 0.87 (s, 9H, (CH$_3$)$_3$C-Si(CH$_3$)$_2$), 0.07 (s, 3H, (CH$_3$)$_3$C-Si(CH$_3$)$_2$), 0.05 ppm (s, 3H, (CH$_3$)$_3$C-Si(CH$_3$)$_2$); ^{13}C NMR (100 MHz, $CDCl_3$): δ = 173.36, 169.93–169.16, 135.15, 128.65, 128.55, 128.27, 75.69, 69.35–68.86, 68.01, 67.22, 60.39, 25.74, 21.30, 21.06, 18.31, 16.89–16.64, 14.24, −4.86, −5.25 ppm; MS (MALDI-TOF): *m/z* calcd for $C_{109}H_{150}O_{65}Si+Na^+$: 2549.81 $[M+Na]^+$; found 2549.81; *m/z* calcd for $C_{85}H_{118}O_{49}Si+K^+$: 2565.78 $[M+K^+]$; found 2565.81.

Synthesis of TBDMS-LLA$_{32}$-Bn (L-**23u**).

Starting with TBDMS protected 16-mer L-**24s** (0.51 g, 0.39 mmol, 1.06 eq), benzyl protected 16-mer L-**22s** (0.48 g, 0.38 mmol, 1 eq), DPTS (0.02 g, 0.07 mmol, 0.2 eq) and EDC·HCl (0.09 g, 0.48 mmol, 1.3 eq), crude double

protected 32-mer L-**23u** was obtained as a light yellow solid (0.93 g) using general method **D**. The material was purified by automated column chromatography using DCM/EtOAc (gradient 90/10 to 80/20) as eluent, giving the pure material as a white solid (0.79 g, 84%). ^{1}H NMR (400 MHz, $CDCl_3$): δ = 7.32–7.29 (m, 5H, Ar-H), 5.16 (q, ^3J = 7.1 Hz, 33H, O-CH(CH_3)-CO and O-CH_2-Ar), 4.39 (q, ^3J = 6.7 Hz, 1H, Si-O-CH(CH_3)-CO), 1.57 (d, ^3J = 7.2 Hz, 87H, O-CH(CH_3)-CO), 1.51 (d, ^3J = 7.1 Hz, 6H, O-CH(CH_3)-CO), 1.43 (d, ^3J = 6.7 Hz, 3H, Si-O-CH(CH_3)-CO), 0.89 (s, 9H, (CH_3)$_3$C-Si(CH_3)$_2$), 0.1 (s, 3H, (CH_3)$_3$C-Si(CH_3)$_2$), 0.07 ppm (s, 3H, (CH_3)$_3$C-Si(CH_3)$_2$); ^{13}C NMR (100 MHz, $CDCl_3$): δ = 173.82, 170.29, 170.19, 170.02, 169.94, 169.89, 169.82, 135.38, 128.93, 128.84, 128.55, 69.59, 69.32, 69.27, 69.12, 68.85, 68.31, 67.53, 26.01, 21.53, 18.59, 17.07, 16.99, 16.96, 16.89, −4.59, −4.98 ppm; MS (MALDI-TOF): *m/z* calcd for $C_{109}H_{150}O_{65}Si+Na^+$: 2549.81 $[M+Na]^+$; found: 2549.84; *m/z* calcd for $C_{109}H_{150}O_{65}Si+K^+$: 2565.78 $[M+K]^+$; found: 2565.74.

Synthesis of TBDMS-DLA$_{32}$-Bn (D-**23u**).

Starting with TBDMS protected 16-mer D-**24s** (0.70 g, 0.55 mmol, 1.06 eq), benzyl protected 16-mer D-**22s** (0.65 g, 0.52 mmol, 1 eq), DPTS (37 mg, 0.23 mmol, 0.2 eq) and EDC·HCl (0.15 g, 0.78 mmol, 1.4 eq), crude double protected 32-mer D-**23u** was obtained as a light yellow solid using general method **D**. The material was purified by automated column chromatography using chloroform/EtOAc (gradient 100/0 to 85/15) as eluent, giving the pure material as a white solid (1.0 g, 73%). ^{1}H NMR (400 MHz, $CDCl_3$): δ = 7.37–7.29 (m, 5H, Ar-H), 5.19–5.09 (m, 33H, O-CH(CH_3)-CO and Ar-CH_2-O), 4.38 (q, ^3J = 6.8 Hz, 1H, Si-O-CH(CH_3)-CO), 1.63–1.42 (m, 96H, O-CH(CH_3)-CO), 0.89 (s, 9H, (CH_3)$_3$C-Si(CH_3)$_2$), 0.09 (s, 3H, (CH_3)$_3$C-Si(CH_3)$_2$), 0.07 ppm (s, 3H, (CH_3)$_3$C-Si(CH_3)$_2$); ^{13}C NMR (100 MHz, $CDCl_3$) δ = 173.64, 170.10, 170.08, 170,02, 169.85, 169. 72, 169.64, 135.18, 128.74, 128.65, 128.36, 69.40, 69.13, 69.08, 68.93, 68.66, 68.12, 67.34, 25.82, 21.34, 18.40, 16.87, 16.77, 16.69, −4.79, −5.18 ppm; MS (MALDI-TOF): *m/z* calcd for $C_{109}H_{150}O_{65}Si+Na^+$: 2549.81 $[M+Na]^+$; found 2549.80; *m/z* calcd for $C_{109}H_{150}O_{65}Si+K^+$: 2565.78 $[M+K^+]$; found 2565.

Synthesis of TBDMS-LLA$_{64}$-Bn (L-**23v**).

Starting with TBDMS protected 32-mer L-**24u** (50 mg, 0.02 mmol, 1.06 eq), benzyl protected 32-mer L-**22u** (50 mg, 0.02 mmol, 1 eq), DPTS (1.14 mg, 3.87 µmol, 0.2 eq) and EDC·HCl (4.82 mg, 0.03 mmol, 1.3 eq), crude double protected 64-mer L-**23v** was obtained as a light yellow solid (0.09 g) using general method **D**. The material was purified by automated column chromatography using DCM/EtOAc (gradient 93/7 to 70/30) as eluent, giving the pure material as a white solid (0.81 g, 87%). ^{1}H NMR (400 MHz, $CDCl_3$): δ = 7.36–7.30 (m, 5H, Ar-H), 5.15 (q, ^3J = 7 Hz, 65H, O-CH(CH_3)-CO and O-CH_2-Ar), 4.39 (q, ^3J = 6.7 Hz, 1H, Si-O-CH(CH_3)-CO), 1.57 (d, ^3J = 7.1 Hz, 183H, O-CH(CH_3)-CO), 1.51 (d, ^3J = 7.1 Hz, 6H, O-CH(CH_3)-CO), 1.43 (d, ^3J = 6.8 Hz, 3H, Si-O-CH(CH_3)-CO), 0.89 (s, 9H, (CH_3)$_3$C-Si(CH_3)$_2$), 0.09 (s, 3H, (CH_3)$_3$C-Si(CH_3)$_2$), 0.07 ppm (s, 3H, (CH_3)$_3$C-Si(CH_3)$_2$); ^{13}C NMR (100 MHz, $CDCl_3$): δ = 173.83, 170.29, 170.20, 170.03, 169.90, 169.83, 135.38, 128.93, 128.84, 128.55, 69.60, 69.32, 69.12, 68.85, 68.31, 67.53, 26.01, 21.53, 18.59, 17.07, 16.96, −4.59, −4.98 ppm; MS (MALDI-TOF): *m/z* calcd for $C_{205}H_{278}O_{129}Si+Na^+$: 4854.49 $[M+Na]^+$; found: 4854.52; *m/z* calcd for $C_{205}H_{278}O_{129}Si+K^+$ = 4870.46 $[M+K]^+$; found: 4870.42.

Synthesis of TBDMS-DLA$_{64}$-Bn (D-**23v**).

Starting with TBDMS protected 32-mer D-**24u** (0.13 g, 0.05 mmol, 1.1 eq), benzyl protected 32-mer D-**22u** (0.11 g, 0.05 mmol, 1 eq), DPTS (5 mg, 0.068 mmol, 0.8 eq) and EDC·HCl (10 mg, 0.06 mmol, 1.1 eq), crude double protected 64-mer D-**23v** was obtained as a light yellow solid using general method **D**. The material was purified by automated column chromatography using chloroform/EtOAc (gradient 95/5 to 75/25) as eluent, giving the pure material as a white solid (0.14 g, 58%). ^{1}H NMR (400 MHz, $CDCl_3$): δ = 7.37–7.28 (m, 5H, Ar-H), 5.18–5.08 (m, 65H, O-CH(CH_3)-CO and Ar-CH_2-O), 4.38 (q, ^3J = 6.8 Hz, 1H, Si-O-CH(CH_3)-CO), 1.65–1.42 (m, 192H, O-CH(CH_3)-CO), 0.88 (s, 9H, (CH_3)$_3$C-Si(CH_3)$_2$), 0.09 (s, 3H, (CH_3)$_3$C-Si(CH_3)$_2$), 0.06 ppm (s, 3H, (CH_3)$_3$C-Si(CH_3)$_2$);

^{13}C NMR (100 MHz, $CDCl_3$): δ = 173.61, 170.08, 169.99, 169.81, 169.72, 169.61, 135.17, 128.72, 128.61, 128.34, 69.38, 69.11, 68.91, 68.63, 68.10, 67.31, 25.80, 21.32, 21.14, 18.38, 16.85, 16.75, 16.68, 16.64, 14.31, −4.80, −5.19 ppm; MS (MALDI-TOF): *m/z* calcd for $C_{205}H_{278}O_{129}Si+Na^+$: 4854.48 $[M+Na]^+$; found 4854; *m/z* calcd for $C_{205}H_{278}O_{129}Si+K^+$: 4870.45 $[M+K^+]$; found 4870.

*General method **E** for removal of the benzyl protective group giving TBDMS-LA$_y$-COOH* (*at*-**24**)*, TBDMS-LLA$_y$-COOH* (L-**24**) *or TBDMS-DLA$_y$-COOH* (D-**24**).

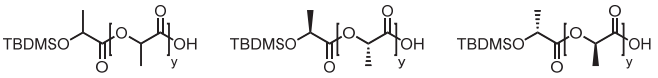

The benzyl protected oligomer **23** (*e.g.*, 45 mmol) was dissolved in ethyl acetate (170 mL, 0.24 M). The solution was purged with argon and Pd/C (10 w% Pd, 0.03 eq of Pd) was added. The mixture was then stirred under a hydrogen atmosphere at room temperature. After 2 h, TLC analysis (hept/EtOAc 50:50; UV and CeMo stain; $R_{f,prod}$ = 0.01–0.50 (tailing)) confirmed that all of the benzyl ester was converted. The black suspension was filtered through a 4 cm thick layer of celite and the filter cake washed with EtOAc (100 mL in small portions). The combined filtrates were concentrated *in vacuo*, giving the title compound **24** in high purity.

Synthesis of TBDMS-LA$_2$-COOH (*at*-**24m**).

Starting from benzyl protected dimer *at*-**23m** (15.00 g, 41 mmol), pure deprotected dimer *at*-**24m** was obtained as a colorless oil (11.32 g, quant.) using general method **E**. ^{1}H NMR (400 MHz, $CDCl_3$): δ = 5.14 (q, ^3J = 7.1 Hz, 1H, O-C<u>H</u>(CH_3)-COOH, 4.40 (q, ^3J = 6.8 Hz, 1H, TBDMSO-C<u>H</u>(CH_3)-CO), 1.56 (d, ^3J = 7.1 Hz, 1H, O-CH(C<u>H</u>$_3$)-COOH), 1.45 (d, ^3J = 6.7 Hz, 1H, TBDMSO-CH(C<u>H</u>$_3$)-CO), 0.91 (s, 9H, (C<u>H</u>$_3$)$_3$C-Si(CH_3)$_2$), 0.10 (s, 3H, (CH_3)$_3$C-Si(C<u>H</u>$_3$)$_2$), 0.08 ppm (s, 3H, (CH_3)$_3$C-Si(C<u>H</u>$_3$)$_2$); ^{13}C NMR (100 MHz, $CDCl_3$): δ = 176.16, 173.67, 68.47, 68.20, 25.79, 21.18, 18.39, 16.86, −4.85, −5.22 ppm; MS (MALDI-TOF): *m/z* calcd for $C_{12}H_{24}O_5Si+Na^+$: 299.13 $[M+Na^+]$; found 299.24.

Synthesis of TBDMS-LLA$_2$-COOH (L-**24m**).

Starting from benzyl protected dimer L-**23m** (7.14 g, 19.5 mmol), pure deprotected dimer L-**24m** was obtained as a colorless oil (5.41 g, quant.) using general method **E**. ^{1}H NMR (400 MHz, $CDCl_3$): δ = 5.12 (q, ^3J = 7.1 Hz, 1H, O-C<u>H</u>(CH_3)-COOH), 4.40 (q, ^3J = 6.8 Hz, 1H, Si-O-C<u>H</u>(CH_3)-CO), 1.55 (d, ^3J = 7.1 Hz, 3H, O-CH(C<u>H</u>$_3$)-COOH), 1.44 (d, ^3J = 6.7 Hz, 3H, O-CH(C<u>H</u>$_3$)-CO), 0.90 (s, 9H, (C<u>H</u>$_3$)$_3$C-Si(CH_3)$_2$), 0.10 (s, 3H, (CH_3)$_3$C-Si(C<u>H</u>$_3$)$_2$), 0.08 ppm (s, 3H, (CH_3)$_3$C-Si(C<u>H</u>$_3$)$_2$); ^{13}C NMR (100 MHz, $CDCl_3$): δ = 176.81, 173.84, 68.70, 68.42, 26.02, 21.50, 18.63, 17.09, −4.97, −4.61 ppm.

Synthesis of TBDMS-DLA$_2$-COOH (D-**24m**).

Starting from benzyl protected dimer D-**23m** (15.4 g, 42.0 mmol), pure deprotected dimer D-**24m** was obtained as a colorless oil (11.5 g, quant.) using general method **E**. ^{1}H NMR (400 MHz, $CDCl_3$): δ = 9.34 (bs, 1H, COO<u>H</u>), 5.12 (q, ^3J = 7.1 Hz, 1H, O-C<u>H</u>(CH_3)-COOH), 4.40 (q, ^3J = 6.8 Hz, 1H, Si-O-C<u>H</u>(CH_3)-CO), 1.57 (d, ^3J = 7.1 Hz, 3H, O-CH(C<u>H</u>$_3$)-COOH), 1.44 (d, ^3J = 6.8 Hz, 3H, Si-O-CH(C<u>H</u>$_3$)-CO), 0.90 (s, 9H, (C<u>H</u>$_3$)$_3$C-Si(CH_3)$_2$), 0.10 (s, 3H, (CH_3)$_3$C-Si(C<u>H</u>$_3$)$_2$), 0.08 ppm (s, 3H, (CH_3)$_3$C-Si(C<u>H</u>$_3$)$_2$); ^{13}C NMR (100 MHz, $CDCl_3$): δ = 176.54, 173.68, 68.52, 68.21, 25.81, 21.30, 18.43, 16.88, −4.82, −5.20 ppm.

Synthesis of TBDMS-LA$_4$-COOH (*at*-**24n**).

Starting from benzyl protected tetramer *at*-**23n** (6.64 g, 13.0 mmol), pure deprotected tetramer *at*-**24n** was obtained as a colorless oil (5.44 g, quant.) using general method **E**. ^{1}H NMR (400 MHz, $CDCl_3$): δ = 5.22–5.08 (m, 3H, O-C<u>H</u>(CH_3)-CO), 4.39 (q, ^3J = 6.7 Hz, 1H, TBDMSO-C<u>H</u>(CH_3)-CO), 1.59–1.49 (m, 9H, O-CH(C<u>H</u>$_3$)-CO), 1.44 (d, ^3J = 6.8 Hz, 3H, TBDMSO-CH(C<u>H</u>$_3$)-CO), 0.89 (s, 9H, (C<u>H</u>$_3$)$_3$C-Si(CH_3)$_2$), 0.10 (s, 3H, (CH_3)$_3$C-Si(C<u>H</u>$_3$)$_2$), 0.08

ppm (s, 3H, $(CH_3)_3C$-Si($C\underline{H}_3)_2$); ^{13}C NMR (100 MHz, $CDCl_3$): δ = 175.78, 175.73, 173.74, 173.60, 170.13, 169.99, 169.78, 169.53, 69.09–68.83, 68.12, 25.81, 21.36, 18.40, 16.96–16.75, −4.80, −5.19 ppm; MS (MALDI-TOF): *m*/*z* calcd for $C_{18}H_{32}O_9Si+Na^+$: 443.17 $[M+Na]^+$; found 443.20; *m*/*z* calcd for $C_{18}H_{31}O_9Si$: 419,17 $[M-H^+]^-$; found 419,24.

Synthesis of TBDMS-LLA$_4$-COOH (L-**24n**).

Starting from benzyl protected tetramer L-**23n** (3.21 g, 6.29 mmol), pure deprotected dimer L-**24n** was obtained as a colorless oil (2.68 g, quant.) using general method **E**. ^1H NMR (400 MHz, $CDCl_3$): δ = 5.26–5.05 (m, 3H, O-C$\underline{H}$(CH_3)-CO), 4.39 (q, ^3J = 6.7 Hz, 1H, Si-O-C$\underline{H}$(CH_3)-CO), 1.26–1.50 (m, 9H, O-CH(C$\underline{H}_3$)-COOH), 1.44 (d, ^3J = 6.8 Hz, 3H, Si-O-CH(C$\underline{H}_3$)-CO), 0.89 (s, 9H, (C$\underline{H}_3$)$_3$C-Si(CH_3)$_2$), 0.10 (s, 3H, $(CH_3)_3$C-Si(C$\underline{H}_3$)$_2$), 0.08 ppm (s, 3H, $(CH_3)_3$C-Si(C$\underline{H}_3$)$_2$); ^{13}C NMR (100 MHz, $CDCl_3$): δ = 176.07, 173.95, 170.35, 169.98, 69.13, 69.07, 68.91, 68.34, 60.88, 26.02, 21.53, 21.37, 18.60, 17.05, 16.97, 16.93, 14.50, −4.59, −4.98 ppm; MS (MALDI-TOF): *m*/*z* calcd for $C_{18}H_{32}O_9Si+Na^+$: 443.17 $[M+Na]^+$; found 443.20; *m*/*z* calcd for $C_{18}H_{32}O_9Si+K^+$: 459.14 $[M+K]^+$; found 459.17.

Synthesis of TBDMS-DLA$_4$-COOH (D-**24n**).

Starting from benzyl protected tetramer D-**23n** (6.39 g, 12.5 mmol), pure deprotected tetramer D-**24n** was obtained as a colorless oil (5.44 g, quant.) using general method **E**. ^1H NMR (400 MHz, $CDCl_3$): δ = 8.87 (bs, 1H, COO$\underline{H}$), 5.22–5.08 (m, 3H, O-C$\underline{H}$(CH_3)-CO), 4.39 (q, ^3J = 6.8 Hz, 1H, Si-O-C$\underline{H}$(CH_3)-CO), 1.63–1.49 (m, 9H, O-CH(C$\underline{H}_3$)-CO), 1.44 (d, ^3J = 6.8 Hz, 3H, Si-O-CH(C$\underline{H}_3$)-CO), 0.90 (s, 9H, (C$\underline{H}_3$)$_3$C-Si(CH_3)$_2$), 0.10 (s, 3H, $(CH_3)_3$C-Si(C$\underline{H}_3$)$_2$), 0.08 ppm (s, 3H, $(CH_3)_3$C-Si(C$\underline{H}_3$)$_2$); ^{13}C NMR (100 MHz, $CDCl_3$): δ = 175.87, 173.78, 170.18, 169.81, 68.93, 68.72, 68.13, 25.82, 21.36, 18.42, 16.86, 16.77, −4.79, −5.18 ppm; MS (MALDI-TOF): *m*/*z* calcd for $C_{18}H_{32}O_9Si+Na^+$: 443.17 $[M+Na]^+$; found 443.17; *m*/*z* calcd for $C_{18}H_{32}O_9Si+K^+$: 459,14 $[M+K^+]^-$; found 459.16.

Synthesis of TBDMS-LA$_8$-COOH (*at*-**24o**).

Starting from benzyl protected octamer *at*-**23o** (3.50 g, 4.38 mmol), pure deprotected octamer *at*-**24o** was obtained as a colorless oil (3.19 g, 98%) using general method **E**. ^1H NMR (400 MHz, $CDCl_3$): δ = 5.26–5.09 (m, 7H, O-C$\underline{H}$(CH_3)-CO), 4.39 (q, ^3J = 6.7 Hz, 1H, TBDMSO-C$\underline{H}$(CH_3)-CO), 1.60–1.52 (m, 21H, O-CH(C$\underline{H}_3$)-CO), 1.44 (d, ^3J = 6.8 Hz, 3H, TBDMSO-CH(C$\underline{H}_3$)-CO), 0.90 (s, 9H, (C$\underline{H}_3$)$_3$C-Si(CH_3)$_2$), 0.10 (s, 3H, $(CH_3)_3$C-Si(C$\underline{H}_3$)$_2$), 0.08 ppm (s, 3H, $(CH_3)_3$C-Si(C$\underline{H}_3$)$_2$); ^{13}C NMR (100 MHz, $CDCl_3$): δ = 175.26, 173.73, 173.56, 170.07–169.32, 69.25–68.74, 68.11, 25.81, 21.36, 18.41, 16.79, −4.80, −5.18 ppm; MS (MALDI-TOF): *m*/*z* calcd for $C_{30}H_{48}O_{17}Si+Na^+$: 731.26 $[M+Na]^+$; found 731.26; *m*/*z* calcd for $C_{30}H_{48}O_{17}Si+K^+$: 747.23 $[M+K^+]$; found 747.24.

Synthesis of TBDMS-LLA$_8$-COOH (L-**24o**).

Starting from benzyl protected octamer L-**23o** (2.57 g, 3.21 mmol), pure deprotected dimer L-**24o** was obtained as a colorless oil (2.25 g, 99%) using general method **E**. The reaction was completed in 5 hours. ^1H NMR (400 MHz, $CDCl_3$): δ = 5.23–5.06 (m, 7H, O-C$\underline{H}$(CH_3)-COOH and O-C$\underline{H}_2$-Ar), 4.39 (q, ^3J = 6.8 Hz, 1H, Si-O-C$\underline{H}$(CH_3)-CO), 1.67–1.49 (m, 21H, O-CH(C$\underline{H}_3$)-COOH), 1.43 (d, ^3J = 6.7 Hz, 3H, Si-O-CH(C$\underline{H}_3$)-CO), 0.89 (s, 9H, (C$\underline{H}_3$)$_3$C-Si(CH_3)$_2$), 0.11 (s, 3H, $(CH_3)_3$C-Si(C$\underline{H}_3$)$_2$), 0.08 ppm (s, 3H, $(CH_3)_3$C-Si(C$\underline{H}_3$)$_2$); ^{13}C NMR (100 MHz, $CDCl_3$): δ = 175.60, 173.91, 170.32, 170.06, 169.98, 169.96, 169.86, 69.34, 69.32, 69.30, 69.16, 69.09, 68.89, 68.33, 26.02, 21.53, 18.60, 17.07, 16.99, 16.97, 16.90, −4.59, −4.97 ppm; MS (MALDI-TOF): *m*/*z* calcd for $C_{30}H_{48}O_{17}Si+Na^+$: 731.26 $[M+Na]^+$; found 731.29 Da; *m*/*z* calcd for $C_{30}H_{48}O_{17}Si+K^+$: 747.23 $[M+K^+]$; found 747.26.

Synthesis of TBDMS-DLA$_8$-COOH (D-**24o**).

Starting from benzyl protected octamer D-**23o** (2.37 g, 2.97 mmol), pure deprotected octamer D-**24o** was obtained as a colorless oil (2.2 g, quant.) using general method **E**. ^1H NMR (400 MHz, $CDCl_3$): δ = 8.18 (bs, 1H, COO$\underline{H}$), 5.20–5.10 (m, 7H, O-C$\underline{H}$(CH_3)-CO), 4.39 (q, ^3J = 6.7 Hz, 1H, Si-O-C$\underline{H}$(CH_3)-CO), 1.63–1.52 (m, 21H, O-CH(C$\underline{H}_3$)-CO), 1.44 (d, ^3J = 6.7 Hz, 3H, Si-O-CH(C$\underline{H}_3$)-CO), 0.89 (s, 9H, (C$\underline{H}_3$)$_3$C-Si(CH_3)$_2$), 0.10 (s, 3H, $(CH_3)_3$C-Si(C$\underline{H}_3$)$_2$), 0.07 ppm (s, 3H, $(CH_3)_3$C-Si(C$\underline{H}_3$)$_2$); ^{13}C NMR (100 MHz, $CDCl_3$): δ = 175.28, 173.71, 170.13, 169.87,

169.77, 169.66, 69.15, 69.12, 69.11, 68.96, 68.88, 68.70, 68.15, 25.83, 21.35, 18.42, 16.88, 16.81, 16.78, 16.71, −4.78, −5.16 ppm; MS (MALDI-TOF): *m/z* calcd for $C_{30}H_{48}O_{17}Si+Na^+$: 731.26 $[M+Na]^+$; found 731.27; *m/z* calcd for $C_{30}H_{48}O_{17}Si+K^+$: 747.23 $[M+K^+]$; found 747.25.

Synthesis of TBDMS-LA$_{10}$-COOH (*at*-**24p**).

Starting from benzyl protected decamer *at*-**23p** (1.05 g, 1.035 mmol), pure deprotected decamer *at*-**24p** was obtained as a colorless oil (0.881 g, quant.) using general method **E**. ^{1}H NMR (400 MHz, $CDCl_3$): δ = 5.26–5.07 (m, 9H, O-C<u>H</u>(CH$_3$)-CO), 4.39 (q, ^3J = 6.7 Hz, 1H, TBDMSO-C<u>H</u>(CH$_3$)-CO), 1.60–1.50 (m, 27H, O-CH(C<u>H</u>$_3$)-CO), 1.43 (d, ^3J = 6.8 Hz, 3H, TBDMSO-CH(C<u>H</u>$_3$)-CO), 0.89 (s, 9H, (C<u>H</u>$_3$)$_3$C-Si(CH$_3$)$_2$), 0.09 (s, 3H, (CH$_3$)$_3$C-Si(C<u>H</u>$_3$)$_2$), 0.07 ppm (s, 3H, (CH$_3$)$_3$C-Si(C<u>H</u>$_3$)$_2$); ^{13}C NMR (100 MHz, $CDCl_3$): δ = 175.09–174.80, 173.74, 173.57, 170.10–169.33, 69.34–68.70, 68.09, 25.82, 21.40–21.19, 18.42, 16.99–16.73, −4.79, −5.18 ppm; MS (MALDI-TOF): *m/z* calcd for C36H56O21Si+Na$^+$: 875.30 $[M+Na]^+$; found 875.28.

Synthesis of TBDMS-LA$_{16}$-COOH (*at*-**24s**).

Starting from benzyl protected 16-mer *at*-**23s** (2.65 g, 1.927 mmol), pure deprotected 16-mer *at*-**24s** was obtained as a colorless oil (2.38 g, 94%) using general method **E**. ^{1}H NMR (400 MHz, $CDCl_3$): δ = 5.22–5.05 (m, 15H, O-C<u>H</u>(CH$_3$)-CO), 4.36 (q, ^3J = 6.7 Hz, 1H, TBDMSO-C<u>H</u>(CH$_3$)-CO), 1.57–1.46 (m, 45H, O-CH(C<u>H</u>$_3$)-CO), 1.40 (d, ^3J = 6.7 Hz, 3H, TBDMSO-CH(C<u>H</u>$_3$)-CO), 0.86 (s, 9H, (C<u>H</u>$_3$)$_3$C-Si(CH$_3$)$_2$), 0.07 (s, 3H, (CH$_3$)$_3$C-Si(C<u>H</u>$_3$)$_2$), 0.05 ppm (s, 3H, (CH$_3$)$_3$C-Si(C<u>H</u>$_3$)$_2$); ^{13}C NMR (100 MHz, $CDCl_3$): δ = 173.66, 173.49, 170.03–169.27, 69.25, 69.12–68.91, 68.07, 25.78, 21.34, 18.37, 16.81–16.74, −4.83, −5.21 ppm; MS (MALDI-TOF): *m/z* calcd for $C_{54}H_{80}O_{33}Si+Na^+$: 1307.42 $[M+Na]^+$; found 1307.42; *m/z* calcd for $C_{54}H_{80}O_{33}Si+K^+$: 1323.40 $[M+K^+]$; found 1323.39.

Synthesis of TBDMS-LLA$_{16}$-COOH (L-**24s**).

Starting from benzyl protected 16-mer L-**23s** (0.73 g, 0.03 mmol), pure deprotected 16-mer L-**24s** was obtained as a colorless solid (0.71 g, quant.) using general method **E**. ^{1}H NMR (400 MHz, $CDCl_3$): δ = 5.18–5.1 (m, 15H, O-C<u>H</u>(CH$_3$)-CO), 4.38 (q, ^3J = 6.7 Hz, 1H, Si-O-C<u>H</u>(CH$_3$)-CO), 1.69–1.48 (m, 45H, O-CH(C<u>H</u>$_3$)-CO), 1.39 (d, ^3J = 6.9 Hz, 3H, Si-O-CH(C<u>H</u>$_3$)-CO), 0.88 (s, 9H, (C<u>H</u>$_3$)$_3$C-Si(CH$_3$)$_2$), 0.08 (s, 3H, (CH$_3$)$_3$C-Si(C<u>H</u>$_3$)$_2$), 0.06 ppm (s, 3H, (CH$_3$)$_3$C-Si(C<u>H</u>$_3$)$_2$); ^{13}C NMR (100 MHz, $CDCl_3$): δ = 175.12, 173.88, 170.29, 170.03, 169.95, 169.91, 169.81, 69.30, 69.12, 69.06, 68.85, 68.29, 25.98, 21.51, 18.57, 17.03, 16.96, 16.93, 16.87, −4.62, −5.01 ppm; MS (MALDI-TOF): *m/z* calcd for $C_{54}H_{80}O_{33}Si+Na^+$: 1307.42 $[M+Na]^+$; found: 1307.44; *m/z* calcd for $C_{54}H_{80}O_{33}Si+K^+$: 1323.40 $[M+K]^+$; found: 1323.41.

Synthesis of TBDMS-DLA$_{16}$-COOH (D-**24s**).

Starting from benzyl protected 16-mer D-**23s** (0.84 g, 0.61 mmol), pure deprotected 16-mer D-**24s** was obtained as a white solid (0.84 g, quant.) using general method **E**. ^{1}H NMR (400 MHz, $CDCl_3$): δ = 5.19–5.09 (m, 15H, O-C<u>H</u>(CH$_3$)-CO), 4.38 (q, ^3J = 6.8 Hz, 1H, Si-O-C<u>H</u>(CH$_3$)-CO), 1.60–1.52 (m, 45H, O-CH(C<u>H</u>$_3$)-CO), 1.43 (d, ^3J = 6.7 Hz, 3H, Si-O-CH(C<u>H</u>$_3$)-CO), 0.89 (s, 9H, (C<u>H</u>$_3$)$_3$C-Si(CH$_3$)$_2$), 0.09 (s, 3H, (CH$_3$)$_3$C-Si(C<u>H</u>$_3$)$_2$), 0.07 ppm (s, 3H, (CH$_3$)$_3$C-Si(C<u>H</u>$_3$)$_2$); ^{13}C NMR (100 MHz, $CDCl_3$): δ = 174.87, 173.69, 170.11, 169.85, 169.77, 169.73, 169.72, 169.63, 69.13, 68.95, 68.87, 68.68, 68.13, 25.82, 21.33, 18.40, 16.87, 16.76, 16.70, −4.79, −5.18 ppm; MS (MALDI-TOF): *m/z* calcd for $C_{54}H_{80}O_{33}Si+Na^+$: 1307.42 $[M+Na]^+$; found 1307.46; *m/z* calcd for $C_{54}H_{80}O_{33}Si+K^+$: 1323.40 $[M+K^+]$; found 1323.43.

Synthesis of TBDMS-LLA$_{32}$-COOH (L-**24u**).

Starting from benzyl protected 32-mer L-**23u** (0.17 g, 0.07 mmol), pure deprotected 32-mer L-***24u*** was obtained as a colorless solid (0.16 g, quant.) using general method **E**. ^{1}H NMR (400 MHz, $CDCl_3$): δ = 5.16 (q, ^3J = 7 Hz, 31H, O-C<u>H</u>(CH$_3$)-CO), 4.39 (q, ^3J = 6.8 Hz, 1H, Si-O-C<u>H</u>(CH$_3$)-CO), 1.58 (d, ^3J = 7.1 Hz, 93H, O-CH(C<u>H</u>$_3$)-CO), 1.44 (d, ^3J = 6.8 Hz, 3H, Si-O-CH(C<u>H</u>$_3$)-CO), 0.9 (s, 9H, (C<u>H</u>$_3$)$_3$C-Si(CH$_3$)$_2$), 0.1 (s, 3H, (CH$_3$)$_3$C-Si(C<u>H</u>$_3$)$_2$), 0.08 ppm (s, 3H,

$(CH_3)_3C$-Si($C\underline{H}_3)_2$); ^{13}C NMR (100 MHz, $CDCl_3$): δ = 174.12, 173.86, 170.31, 170.05, 169.92, 169.82, 69.34, 69.15, 69.06, 68.87, 68.34, 26.03, 21.54, 18.60, 17.08, 16.97, 16.91, −4.58, −4.96 ppm; MS (MALDI-TOF): *m/z* calcd for $C_{102}H_{144}O_{65}Si+Na^+$: 2459.76 $[M+Na]^+$ found: 2459.82; *m/z* calcd for $C_{102}H_{144}O_{65}Si+K^+$: 2475.74 $[M+K]^+$; found: 2475.81.

Synthesis of TBDMS-DLA$_{32}$-COOH (D-**24u**).

Starting from benzyl protected 32-mer D-**23u** (0.29 g, 0.12 mmol), pure deprotected 32-mer D-***24u*** was obtained as a white solid (0.24 g, 86%) using general method **E**. ^1H NMR (400 MHz, $CDCl_3$): δ = 5.21–5.10 (m, 31H, O-C$\underline{H}$(CH_3)-CO), 4.39 (q, ^3J = 6.8 Hz, 1H, Si-O-C$\underline{H}$(CH_3)-CO), 1.61–1.50 (m, 93H, O-CH($C\underline{H}_3$)-CO), 1.43 (d, ^3J = 6.8 Hz, 3H, Si-O-CH($C\underline{H}_3$)-CO), 0.89 (s, 9H, ($C\underline{H}_3)_3$C-Si($CH_3)_2$), 0.10 (s, 3H, $(CH_3)_3$C-Si($C\underline{H}_3)_2$), 0.07 ppm (s, 3H, $(CH_3)_3$C-Si($C\underline{H}_3)_2$); ^{13}C NMR (100 MHz, $CDCl_3$): δ = 174.11, 173.67, 170.11, 169.85, 169.62, 69.14, 68.95, 68.81, 68.67, 68.13, 25.82, 21.34, 18.40, 16.87, 16.79, 16.71, −4.79, −5.17 ppm; MS (MALDI-TOF): *m/z* calcd for $C1_{02}H_{144}O_{65}Si+Na^+$: 2460.77 $[M+Na]^+$; found 2460.76.

Synthesis of benzyl (S)-2-(allyloxy)propanoate (L-**26**).

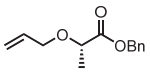

Benzyl-(*S*)-lactate L-**25** (4.882 g, 24.38 mmol) and allyl bromide (4.42 g, 36.6 mmol, 1.5 eq) were dissolved in dry Et_2O (30 mL) in a 250 mL 3-necked round-bottom flask under an argon atmosphere. Silver(I)oxide (5.65 g, 24.38 mmol, 1.0 eq) was added and the resulting black suspension was stirred vigorously under reflux overnight. Afterward, a sample taken from the reaction mixture was checked by ^1H NMR to confirm that the reaction was complete. The suspension was then transferred to a glass centrifuge tube and centrifuged at 1000 rpm for 1 min. The liquid was decanted from the Ag_2O residue and the Ag_2O was resuspended in fresh Et_2O (20 mL). The centrifugation procedure was repeated 4 times and the yellow colored diethyl ether layers were combined. The solvent was then removed in *vacuo*, giving the crude product as a light yellow liquid (5.656 g). The material by automated column chromatography using hept/EtOAc (gradient 95/5 to 85/15) as eluent, giving the pure title compound L-**26** as a colorless liquid (3.24 g, 60%). ^1H NMR (400 MHz, $CDCl_3$): δ = 7.38–7.29 (m, 5H, Ar-$\underline{H}$), 5.90 (ddt, ^3J = 17.2 Hz, ^3J = 10.4 Hz, ^3J = 5.8 Hz, 1H, CH_2=C$\underline{H}$-CH_2), 5.29–5.23 (m, 1H, C$\underline{H}_2$=CH-CH_2 (cis)), 5.21 (d, ^2J = 12.2 Hz, 1H, Ar-C$\underline{H}_2$-O), 5.20–5.16 (m, 1H, C$\underline{H}_2$=CH-CH_2 (trans)), 5.17 (d, ^3J = 12.3 Hz, 1H, Ar-C$\underline{H}_2$-O), 4.17–3.90 (m, 2H, CH_2=CH-C$\underline{H}_2$), 4.06 (q, ^3J = 6.8 Hz, 1H, O-C$\underline{H}$(CH_3)-CO), 1.43 ppm (d, ^3J = 6.9 Hz, 3H, O-CH($C\underline{H}_3$)-CO); ^{13}C NMR (100 MHz, $CDCl_3$): δ = 173.23, 135.79, 134.18, 128.71, 128.47, 128.33, 117.88, 74.12, 71.24, 66.62, 18.77 ppm.

*General hydrosilylation method **F** for the synthesis of Me-Si$_x$-LLA$_1$-Bn* (L-**27**).

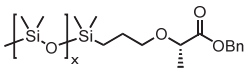

Silyl hydride **14** (*e.g.*, 0.692 mmol) and benzyl (*S*)-2-(allyloxy)propanoate L-**25** (0.657 mmol, 0.95 eq) was dissolved in dry toluene (10 mL) in a 25 mL 2-necked round-bottom flask under an argon atmosphere. To this was added one drop of Karstedt catalyst (soln. in xylene, 2% Pt). The mixture was then stirred at 60 °C for 3 h (the mixture turned from colorless to light yellow/brown in a few min). Afterward, the solvent was removed in *vacuo*. The light brown residue was purified by automated column chromatography to remove residual Karstedt catalyst.

Synthesis of Me-Si$_{15}$-LLA$_1$-Bn (L-**27c**).

Starting with silyl hydride 15-mer **14c** (1.513 g, 1.360 mmol) and benzyl (*S*)-2-allyloxy)propanoate L-**25** (0.285 g, 1.295 mmol, 0.95 eq), crude **Me-Si$_{15}$-LA$_1$-Bn** L-**27c** was obtained as light brown oil (1.915 g) using general method **F**. The material was purified by automated column chromatography using hept/EtOAc (gradient 100/0 to 80/20) as

eluent, giving the product as an almost colorless oil (1.676 g, 97%). Reisdual trace amounts of impurities were removed after the next step. ^{1}H NMR (400 MHz, $CDCl_3$): δ = 7.39–7.29 (m, 5H, Ar-H), 5.19 (ABq, $\Delta\delta_{AB}$ = 0.05, $^2J_{AB}$ = 12.3 Hz, 2H, CO-CH_2-Ar), 4.00 (q, ^3J = 6.8 Hz, 1H, O-CH(CH_3)-CO), 3.52 (dt, ^2J = 8.8 Hz, ^3J = 7.0 Hz, 1H, CH_2-CH_2-O), 3.32 (dt, ^2J = 8.8 Hz, ^3J = 7.1 Hz, 1H, CH_2-CH_2-O), 1.67–1.58 (m, 2H, CH_2-CH_2-O), 1.41 (d, ^3J = 6.8 Hz, 3H, O-CH(CH_3)-CO), 0.56–0.48 (m, 2H, Si(CH_3)$_2$-CH_2-CH_2), 0.10–0.03 ppm (m, 93H, Si(CH_3)); ^{13}C NMR (100 MHz, $CDCl_3$): δ = 173.49, 135.91, 128.72, 128.45, 128.33, 75.09, 73.29, 66.56, 23.69, 18.83, 14.24, 1.94, 1.32, 1.30, 1.22–1.21, 0.26, 0.23 ppm; MS (MALDI-TOF): *m/z* calcd for $C_{44}H_{110}O_{17}Si_{15}$+$Na^+$: 1353.42 $[M+Na]^+$; found 1353.47.

Synthesis of Me-Si$_{23}$-LLA$_1$-Bn (L-**27e**).

Starting with silyl hydride 23-mer **14e** (1.18 g, 0.692 mmol) and benzyl (*S*)-2-allyloxy)propanoate L-**25** (0.145 g, 0.657 mmol, 0.95 eq), crude **Me-Si$_{23}$-LA$_1$-Bn** L-**27e** was obtained as light brown oil (1.497 g) using general method **F**. The material was purified by automated column chromatography using hept/EtOAc (gradient 100/0 to 80/20) as eluent, giving the product as an almost colorless oil (0.843 g, 63%). Residual trace amounts of impurities were removed after the next step. ^{1}H NMR (400 MHz, $CDCl_3$): δ = 7.38–7.29 (m, 5H, Ar-H), 5.19 (ABq, $\Delta\delta_{AB}$ = 0.05, ^2J = 12.3 Hz, 2H, CO-CH2-Ar), 4.00 (q, ^3J = 6.9 Hz, 1H, O-CH(CH3)-CO), 3.52 (dt, ^2J = 8.8 Hz, ^3J = 7.0 Hz, 1H, CH2-CH2-O), 3.32 (dt, ^2J = 8.8 Hz, ^3J = 7.1 Hz, 1H, CH2-CH2-O), 1.67–1.58 (m, 2H, CH2-CH2-O), 1.41 (d, ^3J = 6.8 Hz, 3H, O-CH(CH3)-CO), 0.56–0.48 (m, 2H, Si(CH3)2-CH2-CH2), 0.16 to −0.02 ppm (m, 141H, Si(CH3)); ^{13}C NMR (100 MHz, $CDCl_3$): δ = 173.51, 135.89, 128.72, 128.46, 128.34, 75.09, 73.30, 66.57, 23.69, 18.84, 14.22, 1.94, 1.32, 1.30, 1.23–1.21, 0.26, 0.23 ppm; MS (MALDI-TOF): *m/z* calcd for $C_{60}H_{158}O_{25}Si_{23}$+$Na^+$: 1945.57 $[M+Na]^+$; found 1945.70.

Synthesis of Me-Si$_{27}$-LLA$_1$-Bn (L-**27f**).

Starting with silyl hydride 27-mer **14f** (0.655 g, 0.327 mmol) and benzyl (*S*)-2-allyloxy)propanoate L-**25** (0.068 g, 0.311 mmol, 0.95 eq), crude **Me-Si$_{27}$-LA$_1$-Bn** L-**27f** was obtained as light brown oil (1.915 g) using general method **F**. The material was purified by automated column chromatography using hept/EtOAc (gradient 100/0 to 80/20) as eluent, giving the product as an almost colorless oil (0.538 g, 74%). Residual trace amounts of impurities were removed after the next step. ^{1}H NMR (400 MHz, $CDCl_3$): δ = 7.38–7.30 (m, 5H, Ar-H), 5.19 (ABq, $\Delta\delta_{AB}$ = 0.05, ^2J = 12.3 Hz, 2H, CO-CH_2-Ar), 4.00 (q, ^3J = 6.9 Hz, 1H, O-CH(CH_3)-CO), 3.52 (dt, ^2J = 8.6 Hz, ^3J = 7.1 Hz, 1H, CH_2-CH_2-O), 3.32 (dt, ^2J = 8.8 Hz, ^3J = 7.2 Hz, 1H, CH_2-CH_2-O), 1.68–1.57 (m, 2H, CH_2-CH_2-O), 1.41 (d, ^3J = 6.8 Hz, 3H, O-CH(CH_3)-CO), 0.55–0.47 (m, 2H, Si(CH_3)$_2$-CH_2-CH_2), 0.15–0.02 ppm (m, 165H, Si(CH_3)); ^{13}C NMR (100 MHz, $CDCl_3$): δ = 173.52, 135.88, 128.73, 128.47, 128.35, 75.08, 73.31, 66.57, 23.69, 18.85, 14.21, 1.94, 1.31, 1.21, 0.26, 0.23 ppm; MS (MALDI-TOF): *m/z* calcd for $C_{68}H_{182}O_{29}Si_{27}$+$Na^+$: 2241.64 $[M+Na]^+$; found 2241.65.

Synthesis of Me-Si$_{59}$-LLA$_1$-Bn (L-**27l**).

Starting with silyl hydride 59-mer **14l** (0.374 g, 0.085 mmol) and benzyl (*S*)-2-allyloxy)propanoate L-**25** (20 mg, 0.090 mmol, 1.05 eq), crude **Me-Si$_{59}$-LA$_1$-Bn** L-**27l** was obtained as light brown oil using general method **F**. The material was purified by automated column chromatography using hept/EtOAc (gradient 100/0 to 80/20) as eluent, giving the product as an almost colorless oil (0.301 g, 79%). Residual amounts unfunctionalized siloxane were removed after the next step. ^{1}H NMR (400 MHz, $CDCl_3$): δ = 7.38–7.30 (m, 5H, Ar-H), 5.23–5.16 (m, 2H, CO-CH_2-Ar), 4.00 (q, ^3J = 6.9 Hz, 1H, O-CH(CH_3)-CO), 3.52 (dt, ^3J = 8.6 Hz, ^3J = 7.1 Hz, 1H, CH_2-CH_2-O), 3.32 (dt, ^3J = 8.8 Hz, ^3J = 7.2 Hz, 1H, CH_2-CH_2-O), 1.68–1.58 (m, 2H, CH_2-CH_2-O), 1.41 (d, ^3J = 6.8 Hz, 3H, O-CH(CH_3)-CO), 0.55–0.47 (m, 2H, Si(CH_3)$_2$-CH_2-CH_2), 0.21–0.01 ppm (m, 357H, Si(CH_3)); MS (MALDI-TOF): *m/z* calcd for $C_{132}H_{374}O_{61}Si_{59}$+$Na^+$: 4610.25 $[M+Na]^+$; found 4613.26 (4th isotope peak).

General method ***G*** *for the synthesis of Me-Si$_x$-LLA$_1$-COOH* (L-**28**).

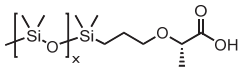

Benzyl ester L-**27** (*e.g.*, 0.396 mmol) was dissolved in ethyl acetate (4 mL, ~0.1 M) in a 50 mL round-bottom flask and Pd/C (10 w% Pd, 0.05 eq of Pd) was added. The mixture was then stirred under a hydrogen atmosphere at room temperature. After 2 h, TLC analysis (hept/EtOAc 80:20; CeMo stain; $R_{f,prod}$ = 0.01–0.30 (tailing)) confirmed that all of the benzyl ester was converted. The black suspension was filtered through a 2 cm thick layer of celite and the filter cake washed with EtOAc (10 mL in small portions). The combined filtrates were concentrated *in vacuo*, giving the crude product L-**28** as a colorless oil. Pure material was obtained after purification by automated column chromatography (see below for details).

Synthesis of Me-Si$_{15}$-LLA$_1$-COOH (L-**28c**).

Starting from benzyl protected **Me-Si$_{15}$-LA$_1$-Bn** L-**27c** (1.576 g, 1.183 mmol), crude deprotected product L-**28c** was obtained as a colorless oil (1.338 g) using general method **G**. The material was purified by automated column chromatography using heptane as eluent, giving the product in pure form as a colorless oil (0.614 g, 42%). ^{1}H NMR (400 MHz, $CDCl_3$): δ = 3.99 (q, ^3J = 6.9 Hz, 1H, O-C<u>H</u>(CH_3)-CO), 3.54 (dt, ^2J = 8.9 Hz, ^3J = 6.9 Hz, 1H, CH_2-C<u>H</u>$_2$-O), 3.44 (dt, ^2J = 8.9 Hz, ^3J = 7.0 Hz, 1H, CH_2-C<u>H</u>$_2$-O), 1.70–1.60 (m, 2H, C<u>H</u>$_2$-CH_2-O), 1.45 (d, ^3J = 6.9 Hz, 3H, O-CH(C<u>H</u>$_3$)-CO), 0.58–0.51 (m, 2H, Si(CH_3)$_2$-C<u>H</u>$_2$-CH_2), 0.17 to −0.03 ppm (m, 93H, Si(C<u>H</u>$_3$)); ^{13}C NMR (100 MHz, $CDCl_3$): δ = 177.18, 74.69, 73.35, 23.69, 18.28, 14.28, 1.94, 1.32, 1.30, 1.21, 0.84, 0.26, 0.25 ppm; MS (MALDI-TOF): *m/z* calcd for $C_{37}H_{104}O_{17}Si_{15}$+$Na^+$: 1263.37 $[M+Na]^+$; found 1263.40; *m/z* calcd for $C_{37}H_{104}O_{17}Si_{15}$+$K^+$: 1279.34 $[M+K]^+$; found 1279.37.

Synthesis of Me-Si$_{23}$-LLA$_1$-COOH (L-**28e**).

Starting from benzyl protected **Me-Si$_{23}$-LA$_1$-Bn** L-**27e** (0.618 g, 0.321 mmol), crude deprotected product L-**28e** was obtained as a colorless oil (0.550 g) using general method **G**. The material was purified by automated column chromatography using hept/EtOAc (gradient 100/0 to 90/10) as eluent, giving the product in pure form as a colorless oil (0.503 g, 85%). ^{1}H NMR (400 MHz, $CDCl_3$): δ = 3.99 (q, ^3J = 6.9 Hz, 1H, O-C<u>H</u>(CH_3)-CO), 3.55 (dt, ^2J = 8.9 Hz, ^3J = 6.9 Hz, 1H, CH_2-C<u>H</u>$_2$-O), 3.43 (dt, ^2J = 8.9 Hz, ^3J = 7.0 Hz, 1H, CH_2-C<u>H</u>$_2$-O), 1.70–1.61 (m, 2H, C<u>H</u>$_2$-CH_2-O), 1.45 (d, ^3J = 6.9 Hz, 3H, O-CH(C<u>H</u>$_3$)-CO), 0.59–0.50 (m, 2H, Si(CH_3)$_2$-C<u>H</u>$_2$-CH_2), 0.18 to −0.02 ppm (m, 141H, Si(C<u>H</u>$_3$)); ^{13}C NMR (100 MHz, $CDCl_3$): δ = 178.10, 74.72, 73.40, 23.72, 18.45, 14.26, 1.95, 1.33, 1.31, 1.24–1.22, 0.28, 0.27 ppm; MS (MALDI-TOF): *m/z* calcd for $C_{53}H_{152}O_{25}Si_{23}$+$Na^+$: 1855.52 $[M+Na]^+$; found 1855.54; *m/z* calcd for $C_{53}H_{152}O_{25}Si_{23}$+$K^+$: 1871.50 $[M+K]^+$; found 1871.71.

Synthesis of Me-Si$_{27}$-LLA$_1$-COOH (L-**28f**).

Starting from benzyl protected **Me-Si$_{27}$-LA$_1$-Bn** L-**27f** (0.583 g, 0.262 mmol), crude deprotected product L-**28f**was obtained as a colorless oil (0.576 g) using general method **G**. The material was purified by automated column chromatography using hept/EtOAc (gradient 100/0 to 90/10) as eluent, giving the product in pure form as a colorless oil (0.287 g, 51%). ^{1}H NMR (400 MHz, $CDCl_3$): δ = 3.99 (q, ^3J = 6.9 Hz, 1H, O-C<u>H</u>(CH_3)-CO), 3.54 (dt, ^2J = 8.8 Hz, ^3J = 6.9 Hz, 1H, CH_2-C<u>H</u>$_2$-O), 3.45 (dt, ^2J = 8.9 Hz, ^3J = 6.9 Hz, 1H, CH_2-C<u>H</u>$_2$-O), 1.71–1.60 (m, 2H, C<u>H</u>$_2$-CH_2-O), 1.45 (d, ^3J = 6.9 Hz, 3H, O-CH(C<u>H</u>$_3$)-CO), 0.59–0.51 (m, 2H, Si(CH_3)$_2$-C<u>H</u>$_2$-CH_2), 0.37 to −0.17 ppm (m, 165H, Si(C<u>H</u>$_3$)); ^{13}C NMR (100 MHz, $CDCl_3$): δ = 177.06, 74.76, 73.35, 23.73, 18.30, 14.29, 1.95, 1.33, 1.30, 1.21, 0.28 ppm; MS (MALDI-TOF): *m/z* calcd for $C_{61}H_{176}O_{29}Si_{27}$+$Na^+$: 2151.60 $[M+Na]^+$; found 2151.61; *m/z* calcd for $C_{61}H_{176}O_{29}Si_{27}$+$K^+$: 2167.57 $[M+K]^+$; found 2167.60.

Synthesis of Me-Si$_{59}$-LLA$_1$-COOH (L-**28l**).

Starting from benzyl protected **Me-Si$_{59}$-LA$_1$-Bn** L-**27l** (0.309 g, 0.067 mmol), crude deprotected product L-**28l** was obtained as a colorless oil using general method **G** (a prolonged reaction time of 20 h was used to reach full conversion). The material was purified by automated column chromatography using hept/EtOAc (gradient 100/0 to 75/25) as eluent, giving the product in pure form as a colorless oil (18 mg, 6%). A substantial amount of **Me-Si$_{59}$-OH** and **Me-Si$_{118}$-Me** (as a mixture) was also isolated. ^{1}H NMR (400 MHz, $CDCl_3$): δ = 3.99 (q, ^3J = 6.9 Hz, 1H, O-C<u>H</u>(CH_3)-CO), 3.54–3.46 (m, ^3J = 6.9 Hz, 2H, CH_2-C<u>H</u>$_2$-O), 1.71–1.58 (m, 2H, C<u>H</u>$_2$-CH_2-O), 1.45 (d, ^3J = 6.9 Hz, 3H, O-CH(C<u>H</u>$_3$)-CO), 0.58–0.50 (m, 2H, Si(CH_3)$_2$-C<u>H</u>$_2$-CH_2), 0.17–0.03 ppm (m, 357H, Si(C<u>H</u>$_3$)); MS (MALDI-TOF): *m/z* calcd for $C_{125}H_{368}O_{61}Si_{59}$+$Na^+$: 4520.20 [M+Na]$^+$; found 4521.30 (2nd isotope peak).

Synthesis of Me-Si$_{15}$-DLA$_1$-COOH (D-**28c**).

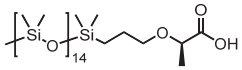

Methyl ester D-**32c** (0.68 g, 0.542 mmol, 1.0 eq) was dissolved in dry dichloroethane (5 mL) in a 25 mL round-bottom flask equipped with cooler under argon atmosphere. To this, trimethyltin hydroxide (0.49 mg, 2.71 mmol, 5 eq) was added and the mixture was stirred for 3 days at 70 °C. The material was diluted with DCM (15 mL) and washed with a mixture of citric acid (6 mL, 0.5 M) and water (15 mL). The organic layer was separated and the aqueous layer was extracted with DCM (2 × 10 mL). The combined organic layers were washed with brine (10 mL), dried with $MgSO_4$ and the solvent was removed in *vacuo*, giving the crude product as a colorless oil. Further purification by automated column chromatography using hept/EtOAc (gradient 95/5 to 60/40) as eluent yielded the pure product D-**28c** (0.50 g, 74%). ^{1}H NMR (400 MHz, $CDCl_3$): δ = 3.99 (q, ^3J = 6.9 Hz, 1H, CH_2-O-C<u>H</u>(CH_3)-CO), 3.54 (dt, ^2J = 8.9 Hz, ^3J = 7.0 Hz, 1H, CH_2-C<u>H</u>$_2$-O), 3.42 (dt, ^2J = 8.9 Hz, ^3J = 7.0 Hz, 1H, CH_2-C<u>H</u>$_2$-O), 1.72–1.58 (m, 2H, Si(CH_3)$_2$-CH_2-C<u>H</u>$_2$-CH_2-O), 1.45 (d, ^3J = 6.9 Hz, 3H, O-CH(C<u>H</u>$_3$)-CO), 0.62–0.47 (m, 2H, Si(CH_3)$_2$-C<u>H</u>$_2$-CH_2-CH_2-O), 0.10–0.04 ppm (m, 93H, Si(C<u>H</u>$_3$)$_2$); ^{13}C NMR (100 MHz, $CDCl_3$): δ = 177.74, 74.90, 73.55, 73.36, 23.89, 18.58, 14.44, 14.14, 3.20, 2.43, 2.30, 2.14, 1.88, 1.86, 1.84, 1.77, 1.58, 1.51, 1.49, 1.40, 1.34, 1.30, 1.24, 1.14, 1.12, 1.03, 0.75, 0.66, 0.61, 0.46 ppm; MS (MALDI-TOF): *m/z* calcd for $C_{37}H_{104}O_{17}Si_{15}$+$Na^+$: 1263.37 [M+Na]$^+$; found 1263.38; *m/z* calcd for $C_{37}H_{104}O_{17}Si_{15}$+$K^+$: 1279.34 [M+K]$^+$; found 1279.30.

Synthesis of Me-Si$_{23}$-DLA$_1$-COOH (D-**28e**).

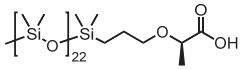

Methyl ester D-**32e** (1.04 g, 0.564 mmol, 1.0 eq) was dissolved in dry dichloroethane (6 mL) in a 25 mL round-bottom flask equipped with cooler under argon atmosphere. To this, trimethyltin hydroxide (0.51 mg, 2.82 mmol, 5 eq) was added and the mixture was stirred for 3 days at 70 °C. The material was diluted with DCM (15 mL) and washed with a mixture of citric acid (6 mL, 0.5 M) and water (15 mL). The organic layer was separated and the aqueous layer was extracted with DCM (2 × 10 mL). The combined organic layers were washed with brine (10 mL), dried with $MgSO_4$ and the solvent was removed in *vacuo*, giving the crude product as a colorless oil. Further purification by automated column chromatography using hept/EtOAc (gradient 95/5 to 60/40) as eluent yielded the pure product D-**28e** (0.50 g, 48%). ^{1}H NMR (400 MHz, $CDCl_3$): δ = 3.94 (q, ^3J = 6.8 Hz, 1H, CH_2-O-C<u>H</u>(CH_3)-CO), 3.54 (dt, ^2J = 8.9 Hz, ^3J = 7.0 Hz, 1H, CH_2-C<u>H</u>$_2$-O), 3.31 (dt, ^2J = 8.9 Hz, ^3J = 7.0 Hz, 1H, CH_2-C<u>H</u>$_2$-O), 1.71–1.57 (m, 2H, Si(CH_3)$_2$-CH_2-C<u>H</u>$_2$-CH_2-O), 1.39 (d, ^3J = 6.8 Hz, 3H, O-CH(C<u>H</u>$_3$)-CO), 0.49–0.39 (m, 2H, Si(CH_3)$_2$-C<u>H</u>$_2$-CH_2-CH_2-O), 0.16 to −0.04 ppm (m, 141H, Si(C<u>H</u>$_3$)$_2$); MS (MALDI-TOF): *m/z* calcd for $C_{53}H_{152}O_{25}Si_{23}$+$Na^+$: 1855.52 [M+Na]$^+$; found 1855.63; *m/z* calcd for $C_{53}H_{152}O_{25}Si_{23}$+$K^+$: 1871.50 [M+K]$^+$; found 1871.62.

*General oDMS–oLA coupling method **H** giving Me-Si$_x$-LA$_y$-Bn* [**Si$_x$-LA$_y$**], *Me-Si$_x$-LLA$_y$-Bn* [**Si$_x$-LLA$_y$**], or *Me-Si$_x$-DLA$_y$-Bn* [**Si$_x$-DLA$_y$**].

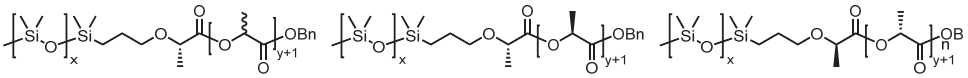

*o*DMS acid **28** (*e.g.*, 0.096 mmol, 1.0 eq) was dissolved in dry DCM (1 mL, ~0.1 M) in a 10 mL schlenk tube under an argon atmosphere. The solution was cooled to 0 °C in ice water and DPTS (0.048 mmol, 0.5 eq) and EDC·HCl (0.193 mmol, 2.0 eq) was added. The mixture stirred for 10 min at 0 °C, followed by the addition of a solution of benzyl protected oLA **22** (0.096 mmol, 1.0 eq) in DCM (0.5 mL). The mixture was then stirred overnight at room temperature (depending on the concentration, sometimes the formation of a suspension of droplets of co-oligomer in DCM was observed). The reaction mixture was diluted with DCM (15 mL) to bring all material in solution, and the mixture was washed with a 50/50 mixture of water and brine (10 mL in total). The org layer was dried with $MgSO_4$ and concentrated in *vacuo*, giving the crude product [**Si$_x$-LA$_y$**], [**Si$_x$-LLA$_y$**] or [**Si$_x$-DLA$_y$**] as a viscous, colorless oil. The material was purified by automated column chromatography, resulting in pure, monodisperse block co-oligomers as a colorless, thick oil or waxy solid.

Synthesis of Me-Si$_{15}$-LA$_9$-Bn [**Si$_{15}$-LA$_9$**].

Starting from oDMS acid **Me-Si$_{15}$-LLA$_1$-COOH** L-**28c** (120 mg, 0.096 mmol, 1 eq), *o*LA **HO-LA$_8$-Bn** *at*-**22o** (66 mg, 0.096 mmol, 1 eq), DPTS (14 mg, 0.048 mmol, 0.5 eq) and EDC·HCl (37 mg, 0.193 mmol, 2 eq), crude co-oligomer [**Si$_{15}$-LA$_9$**] was obtained as a colorless oil (157 mg) using general method **H**. The material was purified by automated column chromatography using hept/EtOAc (gradient 90/10 to 55/45) as eluent, giving the product in pure form as a colorless, thick oil (103 mg, 56%). ^{1}H NMR (400 MHz, $CDCl_3$): δ = 7.40–7.29 (m, 5H, Ar-H), 5.26–5.10 (m, 10H, O-CH(CH$_3$)-CO and O-CH$_2$-Ar), 4.07–3.99 (m, 1H, CH$_2$-O-CH(CH$_3$)-CO), 3.62–3.50 (m, 1H, CH$_2$-O-CH(CH$_3$)-CO), 3.36–3.28 (m, 1H, CH$_2$-O-CH(CH$_3$)-CO), 1.67–1.40 (m, 29H, Si(CH$_3$)$_2$-CH$_2$-CH$_2$-CH$_2$-O and O-CH(CH$_3$)-CO), 0.57–0.50 (m, 2H, Si(CH$_3$)$_2$-CH$_2$-CH$_2$-CH$_2$-O), 0.13–0.01 ppm (m, 93H, Si(CH$_3$)); ^{13}C NMR (100 MHz, $CDCl_3$): δ = 173.19, 173.14, 173.09, 170.09–170.02, 169.91, 169.88, 169.78–169.68, 169.61–169.41, 169.30, 169.27, 135.20, 135.18, 128.75, 128.66, 128.64, 128.38, 128.37, 74.78, 74.66, 73.29, 73.25, 69.41, 69.30, 69.25, 69.20–69.00, 68.58, 68.54, 68.50, 67.35, 67.33, 23.65, 18.82–18.79, 16.92, 16.90–16.70, 14.21, 1.92, 1.30, 1.28, 1.21–1.19, 0.23, 0.20 ppm; MS (MALDI-TOF): *m/z* calcd for $C_{68}H_{142}O_{33}Si_{15}+Na^+$: 1929.59 $[M+Na]^+$; found 1930.58.

Synthesis of Me-Si$_{15}$-LA$_{17}$-Bn [**Si$_{15}$-LA$_{17}$**].

Starting from oDMS acid **Me-Si$_{15}$-LLA$_1$-COOH** L-**28c** (80 mg, 0.064 mmol, 1 eq), oLA **HO-LA$_{16}$.Bn** *at*-**22sn** (81 mg, 0.064 mmol, 1 eq), DPTS (9.5 mg, 0.032 mmol, 0.5 eq) and EDC·HCl (24.7 mg, 0.129 mmol, 2 eq), crude co-oligomer [**Si$_{15}$-LA$_{17}$**] was obtained as a colorless oil (147 mg) using general method **H**. The material was purified by automated column chromatography using hept/EtOAc (gradient 80/20 to 60/40) as eluent, giving the product in pure form as a colorless, waxy substance (115 mg, 72%). ^{1}H NMR (400 MHz, $CDCl_3$): δ = 7.38–7.28 (m, 5H, Ar-H), 5.25–5.09 (m, 18H, O-CH(CH$_3$)-CO and O-CH$_2$-Ar), 4.06–3.97 (m, 1H, CH$_2$-O-CH(CH$_3$)-CO), 3.62–3.48 (m, 1H, CH$_2$-O-CH(CH$_3$)-CO), 3.36–3.27 (m, 1H, CH$_2$-O-CH(CH$_3$)-CO), 1.67–1.39 (m, 53H, Si(CH$_3$)$_2$-CH$_2$-CH$_2$-CH$_2$-O and O-CH(CH$_3$)-CO), 0.57–0.48 (m, 2H, Si(CH$_3$)$_2$-CH$_2$-CH$_2$-CH$_2$-O), 0.14–0.00 ppm (m, 93H, Si(CH$_3$)); ^{13}C NMR (100 MHz, $CDCl_3$): δ = 173.16, 173.10, 173.06, 170.06–169.99, 169.89, 169.85, 169.77–169.63, 169.53–169.39, 169.28, 169.24, 135.20, 135.17, 128.73, 128.64, 128.62, 128.36, 128.34, 74.76, 74.63, 73.26, 73.22, 69.39, 69.29, 69.23, 69.18–69.07, 68.56, 68.52, 68.48, 67.32, 67.30, 23.63, 18.79–18.76, 16.90–16.68, 14.19, 1.90, 1.27, 1.26, 1.18–1.17, 0.21, 0.18 ppm; MS (MALDI-TOF): *m/z* calcd for $C_{92}H_{174}O_{49}Si_{15}+Na^+$: 2505.76 $[M+Na]^+$; found 2505.77; *m/z* calcd for $C_{92}H_{174}O_{49}Si_{15}+K^+$: 2521.73 $[M+K]^+$; found 2521.71.

Synthesis of Me-Si$_{15}$-LLA$_{17}$-Bn [**Si$_{15}$-LLA$_{17}$**]

Starting from *o*DMS acid **Me-Si$_{15}$-LLA$_1$-COOH** L-**28c** (160 mg, 0.13 mmol, 1 eq), **HO-LLA$_{16}$-Bn** L-**22s** (163 mg, 0.13 mmol, 1 eq), DPTS (19 mg, 0.07 mmol, 0.5 eq) and EDC·HCl (50 mg, 0.26 mmol, 2 eq), crude oligomer [**Si$_{15}$-LLA$_{17}$**] was obtained as a colorless oil (252 mg) using general method **H**. The material was purified by automated column chromatography using hept/EtOAc (gradient 80/20 to 60/40) as eluent, giving the product in pure form as a white solid (216 mg, 80%). ^{1}H NMR (400 MHz, $CDCl_3$): δ = 7.44–7.27 (m, 5H, Ar-H), 5.25–5.07 (m, 18H, CO-O-CH(CH$_3$)-CO and O-CH$_2$-Ar), 4.02 (q, ^3J = 6.9 Hz, 1H, CH$_2$-O-CH(CH$_3$)-CO), 3.58 (dt, ^2J = 8.8 Hz, ^3J = 7.0 Hz, 1H, CH$_2$-CH$_2$-O), 3.32 (dt, ^2J = 8.8 Hz, ^3J = 7.0 Hz, 1H, CH$_2$-CH$_2$-O), 1.65–1.6 (m, 2H, Si(CH$_3$)$_2$-CH$_2$-CH$_2$-CH$_2$-O), 1.58 (m, 42H, CO-O-CH(CH$_3$)-CO), 1.51 (m, 6H, CO-O-CH(CH$_3$)-CO), 1.45 (d, ^3J = 6.9 Hz, 3H, CH$_2$-O-CH(CH$_3$)-CO), 0.59–0.49 (m, 2H, Si(CH$_3$)$_2$-CH$_2$-CH$_2$-CH$_2$-O), 0.11–0.01 ppm (m, 93H, Si(CH$_3$)$_2$); ^{13}C NMR (100 MHz, $CDCl_3$): δ = 173.39, 170.28, 170.23, 170.04, 169.98, 169.95, 169.94, 169.92, 169.87, 135.38, 128.96, 128.87, 128.58, 74.86, 73.46, 69.61, 69.34, 69.30, 69.20, 68.73, 67.56, 23.85, 19.02, 17.09, 17.02, 16.98, 16.91, 14.41, 2.13, 1.76, 1.50, 1.49, 1.39, 1.02, 0.43, 0.40, 0.34 ppm; MS (MALDI-TOF): *m/z* calcd for $C_{92}H_{174}O_{49}Si_{15}+Na^+$: 2505.76 $[M+Na]^+$; found 2505.75; *m/z* calcd for $C_{92}H_{174}O_{49}Si_{15}+K^+$: 2521.73 $[M+K]^+$; found 2521.70.

Synthesis of Me-Si$_{15}$-DLA$_{17}$-Bn [**Si$_{15}$-DLA$_{17}$**].

*o*DMS acid **Me-Si$_{15}$-DLA$_1$-COOH** D-**28c** (80 mg, 0.06 mmol, 1 eq) was dissolved in dry DCM (0.5 mL) in a 10 mL schlenk tube under argon. The solution was cooled to 0 °C in ice water and DIPEA (20.8 mg, 0.16 mmol, 2.5 eq) and PyBop (benzotriazol-1-yl-oxytripyrrolidinophosphonium hexafluorophosphate, 50 mg, 0.1 mmol, 1.5 eq) were added. The mixture was stirred for 10 minutes, followed by the addition of **HO-DLA$_{16}$-Bn** D-**22s** (85 mg, 0.07 mmol, 1.05 eq). The mixture was then stirred overnight at room temperature. After full conversion, the mixture was diluted with DCM (10 mL) and washed with a 50/50 mixture of water and brine (total 10 mL). The organic layer was dried with $MgSO_4$ and concentrated in *vacuo* giving the crude product [**Si$_{15}$-DLA$_{17}$**] (222 mg) as a white solid. The material was purified by automated column chromatography, resulting in pure, monodisperse product (26 mg, 16 %). ^{1}H NMR (400 MHz, $CDCl_3$): δ = 7.41–7.29 (m, 5H, Ar-H), 5.26–5.09 (m, 18H, CO-O-CH(CH$_3$)-CO and O-CH$_2$-Ar), 4.02 (q, ^3J = 6.8 Hz, 1H, CH$_2$-O-CH(CH$_3$)-CO), 3.58 (dt, ^2J = 8.8 Hz, ^3J = 7.0 Hz, 1H, CH$_2$-CH$_2$-O), 3.32 (dt, ^2J = 8.8 Hz, ^3J = 7.0 Hz, 1H, CH$_2$-CH$_2$-O), 1.67–1.61 (m, 2H, Si(CH$_3$)$_2$-CH$_2$-CH$_2$-CH$_2$-O), 1.58 (m, 42H, CO-O-CH(CH$_3$)-CO), 1.52 (m, 6H, CO-O-CH(CH$_3$)-CO), 1.45 (d, ^3J = 6.8 Hz, 3H, CH$_2$-O-CH(CH$_3$)-CO), 0.59–0.48 (m, 2H, Si(CH$_3$)$_2$-CH$_2$-CH$_2$-CH$_2$-O), 0.15–0.01 ppm (m, 93H, Si(CH$_3$)$_2$); ^{13}C NMR (100 MHz, $CDCl_3$) δ = 173.39, 170.28, 170.24, 170.04, 169.98, 169.94, 169.92, 169.87, 135.41, 128.97, 128.88, 128.59, 74.88, 73.46, 69.63, 69.35, 69.31, 69.21, 68.75, 67.57, 23.87, 19.02, 17.11, 17.03, 16.99, 16.92, 14.43, 2.13, 1.77, 1.51, 1.49, 1.40, 1.03, 0.45, 0.42, 0.35 ppm; MS (MALDI-TOF): *m/z* calcd for $C_{92}H_{174}O_{49}Si_{15}+Na^+$: 2505.76 $[M+Na]^+$; found 2505.76; *m/z* calcd for $C_{92}H_{174}O_{49}Si_{15}+K^+$: 2521.73 $[M+K]^+$; found 2521.80.

Synthesis of Me-Si$_{23}$-LA$_9$-Bn [**Si$_{23}$-LA$_9$**].

Starting from oDMS acid **Me-Si$_{23}$-LLA$_1$-COOH** L-**28e** (110 mg, 0.060 mmol, 1 eq), oLA **HO-LA$_8$-Bn** *at*-**22o** (41 mg, 0.060 mmol, 1 eq), DPTS (8.8 mg, 0.030 mmol, 0.5 eq) and EDC·HCl (23.0 mg, 0.120 mmol, 2 eq), crude co-oligomer [**Si$_{23}$-LA$_9$**] was obtained as a colorless oil (138 mg) using general method **H**. The material was purified by automated column chromatography using hept/EtOAc (gradient 88/12 to 50/50) as eluent, giving the product in pure form as a colorless, waxy substance (108 mg, 72%). ^{1}H NMR (400 MHz, $CDCl_3$): δ = 7.40–7.29 (m, 5H, Ar-H), 5.26–5.10 (m, 10H, O-CH(CH$_3$)-CO and O-CH$_2$-Ar), 4.08–3.98 (m, 1H, CH$_2$-O-CH(CH$_3$)-CO), 3.63–3.50 (m, 1H, CH$_2$-O-CH(CH$_3$)-CO), 3.37–3.28 (m, 1H, CH$_2$-O-CH(CH$_3$)-CO), 1.67–1.40 (m, 29H, Si(CH$_3$)$_2$-CH$_2$-CH$_2$-CH$_2$-O and O-CH(CH$_3$)-CO), 0.57–0.50 (m, 2H, Si(CH$_3$)$_2$-CH$_2$-CH$_2$-CH$_2$-O), 0.15–0.01 ppm (m, 141H, Si(CH$_3$)); ^{13}C NMR (100 MHz, $CDCl_3$): δ = 173.19, 173.13, 173.09, 170.11–170.03, 169.91, 169.89, 169.76–169.68, 169.56–169.42, 169.31, 169.28, 135.25, 135.22, 128.76, 128.67, 128.65, 128.39, 128.38, 74.81, 74.68, 73.29, 73.26, 69.43, 69.32, 69.26, 69.22–

69.11, 68.60, 68.55, 68.52, 67.36, 67.34, 23.67, 18.81–18.78, 16.93–16.72, 14.24, 1.92, 1.30, 1.28, 1.21–1.19, 0.24, 0.22 ppm; MS (MALDI-TOF): *m/z* calcd for $C_{84}H_{190}O_{41}Si_{23}+Na^+$: 2521.74 [M+Na]$^+$; found 2521.81.

Synthesis of Me-Si$_{23}$-LLA$_9$-Bn [**Si$_{23}$-LLA$_9$**].

Starting from *o*DMS acid **Me-Si$_{23}$-LLA$_1$-COOH** L-**28e** (129 mg, 0.07 mmol, 1 eq), **HO-LLA$_8$-Bn** L-**22o** (48 mg, 0.07 mmol, 1 eq), DPTS (10 mg, 0.04 mmol, 0.5 eq) and EDC·HCl (27 mg, 0.14 mmol, 2 eq), crude oligomer [**Si$_{23}$-LLA$_9$**] was obtained as white solid (145 mg) using general method **H**. The material was purified by automated column chromatography using hept/EtOAc (gradient 90/10 to 65/35) as eluent, giving the product in pure form as a white solid (130 mg, 74 %). ^{1}H NMR (400 MHz, $CDCl_3$): δ = 7.43–7.28 (m, 5H, Ar-H), 5.42–5.05 (m, 10H, CO-O-CH(CH$_3$)-CO and O-CH$_2$-Ar), 4.02 (q, ^3J = 6.9 Hz, 1H, CH$_2$-O-CH(CH$_3$)-CO), 3.59 (dt, ^2J = 8.7 Hz, ^3J = 7.0 Hz, 1H, CH$_2$-CH$_2$-O), 3.32 (dt, ^2J = 8.8 Hz, ^3J = 7.0 Hz, 1H, CH$_2$-CH$_2$-O), 1.69–1.61 (m, 2H, Si(CH$_3$)$_2$-CH$_2$-CH$_2$-CH$_2$-O), 1.58 (m, 18H, CO-O-CH(CH$_3$)-CO), 1.52 (m, 6H, CO-O-CH(CH$_3$)-CO), 1.45 (d, ^3J = 6.9 Hz, 3H, CH$_2$-O-CH(CH$_3$)-CO), 0.61–0.43 (m, 2H, Si(CH$_3$)$_2$-CH$_2$-CH$_2$-CH$_2$-O), 0.10–0.01 ppm (m, 138H, Si(CH$_3$)$_2$); ^{13}C NMR (100 MHz, $CDCl_3$): δ = 173.41, 170.29, 170.25, 170.06, 170.00, 169.96, 169.94, 169.88, 135.40, 128.97, 128.88, 128.60, 74.88, 73.47, 69.63, 69.36, 69.32, 69.21, 68.75, 67.57, 23.87, 19.03, 17.11, 17.03, 17.00, 16.92, 14.42, 2.14, 1.77, 1.51, 1.49, 1.42, 1.40, 1.03, 0.45, 0.42, 0.35 ppm; MS (MALDI-TOF): *m/z* calcd for $C_{84}H_{190}O_{41}Si_{23}+Na^+$: 2521.74 [M+Na]$^+$; found 2521.83; *m/z* calcd for $C_{84}H_{190}O_{41}Si_{23}+K^+$: 2537.71 [M+K]$^+$; found 2537.78.

Synthesis of Me-Si$_{23}$-DLA$_9$-Bn [**Si$_{23}$-DLA$_9$**].

Starting from *o*DMS acid **Me-Si$_{23}$-DLA$_1$-COOH** D-**28e** (100 mg, 0.05 mmol, 1 eq), **HO-DLA$_8$-Bn** D-**22o** (37 mg, 0.05 mmol, 1 eq), DPTS (8.1 mg, 0.03 mmol, 0.5 eq) and EDC·HCl (21 mg, 0.11 mmol, 2 eq), crude oligomer [**Si$_{23}$-DLA$_9$**] was obtained as white solid (141 mg) using general method **H**. The material was purified by automated column chromatography using hept/EtOAc (gradient 95/5 to 65/35) as eluent, giving the product in pure form as a white solid (114 mg, 84 %). ^{1}H NMR (400 MHz, $CDCl_3$): δ = 7.43–7.28 (m, 5H, Ar-H), 5.26–5.08 (m, 10H, CO-O-CH(CH$_3$)-CO and O-CH$_2$-Ar), 4.02 (q, ^3J = 6.8 Hz, 1H, CH$_2$-O-CH(CH$_3$)-CO), 3.59 (dt, ^2J = 8.6 Hz, ^3J = 7.0 Hz, 1H, CH$_2$-CH$_2$-O), 3.32 (dt, ^2J = 8.6 Hz, ^3J = 7.0 Hz, 1H, CH$_2$-CH$_2$-O), 1.70–1.61 (m, 2H, Si(CH$_3$)$_2$-CH$_2$-CH$_2$-CH$_2$-O), 1.58 (m, 18H, CO-O-CH(CH3)-CO), 1.52 (m, 6H, CO-O-CH(CH$_3$)-CO), 1.45 (d, ^3J = 6.8 Hz, 3H, CH$_2$-O-CH(CH$_3$)-CO), 0.61–0.44 (m, 2H, Si(CH$_3$)$_2$-CH$_2$-CH$_2$-CH$_2$-O), 0.17 to −0.06 ppm (m, 141H, Si(CH$_3$)$_2$); ^{13}C NMR (100 MHz, $CDCl_3$) δ = 173.40, 170.29, 170.24, 170.05, 169.99, 169.95, 169.93, 169.88, 135.42, 128.97, 128.88, 128.60, 74.89, 73.47, 69.63, 69.36, 69.32, 69.22, 68.75, 67.57, 23.88, 19.02, 17.11, 17.03, 16.99, 16.92, 14.44, 2.13, 1.76, 1.51, 1.49, 1.40, 1.02, 0.45, 0.42, 0.35 ppm; MS (MALDI-TOF): *m/z* calcd for $C_{84}H_{190}O_{41}Si_{23}+Na^+$: 2521.74 [M+Na]$^+$; found 2521.74; *m/z* calcd for $C_{84}H_{190}O_{41}Si_{23}+K^+$: 2537.71 [M+K]$^+$; found 2537.73.

Synthesis of Me-Si$_{23}$-LA$_{11}$-Bn [**Si$_{23}$-LA$_{11}$**].

Starting from oDMS acid **Me-Si$_{23}$-LLA$_1$-COOH** L-**28e** (112 mg, 0.061 mmol, 1 eq), oLA **HO-LA$_{10}$-Bn** *at*-**22p** (50.7 mg, 0.061 mmol, 1 eq), DPTS (9.0 mg, 0.031 mmol, 0.5 eq) and EDC·HCl (23.5 mg, 0.122 mmol, 2 eq), crude co-oligomer [**Si$_{23}$-LA$_{11}$**] was obtained as a colorless oil (168 mg) using general method **H**. The material was purified by automated column chromatography using hept/EtOAc (gradient 88/12 to 50/50) as eluent, giving the product in pure form as a colorless, waxy substance (108 mg, 67%). ^{1}H NMR (400 MHz, $CDCl_3$): δ = 7.40–7.29 (m, 5H, Ar-H), 5.27–5.09 (m, 12H, O-CH(CH$_3$)-CO and O-CH$_2$-Ar), 4.08–3.98 (m, 1H, CH$_2$-O-CH(CH$_3$)-CO), 3.63–3.50 (m, 1H, CH$_2$-O-CH(CH$_3$)-CO), 3.37–3.28 (m, 1H, CH$_2$-O-CH(CH$_3$)-CO), 1.77–1.37 (m, 35H, Si(CH$_3$)$_2$-CH$_2$-CH$_2$-CH$_2$-O and O-CH(CH$_3$)-CO), 0.58–0.49 (m, 2H, Si(CH$_3$)$_2$-CH$_2$-CH$_2$-CH$_2$-O), 0.10–0.02 ppm (m, 141H, Si(CH$_3$)); ^{13}C NMR (100 MHz, $CDCl_3$): δ = 173.18, 173.13, 173.08, 170.10–170.02, 169.91–169.85, 169.80–169.66, 169.56–169.41, 169.31, 169.27, 135.24, 135.22, 128.76, 128.67, 128.65, 128.39, 128.37, 74.80, 74.68, 73.29, 73.25, 69.43, 69.32, 69.26–69.11, 68.59, 68.55, 68.51, 67.36, 67.34, 23.67, 18.81–18.78, 16.93–16.71, 14.24, 1.92, 1.30, 1.28, 1.20–1.18, 0.24, 0.21 ppm; MS (MALDI-TOF): *m/z* calcd for $C_{90}H_{198}O_{45}Si_{23}+Na^+$: 2665.78 [M+Na]$^+$; found 2665.85.

Synthesis of Me-Si$_{23}$-LA$_{13}$-Bn [**Si$_{23}$-LA$_{13}$**].

Starting from oDMS acid **Me-Si$_{23}$-LLA$_1$-COOH** L-**28e** (125 mg, 0.068 mmol, 1 eq), *o*LA **HO-LA$_{12}$-Bn** *at*-**22q** (72.9 mg, 0.075 mmol, 1.1 eq), DPTS (10.1 mg, 0.034 mmol, 0.5 eq) and EDC·HCl (26.2 mg, 0.137 mmol, 2 eq), crude co-oligomer [**Si$_{23}$-LA$_{13}$**] was obtained as a colorless oil (208 mg) using general method **H**. The material was purified by automated column chromatography using hept/EtOAc (gradient 88/12 to 50/50) as eluent, giving the product in pure form as a colorless, waxy substance (87.3 mg, 46%). ^{1}H NMR (400 MHz, $CDCl_3$): δ = 7.39–7.29 (m, 5H, Ar-H), 5.26–5.09 (m, 14H, O-CH(CH$_3$)-CO and O-CH$_2$-Ar), 4.07–3.98 (m, 1H, CH$_2$-O-CH(CH$_3$)-CO), 3.62–3.49 (m, 1H, CH$_2$-O-CH(CH$_3$)-CO), 3.36–3.28 (m, 1H, CH$_2$-O-CH(CH$_3$)-CO), 1.67–1.38 (m, 41H, Si(CH$_3$)$_2$-CH$_2$-CH$_2$-CH$_2$-O and O-CH(CH$_3$)-CO), 0.57–0.48 (m, 2H, Si(CH$_3$)$_2$-CH$_2$-CH$_2$-CH$_2$-O), 0.18 to −0.04 ppm (m, 141H, Si(CH$_3$)); ^{13}C NMR (100 MHz, $CDCl_3$): δ = 173.15, 170.06, 169.92, 169.76, 169.49, 169.28, 135.19, 128.75, 128.65, 128.38, 74.77, 74.64, 73.28, 69.40, 69.30, 69.12, 68.53, 67.33, 23.64, 18.81, 16.88–16.79, 14.20, 1.92, 1.29, 1.20–1.18, 0.23, 0.20 ppm; MS (MALDI-TOF): *m/z* calcd for $C_{96}H_{206}O_{49}Si_{23}+Na^+$: 2809.82 $[M+Na]^+$; found 2809.80.

Synthesis of Me-Si$_{23}$-LLA$_{13}$-Bn [**Si$_{23}$-LLA$_{13}$**].

Starting from *o*DMS acid **Me-Si$_{23}$-LLA$_1$-COOH** L-**28e** (129 mg, 0.07 mmol, 1 eq), **HO-LLA$_{12}$-Bn** L-**22q** (68 mg, 0.07 mmol, 1 eq), DPTS (10 mg, 0.04 mmol, 0.5 eq) and EDC·HCl (27 mg, 0.14 mmol, 2 eq), crude oligomer [**Si$_{23}$-LLA$_{13}$**] was obtained as white solid (181 mg) using general method **H**. The material was purified by automated column chromatography using hept/EtOAc (gradient 90/10 to 55/45) as eluent, giving the product in pure form as a white solid (161 mg, 82 %). ^{1}H NMR (400 MHz, $CDCl_3$): δ = 7.42–7.28 (m, 5H, Ar-H), 5.26–5.07 (m, 14H, CO-O-CH(CH$_3$)-CO and O-CH$_2$-Ar), 4.02 (q, ^3J = 6.8 Hz, 1H, CH$_2$-O-CH(CH$_3$)-CO), 3.58 (dt, ^2J = 8.7 Hz, ^3J = 7.0 Hz, 1H, CH$_2$-CH$_2$-O), 3.32 (dt, ^2J = 8.7 Hz, ^3J = 7.0 Hz, 1H, CH$_2$-CH$_2$-O), 1.68–1.61 (m, 2H, Si(CH$_3$)$_2$-CH$_2$-CH$_2$-CH$_2$-O), 1.58 (m, 30H, CO-O-CH(CH$_3$)-CO), 1.52 (m, 6H, CO-O-CH(CH$_3$)-CO), 1.45 (d, ^3J = 6.9 Hz, 3H, CH$_2$-O-CH(CH$_3$)-CO), 0.59–0.48 (m, 2H, Si(CH$_3$)$_2$-CH$_2$-CH$_2$-CH$_2$-O), 0.10–0.00 ppm (m, 138H, Si(CH$_3$)$_2$); ^{13}C NMR (100 MHz, $CDCl_3$): δ = 173.38, 170.27, 170.22, 170.04, 169.98, 169.94, 169.93, 169.91, 169.86, 135.39, 128.95, 128.87, 128.58, 74.86, 73.45, 69.61, 69.35, 69.34, 69.30, 69.20, 68.74, 67.55, 23.86, 19.02, 17.09, 17.01, 16.98, 16.90, 14.41, 3.18, 2.12, 1.82, 1.75, 1.54, 1.50, 1.48, 1.38, 1.01, 0.43, 0.40, 0.33 ppm; MS (MALDI-TOF): *m/z* calcd for $C_{96}H_{206}O_{49}Si_{23}+Na^+$: 2809.82 $[M+Na]^+$; found 2809.93; *m/z* calcd for $C_{96}H_{206}O_{49}Si_{23}+K^+$: 2825.80 $[M+K]^+$; found 2825.92.

Synthesis of Me-Si$_{23}$-DLA$_{13}$-Bn [**Si$_{23}$-DLA$_{13}$**].

Starting from *o*DMS acid **Me-Si$_{23}$-DLA$_1$-COOH** D-**28e** (137 mg, 0.07 mmol, 1 eq), **HO-DLA$_{12}$-Bn** D-**22q** (70 mg, 0.07 mmol, 1 eq), DPTS (11 mg, 0.04 mmol, 0.5 eq) and EDC·HCl (28 mg, 0.14 mmol, 2 eq), crude oligomer [**Si$_{23}$-DLA$_{13}$**] was obtained as white solid (211 mg) using general method **H**. The material was purified by automated column chromatography using hept/EtOAc (gradient 90/10 to 65/35) as eluent, giving the product in pure form as a white solid (196 mg, 95 %). ^{1}H NMR (400 MHz, $CDCl_3$): δ = 7.45–7.27 (m, 5H, Ar-H), 5.28–5.07 (m, 15H, CO-O-CH(CH$_3$)-CO and O-CH$_2$-Ar), 4.02 (q, ^3J = 6.8 Hz, 1H, CH$_2$-O-CH(CH$_3$)-CO), 3.59 (dt, ^2J = 8.8 Hz, ^3J = 7.0 Hz, 1H, CH$_2$-CH$_2$-O), 3.32 (dt, ^2J = 8.8 Hz, ^3J = 7.0 Hz, 1H, CH$_2$-CH$_2$-O), 1.69–1.61 (m, 2H, Si(CH$_3$)$_2$-CH$_2$-CH$_2$-CH$_2$-O), 1.58 (m, 30H, CO-O-CH(CH$_3$)-CO), 1.52 (m, 6H, CO-O-CH(CH$_3$)-CO), 1.45 (d, ^3J = 6.8 Hz, 3H, CH$_2$-O-CH(CH$_3$)-CO), 0.58–0.46 (m, 2H, Si(CH$_3$)$_2$-CH$_2$-CH$_2$-CH$_2$-O), 0.18 to −0.05 ppm (m, 141H, Si(CH$_3$)$_2$); ^{13}C NMR (100 MHz, $CDCl_3$) δ = 173.39, 170.29, 170.24, 170.05, 169.99, 169.95, 169.87, 135.42, 128.97, 128.88, 128.60, 74.88, 73.47, 69.63, 69.36, 69.22, 68.75, 67.57, 23.88, 19.02, 17.11, 17.03, 17.00, 16.92, 14.43, 2.13, 1.76, 1.51, 1.49, 1.40, 1.02, 0.45, 0.42, 0.35 ppm; MS (MALDI-TOF): *m/z* calcd for $C_{96}H_{206}O_{49}Si_{23}+Na^+$: 2809.82 $[M+Na]^+$; found 2809.87; *m/z* calcd for $C_{96}H_{206}O_{49}Si_{23}+K^+$: 2825.80 $[M+K]^+$; found 2825.86.

Synthesis of Me-Si$_{23}$-LA$_{15}$-Bn [**Si$_{23}$-LA$_{15}$**].

Starting from oDMS acid **Me-Si$_{23}$-LLA$_1$-COOH** L-**28e** (123mg, 0.067 mmol, 1 eq), oLA **HO-LA$_{14}$-Bn** *at*-**22r** (75 mg, 0.067 mmol, 1 eq), DPTS (9.3 mg, 0.034 mmol, 0.5 eq) and EDC·HCl (25.6 mg, 0.134 mmol, 2 eq), crude co-oligomer [**Si$_{23}$-LA$_{15}$**] was obtained as a colorless oil (198 mg) using general method **H**. The material was purified by automated column chromatography using hept/EtOAc (gradient 88/12 to 50/50) as eluent, giving the product in pure form as a colorless, waxy substance (100 mg, 51%). ^{1}H NMR (400 MHz, $CDCl_3$): δ = 7.39–7.29 (m, 5H, Ar-H), 5.29–5.06 (m, 16H, O-CH(CH$_3$)-CO and O-CH$_2$-Ar), 4.10–3.96 (m, 1H, CH$_2$-O-CH(CH$_3$)-CO), 3.65–3.46 (m, 1H, CH$_2$-O-CH(CH$_3$)-CO), 3.39–3.24 (m, 1H, CH$_2$-O-CH(CH$_3$)-CO), 1.67–1.37 (m, 47H, Si(CH$_3$)$_2$-CH$_2$-CH$_2$-CH$_2$-O and O-CH(CH$_3$)-CO), 0.59–0.47 (m, 2H, Si(CH$_3$)$_2$-CH$_2$-CH$_2$-CH$_2$-O), 0.22 to −0.07 ppm (m, 141H, Si(CH$_3$)); ^{13}C NMR (100 MHz, $CDCl_3$): δ = 173.19, 170.05, 169.75, 169.46, 169.27, 135.19, 128.74, 128.65, 128.37, 74.64, 73.24, 69.40, 69.30, 69.11, 68.52, 67.32, 23.64, 18.81, 16.87–16.78, 14.19, 1.91, 1.28, 1.18, 0.21 ppm; MS (MALDI-TOF): *m/z* calcd for $C_{102}H_{214}O_{53}Si_{23}+Na^+$: 2953.86 $[M+Na]^+$; found 2953.86.

Synthesis of Me-Si$_{23}$-LA$_{17}$-Bn [**Si$_{23}$-LA$_{17}$**].

Starting from oDMS acid **Me-Si$_{23}$-LLA$_1$-COOH** L-**28e** (101 mg, 0.055 mmol, 1 eq), oLA **HO-LA$_{16}$-Bn** *at*-**22s** (69.4 mg, 0.055 mmol, 1 eq), DPTS (8.1 mg, 0.028 mmol, 0.5 eq) and EDC·HCl (21.1 mg, 0.110 mmol, 2 eq), crude co-oligomer [**Si$_{23}$-LA$_{17}$**] was obtained as a colorless oil (157 mg) using general method **H**. The material was purified by automated column chromatography using hept/EtOAc (gradient 78/22 to 55/45) as eluent, giving the product in pure form as a colorless, waxy substance (154 mg, 91%). ^{1}H NMR (400 MHz, $CDCl_3$): δ = 7.39–7.29 (m, 5H, Ar-H), 5.26–5.09 (m, 18H, O-CH(CH$_3$)-CO and O-CH$_2$-Ar), 4.07–3.98 (m, 1H, CH$_2$-O-CH(CH$_3$)-CO), 3.62–3.49 (m, 1H, CH$_2$-O-CH(CH$_3$)-CO), 3.36–3.27 (m, 1H, CH$_2$-O-CH(CH$_3$)-CO), 1.66–1.39 (m, 53H, Si(CH$_3$)$_2$-CH$_2$-CH$_2$-CH$_2$-O and O-CH(CH$_3$)-CO), 0.57–0.49 (m, 2H, Si(CH$_3$)$_2$-CH$_2$-CH$_2$-CH$_2$-O), 0.16 to −0.05 ppm (m, 141H, Si(CH$_3$)); ^{13}C NMR (100 MHz, $CDCl_3$): δ = 173.12, 170.04, 169.73, 169.54, 169.47, 169.44, 169.26, 135.22, 128.75, 128.66, 128.64, 128.36, 74.78, 74.65, 73.24, 69.41, 69.31, 69.12, 68.53, 67.32, 23.65, 18.77, 16.87–16.73, 14.21, 1.91, 1.29, 1.27, 1.20–1.17, 0.23, 0.20 ppm; MS (MALDI-TOF): *m/z* calcd for $C_{108}H_{222}O_{57}Si_{23}+Na^+$: 3097.91 $[M+Na]^+$; found 3097.99.

Synthesis of Me-Si$_{23}$-LLA$_{17}$-Bn [**Si$_{23}$-LLA$_{17}$**].

Starting from *o*DMS acid **Me-Si$_{23}$-LLA$_1$-COOH** L-**28e** (129 mg, 0.07 mmol, 1 eq), **HO-LLA$_{16}$-Bn** L-**22s** (88 mg, 0.07 mmol, 1 eq), DPTS (10 mg, 0.04 mmol, 0.5 eq) and EDC·HCl (27 mg, 0.14 mmol, 2 eq), crude oligomer **[Si$_{23}$-LLA$_{17}$]** was obtained as white solid (222 mg) using general method **H**. The material was purified by automated column chromatography using hept/EtOAc (gradient 90/10 to 50/50) as eluent, giving the product in pure form as a white solid (204 mg, 95 %). ^{1}H NMR (400 MHz, $CDCl_3$): δ = 7.44–7.27 (m, 5H, Ar-H), 5.27–5.07 (m, 18H, CO-O-CH(CH$_3$)-CO and O-CH$_2$-Ar), 4.02 (q, ^3J = 6.8 Hz, 1H, CH$_2$-O-CH(CH$_3$)-CO), 3.58 (dt, ^2J = 8.7 Hz, ^3J = 7.0 Hz, 1H, CH$_2$-CH$_2$-O), 3.32 (dt, ^2J = 8.8 Hz, ^3J = 7.0 Hz, 1H, CH$_2$-CH$_2$-O), 1.67–1.61 (m, 2H, Si(CH$_3$)$_2$-CH$_2$-CH$_2$-CH$_2$-O), 1.61–1.54 (m, 42H, CO-O-CH(CH$_3$)-CO), 1.52 (m, 6H, CO-O-CH(CH$_3$)-CO), 1.45 (d, ^3J = 6.9 Hz, 3H, CH$_2$-O-CH(CH$_3$)-CO), 0.57–0.5 (m, 2H, Si(CH$_3$)$_2$-CH$_2$-CH$_2$-CH$_2$-O), 0.11 to −0.02 ppm (m, 138H, Si(CH$_3$)$_2$); ^{13}C NMR (100 MHz, $CDCl_3$): δ = 173.39, 170.28, 170.22, 170.04, 169.98, 169.93, 169.86, 135.38, 128.95, 128.86, 128.58, 74.85, 73.45, 69.61, 69.49, 69.33, 69.29, 69.19, 68.73, 67.55, 23.85, 19.02, 17.08, 17.01, 16.98, 16.90, 14.40, 3.18, 2.12, 1.75, 1.49, 1.48, 1.38, 1.20, 1.01, 0.43, 0.40, 0.33 ppm; MS (MALDI-TOF): *m/z* calcd for $C_{108}H_{222}O_{57}Si_{23}+Na^+$: 3097.91 $[M+Na]^+$; found 3098.04; *m/z* calcd for $C_{108}H_{222}O_{57}Si_{23}+K^+$: 3113.88 $[M+K]^+$; found 3114.05.

Synthesis of Me-Si$_{23}$-DLA$_{17}$-Bn [**Si$_{23}$-DLA$_{17}$**].

Starting from *o*DMS acid **Me-Si$_{23}$-DLA$_1$-COOH** D-**28e** (89 mg, 0.05 mmol, 1 eq), **HO-DLA$_{16}$-Bn** D-**22s** (61 mg, 0.05 mmol, 1 eq), DPTS (7.1 mg, 0.02 mmol, 0.5 eq) and EDC·HCl (19 mg, 0.1 mmol, 2 eq), crude oligomer **[Si$_{23}$-DLA$_{17}$]** was obtained as white solid (122 mg) using general method **H**. The material was purified by automated

column chromatography using hept/EtOAc (gradient 90/10 to 50/50) as eluent, giving the product in pure form as a white solid (90 mg, 60 %). ^{1}H NMR (400 MHz, $CDCl_3$): δ = 7.44–7.27 (m, 5H, Ar-H), 5.26–5.08 (m, 18H, CO-O-CH(CH$_3$)-CO and O-CH$_2$-Ar), 4.02 (q, ^3J = 6.8 Hz, 1H, CH2-O-CH(CH$_3$)-CO), 3.58 (dt, ^2J = 8.8 Hz, ^3J = 7.0 Hz, 1H, CH$_2$-CH$_2$-O), 3.32 (dt, ^2J = 8.8 Hz, ^3J = 7.1 Hz, 1H, CH$_2$-CH$_2$-O), 1.67–1.61 (m, 2H, Si(CH$_3$)$_2$-CH$_2$-CH$_2$-CH$_2$-O), 1.58 (m, 42H, CO-O-CH(CH$_3$)-CO), 1.52 (m, 6H, CO-O-CH(CH$_3$)-CO), 1.45 (d, ^3J = 6.8 Hz, 3H, CH$_2$-O-CH(CH$_3$)-CO), 0.65–0.42 (m, 2H, Si(CH$_3$)$_2$-CH$_2$-CH$_2$-CH$_2$-O), 0.17 to −0.06 ppm (m, 141H, Si(CH$_3$)$_2$); ^{13}C NMR (100 MHz, $CDCl_3$) δ = 173.39, 170.28, 170.24, 170.05, 169.98, 169.94, 169.87, 135.41, 128.97, 128.88, 128.59, 74.88, 73.46, 69.63, 69.35, 69.21, 68.75, 67.57, 23.87, 19.02, 17.10, 17.03, 16.99, 16.92, 14.43, 2.13, 1.76, 1.50, 1.49, 1.39, 1.02, 0.44, 0.41, 0.34 ppm; MS (MALDI-TOF): *m/z* calcd for $C_{108}H_{222}O_{57}Si_{23}+Na^+$: 3097.91 $[M+Na]^+$; found 3097.93; *m/z* calcd for $C_{108}H_{222}O_{57}Si_{23}+K^+$: 3113.88 $[M+K]^+$; found 3114.90 (2nd isotope peak).

Synthesis of Me-Si$_{23}$-LA$_{25}$-Bn [**Si$_{23}$-LA$_{25}$**].

Starting from oDMS acid **Me-Si$_{23}$-LLA$_1$-COOH** L-**28e** (91 mg, 0.050 mmol, 1 eq), oLA **HO-LA$_{24}$-Bn** *at*-**22t** (91 mg, 0.050 mmol, 1 eq), DPTS (7.3 mg, 0.025 mmol, 0.5 eq) and EDC·HCl (19.0 mg, 0.099 mmol, 2 eq), crude co-oligomer [**Si$_{23}$-LA$_{25}$**] was obtained as a colorless oil (171 mg) using general method **H**. The material was purified by automated column chromatography using hept/EtOAc (gradient 70/30 to 40/60) as eluent, giving the product in pure form as a colorless, waxy substance (174 mg, 96%). ^{1}H NMR (400 MHz, $CDCl_3$): δ = 7.38–7.29 (m, 5H, Ar-H), 5.29–5.09 (m, 26H, O-CH(CH$_3$)-CO and O-CH$_2$-Ar), 4.06–3.98 (m, 1H, CH$_2$-O-CH(CH$_3$)-CO), 3.62–3.49 (m, 1H, CH$_2$-O-CH(CH$_3$)-CO), 3.36–3.27 (m, 1H, CH$_2$-O-CH(CH$_3$)-CO), 1.67–1.39 (m, 77H, Si(CH$_3$)$_2$-CH$_2$-CH$_2$-CH$_2$-O and O-CH(CH$_3$)-CO), 0.56–0.49 (m, 2H, Si(CH$_3$)$_2$-CH$_2$-CH$_2$-CH$_2$-O), 0.14 to −0.03 ppm (m, 141H, Si(CH$_3$)); ^{13}C NMR (100 MHz, $CDCl_3$): δ = 173.10, 173.06, 170.02, 169.99, 169.89, 169.86, 169.73–169.66, 169.52–169.39, 169.29, 169.24, 135.20, 128.73, 128.64, 128.62, 128.36, 128.34, 74.76, 74.64, 73.26, 73.22, 69.40, 69.29, 69.23, 69.15–69.07, 68.52, 68.48, 67.32, 67.30, 23.63, 18.76, 16.89–16.68, 14.19, 1.89, 1.27, 1.25, 1.18–1.16, 0.21, 0.18 ppm; MS (MALDI-TOF): *m/z* calcd for $C_{132}H_{254}O_{73}Si_{23}+Na^+$: 3674.08 $[M+Na]^+$; found 3674.11.

Synthesis of Me-Si$_{23}$-LLA$_{25}$-Bn [**Si$_{23}$-LLA$_{25}$**].

Starting from *o*DMS acid **Me-Si$_{23}$-LLA$_1$-COOH** L-**28e** (137 mg, 0.07 mmol, 1 eq), **HO-LLA$_{24}$-Bn** L-**22t** (70 mg, 0.07 mmol, 1 eq), DPTS (11 mg, 0.04 mmol, 0.5 eq) and EDC·HCl (28 mg, 0.14 mmol, 2 eq), crude oligomer **[Si$_{23}$-LLA$_{25}$]** was obtained as white solid (228 mg) using general method **H**. The material was purified by automated column chromatography using hept/EtOAc (gradient 70/30 to 40/60) as eluent, giving the product in pure form as a white solid (196 mg, 95%). ^{1}H NMR (400 MHz, $CDCl_3$): δ = 7.42–7.27 (m, 5H, Ar-H), 5.36–5.06 (m, 26H, CO-O-CH(CH$_3$)-CO and O-CH$_2$-Ar), 4.02 (q, ^3J = 6.9 Hz, 1H, CH$_2$-O-CH(CH$_3$)-CO), 3.58 (dt, ^2J = 8.8 Hz, ^3J = 7.0 Hz, 1H, CH$_2$-CH$_2$-O), 3.32 (dt, ^2J = 8.8 Hz, ^3J = 7.0 Hz, 1H, CH$_2$-CH$_2$-O), 1.65–1.61 (m, 2H, Si(CH$_3$)$_2$-CH$_2$-CH$_2$-CH$_2$-O), 1.58 (m, 66H, CO-O-CH(CH$_3$)-CO), 1.52 (m, 6H, CO-O-CH(CH$_3$)-CO), 1.45 (d, ^3J = 6.9 Hz, 3H, CH$_2$-O-CH(CH$_3$)-CO), 0.59–0.48 (m, 2H, Si(CH$_3$)$_2$-CH$_2$-CH$_2$-CH$_2$-O), 0.11 to −0.03 ppm (m, 138H, Si(CH$_3$)$_2$); ^{13}C NMR (100 MHz, $CDCl_3$): δ = 173.36, 170.26, 170.20, 170.02, 169.91, 169.84, 135.40, 128.94, 128.85, 128.57, 74.86, 73.43, 69.61, 69.33, 69.19, 68.72, 67.54, 23.85, 18.99, 17.07, 16.97, 16.89, 14.41, 2.10, 1.74, 1.48, 1.46, 1.37, 1.00, 0.42, 0.39 ppm; MS (MALDI-TOF): *m/z* calcd for $C_{132}H_{254}O_{73}Si_{23}+Na^+$: 3674.08 $[M+Na]^+$; found 3674.15.

Synthesis of Me-Si$_{23}$-LLA$_{33}$-Bn [**Si$_{23}$-LLA$_{33}$**].

Starting from *o*DMS acid **Me-Si$_{23}$-LLA$_1$-COOH** L-**28e** (28 mg, 15 µmol, 1 eq), **HO-LLA$_{32}$-Bn** L-**22u** (40 mg, 17 µmol, 1.1 eq), DPTS (2.7 mg, 9.2 µmol, 0.6 eq) and EDC·HCl (8.8 mg, 46 µmol, 2 eq), crude oligomer **[Si$_{23}$-LLA$_{33}$]** was obtained as white solid (55 mg) using general method **H**. The material was purified by automated column chromatography using hept/EtOAc (gradient 70/30 to 40/60) as eluent, giving the product in pure form as a white solid (47 mg, 73%). ^{1}H NMR (400 MHz, $CDCl_3$): δ = 7.39–7.29 (m, 5H, Ar-H), 5.22–5.10 (m, 34H, O-CH(CH$_3$)-CO and O-CH$_2$-Ar), 4,02 (q, ^3J = 6,9 Hz, 1H, CH$_2$-O-CH(CH$_3$)-CO), 3,58 (dt, ^3J = 8,7 Hz, ^3J = 6,9 Hz, 1H, CH$_2$-O-

CH(CH$_3$)-CO), 3,32 (dt, ^3J = 8,7 Hz, ^3J = 7 Hz, 1H, CH$_2$-O-CH(CH$_3$)-CO), 1.66–1.54 (m, 92H, Si(CH$_3$)$_2$-CH$_2$-CH$_2$-CH$_2$-O and O-CH(CH$_3$)-CO), 1.53–1.49 (m, 6H, O-CH(CH$_3$)-CO), 1,45 (dt, ^3J = 6,9 Hz, 3H, O-CH(CH$_3$)-CO), 0.57–0.50 (m, 2H, Si(CH$_3$)$_2$-CH$_2$-CH$_2$-CH$_2$-O), 0.09–0.03 ppm (m, 141H, Si(CH$_3$)); ^{13}C NMR (100 MHz, CDCl$_3$): δ = 173.16, 170.06, 170.02, 169.82, 169.71, 135.23, 128.76, 128.66, 128.38, 74.68, 73.24, 69.43, 69.15, 69.01, 68.54, 67.35, 23.67, 18.79, 16.89, 16.79, 16.71, 14.25, 1.92, 1.29, 1.27, 1.18, 0.24, 0.21 ppm; MS (MALDI-TOF): *m/z* calcd for C$_{156}$H$_{286}$NaO$_{89}$Si$_{23}$+Na$^+$: 4250.24 [M+Na]$^+$; found: 4250.49; *m/z* calcd for C$_{156}$H$_{286}$NaO$_{89}$Si$_{23}$+K$^+$: 4266.22 [M+K]$^+$; found: 4266.50.

Synthesis of Me-Si$_{27}$-LA$_{15}$-Bn [**Si$_{27}$-LA$_{15}$**].

Starting from oDMS acid **Me-Si$_{27}$-LLA$_1$-COOH** L-**28f** (131 mg, 0.061 mmol, 1 eq), oLA **HO-LA$_{14}$-Bn** *at*-**22r** (68.7 mg, 0.061 mmol, 1 eq), DPTS (9.1 mg, 0.031 mmol, 0.5 eq) and EDC·HCl (23.6 mg, 0.123 mmol, 2 eq), crude co-oligomer [**Si$_{27}$-LA$_{15}$**] was obtained as a colorless oil (278 mg) using general method **H**. The material was purified by automated column chromatography using hept/EtOAc (gradient 90/10 to 50/50) as eluent, giving the product in pure form as a colorless, waxy substance (156 mg, 78%). ^{1}H NMR (400 MHz, CDCl$_3$): δ = 7.39–7.28 (m, 5H, Ar-H), 5.25–5.09 (m, 16H, O-CH(CH$_3$)-CO and O-CH$_2$-Ar), 4.07–3.98 (m, 1H, CH$_2$-O-CH(CH$_3$)-CO), 3.62–3.49 (m, 1H, CH$_2$-O-CH(CH$_3$)-CO), 3.36–3.28 (m, 1H, CH$_2$-O-CH(CH$_3$)-CO), 1.68–1.39 (m, 47H, Si(CH$_3$)$_2$-CH$_2$-CH$_2$-CH$_2$-O and O-CH(CH$_3$)-CO), 0.58–0.49 (m, 2H, Si(CH$_3$)$_2$-CH$_2$-CH$_2$-CH$_2$-O), 0.16 to −0.04 ppm (m, 165H, Si(CH$_3$)); ^{13}C NMR (100 MHz, CDCl$_3$): δ = 173.13, 173.08, 170.04–169.98, 169.85, 169.78, 169.74–169.63, 169.54, 169.51, 169.49, 169.44–169.38, 169.28, 169.24, 135.27, 135.24, 128.74, 128.64, 128.62, 128.34, 74.80, 74.68, 73.22, 69.42, 69.31, 69.17–69.10, 69.00, 68.53, 68.50, 67.30, 23.66, 18.77–18.73, 16.90–16.69, 14.24, 1.89, 1.27, 1.24, 1.15, 0.22, 0.19 ppm; MS (MALDI-TOF): *m/z* calcd for C$_{110}$H$_{238}$O$_{57}$Si$_{27}$+Na$^+$: 3249.94 [M+Na]$^+$; found 3250.02.

Synthesis of Me-Si$_{27}$-LLA$_1$-COCl (L-**29f**).

Free acid **Me-Si$_{27}$-LLA$_1$-COOH** L-**28f** (58 mg, 0.027 mmol) was dissolved in dry DCM (1 mL) in a 10 mL schlenk tube under an argon atmosphere. The mixture was cooled in ice water and Ghosez's reagent (1-chloro-*N*,*N*,2-trimethyl-1-propenylamine, 36 mg, 0.27 mmol, 10 eq) was added. The resulting mixture was stirred for 30 min at 0 °C and then at room temperature overnight. Afterward, all solvent was removed in a stream of nitrogen and the remaining material dried under vacuum (1 mbar) for 30 min. The crude mixture, containing the acid chloride, was directly used for the next step.

Synthesis of Me-Si$_{27}$-LA$_{25}$-Bn [**Si$_{27}$-LA$_{25}$**].

The crude mixture containing acid chloride **Me-Si$_{27}$-LLA$_1$-COCl** L-**29f** (~0.027 mmol) was dissolved in dry DCM (0.5 mL) in a 10 mL schlenk tube under an argon atmosphere. In a second schlenk tube (also under an argon atmosphere), benzyl protected oLA *at*-**22t** (50 mg, 0.027 mmol, 1 eq) and dry pyridine (22 mg, 0.27 mmol, 10 eq) was dissolved in dry DCM (0.5 mL). This colorless solution was cooled in ice water, and the acid chloride solution was added dropwise. The resulting mixture turned yellow and was stirred for 20 min at 0 °C, followed by stirring for another 5 h at room temperature. Next the solvent was removed in a stream of nitrogen and by further drying in vacuum (1 mbar), giving the crude product as a yellow, waxy material. The material was purified by automated column chromatography using hept/EtOAc (gradient 90/10 to 0/100) as eluent, giving the product [**Si$_{27}$-LA$_{25}$**] in pure form as a colorless, waxy solid (52 mg, 60% (two steps)). ^{1}H NMR (400 MHz, CDCl$_3$): δ = 7.40–7.29 (m, 5H, Ar-H), 5.29–5.08 (m, 26H, O-CH(CH$_3$)-CO and O-CH$_2$-Ar), 4.07–3.97 (m, 1H, CH$_2$-O-CH(CH$_3$)-CO), 3.62–3.49 (m, 1H, CH$_2$-O-CH(CH$_3$)-CO), 3.36–3.27 (m, 1H, CH$_2$-O-CH(CH$_3$)-CO), 1.69–1.39 (m, 77H, Si(CH$_3$)$_2$-CH$_2$-CH$_2$-CH$_2$-O and O-CH(CH$_3$)-CO), 0.57–0.49 (m, 2H, Si(CH$_3$)$_2$-CH$_2$-CH$_2$-CH$_2$-O), 0.23 to −0.04 ppm (m, 165H, Si(CH$_3$)); ^{13}C NMR (100 MHz, CDCl$_3$): δ = 173.13, 173.08, 170.05–170.03, 169.88, 169.73, 169.55, 169.48, 169.45, 169.27, 135.24, 135.22, 128.76, 128.67, 128.65, 128.37, 74.80, 74.67, 73.29, 73.25, 69.43, 69.32, 69.18–69.10, 68.54,

68.51, 67.36–67.34, 23.66, 18.79, 16.90–16.88, 16.82–16.75, 14.24, 1.92, 1.30, 1.28, 1.18, 0.24, 0.21 ppm; MS (MALDI-TOF): *m/z* calcd for $C_{140}H_{278}O_{77}Si_{27}+Na^+$: 3970.15 $[M+Na]^+$; found 3970.74.

Synthesis of Me-Si$_{59}$-LLA$_1$-COCl (L-**29l**).

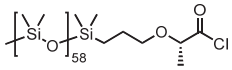

Free acid Me-Si$_{59}$-LLA$_1$-COOH L-**28l** (18 mg, 4.0 µmol) was dissolved in dry DCM (1 mL) in a 10 mL schlenk tube under an argon atmosphere. The mixture was cooled in ice water and Ghosez's reagent (1-chloro-*N,N*,2-trimethyl-1-propenylamine, 5.4 mg, 40 µmol, 10 eq) was added. The resulting mixture was stirred for 30 min at 0 °C and then at room temperature overnight. Afterward, all solvent was removed in a stream of nitrogen and the remaining material dried under vacuum (1 mbar) for 30 min. The crude mixture, containing the acid chloride, was directly used for the next step.

Synthesis of Me-Si$_{59}$-LA$_{33}$-Bn [**Si$_{59}$-LA$_{33}$**].

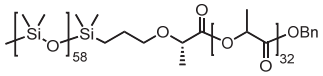

The crude mixture containing acid chloride Me-Si$_{59}$-LLA$_1$-COCl L-**29l** (~4 µmol) was dissolved in dry DCM (0.5 mL) in a 10 mL schlenk tube under an argon atmosphere. In a second schlenk tube (also under an argon atmosphere), benzyl protected oLA *at*-**22u** (10.6 mg, 4.4 µmol, 1.1 eq) and dry pyridine (3.2 mg, 40 µmol, 10 eq) was dissolved in dry DCM (0.5 mL). This colorless solution was cooled in ice water, and the acid chloride solution was added dropwise. The resulting mixture turned yellow and was stirred for 20 min at 0 °C, followed by stirring overnight at room temperature. Next the solvent was removed in a stream of nitrogen and by further drying in vacuum (1 mbar), giving the crude product as a yellow, waxy material. The material was purified by automated column chromatography using hept/EtOAc (gradient 90/10 to 0/100) as eluent, giving the product [**Si$_{59}$-LA$_{33}$**] as a colorless, waxy solid (5 mg, 18% (two steps)). In the ^{1}H NMR spectrum only a tiny amount of (unknown) impurity was found at 2.33 ppm. ^{1}H NMR (400 MHz, $CDCl_3$): δ = 7.40–7.30 (m, 5H, Ar-H), 5.26–5.10 (m, 34H, O-CH(CH$_3$)-CO and O-CH$_2$-Ar), 4.08–3.97 (m, 1H, CH$_2$-O-CH(CH$_3$)-CO), 3.62–3.50 (m, 1H, CH$_2$-O-CH(CH$_3$)-CO), 3.36–3.27 (m, 1H, CH$_2$-O-CH(CH$_3$)-CO), 1.67–1.39 (m, 101H, Si(CH$_3$)$_2$-CH$_2$-CH$_2$-CH$_2$-O and O-CH(CH$_3$)-CO), 0.57–0.49 (m, 2H, Si(CH$_3$)$_2$-CH$_2$-CH$_2$-CH$_2$-O), 0.13–0.02 ppm (m, 357H, Si(CH$_3$)); MS (MALDI-TOF): *m/z* calcd for $C_{228}H_{502}O_{125}Si_{59}+Na^+$: 6914.92 $[M+Na]^+$; found 6924.78 (11th isotope peak).

Synthesis of methyl (R)-2-(allyloxy)propanoate (D-**31**).

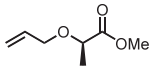

Methyl D-lactate D-**30** (4.67 g, 44.8 mmol, 1.0 eq) and allyl bromide (8.16 g, 5.85 mL, 67.2 mmol, 1.5 eq) were dissolved in dry diethyl ether (40 mL) in a 3-necked round-bottom flask under an argon atmosphere. Silver(I) oxide (10.39 g, 44.8 mmol, 1.0 eq) was added and the mixture was stirred for 2 days under reflux. The mixture was cooled to room temperature, transferred to centrifuge tubes and centrifuged at 2000 rpm for 2 minutes. The supernatant was transferred to a 250 mL round-bottom flask. The residue was washed with Et_2O (15 mL) and centrifuged (two times). The combined organic layers were concentrated in *vacuo*, giving crude product D-**31** as a light yellow liquid. The mixture was purified by automated column chromatography (pentane/DCM gradient 20/80 to 0/100), giving the pure material (4.4 g, 68 %). ^{1}H NMR (400 MHz, $CDCl_3$): δ = 5.97–5.84 (m, 1H, CH$_2$-CH=CH$_2$), 5.29 (d, ^3J = 10.4 Hz, 1H, CH$_2$-CH=CH$_2$), 5.19 (d, ^3J = 10.4 Hz, 1H, CH$_2$-CH-CH$_2$ (trans)), 4.13 (dd, ^2J = 12.5 Hz, ^3J = 5.6 Hz, 1H, CH$_2$-O-CH(CH$_3$)), 4.02 (q, ^3J = 6.9 Hz, 1H, O-CH(CH$_3$)-CO), 3.93 (dd, ^2J = 12.5 Hz, ^3J = 6.1 Hz, 1H, CH$_2$-O-

CH(CH$_3$)), 3.74 (s, 3H, CO-O-C<u>H</u>$_3$), 1.41 ppm (d, ^3J = 6.8 Hz, 3H, O-CH(C<u>H</u>$_3$)-CO); ^{13}C NMR (100 MHz, CDCl$_3$) δ = 174.05, 134.38, 118.06, 74.28, 71.43, 53.75, 52.23, 18.97 ppm.

Synthesis of Me-Si$_{15}$-DLA$_1$-Me (D-**32c**).

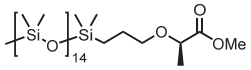

Silyl hydride **14c** (0.79 g, 0.71 mmol, 1 eq) and methyl (*R*)-2-(allyloxy)propanoate D-**31** (0.12 g, 0.85, 1.2 eq) were dissolved in dry toluene (3 mL) in a 25 mL round-bottom flask under an argon atmosphere. To this was added one drop of Karstedt catalyst (soln. in xylene, 2% Pt). The mixture was stirred at 60 °C for 3 hours (the mixture turned from colorless to light yellow/brown in a few minutes). Afterward, the solvent was removed in *vacuo*. The light brown residue was purified by automated column chromatography using hept/EtOAc (gradient 100/0 to 90/20) as eluent, giving the pure material D-**32c** (700 mg, 79 %). ^{1}H NMR (400 MHz, CDCl$_3$): δ = 3.96 (q, ^3J = 6.8 Hz, 1H, CH$_2$-O-C<u>H</u>(CH$_3$)-CO), 3.74 (s, 3H, CO-O-C<u>H</u>$_3$), 3.52 (dt, ^2J = 8.9 Hz, ^3J = 7.0 Hz, 1H, CH$_2$-C<u>H</u>$_2$-O), 3.32 (dt, ^2J = 8.8 Hz, ^3J = 7.1 Hz, 1H, CH$_2$-C<u>H</u>$_2$-O), 1.68–1.58 (m, 2H, Si(CH$_3$)$_2$-CH$_2$-C<u>H</u>$_2$-CH$_2$-O), 1.4 (d, ^3J = 6.8 Hz, 3H, O-CH(C<u>H</u>$_3$)-CO), 0.59–0.48 (m, 2H, Si(CH$_3$)$_2$-C<u>H</u>$_2$-CH$_2$-CH$_2$-O), 0.13–0.02 ppm (m, 93H, Si(C<u>H</u>$_3$)$_2$); ^{13}C NMR (100 MHz, CDCl$_3$) δ = 174.34, 75.28, 73.51, 52.17, 23.88, 19.07, 14.40, 2.14, 1.50, 1.41, 0.67, 0.44 ppm; MS (MALDI-TOF): *m/z* calcd for $C_{38}H_{106}O_{17}Si_{15}$+Na$^+$: 1277.39 [M+Na]$^+$; found 1277.46.

Synthesis of Me-Si$_{23}$-DLA$_1$-Me (D-**32e**).

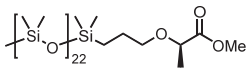

Silyl hydride **14e** (1.08 g, 0.63 mmol, 1 eq) and methyl (*R*)-2-(allyloxy)propanoate D-**31** (0.11 g, 0.76, 1.2 eq) were dissolved in dry toluene (6 mL) in a 25 mL round-bottom flask under an argon atmosphere. To this was added one drop of Karstedt catalyst (soln. in xylene, 2% Pt). The mixture was stirred at 60 °C for 3 hours (the mixture turned from colorless to light yellow/brown in a few minutes). Afterward, the solvent was removed in *vacuo*. The light brown residue was purified by automated column chromatography using hept/EtOAc (gradient 100/0 to 78/22) as eluent, giving the pure material D-**32e** (772 mg, 79 %). ^{1}H NMR (400 MHz, CDCl$_3$): δ = 3.96 (q, ^3J = 6.9 Hz, 1H, CH$_2$-O-C<u>H</u>(CH$_3$)-CO), 3.74 (s, 3H, CO-O-C<u>H</u>$_3$), 3.52 (dt, ^2J = 8.9 Hz, ^3J = 7.0 Hz, 1H, CH$_2$-C<u>H</u>$_2$-O), 3.32 (dt, ^2J = 8.8 Hz, ^3J = 7.1 Hz, 1H, CH$_2$-C<u>H</u>$_2$-O), 1.71–1.56 (m, 2H, Si(CH$_3$)$_2$-CH$_2$-C<u>H</u>$_2$-CH$_2$-O), 1.4 (d, ^3J = 6.8 Hz, 3H, O-CH(C<u>H</u>$_3$)-CO), 0.59–0.48 (m, 2H, Si(CH$_3$)$_2$-C<u>H</u>$_2$-CH$_2$-CH$_2$-O), 0.2 to −0.05 ppm (m, 141H, Si(C<u>H</u>$_3$)$_2$); ^{13}C NMR (100 MHz, CDCl$_3$) δ = 174.32, 75.29, 73.51, 52.16, 52.14, 23.90, 19.05, 14.42, 2.14, 2.13, 1.77, 1.52, 1.50, 1.48, 1.40, 1.03, 0.45, 0.35 ppm; MS (MALDI-TOF): *m/z* calcd for $C_{54}H_{154}O_{25}Si_{23}$+Na$^+$: 1869.54 [M+Na]$^+$; found 1869.56.

2.7 References

(1) Mülhaupt, R. *Angew. Chemie Int. Ed.* **2004**, *43*, 1054.

(2) Park, S.; Kwon, K.; Cho, D.; Lee, B.; Ree, M.; Chang, T. *Macromolecules* **2003**, *36*, 4662.

(3) Sun, J.; Teran, A. A.; Liao, X.; Balsara, N. P.; Zuckermann, R. N. *J. Am. Chem. Soc.* **2013**, *135*, 14119.

(4) Sun, J.; Teran, A. A.; Liao, X.; Balsara, N. P.; Zuckermann, R. N. *J. Am. Chem. Soc.* **2014**, *136*, 2070.

(5) Zeng, F.; Zimmerman, S. C. *Chem. Rev.* **1997**, *97*, 1681.

(6) Paynter, O. I.; Simmonds, D. J.; Whiting, M. C. *J. Chem. Soc. Chem. Commun.* **1982**, 1165.

(7) Bidd, I.; Whiting, M. C. *J. Chem. Soc. Chem. Commun.* **1985**, 543.

(8) Brooke, G. M.; Burnett, S.; Mohammed, S.; Proctor, D.; Whiting, M. C. *J. Chem. Soc. Perkin Trans. 1* **1996**, 1635.

(9) Lee, K. S.; Wegner, G. *Die Makromol. Chemie, Rapid Commun.* **1985**, *6*, 203.
(10) Fordyce, R.; Lovell, E. L.; Hibbert, H. *J. Am. Chem. Soc.* **1939**, *61*, 1905.
(11) Loiseau, F. A.; Hii, K. K.; Hill, A. M. *J. Org. Chem.* **2004**, *69*, 639.
(12) Ahmed, S. A.; Tanaka, M. *J. Org. Chem.* **2006**, *71*, 9884.
(13) French, A. C.; Thompson, A. L.; Davis, B. G. *Angew. Chemie Int. Ed.* **2009**, *48*, 1248.
(14) Székely, G.; Schaepertoens, M.; Gaffney, P. R. J.; Livingston, A. G. *Chemistry* **2014**, *20*, 10038.
(15) Li, Y.; Guo, Q.; Li, X.; Zhang, H.; Yu, F.; Yu, W.; Xia, G.; Fu, M.; Yang, Z.; Jiang, Z.-X. *Tetrahedron Lett.* **2014**, *55*, 2110.
(16) Shi, W.; McGrath, A. J.; Li, Y.; Lynd, N. A.; Hawker, C. J.; Fredrickson, G. H.; Kramer, E. J. *Macromolecules* **2015**, *48*, 3069.
(17) Percec, V.; Asandei, A. D. *Macromolecules* **1997**, *30*, 7701.
(18) Hawker, C. J.; Malmström, E. E.; Frank, C. W.; Kampf, J. P. *J. Am. Chem. Soc.* **1997**, *119*, 9903.
(19) Lengweiler, U. D.; Fritz, M. G.; Seebach, D. *Helv. Chim. Acta* **1996**, *79*, 670.
(20) Williams, J. B.; Chapman, T. M.; Hercules, D. M. *Macromolecules* **2003**, *36*, 3898.
(21) Takizawa, K.; Tang, C.; Hawker, C. J. *J. Am. Chem. Soc.* **2008**, *130*, 1718.
(22) Takizawa, K.; Nulwala, H.; Hu, J.; Yoshinaga, K.; Hawker, C. J. *J. Polym. Sci. Part A Polym. Chem.* **2008**, *46*, 5977.
(23) Aratani, N.; Osuka, A.; Kim, Y. H.; Jeong, D. H.; Kim, D. *Angew. Chemie Int. Ed.* **2000**, *39*, 1458.
(24) Inouchi, K.; Kobashi, S.; Takimiya, K.; Aso, Y.; Otsubo, T. *Org. Lett.* **2002**, *4*, 2533.
(25) Izumi, T.; Kobashi, S.; Takimiya, K.; Aso, Y.; Otsubo, T. *J. Am. Chem. Soc.* **2003**, *125*, 5286.
(26) Aratani, N.; Takagi, A.; Yanagawa, Y.; Matsumoto, T.; Kawai, T.; Yoon, Z. S.; Kim, D.; Osuka, A. *Chem. – A Eur. J.* **2005**, *11*, 3389.
(27) Koch, F. P. V; Smith, P.; Heeney, M. *J. Am. Chem. Soc.* **2013**, *135*, 13695.
(28) Eggen, M.; Nair, S. K.; Georg, G. I. *Org. Lett.* **2001**, *3*, 1813.
(29) Karstedt, B. D. Platinum complexes of unsaturated siloxanes and platinum containing organopolysiloxanes. US3775452, 1973.
(30) Devos, A.; Remion, J.; Frisque-Hesbain, A.-M.; Colens, A.; Ghosez, L. *J. Chem. Soc. Chem. Commun.* **1979**, 1180.
(31) Pitet, L. M.; Wuister, S. F.; Peeters, E.; Kramer, E. J.; Hawker, C. J.; Meijer, E. W. *Macromolecules* **2013**, *46*, 8289.

♦ Chapter 3 ♦

Discrete contra Disperse: Consequences of Molecular Uniformity on Block Co-Oligomer Phase Behavior

Abstract: Most of the theoretical and computational descriptions of the phase behavior of block copolymers describe chain ensembles of perfect and uniform polymers. In contrast, experimental studies on block copolymers always employ materials with disperse molecular makeup. Here, we describe properties of a series of discrete-length oligodimethylsiloxane–oligolactic acid (*o*DMS–*o*LA) block co-oligomers, featuring ultralow molar mass dispersities ($Đ \leq 1.00002$) and unique control over the co-oligomer composition. The formation of cylindrical, gyroid, and lamellar nanostructures was revealed by DSC, SAXS, and AFM. The low DP and discrete nature of the block co-oligomers results in exceptionally small feature sizes (down to 3.5 nm) and long-range organization. Partial introduction of dispersity in either one or both of the BCO blocks results in materials with dispersities ranging from <1.00001 to 1.09. Compared to the well-organized lamellae formed by discrete *o*DMS–*o*LA, we observe that an increase in the dispersity of these BCOs results in: 1) an increase of the *stability* of the microphase-segregated state, 2) a decrease of the overall *degree of ordering*, and 3) an increase of the *domain spacing*.

Part of this work has been published:
van Genabeek, B.; de Waal, B. F. M.; Gosens, M. M. J.; Pitet, L. M.; Palmans, A. R. A.; Meijer, E. W. *J. Am. Chem. Soc.* **2016**, *138*, 4210.
van Genabeek, B.; de Waal, B. F. M.; Ligt, B.; Palmans, A. R. A.; Meijer, E. W. *ACS Macro Lett.* **2017**, *6*, 674.

"The best science is carried out on pure compounds."
—Mark C. Whiting, 1997.[1]

3.1 Introduction

Block copolymers (BCPs) represent an important class of self-organizing materials and have been studied intensively for many decades. The propensity to microphase-segregate into various structures having domain sizes close to the length scale of individual chains makes such materials ideally suited for various nanotechnologies. Lithographic resists for nanoscale patterns,[2–10] ultrafiltration membranes,[11–13] stimuli-responsive materials,[14] and next-generation organic solar cells[15] highlight only few of these possible applications. Of the many different BCPs synthesized and studied, diblock copolymers are the ones that attracted most attention.

Diblock copolymers comprise two chemically distinct polymeric entities, covalently linked to generate a linear macromolecule. The microphase separation between these polymer blocks is well understood—both theoretically and experimentally—and enables chemists to control morphologies as well as feature sizes. This is mainly achieved by fine-tuning three parameters: the Flory–Huggins interaction parameter, χ; the average number of polymer segments, N;[i] and the volumetric ratio of the two blocks, expressed as the volume fraction of block A (f_A) or block B ($f_B = 1 - f_A$).[16]

Several theoretical studies have emerged that enable computations to accurately predict the properties and self-assembly behavior of block copolymers.[17–21] However, only relatively few models have accounted for chain length dispersity, mostly because of the disproportionally longer calculation times typically required for disperse systems.[22–25] On the contrary, almost every reported synthetic diblock copolymer, although called "monodisperse", exhibits molar mass dispersity to a certain extent due to remaining challenges in preparing well-defined polymers.[26] As a result, the number of examples of uniform synthetic block copolymers with high χ-parameter reported to date is very limited.[27–29]

Developing and evaluating (diblock) copolymer systems with no chain-length dispersity is very rewarding in light of increasing the fundamental understanding of molecular self-assembly behavior, allowing validation of theoretical models and from a practical point of

[i] N is the number of polymer segments, based on a predefined reference volume v. The average DP and N are related via the polymer/block density ρ and reference volume v.

view (*e.g.*, obtaining smaller feature sizes or improved long-range order. The increasing attractiveness of BCPs for emerging fields such as nanopatterning and nanofiltration initiated a desire to decrease the feature sizes and increase the long-range order of the formed morphologies, while pushing the materials ever closer to the border of (micro)phase separation.[30] Although it is rarely specifically addressed, this trend inevitably results in a higher sensitivity of the material toward absolute changes in the (average) degree of polymerization. A simple calculation shows that elongation of the A block of a A_{15}-B_{15} type BCP (*i.e.*, a BCP comprising 2 blocks of 15 A-monomers and 15 B-monomers) by only a single A-monomer already results in a ~3.3% increase in both N and f_A, which consequently may lead to complete alteration of the phase behavior. Inevitably, this also raises the question how the phase behavior is affected by chain length and composition dispersities, both of which result in *chain-to-chain* variations in N and f_A around the average values. Of particular consideration is the fact that even low disperse polymers comprise polymer chains differing up to tens of repeat units.

Recently, our group reported on the self-assembly behavior of polydimethylsiloxane-*block*-polylactide (PDMS-*b*-PLA) BCPs.[7,31] The exceptionally high χ-parameter for these two constituents[4] allows the formation of microphase-separated structures even at low N. Despite having a low dispersity, still MW dispersities $Đ > 1.05$ were obtained in all cases. In Figure 3–1, a calculated curve (Schulz–Zimm distribution) representing the molar mass distribution for a polymer dispersity $Đ = 1.05$ is shown (purple curve). Although the low dispersity value suggests otherwise, a relatively broad distribution of chain lengths is found. On the contrary, in Chapter 2 we described the synthetic routes toward perfectly uniform ($Đ \approx 1.000001$) diblock co-oligomers (BCOs) based on oligodimethylsiloxane (*o*DMS) and atactic oligolactic

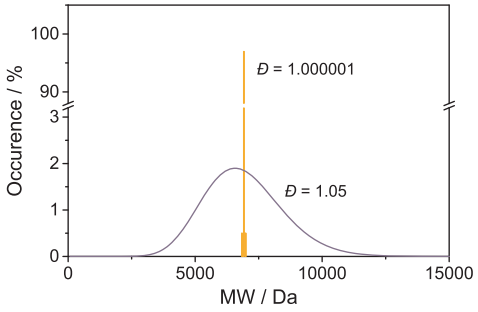

Figure 3–1. Graphical representation (calculated curves) of the Schulz–Zimm molar mass distribution of a BCP ($M_n \approx 6.9$ kDa) with a dispersity of 1.05 (in purple) and 1.000001 (in orange). The y-axis region between 3 and 90% is omitted for clarity.

acid (*at*-*o*LA). A representation for the molar mass distribution corresponding to $Đ$ = 1.000001 is provided in Figure 3–1 as the orange curve. Stimulated by the large (graphical) discrepancy between $Đ$ = 1.05 and $Đ$ = 1.000001, we studied the (microphase segregation) properties of discrete-length *o*DMS–*o*LA in detail. Also, the effect of stepwise introduction of dispersity in either one or both of the blocks is addressed.

3.2 Physical properties of atactic, discrete-length BCOs

Chapter 2 described the synthesis and molecular characterization of a library of [**Si$_x$-LA$_y$**] BCOs, comprising discrete-length *o*DMS and *at*-*o*LA. An overview of all uniform BCOs that are considered in this chapter is provided in Table 3–1, entries 1–11. As follows from the calculated number of segments N and lactic acid volume fractions f_{LA}, the materials presumably reside near the microphase segregation boundary of the BCP phase diagram, spanning multiple morphological domains. For comparison, two disperse reference PDMS–PLA block copolymers [**2.5k-Ref**] and [**10k-Ref**] (entries 12–13) are included. The reference materials were synthesized following known procedures[7] and exhibited molar mass

Table 3–1. Molecular characterization data for monodisperse block co-oligomers.

Entry	BCO[a]	M_n [Da]	N[b]	f_{LA}[c]	$Đ$[d]	T_g[e] [°C]	T_{ODT}[f] [°C]	Phase[g]	d^*[h] [nm]
1	**[Si$_{15}$-LA$_9$]**	1909	25.6	0.34	<1.00001	−32.7	-	DIS	-
2	**[Si$_{15}$-LA$_{17}$]**	2486	32.6	0.48	<1.00001	0.5	72.9	LAM[k]	7.1
3	**[Si$_{23}$-LA$_9$]**	2502	35.0	0.25	<1.00001	−32.0	20.7	DIS	-
4	**[Si$_{23}$-LA$_{11}$]**	2646	36.8	0.29	<1.00001	−21.1	42.2	CYL[k]	6.5
5	**[Si$_{23}$-LA$_{13}$]**	2791	38.5	0.32	<1.00001	−17.2	52.3	CYL	7.1
6	**[Si$_{23}$-LA$_{15}$]**	2935	40.3	0.35	<1.00001	−7.6	70.8	GYR	7.4
7	**[Si$_{23}$-LA$_{17}$]**	3079	42.0	0.37	1.00001	−6.8	82.5	GYR	7.8
8	**[Si$_{23}$-LA$_{25}$]**	3655	49.0	0.46	1.00001	9.1	148.9	LAM	8.6
9	**[Si$_{27}$-LA$_{15}$]**	3231	45.0	0.31	<1.00001	−6.6	91.3	CYL	8.0
10	**[Si$_{27}$-LA$_{25}$]**	3952	53.7	0.42	<1.00001	5.8	151.3	LAM	9.3
11	**[Si$_{59}$-LA$_{33}$]**	6901	98.5	0.30	1.00002	15.0	>250	CYL	13.7
12	**[2.5k-Ref]**	2554[i]	33.5	0.46	1.15[j]	n.d.	n.d.	DIS	-
13	**[10k-Ref]**	9700[i]	133	0.40	1.10[j]	n.d.	n.d.	CYL	17.9

[a] Number of siloxane and lactic acid repeat units, respectively; [b] Number of segments based on a 110 Å^3 reference volume; [c] Lactic acid volume fraction, calculated using bulk densities for PDMS and PLA (0.95 g/mL and 1.24 g/mL, respectively); [d] Calculated from the relative peak intensities in the MALDI-TOF mass spectra; [e] Glass transition temperature of the *at*-*o*LA block; [f] Order–disorder temperature; [g] Bulk morphology determined with SAXS at room temperature. DIS = disordered, CYL = cylindrical, GYR = gyroid, LAM = lamellar; [h] Domain spacing, calculated as $d^* = 2\pi/q^*$; [i] Calculated from ^{1}H NMR integral ratios; [j] Determined by SEC; [k] After aging for 6 months at room temperature; n.d. = not determined.

dispersities $Đ$ = 1.15 and $Đ$ = 1.10 (determined by size exclusion chromatography, SEC), respectively. In contrast, the ultralow dispersities for the discrete-length materials were confirmed by MALDI-TOF MS analysis. Based on the relative intensities of the signals corresponding to the correct and incorrect masses, dispersity values were calculated for each BCO. As already discussed in Chapter 2, only upper values for the dispersity could be extracted from the MALDI-TOF data for most BCOs because of the near-absence of molecules with the incorrect length.

3.2.1 Thermal properties of BCOs

Differential scanning calorimetry (DSC) was used to investigate the effect of chain length on the thermal transitions of the block co-oligomers. Figure 3–2 exhibits a selection of DSC traces of the [**Si$_{23}$-LA$_y$**] family. For all those BCOs, a glass transition was observed in both the heating and cooling traces. As summarized in Table 3–1, values for T_g varied between −32.0 °C and +9.1 °C, monotonically increasing with increasing f_{LA}. In addition, all block co-oligomers in the [**Si$_{23}$-LA$_y$**] series showed a second thermal transition at higher temperatures (indicated with an asterisk in Figure 3–2). In most cases, the transition was only clearly visible in the heating run, having a relatively small enthalpic footprint of 1–2 kJ mol^{-1}.

The BCOs that are not depicted in Figure 3–2 showed similar thermal behavior. Only for shortest ([**Si$_{15}$-LA$_9$**]) and longest ([**Si$_{59}$-LA$_{33}$**]) BCOs no second transition was observed in the temperature range −70 to 250 °C. For co-oligomers [**Si$_{15}$-LA$_{17}$**] and [**Si$_{23}$-LA$_{25}$**], the second transition was very narrow (less than 1 °C broad), despite the intermediate heating/cooling rate of 10 °C min^{-1}. BCOs with a lower f_{LA} showed a broader transition (over a temperature range of 5 to 6 °C). The use of a temperature ramp of 5 °C min^{-1} or 1 °C min^{-1} did not change the results significantly.

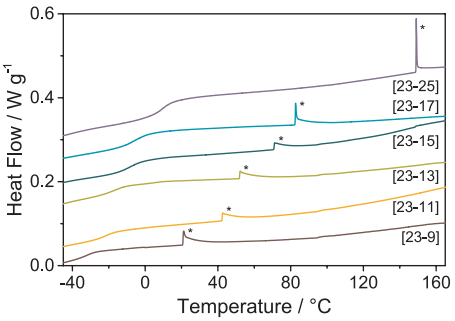

Figure 3–2. DSC traces (second heating run) of discrete-length [**Si$_{23}$-LA$_y$**] BCOs, containing 23 siloxane units. The data are shifted for clarity. Order–disorder transitions are indicated with an asterisk (*). A heating/cooling rate of 10 °C min^{-1} was used. Endothermic heatflows have a positive value.

Typically, a microphase-segregated diblock copolymer reveals two separate glass transitions, each corresponding to the glass transitions of the individual blocks. Consequently, the observation of only a single glass transition normally is indicative for a disordered (DIS) state in which mutual interactions between both molecular fragments are present. However, the T_g value of the *o*DMS blocks that were incorporated in these materials is too low to be observed with our available DSC set-up (T_g (*o*DMS) ≪ −50 °C). The single glass transition that was found for each BCO was located at considerably lower temperatures than that of the corresponding, pure *at*-*o*LA blocks (*e.g.*, for HO-LA_{16}-Bn *at*-**22s** a T_g of 19.1 °C was found). Yet, the T_g values obtained were in most cases still higher than those predicted by the Fox equation for a disordered system,[32] which suggested that the system was—at least partially—microphase-segregated. As a result, the small endothermic transition at higher temperature was attributed the order–disorder transition (ODT), during which the material converts from a microphase-segregated state into the disordered melt. Apart from a limited number of examples,[8,9,33,34] such a transition is rarely observed in DSC analyses of block copolymers. Small-angle X-ray scattering (SAXS) experiments (*vide infra*) confirm that the samples are microphase-segregated and well-organized at temperatures below the order–disorder temperature (T_{ODT}). Presumably, the lower T_g of the *at*-*o*LA blocks in the BCOs compared to that of the unfunctionalized blocks is a result of the small domain sizes in the microphase segregated system. This leads to a significant number of *o*LA–*o*DMS interactions at the domain interface, partially shifting the T_g of both blocks to a single, average value.

Additionally, an increase of T_{ODT} was observed for BCOs with increasing chain length but similar f_{LA}: [**Si_{15}-LA_{17}**], [**Si_{23}-LA_{25}**] and [**Si_{27}-LA_{25}**] (Table 3–1; entries 2, 8, and 10, respectively). Indeed, it is expected that the value for T_{ODT} increases for higher N and constant f_{LA} because of the inverse relation between the temperature and χ. Consequently, an increase in the BCO length (increase in N) should automatically lead to an increase of the temperature T for which $\chi N(T) = \chi N(T_{ODT}) \approx 10.5$.[ii]

3.2.2 Microphase segregation in bulk

Triggered by the apparent existence of an order–disorder transition above room temperature for most diblock co-oligomers, the microphase-segregated state was studied in detail by means of small-angle X-ray scattering experiments on the bulk material at room temperature. Prior to measuring, all samples were heated to a temperature 20 °C above the

[ii] Although the value for χN at T_{ODT} most certainly is not equal to 10.495 (the value for $\chi N(T_{ODT})$ for symmetrical BCOs in the strong segregation limit),[59] for simplicity we assume that, regardless of the exact values, $\chi N(T_{ODT})$ is equal for all discrete polymers studied here, and χ does not depend on N.

aforementioned T_{ODT} and slowly cooled down to room temperature. Azimuthal integration of the 2-D transmission scattering data resulted in 1-D patterns. A selection of the data collected for BCOs [**Si$_{23}$-LA$_y$**] is shown in Figure 3–3A. It was observed that most BCOs revealed a sharp principal scattering peak along with a number of (weak) higher-order

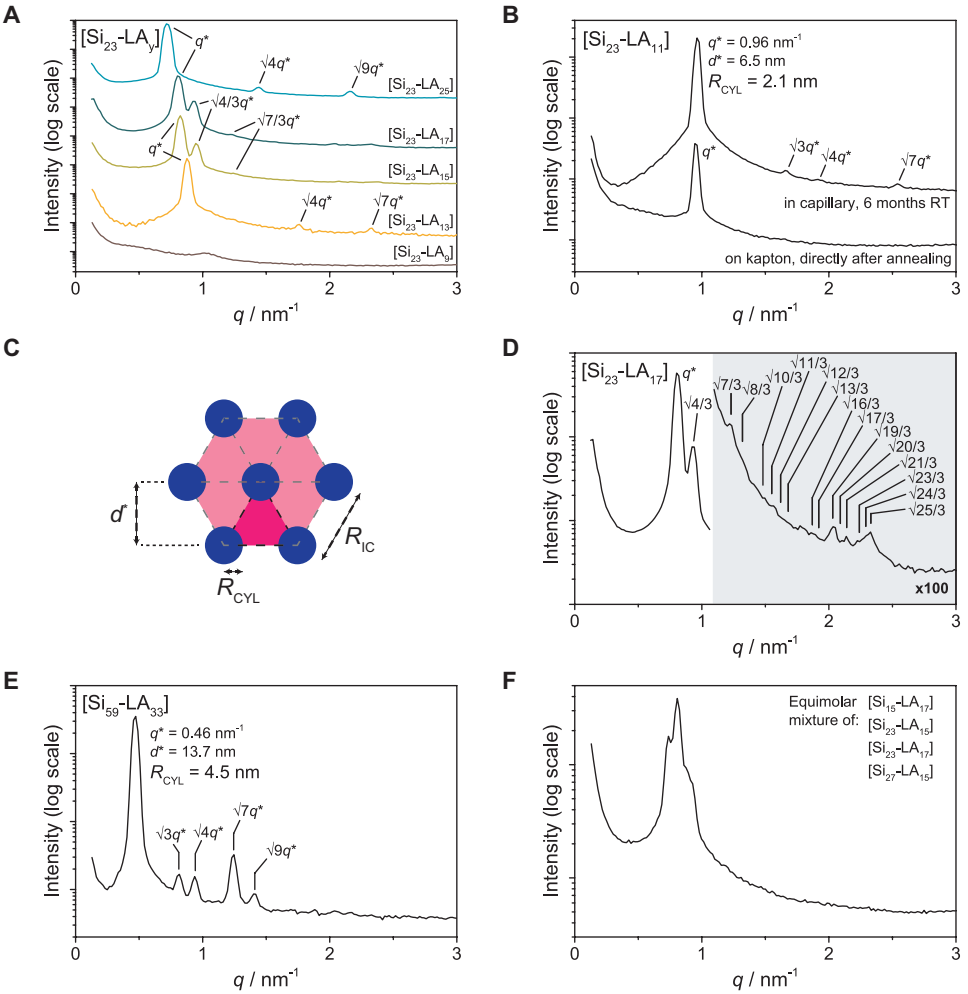

Figure 3–3. Reduced transmission-SAXS data for: (**A**) Discrete [**Si$_{23}$-LA$_y$**] BCOs. The data are shifted vertically for clarity; (**B**) BCO [**Si$_{23}$-LA$_{11}$**] directly after preparation of the sample (bottom) and after aging for 6 months in a sealed 1 mm glass capillary at room temperature (top); (**C**) Cartoon of the hexagonal packing in the cylindrical BCO morphology, including the domain spacing d^*, cylinder-to-cylinder distance R_{IC} and cylinder radius R_{CYL} of the minor block (pink = *o*DMS, blue = *at*-*o*LA); (**D**) BCO [**Si$_{23}$-LA$_{17}$**]. Expected reflections for a gyroid morphology are indicated. The signal in the blue-gray region is multiplied with a factor 100; (**E**) BCO [**Si$_{59}$-LA$_{33}$**]; (**F**) An equimolar mixture of BCOs [**Si$_{15}$-LA$_{17}$**], [**Si$_{23}$-LA$_{15}$**], [**Si$_{23}$-LA$_{17}$**] and [**Si$_{27}$-LA$_{15}$**]. Higher-order Bragg reflections are indicated for all scattering curves if present. All data were recorded at room temperature.

reflections, indicative for microphase separation at room temperature. The q-values for the maxima of the primary and higher-order reflections are labelled q^* and $\sqrt{n}q^*$, respectively, where $\sqrt{n}$ is a multiplication factor.

The scattering profile of the short, compositionally asymmetric BCOs with a low f_{LA} value, **[Si$_{15}$-LA$_9$]** and **[Si$_{23}$-LA$_9$]**, showed only low-intensity and broad principal scattering peaks at 1.17 and 1.03 nm^{-1}, respectively. This suggested that these co-oligomers were disordered, with only a weak composition inhomogeneity present at room temperature. Furthermore, repeating the measurement at −5 °C did not result in any additional ordering for both samples. This is in accordance with the absence of an ODT in the DSC trace of compound **[Si$_{15}$-LA$_9$]**. However, the presence of an ODT signature for the **[Si$_{23}$-LA$_9$]** BCO at 20.7 °C suggested that this co-oligomer should adopt a more ordered state at −5 °C. Possibly, phase segregation at a molecular level (resulting in the ODT observed by DSC) does not instantaneously lead to a (ordered) microphase-segregated system (*i.e.*, observable with SAXS). Formation of the latter might be retarded as a result of the small thermodynamic driving force for the ODT (*vide infra*),[34] requiring prolonged annealing times at temperatures between T_g and T_{ODT}.

Similarly, the scattering profile of the disperse polymer [**2.5k-Ref**] ($Đ$ = 1.15) lacked any evidence for phase segregation or composition fluctuations. In contrast, the scattering profile of the BCO **[Si$_{15}$-LA$_{17}$]**, which has comparable values for χN and f_{LA}, was dominated by a very narrow, high-intensity principal peak at q^* = 0.89 nm^{-1}. Still, the absence of higher-order reflections suggested that the presence of this scattering peak merely is a result of very strong, local composition fluctuations [iii] in the bulk material, lacking any long-range ordering. Interestingly, repetition of the scattering experiment with a sample that was stored in a glass capillary at room temperature for 6 months[iv] revealed additional reflections positioned at $\sqrt{4}q^*$ and $\sqrt{9}q^*$, indicative for a lamellar phase. Later, we found that slower cooling after annealing of the **[Si$_{15}$-LA$_{17}$]** BCO yielded samples that directly gave higher-order scattering reflections. From the position of the principal scattering peak, a principal interplanar (domain) spacing ($d^* = 2\pi/q^*$) of 7.1 nm was calculated.[v] For lamellae, this domain spacing is equal to the interlamellar distance (*i.e.*, the sum of the lamellar thicknesses of both domains of the BCO). Given the nearly symmetrical block-volume ratio, the lamellar thickness of the

[iii] The term 'microphase separation' can already be used here.

[iv] No kinetic measurements were performed; the aging period of 6 months was taken arbitrarily.

[v] Because of the limited number of detector pixels of the SAXS machine, the q-scale resolution is approximately 0.018 nm^{-1} at q = 1 nm^{-1}. Therefore, we estimate a maximum error of 2% in the domain spacings calculated from the SAXS data after calibration of the machine with silver behenate.

individual blocks is approximately 3.5 nm each. Similar behavior was observed for BCO [**Si$_{23}$-LA$_{11}$**] (Figure 3–3B). First, a singular, strong scattering peak was visible at $q^* = 0.96$ nm^{-1}, without additional Bragg reflections at higher q-values. After aging for 6 months at room temperature, the formation of hexagonally packed cylinders of the minor block (*o*LA) in a matrix of the major block (*o*DMS) was observed, as is evident from additional reflections at $\sqrt{3}q^*$, $\sqrt{4}q^*$ and $\sqrt{7}q^*$. From the value for the domain spacing ($d^* = 6.5$ nm), a cylinder-to-cylinder distance ($R_{IC} = 2d^*/\sqrt{3}$) of 7.5 nm was extracted (see also Figure 3–3C). Additionally, the following trigonometric relation can be derived, which allows an estimation of the radius of the *at-o*LA cylinders (R_{CYL}):

$$R_{CYL} = \left(\frac{2f_{LA}d^{*2}}{\sqrt{3}\times\pi}\right)^{\frac{1}{2}}$$

Using $f_{LA} \approx 0.29$ for [**Si$_{23}$-LA$_{11}$**], an *at-o*LA cylinder radius $R_{CYL} \approx 2.1$ nm was calculated. To the best of our knowledge, the dimensions of the lamellar and cylindrical structures formed by co-oligomers [**15-17**] and [**23-11**], respectively, belong to the smallest reported for a pristine diblock BCP system at the moment of discovery.[3,5,8,9,34–36] This is the more remarkable, since literature typically reports that monodisperse polymers are less able to microphase separate at low χN values.[25,37,38]

For BCO [**Si$_{23}$-LA$_{13}$**], with two additional lactic acid repeat units, no prolonged aging times were required to generate a microphase-separated system. The scattering pattern with $q^* = 0.89$ nm^{-1} ($d^* = 7.1$ nm) and additional reflections at $\sqrt{4}q^*$ and $\sqrt{7}q^*$ suggested a cylindrical morphology with $R_{IC} = 8.2$ nm and $R_{CYL} \approx 2.4$ nm. Upon further increasing f_{LA} ([**Si$_{23}$-LA$_{15}$**] and [**Si$_{23}$-LA$_{17}$**]), characteristic peaks at for instance $\sqrt{4/3}q^*$ and $\sqrt{7/3}q^*$ suggest the adoption of a gyroid morphology. In case of the [**Si$_{23}$-LA$_{17}$**] BCO, even the 16th (theoretical) reflection at $\sqrt{25/3}q^*$ could be observed (Figure 3–3D), reflecting the high level of long-range ordering in this sample. A lamellar structure was observed for BCO [**Si$_{23}$-LA$_{25}$**], with $d^* = 8.6$ nm ($q^* = 0.73$ nm^{-1}) and higher reflections at $\sqrt{4}q^*$ and $\sqrt{9}q^*$. The two 27-siloxane co-oligomers [**Si$_{27}$-LA$_{15}$**] and [**Si$_{27}$-LA$_{25}$**] showed cylindrical ($d^* = 8.0$ nm, $R_{IC} = 9.2$ nm, $R_{CYL} \approx 2.7$ nm) and lamellar ($d^* = 9.3$ nm) morphologies, respectively. This is in line with the expected structures based on the *at-o*LA volume fractions. A cylindrical structure ($d^* = 13.7$ nm, $R_{IC} = 15.8$ nm, $R_{CYL} \approx 4.5$ nm) was found for the longest co-oligomer [**Si$_{59}$-LA$_{33}$**] (Figure 3–3E). This longest BCO revealed stronger reflections at $\sqrt{3}q^*$, $\sqrt{4}q^*$, $\sqrt{7}q^*$ and $\sqrt{9}q^*$ than the shorter homologues, reminiscent of a stronger phase-segregated state and increased long-range order. The morphologies and d^* values for all BCOs are listed in Table 3–1.

To probe the effect of low-level dispersity on the self-assembly behavior of the BCOs discussed above, a 1:1:1:1-mixture of 4 BCOs (each with a different length and composition) was prepared. Equimolar amounts of BCOs [**Si$_{15}$-LA$_{17}$**], [**Si$_{23}$-LA$_{15}$**], [**Si$_{23}$-LA$_{17}$**] and [**Si$_{27}$-LA$_{15}$**] were dissolved in DCM, followed by removal of the solvent and annealing of the residual mixture above the T_{ODT} of component [**Si$_{27}$-LA$_{15}$**]. The resulting mixture had a calculated dispersity $Đ$ = 1.0090 (*i.e.*, still much lower than reference compound [**2.5k-Ref**]). The diffraction pattern of the mixture is provided in Figure 3–3F. Interestingly, not a single principal diffraction peak was obtained. Instead, the scattering data revealed a multitude of overlapping reflections. This might indicate the co-existence of multiple microphase-separated states—featuring dissimilar domain spacings—which are the result of macrophase segregation or self-sorting of the different components of the mixture. Macrophase separation has been predicted[25,39] and observed[40–43] for diblock and triblock copolymers, however, only for systems with dispersities that are considerably larger ($Đ$ > 1.5) and in a very narrow composition window, or for BCPs blends with a substantial MW difference.[44] Possibly, the discontinuous distribution of chain lengths, large differences in BCO composition of each component, or weak overall segregation resulted in the observed behavior. However, definite conclusions could not be drawn from this and other mixing experiments. The effect of dispersity on [**Si$_x$-LA$_y$**] BCO phase behavior using molecular weight distributions that better represent conventional polymers will be adressed in Section 3.3.

For a selection of co-oligomers, variable temperature SAXS experiments were performed. In Figure 3–4A, the data for BCO [**Si$_{27}$-LA$_{15}$**] are plotted. At temperatures below the T_{ODT} value found with DSC (T_{ODT} = 91.3 °C for BCO [**Si$_{27}$-LA$_{15}$**]), a sharp principal scattering peak was observed, similar to the scattering pattern found at room temperature. Apart from a slight shift of the scattering maximum at q^* to higher q-values and a gradual disappearance of higher-order reflections, almost no changes were observed in the region around the principal scattering peak upon increasing temperature to 91°C (slightly below the expected T_{ODT} value). Conversely, at T = 93 °C a discontinuous drop in the maximum scattering intensity and significant broadening of the principal scattering peak was observed. A further increase of the temperature resulted in continued broadening and loss of scattering intensity. The evolution of the inverse of the maximum scattering intensity at q^* (I^{-1}) and the squared value of the full width at half maximum of the principal scattering peak (σ^2) as function of the inverse of the temperature is plotted in Figure 3–4B. This plot clearly shows the discontinuity in both variables at $T = T_{ODT}$ as well as two linear trends at high temperatures.

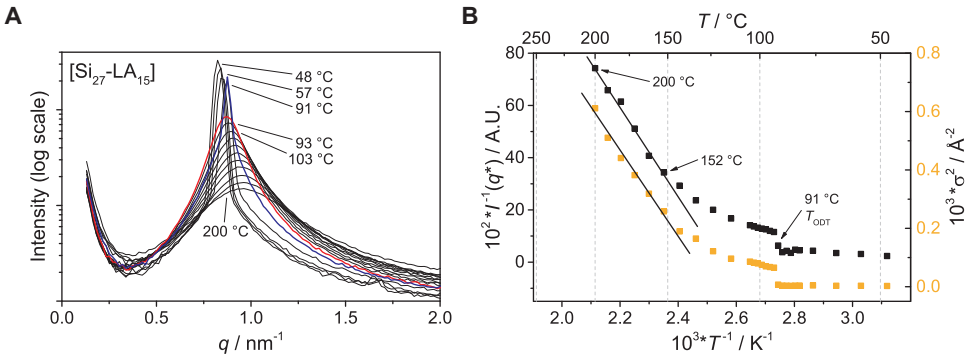

Figure 3–4. (**A**) Reduced variable temperature transmission-SAXS profiles of uniform BCO [**Si$_{27}$-LA$_{15}$**]. The blue and red curves represent the scattering profiles directly below (T = 91 °C) and above (T = 93 °C) the order–disorder transition temperature; (**B**) Inverse of the maximum scattering intensity at q^* ($I^{-1}(q^*)$, left y-axis, black squares) and the squared value of the full width at half maximum of the principal scattering peak (σ^2, right y-axis, orange squares) of BCO [**Si$_{27}$-LA$_{15}$**] as function of the inverse of the absolute temperature (T^{-1}). For convenience, the temperature in °C is provided as the top x-axis. Black, continuous lines are linear fits though data points for T = 152 °C and higher.

The latter is perfectly in line with mean-field theory predictions using the random phase approximation.[16,45] Deviation of the data from the linear curve at lower T is a direct result of the thermal fluctuation effect, and can be seen as non-mean-field behavior.

3.2.3 Thin-film morphologies

After the observation of microphase-segregated structures by X-ray scattering, we evaluated the presence of ordered nanostructures in a thin film (thickness < 20 nm) of the co-oligomers [**Si$_{27}$-LA$_{15}$**] and [**Si$_{59}$-LA$_{33}$**] with tapping-mode atomic force microscopy (TM-AFM). As a control, we also studied a 10 kDa PDMS–PLA reference compound [**10k-Ref**] ($Đ$ = 1.10, Table 3–1, entry 13). All three compounds formed cylindrical structures in the bulk materials. A uniform, thin co-oligomer film was prepared by spincoating of a 0.6 wt % solution of the BCO in methylcyclohexane (MCH) onto a flat silicon substrate with an anti-reflective top-coating (ARC) of 93 nm thick. Important to note here is that initially no annealing steps were applied after the preparation of the thin layer.

The AFM height image of the spincoated compound [**Si$_{27}$-LA$_{15}$**] revealed terrace formation (Figure 3–5A). Height profiles, extracted from different regions of the image (see for example Figure 3–5B), indicated that height fluctuations at each terrace were small (<1 nm). Moreover, a constant height difference of 8.5±1 nm was found between two consecutive layers. This value is commensurate with the domain spacing that was extracted from the SAXS data for this BCO (d^* = 8.0 nm). Based on these results and the tendency for this

material to form a cylindrical microstructure in bulk, we assume that the film consists of a matrix of *o*DMS, in which *o*LA rich cylinders are present as discrete layers, oriented parallel to the wafer surface (Figure 3–5C). This is in accordance with previous results obtained with a similar (disperse) PDMS–PLA system[7] and confirmed by the presence of a fingerprint-like line pattern in the phase image at 500 × 500 nm resolution (Figure 3–5D).The alternating light and dark lines in this image correspond to the cylinders of *at*-*o*LA and the *o*DMS matrix, respectively. A clearer image was obtained at 150 × 150 nm resolution (inset). Yet, obtaining images with enough contrast (*i.e.*, phase difference) proved to be extremely difficult. In the most optimal case, a maximal phase difference between the *o*DMS and *o*LA regions of approximately 2 degrees was found. Probably, the low contrast is a result of the slight intermixing of the *at*-*o*LA and *o*DMS blocks, decreasing the difference in Young's moduli and thus phase difference between the two segregated blocks. Moreover, the surface of the

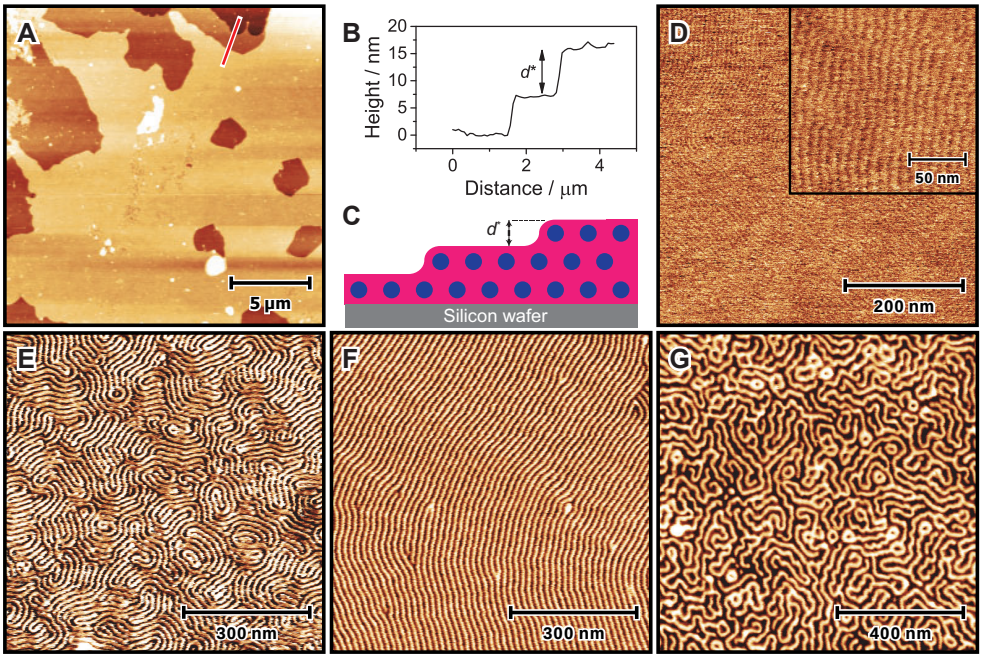

Figure 3–5. Tapping mode AFM images of BCOs [**Si$_{27}$-LA$_{15}$**] **(A–D)**, [**Si$_{59}$-LA$_{33}$**] **(E–F)** and [**10k-Ref**] **(G)** as thin films on an ARC-modified silicon wafer: (**A**) Height image (light = high, dark = low regions). with (**B**) extracted height profile along the red line and (**C**) cartoon of the cross-section perpendicular to the wafer surface along the red line (pink = *o*DMS, blue = *at*-*o*LA). Although the cartoon suggests that the *o*DMS block wets the wafer surface, the exact morphology of the wetting layer is unknown; (**D**) Phase image of BCO [**Si$_{27}$-LA$_{15}$**] monolayer, including an inset at higher magnification; (**E**) Phase image of BCO [**Si$_{59}$-LA$_{33}$**] before annealing; (**F**) Phase image of BCO [**Si$_{59}$-LA$_{33}$**] after annealing; (**G**) Phase image of disperse BCP [**10k-Ref**] after annealing. Light = *at*-*o*LA, dark = *o*DMS.

BCO film is anticipated to be covered with a soft and sticky *o*DMS layer, because of the low surface energy of this material with respect to that of *at*-*o*LA.[36,46] In combination with the extremely small feature sizes, this further complicates the visualization of the underlying small cylinders.[36] Nevertheless, a cylinder-to-cylinder distance of 9.1 nm could be extracted from the phase image by fast Fourier transform analysis, which agrees very well with the value found with X-ray scattering (R_{IC} = 9.2 nm).

As expected, co-oligomer [**Si$_{59}$-LA$_{33}$**] formed a similar type of microstructure, composed of an *o*DMS matrix with *at*-*o*LA cylinders ($R_{IC,\ AFM}$ = 15.1 nm) parallel to the wafer surface (Figure 3–5E). Due to the stronger segregation of this longer BCO and slightly larger features, a more pronounced phase difference between the *at*-*o*LA and *o*DMS blocks was measured, resulting in better contrast in the phase images. Interestingly, the image revealed less long-range ordering of the *o*LA cylinders compared to the structure formed by BCO [**Si$_{27}$-LA$_{15}$**]. We propose that this decreased order is a direct result of the higher stiffness and thus lower chain mobility of the longer BCO at room temperature. Indeed, after thermal annealing of the spincoated sample for 2 hours in vacuum at 120 °C, a system with much improved long range ordering was obtained (Figure 3–5F).

Cylindrical features oriented parallel to the substrate could also be observed for disperse reference BCP [**10k-Ref**]. In Figure 3–5G, an AFM phase image for the reference BCP is provided, representing the best possible quality of long-range ordering that could be obtained after annealing. Again, the intercylinder distance that was extracted from the micrographs (22 nm) was in good agreement with the value obtained from SAXS experiments (R_{IC} = 21 nm). However, the cylindrical structures are less aligned than the corresponding structures observed for discrete-length [**Si$_{59}$-LA$_{33}$**]. Also, the variability in the thickness of the intercylinder *o*DMS domains is larger.

3.2.4 Self-assembly in confined space

A promising strategy to gain more control over BCP self-assembly is the use of substrates containing prefabricated, nanoscopic structures that can act as a template to guide the orientation of the (smaller) microphase-separated domains of the BCP.[47] Apart from introducing better long-range order, this form of templated or directed self-assembly enables better spatial control—ideally extended into the micron to millimeter regime—over the nanometer-sized BCP features. However, it has been observed that the combination of strong spatial confinement and weakly segregating (*i.e.*, low-MW) BCPs often leads to the formation of mixed morphologies.[48] Such defects represent an obstacle to harnessing the full potential of directed BCP self-assembly in down-stream fabrication processes.

To evaluate the effect of packing frustration on the phase separation of uniform BCOs, a custom made silicon wafer substrate was used. The substrate contained hexagonal or rectangular arrays of cylindrical contact holes (CHs) with diameters ranging from 20 to 70 nm and was generously provided by Imec (Leuven, Belgium). Discrete BCO [**Si_{59}-LA_{33}**] or disperse control [**10k–Ref**] were spincoated from a 0.5–1 w% solution in MCH onto the substrate, and subsequently annealed for 30 minutes in vacuum at 130 °C. The samples were then studied with TM-AFM. Representative AFM height images are depicted in Figure 3–6A–C. Figure 3–6A shows a small region of the bare wafer (without polymer). In the image, a square 10 × 10 micron array of 48 nm diameter CHs could be observed (appearing as dark, individual dots; depth ≈ 70 nm), with a hole-to-hole spacing of 200 nm (approximately 2500 contact holes in total for this array). In contrast, the wafer that was treated with the 1 w% BCO [**Si_{59}-LA_{33}**] solution was almost fully covered with the polymeric material (Figure 3–6B). Three regions with different heights could be distinguished, having height differences matching the bulk domain spacing of the cylinder-forming BCO. This observation conforms to the results obtained with the thin-film studies in the previous section. Most probably, from the highest to the lowest, these three regions correspond to the wafer that is covered with a BCO layer with a thickness of two, one and zero times the domain spacing, respectively. The latter resembles the uncovered wafer, in which only the contact holes are filled with the BCO due to strong capillary forces.

To have a clear view on the BCO morphologies that are formed inside the contact holes, it was desirable to decrease the coverage of the wafer with excess BCO as far as possible, whilst keeping completely filled contact holes. Therefore, the polymer concentration in the solution used for spincoating was lowered to 0.5 w%. Indeed, a wafer treated with this polymer solution only exhibited regions with either no material or a monolayer of BCO (Figure 3–6C).

At 1400 × 1400 nm resolution, it was possible to observe the microphase segregation of the BCO (both inside the CHs as well as in the monolayer covering a portion of the wafer, see Figure 3–6D-I). First, we imaged a wafer that was spincoated with disperse reference BCP [**10k-Ref**]. The region of the wafer that represented in Figure 3–6D contained 50 nm contact holes. We observed that roughly 70% of the wafer surface contained no polymeric material on top of the CH features. Here, only material was present inside the contact holes. The remainder was covered with a microphase-segregated monolayer of BCP, comprising *at-o*LA cylinders that were oriented parallel to the surface. This layer closely resembled the structures formed by the disperse BCP on a flat wafer, as provided in Figure 3–5G. A closer look to the

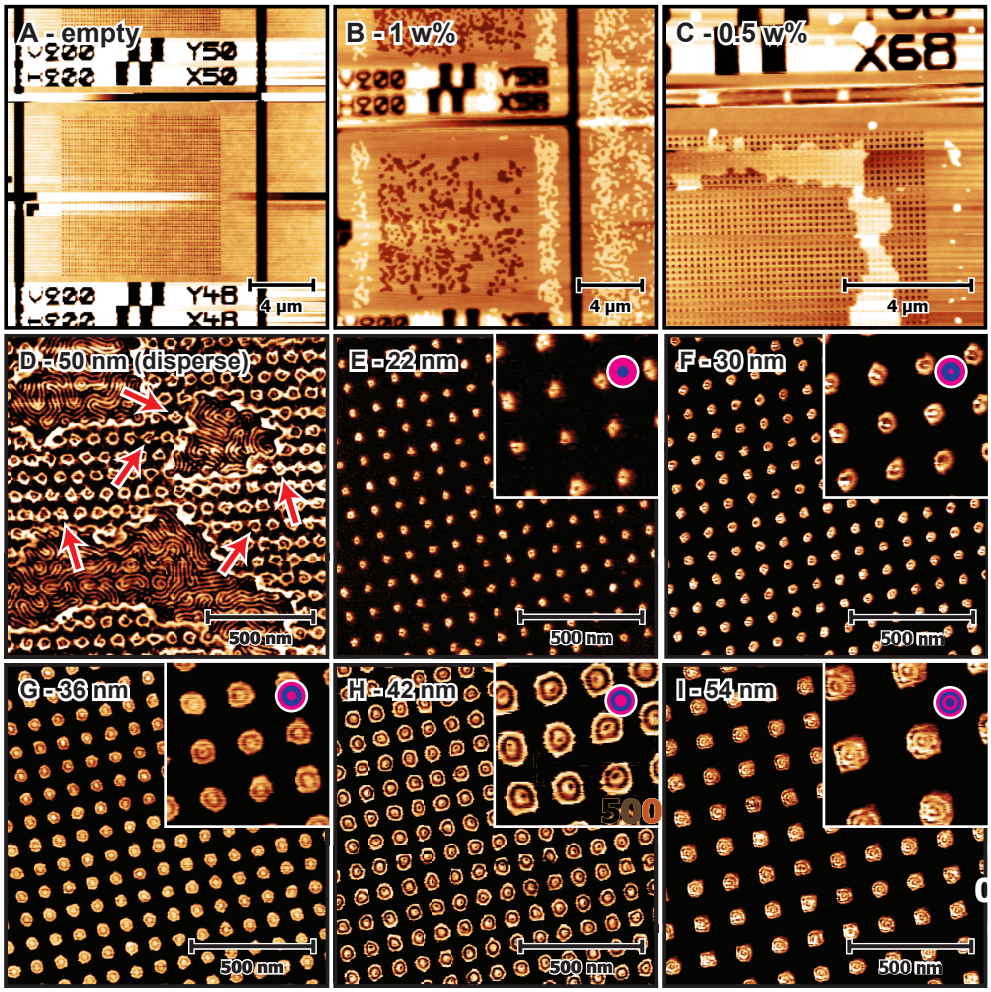

Figure 3–6. (**A–C**) AFM height images (tapping mode) of a silicon wafer with contact holes: (**A**) 48 nm diameter contact holes without polymer (bare wafer); (**B**) 56 nm diameter contact holes after spincoating with a 1 w% solution of monodisperse BCO [**Si$_{59}$-LA$_{33}$**] in MCH; (**C**) 66 nm diameter contact holes after a similar treatment as image (B), but using a 0.5 w% solution of BCO. High regions appear light, low regions appear dark; (**D**) AFM phase image (tapping mode) of disperse polymer [**10k-Ref**], spincoated from 0.5 w% MCH solution in contact holes with a diameter of 50 nm. A select number of odd structures is indicated with the red arrows; (**E–I**) AFM phase images (tapping mode) of monodisperse BCO [**Si$_{59}$-LA$_{33}$**], spincoated from 0.5 w% MCH solution in contact holes with a diameter of: (**E**) 22 nm; (**F**) 30 nm; (**G**) 36 nm; (**H**) 42 nm, (**I**) 54 nm. All samples were thermally annealed for 30 minutes at 130 °C in vacuum after spincoating. The insets show a 2× magnified detail of the original micrograph. Graphical representations of the formed morphologies are included for images (E-I) (pink = *o*DMS, blue = *at*-oLA).

polymeric material inside the contact holes revealed that hollow-cylinder-type morphologies were generated. However, also a large number of odd morphologies could be observed (a select number is indicated with the red arrows). These results were in good accordance with measurements conducted before.[48]

Subsequently, the self-assembly of discrete-length [**Si_{59}-LA_{33}**] in various contact hole sizes was examined. A selection of micrographs is shown in Figure 3–6E–I. For CH diameters smaller than 50 nm, remarkably uniform and (centro)symmetrical structures were found for each CH size. Yet, a clear dependence of the morphology on the CH diameter was noticeable. First, the smallest contact holes (⌀22–24 nm) contained structures consisting (probably) of a cylindrical *o*LA core, surrounded by *o*DMS (Figure 3–6E). Upon increasing the CH diameter to 26–36 nm, a new structure was formed, consisting of a hollow *o*LA cylinder with a *o*DMS core and outer shell (Figure 3–6F–G). Here, a larger number of defects was found. Again, a new structure was found for CH dimensions between 40 and 46 nm (Figure 3–6H), containing an additional *o*LA core. Further increasing the CH size lead to more distorted morphologies (Figure 3–6I). However, all structures are by far more uniform than those found for the disperse BCP.

Finally, a remark has to be placed here regarding the wall-coverage and 3-D morphology of the BCOs inside the CHs. In the cartoons, we image the CH wall to be always in contact with the *o*DMS block. This is based on the combined observations in the AFM phase images (as described above) and the simultaneously obtained height images that revealed the CH edges. However, it is known that *o*DMS has very poor wettability characteristics for nearly all surfaces, including the wafer top-layer. Hence, it might be possible that the outer shell of the self-assembled BCO structures, which is in contact with the CH template, consists of a very thin *at-o*LA layer that could not be observed here due to the limited resolution. Additionally, we are unsure of the 3-D morphology of the BCO inside the CHs. Although it is desirable and tempting to assume that the *cylinder-in-cylinder* structures remain uniform throughout the full depth of the CH, simulations already showed that more exotic structures may form.[17] As a follow-up study, selective removal of the *o*LA block by, for example, reactive ion etching, followed by evaluation of the remaining silica nano-objects by scanning electron microscopy might provide more insight into the exact 3-D structure.

3.3 A systematic introduction of dispersity in diblock co-oligomers

In the previous section, an intriguing difference in microphase behavior was noticed between the discrete-length *o*DMS–*o*LA BCO [**Si$_{15}$-LA$_{17}$**] and the analogous, disperse PDMS–PLA reference material [**2.5k-Ref**] with a dispersity $Đ$ = 1.15. This encouraged us to perform a more systematic study of discrete *versus* disperse blocks in low-MW BCOs, particularly since our observations contradict the work of Hillmyer *et al.*,[22,38,49] Mahanthappa *et al.*,[40,50,51] Matsushita *et al.*,[42,52] and numerous theoretical models.[24,37,53]

3.3.1 Synthesis and molecular characterization

To isolate block dispersity as the only variable that can influence the BCO properties, it is important to recognize the differences in endgroups and interblock connectivity that are present within the couple [**Si$_{15}$-LA$_{17}$**] and [**2.5k-Ref**]. Despite the similar (average) molecular weight and *at-o*LA volume fraction, these variations might induce phase behavior differences that are not solely the result of chain length dispersity. Therefore, we envisioned a new set of co-oligomers that have almost identical endgroups and interblock connectivity, but embody four different types of dispersity: 1) discrete *o*DMS + discrete *at-o*LA; 2) disperse *o*DMS + discrete *at-o*LA; 3) discrete *o*DMS + disperse *at-o*LA; 4) disperse *o*DMS + disperse *at-o*LA (Figure 3–7). Both for practical reasons (commercial availability of the starting materials) and to minimize the risk of encountering undesired morphology changes upon changing the dispersity, we aimed for a symmetric BCO ($f_{LA} \approx 0.5$) with (average) block lengths of 15 siloxane and 17 lactic acid repeat units.

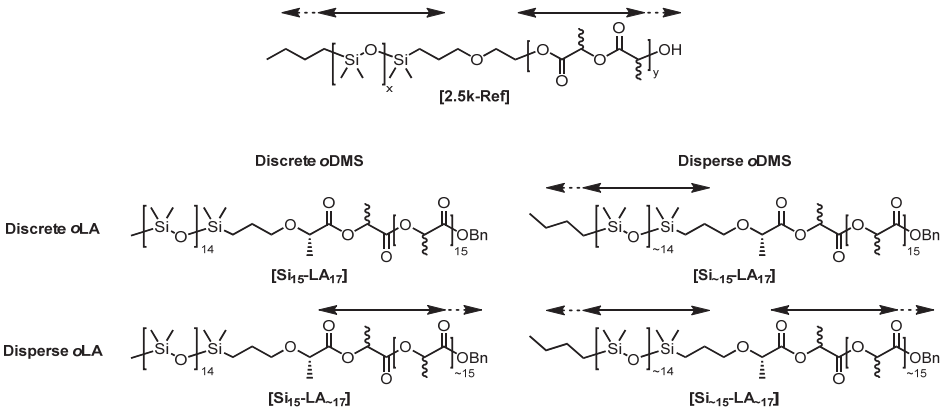

Figure 3–7. Molecular structure of disperse BCP [**2.5k-Ref**] (top), and design of (partially) disperse *o*DMS–*o*LA BCOs with average block sizes of 15 siloxane and 17 lactic acid repeat units (bottom). The double-headed arrow with variable length and the tilde (~) character indicate dispersity.

The design required the synthesis of disperse variants of the acid functionalized *o*DMS L-**28c** and *at*-*o*LA *at*-**22s**. Then disperse and discrete *o*DMS and *at*-*o*LA can be coupled using the same carbodiimide-facilitated esterification as described in Chapter 2. In this way, the dispersity in each of the 2 blocks can be tuned independently. Disperse *o*LA *at*-**34-PC** was synthesized with an uncontrolled condensation reaction of racemic lactic acid dimer **21**, which was initially obtained via ring-opening of DL-lactide **20** with water (Scheme 3–1, top). A subsequent, carbodiimide-mediated polycondensation (PC) reaction of this compound with the appropriate amount of benzyl alcohol as a chain stopper resulted in the desired disperse block. For comparison, we also prepared another disperse *o*LA block *at*-**34-ROP** by a more commonly employed ring-opening polymerization (ROP) of DL-lactide with benzyl alcohol, in the presence of catalytic amounts of 1,8-diazabicyclo[5.4.0]undec-7-ene (DBU).

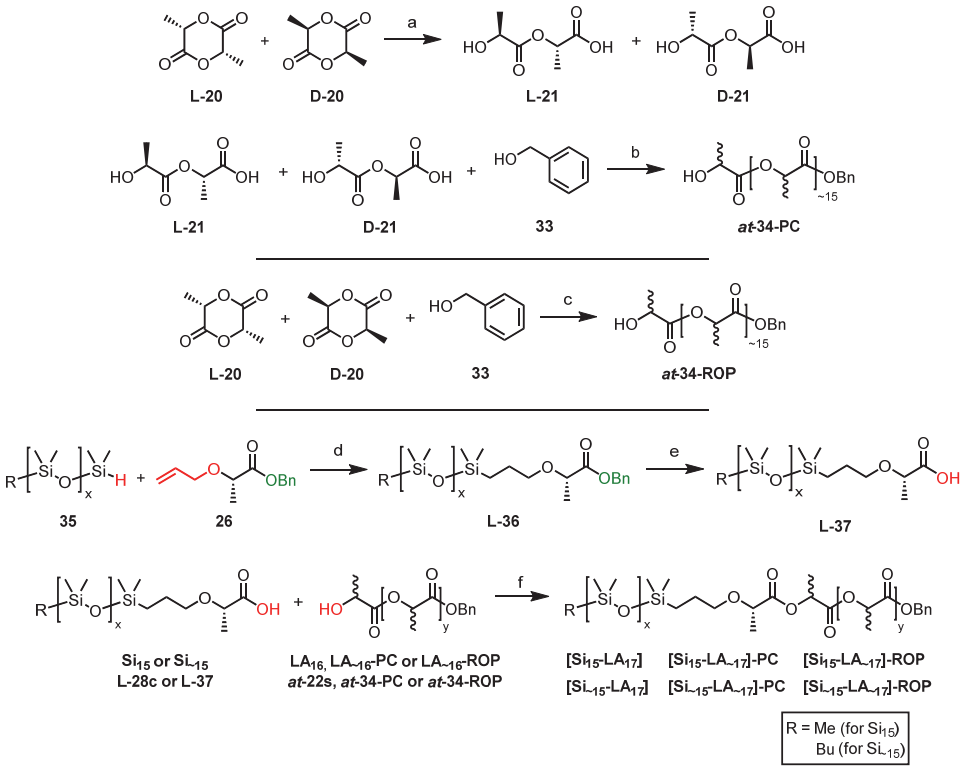

Scheme 3–1. Synthesis of disperse *at*-*o*LA by polycondensation (top) and ring-opening polymerization (middle), and synthesis of (partially) disperse [$\mathbf{Si_x}$-$\mathbf{LA_y}$] BCOs (bottom). Dormant and reactive endgroups are depicted in green and red, respectively. Reagents and conditions: (a) water, 60 °C, 4 h (97%); (b and f) EDC·HCl, DPTS, DCM, RT, O/N (41–82%); (c) DBU, DCM, RT, 1 h (quant.); (d) Karstedt catalyst, toluene, 60 °C, 3 h (86%); (e) H_2, Pd/C, EtOAc, RT, 2 h (56%). EDC·HCl = *N*-(3-dimethylaminopropyl)-*N*'-ethylcarbodiimide hydrochloride, DPTS = 4-(dimethylamino)pyridinium 4-toluenesulfonate, DBU = 1,8-diazabicyclo[5.4.0]undec-7-ene.

The disperse *o*DMS block L-**37** was prepared from commercially available *o*DMS hydride **35** (DP ≈ 15; M_n ≈ 1150 Da) (Scheme 3–1, bottom). Although this material is endcapped with a butyl instead of a methyl group, we assume that this has a negligible effect on the material properties. Following the strategy described in Chapter 2, derivatization of this hydride with allyl functionalized L-lactic acid and subsequent removal of the peripheral benzyl group gave the required disperse siloxane block.

Finally, coupling of the two different *o*DMS and three different *at*-*o*LA blocks resulted in 6 BCOs: [**Si$_{15}$-LA$_{17}$**],[vi] [**Si$_{\sim 15}$-LA$_{17}$**], [**Si$_{15}$-LA$_{\sim 17}$**]-**PC**, [**Si$_{\sim 15}$-LA$_{\sim 17}$**]-**PC**, [**Si$_{15}$-LA$_{\sim 17}$**]-**ROP** and [**Si$_{\sim 15}$-LA$_{\sim 17}$**]-**ROP**. The disperse blocks are indicated with a tilde (~) character preceding the (desired) average block lengths, and the methods used for the synthesis of the *at*-*o*LA blocks are abbreviated as **PC** and **ROP** for polycondensation and ring-opening polymerization, respectively. All newly synthesized materials were purified by automated column chromatography. As expected, the product peak in the elution profiles of the disperse blocks

Table 3–2. Molecular characterization data for the block co-oligomers and separate blocks.

Entry	Compound[a]	#Si[b]	#LA[c]	$M_{n,NMR}$[d] [Da]	$M_{n,SEC}$ [Da]	$Đ$	N[e]	f_{LA}[f]	T_{ODT}[g] [°C]	d^*[h] [nm]
1	**Si$_{15}$**	15	-	1242	n.d.	<1.00001[j]	17.7	-	-	-
2	**Si$_{\sim 15}$**	15.2[i]	-	1299[i]	1360	1.15	18.7[i]	-	-	-
3	**LA$_{16}$**	-	16	1261	n.d.	<1.00001[j]	12.7	-	-	-
4	**LA$_{\sim 16}$-PC**	-	16.0[i]	1261[i]	1787	1.24	12.7[i]	-	-	-
5	**LA$_{\sim 16}$-ROP**	-	17.9[i]	1398[i]	2265	1.23	14.2[i]	-	-	-
6	[**Si$_{15}$-LA$_{17}$**]	15	17	2486	3852	<1.00001[j]	32.6	0.48	72.9	7.10
7	[**Si$_{\sim 15}$-LA$_{17}$**]	15.2[i]	17	2543[i]	4118	1.05	32.8[i]	0.47[i]	77.1	7.34
8	[**Si$_{15}$-LA$_{\sim 17}$**]-**PC**	15	16.2[i]	2429[i]	4015	1.08	30.5[i]	0.44[i]	82.9	7.20
9	[**Si$_{\sim 15}$-LA$_{\sim 17}$**]-**PC**	15.0[i]	16.7[i]	2464[i]	3999	1.09	30.9[i]	0.45[i]	-	7.45
10	[**Si$_{15}$-LA$_{\sim 17}$**]-**ROP**	15	21.0[i]	2774[i]	4964	1.07	36.1[i]	0.52[i]	79.5	7.72
11	[**Si$_{\sim 15}$-LA$_{\sim 17}$**]-**ROP**	15.0[i]	19.4[i]	2701[i]	4547	1.09	34.7[i]	0.51[i]	83.0	-

[a] **Si$_x$** and **LA$_y$** are a shorthand notation for Me-Si$_x$-LLA$_1$-COOH and HO-LA$_y$-Bn, respectively. Disperse blocks are indicated with a tilde (~) character preceding the (desired) average block lengths; [b] Number of siloxane repeat units; [c] Number of lactic acid repeat units. Determined with ^{1}H NMR; [d] Determined from the number of Si and LA repeat units; [e] Number of segments based on a 110 Å^3 reference volume; [f] Lactic acid volume fraction, calculated using bulk densities for PDMS and PLA (0.95 g/mL and 1.24 g/mL, respectively); [g] The reported values are for the heating run; [h] Domain spacing attributed to lamellar ordering; [i] Average value; [j] Calculated from relative peak intensities in the MALDI-TOF spectra.

[vi] The synthesis and properties of [**Si$_{15}$-LA$_{17}$**] are already described in Chapter 2 and preceding sections of this chapter.

and BCOs showed a significant broadening with respect to that of the discrete versions. To some extent, overlap with impure fractions was observed. Care was taken not to alter the molecular weight distribution of the disperse materials significantly by collecting small fractions and recombining all fractions with high enough purity. Full molecular analysis with ^{1}H NMR, ^{13}C NMR, MALDI-TOF MS, and SEC confirmed the excellent purity of all compounds.

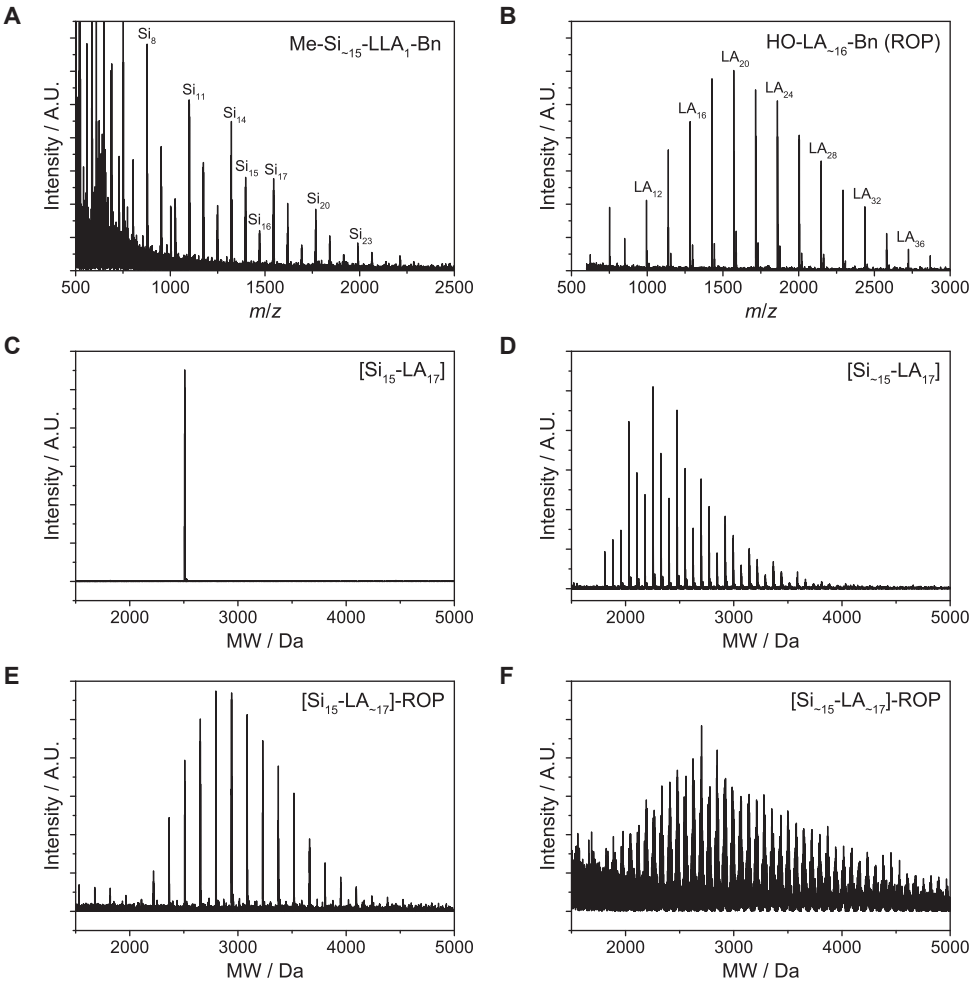

Figure 3–8. MALDI-TOF MS spectra (DCTB matrix) of (**A**) Disperse *o*DMS **36**; (**B**) Disperse *at-o*LA **34-ROP**; (**C–F**) [$\mathbf{Si_x}$-$\mathbf{LA_y}$] BCOs with various dispersities.

As depicted in Table 3–2, entries 1–5, comparable values for $M_{n,NMR}$ are found for the disperse blocks and the related discrete versions. These average MWs were calculated using the number of siloxane and lactic acid repeat units (determined with ^{1}H NMR) in the individual blocks or BCOs The M_n values of the *o*LA blocks and BCOs found with SEC differ significantly from those calculated from the number of repeat units as a result of the larger hydrodynamic volume of the *o*LA block in the SEC eluent (THF), thus resulting in a shorter elution time compared to the polystyrene standards with which the machine was calibrated. Nevertheless, dispersity values could be extracted from the elution data. Also, MALDI-TOF MS revealed the stark contrast between disperse and discrete samples for both the *o*DMS and *at*-*o*LA blocks. The disperse variants contained at least 15 different oligomers (spectra for disperse *o*DMS and *at*-*o*LA are depicted in Figure 3–8A and B). Similar observations were made for the BCOs (entries 6–11; Figure 3–8C–F). Here, purification of the final product by column chromatography led to a slightly larger offset in the average *at*-*o*LA block length for the BCOs with a disperse *at*-*o*LA block obtained by ROP (entries 10 and 11). Still, all BCOs exhibited *at*-*o*LA volume fractions that were close to the desired fully symmetrical composition. Finally, dispersities of the BCOs ranged between $Đ < 1.00001$ for the uniform BCO and $Đ = 1.09$ for both BCOs with two disperse blocks. Intermediate values for $Đ$ were found for the BCOs comprised of one discrete and one disperse block. Hence, this set of polymers is a perfect addition to previously studied BCOs that only explored the regime $Đ > 1.10$.[22,38,49]

3.3.2 Thermal behavior

The thermal behavior of the BCOs was studied with differential scanning calorimetry (DSC). As shown in Figure 3–9A and summarized in Table 3–2, entries 6–11, this afforded the temperatures of the order–disorder transitions, represented by endo- and exothermal transitions in the heating and cooling curves, respectively.[34] Interestingly, the ODT of nearly each BCO could be visualized by DSC, regardless of the presence of dispersity in either of the blocks. Only for BCO [**Si**$_{\sim 15}$-**LA**$_{\sim 17}$]-**PC**, no ODT was observed. For the other BCOs, the sharpness and position of the peaks varied significantly. Compounds [**Si**$_{15}$-**LA**$_{17}$] and [**Si**$_{\sim 15}$-**LA**$_{17}$], both with discrete-length *at*-*o*LA blocks, gave narrow ODT signatures. In contrast, dispersity in the lactic acid block ([**Si**$_{15}$-**LA**$_{\sim 17}$]-**PC**, [**Si**$_{15}$-**LA**$_{\sim 17}$]-**ROP** and [**Si**$_{\sim 15}$-**LA**$_{17}$]-**ROP**) resulted in significantly broader order–disorder transitions. Although not fully understood, this is probably related to the somewhat higher dispersity of the *at*-*o*LA block with respect to the *o*DMS block. In addition, a strong correlation between T_{ODT} and the dispersity was observed: T_{ODT} increased from $T_{ODT} = 72.9$ °C for the monodisperse [**Si**$_{15}$-**LA**$_{17}$]

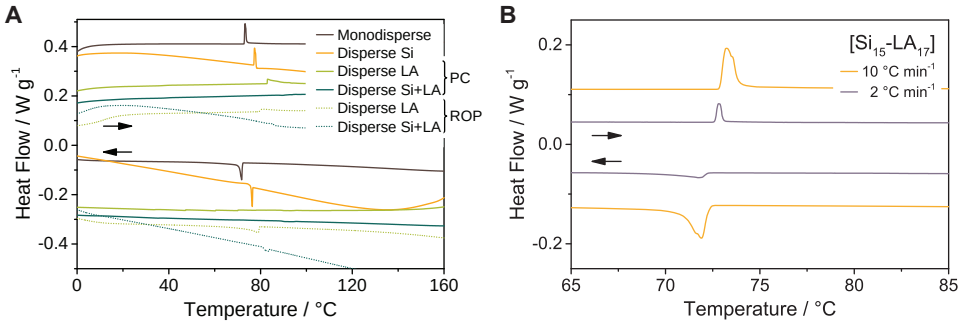

Figure 3–9. DSC traces (second cycle) for: (**A**) *o*DMS–*o*LA with various dispersities. Dotted lines represent BCOs containing *at*-*o*LA blocks obtained by ROP. A heating/cooling rate of 10 °C min^{-1} was used; (**B**) BCO [**Si$_{15}$-LA$_{17}$**] using a heating/cooling rate of 10 °C min^{-1} (orange trace) or 2 °C min^{-1} (purple trace). The data are shifted vertically for clarity. Endothermic heatflows have a positive value.

up to T_{ODT} = 83.0 °C for BCO [**Si$_{\sim 15}$-LA$_{\sim 17}$**]-**ROP** that has the highest dispersity ($Đ$ = 1.09). This suggests that the materials with higher dispersity are stable for lower values of χN ($\chi \propto T^{-1}$), and hence can be considered to have a more stable microphase-segregated state, exactly as described by theoretical and experimental work.[38,54] Noteworthy here is the assumption that kinetic effects do not play a dominant role in the determination of T_{ODT} with DSC. The justifiability of this assumption follows from the small hysteresis between the transitions of each BCO in the heating and cooling run, as well as the negligible shift of T_{ODT} of, for example, [**Si$_{15}$-LA$_{17}$**] or [**Si$_{\sim 15}$-LA$_{17}$**] when the DSC measurement was repeated at 5 and 20 times lower heating and cooling rates (*i.e.*, 2 °C min^{-1} and 0.5 °C min^{-1}, respectively; see Figure 3–9B).

3.3.3 Microphase behavior

The extent of microphase separation in the BCOs was studied with SAXS at room temperature. Azimuthal integration of the 2-D transmission scattering data resulted in 1-D patterns depicted in Figure 3–10. When focussing on the q-range 0.1–4 nm^{-1}, which corresponds to a size domain of approx. 1.6–60 nm, both [**Si$_{15}$-LA$_{17}$**] and [**Si$_{\sim 15}$-LA$_{17}$**] revealed a sharp principal scattering peak at q^* = 0.885 nm^{-1} and q^* = 0.856 nm^{-1}, respectively.[vii] This corresponds to domain spacings d^* = 2π/q^* = 7.10 nm for [**Si$_{15}$-LA$_{17}$**] and d^* = 7.34 nm for [**Si$_{\sim 15}$-LA$_{17}$**]. Additional reflections at q-values $\sqrt{4}q^*$ (both BCOs) and $\sqrt{9}q^*$ (uniform BCO only) confirmed the lamellar ordering of the samples. Increasing the dispersity in the *o*DMS block had a negative—albeit small—effect on the quality of microphase separation. Besides, a small but significant decrease in q^* (*i.e.*, an increase of the domain spacing) was observed after introduction of dispersity in the siloxane block. This is in line with SCFT predictions

[vii] The relative difference is significantly larger than the estimated machine resolution.

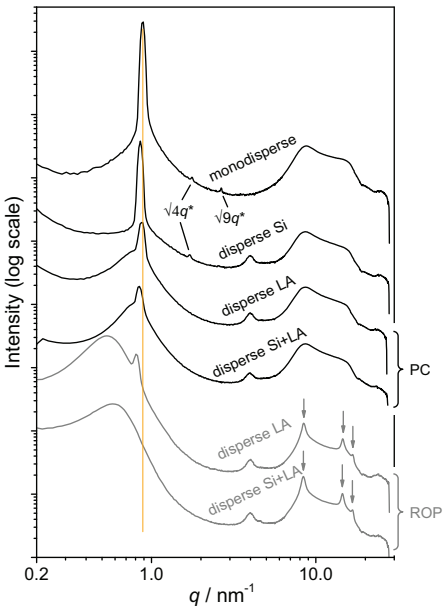

Figure 3–10. Reduced transmission-SAXS data for discrete and (partially) disperse BCOs. The data are shifted vertically for clarity. Higher-order Bragg reflections are indicated if present. The peak at q = 4 nm^{-1} results from background scattering (kapton tape). The vertical red line at q = 0.885 nm^{-1} is there to guide the eye. All data were recorded at room temperature.

and previous experimental work,[22] but never observed for materials with such low dispersities. In sharp contrast, the scattering curves of BCOs with a disperse *at-o*LA block lacked any higher-order reflections, and were largely dominated by a broad reflection that is typical for a disordered BCP.[16,55] This reflection nearly overshadowed the aforementioned primary peak that belongs to the microphase-segregated state, and was the only observable reflection at low q for BCO [**Si**$_{\sim 15}$-**LA**$_{\sim 17}$]-**ROP**. It is currently unclear why [**Si**$_{\sim 15}$-**LA**$_{\sim 17}$]-**ROP** is seemingly disordered according to SAXS, but still gives a weak thermal signature in the DSC traces. Again, this might be related to kinetic effects (similar to those in uniform BCO [**Si**$_{23}$-**LA**$_{9}$]) that impede the self-assembly process, even though all samples were annealed prior to the measurements and did not show significant changes in their scattering profiles when remeasured after storage for one week at room temperature. Overall, the scattering data revealed that all of the BCOs with a disperse *at-o*LA block primarily reside in a disordered state, although partially ordered (lamellar) domains coexist in most samples. Apparently, increasing dispersity in either the *o*DMS or *o*LA block affects the lamellar organization to a different extent. The origin hereof is not entirely understood but is likely related to the

disparate molecular make-up of the blocks, different block length distributions or differences in statistical segment lengths.

Initially, we were intrigued by the higher level of disordered regions in the set of BCOs with a disperse *at*-*o*LA block obtained via ROP compared to those obtained by polycondensation. First, the dispersities of [**Si$_{15}$-LA$_{\sim 17}$**]-**PC** and [**Si$_{15}$-LA$_{\sim 17}$**]-**ROP** are nearly equal, as are the dispersities of [**Si$_{\sim 15}$-LA$_{\sim 17}$**]-**PC** and [**Si$_{\sim 15}$-LA$_{\sim 17}$**]-**ROP**. Besides, *N* is slightly higher for both BCOs produced with ROP than the PC analogues, which principally should lead to a more facile formation of an *ordered* structure. However, additional scattering experiments in the *q*-range 4–30 nm^{-1} (size domain of approx. 2–16 Å) revealed a clear contrast between the materials obtained by PC or ROP. As expected, two partially resolved, broad peaks at q = 8.6 nm^{-1} and q = 14.8 nm^{-1} were found in the scattering data of the BCOs for which polycondensation was employed. These reflections represent the siloxane and oligolactic acid halos of the two amorphous constituents of the BCO, respectively, and are identical to the halos that were observed for [**Si$_{15}$-LA$_{17}$**] and [**Si$_{\sim 15}$-LA$_{17}$**] (*i.e.*, BCOs with a discrete-length *at*-*o*LA block). Contrarily, three additional, sharper peaks appeared in the scattering profiles of the BCO with disperse *o*LA blocks obtained by ROP (marked with arrows in Figure 3–10). The location of these peaks is in exact correspondence with those found for the stereocomplex of isotactic, crystalline PLA,[56] which is suggestive of a higher degree of isotacticity in the disperse *o*LA blocks. Indeed, a comparison of the ^{13}C NMR data for BCOs [**Si$_{15}$-LA$_{17}$**], [**Si$_{15}$-LA$_{17}$**]-**PC** and [**Si$_{15}$-LA$_{\sim 17}$**]-**ROP** revealed distinct differences between the first two and the latter (Figure 3–11). For the signals originating from the

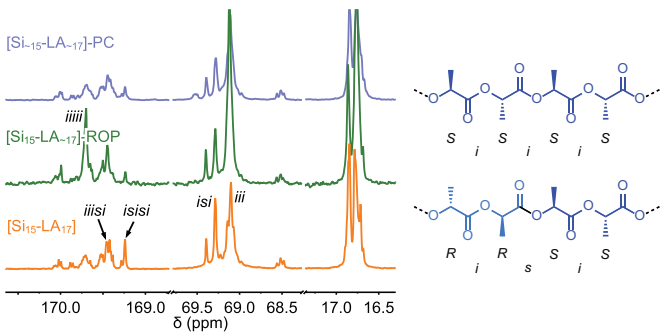

Figure 3–11. Partial ^{13}C NMR traces of [**Si$_{15}$-LA$_{17}$**], [**Si$_{15}$-LA$_{\sim 17}$**]-**ROP** and [**Si$_{15}$-LA$_{\sim 17}$**]-**PC**. Peaks belonging to specific tetrads or hexads are assigned based on literature examples. The chemical structures show both possible diad configurations (isotactic (*i*) and syndiotactic (*s*)), belonging to neighboring lactic acid repeat units with equal or complementary absolute configuration of the asymmetric carbon atom, respectively.

carbonyl and methine carbons, particular tetrad or hexad configurations[viii] could be assigned based on literature data.[57,58] An above-average amount of isotactic tetrads and hexads was observed for the BCOs containing a disperse *o*LA block that was obtained via ROP as opposed to those with the discrete block or disperse block made by polycondensation. Clearly, the higher degree of isotacticity—and, probably, crystallinity—amplifies the adverse effect of dispersity in the *o*LA block on the formation of an ordered structure.

3.4 Conclusions

We demonstrated that discrete-length [$\mathbf{Si_x}$-$\mathbf{LA_y}$] BCOs with low MW possess sharp order–disorder transitions of microphase-separated morphologies, which could reliably be captured by differential scanning calorimetry. The observations were corroborated by X-ray scattering data that confirmed the formation well-ordered microphase-segregated structures. Despite their relatively low MW, the BCOs self-assemble into morphologies that match the structures expected for traditional high-MW BCPs.

We showed that minor changes in block lengths (*i.e.*, 2 lactic acid units difference) have a major effect on the type of well-ordered microstructure that is formed. This supported our expectation that the introduction of dispersity—which easily results in a mixture of BCOs differing up to tens of repeat units in length—might have a tremendous negative impact on the microphase behavior in these low-MW systems. Indeed, the uniform BCOs allowed the exploration of far smaller feature sizes, in the form of 3.5 nm thin lamellae and cylinders with a 2.1 nm radius. Structures of this size were not obtained with disperse analogues. Finally, we showed that the excellent long-term stability and low T_{ODT} values provide convenient processing conditions for the discrete-length BCOs at ambient or slightly elevated temperatures.

The cylindrical structures formed by the longest BCO [$\mathbf{Si_{59}}$-$\mathbf{LA_{33}}$] proved to be large enough for direct observation by AFM. Unfortunately, technical limitations prevented the clear visualization of the smallest features formed by the lower MW compounds. Nevertheless, compelling differences were found when comparing the self-assembled structures of the discrete BCO and a disperse reference co-polymer. The intriguing improvement of long-range order in thin films and uniformity of self-assembled structures in confined space further stress the potential benefits of eliminating dispersity to boost the degree organization without the need for elaborate post-processing techniques.

[viii] Tetrad: 3 sequential diads; hexad: 5 sequential diads.

In a more in-depth study, the effect of (partial) introduction of dispersity in amorphous [$\mathbf{Si_x\text{-}LA_y}$] BCOs was examined. While monitoring changes in BCO properties and microphase behavior upon switching from a uniform to a considerably less 'monodisperse' BCO, three main trends were noticed. First, two important terms that quantify and qualify phase behavior—and are often erroneously used interchangeably—show two pronounced, yet exactly opposite drifts: 1) an increase of the *stability* of the microphase-segregated state, expressed as an increase of the T_{ODT}; accompanied by 2) a decrease of the overall *degree of ordering* in the samples. Lastly, an increase of dispersity results in 3) widening of the *domain spacing*. As a bonus, our samples illustrated that variations in local stereoregularity have a strong influence on BCO phase behavior.

In general, the effect of all intermolecular interactions resulting from the endgroups and interblock connectivities in low-MW polymers can no longer be neglected. For example, in a related publication, the Hawker research group described a set of BCOs with comparable length and dispersities, but incorporating different chemical structures.[29] Here, they reveal an exactly opposite trend of T_{ODT} *versus* dispersity, yet a very similar effect on the domain spacings. These apparent differences should not be conceived purely as contradictory behavior, but merely highlight that the (phase) behavior of high χ–low N block copolymers still is highly unpredictable.

In that respect, we conclude that the discrete-length BCOs can be considered as a subset of 'normal' BCPs, sharing typical (self-assembly) behavior. However, their discrete and low MW provides these materials with some unique properties. Therefore care should be taken not to over-extrapolate the results to (much) higher MW compounds. In view of the forthgoing trend toward materials that are becoming too exclusive to be classified either polymers or small molecules (*e.g.*, thermotropic liquid crystals), the explorative work on discrete-length oligomeric materials is continued in Chapter 4.

3.5 Experimental

3.5.1 Materials and methods

All chemicals were purchased from commercial sources and used without further purification. The synthesis of discrete Me-Si_{15}-H **14c**, benzyl (*S*)-2-(allyloxy)propanoate L-**26**, discrete HO-LA_{16}-Bn *at*-**22s** and discrete Me-Si_{15}-LLA_1-COOH L-**28c** is described in Chapter 2. Dry solvents were obtained with an MBRAUN Solvent Purification System (MB-SPS). Toluene was dried over 4Å molecular sieves before use. Oven-dried glassware (120 °C) was used for all reactions carried out under argon atmosphere. Reactions were followed by thin-layer chromatography (TLC) using 60-F254 silica gel plates from Merck and visualized by UV light at 254 nm and/or cerium molybdate (CeMo)

staining. Automated column chromatography was conducted on a Grace Reveleris X2 Flash Chromatography System using Reveleris Silica Flash Cartridges. Elution gradients are specified in column volumes (CVs).

NMR spectra were recorded on Varian Mercury Vx 400 MHz, Varian 400MR 400 MHz, Bruker 400 MHz Ultrashield (400 MHz for ^{1}H NMR), and/or Varian Inova 500 MHz (500 MHz for ^{1}H NMR) spectrometers. Deuterated solvents used are indicated in each case. Chemical shifts (δ) are expressed in ppm and are referred to the residual peak of the solvent. Peak multiplicity is abbreviated as s: singlet; d: doublet; t: triplet; dt: doublet of triplets; ddt: doublet of doublets of triplets; td: triplet of doublets; tt: triplet of triplets; q: quartet; ABq: AB quartet; qd: quartet of doublets; sept: septet; m: multiplet; bs: broad singlet. **Matrix assisted laser desorption/ionization time-of-flight** (MALDI-TOF) mass spectra were obtained on a PerSeptive Biosystems Voyager DE-PRO spectrometer using α-cyano-4-hydroxycinnamic acid (CHCA) or *trans*-2-[3-(4-*tert*-butylphenyl)-2-methyl-2-propenylidene]-malononitrile (DCTB) as matrix. **Size exclusion chromatography** (SEC) measurements were conducted on a Shimadzu Prominence-i LC-2030C 3D with a Shimadzu RID-20A Refractive index detector, using an eluent flow of 1 mL min^{-1} (THF or $CHCl_3$). The molecular weight is determined based on narrow dispersity polystyrene standards purchased from Polymer Source Inc. **Differential scanning calorimetry** (DSC) data were collected on a DSC Q2000 from TA instruments, calibrated with an indium standard. The samples (4–8 mg) were weighed directly into aluminum pans and hermetically sealed. The samples were initially heated to 180 °C and then subjected to two cooling/heating cycles, typically from -50 °C to 180 °C with a rate of 10 °C min^{-1}. The data that are presented, represent the second heating/cooling cycle unless stated otherwise. Bulk **small-angle X-ray scattering** (SAXS) was performed on an instrument from Ganesha Lab. The flight tube and sample holder are all under vacuum in a single housing, with a GeniX-Cu ultra-low divergence X-ray generator. The source produces X-rays with a wavelength (λ) of 0.154 nm and a flux of 1×10^8 ph s^{-1}. All samples were annealed by heating to a temperature 20 °C above the (expected) ODT and slow (0.5 °C min^{-1}) cooling to room temperature. For room temperature measurements, the material was smeared onto glass or kapton tape, and positioned directly in the beamline. Samples for variable temperature SAXS (VT-SAXS) were molten into 1 mm diameter glass capillaries and measured at elevated temperatures using a Linkam heating stage. Samples were equilibrated at each temperature for 5 minutes prior to measuring and a heating/cooling rate of 5 °C min^{-1} was used in between the measurements. Scattered X-rays were captured on a 2-dimensional Pilatus 300K detector with 487 × 619 pixel resolution. Samples were measured in MAXS mode for 1200 seconds and WAXS mode for 300 seconds. The sample-to-detector distance was 0.084 m (WAXS mode) or 0.431 m (MAXS mode). The instrument was calibrated with diffraction patterns from silver behenate. The raw data files were calibrated and reduced to 1-D data with the SAXSGui software provided by JJ X-Ray Systems ApS. MAXS and WAXS regions were merged into a single data file using the SAXSutilities software package provided by Michael Sztucki.

3.5.2 Synthetic procedures

Synthesis of disperse Bu-Si$_{\sim 15}$-LLA$_1$-Bn (L-**36**).

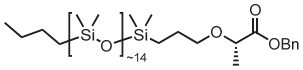

Silyl hydride **35** (1.5 g, ~1.30 mmol, 1 eq, DP~15) and benzyl (*S*)-2-(allyloxy)propanoate L-**26** (0.343 g, 1.56 mmol, 1.2 eq) were dissolved in dry toluene (6 mL) in a 25 mL 2-necked round-bottom flask under an argon atmosphere. One drop of Karstedt catalyst (soln. in xylene, 2% Pt) was added, and the stirred mixture was then heated to 60 °C (the mixture turned from colorless to light yellow/brown in a few minutes). After 4 h, all hydride was converted (checked with ^{1}H NMR). The solvent was removed in *vacuo*, and the residual light brown oil was purified by automated column chromatography using hept/EtOAc (gradient 100/0 to 80/20) as eluent, giving the product L- **36** as an almost colorless oil (1.532 g, 86%). Residual trace amounts of impurities were removed after the

next step. ^{1}H NMR (400 MHz, $CDCl_3$): δ = 7.40–7.29 (m, 5H, Ar-H), 5.25–5.13 (ABq, $\Delta\delta_{AB}$ = 0.05, J_{AB} = 12.5 Hz, 2H, CO-C$\underline{H}_2$-Ar), 4.00 (q, ^3J = 6.8 Hz, 1H, O-C$\underline{H}$(CH_3)-CO), 3.52 (dt, ^2J = 8.8 Hz, ^3J = 7.0 Hz, 1H, CH_2-C$\underline{H}_2$-O), 3.32 (dt, ^2J = 8.9 Hz, ^3J = 7.0 Hz, 1H, CH_2-C$\underline{H}_2$-O), 1.68–1.57 (m, 2H, C$\underline{H}_2$-CH_2-O), 1.41 (d, ^3J = 6.8 Hz, 3H, O-CH(C$\underline{H}_3$)-CO), 1.37–1.24 (m, 4H, CH_3-C$\underline{H}_2$-C$\underline{H}_2$), 0.89 (t, ^3J = 7.3 Hz, 3H, C$\underline{H}_3$-CH_2), 0.61–0.47 (m, 4H, Si(CH_3)$_2$-C$\underline{H}_2$-CH_2 and CH_2-C$\underline{H}_2$-Si(CH_3)$_2$), 0.13–0.02 ppm (m, 90H, Si(C$\underline{H}_3$)); ^{13}C NMR (100 MHz, $CDCl_3$): δ = 173.70, 136.10, 128.65, 128.53, 75.29, 73.49, 66.76, 26.72, 25.80, 23.89, 19.02, 18.31, 14.43, 14.16, 1.52–1.40, 0.52, 0.45, 0.42 ppm; MS (MALDI-TOF): *m/z* calcd for $C_{47}H_{116}O_{17}Si_{15}$+$Na^+$: 1395.46 $[M+Na]^+$; found 1395.60 (multiple, equally spaced (74.02 Da) peaks were found between 500–2500 Da, each corresponding to the desired product with a different DP); SEC ($CHCl_3$): M_n = 1160 Da; $Đ$ = 1.15.

Synthesis of disperse Bu-Si$_{\sim 15}$-LA$_1$-COOH (L-**37**).

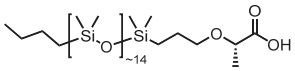

Benzyl ester L- **36** (465 mg, 0.338 mmol, 1 eq) was dissolved in ethyl acetate (5 mL) in a 50 mL round-bottom flask, and Pd/C (10 w% Pd, 18 mg, 0.05 eq of Pd) was added. The mixture was then stirred under a hydrogen atmosphere at room temperature. After 4 h, TLC analysis (hept/EtOAc 80/20; CeMo stain; $R_{f,prod}$ = 0.01–0.30 (tailing)) confirmed that all of the benzyl ester was converted. The black suspension was filtered through a 2 cm thick layer of celite and the filter cake washed with EtOAc (3 × 5 mL). The combined filtrates were concentrated in *vacuo*, giving the crude product as a colorless oil. The material was purified by automated column chromatography using hept/EtOAc (gradient 100/0 to 70/30), giving the product L-**37** in pure form as a colorless oil (245 mg, 56%). ^{1}H NMR (400 MHz, $CDCl_3$): δ = 3.99 (q, ^3J = 6.9 Hz, 1H, O-C$\underline{H}$(CH_3)-CO), 3.54 (dt, ^2J = 8.9 Hz, ^3J = 6.9 Hz, 1H, CH_2-C$\underline{H}_2$-O), 3.44 (dt, ^2J = 8.9 Hz, ^3J = 7.0 Hz, 1H, CH_2-C$\underline{H}_2$-O), 1.73–1.55 (m, 2H, C$\underline{H}_2$-CH_2-O), 1.45 (d, ^3J = 6.9 Hz, 3H, O-CH(C$\underline{H}_3$)-CO), 1.39–1.23 (m, 4H, CH_3-C$\underline{H}_2$-C$\underline{H}_2$), 0.88 (t, ^3J = 7.0 Hz, 3H, C$\underline{H}_3$-CH_2), 0.61–0.48 (m, 4H, Si(CH_3)$_2$-C$\underline{H}_2$-CH_2 and CH_2-C$\underline{H}_2$-Si(CH_3)$_2$), 0.17 to −0.03 ppm (m, 90H, Si(C$\underline{H}_3$)); ^{13}C NMR (100 MHz, $CDCl_3$): δ = 177.47, 74.70, 73.35, 26.53, 25.61, 23.69, 18.34, 18.12, 14.23, 13.96, 1.57, 1.32, 1.20, 0.83, 0.33, 0.25 ppm; MS (MALDI-TOF): *m/z* calcd for $C_{40}H_{110}O_{17}Si_{15}$+$Na^+$: 1305.42 $[M+Na]^+$; found 1307.46 (peak belonging to the 3rd isotopic mass) (multiple, equally spaced (74.02 Da) peaks were found between 500–2000 Da, each corresponding to the desired product with a different DP).

Synthesis of HO-LA$_2$-COOH (*rac*-**21**).

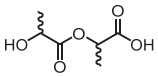

DL-Lactide *rac*-**20** (10.01 g, 69.5 mmol) was suspended in water (60 mL) in a 250 mL round-bottom flask. The mixture was stirred at 65 °C until all starting material was converted (4 hours, the mixture became clear, conversion checked with ^{1}H NMR). The water was removed by freeze-drying, giving the racemic product (10.98 g, 97%) as a mixture of dimer (~85%) and lactic acid monomer (~15%). The mixture was used for the next reaction as-is. Average MW ≈ 151.3 g/mol; average DP ≈ 1.85. ^{1}H NMR (400 MHz, $CDCl_3$): δ = 6.64 (bs, 1H, H$\underline{O}$-CH(CH_3)-CO), 5.13 (q, ^3J = 7.1 Hz, 1H, O-C$\underline{H}$(CH_3)-CO), 4.37 (q, ^3J = 7.0 Hz, 1H, HO-C$\underline{H}$(CH_3)-CO), 1.52 (d, ^3J = 7.1 Hz, 3H, O-CH(C$\underline{H}_3$)-CO), 1.45 ppm (d, ^3J = 7.0 Hz, 3H, HO-CH(C$\underline{H}_3$)-CO); ^{13}C NMR (100 MHz, $CDCl_3$): δ = 175.07, 174.24, 69.22, 66.96, 20.11, 16.74 ppm.

Synthesis of disperse HO-LA$_{\sim 16}$-Bn (polycondensation) (*at*-**34-PC**).

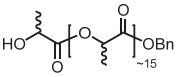

Lactic acid dimer/monomer mixture *rac*-**21** (1.54 g, 10.2 mmol, 8.6 eq) was dissolved in dry DCM (15 mL) in a 50 mL round-bottom flask under argon. Dry benzyl alcohol (0.128 g, 1.18 mmol, 1 eq) and 4-(dimethylamino)pyridinium 4-toluenesulfonate (DPTS, 1.28 g, 5.1 mmol, 4.3 eq) were added. The mixture was cooled to 0 °C in ice water, *N*-(3-dimethylaminopropyl)-*N*'-ethylcarbodiimide hydrochloride (EDC·HCl, 3.91 g, 20.4 mmol, 16.2 eq) was added and the mixture was stirred for 10 minutes at 0 °C. Next, the mixture was allowed to reach room temperature, and stirring was continued overnight. The mixture was then diluted with DCM (20 mL) and washed with a 50/50 mixture of water and brine (20 mL in total). The organic layer was dried with $MgSO_4$ and concentrated in *vacuo*, giving the crude product *at*-**34-PC** (1.67 g) as a waxy solid. The material was purified by automated column chromatography using hept/EtOAc (gradient 90/10 to 0/100) as eluent, giving the pure oligomer as a colorless, waxy substance (571 mg, 41%). ^{1}H NMR (400 MHz, $CDCl_3$): δ = 7.36–7.26 (m, 5H, Ar-H), 5.26–5.05 (m, 17H, O-CH(CH$_3$)-CO and Ar-CH$_2$-O), 4.31 (q, ^3J = 7.0 Hz, 1H, HO-CH(CH$_3$)-CO), 2.86 (bs, 1H, HO-CH(CH$_3$)-CO), 1.58–1.42 ppm (m, 48H, O-CH(CH$_3$)-CO); ^{13}C NMR (100 MHz, $CDCl_3$): δ = 175.15, 175.04, 170.41–169.12, 135.16, 128.70–128.30, 69.37–69.04, 67.30, 67.28, 66.79, 66.75, 20.59, 16.84–16.72 ppm; MS (MALDI-TOF): *m/z* calcd for $C_{55}H_{72}O_{33}$+Na^+: 1283.38 $[M+Na]^+$; found 1283.38; *m/z* calcd for $C_{55}H_{72}O_{33}$+K^+: 1299.36 $[M+K]^+$; found 1299.37 (multiple, equally spaced (72.02 m/z) peaks were found between 500–3000 Da, each corresponding to the desired product with a different DP); SEC (THF): M_n = 1787 Da; $Đ$ = 1.24.

Synthesis of disperse HO-LA$_{\sim 16}$-Bn (ring-opening polymerization) (*at*-**34-ROP**).

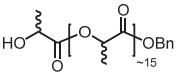

DL-lactide (a 1:1 mixture of (*S,S*)-**20** and (*R,R*)-**20**) was dried for 6 hours at 45 °C under vacuum. The dry material (231 mg, 1.60 mmol, 8 eq) was dissolved in dry DCM (3 mL, 0.5 M) in a dry 10 mL Schlenk tube under an argon atmosphere. Dry benzyl alcohol **4** (21.6 mg, 0.20 mmol, 1 eq) was added. Next, a 10 w% solution of 1,8-diazabicyclo[5.4.0]undec-7-ene (DBU) in dry DCM was prepared. Then, 24 mg of the DBU solution (2.4 mg, 0.016 mmol, 0.08 eq DBU) was added to the stirred reaction mixture. The reaction progress was followed with TLC (hept/EtOAc 50/50; CeMo stain). After completion (~1 h), benzoic acid (5.9 mg, 0.048 mmol, 0.24 eq) was added to quench the reaction, and the solution was concentrated in *vacuo* to give crude disperse oligolactic acid as a yellowish wax. The material was purified by automated column chromatography using hept/EtOAc (gradient 88/12 to 15/85) as eluent. The pure product *at*-**34-ROP** was obtained as a colorless, waxy solid (251 mg, quant.). ^{1}H NMR (400 MHz, $CDCl_3$): δ = 7.39–7.28 (m, 5H, Ar-H), 5.25–5.07 (m, 17H, O-CH(CH$_3$)-CO and Ar-CH$_2$-O), 4.35 (q, ^3J = 7.0 Hz, 1H, HO-CH(CH$_3$)-CO), 2.61 (bs, 1H, HO-CH(CH$_3$)-CO), 1.63–1.41 ppm (m, 48H, O-CH(CH$_3$)-CO); ^{13}C NMR (100 MHz, $CDCl_3$): δ = 175.18, 175.04, 170.00–169.20, 135.21, 128.80–128.34, 69.43–69.05, 67.30, 67.29, 66.74, 20.61, 16.86–16.72 ppm; MS (MALDI-TOF): *m/z* calcd for $C_{55}H_{72}O_{33}$+Na^+: 1283.38 $[M+Na]^+$; found 1283.43; *m/z* calcd for $C_{55}H_{72}O_{33}$+K^+: 1299.36 $[M+K]^+$; found 1299.35 (multiple, equally spaced (144.04 m/z) peaks were found between 500–3000 Da, each corresponding to the desired product with a different DP); SEC (THF): M_n = 2265; $Đ$ = 1.23.

*General procedure **A** for the oDMS–oLA coupling reactions giving Me/Bu-Si$_x$-LA$_y$-Bn* ([**Si$_x$-LA$_y$**]).

*o*DMS acid (L-**28c** or L-**37**) (*e.g.*, 0.047 mmol, 1.0 eq) was dissolved in dry DCM (0.5 mL, ~0.1 M) in a 10 mL Schlenk tube under an argon atmosphere. The solution was cooled to 0 °C in ice water and DPTS (0.023 mmol, 0.5 eq) and EDC·HCl (0.094 mmol, 2.0 eq) were added. The mixture was stirred for 10 min at 0 °C, followed by the addition of a solution of benzyl protected *at*-*o*LA (*at*-**22s**, *at*-**34-PC** or *at*-**34-ROP**) (0.047 mmol, 1.0 eq) in DCM

(0.5 mL). The mixture was then stirred overnight at room temperature (depending on the concentration, sometimes the formation of a suspension of droplets of co-oligomer in DCM was observed). The reaction mixture was diluted with DCM (15 mL) to bring all material in solution, and the mixture was washed with a 50/50 mixture of water and brine (10 mL in total). The organic layer was dried with $MgSO_4$ and concentrated in *vacuo*, giving the crude product [**Si$_x$-LA$_y$**] as a viscous, colorless oil. The material was purified by automated column chromatography, resulting in the pure block co-oligomer as a colorless, thick oil or waxy solid.

Synthesis of Bu-Si$_{\sim 15}$-LA$_{17}$-Bn ([**Si$_{\sim 15}$-LA$_{17}$**]).

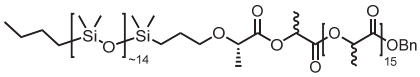

Starting from *o*DMS acid L-**37** (60 mg, 0.047 mmol, 1 eq), *o*LA *at*-**22s** (59 mg, 0.047 mmol, 1 eq), DPTS (6.9 mg, 0.023 mmol, 0.5 eq) and EDC·HCl (18 mg, 0.094 mmol, 2 eq), crude co-oligomer [**Si$_{\sim 15}$-LA$_{17}$**] was obtained as a colorless wax using general procedure **A**. The material was purified by automated column chromatography using hept/EtOAc (gradient 80/20 to 60/40) as eluent, giving the product in pure form as a colorless, waxy substance (97 mg, 82%). ^{1}H NMR (400 MHz, $CDCl_3$): δ = 7.39–7.28 (m, 5H, Ar-H), 5.25–5.08 (m, 18H, O-CH(CH$_3$)-CO and O-CH$_2$-Ar), 4.07–3.37 (m, 1H, CH$_2$-O-CH(CH$_3$)-CO), 3.62–3.49 (m, 1H, CH$_2$-O-CH(CH$_3$)-CO), 3.32 (dt, ^2J = 9.1 Hz, ^3J = 7.0 Hz, 1H, CH$_2$-O-CH(CH$_3$)-CO), 1.65–1.40 (m, 53H, Si(CH$_3$)$_2$-CH$_2$-CH$_2$-CH$_2$-O and O-CH(CH$_3$)-CO), 1.36–1.22 (m, 4H, CH$_3$-CH$_2$-CH$_2$), 0.93–0.81 (m, 3H, CH$_3$-CH$_2$), 0.58–0.46 (m, 4H, Si(CH$_3$)$_2$-CH$_2$-CH$_2$-CH$_2$-O and CH$_2$-CH$_2$-Si(CH$_3$)$_2$), 0.11– 0.01 ppm (m, 90H, Si(CH$_3$)); ^{13}C NMR (100 MHz, $CDCl_3$): δ = 173.11, 170.03–169.25, 135.22, 128.74, 128.63, 128.35, 74.78, 73.27, 69.41–69.09, 67.32, 26.47, 25.56, 23.64, 18.76, 18.07, 16.86–16.69, 14.21, 13.92, 1.53, 1.28, 1.17, 0.79, 0.30, 0.22, 0.19 ppm; MS (MALDI-TOF): *m/z* calcd for $C_{95}H_{180}O_{49}Si_{15}$+Na$^+$: 2547.80 [M+Na]$^+$; found 2547.86 (multiple, equally spaced (74.02 m/z) peaks were found between 1500–4000 Da, each corresponding to the desired product with a different DP); SEC (THF): M_n = 4118; $Đ$ = 1.05.

Synthesis of Me-Si$_{15}$-LA$_{\sim 17}$-Bn (PC) ([**Si$_{15}$-LA$_{\sim 17}$**]-**PC**).

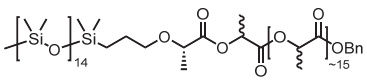

Starting from *o*DMS acid L-**28c** (100 mg, 0.08 mmol, 1 eq), *o*LA *at*-**34-PC** (104 mg, 0.08 mmol, 1 eq), DPTS (11.8 mg, 0.04 mmol, 0.5 eq) and EDC·HCl (30.7 mg, 0.16 mmol, 2 eq), crude co-oligomer [**Si$_{15}$-LA$_{\sim 17}$**]-**PC** was obtained as a colorless wax using general procedure **A**. The material was purified by automated column chromatography using hept/EtOAc (gradient 95/5 to 30/70) as eluent, giving the product in pure form as a colorless, waxy substance (117 mg, 59%). ^{1}H NMR (400 MHz, $CDCl_3$): δ = 7.38–7.27 (m, 5H, Ar-H), 5.26–5.07 (m, 18H, O-CH(CH$_3$)-CO and O-CH$_2$-Ar), 4.08–3.23 (m, 1H, CH$_2$-O-CH(CH$_3$)-CO), 3.63–3.48 (m, 1H, CH$_2$-O-CH(CH$_3$)-CO), 3.36–3.27 (m, 1H, CH$_2$-O-CH(CH$_3$)-CO), 1.81–1.35 (m, 53H, Si(CH$_3$)$_2$-CH$_2$-CH$_2$-CH$_2$-O and O-CH(CH$_3$)-CO), 0.57–0.49 (m, 2H, Si(CH$_3$)$_2$-CH$_2$-CH$_2$-CH$_2$-O), 0.15 to 0.05 ppm (m, 93H, Si(CH$_3$)); ^{13}C NMR (100 MHz, $CDCl_3$): δ = 173.09, 170.07–169.24, 135.21, 128.72, 128.61, 128.33, 74.76, 74.64, 73.24, 73.21, 69.52–68.98, 68.52, 67.29, 23.62, 18.74, 16.85–16.64, 14.20, 1.89, 1.52, 1.26, 1.24, 1.15–1.13, 0.78, 0.20, 0.18 ppm; MS (MALDI-TOF): *m/z* calcd for $C_{92}H_{174}O_{49}Si_{15}$+Na$^+$: 2505.76 [M+Na]$^+$; found 2505.89 (multiple, equally spaced (72.02 m/z) peaks were found between 1500–4500 Da, each corresponding to the desired product with a different DP); SEC (THF): M_n = 4015; $Đ$ = 1.08.

Synthesis of Bu-Si$_{\sim 15}$-LA$_{\sim 17}$-Bn (PC) ([**Si**$_{\sim 15}$-**LA**$_{\sim 17}$]-**PC**).

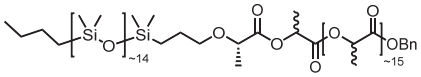

Starting from *o*DMS acid L-**37** (97 mg, 0.076 mmol, 1.25 eq), *o*LA *at*-**34**-**PC** (77 mg, 0.061 mmol, 1 eq), DPTS (9.1 mg, 0.031 mmol, 0.5 eq) and EDC·HCl (23.4 mg, 0.122 mmol, 2 eq), crude co-oligomer [**Si**$_{\sim 15}$-**LA**$_{\sim 17}$]-**PC** was obtained as a colorless wax using general procedure **A**. The material was purified by automated column chromatography using hept/EtOAc (gradient 90/10 to 55/45) as eluent, giving the product in pure form as a colorless, waxy substance (90 mg, 58%). ^{1}H NMR (400 MHz, $CDCl_3$): δ = 7.37–7.26 (m, 5H, Ar-H), 5.26–5.06 (m, 18H, O-CH(CH$_3$)-CO and O-CH$_2$-Ar), 4.08–3.45 (m, 1H, CH$_2$-O-CH(CH$_3$)-CO), 3.64–3.49 (m, 1H, CH$_2$-O-CH(CH$_3$)-CO), 3.32 (td, ^3J = 7.6 Hz, ^3J = 7.6 Hz, 1H, CH$_2$-O-CH(CH$_3$)-CO), 1.68–1.39 (m, 53H, Si(CH$_3$)$_2$-CH$_2$-CH$_2$-CH$_2$-O and O-CH(CH$_3$)-CO), 1.36–1.26 (m, 4H, CH$_3$-CH$_2$-CH$_2$), 0.91–0.83 (m, 3H, CH$_3$-CH$_2$), 0.58–0.48 (m, 4H, Si(CH$_3$)$_2$-CH$_2$-CH$_2$-CH$_2$-O and CH$_2$-CH$_2$-Si(CH$_3$)$_2$), 0.11–0.00 ppm (m, 90H, Si(CH$_3$)); ^{13}C NMR (100 MHz, $CDCl_3$): δ = 173.09, 170.00–169.24, 135.21, 128.72, 128.61, 128.34, 74.76, 74.64, 73.24, 73.21, 69.52–69.08, 68.52, 67.30, 26.46, 25.55, 23.63, 18.75, 18.05, 16.85–16.67, 14.20, 13.90, 1.52, 1.27, 1.15, 0.78, 0.28, 0.20, 0.18 ppm; MS (MALDI-TOF): *m/z* calcd for $C_{95}H_{180}O_{49}Si_{15}+Na^+$: 2547.80 $[M+Na]^+$; found 2547.83 (a range of masses was found between 1500–4500 Da, each corresponding to the desired product with a different DP); SEC (THF): M_n = 3999; $Đ$ = 1.09.

Synthesis of Me-Si$_{15}$-LA$_{\sim 17}$-Bn (ROP) ([**Si$_{15}$**-**LA**$_{\sim 17}$]-**ROP**).

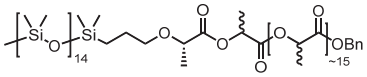

Starting from *o*DMS acid L-**28c** (72 mg, 0.058 mmol, 1 eq), *o*LA *at*-**34**-**ROP** (73 mg, 0.058 mmol, 1 eq), DPTS (8.6 mg, 0.029 mmol, 0.5 eq) and EDC·HCl (22.3 mg, 0.116 mmol, 2 eq), crude co-oligomer [**Si$_{15}$**-**LA**$_{\sim 17}$]-**ROP** was obtained as a colorless wax using general procedure **A**. The material was purified by automated column chromatography using hept/EtOAc (gradient 80/20 to 60/40) as eluent, giving the product in pure form as a colorless, waxy substance (98 mg, 67%). ^{1}H NMR (400 MHz, $CDCl_3$): δ = 7.39–7.28 (m, 5H, Ar-H), 5.28–5.01 (m, 18H, O-CH(CH$_3$)-CO and O-CH$_2$-Ar), 4.10–3.43 (m, 1H, CH$_2$-O-CH(CH$_3$)-CO), 3.63–3.47 (m, 1H, CH$_2$-O-CH(CH$_3$)-CO), 3.32 (dt, ^2J = 9.2 Hz, ^3J = 7.0 Hz, 1H, CH$_2$-O-CH(CH$_3$)-CO), 1.77–1.37 (m, 53H, Si(CH$_3$)$_2$-CH$_2$-CH$_2$-CH$_2$-O and O-CH(CH$_3$)-CO), 0.58–0.48 (m, 2H, Si(CH$_3$)$_2$-CH$_2$-CH$_2$-CH$_2$-O), 0.13 to 0.02 ppm (m, 93H, Si(CH$_3$)); ^{13}C NMR (100 MHz, $CDCl_3$): δ = 173.10, 169.99–169.24, 135.19, 128.73, 128.64, 128.35, 74.77, 74.64, 73.22, 69.40–69.12, 67.32, 23.63, 18.76, 16.86–16.68, 14.21, 1.90, 1.54, 1.28–1.17, 0.80, 0.22, 0.19 ppm; MS (MALDI-TOF): *m/z* calcd for $C_{92}H_{174}O_{49}Si_{15}+Na^+$: 2505.76 $[M+Na]^+$; found 2505.82 (multiple, equally spaced (144.04 m/z) peaks were found between 2000–4500 Da, each corresponding to the desired product with a different DP); SEC (THF): M_n = 4964; $Đ$ = 1.07.

Synthesis of Bu-Si$_{\sim 15}$-LA$_{\sim 17}$-Bn (ROP)] ([**Si**$_{\sim 15}$-**LA**$_{\sim 17}$-**ROP**).

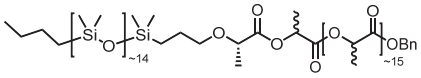

Starting from *o*DMS acid L-**37** (60 mg, 0.046 mmol, 1.25 eq), *o*LA *at*-**34**-**ROP** (58 mg, 0.046 mmol, 1 eq), DPTS (6.8 mg, 0.023 mmol, 0.5 eq) and EDC·HCl (18 mg, 0.093 mmol, 2 eq), crude co-oligomer [**Si**$_{\sim 15}$-**LA**$_{\sim 17}$]-**ROP** was obtained as a colorless wax using general procedure **A**. The material was purified by automated column chromatography using hept/EtOAc (gradient 80/20 to 60/40) as eluent, giving the product in pure form as a colorless, waxy substance (72 mg, 62%). ^{1}H NMR (400 MHz, $CDCl_3$): δ = 7.39–7.28 (m, 5H, Ar-H), 5.27–5.08 (m, 18H, O-CH(CH$_3$)-CO and O-CH$_2$-Ar), 4.09–3.54 (m, 1H, CH$_2$-O-CH(CH$_3$)-CO), 3.63–3.49 (m, 1H, CH$_2$-O-CH(CH$_3$)-CO), 3.32 (dt, ^2J = 9.1 Hz, ^3J = 7.0 Hz, 1H, CH$_2$-O-CH(CH$_3$)-CO), 1.78–1.39 (m, 53H, Si(CH$_3$)$_2$-CH$_2$-CH$_2$-CH$_2$-O and O-

CH(C$\underline{H}_3$)-CO), 1.36–1.26 (m, 4H, CH_3-C$\underline{H}_2$-C$\underline{H}_2$), 0.94–0.81 (m, 3H, C$\underline{H}_3$-CH_2), 0.58–0.49 (m, 4H, $Si(CH_3)_2$-C$\underline{H}_2$-CH_2-CH_2-O and CH_2-C$\underline{H}_2$-$Si(CH_3)_2$), 0.15 to 0.02 ppm (m, 90H, $Si(C\underline{H}_3)$); ^{13}C NMR (100 MHz, $CDCl_3$): δ = 173.11, 170.03–169.26, 135.20, 128.74, 128.65, 128.37, 74.78, 74.66, 73.26, 69.41–69.10, 67.34, 26.48, 25.56, 23.64, 18.76, 18.07, 16.87–16.69, 14.22, 13.92, 1.54, 1.29–1.17, 0.80, 0.30, 0.22, 0.19 ppm; MS (MALDI-TOF): *m/z* calcd for $C_{95}H_{180}O_{49}Si_{15}+Na^+$: 2547.80 $[M+Na]^+$; a range of masses was found between 1500–4500 Da; SEC (THF): M_n = 4547; $Đ$ = 1.09.

3.6 References

(1) Brooke, G. M.; Mohammed, S.; Whiting, M. C. *J. Chem. Soc. Perkin Trans. 1* **1997**, 3371.

(2) Kim, S. H.; Misner, M. J.; Russell, T. P. *Adv. Mater.* **2004**, *16*, 2119.

(3) Park, S.; Lee, D. H.; Xu, J.; Kim, B.; Hong, S. W.; Jeong, U.; Xu, T.; Russell, T. P. *Science* **2009**, *323*, 1030.

(4) Rodwogin, M. D.; Spanjers, C. S.; Leighton, C.; Hillmyer, M. A. *ACS Nano* **2010**, *4*, 725.

(5) Cushen, J. D.; Bates, C. M.; Rausch, E. L.; Dean, L. M.; Zhou, S. X.; Willson, C. G.; Ellison, C. J. *Macromolecules* **2012**, *45*, 8722.

(6) Cushen, J. D.; Otsuka, I.; Bates, C. M.; Halila, S.; Fort, S.; Rochas, C.; Easley, J. A.; Rausch, E. L.; Thio, A.; Borsali, R.; Willson, C. G.; Ellison, C. J. *ACS Nano* **2012**, *6*, 3424.

(7) Pitet, L. M.; Wuister, S. F.; Peeters, E.; Kramer, E. J.; Hawker, C. J.; Meijer, E. W. *Macromolecules* **2013**, *46*, 8289.

(8) Sweat, D. P.; Kim, M.; Larson, S. R.; Choi, J. W.; Choo, Y.; Osuji, C. O.; Gopalan, P. *Macromolecules* **2014**, *47*, 6687.

(9) Kennemur, J. G.; Yao, L.; Bates, F. S.; Hillmyer, M. A. *Macromolecules* **2014**, *47*, 1411.

(10) Keen, I.; Cheng, H.-H.; Yu, A.; Jack, K. S.; Younkin, T. R.; Leeson, M. J.; Whittaker, A. K.; Blakey, I. *Macromolecules* **2014**, *47*, 276.

(11) Lee, H.-C.; Hsueh, H.-Y.; Jeng, U.-S.; Ho, R.-M. *Macromolecules* **2014**, *47*, 3041.

(12) Jackson, E. A.; Hillmyer, M. A. *ACS Nano* **2010**, *4*, 3548.

(13) Qiu, X.; Yu, H.; Karunakaran, M.; Pradeep, N.; Nunes, S. P.; Peinemann, K.-V. *ACS Nano* **2013**, *7*, 768.

(14) Kang, Y.; Walish, J. J.; Gorishnyy, T.; Thomas, E. L. *Nat. Mater.* **2007**, *6*, 957.

(15) Darling, S. B. *Energy Environ. Sci.* **2009**, *2*, 1266.

(16) Leibler, L. *Macromolecules* **1980**, *13*, 1602.

(17) Chen, P.; Liang, H.; Shi, A.-C. *Macromolecules* **2007**, *40*, 7329.

(18) Matsen, M. W.; Bates, F. S. *Macromolecules* **1996**, *29*, 1091.

(19) Matsen, M. W.; Bates, F. S. *J. Polym. Sci. Part B Polym. Phys.* **1997**, *35*, 945.

(20) Yu, B.; Li, B.; Jin, Q.; Ding, D.; Shi, A.-C. *Soft Matter* **2011**, *7*, 10227.

(21) Durand, W. J.; Blachut, G.; Maher, M. J.; Sirard, S.; Tein, S.; Carlson, M. C.; Asano, Y.; Zhou, S. X.; Lane, A. P.; Bates, C. M.; Ellison, C. J.; Willson, C. G. *J. Polym. Sci. Part A Polym. Chem.* **2015**, *53*, 344.

(22) Lynd, N. A.; Hillmyer, M. A. *Macromolecules* **2005**, *38*, 8803.

(23) Matsen, M. W. *Eur. Phys. J. E* **2013**, *36*, 44.

(24) Beardsley, T. M.; Matsen, M. W. *Macromolecules* **2011**, *44*, 6209.

(25) Matsen, M. W. *Phys. Rev. Lett.* **2007**, *99*, 148304.

(26) Lutz, J.-F.; Ouchi, M.; Liu, D. R.; Sawamoto, M. *Science* **2013**, *341*, 1238149.

(27) Sun, J.; Teran, A. A.; Liao, X.; Balsara, N. P.; Zuckermann, R. N. *J. Am. Chem. Soc.* **2014**, *136*, 2070.

(28) Sun, J.; Teran, A. A.; Liao, X.; Balsara, N. P.; Zuckermann, R. N. *J. Am. Chem. Soc.* **2013**, *135*, 14119.

(29) Oschmann, B.; Lawrence, J.; Schulze, M. W.; Ren, J. M.; Anastasaki, A.; Luo, Y.; Nothling, M. D.; Pester, C. W.; Delaney, K. T.; Connal, L. A.; McGrath, A. J.; Clark, P. G.; Bates, C. M.; Hawker, C. J. *ACS Macro Lett.* **2017**, *6*, 668.

(30) Sinturel, C.; Bates, F. S.; Hillmyer, M. A. *ACS Macro Lett.* **2015**, *4*, 1044.

(31) Pitet, L. M.; van Loon, A. H. M.; Kramer, E. J.; Hawker, C. J.; Meijer, E. W. *ACS Macro Lett.* **2013**, *2*, 1006.

(32) Fox, T. G. *Bull. Am. Phys. Soc.* **1956**, 123.

(33) Kim, J. K.; Lee, H. H.; Gu, Q.-J.; Chang, T.; Jeong, Y. H. *Macromolecules* **1998**, *31*, 4045.

(34) Lee, S.; Gillard, T. M.; Bates, F. S. *AIChE J.* **2013**, *59*, 3502.

(35) Isono, T.; Otsuka, I.; Suemasa, D.; Rochas, C.; Satoh, T.; Borsali, R.; Kakuchi, T. *Macromolecules* **2013**, *46*, 8932.

(36) Luo, Y.; Montarnal, D.; Kim, S.; Shi, W.; Barteau, K. P.; Pester, C. W.; Hustad, P. D.; Christianson, M. D.; Fredrickson, G. H.; Kramer, E. J.; Hawker, C. J. *Macromolecules* **2015**, *48*, 3422.

(37) Lynd, N. A.; Meuler, A. J.; Hillmyer, M. A. *Prog. Polym. Sci.* **2008**, *33*, 875.

(38) Lynd, N. A.; Hillmyer, M. A. *Macromolecules* **2007**, *40*, 8050.

(39) Matsen, M. W. *Eur. Phys. J. E* **2013**, *36*, 44.

(40) Schmitt, A. L.; Mahanthappa, M. K. *Soft Matter* **2012**, *8*, 2294.

(41) Schmitt, A. K.; Mahanthappa, M. K. *Macromolecules* **2017**, *50*, 6779.

(42) Matsushita, Y.; Noro, A.; Iinuma, M.; Suzuki, J.; Ohtani, H.; Takano, A. *Macromolecules* **2003**, *36*, 8074.

(43) Noro, A.; Iinuma, M.; Suzuki, J.; Takano, A.; Matsushita, Y. *Macromolecules* **2004**, *37*, 3804.

(44) Williamson, L. D.; Nealey, P. F. *Macromolecules* **2015**, *48*, 3997.

(45) Sakamoto, N.; Hashimoto, T. *Macromolecules* **1995**, *28*, 6825.

(46) Ringard-Lefebvre, C.; Baszkin, A. *Langmuir* **1994**, *10*, 2376.

(47) Hu, H.; Gopinadhan, M.; Osuji, C. O. *Soft Matter* **2014**, *10*, 3867.

(48) Pitet, L. M.; Alexander-Moonen, E.; Peeters, E.; Druzhinina, T. S.; Wuister, S. F.; Lynd, N. A.; Meijer, E. W. *ACS Nano* **2015**, *9*, 9594.

(49) Lynd, N. A.; Hamilton, B. D.; Hillmyer, M. A. *J. Polym. Sci. Part B Polym. Phys.* **2007**, *45*, 3386.

(50) Widin, J. M.; Schmitt, A. K.; Schmitt, A. L.; Im, K.; Mahanthappa, M. K. *J. Am. Chem. Soc.* **2012**, *134*, 3834.

(51) Widin, J. M.; Kim, M.; Schmitt, A. K.; Han, E.; Gopalan, P.; Mahanthappa, M. K. *Macromolecules* **2013**, *46*, 4472.

(52) Noro, A.; Cho, D.; Takano, A.; Matsushita, Y. *Macromolecules* **2005**, *38*, 4371.

(53) Beardsley, T. M.; Matsen, M. W. *Eur. Phys. J. E* **2008**, *27*, 323.

(54) Pandav, G.; Ganesan, V. *J. Chem. Phys.* **2013**, *139*, 214905.

(55) Bates, F. S. *Macromolecules* **1985**, *18*, 525.

(56) Tsuji, H. *Macromol. Biosci.* **2005**, *5*, 569.

(57) Kasperczyk, J. E. *Macromolecules* **1995**, *28*, 3937.

(58) Zhao, P.; Qin-Feng, W.; Zhong, Q.; Nai-Wen, Z.; Ren, J. *J. Appl. Polym. Sci.* **2010**, *115*, 2955.

(59) Fredrickson, G. H.; Helfand, E. *J. Chem. Phys.* **1987**, *87*, 697.

♦ Chapter 4 ♦

The Subtle Interplay of Crystalline Interactions and Molecular Uniformity in Block Co-Oligomer Systems

Abstract: Crystallization is seldomly utilized as part of the microphase segregation process in ultra-low-MW block copolymers, despite being a very common property of many commodity polymers. Here, we show the properties of discrete, isotactic oligolactic acid and their conjugates with oligodimethylsiloxane. The self-assembly of these uniform blocks and block co-oligomers (BCOs) results in lamellar structures. Accordingly, a select number of BCOs displays an unprecedented uniformity in the domain spacing. A well-balanced blend of crystallization kinetics and molecular pre-organization is key for obtaining perfectly organized structures. Furthermore, a systematic introduction of dispersity reveals the extreme sensitivity of the microphase segregation process toward chain length dispersity in the crystalline block.

This work was performed in close collaboration with Brigitte Lamers.

Part of this work has been published:
van Genabeek, B.; Lamers, B. A. G.; de Waal, B. F. M.; van Son, M. H. C.; Palmans, A. R. A.; Meijer, E. W. *J. Am. Chem. Soc.* **2017**, *139*, 14869.

"I would like to describe a field, in which little has been done, but in which an enormous amount can be done in principle."

—Richard P. Feynman, in *There's Plenty of Room at the Bottom*, 1959.

4.1 Introduction

Self-organization in (di)block copolymers (BCPs) has proven itself, both theoretically and experimentally, as a robust and well-established strategy to generate organized structures at nano- and mesoscopic length scales reaching beyond that of small, organic molecules.[1–3] Yet, the gap between small, perfectly defined molecules and traditional polymers is slowly fading.[4,5] In the previous chapters, we illustrated our efforts to amalgamate full synthetic control and BCP self-assembly. Low-MW block co-oligomers composed of discrete-length oligodimethylsiloxane (*o*DMS) and atactic oligolactic acid (*o*LA) exhibited self-assembly behavior that is qualitatively analogous to that of traditional, disperse block copolymers, but allowed the exploration of a far lower molecular weight regime. In conjunction with that work, Hawker and coworkers simultaneously reported similar observations.[6]

To evolve nano- and mesoscale organization of BCOs into a higher level of perfection, the introduction of additional interactions that further guide self-assembly and increase the effective interaction parameter χ of the incompatible blocks is required. Such interactions can be diverse in nature—Van der Waals, dipole, π–π, and others—and have already been exploited in, for example, the molecular designs of liquid crystalline materials.[7] Also the use of one or two (semi)crystalline blocks in (diblock) BCPs has received a great deal of attention.[8–10] Furthermore, numerous examples highlight the importance of molecular perfection (*i.e.*, sequence control) in other classes of self-assembling oligomeric sequences.[11,12]

In the context of a 'simple' diblock copolymer design, understanding *and* exploiting the optimal blend of (directional) molecular interactions and full synthetic control still is in its infancy. Even though the development of 'high χ–low N' BCPs has led to ever smaller domain spacings, the general trend is to evade the use of crystalline blocks, and the extent of long-range order in the resulting systems is often limited.[6,13–16] A notable exception here is the work of Booth and coworkers on poly(ethylene oxide-*block*-propylene oxide),[17–19] poly(ethylene oxide-*block*-butylene oxide)[20–22] and poly(ethylene oxide-*block*-methylene)[23–27] in di- and triblock configurations.

Triggered by the beneficial influence of a discrete MW on the self-assembly characteristics of fully amorphous *o*DMS–*o*LA, we envisioned a new type of uniform BCOs, consisting of amorphous *o*DMS linked to an isotactic oligo-L-lactic acid (*o*LLA) or oligo-D-lactic acid

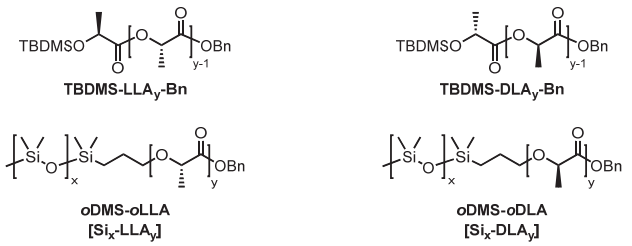

Figure 4–1. Chemical structures of isotactic *o*LA blocks (TBDMS-LLA$_y$-Bn and TBDMS-DLA$_y$-Bn), *o*DMS–*o*LLA [**Si$_x$-LLA$_y$**] and *o*DMS–*o*DLA [**Si$_x$-DLA$_y$**].

(*o*DLA) block (Figure 4–1). As shown before, discrete-length, isotactic oligo-L-lactic acid (*o*LLA) is crystalline, forming well-defined lamellea.[28] Also, having available both enantiomeric forms of isotactic *o*LA (*i*-*o*LA) enables the exploration of stereocomplex formation within the *o*LA domain and its effect on BCO self-assembly.[29] As described in Chapter 2, a library of isotactic *o*LLA and *o*DLA blocks consisting of 2–64 repeat units was generated. Additionally, these isotactic blocks were ligated with discrete-length *o*DMS, resulting in BCOs comprising an amorphous and a crystalline block. This chapter focusses on the thermal and morphological properties of the discrete-length *o*LLA (previously studied in the Hawker research group)[28] and *o*DLA blocks, as well as their *o*DMS conjugates. Furthermore, in line with the work presented in Chapter 3, we will study the dispersity influence in *o*DMS–*o*LLA in more detail.

4.2 Crystallization of discrete-length, isotactic oligolactic acid

In contrast to atactic lactic acid oligomers of comparable length, most of L- and D-lactic acid derived oligomers were obtained as white, crystalline solids at room temperature, regardless of the endgroups. Only the shortest oligomers (up to 8 lactic acid units) did not directly crystallize upon cooling down a sample that was molten at elevated temperatures, but initially formed viscous oils.

4.2.1 Thermal behavior

All materials were studied with differential scanning calorimetry (DSC) over a broad temperature range with a fixed temperature gradient (typically −50 to +180 °C with 10 °C min^{-1}). For clarity, throughout this chapter we will only discuss the oligomers that have both protective groups attached (TBDMS-LLA$_y$-Bn L-**23** or TBMDS-DLA$_y$-Bn D-**23**, see Figure 4–1), unless mentioned otherwise. However, alteration of the thermal behavior after removal of one or both of the endgroups was also examined and turned out to be minimal. The data obtained are summarized in Table 4–1. The thermal profiles can be roughly divided into 3

categories: A, B and C. Each category will be discussed below, and a representative DSC trace is shown in Figure 4–2. Category A represents all materials that do not directly crystallize upon cooling from the isotropic melt but enter a glassy state. Furthermore, upon heating, only a glass transition around $T = T_g$ is observed. All lactic acid oligomers with 2, 4, 8 or 12 repeat units showed this behavior. After prolonged storage at room temperature (up to 12 months), most of these materials crystallized. DSC analyses of the crystallized samples showed the absence of a glass transition and the appearance of a melting transition at $T = T_m$. After melting of the samples during the first heating ramp, only glass transitions could be observed in successive cycles (see Figure 4–2A). Oligomers TBMDS-LLA$_2$-Bn, TBDMS-DLA$_2$-Bn and TBDMS-LLA$_8$-Bn did not crystallize within a 24 month timeframe. It is not fully understood why the latter did not crystallize, whereas the enantiomeric TBDMS-DLA$_8$-Bn did. Probably, the rate of nucleation is extremely slow and very sensitive to remaining traces of solvent or heterogeneous impurities.

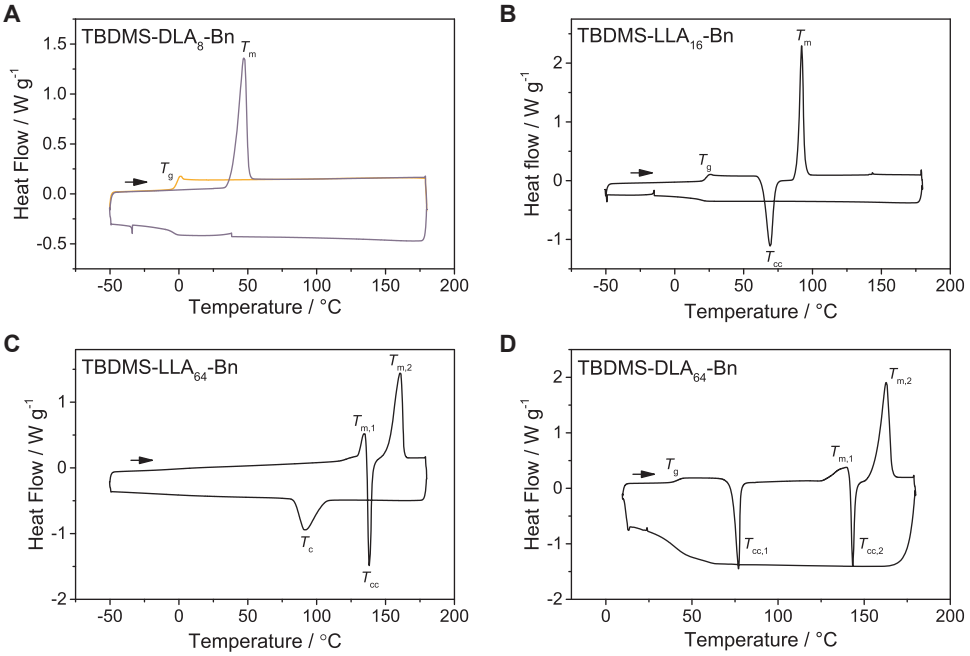

Figure 4–2. DSC traces (second cycle) representative for the 3 categories of thermal profiles for lactic acid oligomers, as described in the main text: (**A**) TBDMS-DLA$_8$-Bn (category A) (purple: first heating/cooling run of a crystallized sample, orange: second cycle). Artefacts at −34 °C and 38 °C in the cooling run are not sample-related; (**B**) TBDMS-LLA$_{16}$-Bn (category B). Artefacts at −15 °C and 144 °C are not sample-related; (**C**) TBDMS-LLA$_{64}$-Bn (category C). For (A–C), a temperature ramp of 10 °C min^{-1} was used; (**D**) TBDMS-DLA$_{64}$-Bn with a cooling rate of 40 °C min^{-1}. Endothermic heatflows have a positive value.

Oligomers in category B (16 and 24 lactic acid repeat units) also did not crystallize upon cooling from the isotropic melt. However, during heating, a glass transition was followed by an exothermic cold-crystallization transition at T_{cc} and finally by a sharp melting transition (Figure 4–2B).

Category C holds the remaining highest MW oligomers with 32 or 64 repeat units. These materials directly crystallized when cooled down from the isotropic melt with 10 °C min^{-1}, yet at temperatures that were significantly lower than the values for T_m ($\Delta T > 30$ °C). No glass transitions were found, revealing the highly crystalline character of these materials. Additionally, oligomers TBDMS-LLA$_{64}$-Bn and TBDMS-DLA$_{64}$-Bn revealed not a single melting transition, but a combination of a melting transition at $T_{m,1}$, followed by an exothermic crystallization, and subsequently a second melting transition at $T_{m,2}$ (see Figure 4–2C). Very similar results were obtained by Hawker and coworkers.[28] Next, compounds TBDMS-DLA$_{32}$-Bn and TBDMS-DLA$_{64}$-Bn were forced into a glassy state by rapid cooling (rate = 40 °C min^{-1}) from the isotropic melt (see Figure 4–2D). Because of the high cooling rate, nucleation was retarded and a glass transition was observed instead. During heating, cold crystallization occurred, followed by melting transitions, as described above.

Table 4–1. Overview of TBDMS-LLA$_y$-Bn and TBDMS-DLA$_y$-Bn oligomers, including thermal and scattering data.

Entry	Type and length[a]		M_n [Da]	T_g [°C]	T_m [°C]	ΔH_{fus} [kJ mol^{-1}]	Cat.[b]	d_{LAM} [nm]
1	LLA	2	366.53	n.d.	-	-	A	-
2	DLA			−66.7	-	-	A	-
3	LLA	4	510.66	−32.0	42.0	33.1	A	-
4	DLA			−32.5	39.0	35.2	A	-
5	LLA	8	798.91	−3.8	-	-	A	-
6	DLA			−1.2	39.3	44.9	A	3.35
7	LLA	12	1087.16	10.9	64.4	39.1	A	4.65
8	DLA			12.8	65.8	73.4	A	4.65
9	LLA	16	1374.41	23.2	89.6	70.9	B	5.95
10	DLA			23.1	89.4	73.5	B	5.89
11	LLA	24	1951.92	29.7	120.9	101.1	B	8.19
12	LLA	32	2528.42	n.d.	139.9	195.9	C	10.65
13	DLA			37.7	135.4	189.8	C	10.73
14	LLA	64	4834.44	n.d.	152.0[c]	291.9	C	10.1, 15.8[d]
15	DLA			42.1	159.5[c]	377.5	C	10.64

[a] Lactic acid oligomers are endcapped with a TBDMS and benzyl group. The number represents the number of lactic acid repeat units (*e.g.*, DLA 12 = TBDMS-DLA$_{12}$-Bn); [b] Thermal behavior category, see main text; [c] Two melting transitions were observed. The listed value is the highest T_m; [d] Two coexisting lamellar structures were observed.

The melting enthalpies obtained were compared to the reported value for 100% crystalline PLLA:[30] 6.55 kJ (mol LA units)$^{-1}$. The ΔH_{fus} values reported in Table 4–1 were divided by the number of LA units per oligomer, giving values that are 70–94% of the literature value. No correlation was found between the oligomer length and heat of fusion per LA unit. Likely, the conditions under which the DSC measurements were performed were not ideal to generate 100% crystalline samples.

4.2.2 X-ray scattering

The formation of an organized structure was examined for all crystalline lactic acid oligomers with small-angle X-ray scattering (SAXS). 2-D transmission-scattering data were acquired in medium- and wide-angle modes (MAXS and WAXS; $0.1 < q < 30$ nm^{-1}), resulting in 1-D scattering profiles that captured all potential organization over a size range of 0.2–60 nm. To prevent the undesired formation of amorphous regions, samples were prepared by very slow cooling from the melt (0.5 °C min^{-1}). A selection of scattering profiles is shown in Figure 4–3. Clearly, all solidified lactic acid oligomers with 8 or more repeat units exhibit very well structured lamellar macrolattices, indicated by the sharp, equally spaced scattering peaks in the MAXS region (Figure 4–3A). Non-crystallized oligomers (*e.g.*, TBDMS-LLA$_8$-Bn), as well as crystalline TBDMS-LLA$_4$-Bn and TBDMS-DLA$_4$-Bn, did not show any (sharp) reflections in this q-region. Interestingly, sample TBDMS-LLA$_{64}$-Bn seems to consist of two lamellar structures with a different lamellar thickness, of which we labeled the two sets of principal and related higher-order reflections with q^* and q_2^*, respectively. Lamellar spacings (d_{LAM}) could be extracted from the position of the primary scattering peak at $q = q^*$ via the relation $d_{LAM} = 2\pi/q^*$. These values are listed in Table 4–1 and plotted as a function of the number of repeat units in Figure 4–3C. Separate linear fits through the data points for both enantiomeric sets (excluding the points for the oligomers with 64 repeat units) reveal near-perfect linear correlations between the number of repeat units and the lamellar thickness. An increase of 0.306±0.003 nm and 0.298±0.003 nm per monomeric residue was found for *o*LLA and *o*DLA, respectively.

Furthermore, additional scattering reflections owing to the oligolactic acid crystal lattice were present in the WAXS domain (q = 5–20 nm^{-1}; see Figure 4–3B). Obviously, non-crystallized oligomers TBDMS-LLA$_2$-Bn, TBDMS-DLA$_2$-Bn and TBDMS-LLA$_8$-Bn showed no scattering reflections in this region. Although a large number of sharp, yet not fully resolved, reflections were present for the shortest crystalline oligomer TBDMS-LLA$_4$-Bn—for which no reflections at lower q-values were found—only broad, overlapping reflections remained for the longer oligomers. For oligomers with 16 repeat units or more, the positions

of three most pronounced reflections at 10.4, 11.8 and 13.4 nm^{-1} are indicated with the red, dashed lines. Those reflections perfectly matched the ones found for crystalline PLLA.[31] Consequently, we may assume that these oligomers crystallize in a pseudo-orthorhombic unit cell containing two oligolactic acid molecules oriented in 10_3 helices parallel to the unit cell *c*-axis (cell dimensions: a = 1.07 nm, b = 0.595 nm, and c = 2.78 nm).

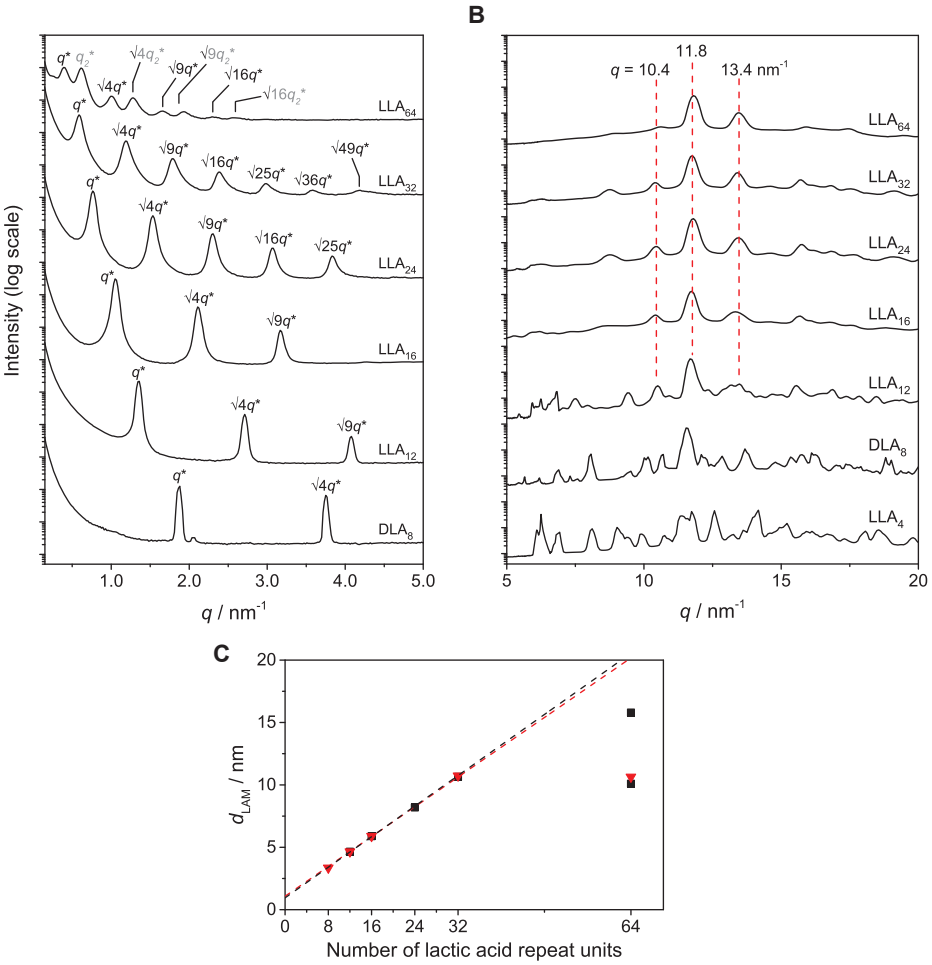

Figure 4–3. (**A–B**) Reduced transmission-SAXS data for lactic acid oligomers (with protective groups present) of various lengths in the low-q range (**A**) and high-q range (**B**). The dashed, red lines mark the position of the three most prominent reflections in the WAXS region. The data are shifted vertically for clarity. Higher-order Bragg reflections are indicated for all scattering curves if present. All data were recorded at room temperature; (**C**) Lamellar domain spacing d_{LAM} of TBDMS-LLA$_y$-Bn (■) and TBDMS-DLA$_y$-Bn (▼) as a function of the number of repeat units. The dashed lines are individual linear fits for both enantiomeric sets (black for *o*LLA, red for *o*DLA) through all data points except those for the oligomers with 64 repeat units.

Since the 10_3 *o*LLA helix spans the full 2.78 nm of the unit cell, it follows that fully extended chains should elongate by 0.278 nm for each additional lactic acid residue. Indeed, this value is very close to the experimentally found increase of approximately 0.3 nm per monomeric residue (*vide supra*). As such, the lamellar domains described above most probably consist of unfolded *o*LLA or *o*DLA molecules—in a 10_3 helix—that are oriented perpendicular to the lamellar planes. *o*LLA_{64} and *o*DLA_{64}, both having lower values for d_{LAM} than expected, form an exception. For these lengths the gain of entropy that results from chain folding most likely overcomes the enthalpic penalty that is associated with this packing mode. Similarly, conventional, high-MW PLLA also adopts a folded structure, with an average lamellar domain spacing of around 24 nm.[32]

4.3 Microphase behavior of *o*DMS-*o*LLA and *o*DMS-*o*DLA

In contrast to the atactic BCOs discussed in Chapter 3, which were obtained as soft, waxy substances at room temperature, we found that the BCOs containing an isotactic *o*LLA or *o*DLA block appeared as crystalline, white solids. Only [**Si_{23}-LLA_9**] and [**Si_{23}-DLA_9**] remained liquid-like at room temperature. Similar to the oligolactic acid homoblocks, the isotactic BCOs were subjected to DSC and SAXS analyses, using identical measurement conditions. The examined BCOs are listed in Table 4–2.

4.3.1 Thermal properties

Figure 4–4 displays DSC thermograms (heating traces) for a selection of BCOs. Typically, two (reversible) transitions can be observed: a major endothermic transition ($\gg$ 10 kJ (mol BCO)$^{-1}$) and a second, much weaker endotherm (~2 kJ (mol BCO)$^{-1}$) at higher temperatures (the latter is indicated with an asterisk). A hysteresis in the position of the highest intensity transition was found when comparing the heating and cooling runs. This hysteresis varied between 5 and 20 °C, and increased with decreasing *o*LA block lengths. For BCOs [**Si_{15}-LLA_{17}**] and [**Si_{15}-DLA_{17}**], the highly enthalpic transition was the only observable transition in the heating run. However, during the cooling run of enantiomer [**Si_{15}-LLA_{17}**] a weak shoulder was visible at the high-temperature side of the exothermic peak (see Figure 4–11A and more details in Section 4.5.2). Finally, the two BCOs [**Si_{23}-LLA_9**] and [**Si_{23}-DLA_9**] only exhibited a single, weak (~2 kJ (mol BCO)$^{-1}$) transition.

The weak thermal effect is ascribed to the order–disorder transition, given the low enthalpic footprint[33–36] and comparability of the order–disorder transition temperatures (T_{ODT}) with those of fully amorphous *o*DMS-*o*LA BCOs that comprise an atactic oligolactic

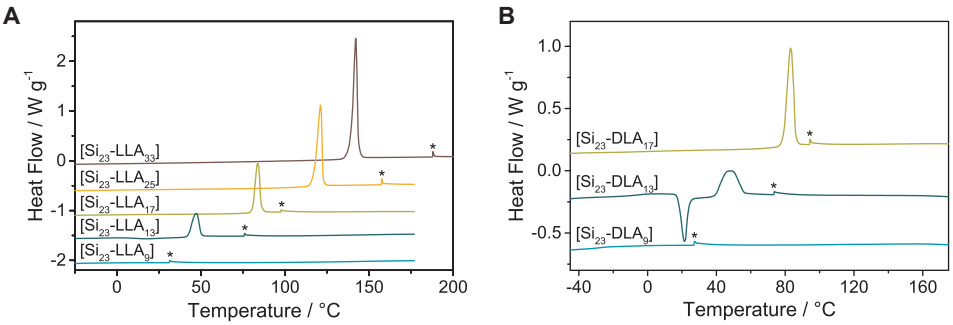

Figure 4–4. DSC traces (second heating run) for a selection of (**A**) [$\mathbf{Si_x\text{-}LLA_y}$] and (**B**) [$\mathbf{Si_x\text{-}DLA_y}$] BCOs. Endothermic heatflows have a positive value. The data are shifted vertically for clarity. The order–disorder transitions, unrelated to the crystallization process, are indicated with an asterisk. A temperature ramp of 10 °C min^{-1} was used.

acid block (see Chapter 3). Still, the T_{ODT} values of the BCOs that contain an isotactic lactic acid block are systematically higher (6 to 20 °C difference) than those of amorphous *o*DMS-*o*LA BCOs of equal length and composition. This suggests that the effective interaction parameter, χ_{eff}, between *o*DMS and *o*LLA or *o*DLA blocks is larger than that of the combination *o*DMS and atactic *o*LA.

We attribute the prominent peaks that typically preceded the ODTs in the heating runs, to a melting event (and related crystallization event upon cooling) of the oligolactic acid block. This is supported by similar values for the melting enthalpies of the individual oligolactic acid blocks and BCOs derived thereof (*e.g.*, TBDMS-LLA_{12}-Bn (ΔH_{fus} = 39.1 kJ mol^{-1}) and [$\mathbf{Si_{23}\text{-}LLA_{13}}$] ($\Delta H_{fus}$ = 38.2 kJ (mol BCO)$^{-1}$)), although in some cases the values are more divergent (*viz.*, TBDMS-LLA_{24}-Bn and [$\mathbf{Si_{23}\text{-}LLA_{25}}$]). Nevertheless, it is safe to assume that in the crystallized BCOs, a major part of the oligolactic acid block is incorporated in a crystalline phase (provided that the *o*DMS block does not contribute to the crystalline phase, *vide infra*). Apparently, in BCOs [$\mathbf{Si_{15}\text{-}LLA_{17}}$] and [$\mathbf{Si_{15}\text{-}DLA_{17}}$], the crystalline interactions within the *o*LA block are strong enough to preserve the organized—*i.e.*, crystallized—system at temperatures above the (expected) T_{ODT} (for example, T_{ODT} = 72.9 °C for amorphous [$\mathbf{Si_{15}\text{-}LA_{17}}$]). Only as a result of the 7 °C hysteresis in the crystallization temperature, BCO [$\mathbf{Si_{15}\text{-}LLA_{17}}$] shows an ordinary order–disorder transition preceding the crystallization peak, which corresponds to the microphase segregation of the (still) amorphous *o*LLA and *o*DMS blocks.

Table 4–2. Examined block co-oligomers: thermal and scattering data.

Entry	BCO	M_n [Da]	N^a	$f_{LA}{}^b$	T_m [°C]	$\Delta H_{fus}{}^c$ [kJ mol^{-1}]	T_{ODT} [°C]	$d_{cryst}{}^d$ [nm]	$d_{amorph}{}^e$ [nm]
1	[**Si$_{15}$-LLA$_{17}$**]	2486	32.0	0.47	85.1	78.3	79.1[g]	11.7	-
2	[**Si$_{15}$-DLA$_{17}$**]				81.5	76.1	-	12.1	-
3	[**Si$_{23}$-LLA$_{9}$**]	2502	34.7	0.25	−24.8[f]	-	31.2	-	6.3 (CYL, 25 °C)
4	[**Si$_{23}$-DLA$_{9}$**]				−31.4[f]	-	26.9	-	6.4 (CYL, 25 °C)
5	[**Si$_{23}$-LLA$_{13}$**]	2791	38.1	0.31	42.5	38.2	75.7	11.3	7.1 (CYL, 55 °C)
6	[**Si$_{23}$-DLA$_{13}$**]				39.5	34.3	73.4	11.6	n.d.
7	[**Si$_{23}$-LLA$_{17}$**]	3079	41.4	0.36	80.8	63.7	97.5	12.8	7.7 (GYR, 91 °C)
8	[**Si$_{23}$-DLA$_{17}$**]				78.9	66.5	94.2	12.8	n.d.
9	[**Si$_{23}$-LLA$_{25}$**]	3655	48.2	0.45	117.2	130.8	157.3	12.8	8.3 (LAM, 145 °C)
10	[**Si$_{23}$-LLA$_{33}$**]	4232	54.9	0.52	139.2	205.5	187.7	15.2	9.1 (LAM, 145 °C)

[a] Number of segments based on a 110 Å^3 reference volume; [b] Volume fraction of the crystalline *o*LA block, calculated using bulk densities for PDMS (0.95 g mL^{-1}) and PLLA (1.29 g mL^{-1});[29] [c] Melting enthalpy in kJ per mole of BCO; [d] Domain spacing of the crystalline, lamellar microphase; [e] Domain spacing of the amorphous microphase. The morphology and sample temperature are in between brackets; [f] T_g instead of T_m; [g] The transition was only observed in the cooling run. n.d.: not determined.

Interestingly, nearly all BCOs with an oligolactic acid block with more than 9 monomeric residues directly crystallized upon cooling. As opposed to a number of the individual *o*LLA and *o*DLA molecules, no glass transitions or cold-crystallization effects could be observed. Also, the hysteresis that was found between the melting and crystallization temperatures is smaller for the crystalline *o*LA blocks within the BCO than for the individual blocks. This indicates a more facile formation of an oligolactic acid nucleus if ligated with an *o*DMS block, which very likely is related to the fact that crystallization within the *i*-*o*LLA domains is confined.[i] A single exception was BCO [**Si$_{23}$-DLA$_{13}$**], for which a T_g and T_{CC} could be determined. The origin of this anomaly—enantiomer [**Si$_{23}$-LLA$_{13}$**] did crystallize directly upon cooling—is not known. However, it suggests that the crystallization kinetics of the shortest crystalline oligolactic acid blocks presumably remain very sensitive toward external factors (*e.g.*, traces of solvent). When comparing the melting points of the BCOs with those of pristine *o*LLA and *o*DLA, we noticed that the melting points of the BCOs (following the red dashed line in Figure 4–5) typically are lower than those of the oligolactic acid building blocks, and this offset increases with decreasing number of repeat units. Extrapolation of the red dashed line for even shorter oligolactic acid block lengths shows that the location of the melting point rapidly approaches that of the glass transition of the *i*-*o*LA block. This

[i] *o*LLA or *o*DLA domains are always flanked by (covalently bound) *o*DMS regions, and therefore greatly differ from the *o*LLA and *o*DLA bulk material.

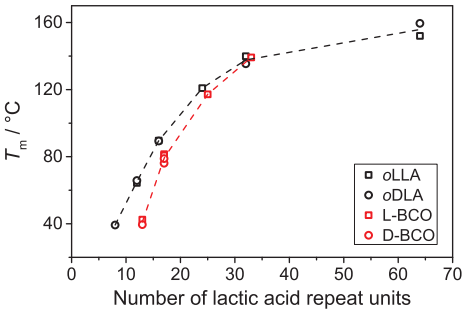

Figure 4–5. Melting points of TBDMS-LLA$_y$-Bn L-**23** (black, open squares), TBDMS-DLA$_y$-Bn D-**23** (black, open circles), [**Si$_x$-LLA$_y$**] (red, open squares) and [**Si$_x$-DLA$_y$**] (red, open circles) as a function of the number of lactic acid repeat units *y*. The dashed black and red lines are added to guide the eye.

corroborates the absence of a crystalline phase in BCOs [**Si$_{23}$-LLA$_9$**] and [**Si$_{23}$-DLA$_9$**] even after storage of these compounds for multiple weeks at 4 or −20 °C. Extrapolation to higher lengths leads to a plateau value, which for high-MW PLLA is found at 180 °C.[31]

4.3.2 Microphase separation

The expected existence of microphase-separated structures below T_m (or T_{ODT}) was examined with SAXS at room temperature. To minimalize the formation of kinetically trapped states during crystallization, samples were cooled down from temperatures above T_{ODT} with a rate of 0.5 °C min^{-1} inside thin-walled glass capillaries. A selection of 1-D scattering profiles resulting from the radial averaging of the scattering data are depicted in Figure 4–6. All BCOs showed a primary reflection peak at $q^* < 1$ nm^{-1} and two or more higher-order reflections, confirming the presence of an ordered (microphase-separated) structure at room temperature. Related domain sizes were calculated as $d = 2\pi/q^*$ and tabulated as d_{cryst} for the BCOs that are crystalline (see Table 4–2).

Figure 4–6A shows scattering profiles (MAXS region) of BCOs containing an *o*DMS with 23 siloxane repeat units, connected to *o*LLA of various lengths. The results for [**Si$_x$-DLA$_y$**] BCOs are nearly identical to those obtained for [**Si$_x$-LLA$_y$**]. Therefore, we will only discuss the results for the *o*LLA containing BCOs here, but these are valid for oDMS-*o*DLA BCOs as well. BCO [**Si$_{23}$-LLA$_9$**]—the sole block length combination that did not show a crystallization transition in DSC analysis—exhibited scattering reflections at q^*, $\sqrt{3}q^*$ and $\sqrt{7}q^*$. This is consistent with a morphology of hexagonally packed cylinders with a domain spacing $d_{10} = d^* = 6.3$ nm. All BCOs with a longer *o*LLA block showed a significant shift of the primary scattering peak positions to lower *q*-values. Higher-order reflections reflections at integer multiples of q^* (*i.e.*, $\sqrt{4}q^*$, $\sqrt{9}q^*$, $\sqrt{16}q^*$, …) were most prominent, indicative for the presence

of a lamellar structure. However, the scattering patterns of [**Si$_{23}$-LLA$_{13}$**] and [**Si$_{23}$-LLA$_{17}$**] looked distorted, mostly expressed as broadened reflections and a shoulders at the low-q side of the $\sqrt{4}q^*$ peaks.

BCO [**Si$_{15}$-LLA$_{17}$**] revealed an unprecedentedly high number of equally spaced reflection peaks (q/q^* up to $\sqrt{169}$), indicative for a high degree of long-range order (Figure 4–6B, orange curve). Again, the distance between the reflections unambiguously pointed to the presence of a lamellar structure with a lamellar domain spacing d^* = 11.7 nm. Comparison of the scattering data of [**Si$_{15}$-LLA$_{17}$**] with BCO [**Si$_{15}$-LA$_{17}$**] (purple curve) further emphasized the sharp contrast in the level of organization of BCOs with an isotactic or atactic *o*LA block, as well as a significant increase of the lamellar domain spacing of the semicrystalline BCO by almost 65%.

At higher q-values, additional scattering peaks reveal further interchain organization in BCO [**Si$_{15}$-LLA$_{17}$**]. Similar to the BCO with the atactic *o*LA block, a broad reflection at $q \approx 8.6$

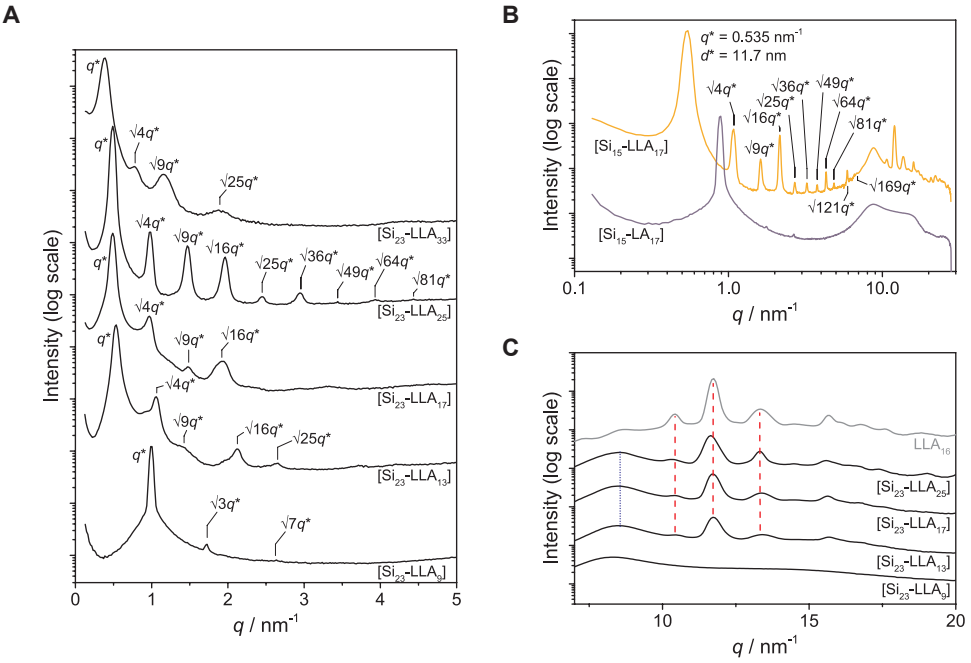

Figure 4–6. Reduced transmission-SAXS data for: (**A**) [**Si$_{23}$-LLA$_{Y}$**] BCOs; (**B**) [**Si$_{15}$-LLA$_{17}$**] (in orange) and atactic [**Si$_{15}$-LA$_{17}$**] (in purple); (**C**) [**Si$_{23}$-LLA$_{Y}$**] BCOs in the high-q region. Scattering data for TBDMS-LLA$_{16}$-Bn are plotted in gray. The dashed red lines indicate the three most prominent *o*LLA-related WAXS reflections. The dotted blue line marks the scattering maxima of the siloxane halos. At scattering measurements were performed at room temperature. The data are shifted vertically for clarity. A selection of higher–order Bragg reflections in the MAXS region is indicated.

nm^{-1} was attributed to the amorphous siloxane block. However, additional, sharp reflections at larger q were only present in [**Si$_{15}$-LLA$_{17}$**], whereas amorphous [**Si$_{15}$-LA$_{17}$**] only exhibited a second broad reflection originating from the amorphous *o*LA domains.

As is shown in more detail Figure 4–6C, sharp scattering reflections were observed in the q-range 5–20 nm^{-1} for all *o*LLA containing BCOs except [**Si$_{23}$-LLA$_{9}$**]. Three reflections around 10.4, 11.8 and 13.4 nm^{-1} dominated in the WAXS region (indicated with the red, dashed lines). For comparison, scattering data of TBDMS-LLA$_{16}$-Bn are added. The close resemblance of the data suggests that within the lamellar domains generated by the *o*LLA blocks, an *o*LLA crystal structure similar to that of *o*LLA homoblocks was present. The lack of clear reflections in the scattering pattern of [**Si$_{23}$-LLA$_{9}$**] confirms the non-crystalline state of this BCO, as was already suggested by the DSC data. Similar to BCO [**Si$_{15}$-LLA$_{17}$**], a broad reflection with a maximum at $q \approx 8.6$ nm^{-1} (blue, dotted line) was found in the scattering profiles of all other BCOs and could be ascribed to the amorphous chain organization in the *o*DMS domain.

Additionally, variable temperature (VT-)SAXS measurements were conducted for most BCOs, with the aim to capture any structural transformations related to the transitions that were observed with the DSC measurements. A selection of 1-D scattering profiles for BCOs [**Si$_{15}$-LLA$_{17}$**], [**Si$_{23}$-LLA$_{13}$**], [**Si$_{23}$-LLA$_{17}$**], and [**Si$_{23}$-LLA$_{25}$**] at various temperatures is presented in Figure 4–7. Generally, little to no changes in the scattering data for any of the four BCOs were observed upon heating from 25 °C to slightly below the melting temperature. In contrast, subsequent melting of the sample within a narrow temperature window around T_m resulted in significant changes in the scattering profiles. As pictured in Figure 4–7A, all sharp reflections in the WAXS region disappeared above T_m (T_m = 85.1 °C for [**Si$_{15}$-LLA$_{17}$**]), which was indicative for the transformation of the crystalline *o*LLA domain into an amorphous (molten) phase. Similar transitions were observed for the other BCOs. Also, a loss of the scattering reflections at integer values of q^* was observed, consistent with the disappearance of the (crystalline) lamellar phase of the BCOs. After melting of the crystalline *o*LLA blocks, BCO [**Si$_{15}$-LLA$_{17}$**] entered a disordered state, indicated by the single remaining, broad reflection. In contrast, the formation of a differently ordered morphologies was observed for BCOs [**Si$_{23}$-LLA$_{13}$**], [**Si$_{23}$-LLA$_{17}$**], and [**Si$_{23}$-LLA$_{25}$**]. This followed from the appearance of new, primary scattering peaks, denoted q_2^* in Figure 4–7B–D. Additionally, all three BCOs showed a number of associated higher-order reflections. BCO [**Si$_{23}$-LLA$_{13}$**] revealed a new reflection at $q_2^* = 0.89$ nm^{-1} and two additional reflections at $\sqrt{4}q_2^*$ and $\sqrt{7}q_2^*$. This conformed to a structure consisting of hexagonally packed *o*LLA cylinders (d_{amorph} = 7.10 nm), similar to that

of [**Si$_{23}$-LLA$_9$**]. Scattering reflections observed at $q_2^* = 0.81$ nm^{-1} and $\sqrt{4/3}q_2^*$ indicated the formation of a gyroid microphase with $d_{amorph} = 7.7$ nm in BCO [**Si$_{23}$-LLA$_{17}$**] above T_m. Finally, [**Si$_{23}$-LLA$_{25}$**] most likely remained in a lamellar morphology after melting of the crystalline block. However, a new primary peak at higher q-value ($q_2^* = 0.76$ nm^{-1}) indicated a significant decrease of the domain spacing to $d_{amorph} = 8.3$ nm. Further increase of the temperature ultimately lead to the complete loss of ordering in polymer [**Si$_{23}$-LLA$_{17}$**] above T_{ODT}. It is still unclear why [**Si$_{23}$-LLA$_{13}$**] and [**Si$_{23}$-LLA$_{25}$**] did not enter the disordered state above T_{ODT}. Presumably, this is related to an offset in the calibration of the temperature probe in the sample heating stage. During cooling of the samples, the reverse transitions were observed, leading to a crystalline, lamellar structure at room temperature for all BCOs.

The microphase-segregated structures for BCOs [**Si$_{23}$-LLA$_{13}$**], [**Si$_{23}$-LLA$_{17}$**], and [**Si$_{23}$-LLA$_{25}$**] above T_m were fully consistent with the amorphous state morphologies observed for the sister compounds [**Si$_{23}$-LA$_y$**] that were studied in Chapter 3. Furthermore, the data confirmed the proper assignment of both the intense and weak transitions in the DSC traces

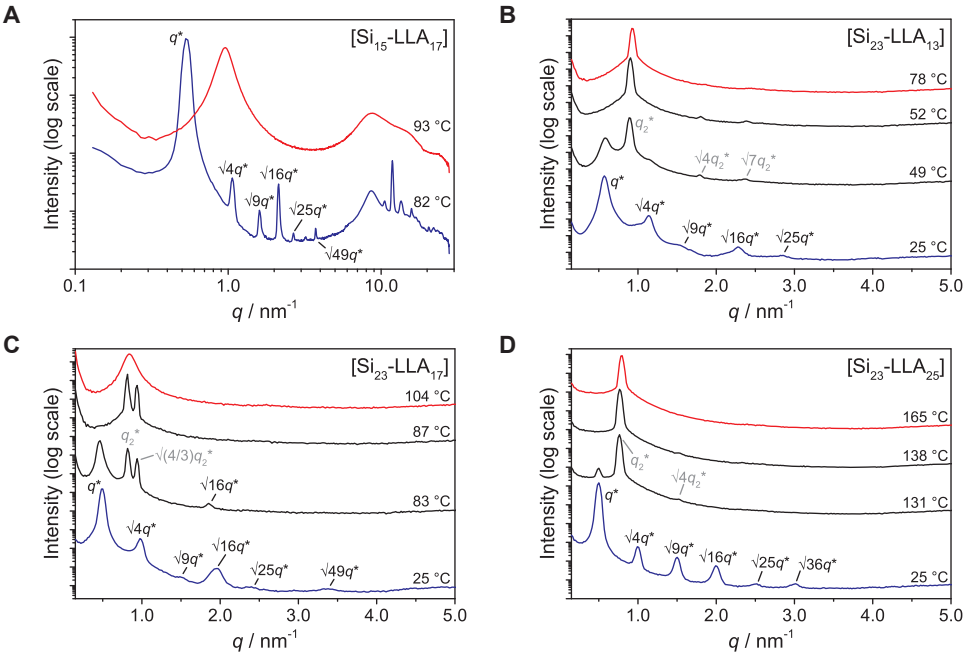

Figure 4–7. Reduced variable temperature transmission-SAXS data for: (**A**) [**Si$_{15}$-LLA$_{17}$**]; (**B**) [**Si$_{23}$-LLA$_{13}$**]; (**C**) [**Si$_{23}$-LLA$_{17}$**]; (**D**) [**Si$_{23}$-LLA$_{25}$**]. The data are shifted vertically for clarity. Lowest and highest temperature data are plotted in blue and red, respectively. (Higher–order) Bragg reflections of the crystalline phase are indicated for all scattering curves in black if present. Reflections indicated in gray belong to the microphase-segregated state above the melting point of the *o*LLA block.

as being the melting and order–disorder transitions, respectively. Indeed, below T_m, all BCOs formed a lamellar structure, consisting of alternating, amorphous *o*DMS blocks and crystalline *o*LA blocks. Here, the formation of the lamellar phase presumably is governed by the preferred parallel orientation of the *o*LA chains in the crystalline state. Above T_m, most BCOs remained microphase-segregated and rearranged to the preferred morphology for an amorphous BCO, determined by the *o*LLA volume fraction. The absence of an amorphous, microphase-separated structure in [**Si$_{15}$-LLA$_{17}$**] corroborates the absence of a separate ODT for this BCO in the DSC data.

4.3.3 Molecular orientation

In Section 4.2.2, it was deduced that the *o*LLA or *o*DLA chains crystallize into lamellar domains, in which the individual oligomers are present as unfolded (*i.e.*, stretched) molecules, with their molecular long-axis oriented perpendicular to the lamellar planes. A very schematic illustration of the *o*LLA orientation (projected as a 2-D image) is provided in Figure 4–8A. Here the lamellar domain spacing (d_{LAM}) that was obtained with SAXS measurements corresponds to the interlamellar spacing, and thus roughly to the length of the extended *o*LLA molecule. The lamellar domain spacings are plotted in Figure 4–8B as the brown squares.

The BCOs that contain crystallized *i*-*o*LA domains at room temperature also form a lamellar structure, consisting of alternating *o*DMS (amorphous) and *i*-*o*LA (crystalline) regions. Under the assumption that the molecular *o*DMS and *i*-*o*LA fragments are fully incorporated in their respective domains, the thickness of the individual *o*DMS and *i*-*o*LA lamellae can be estimated by multiplication of the total domain spacing (d^*) with the volume fraction of the respective BCO blocks (*i.e.*, the thickness of the *i*-*o*LA lamellae $d_{LA} = f_{LA} \times d^*$). In Figure 4–8B, the estimated thicknesses of the crystalline *o*LLA domains of BCOs [**Si$_{15}$-LLA$_{17}$**] and [**Si$_{23}$-LLA$_y$**] are plotted as the single orange triangle and olive green circles, respectively.

Interestingly, the thickness of the *o*LLA domain in BCO [**Si$_{15}$-LLA$_{17}$**] matches closely with the expected value for the length of an extended LLA$_{17}$ chain that follows from interpolation of the known domain spacing of the loose *o*LLA blocks.[ii] Therefore, we propose that the *o*LLA domain of the lamellar BCO structure is composed fully stretched *o*LLA chains, aligned perpendicular to the domain boundary (see Figure 4–8C). Subsequently, the *o*DMS domain

[ii] It should be taken into account that the *o*LLA block in [**Si$_{15}$-LLA$_{17}$**] lacks the TDBMS group that is present in the pure *o*LLA blocks.

consists of a highly asymmetric, amorphous *o*DMS coil, elongated perpendicular to the lamellar domains. Since we may safely assume that the covalent links between *o*DMS and *o*LLA are localized at both the top and bottom domain boundaries of the *o*LLA domain that is sketched in Figure 4–8C, the *o*LLA chains will adopt an interdigitated structure.

In case of the [**Si$_{23}$-LLA$_y$**] BCOs, we observed a significant deviation of the *o*LLA lamellar thickness (olive green circles in Figure 4–8B) to lower values compared to those of the *o*LLA homoblocks. Most likely, the lower-than-expected d_{LA} is caused by tilting of the extended *o*LLA chains away from the normal of the lamellar domain boundaries, which in turn causes a reduction of the domain thickness. This decrease of d^* allows the *o*DMS chain to adopt a more random coil conformation, which greatly minimizes the entropic penalty resulting from the severe chain stretching of the *o*DMS backbone, thus lowering the overall Gibbs free energy of the system.

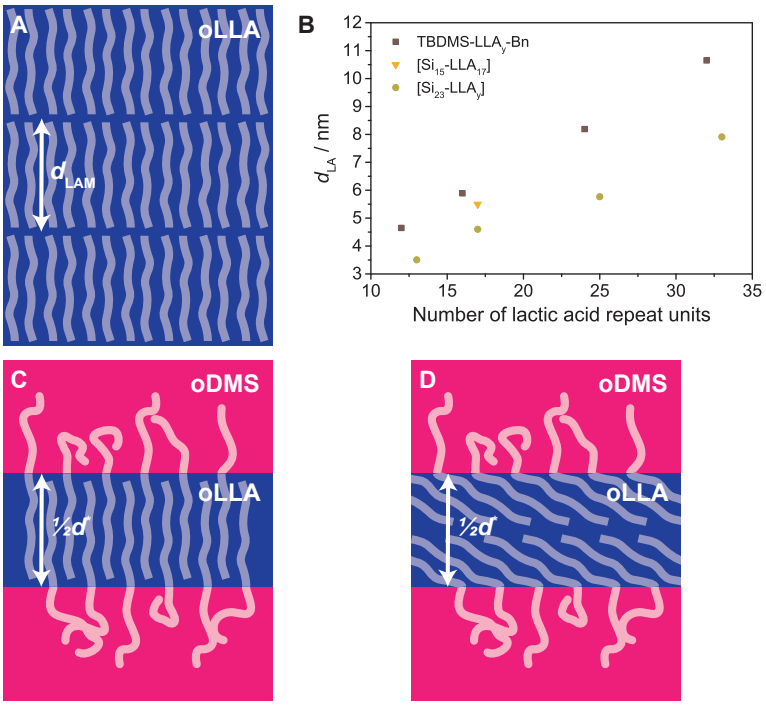

Figure 4–8. Schematic 2-D projections of: (**A**) *o*LLA crystal structure; (**C**) BCO [**Si$_{15}$-LA$_{17}$**] at room temperature, with interdigitated *o*LLA chains oriented perpendicular to the lamellar domains; (**D**) BCO [**Si$_{15}$-LA$_{17}$**] at room temperature, with a double layer of *o*LLA chains in a tilted configuration (with respect to the lamellar domains). Blue = *o*LLA, pink = *o*DMS; (**B**) Thickness of the *o*LLA lamellae for a selection of TBMDS-LLA$_y$-Bn L-**23** and [**Si$_x$-LLA$_y$**] BCOs.

Finally, an alternative *o*LLA chain orientation is pictured for BCO [**Si$_{15}$-LLA$_{17}$**] in Figure 4–8D. Here, a tilt of the extended *o*LLA chains away from the normal of the lamellar domain boundaries is proposed. As a result, the *o*LLA domain consists of two stacked, non-interdigitated *o*LLA lamellae, with a combined thickness of $d_{LA} \approx \frac{1}{2}d^*$.

4.4 Stereocomplex formation in discrete-length (co-)oligomers

The formation and behavior of PLLA and PDLA stereocomplexes is known and studied for a long time already,[29,31] but remains open for debate.[37] Here, we briefly studied the stereocomplex (sc) formation in the *i*-*o*LA homoblocks and the related [**Si$_x$-LLA$_y$**] and [**Si$_x$-DLA$_y$**] BCOs by following changes in the thermal and self-assembly behavior. Stereocomplex formation was induced by physical mixing of both enantiomeric forms of *i*-*o*LA of equal length, or, similarly, mixing of [**Si$_x$-LLA$_y$**] and [**Si$_x$-DLA$_y$**] of equal MW and composition. We will abbreviate the stereocomplexes as sc-LA$_y$ and sc-[**Si$_x$-LA$_y$**]. Mixing was performed in solution (DCM). After removal of the solvent, the stereocomplex mixtures were fully dried under high vacuum. In all cases a 1 to 1 mixing ratio was used. The stereocomplexes studied are summarized in Table 4–3.

4.4.1 Stereocomplexes of *o*LLA and *o*DLA

Interestingly, all stereocomplexes of the *i*-*o*LA blocks (entries 1–6) were solid at room temperature. Most samples crystallized directly after preparation, except sc-LA$_8$, which crystallized after storage for 4 months at room temperature. DSC analysis of all samples

Table 4–3. Thermal and scattering data for stereocomplexes of *i*-*o*LA, and [**Si$_x$-LLA$_y$**] and [**Si$_x$-DLA$_y$**] BCOs.

Entry	Stereocomplex[a]	T_g [°C]	T_m [°C]	ΔH_{fus}[b] [kJ mol^{-1}]	d_{cryst}[c] [nm]
1	LLA$_4$ + DLA$_4$	−33.5	33.2	34.3	1.75
2	LLA$_8$ + DLA$_8$	−11.9	41.6	25.9	3.82
3	LLA$_{12}$ + DLA$_{12}$	-	87.7	59.7	4.52
4	LLA$_{16}$ + DLA$_{16}$	-	143.2	302.4	5.39
5	LLA$_{32}$ + DLA$_{32}$	-	202.9	302.4	10.4
6	LLA$_{64}$ + DLA$_{64}$	-	227.3	549.2	18.6
7	[**Si$_{15}$-LLA$_{17}$**] + [**Si$_{15}$-DLA$_{17}$**]	-	142.7	126.8	11.7
8	[**Si$_{23}$-LLA$_9$**] + [**Si$_{23}$-DLA$_9$**]	-	47.2	41.8	9.93
9	[**Si$_{23}$-LLA$_{13}$**] + [**Si$_{23}$-DLA$_{13}$**]	-	103.8	89.3	11.7
10	[**Si$_{23}$-LLA$_{17}$**] + [**Si$_{23}$-DLA$_{17}$**]	-	137.5	134.9	13.4

[a] A 1 to 1 physical mixture of both components; [b] Melting enthalpy per mole of individual oligomer or BCO; [c] Domain spacing of the crystalline, lamellar microphase.

revealed a significant increase of the melting temperatures and melting enthalpies, compared to those of the homochiral constituents. Stereocomplexes sc-LA_4 or sc-LA_8 melted only once. In consecutive heating/cooling cycles, only a glass transition was observed (*i.e.*, a category A thermal profile, see Section 4.2.1). Stereocomplexes of the longer oligomers all conformed to category C: direct crystallization when cooled down from the isotropic melt with 10 °C min^{-1}. Typically, undercooling temperatures of 10–50 °C were observed. For these stereocomplexes, no glass transitions were found. Also, in no case signs of cold-crystallization or double melting transitions were observed, as was the case for a number of *o*LLA and *o*DLA blocks.

The formation of a lamellar crystal structure was confirmed by SAXS, evident from the equally spaced, strong reflections in the MAXS region of the scattering profiles (Figure 4–9A). A lamellar domain spacing could be extracted for all *i*-*o*LA stereocomplexes (sc-LA_4 to sc-LA_{64}), and can be found in in Table 4–3. Most domain spacings were almost equal to those found for the homochiral blocks. Surprisingly, the domain spacing of sc-LA_{64} was nearly double that of sc-LA_{32}, indicative for fully stretched *i*-*o*LA chains in the stereocomplex of both oligomer lengths. In contrast to the homoblocks, the enthalpic penalty for chain folding in the stereocomplex sc-LA_{64} probably is much higher, which outweighs the potential increase in entropy that would result from chain folding, and forces the molecules in fully stretched conformation.

Additional scattering measurements in the WAXS region resulted in scattering profiles that looked very similar for all evaluated stereocomplex *o*LA mixtures (Figure 4–9B). Typically, three strong reflections were observed at q = 8.4, 14.6, and 16.9 nm^{-1}. The location of these peaks exactly corresponds to experimentally observed reflections for the well-studied PLA stereocomplex,[29,31,37] and is suggestive for crystallization in a triclinic crystal system. Ideally, the crystal lattice contains parallel packed, alternating *o*LLA and *o*DLA chains that adopt a 3_1-helix (instead of the 10_3 helix that was observed for the individual *o*LLA and *o*DLA components).

4.4.2 Stereocomplexes of [Si_x-LLA_y] and [Si_x-DLA_y]

Stereocomplex formation was also observed in 1 to 1 mixtures of [**Si_x-LLA_y**] and [**Si_x-DLA_y**] (Table 4–3, entries 7–10). The evaluated BCO stereocomplexes were all solids at room temperature and showed melting and crystallization transitions at approximately 60 °C higher temperatures than the homochiral BCOs. In particular for sc-[**Si_{15}-LLA_{17}**], a very sharp crystallization transition was observed in DSC measurements (Figure 4–9C). Stereocomplex sc-[**Si_{23}-LLA_9**] showed a single melting transition, similar to the other

stereocomplexes in the sc-[**Si$_{23}$-LLA$_y$**] series (Figure 4–9D), which contrasts with the behavior of the separate components that both did not crystallize.

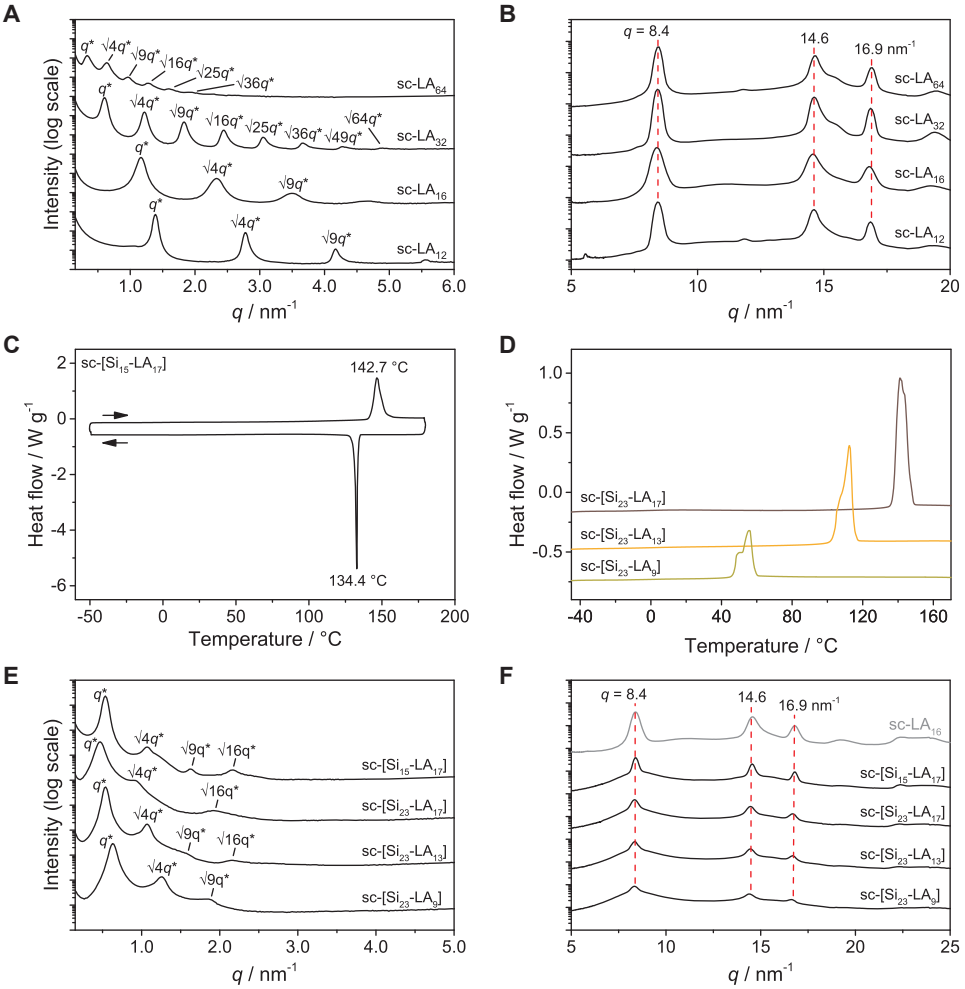

Figure 4–9. (**A–B**) Reduced transmission-SAXS data for stereocomplex lactic acid oligomers in the low-*q* range (**A**) and high-*q* range (**B**); (**C–D**) DSC traces (second heating run) of stereocomplex BCOs: (**C**) sc-[**Si$_{15}$-LA$_{17}$**]; (**D**) sc-[**Si$_{23}$-LA$_y$**]. A temperature ramp of 10 °C min^{-1} was used. Endothermic heatflows have a positive value; (**E–F**) Reduced transmission-SAXS data for various BCO stereocomplexes in the low-*q* range (**E**) and high-*q* range (**F**). Scattering data for sc-LA$_{16}$ are plotted in gray for comparison. The data are shifted vertically for clarity. In the scattering plots, the dashed, red lines mark the position of the three most prominent reflections in the WAXS region. Higher-order Bragg reflections are indicated for all scattering curves if present. The scattering profiles were all recorded at room temperature.

Probing of the self-assembled, crystalline structure with SAXS gave a collection of scattering profiles in the MAXS and WAXS region. The anticipated existence of a lamellar microphase-separated structure was confirmed by the appearance of equally spaced reflections in the MAXS region (Figure 4–9E). Furthermore, three reflections at higher q perfectly overlapped with the aforementioned reflections indicative for the triclinic unit cell of stereocomplex PLA (Figure 4–9F). This confirmed the presence of stereocomplex interactions within the *i*-*o*LA domain. Unexpectedly, a significant broadening of the reflections that originated from the lamellar organization was observed. The broadening indicated an increase in the local level of defects in the lamellar packing (*e.g.*, higher variations in lamellar thickness and a diminished long-range order). Currently, it is unclear why the stereocomplex BCOs show this behavior. We propose that there is a relation with the faster kinetics and larger thermodynamic driving force for crystallization, which impedes defect minimization during the crystallization process. For example, broadening of the scattering peak is also observed for the longer *o*LLA and *o*DLA blocks, and very likely results from an unbalance of the relative crystallization and diffusion kinetics of the individual *i*-*o*LA (or BCO) chains. Besides, it is known that neighboring molecules in the PLA stereocomplex are prone to exhibit shift-disorder, which might further contribute to broadening of the scattering reflections.[29]

4.5 Dispersity effects in crystalline BCOs

The exceptionally high number of observed reflection peaks in the semicrystalline [$\mathbf{Si_x}$-$\mathbf{LLA_y}$] BCOs, with BCO [$\mathbf{Si_{15}}$-$\mathbf{LLA_{17}}$] being the most impressive example, is uncommon for BCPs, particularly in such low-MW materials.[25,38,39] According to paracrystalline theory,[40] the high number of reflections observed permits only a small variability in the lamellar thickness throughout the microphase-segregated sample. Although crystallinity undoubtedly enhances the uniformity of the lamellar domains, we wondered to what extent the discrete nature of the materials plays a role in obtaining such highly organized structures. This is all the more interesting because it was already observed that the unintentional introduction of crystalline interactions in (partially) disperse [$\mathbf{Si_{15}}$-$\mathbf{LA_{\sim 17}}$] and [$\mathbf{Si_{\sim 15}}$-$\mathbf{LA_{\sim 17}}$] actually hampered the formation of an ordered structure (see Section 3.3). We therefore envisioned three additional BCOs: [$\mathbf{Si_{\sim 15}}$-$\mathbf{LLA_{17}}$], [$\mathbf{Si_{15}}$-$\mathbf{LLA_{\sim 17}}$] and [$\mathbf{Si_{\sim 15}}$-$\mathbf{LLA_{\sim 17}}$], incorporating disperse *o*DMS, disperse *o*LLA or two disperse blocks, respectively. This allows a systematic screening of the effect of a discrete *versus* a disperse block on the crystallization of the fully isotactic

*o*LLA and subsequent microphase separation of the BCO. In the abbreviations, disperse blocks are indicated with a tilde (~) character preceding the (desired) average block lengths.

4.5.1 Synthesis and molecular characterization

The synthesis of the disperse materials is shown in Scheme 4–1 and is analogous to the synthesis of disperse, amorphous [$\mathbf{Si_x\text{-}LA_y}$] compounds described in Chapter 3. The synthesis of most of the required discrete and disperse components (*o*DMS L-**28c** and L-**37**, and *o*LLA L-**22s**) is already discussed in preceding chapters. Disperse *o*LLA L-**34** with an average length of 16 L-LA repeat units was prepared by the ring-opening of L-lactide L-**20** with benzyl alcohol in the presence of catalytic amounts of 1,8-diazabicyclo[5.4.0]undec-7-ene (DBU). Again, we assume that the different endgroups *R* of the discrete and disperse siloxane blocks (Me and *n*-Bu, respectively) do not cause notable changes in the material properties. Coupling of the different *o*DMS and *o*LLA blocks resulted in 4 different BCOs: [$\mathbf{Si_{15}\text{-}LLA_{17}}$],[iii] [$\mathbf{Si_{\sim 15}\text{-}LLA_{17}}$], [$\mathbf{Si_{15}\text{-}LLA_{\sim 17}}$] and [$\mathbf{Si_{\sim 15}\text{-}LLA_{\sim 17}}$]. All newly synthesized materials were purified by automated column chromatography. Similar to what was observed for the non-crystalline materials, the product peak in the elution profiles of the disperse crystalline block and BCOs showed a significant broadening with respect to that of the fully discrete versions. After purification, all materials were analyzed with ^{1}H NMR, ^{13}C NMR, MALDI-TOF MS, and size exclusion chromatography (SEC), confirming good purity of all compounds (*e.g.*, endgroup fidelity and absence of loose *o*DMS or *o*LLA blocks), as well as the presence of a chain-length distribution in the disperse materials.

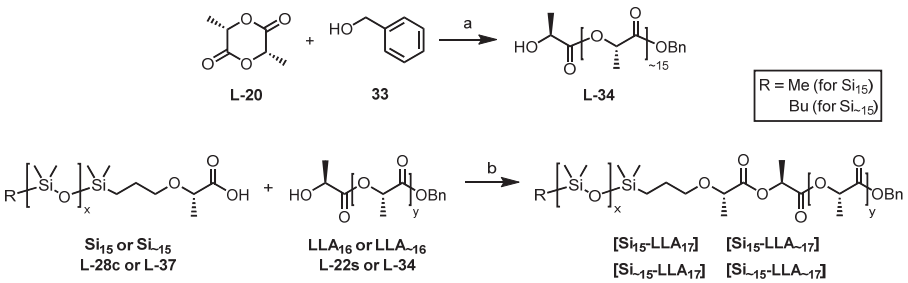

Scheme 4–1. Synthesis of disperse *o*LLA L-**34** by ring-opening polymerization and formation of disperse *o*DMS–*o*LLA BCOs. Reagents and conditions: (a) DBU, DCM, room temperature, 1 h (92%); (b) EDC·HCl, DPTS, DCM, room temperature, O/N (64–90%). DBU = 1,8-diazabicyclo[5.4.0]undec-7-ene, EDC·HCl = *N*-(3-dimethylaminopropyl)-*N'*-ethylcarbodiimide hydrochloride, DPTS = 4-(dimethylamino)pyridinium 4-toluenesulfonate.

[iii] The synthesis and properties of [$\mathbf{Si_{15}\text{-}LLA_{17}}$] are already described in Chapter 2 and preceding sections of this chapter.

Table 4–4. Molecular and morphologic characterization data for BCOs with various dispersity levels.

Entry	Compound[a]	#Si[b]	#LLA[b]	$M_{n,NMR}$[c] [Da]	$Đ$	N[d]	f_{cr}[e]	T_m [°C]	ΔH_{fus}[f] [kJ mol^{-1}]	T_{ODT} [°C]	d^* [nm]
1	[**Si$_{15}$-LLA$_{17}$**]	15	17	2486	<1.00001[h]	32.0	0.47	85.1	78	79.1	11.7
2	[**Si$_{\sim 15}$-LLA$_{17}$**]	15.8[g]	17	2587	1.04	33.0	0.45	87.9	80	83.5	12.4
3	[**Si$_{15}$-LLA$_{\sim 17}$**]	15	15.2[g]	2356	1.13	30.5	0.44	87–125[i]	42	n.o.	12.7
4	[**Si$_{\sim 15}$-LLA$_{\sim 17}$**]	15[g]	16.2[g]	2470	1.13	31.3	0.45	90–129[i]	25	n.o.	18.3

[a] Disperse blocks are indicated with a tilde (~) character preceding the (desired) average block lengths; [b] Number of siloxane or L-lactic acid repeat units. Determined with ^{1}H NMR; [c] Determined from the number of Si and LA repeat units; [d] Number of segments based on a 110 Å^3 reference volume; [e] Volume fraction of the crystalline block, calculated using bulk densities for PDMS (0.95 g mL^{-1}) and PLLA (1.29 g mL^{-1});[29] [f] Heat effect per mole of BCO; [g] Average value, determined with ^{1}H NMR; [h] Calculated from relative peak intensities in the MALDI-TOF spectra; [i] A broad melting range was observed. n.o.: not observed.

As summarized in Table 4–4, *o*DMS and *o*LLA block lengths and M_n values of the (partially) disperse materials were close to those of the discrete analogues. The average number of repeat units in the disperse materials was determined from integral ratios of the backbone signals in the ^{1}H NMR spectra of the BCOs. Values for the molar mass dispersity (determined by SEC) increased after introduction of one or two disperse blocks, although the maximum value of $Đ$ = 1.13 (for both [**Si$_{15}$-LLA$_{\sim 17}$**] and [**Si$_{\sim 15}$-LLA$_{\sim 17}$**]) still can be considered

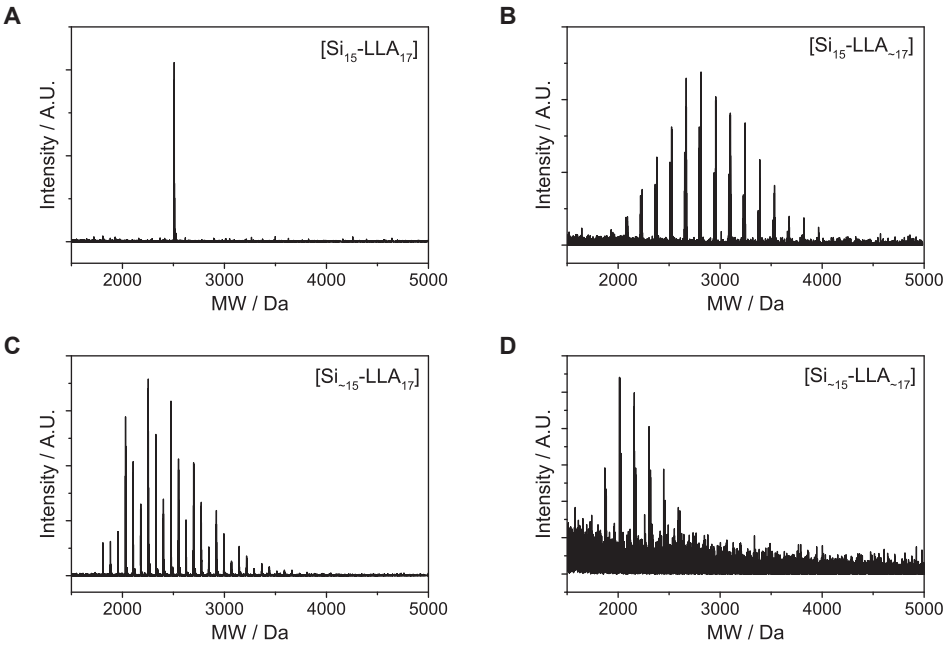

Figure 4–10. MALDI-TOF MS data (DCTB matrix) of crystalline [**Si$_x$-LLA$_y$**] BCOs with various dispersities.

as relatively low. Mass spectrometry nicely captured the striking differences between 'no' and 'low' dispersity (Figure 4–10). Probably, complications with the ionization of [**Si**$_{\sim 15}$-**LLA**$_{\sim 17}$] resulted in the noisy mass spectrum and slightly skewed representation of the chain-length distribution in this BCO (Figure 4–10D).

4.5.2 Shifts in phase transitions

The thermal behavior the disperse BCOs was captured with DSC measurements and is plotted in Figure 4–11A. Both [**Si**$_{15}$-**LLA**$_{17}$] and [**Si**$_{\sim 15}$-**LLA**$_{17}$] showed similar thermal profiles. In both cases, a relatively narrow melting and crystallization transition was observed, with a heat effect ΔH_{fus} = 80 kJ (mol BCO)$^{-1}$. Interestingly, the *o*LLA block that was conjugated to disperse *o*DMS melted at slightly higher temperatures ([**Si**$_{\sim 15}$-**LLA**$_{17}$], T_m = 87.9 °C) than the material consisting of two discrete blocks ([**Si**$_{15}$-**LLA**$_{17}$], T_m = 85.1 °C). Currently, we do not have an explanation for this observation. Additionally, both co-oligomers reveal an ODT at temperatures just above the crystallization temperature (see the transitions marked with an asterisk in Figure 4–11A). Again, an upward shift of T_{ODT} was found with increasing dispersity, similar to the trend observed for the atactic BCOs (see Chapter 3) and in line with the theoretical and experimental work of others.[41,42] Interestingly, we found significant changes in the thermal behavior if a disperse *o*LLA block is incorporated. Instead of a sharp melting transition, melting occurs over a broad temperature range. Moreover, ΔH_{fus} decreased by 45–70%, albeit that the determination of ΔH_{fus} became less accurate as a result of the peak broadening. The crystallization transitions of BCOs [**Si**$_{15}$-**LLA**$_{\sim 17}$] and [**Si**$_{\sim 15}$-**LLA**$_{\sim 17}$] were less broadened, but showed a similar decrease of the net heat effect. No

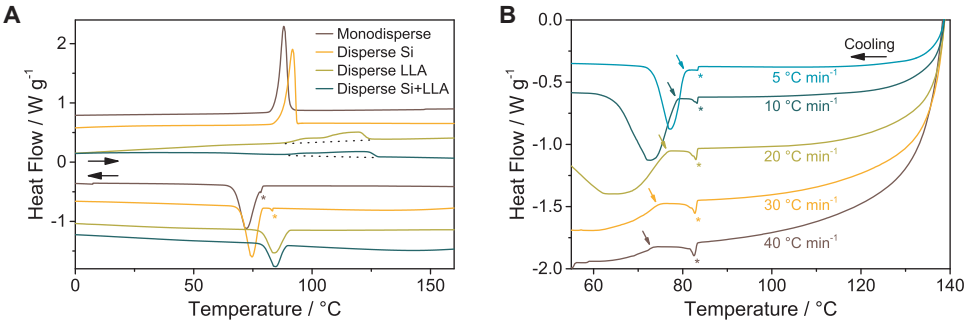

Figure 4–11. DSC traces (second cycle) of: (**A**) *o*DMS–*o*LLA BCOs with different levels of dispersity. A heating/cooling rate of 10 °C min^{-1} was used. As a guide to the eye, continuation of the baseline is provided as a dotted line under the melting transitions of [**Si**$_{15}$-**LLA**$_{\sim 17}$] and [**Si**$_{\sim 15}$-**LLA**$_{\sim 17}$]. Endothermic heatflows have a positive value. The data are shifted vertically for clarity. (**B**) BCO [**Si**$_{\sim 15}$-**LLA**$_{17}$] at different cooling speeds. The different onsets of crystallization are marked with the colored arrows. Order–disorder transitions unrelated to the crystallization process are indicated with an asterisk.

ODTs were observed for these two BCOs. Most likely, we can attribute the broadened melting transitions to the manifestation of numerous melting events—each linked to a certain *o*LLA block length within the crystalline domain of the BCOs—occurring over a broad temperature window. This is supported by the strong dependence of T_m on the number of L-LA repeat units in uniform *o*LLA (and related BCOs), particularly for block lengths below 32 units. Possibly, the smaller temperature window for crystallization is the result of a higher degree of undercooling (*i.e.*, temperature difference between the onset of crystallization and high-temperature limit of the melting peak) in [**Si$_{15}$-LLA$_{\sim 17}$**] and [**Si$_{\sim 15}$-LLA$_{\sim 17}$**], causing most of the *o*LLA fragments to crystallize simultaneously after the formation of small, crystalline nuclei.

Repetition of the DSC experiments with cooling rates other than 10 °C min^{-1} revealed a continuous lowering of the crystallization temperature and broadening of the crystallization peak with increasing cooling rate, as expected (Figure 4–11B). In contrast, almost no change in T_{ODT} was observed, even at a cooling rate of 40 °C min^{-1}, underlining the major differences in nucleation phenomena that initiate each of the two phase transitions.

4.5.3 Dispersity induced disorder

The phase behavior of the disperse co-oligomers at room temperature was studied with SAXS (Figure 4–12). Discrete [**Si$_{15}$-LLA$_{17}$**] and the BCO with a disperse Si block [**Si$_{\sim 15}$-LLA$_{17}$**] reveal a very similar scattering pattern. As discussed above, this was indicative for a highly ordered lamellar structure. Introduction of a disperse *o*DMS block caused a 6% increase of the domain spacing (d^* = 12.4 nm). This is accompanied by a broadening of the principal scattering peak, indicated by a 35% increase of the full width at half maximum value (see Figure 4–12). Remarkably, the degree of ordering decreases dramatically in the two BCOs comprising a disperse *o*LLA block. Here, the principal scattering peak at low q-values becomes very broad and only a single, very weak second reflection is visible (indicated with the black triangles in Figure 4–12). In contrast, all scattering patterns look similar at large scattering angles. This is suggestive for a very similar orthorhombic sub-unit cell in the crystalline *o*LLA domain of all four BCOs, albeit that the DSC data show that a fraction of the disperse *o*LLA blocks resides in an amorphous state.

We propose that the crystalline nature of the *o*LLA precisely aligns the chains in a parallel manner, unaffected by dispersity in the block. In case of the BCOs with discrete-length *o*LLA chains, this results in near-perfect localization of the chain-ends and interblock connections

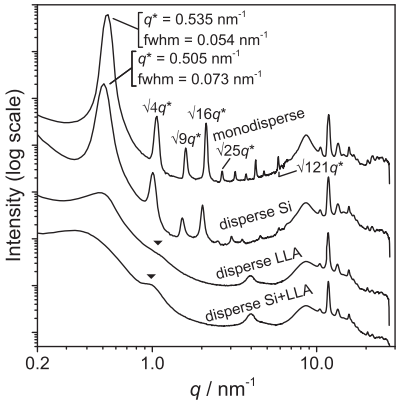

Figure 4–12. Reduced transmission-SAXS data for discrete and (partially) disperse *o*DMS-*o*LLA BCOs. The data are shifted vertically for clarity. A selection of higher-order Bragg reflections are indicated as q/q^* values or with black triangles. The scattering profiles were all recorded at room temperature. The broad peak at $q = 4$ nm^{-1} results from background scattering (Kapton tape). fwhm = full width at half maximum.

in three-dimensional space, greatly reducing any variations and fluctuations in domain spacing that generally exist in completely amorphous systems. Apparently, the impact of the extremely organized, crystalline *o*LLA domains on the lamellar ordering of alternating *o*DMS and *o*LLA domains is dominating insofar that a (low) degree of dispersity in the amorphous counterblock is very well tolerated. On the contrary, dispersity in the crystalline block (primarily) forces the ordering of the block links along the domain boundary out of alignment. This results in an increased variation of the lamellar thickness, at the cost of (long-range) order. Likely, this effect is amplified by the absence of chain folds in this low-MW system that can act as a buffer for variations in chain length during the crystallization process.

4.6 Conclusions

In summary, we studied the thermal and self-assembly behavior of isotactic *o*LLA, *o*DMS-*o*LLA, its enantiomers, and stereocomplexes thereof. Compared to the atactic analogues, discrete-length *i*-*o*LA has a strong tendency to form a well-organized crystalline phase at room temperature. After prolonged aging periods, even the very low-MW *o*LLA tetrameric and octameric materials were capable of forming crystalline domains, contradictory to what previously has been reported.[43] The observed propensity to crystallize into a lamellar macrolattice in which the individual *i*-*o*LA chains adopt an extended-chain conformation was exploited in the self-assembly of *o*DMS–*o*LLA or *o*DMS–*o*DLA BCOs. Our results showed that the introduction of crystallinity completely alters and, in many cases, improves the organization in phase-segregated BCOs, provided that the crystalline block is

discrete. Consequently, we were able to create exceptionally uniform microphase-segregated domains, which opens new avenues to further decrease feature sizes. Additionally, stereocomplex formation can be employed as a second handle to further fine-tune the self-assembly behavior.

However, attaining perfect ordering in low-MW block co-oligomer systems requires special consideration of two factors: kinetics and dispersity. First, we found that an optimal balance between crystallization kinetics, pre-organization in the amorphous state and the dimensions of the anticipated crystalline structure are key for obtaining the best possible organization. Typically, we can conclude that break-out crystallization is very likely to occur, as most of the systems either stay disordered of reside in a very weakly phase-segregated, amorphous state at temperatures above T_m of the crystalline blocks.[9] However, the crystallization-induced transformation of the disordered or amorphous phase-segregated state into the alternating crystalline–amorphous lamellar domains incidentally requires the (local) migration of a huge number of molecules. Arguably, displacement of low-MW molecules and pre-organization of the BCOs in a phase that already resembles that of the final, crystalline state (*e.g.*, in [**Si$_{23}$-LLA$_{25}$**]), is very beneficial. Contrarily, materials that initially formed non-lamellar morphologies gave more distorted lamellar structures after crystallization. (*e.g.*, [**Si$_{23}$-LLA$_{13}$**]).

Secondly, dispersity plays an even more crucial role in the formation of ordered structures, causing a nearly complete loss of ordering if the crystalline block has a non-uniform length. Although this is easily explained with a simple, intuition-based molecular picture, no comparative experimental studies exist to date. In the next, and final chapter, we further elucidate the exact molecular organization and intriguing temperature dependent behavior in semicrystalline BCOs by using a new block combination and other BCO architectures.

4.7 Experimental

4.7.1 Materials and methods

All chemicals were purchased from commercial sources and used without further purification. The synthesis of discrete Me-Si$_{15}$-LLA$_1$-COOH L-**28c**, disperse Bu-Si$_{\sim 15}$-LLA$_1$-COOH L-**37**, and discrete HO-LLA$_{16}$-Bn L-**22s** is described in preceding chapters. Dry solvents were obtained with an MBRAUN Solvent Purification System (MB-SPS). Oven-dried glassware (120 °C) was used for all reactions carried out under argon atmosphere. Reactions were followed by thin-layer chromatography (TLC) using 60-F254 silica gel plates from Merck and visualized by UV light at 254 nm and/or cerium molybdate (CeMo) staining. Automated column chromatography was conducted on a

Grace Reveleris X2 Flash Chromatography System using Reveleris Silica Flash Cartridges. Elution gradients are specified in column volumes (CVs).

NMR spectra were recorded on Varian Mercury Vx 400 MHz, Varian 400MR 400 MHz, Bruker 400 MHz Ultrashield (400 MHz for ^{1}H NMR), and/or Varian Inova 500 MHz (500 MHz for ^{1}H NMR) spectrometers. Deuterated solvents used are indicated in each case. Chemical shifts (δ) are expressed in ppm and are referred to the ressidual peak of the solvent. Peak multiplicity is abbreviated as s: singlet; d: doublet; t: triplet; dt: doublet of triplets; ddt: doublet of doublets of triplets; td: triplet of doublets; tt: triplet of triplets; q: quartet; ABq: AB quartet; qd: quartet of doublets; sept: septet; m: multiplet; bs: broad singlet. **Matrix assisted laser desorption/ionization time-of-flight** (MALDI-TOF) mass spectra were obtained on a PerSeptive Biosystems Voyager DE-PRO spectrometer using α-cyano-4-hydroxycinnamic acid (CHCA) or *trans*-2-[3-(4-*tert*-butylphenyl)-2-methyl-2-propenylidene]-malononitrile (DCTB) as matrix. **Gas chromatography-mass spectrometry** (GC-MS) measurements were conducted on a Shimadzu GC-17A gas chromatograph with a Shimadzu AOC-20i auto injector, Shimadzu GCMS-QP5000 gas chromatograph mass spectrometer and Phenomenex Zebron ZB-35 column (l = 30 meters, ID = 0.25 mm, film thickness = 0.25 μm). **Size exclusion chromatography** (SEC) measurements were conducted on a Shimadzu Prominence-i LC-2030C 3D with a Shimadzu RID-20A Refractive index detector, using an eluent flow of 1 mL min^{-1} (THF or $CHCl_3$). The molecular weight is determined based on narrow dispersity polystyrene standards purchased from Polymer Source Inc. **Differential scanning calorimetry** (DSC) data were collected on a DSC Q2000 from TA instruments, calibrated with an indium standard. The samples (4–8 mg) were weighed directly into aluminum pans and hermetically sealed. The samples were initially heated to 180 °C and then subjected to two cooling/heating cycles, typically from −50 °C to 180 °C with a rate of 10 °C min^{-1}. The data that are presented, represent the second heating/cooling cycle unless stated otherwise. **Polarized optical microscopy** (POM) images were obtained with a Jenaval polarization microscope equipped with a Linkam THMS 600 temperature controller. Images were captured with crossed polarizers. The samples were positioned between two coverslips and mounted directly on the Linkam heating stage. Micrographs were taken during cooling runs at a rate of 0.1–1 °C min^{-1}, starting from the molten (isotropic) state. Bulk **small-angle X-ray scattering** (SAXS) was performed on an instrument from Ganesha Lab. The flight tube and sample holder are all under vacuum in a single housing, with a GeniX-Cu ultra-low divergence X-ray generator. The source produces X-rays with a wavelength (λ) of 0.154 nm and a flux of 1×10^8 ph s^{-1}. Samples were put inside 1 mm diameter glass capillaries, and annealed by heating above the (expected) melting point and slow (0.5 °C min^{-1}) cooling to room temperature. Disperse samples [**Si$_{15}$-LLA$_{\sim 17}$**] and [**Si$_{\sim 15}$-LLA$_{\sim 17}$**] were annealed in a glass vial and then smeared onto Kapton tape. For room temperature measurements, the samples were positioned directly in the beamline. Variable temperature measurements (VT-SAXS) were performed using a Linkam heating stage. Samples were equilibrated at each temperature for 5 minutes prior to measuring and a heating/cooling rate of 5 °C min^{-1} was used in between the measurements. Scattered X-rays were captured on a 2-dimensional Pilatus 300K detector with 487 × 619 pixel resolution. Samples were measured in MAXS mode for 1200 seconds and WAXS mode for 300 seconds. The sample-to-detector distance was 0.084 m (WAXS mode) or 0.431 m (MAXS mode). The instrument was calibrated with diffraction patterns from silver behenate. The raw data files were calibrated and reduced to 1-D data with the SAXSGui software provided by JJ X-Ray Systems ApS. MAXS and WAXS regions were merged into a single data file using the SAXSutilities software package provided by Michael Sztucki.

4.7.2 Synthetic procedures

Synthesis of disperse HO-LLA$_{\sim 16}$-Bn (ring-opening polymerization) (L-**34**).

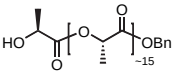

L–lactide L-**20** was dried for 6 hours at 45 °C under vacuum. The lactide (202.0 mg, 1.40 mmol, 8 eq) was dissolved in dry DCM (3 mL) in a dry 10 mL Schlenk tube under an argon atmosphere. Dry benzyl alcohol **33** (19.0 mg, 0.175 mmol, 1 eq) was added. Next, a 10 w% solution of 1,8- diazabicyclo[5.4.0]undec-7-ene (DBU) in dry DCM was prepared. Then, 21 mg of the DBU solution (2.1 mg, 0.014 mmol, 0.08 eq DBU) was added to the stirred reaction mixture. The reaction progress was checked with TLC (hept/EtOAc 50/50; CeMo stain). After completion (~1 h), benzoic acid (0.24 eq) was added to quench the reaction, and the solution was concentrated in *vacuo* to give crude disperse oligolactic acid as a yellowish wax. The material was purified by automated column chromatography using hept/EtOAc (gradient 88/12 to 15/85) as eluent. The pure product L-**34** was obtained as a white, waxy solid (203 mg, 92%). ^{1}H NMR (400 MHz, $CDCl_3$): δ = 7.38–7.27 (m, 5H, Ar-H), 5.23–5.08 (m, 17H, O-CH(CH_3)-CO and Ar-CH_2-O), 4.33 (q, ^3J = 6.2 Hz, 1H, HO-CH(CH_3)-CO), 1.62–1.35 ppm (m, 54H, O-CH(CH_3)-CO); ^{13}C NMR (100 MHz, $CDCl_3$): δ = 174.96, 169.85–169.04, 134.99, 128.56–128.41, 128.13, 69.37, 68.91, 67.08, 66.59, 20.39, 16.72–16.32 ppm; MS (MALDI-TOF): *m/z* calcd for $C_{55}H_{72}O_{33}$+Na^+ (HO-LLA$_{16}$-Bn): 1283.38 $[M+Na]^+$; found 1283.40; (multiple, equally spaced (144.04 *m/z*) peaks were found between 500–3000 Da, each corresponding to the desired product with a different DP); SEC (THF): M_n = 1905; $Đ$ = 1.49.

*General procedure **A** for the oDMS–oLLA coupling reactions giving Me/Bu-Si$_x$-LLA$_y$-Bn* ([**Si$_x$-LLA$_y$**]).

*o*DMS acid L-**28c** or L-**37** (*e.g.*, 0.16 mmol, 1.0 eq) was dissolved in dry DCM (1 mL, ~0.15 M) in a 10 mL Schlenk tube under an argon atmosphere. The solution was cooled to 0 °C in ice water and 4-(dimethylamino)pyridinium 4-toluenesulfonate (DPTS, 0.08 mmol, 0.5 eq) and *N*-(3-dimethylaminopropyl)-*N'*-ethylcarbodiimide hydrochloride (EDC·HCl, 0.322 mmol, 2.0 eq) were added. The mixture was stirred for 10 minutes at 0 °C, followed by the addition of benzyl protected *o*LLA L-**22s** or L-**34** (0.16 mmol, 1.0 eq). The mixture was then stirred overnight at room temperature, during which the formation of a suspension/emulsion of co-oligomer in DCM was observed. The reaction mixture was diluted with DCM (15 mL) to bring all material in solution and the material was washed with a 50/50 mixture of water and brine (10 mL in total). The organic layer was dried with $MgSO_4$ and concentrated in *vacuo*, giving the crude product [**Si$_x$-LLA$_y$**]. The material was purified by automated column chromatography.

Bu-Si$_{\sim 15}$-LLA$_{17}$-Bn ([**Si$_{\sim 15}$-LLA$_{17}$**]).

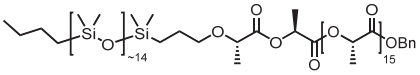

Starting from *o*DMS acid L-**37** (61.4 mg, 0.048 mmol, 1 eq), *o*LLA L-**22s** (58 mg, 0.046 mmol, 1 eq), DPTS (7 mg, 0.023 mmol, 0.5 eq) and EDC·HCl (18 mg, 0.093 mmol, 2 eq), crude oligomer [**Si$_{\sim 15}$-LLA$_{17}$**] was obtained as a white solid using general method **A**. The material was purified by automated column chromatography using hept/EtOAc (gradient 80/20 to 60/40) as eluent, giving the product in pure form as a white solid (102 mg, 88%). ^{1}H NMR (400 MHz, $CDCl_3$): δ = 7.39–7.28 (m, 5H, Ar-H), 5.22–5.11 (m, 18H, CO-O-CH(CH_3)-CO and O-CH_2-Ar), 4.02 (q, ^3J = 6.9 Hz, 1H, CH_2-O-CH(CH_3)-CO), 3.58 (dt, ^2J = 8.8 Hz, ^3J = 6.9 Hz, 1H, CH_2-O-CH(CH_3)-CO), 3.32 (dt, ^2J = 8.8 Hz, ^3J = 7.1 Hz, 1H, CH_2-O-CH(CH_3)-CO), 1.68–1.42 (m, 53H, Si(CH_3)$_2$-CH_2-CH_2-CH_2-O and O-CH(CH_3)-CO), 1.36–1.23 (m, 4H, CH_3-CH_2-CH_2), 0.87 (t, ^3J = 6.8 Hz, 3H, CH_3-CH_2-CH_2), 0.56–0.49 (m, 4H, Si(CH_3)$_2$-CH_2-CH_2-CH_2-O and CH_2-CH_2-Si(CH_3)$_2$), 0.10–0.01 ppm (m, 90H, Si(CH_3)$_2$-CH_2); ^{13}C NMR (100 MHz, $CDCl_3$): δ = 173.16, 170.05, 170.00, 169.82, 169.76, 169.71, 169.64, 135.19, 128.74, 128.65, 128.37, 74.66, 73.23, 69.41, 69.13, 68.99, 68.53, 67.34, 26.48, 25.57, 23.65, 18.79, 18.07, 16.87, 16.83–16.73, 16.69, 14.21, 13.92, 1.29, 1.17, 0.30,

0.22, 0.19 ppm; MS (MALDI-TOF): *m/z* calcd for $C_{95}H_{180}O_{49}Si_{15}+Na^+$: 2547.80 $[M+Na]^+$; found 2547.82 (multiple, equally spaced (74.02 *m/z*) peaks were found between 1700–4000 Da, each corresponding to the desired product with a different DP); SEC (THF): M_n = 4444; $Đ$ = 1.04.

Synthesis of Me-Si$_{15}$-LLA$_{\sim 17}$-Bn ([**Si$_{15}$-LLA$_{\sim 17}$**]).

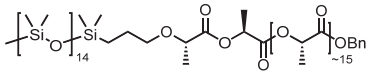

Starting from *o*DMS acid L-**28c** (93 mg, 0.075 mmol, 1.2 eq), *o*LLA L-**34** (79 mg, 0.062 mmol, 1 eq), DPTS (11 mg, 0.037 mmol, 0.6 eq) and EDC·HCl (29 mg, 0.15 mmol, 2.4 eq), crude oligomer [**Si$_{15}$-LLA$_{\sim 17}$**] was obtained as a white wax using general method **A**. The material was purified by automated column chromatography using hept/EtOAc (gradient 80/20 to 60/40) as eluent, giving the product in pure form as a white, waxy solid (140 mg, 90%). ^{1}H NMR (400 MHz, $CDCl_3$): δ = 7.40–7.30 (m, 5H, Ar-H), 5.22–5.10 (m, 18H, CO-O-CH(CH_3)-CO and O-CH_2-Ar), 4.02 (q, ^3J = 6.9 Hz, 1H, CH_2-O-CH(CH_3)-CO), 3.58 (dt, ^2J = 8.7 Hz, ^3J = 6.9 Hz, 1H, CH_2-O-CH(CH_3)-CO), 3.32 (dt, ^2J = 8.7 Hz, ^3J = 6.9 Hz, 1H, CH_2-O-CH(CH_3)-CO), 1.69–1.42 (m, 53H, Si(CH_3)$_2$-CH_2-CH_2-CH_2-O and O-CH(CH_3)-CO), 0.58–0.48 (m, 2H, Si(CH_3)$_2$-CH_2-CH_2-CH_2-O), 0.10–0.03 ppm (m, 93H, Si(CH_3)$_2$); ^{13}C NMR (100 MHz, $CDCl_3$): δ = 173.14, 170.04, 169.99, 169.80, 169.73, 169.69, 169.62, 135.20, 128.73, 128.64, 128.35, 74.66, 73.21, 69.40, 69.13, 68.98, 68.52, 67.32, 23.64, 18.77, 16.86, 16.75, 16.68, 14.21, 1.89, 1.27, 1.25, 1.16, 0.21, 0.19 ppm; MS (MALDI-TOF): *m/z* calcd for $C_{92}H_{174}O_{49}Si_{15}+Na^+$: 2505.76 $[M+Na]^+$; found 2505.82 (multiple, equally spaced (144.04 *m/z*) peaks were found between 1500–4000 Da, each corresponding to the desired product with a different DP); SEC (THF): M_n = 4482; $Đ$ = 1.13.

Synthesis of Bu-Si$_{\sim 15}$-LLA$_{\sim 17}$-Bn ([**Si$_{\sim 15}$-LLA$_{\sim 17}$**]).

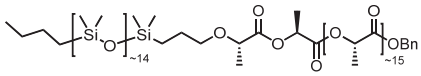

Starting from *o*DMS acid L-**37** (59.5 mg, 0.046 mmol, 1 eq), *o*LLA L-**34** (58.4 mg, 0.046 mmol, 1 eq), DPTS (6.8 mg, 0.023 mmol, 0.5 eq) and EDC·HCl (18 mg, 0.093 mmol, 2 eq), crude oligomer [**Si$_{\sim 15}$-LLA$_{\sim 17}$**] was obtained as a waxy solid using general method **A**. The material was purified by automated column chromatography using hept/EtOAc (gradient 80/20 to 60/40) as eluent, giving the product in pure form as a white wax (74.5 mg, 64%). ^{1}H NMR (400 MHz, $CDCl_3$): δ = 7.39–7.29 (m, 5H, Ar-H), 5.23–5.09 (m, 18H, CO-O-CH(CH_3)-CO and O-CH_2-Ar), 4.02 (q, ^3J = 6.9 Hz, 1H, CH_2-O-CH(CH_3)-CO), 3.58 (dt, ^2J = 8.8 Hz, ^3J = 7 Hz, 1H, CH_2-O-CH(CH_3)-CO), 3.32 (dt, ^2J = 8.8 Hz, ^3J = 7 Hz, 1H, CH_2-O-CH(CH_3)-CO), 1.68–1.43 (m, 53H, Si(CH_3)$_2$-CH_2-CH_2-CH_2-O and O-CH(CH_3)-CO), 1.37–1.24 (m, 4H, CH_3-CH_2-CH_2), 0.88 (t, ^3J = 6.8 Hz, 3H, CH_3-CH_2-CH_2), 0.57–0.50 (m, 4H, Si(CH_3)$_2$-CH_2-CH_2-CH_2-O and CH_2-CH_2-Si(CH_3)$_2$), 0.10–0.02 ppm (m, 90H, Si(CH_3)$_2$-CH_2); ^{13}C NMR (100 MHz, $CDCl_3$): δ = 173.18, 170.07, 170.02, 169.83, 169.77, 169.72, 169.66, 135.21, 128.75, 128.66, 128.38, 74.67, 73.25, 69.42, 69.15–69.11, 69.00, 68.54, 67.35, 26.49, 25.58, 23.66, 18.80, 18.08, 16.89, 16.81–16.78, 16.70, 14.22, 13.93, 1.30, 1.18, 0.31, 0.23, 0.20 ppm; MS (MALDI-TOF): *m/z* calcd for $C_{95}H_{180}O_{49}Si_{15}+Na^+$: 2547.80 $[M+Na]^+$; found 2547.94 (a range of masses was found between 1500–4000 Da, each corresponding to the desired product with a different DP); SEC (THF): M_n = 4063; $Đ$ = 1.13.

4.8 References

(1) Leibler, L. *Macromolecules* **1980**, *13*, 1602.

(2) Bates, C. M.; Bates, F. S. *Macromolecules* **2017**, *50*, 3.

(3) Schacher, F. H.; Rupar, P. a; Manners, I. *Angew. Chemie Int. Ed.* **2012**, *51*, 7898.

(4) Sinturel, C.; Bates, F. S.; Hillmyer, M. A. *ACS Macro Lett.* **2015**, *4*, 1044.
(5) Hawker, C. J. *Science* **2005**, *309*, 1200.
(6) Oschmann, B.; Lawrence, J.; Schulze, M. W.; Ren, J. M.; Anastasaki, A.; Luo, Y.; Nothling, M. D.; Pester, C. W.; Delaney, K. T.; Connal, L. A.; McGrath, A. J.; Clark, P. G.; Bates, C. M.; Hawker, C. J. *ACS Macro Lett.* **2017**, *6*, 668.
(7) Goodby, J. W.; Davis, E. J.; Mandle, R. J.; Cowling, S. J. *Handbook of Liquid Crystals*; Goodby, J. W.; Tschierske, C.; Raynes, P.; Gleeson, H.; Kato, T.; Collings, P. J., Eds.; Wiley-VCH Verlag GmbH & Co. KGaA: Weinheim, Germany, 2014.
(8) He, W.-N.; Xu, J.-T. *Prog. Polym. Sci.* **2012**, *37*, 1350.
(9) Nandan, B.; Hsu, J.-Y.; Chen, H.-L. *J. Macromol. Sci. Part C Polym. Rev.* **2006**, *46*, 143.
(10) Hamley, I. W. In *Interfaces Crystallization Viscoelasticity*; Springer Berlin Heidelberg: Berlin, Heidelberg, 1999; pp. 113–137.
(11) Sun, J.; Zuckermann, R. N. *ACS Nano* **2013**, *7*, 4715.
(12) Badi, N.; Chan-Seng, D.; Lutz, J.-F. *Macromol. Chem. Phys.* **2013**, *214*, 135.
(13) Jeong, G.; Yu, D. M.; Mapas, J. K. D.; Sun, Z.; Rzayev, J.; Russell, T. P. *Macromolecules* **2017**, *50*, 7148.
(14) Kwak, J.; Mishra, A. K.; Lee, J.; Lee, K. S.; Choi, C.; Maiti, S.; Kim, M.; Kim, J. K. *Macromolecules* **2017**, *50*, 6813.
(15) Nowak, S. R.; Hwang, W.; Sita, L. R. *J. Am. Chem. Soc.* **2017**, *139*, 5281.
(16) Carter, M. C. D.; Jennings, J.; Speetjens, F. W.; Lynn, D. M.; Mahanthappa, M. K. *Macromolecules* **2016**, *49*, 6268.
(17) Booth, C.; Pickles, C. J. *J. Polym. Sci. Part A-2 Polym. Phys.* **1973**, *11*, 249.
(18) Viras, F.; Luo, Y.-Z.; Viras, K.; Mobbs, R. H.; King, T. A.; Booth, C. *Die Makromol. Chemie* **1988**, *189*, 459.
(19) Šimek, L.; Petřík, S.; Hadobaš, F.; Bohdanecký, M. *Eur. Polym. J.* **1990**, *26*, 371.
(20) Yang, Y.-W.; Tanodekaew, S.; Mai, S.-M.; Booth, C.; Ryan, A. J.; Bras, W.; Viras, K. *Macromolecules* **1995**, *28*, 6029.
(21) Mai, S.-M.; Fairclough, J. P. A.; Viras, K.; Gorry, P. A.; Hamley, I. W.; Ryan, A. J.; Booth, C. *Macromolecules* **1997**, *30*, 8392.
(22) Ryan, A. J.; Fairclough, J. P. A.; Hamley, I. W.; Mai, S.-M.; Booth, C. *Macromolecules* **1997**, *30*, 1723.
(23) Cooper, D. R.; Leung, Y.-K.; Heatley, F.; Booth, C. *Polymer* **1978**, *19*, 309.
(24) Domszy, R. .; Mobbs, R. .; Leung, Y.-K.; Heatley, F.; Booth, C. *Polymer* **1979**, *20*, 1204.
(25) Swales, T. G. E.; Domszy, R. C.; Beddoes, R. L.; Price, C.; Booth, C. *J. Polym. Sci. Polym. Phys. Ed.* **1985**, *23*, 1585.
(26) Yeates, S. G.; Booth, C. *Eur. Polym. J.* **1985**, *21*, 217.
(27) Campbell, C.; Viras, K.; Richardson, M. J.; Masters, A. J.; Booth, C. *Die Makromol. Chemie* **1993**, *194*, 799.
(28) Takizawa, K.; Nulwala, H.; Hu, J.; Yoshinaga, K.; Hawker, C. J. *J. Polym. Sci. Part A Polym. Chem.* **2008**, *46*, 5977.
(29) Okihara, T.; Tsuji, M.; Kawaguchi, A.; Katayama, K.-I.; Tsuji, H.; Hyon, S.-H.; Ikada, Y. *J. Macromol. Sci. Part B* **1991**, *30*, 119.
(30) Pyda, M.; Bopp, R. .; Wunderlich, B. *J. Chem. Thermodyn.* **2004**, *36*, 731.
(31) Tsuji, H. *Macromol. Biosci.* **2005**, *5*, 569.
(32) Zhou, C.; Li, H.; Zhang, W.; Li, J.; Huang, S.; Meng, Y.; de Claville Christiansen, J.; Yu, D.; Wu, Z.; Jiang, S. *CrystEngComm* **2016**, *18*, 3237.

(33) Sweat, D. P.; Kim, M.; Larson, S. R.; Choi, J. W.; Choo, Y.; Osuji, C. O.; Gopalan, P. *Macromolecules* **2014**, *47*, 6687.
(34) Kennemur, J. G.; Yao, L.; Bates, F. S.; Hillmyer, M. A. *Macromolecules* **2014**, *47*, 1411.
(35) Kim, J. K.; Lee, H. H.; Gu, Q.-J.; Chang, T.; Jeong, Y. H. *Macromolecules* **1998**, *31*, 4045.
(36) Lee, S.; Gillard, T. M.; Bates, F. S. *AIChE J.* **2013**, *59*, 3502.
(37) Tashiro, K.; Kouno, N.; Wang, H.; Tsuji, H. *Macromolecules* **2017**, *50*, 8048.
(38) Lynd, N. A.; Hamilton, B. D.; Hillmyer, M. A. *J. Polym. Sci. Part B Polym. Phys.* **2007**, *45*, 3386.
(39) Hashimoto, T.; Tanaka, H.; Hasegawa, H. *Macromolecules* **1985**, *18*, 1864.
(40) Hosemann, R.; Bagchi, S. N. *Direct Analysis of Diffraction by Matter*; North-Holland Publishing: Amsterdam, 1962.
(41) Lynd, N. A.; Hillmyer, M. A. *Macromolecules* **2007**, *40*, 8050.
(42) Pandav, G.; Ganesan, V. *J. Chem. Phys.* **2013**, *139*, 214905.
(43) de Jong, S. J.; van Dijk-Wolthuis, W. N. E.; Kettenes-van den Bosch, J. J.; Schuyl, P. J. W.; Hennink, W. E. *Macromolecules* **1998**, *31*, 6397.

♦ Chapter 5 ♦

Molecular Organization of Oligodimethylsiloxane–Oligomethylene Di- and Triblock Co-Oligomers

Abstract: A new class of discrete-length block co-oligomers comprising oligodimethylsiloxane (*o*DMS) and oligomethylene (*o*M) is presented. For this, *o*M blocks containing up to 69 backbone carbons are synthesized *via* an iterative, Wittig reaction based strategy. Ligation with *o*DMS hydrides permits the formation of a library of block co-oligomers (BCOs) in which block configuration, MW, and composition can be tuned. Differential scanning calorimetry and small-angle X-ray scattering shows that all BCOs exhibit microphase separation into well-ordered lamellar morphologies, driven by the crystallization of the *o*M block. Pre-melting order–order transitions are present for a number of BCOs, resulting in an alteration of the *o*M crystal packing as well as in changes of the overall microphase-segregated structure. As a result of the discrete nature of the BCO chains, we propose models that describe the molecular organization within the microphase-segregated structures by evaluating the changes in the lamellar thickness upon varying the BCO architecture.

Part of this work has been published:
van Genabeek, B.; Lamers, B. A. G.; de Waal, B. F. M.; van Son, M. H. C.; Palmans, A. R. A.; Meijer, E. W. *J. Am. Chem. Soc.* **2017**, *139*, 14869.

"Even though alkanes are relatively unreactive and rarely involved in chemical reactions, they nevertheless provide a useful vehicle for introducing some important general ideas."

—John McMurry, 2012.

5.1 Introduction

As already pointed out in Chapter 1, a significant share of recent block copolymer (BCP) research focusses on designing new block combinations that allow a decrease of feature sizes without compromising on the (long range) order in the formed morphologies.[1–5] In the previous chapters, we added a new dimension to this research by discussing the synthesis and phase behavior of low-MW, uniform ($Đ$ = 1) block co-oligomers (BCOs), comprising oligolactic acid (*o*LA) and oligodimethylsiloxane (*o*DMS). With these materials, we unveiled the impact of monodispersity on low-MW BCP phase behavior. In addition, we showed the stabilizing effect of crystallinity on the overall ordering of the BCO domains in Chapter 4.

By now, it is clear that the boundary between BCP or BCO microphase segregation and the self-assembly of liquid crystals[6–9] or so-called 'block molecules' (BMs)[10–12] may virtually be non-existent. Yet, a full understanding of the molecular organization within such systems is often lacking, particularly in the first-mentioned category of materials. On the contrary, elucidating the atom-by-atom positioning in other (well-defined) self-assembling systems such as proteins and other natural structures—mainly by extensive X-ray scattering studies—provided key insights into structure-property relationships and system dynamics.[13]

However, understanding the exact molecular orientation in polymeric systems is not that trivial, and literature is not always in agreement. For example, models for semicrystalline polymers and polymer-like materials typically show the formation of crystalline lamellae, in which the polymer chains are oriented perpendicular to the lamellar planes.[14–16] Contradictory, other work suggests that chains might be tilted away from the perpendicular position.[17–19] A very recent paper concerning the location of the chain-ends in semicrystalline polyethylene—a polymer of which no less than 80 million metric tons are produced annually[20]—further illustrates the complexity of extracting full molecular organization details from a seemingly simple molecule.[21]

Clearly, a sound knowledge of the relation between the molecular structure and mesoscale organization is key to develop new materials that exhibit tailor-made properties and behavior, particularly if little modifications in the molecular structure can induce large morphological changes. For this purpose, this final chapter focusses on the synthesis and properties of a new set of BCOs, consisting of *o*DMS and discrete-length oligomethylene

(*o*M) blocks (Figure 5–1). The *o*M block was chosen for the known (semi)crystalline properties of oligo- and polymethylene.[i] In these molecules, non-directional London dispersion forces result in a lamellar type organization.[22] Mostly, we are interested in how the potential crystalline properties of the alkane blocks affect the phase behavior and stability of different morphologies. Also, we hope to increase our understanding of how the molecular architecture of a semicrystalline BCO results in a particular microphase-segregated structure.

5.2 Synthesis of uniform AB-, ABA- and BAB-type co-oligomers

We explored three linear block co-oligomer configurations, subdivided into two main categories: diblock (AB-type) and symmetrical triblock (ABA- or BAB-type) co-oligomers. Here A and B stand for an *o*DMS and *o*M block, respectively. To discriminate between di- and triblock co-oligomers, the abbreviations di-BCO and tri-BCO will be used throughout this chapter. *o*DMS–*o*M BCOs will be designated as [$\mathbf{Si_x\text{-}M_z}$], [$\mathbf{Si_x\text{-}M_z\text{-}Si_x}$] or [$\mathbf{M_z\text{-}Si_x\text{-}M_z}$], where *x* and *z* quantify the number of siloxane and methylene repeat units, respectively.[ii] The synthetic strategy toward these discrete-length siloxane–alkane co-oligomers employed the efficient and selective Karstedt hydrosilylation as a key reaction step.[23] This allowed the use of discrete-length oligodimethylsiloxane hydrides and linear α-olefins (either homo- or

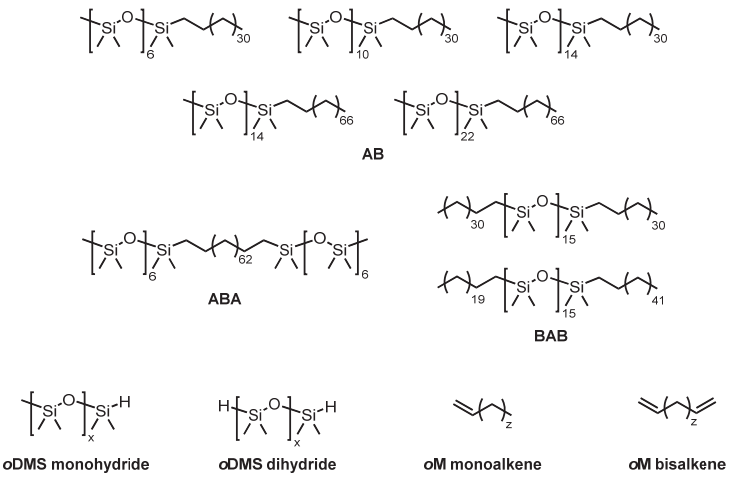

Figure 5–1. Molecular structures for *o*DMS–*o*M di- and tri-BCOs (top) and required *o*DMS and *o*M building blocks (bottom).

[i] Better known as polyethylene, PE

[ii] 'Methylene' should be conceived in a broader sense. For example, including the methyl endgroup or ignoring the internal double bonds that are present in the *o*M intermediates. In general, *z* represents the number of backbone carbons in the *o*M block.

heterotelechelic). The synthesis of the required siloxane hydrides is described in full detail in Chapter 2. Commercial availability of linear alkenes containing 20 or more carbon atoms is very limited, and the purity—or better: monodispersity—is questionable. Therefore, a library of olefins with one or two terminal double bonds was first synthesized, after which ligation with the available *o*DMS hydrides was conducted.

5.2.1 Block co-oligomer design

As shown in Figure 5–1, we aimed for di-BCOs of which the block lengths varied between 7 and 23 siloxane repeat units, and either 33 or 69 methylene repeat units: [**Si$_7$-M$_{33}$**], [**Si$_{11}$-M$_{33}$**], [**Si$_{15}$-M$_{33}$**], [**Si$_{15}$-M$_{69}$**], and [**Si$_{23}$-M$_{69}$**]. The combination of various block lengths resulted in a variation of the oligomethylene volume fractions (f_M) between 0.33 and 0.51. In addition, we designed three tri-BCOs; one ABA-type and two of the BAB-type. The (symmetrical) ABA-type triblock [**Si$_7$-M$_{66}$-Si$_7$**] was prepared to study the effect of hypothetical dimerization of di-BCO [**Si$_7$-M$_{33}$**] *via* the methyl endgroups. Moreover, [**Si$_7$-M$_{66}$-Si$_7$**] is in terms of mass and average composition closely related to di-BCO [**Si$_{15}$-M$_{69}$**], the only difference being that in the former the total *o*DMS block length is distributed equally at both sides of the *o*M block. Likewise, BAB-type triblock [**M$_{33}$-Si$_{16}$-M$_{33}$**] was nearly equal to the siloxane dimer of [**Si$_7$-M$_{33}$**]. Lastly, with BCO [**M$_{22}$-Si$_{16}$-M$_{44}$**] we intended to study the effect of an uneven distribution of the *o*M block lengths. All tri-BCOs had nearly double the MW of di-BCO [**Si$_7$-M$_{33}$**] but almost identical volume fraction of $f_M \approx 0.5$. This was chosen to match the expected lamellar organization for this composition with the (expected) lamellar ordering of crystalline *o*M (vide supra).

5.2.2 Aldehyde precursors

For the formation of end-functionalized long hydrocarbons, we were inspired by the elaborate work of Whiting and coworkers from the mid-1980s.[24–27] The route we followed focusses on the preparation of linear-chain aldehydes (or bisaldehydes) with 22 to 66 carbon atoms by stepwise chain-extensions with a bifunctional M_{22} building block (Scheme 5–1 and Scheme 5–2), which in a later process were extended to obtain the terminal alkenes (Scheme 5–3).

The synthesis of longer aldehydes required a systematic carbon-carbon ligation strategy of lower MW building blocks. Parallel to the work of Whiting *et al.*, we selected the Wittig reaction as the method of choice. However, we significantly modified the original procedures[24–26] to optimize the yields and improve the purity of the final molecules.

In collaboration with Bas de Waal, a bifunctional M_{22} building block **44** was prepared (Scheme 5–1). This building block consisted of a triphenylphosphonium salt and an aldehyde protected as the ethylene acetal. Both functionalities were linked though a linear, monounsaturated aliphatic spacer of 21 carbons with a double bond (a mixture of *cis* and *trans*) between carbon 11 and 12. As such, this block can be used to chain-extend existing aldehydes with 22 methylene units.[iii] An added bonus of this strategy is the incorporation of one double bond after every 9 methylene residues, which greatly enhances the solubility of the materials with longer chain lengths.

To obtain the building block, 11-bromoundecanol **38** was first oxidized to bromoaldehyde **39** under mild oxidation conditions (TEMPO/*N*-chlorosuccinimide) in a biphasic (DCM/water) reaction mixture.[28] The material was obtained as a white solid in 85% yield. Next, part of the material was converted to the corresponding ethylene acetal **41** in a two-step procedure. First, the dimethyl acetal **40** was prepared in 85% yield by stirring the aldehyde in an excess of methanol with *p*-toluene sulfonic acid (TsOH) as a catalyst and trimethyl orthoformate as a water scavenger. Subsequently, ethylene acetal **41** was obtained by the acid-catalyzed reaction of the dimethyl acetal with ethylene glycol at elevated temperatures under the continuous removal of methanol by evaporation. The material was then reacted with triphenylphosphine in refluxing acetonitrile, followed by trituration of the

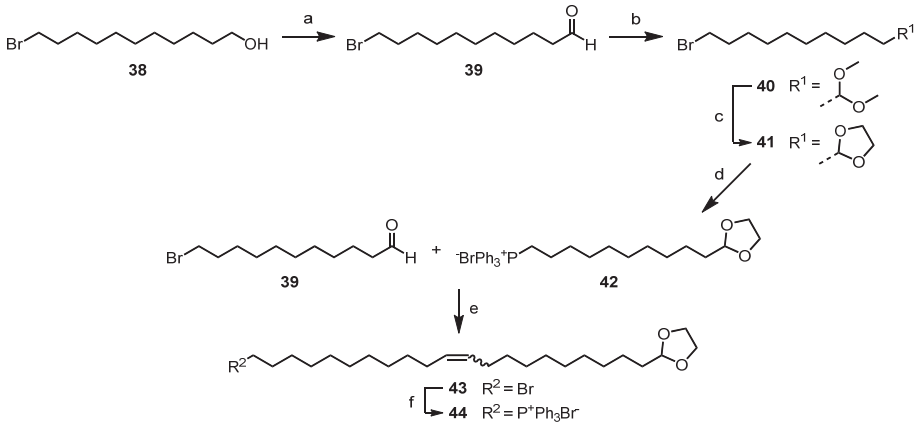

Scheme 5–1. Synthesis of bifunctional M_{22} building block **44**. Reagents and conditions: (a) TEMPO, tetrabutylammonium chloride, *N*-chlorosuccinimide, $NaHCO_3$, K_2CO_3, DCM, water, room temperature, 24 h (85%); (b) methanol, trimethyl orthoformate, TsOH, room temperature, 6 h (85%); (c) ethylene glycol, TsOH, toluene, 95 °C, 3.5 h (99%); (d and f) triphenylphosphine, 2,2-dimethyl-1,3-dioxolane, acetonitrile, reflux, 24 h (79–80%); (e) KO*t*Bu, THF, 0–20 °C, 24 h (58%). TsOH = *p*-toluene sulfonic acid.

[iii] See footnote [ii] on page 151.

solids formed with ethyl acetate. This gave pure phosphonium salt **42** in good yield (79%). Initially, we observed the formation of minor amounts of aldehyde byproduct, resulting from degradation of the ethylene acetal. Therefore, 2,2-dimethyl-1,3-dioxolane was added during the preparation of the phosphonium salt to compensate for this side-reaction. The Wittig reaction between the phosphonium salt and 11-bromoundecanal **39** in THF using KO*t*Bu as a base gave the M_{22} bromo acetal **43** in decent yield (58%). Finally, the material was converted to phosphonium salt **44** under the same conditions as described above. In this case, the material was purified by precipitation in hexane from a solution in ethyl acetate. The compound was obtained as a white solid in good yield (80%) and stored under argon to prevent uptake of moisture.

The synthesis of aliphatic aldehydes is depicted in Scheme 5–2. The lowest MW aldehyde, docosanal **46**, was obtained in one step from commercially available compounds. For this, docosanol **45** was converted to the aldehyde under similar conditions as those for the oxidation of 11-bromoundecanol. Large amounts of M_{22} aldehyde **46** (20–30 g) could be obtained in good yield (78%).

The Wittig reaction between building block **44** and undecanal **47** in THF with using KO*t*Bu as a base gave unsaturated M_{33} aldehyde **48** in good yield (73%). Notable is the presence of both *cis*- and *trans* configurations in the two double bonds (approximately 80% *cis*, determined with ^{1}H NMR), resulting in four different isomers. As expected from the Wittig reaction, formation of the *cis*-isomer is preferred under these conditions.[29]

For the deprotection of ethylene acetal **48** we developed a two-step procedure, since other methods proved to be too unsuccessful or unpractical.[25] First, ethylene acetal **48** was converted to diethyl acetal **49** by stirring a solution of the protected aldehyde in a large excess of refluxing ethanol in the presence of TsOH as a catalyst. After completion of the reaction, the mixture was basified with powdered KOH. Extraction with heptane and removal of the solvent afforded the M_{33} diethyl acetal in an excellent yield (97%).[iv] Without further purification, the acetal was then reacted with an excess of acetone, again in the presence of catalytic amounts of TsOH. Basic work-up gave the deprotected M_{33} acetal (M_{33} aldehyde) **50** in 95% yield.

[iv] Quenching the reaction with a base is key to prevent the back-reaction from occurring during the isolation of the product. Under acidic conditions, a continuous equilibration of the reaction mixture will take place during removal of the ethanol. The high-boiling ethylene glycol remains, eventually resulting in reformation of the starting material.

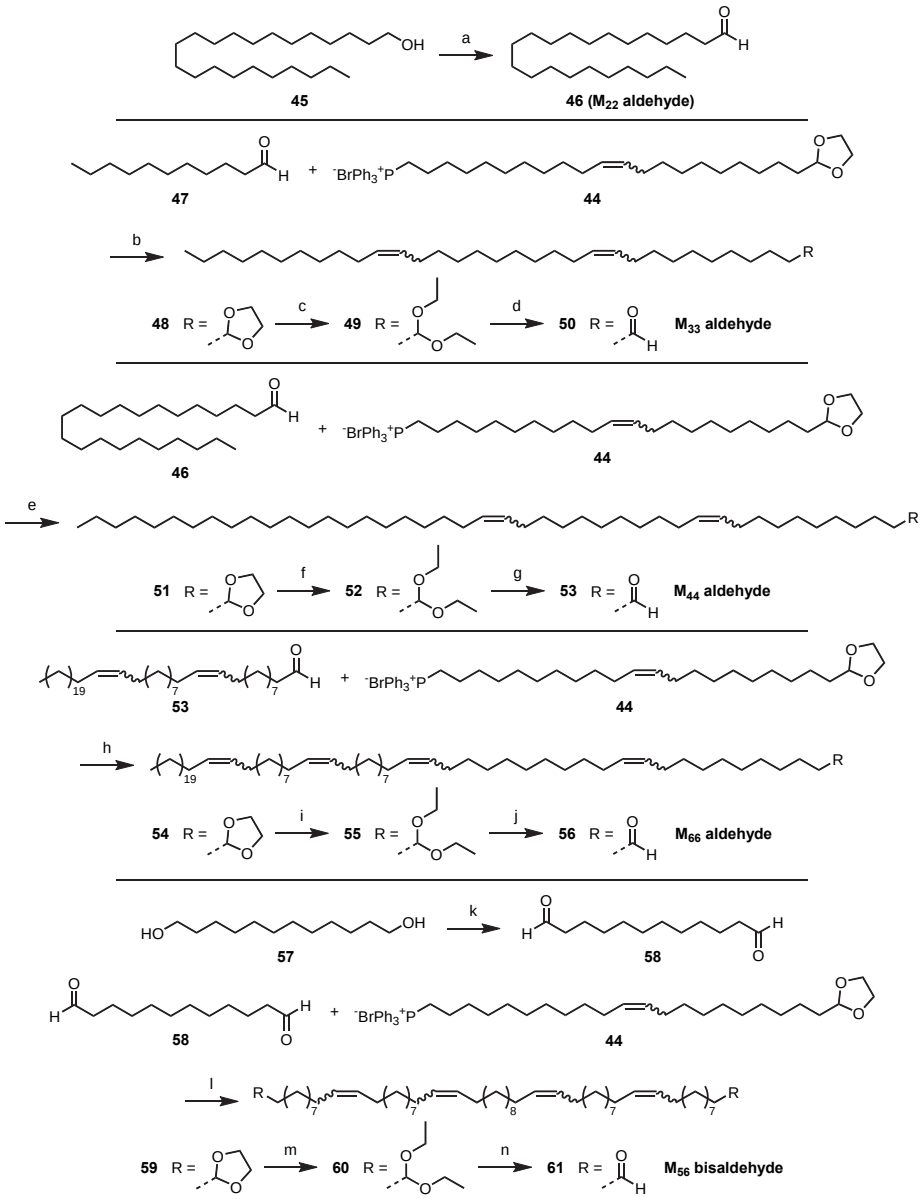

Scheme 5–2. Synthesis of unsaturated, long-chain aldehydes. Reagents and conditions: (a and k) TEMPO, tetrabutylammonium chloride, *N*-chlorosuccinimide, $NaHCO_3$, K_2CO_3, DCM, water, room temperature, 20 h (45–86%); (b, e, h and l) KO*t*Bu, THF, 0–20 °C, 1–21 h (60–77%); (c, f, i and m) EtOH, TsOH, reflux, 1–2 h (88–100%); (d, g, j and n) acetone, TsOH, room temperature, 1–3 h (95–99%). TEMPO = (2,2,6,6-tetramethylpiperidin-1-yl)oxyl.

A similar strategy was used to obtain M_{44} aldehyde **53**. Starting from docosanal **46**, ethylene acetal **51** was produced in 78% yield. Deprotection in two steps gave the M_{44} diethyl acetal **52** and M_{44} aldehyde **53** in 88% and 74% yield, respectively. Part of the aldehyde was subsequently converted to M_{66} ethylene acetal **54**, diethyl acetal **55** and aldehyde **56** in a good overall yield of 62%. For the deprotection of the longer acetals, chloroform was added as a co-solvent.

For the synthesis of homotelechelic M_{56} bisaldehyde, dodecanediol **57** was oxidized to bisaldehyde **58** under similar conditions as those for the oxidation of docosanol. The material was obtained as a white solid in 45% yield. Reaction with two equivalents of M_{22} building block **44** using the procedures described above, followed by removal of the acetal protective groups finally gave M_{56} bisaldehyde **61** in 71% yield over 3 steps.

5.2.3 α-Alkene and α,ω-bisalkene building blocks

The aldehydes were extended with terminal-alkene-containing phosphonium salts **65–67** to give a library of discrete-length α-alkenes and an α,ω-bisalkene (Scheme 5–3). The phosphonium salts were obtained from the reaction of ω-bromoalkenes **62–64** with triphenylphosphine in refluxing acetonitrile, followed by trituration of the formed solids with diethyl ether or washing of the acetonitrile solution with heptane. This gave the corresponding phosphonium salt either as crystalline, white compounds (**65** and **66**), or as a very viscous, light yellow oil (**67**) in good yields (84–92%). Hygroscopic compound **67** was dried thoroughly in high vacuum at 50 °C to remove any traces of water before using the compound in the Wittig reaction with the long-chain aldehydes.

Next, phosphonium salt **67** was reacted with undecanal **47**, docosanal **46**, and M_{33} aldehyde **50**. The reaction conditions were similar to those described for the Wittig reactions above. This afforded three linear alkenes: M_{22} alkene **68**, M_{33} alkene **69**, and M_{44} alkene **70**. The yields were 32%, 62%, and 28%, respectively. The low yields most likely are a result of competing reactions involving remaining water in phosphonium salt **67**. The longest alkene (M_{69} alkene **71**) was the product of the Wittig reaction between M_{66} aldehyde **56** and phosphonium salt **65** (46% yield). Lastly, homotelechelic M_{66} bisalkene **72** was obtained from the reaction of M_{56} bisaldehyde **61** with two equivalents of phosphonium salt **66** in 72% yield. All alkenes were obtained as colorless oils after purification by automated column chromatography. Confirmation of the purity of the alkene block with ^{1}H and ^{13}C NMR was straightforward. However, obtaining the MW of the materials with MALDI-TOF MS or GC-

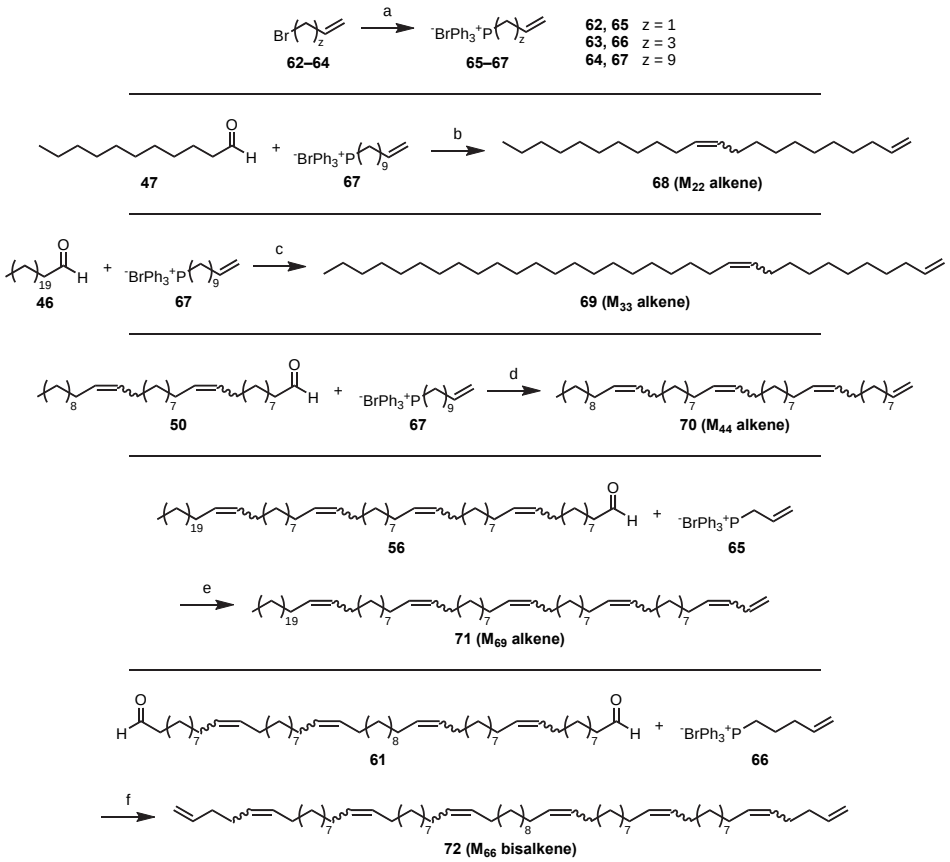

Scheme 5–3. Synthesis of unsaturated, terminal alkenes. Reagents and conditions: (a) PPh_3, acetonitrile, reflux, 1–24 h (84–92%); (b–f) KO*t*Bu, THF, 0–20 °C, 2 h (28–72%).

MS (electron ionization) proved to be very difficult. With the latter technique, only low-MW fragments were observed.

5.2.4 Formation of *o*DMS–*o*M conjugates

The high selectivity of the Karstedt platinum complex for monosubstituted (*i.e.*, terminal) olefins over internal double bonds permitted the direct hydrosilylation of M_{33} alkene **69** with siloxane monohydrides containing 7, 11, or 15 siloxane repeat units (**14a**–**c**) (see Scheme 5–4). We found that the reaction proceeded very well in DCM (a good solvent for both the starting materials and the BCO product) at room temperature, resulting in *o*M that was substituted with an *o*DMS block only at the terminal carbon in 59–81% yield. No isomerization of the double bond[30] or reaction with the internal double bond was found by

^{1}H NMR or MALDI-TOF MS. All compounds were obtained as colorless oils after purification by automated column chromatography.

Finally, the remaining internal double bond was hydrogenated by classical Pd/C catalyzed hydrogenation at atmospheric pressure, giving the fully saturated siloxane–alkane BCOs [**Si$_7$-M$_{33}$**], [**Si$_{11}$-M$_{33}$**], [**Si$_{15}$-M$_{33}$**] in excellent yields (92–100%). Because of the better

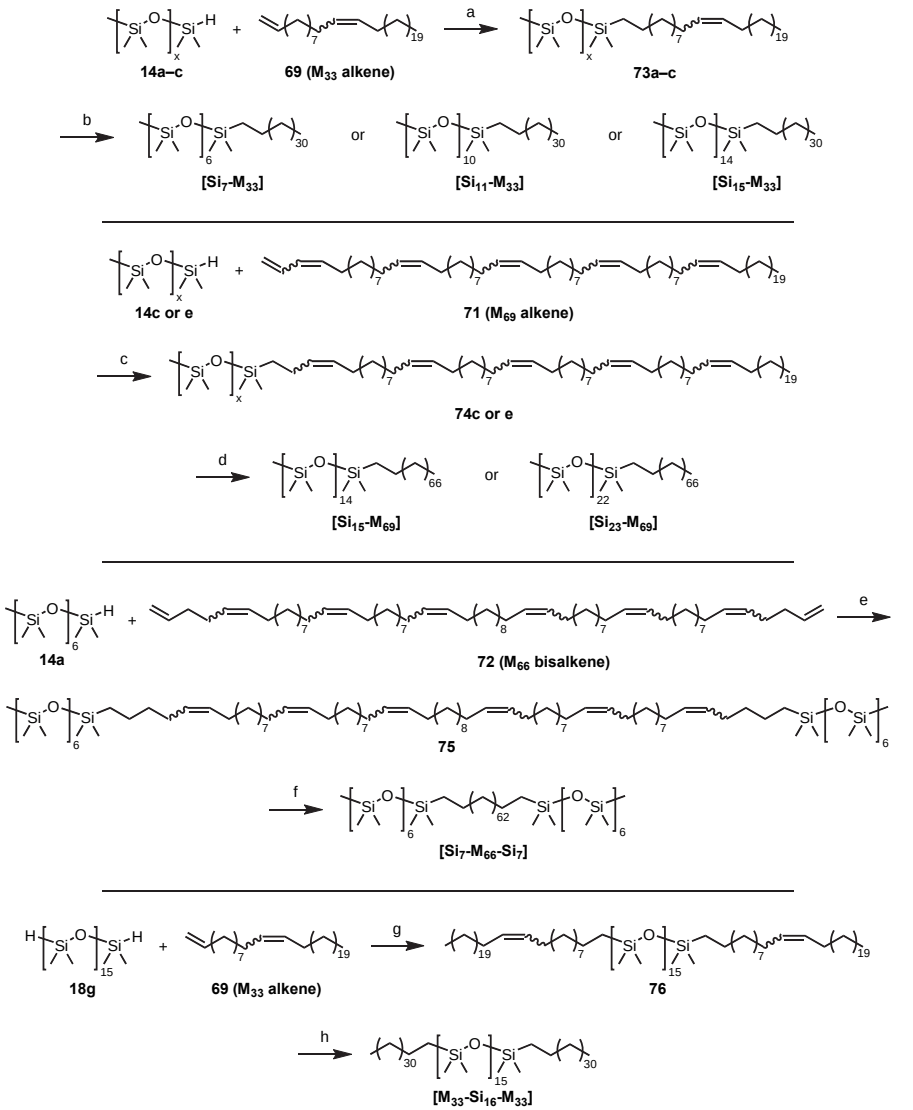

Scheme 5–4. Formation of BCOs [**Si$_x$-M$_z$**], [**Si$_7$-M$_{66}$-Si$_7$**] and [**M$_{33}$-Si$_{16}$-M$_{33}$**]. Reagents and conditions: (a, c, e and g) Karstedt catalyst, DCM, room temperature, 0.5–1 h (35–81%); (b, d, f and h) H_2, Pd/C, EtOAc, 20–70 °C, 3 h (54–100%).

ionizability of the BCOs than the separate *o*M blocks, the high purity of both BCOs and absence of oligomers with a different number of repeat units could be confirmed with both NMR and MALDI-TOF MS. In addition, the pure alkane $C_{33}H_{68}$ was prepared by hydrogenation of the unsaturated alkane M_{33} alkene **69**, and served as a reference compound.

Higher MW BCOs [**Si$_{15}$-M$_{69}$**] and [**Si$_{23}$-M$_{69}$**] were obtained from the reaction of M_{69} alkene **71** with monohydrides Me-Si$_{15}$-H **14c** and Me-Si$_{23}$-H **14e** under similar reaction conditions. However, during hydrogenation of the unsaturated BCOs at room temperature, we observed the formation of a gray reaction mixture. This was a result of the precipitation of (partially) hydrogenated BCOs (white solids) in combination with the black Pd/C catalyst. Therefore, the reaction mixture was heated to 60 °C. At this temperature, the initial deep black color returned, indicating full dissolution of the BCOs. After full hydrogenation of all double bonds, the reaction mixture was filtered whilst still hot to prevent premature precipitation of the products. The products were further purified by automated column chromatography.

For the preparation of tri-BCOs [**Si$_7$-M$_{66}$-Si$_7$**] and [**M$_{33}$-Si$_{16}$-M$_{33}$**], the outer blocks (*o*DMS and *o*M, respectively) were used in a slightly over two-fold excess to ensure a 100% formation of the triblock in the Karstedt reaction. The subsequent hydrogenation leading to [**Si$_7$-M$_{66}$-Si$_7$**] again needed heating of the reaction mixture. Formation of [**M$_{33}$-Si$_{16}$-M$_{33}$**] was achieved at room temperature.

Because of the limited separation of alike *o*DMS–*o*M BCOs with column chromatography, it was not possible to directly obtain pure, asymmetrical tri-BCO [**M$_{22}$-Si$_{16}$-M$_{44}$**] with the procedures above. Although it was perfectly possible to form the statistical mixture of the unsaturated versions of [**M$_{22}$-Si$_{16}$-M$_{22}$**] (**78**), [**M$_{22}$-Si$_{16}$-M$_{44}$**] (**77**), and [**M$_{44}$-Si$_{16}$-M$_{44}$**] (**79**) by reacting H-Si$_{16}$-H **18g** with equimolar amounts of M_{22} alkene **68** and M_{44} alkene **70**, separation of the mixture was impossible (Scheme 5–5, top). Also first reacting the *o*DMS dihydride with 1 equivalent of only one type of alkene to desymmetrize the molecule gave inseparable mixtures.

In order to obtain pure [**M$_{22}$-Si$_{16}$-M$_{44}$**], desymmetrization of the siloxane was needed at an earlier stage in the synthesis. The route depicted in the bottom part of Scheme 5–5 was followed. First, disilanol HO-Si$_8$-OH **17g** was reacted with 1 equivalent of chlorosilane building block **11** in toluene, using pyridine as a base. The procedure was equal to that described in Chapter 2, Section 2.2.1 for the desymmetrization of disilanol HO-Si$_{40}$-OH **17k**. The resulting mixture of product HO-Si$_{12}$-H **80**, remaining starting material HO-Si$_8$-OH, and disubstituted byproduct H-Si$_{16}$-H could be separated in a straightforward manner by

automated column chromatography because of the large differences in affinity of the different components for the column material. Thus, monohydride **80** was obtained in a very good yield of 44%.[v]

Next, monohydride **80** was coupled to M_{44} alkene **70** with the Karstedt catalyst, resulting in diblock-like molecule **81**. During the reaction and purification, the silanol remained fully

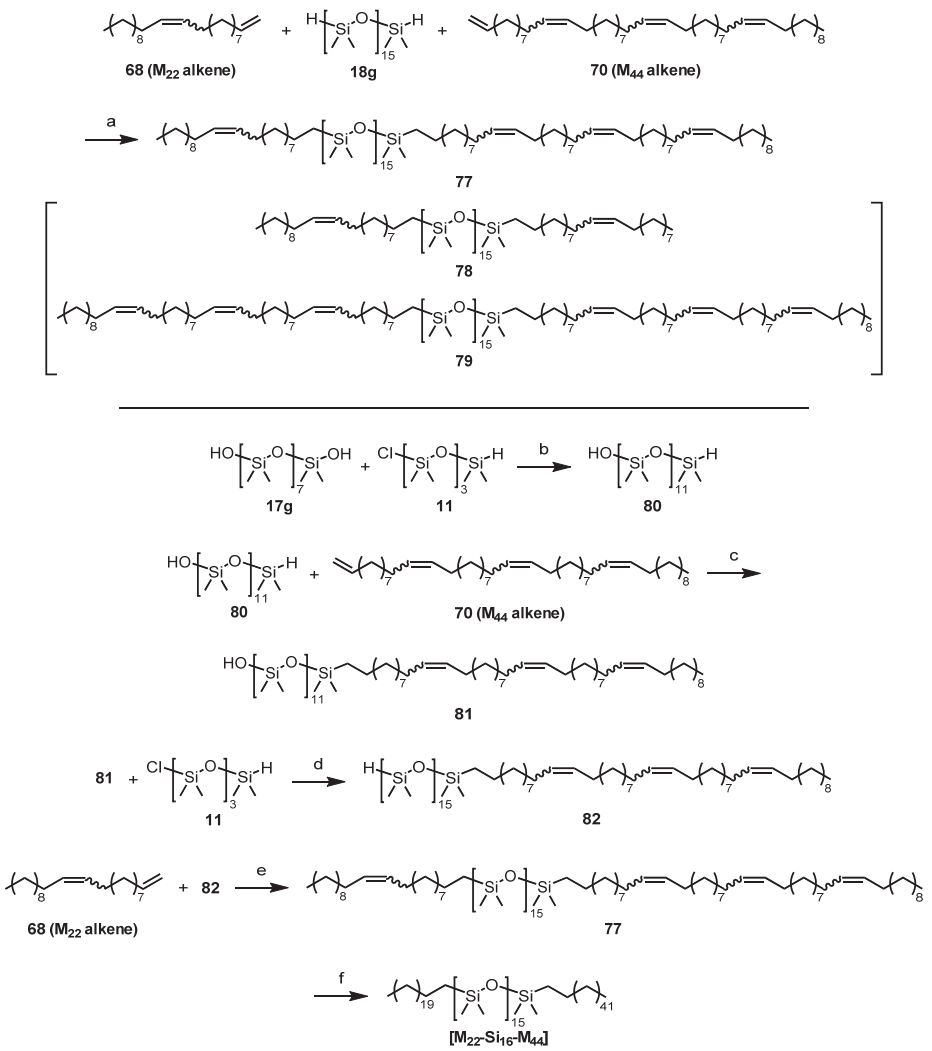

Scheme 5–5. Formation of asymmetric BCO [$\mathbf{M_{22}}$-$\mathbf{Si_{16}}$-$\mathbf{M_{44}}$]. Reagents and conditions: (a, c and e) Karstedt catalyst, DCM, room temperature, 1 h (27–75%); (b) pyridine, toluene, room temperature, 2.5–3h (44–80%); (f) H_2, Pd/C, EtOAc, 60 °C, 3 h (88%).

[v] A maximum (theoretical) yield of 50% is expected.

intact, as was evidenced by ^{1}H NMR and MALDI-TOF MS. Subsequent reaction with one additional equivalent of chlorosilane building block **11** gave compound **82**, with the required length of 16 siloxane repeat units, in good yield (80%). The new hydride functionality in this molecule was used to attach the shorter M_{22} alkene **68**, giving unsaturated BCO **77** in pure form after column chromatography. Care was taken to select only the purest fractions for the last hydrogenation step, hence the low yield of 27%. Finally, the molecule was hydrogenated at 60 °C with the standard procedure, giving the pure tri-BCO [$\mathbf{M_{22}}$-$\mathbf{Si_{16}}$-$\mathbf{M_{44}}$] in good yield (88%). The high purity of all BCOs and absence of oligomers with a different number of repeat units was confirmed with NMR and mass spectrometry.

5.3 Experimental evidence for microphase segregation in *o*DMS–*o*M

The following section deals with extensive structural analysis for all BCOs with differential scanning calorimetry (DSC) and small-angle X-ray scattering (SAXS) experiments. For clarity, we reserved a separate section (Section 5.4) in which we translate the measurement data to our view on the molecular organization in the self-assembled BCOs and its relation to molecular architecture.

In Table 5–1, an overview is presented of all BCOs synthesized (entries 1–8). Entry 9 shows the data for reference molecule tritriacontane (*n*-$C_{33}H_{68}$). Notably, all saturated BCOs—in contrast to the unsaturated precursors—were solids at room temperature, forming flaky solids that were reminiscent of brittle candle wax (*i.e.*, a typical texture for low-MW alkanes). This was a direct indication that at least part of the crystalline behavior of the alkane block remained intact within the BCO, and suggested that microphase separation occurred in all materials. Also, we observed a dramatic difference between the solubility of the BCOs and the tritriacontane reference molecule. Whereas all BCOs readily dissolved in most common solvents (DCM, heptane, ethyl acetate) at room temperature or after slight heating, hardly any of the pure alkane dissolved under these conditions. Significantly higher temperatures (*e.g.*, boiling heptane) were required to dissolve the tritriacontane.

5.3.1 Thermal transitions

The thermal signatures of all BCOs were captured with differential scanning calorimetry (DSC). The data are summarized in Table 5–1. In Figure 5–2A–C, the DSC traces for all BCOs are provided. The BCOs revealed at least one strong endothermic transition, denoted with T_m. This this transition was broadened and consisted of more than one maximum for compounds [$\mathbf{Si_{15}}$-$\mathbf{M_{33}}$] and [$\mathbf{Si_{15}}$-$\mathbf{M_{69}}$]. Additionally, most compounds gave a second, weaker

Table 5–1. Molecular characterization data for monodisperse block co-oligomers.

Entry	Compound	M_n [Da]	N[a]	f_M[b]	T_{OOT}[c] [°C]	ΔH_{OOT}[c] [kJ mol^{-1}]	T_m[c] [°C]	ΔH_{fus}[c] [kJ mol^{-1}]	d_{LAM}[d] [nm]	2nd phase (d_2^* [nm])[e]
1	**[Si$_7$-M$_{33}$]**	982.0	15.6	0.51	35.8	10.8	43.8	71.2	5.77	LAM (5.6)
2	**[Si$_{11}$-M$_{33}$]**	1279	20.0	0.40	32.2	6.2	38.7	63.4	6.76	CYL (7.0)
3	**[Si$_{15}$-M$_{33}$]**	1575	24.4	0.33	24.7	7.2	35.6	58.9	8.06[h]	CYL (7.8)
4	**[Si$_{15}$-M$_{69}$]**	2080	33.1	0.50	n.o.	-	81.9	148.5	11.2	n.d.
5	**[Si$_{23}$-M$_{69}$]**	2673	41.9	0.40	n.o.	-	83.3	166.4	12.5	n.d.
6	**[Si$_7$-M$_{66}$-Si$_7$]**	1962	31.3	0.51	46.6	10.5	71.8	180.3	5.91	n.o.
7	**[M$_{33}$-Si$_{16}$-M$_{33}$]**	2098	33.5	0.48	34.9	18.7	47.8	126.6	5.86	LAM (8.6)[i]
8	**[M$_{22}$-Si$_{16}$-M$_{44}$]**	2098	33.5	0.48	3.6[f]	30.4	50.8	108.0	12.0	LAM (11.1)
9	**C$_{33}$H$_{68}$**	464.9	7.9	-	n.o.	n.o.	72[g]	79.5[g]	4.44	n.o.

[a] Number of segments based on a 110 Å^3 reference volume; [b] Oligomethylene volume fraction, calculated using bulk densities for PDMS (0.95 g mL^{-1}) and tritriacontane (0.82 g mL^{-1}); [c] Pre-melting, endothermic order–order transition (T_{OOT}), associated heat effect (ΔH_{OOT}), melting temperature (T_m), and enthalpy of fusion of the *o*M block (ΔH_{fus}). Determined with DSC using a heating rate of 10 °C min^{-1} Enthalpic values are per mole of BCO; [d] Lamellar domain spacing determined with SAXS at room temperature, calculated as $d_{LAM} = 2\pi/q^*$; [e] Morphology above T_{OOT} (principal domain spacing in between brackets). CYL = cylindrical, LAM = lamellar; [f] A very broad transition was observed; [g] Literature value;[31] [h] Determined at −4 °C; [i] The domain spacing for the second set of lamellar reflections below T_{OOT}; n.d. = not determined, n.o. = not observed.

transition that preceded T_m (denoted with an asterisk). In some cases, this second peak was very broad ([**M$_{22}$-Si$_{16}$-M$_{44}$**]) or completely absent ([**Si$_{15}$-M$_{69}$**] and [**Si$_{23}$-M$_{69}$**]).

Interestingly, all transitions were found well below the melting point of the corresponding, unfunctionalized alkane block. For example, BCO [**Si$_7$-M$_{33}$**] (entry 1) showed transitions at 36 and 44 °C, whereas pure tritriacontane has a reported melting point at 72 °C[31] (this temperature is indicated with the blue-green arrow in Figure 5–2A). However, the enthalpy associated with the transition at 44 °C (71 kJ (mol BCO)$^{-1}$) has a similar value as the enthalpy of fusion of tritriacontane (79.5 kJ mol^{-1}).[31] Analogously, the highest-temperature transitions for the BCOs with M_{66} or M_{69} blocks are 20–25 °C lower than those of related *n*-$C_{64}H_{130}$ or *n*-$C_{70}H_{142}$.[32]

For all BCOs, we attribute the endothermic transitions at the highest temperatures to melting transitions of the alkane blocks and the formation of an isotropic state. This was later corroborated by polarized optical microscopy and SAXS (*vide infra*) experiments at temperatures above and below these transitions. Evidently, the observed reduction in T_m compared to that of the pure alkanes is the result of changes in the alkane crystal packing, induced by the attached *o*DMS blocks. These changes can, for example, be induced by nanoconfinement of the crystalline domains[33] or alkyl chain folding.[34] Also, partially

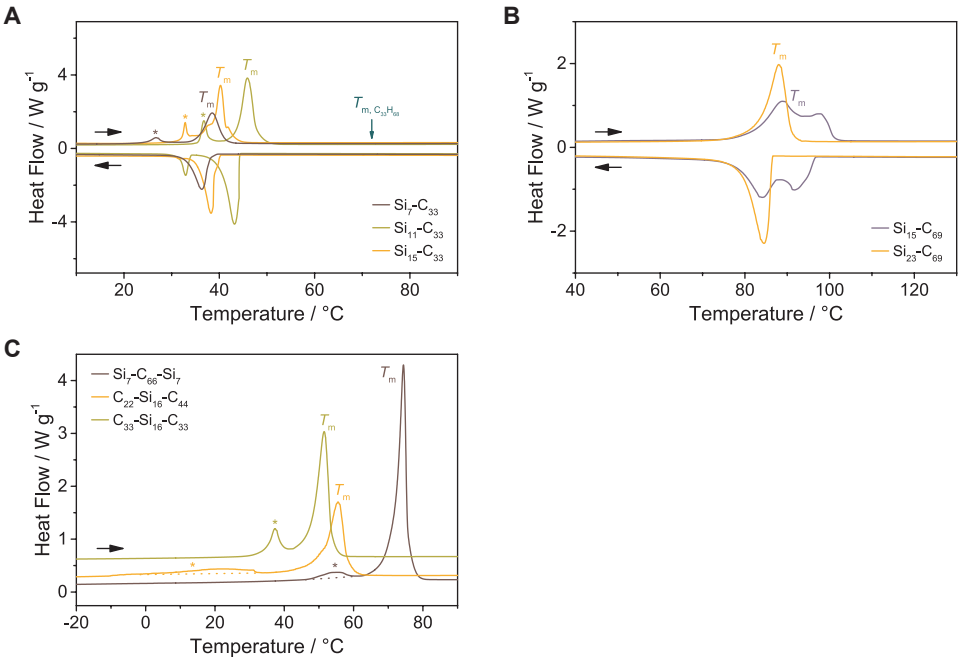

Figure 5–2. DSC traces (second cycle) for: (**A**) di-BCOs [$\mathbf{Si_x\text{-}M_{33}}$]; (**B**) di-BCOs [$\mathbf{Si_x\text{-}M_{69}}$]; (**C**) tri-BCOs. Endothermic heatflows have a positive value. The data are shifted vertically for clarity. Order–order transitions preceding the melting transition are indicated with an asterisk. As a guide to the eye, continuation of the baseline is provided as a dotted line under the OOTs of [$\mathbf{Si_7\text{-}M_{66}\text{-}Si_7}$] and [$\mathbf{M_{22}\text{-}Si_{16}\text{-}M_{44}}$]. A temperature ramp of 10 °C min^{-1} was used.

amorphous alkanes block may lead to a lower melting temperature. This trend is for example visible for the [$\mathbf{Si_x\text{-}M_{33}}$] family, in which a longer siloxane block leads to both lower melting points and a decrease of ΔH_{fus} per mol of BCO (see Figure 5–2A and Table 5–1, entries 1–3).

Interestingly, the changes in melting temperatures were much more prominent in the *o*DMS–*o*M systems than in the semicrystalline *o*DMS–*o*LA system described in Chapter 4 (see Section 4.3.1). Here, much less difference between the melting points of the pure *o*LLA or *o*DLA blocks and their *o*DMS conjugates was found. Likely, this is predominantly related to the much smaller oligomethylene chain length in the *o*DMS–*o*M materials studied (*i.e.*, one single lactic acid repeat unit contains three backbone atoms (–carbon–carbon–oxygen–) *versus* only a single carbon atom per methylene residue).

Finally, we ascribe the second transition, preceding the melting transitions, to an order–order phase transition (OOT) involving a reorganization of the alkyl chains. Similar pre-melting phase behavior has been observed in normal paraffins with comparable length.[31,35–37] However, the appearance and sharpness of this transition in the DSC measurements varied

significantly between the BCOs and was also strongly dependent on the heating/cooling rate with which the measurement was executed. Therefore, we performed a more thorough study of the BCO phase behavior with SAXS experiments at room temperature and elevated temperatures.

5.3.2 X-ray scattering in di-BCOs at room temperature

The formation of an ordered crystalline state was first investigated with SAXS at room temperature. Transmission-scattering profiles were recorded in medium- (MAXS) and wide-angle (WAXS) operating modes. The 2-D scattering data were reduced to 1-D profiles, and MAXS and WAXS regions were merged. Figure 5–3A reveals the scattering data over the entire q-range for BCOs [$\mathbf{Si_x}$-$\mathbf{M_{33}}$]. In addition, the scattering profile of $C_{33}H_{68}$ is provided (gray curve). The samples were not thermally annealed prior to the measurements. In all traces, a sharp principal scattering peak, denoted q^*, was observed at low q-values. Additional higher-order reflections at equidistant q-values ($\sqrt{4}q^*$, $\sqrt{9}q^*$, and $\sqrt{16}q^*$) were observed for BCO [$\mathbf{Si_7}$-$\mathbf{M_{33}}$] and alkane $C_{33}H_{68}$, indicative for the formation of an ordered, lamellar structure. For BCO [$\mathbf{Si_{11}}$-$\mathbf{M_{33}}$] only 1 additional, clear reflection at $\sqrt{9}q^*$ was found, whereas [$\mathbf{Si_{15}}$-$\mathbf{M_{33}}$] revealed more peaks at $\sqrt{3}q^*$, $\sqrt{4}q^*$, $\sqrt{7}q^*$, $\sqrt{9}q^*$, and $\sqrt{12}q^*$. The latter is typical for a cylindrical BCP morphology. However, the scattering profiles of [$\mathbf{Si_{11}}$-$\mathbf{M_{33}}$] and [$\mathbf{Si_{15}}$-$\mathbf{M_{33}}$] looked distorted. The $\sqrt{9}q^*$ reflection in [$\mathbf{Si_{11}}$-$\mathbf{M_{33}}$] displayed a shoulder at the low-q side, and most higher-order reflections of [$\mathbf{Si_{15}}$-$\mathbf{M_{33}}$] were broadened.

To eliminate kinetically trapped states, all samples were remeasured again after annealing. The annealing strategy was similar to that described in the previous chapters, and involved

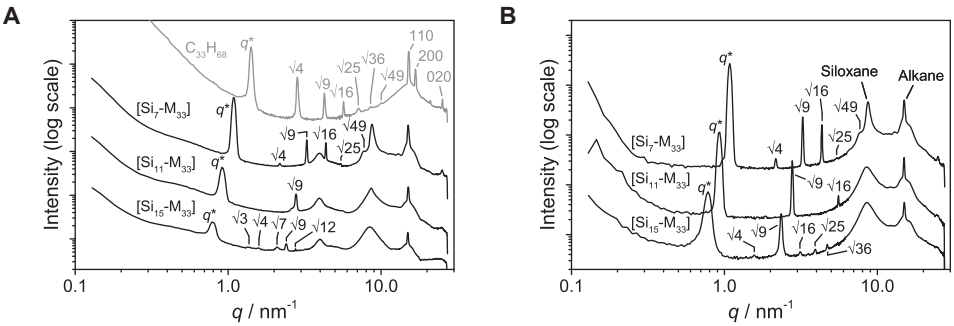

Figure 5–3. Reduced transmission-SAXS data for: (**A**) BCOs [$\mathbf{Si_x}$-$\mathbf{M_{33}}$] and alkane $C_{33}H_{68}$ at room temperature before annealing; (**B**) BCOs [$\mathbf{Si_x}$-$\mathbf{M_{33}}$] at room temperature (T = −4 °C for [$\mathbf{Si_{15}}$-$\mathbf{M_{33}}$]) after annealing. The data are shifted vertically for clarity. A selection of higher-order Bragg reflections are indicated as q/q^* values. Additionally, the three most alkane reflections in the WAXS region are labeled. The broad peak at q = 4 nm^{-1} results from background scattering (Kapton tape).

heating the material to a temperature 20 degrees above T_m, followed by cooling down to room temperature with 0.5 °C min^{-1}. In addition, the measurement of BCO [**Si$_{15}$-M$_{33}$**] was conducted at −4 °C instead of room temperature. The reason for this is the manifestation of an exothermic transition around 6 °C in the DSC cooling curve of [**Si$_{15}$-M$_{33}$**], which is presumed to be the same OOT as was found around 25 °C in the heating run for this BCO. Interestingly, the annealed samples showed a significant improvement in the level of organization in the microphase-segregated state (Figure 5–3B). A remarkably large number of equally spaced reflections was observed, including a rarely observed, high intensity 7th order reflection.[38–40] This indicated that extremely organized lamellar structure were formed in all three samples, despite the very low MW of these compounds and existence of only weak London dispersion interactions between the alkane chains. Lamellar domain spacings were calculated as $d_{LAM} = 2\pi/q^*$, which resulted in values of 5.8, 6.8, and 8.1 nm for BCOs [**Si$_7$-M$_{33}$**], [**Si$_{11}$-M$_{33}$**], and [**Si$_{15}$-M$_{33}$**], respectively. To our knowledge, the domain spacing of [**Si$_7$-M$_{33}$**] was the smallest hitherto observed for a BCP analogue at the moment of discovery, although very recently an even smaller domain spacing was reported.[1]

At higher q-values, additional scattering peaks revealed further interchain organization, both in annealed as well as non-annealed samples. First, a reflection at q = 8.6 nm^{-1} was attributed to the amorphous *o*DMS block. A siloxane reflection at this location was also observed for the crystalline [**Si$_x$-LLA$_y$**] and [**Si$_x$-DLA$_y$**] BCOs in Chapter 4. Also, a sharp peak at 15.0 nm^{-1}, a shoulder around q = 16.7 nm^{-1}, and a weak reflection at 25.0 nm^{-1} were found. The locations of these reflections perfectly coincide with the 110, 200, and 020 reflections for the orthorhombic sub-unit cell of alkanes[41,42] (cell dimensions: a = 7.42 Å, b = 4.95 Å, and c = 2.55 Å; see Figure 5–3B, gray curve), which suggests that the alkane blocks crystallize in the same orthorhombic substructure as simple, linear alkanes.

Interestingly, BCO [**Si$_7$-M$_{33}$**] gave a significantly more narrow siloxane reflection band than the other two di-BCOs, which is an indication that the variability of interchain distances within the *o*DMS block is smaller in [**Si$_7$-M$_{33}$**] compared to that in the other BCOs. We did not anticipate to observe this increase in the ordering of the *o*DMS chains because of the extraordinary high flexibility of the siloxane backbone. Nevertheless, we presume that the combined effect of crystallinity in the *o*M block, the short stretched-chain length of the *o*DMS block, and very high density of *o*DMS–*o*M links at the domain boundaries of BCO [**Si$_7$-M$_{33}$**] forces the *o*DMS chains in an entropically unfavorable, but more uniform conformation. Similar—but less extreme—non-Gaussian chain conformations are well known in brush type polymers with high grafting density.[43]

The scattering patterns of [**Si**$_{15}$-**M**$_{69}$] and [**S**$_{23}$-**M**$_{69}$] were both recorded only after annealing of the samples and showed typical reflections for a lamellar structure (up to reflection $\sqrt{81}q^*$ for BCO [**Si**$_{23}$-**M**$_{69}$]). The domain spacings were 11.2 and 12.5 nm, respectively. In the WAXS region, the 110, 200, and 020 reflections for an orthorhombic crystal lattice were clearly visible. The scattering data for the tri-BCOs will be treated in Section 5.3.4.

In conjunction with Section 4.3.2, we assumed that the formation of a lamellar structure at low temperatures in all di-BCOs again is driven by the preferred parallel orientation of the alkyl fragments within the crystalline *o*M domain. However, the origin of the pre-melting transitions and unexpected reflections that were observed for the non-annealed, asymmetrical BCOs were not fully understood and required additional scattering measurements. As already mentioned in the beginning of Section 5.3, we further elaborate on the molecular organization the self-assembled BCOs in Section 5.4.

5.3.3 Variable temperature X-ray scattering for di-BCOs

The presence of pre-melting transitions in the DSC traces of most BCOs and the observed formation of kinetically trapped, non-lamellar morphologies in BCO [**Si**$_{15}$-**M**$_{33}$] served as a trigger for a more detailed study of the morphology development at temperatures above and below room temperature. BCOs [**Si**$_x$-**M**$_{33}$] were examined over the full temperature range spanned by the transitions that were detected with DSC. For this, X-ray scattering images were collected at regular intervals while heating up annealed samples from their crystalline state (at or below room temperature) to the isotropic state (above T_m). Also, scattering data were recorded during cooling down of the sample. Similar measurements were performed for tri-BCOs [**Si**$_7$-**M**$_{66}$-**Si**$_7$], [**M**$_{33}$-**Si**$_{16}$-**M**$_{33}$], and [**M**$_{22}$-**Si**$_{16}$-**M**$_{44}$] (see the next section). A select number of scattering profiles, which captured all observed morphological changes, is plotted in Figure 5–4.

Figure 5–4A and B show the data for BCO [**Si**$_7$-**M**$_{33}$]. Heating of the sample from 22 to 36 °C did not resulted in a change of the scattering patterns that we attributed to a lamellar packing in the previous section. Also no alteration of the alkane packing was observed. As indicated with the red arrow in Figure 5–4A, increasing the temperature to 37 °C resulted in the loss of the strongest WAXS reflection at q = 15.0 nm^{-1} (blue, dashed line), and the appearance of a new reflection at q = 14.2 nm^{-1} (red, dashed line). Also, a significant broadening of the WAXS reflection of the siloxane block (around q = 8.6 nm^{-1}) was seen. Simultaneously, a very small shift of the low-q reflections to higher q-values was observed. This shift was not a result of a calibration error, since at 37 °C clearly two nearby peaks

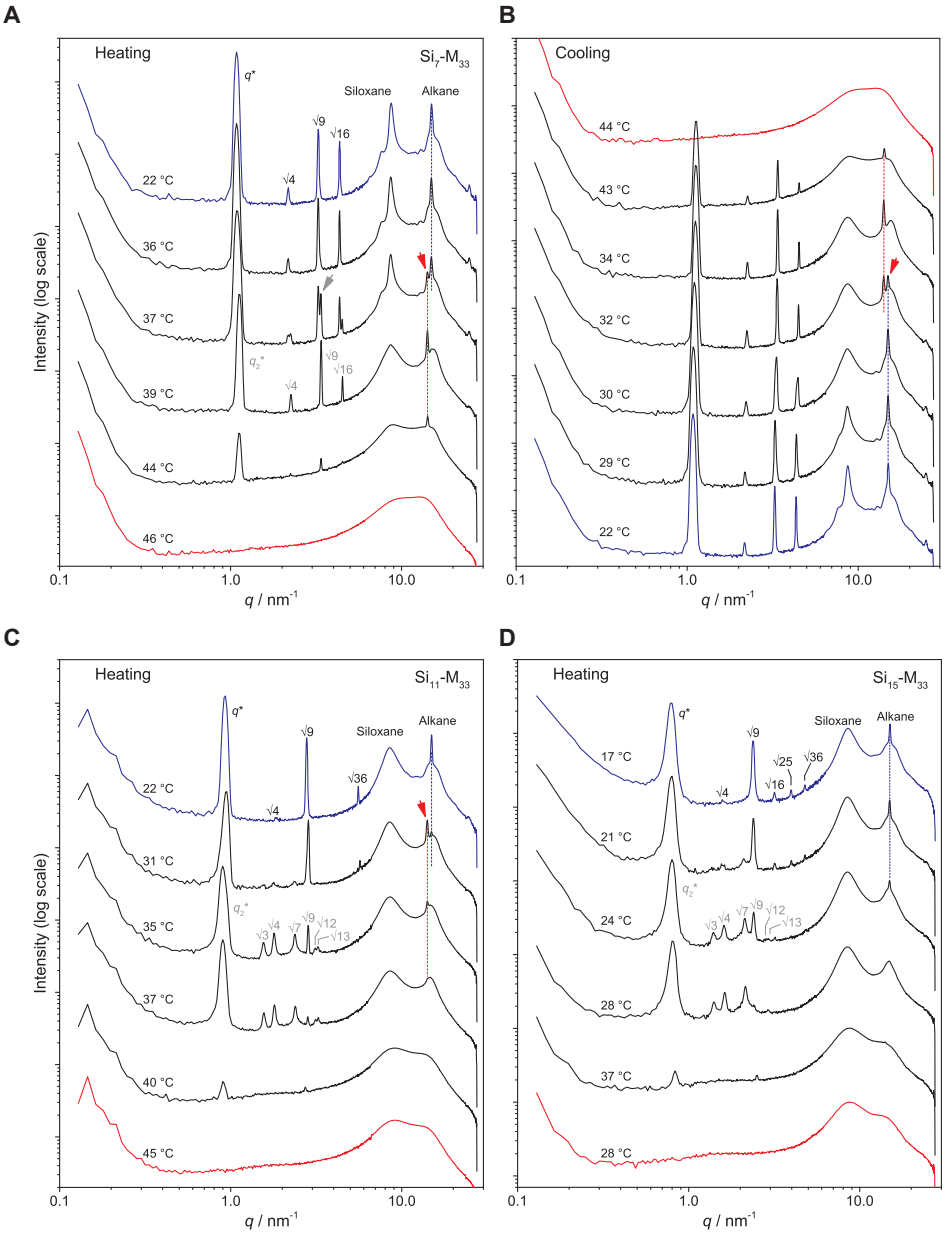

Figure 5–4. Reduced variable temperature transmission-SAXS data for [**Si$_7$-M$_{33}$**] (**A–B**), [**Si$_{11}$-M$_{33}$**] (**C**), and [**Si$_{15}$-M$_{33}$**] (**D**). The data are shifted vertically for clarity. Lowest and highest temperature data are plotted in blue and red, respectively. A selection of (higher-order) Bragg reflections of the crystalline phase below the OOT is indicated is indicated as q/q^* values (in black). Reflections indicated in gray belong to the microphase-segregated state above the OOT. The blue and red, vertical, dashed lines follow the most intense alkane reflection in the WAXS region.

belonging to the $\sqrt{9}q^*$ and $\sqrt{9}q_2^*$ reflections (*i.e.*, reflections attributed to the morphologies before and after the shift, respectively) can be discriminated (indicated with the gray arrow). Further increase of the temperature finally lead to the disappearance of all sharp reflections in both the MAXS and WAXS region of the scattering plots around 44 °C, indicative for the formation of a disordered (isotropic) state.

The reversibility of the transitions was confirmed by the scattering profiles recorded during cooling of the sample (Figure 5–4B). Reappearance of scattering reflections occurred around 37 °C. The scattering profile closely resembled the pre-melting profile that was captured in the heating run. At 32 °C, a reorganization of the initially formed structure was evidenced from a discontinous change in the location of the alkane WAXS reflection, again indicated with the red arrow. No further changes were observed upon further cooling down of the sample, and the scattering profiles at room temperature before and after the VT-SAXS measurements were identical.

The temperatures at which both the solid–solid transition and the melting transition were observed matched with the DSC values (T_{OOT} = 35.8 °C and T_m = 43.8 °C). Also a hysteresis for the order–order transition (OOT) was observed with both techniques. Evidently, crystalline interactions within the *o*M blocks are preserved above the OOT, given the sharp reflection at q = 14.2 nm^{-1} and highly enthalpic melting transition at T_m. However, we did not succeed in assigning a particular spacegroup to the alkane packing in this block.

For BCOs [$\mathbf{Si_{11}}$-$\mathbf{M_{33}}$] and [$\mathbf{Si_{15}}$-$\mathbf{M_{33}}$] also two distinct transitions were observed in the VT-SAXS measurements (Figure 5–4C and D). BCO At 31 °C, [$\mathbf{Si_{11}}$-$\mathbf{M_{33}}$] exhibited a change in the WAXS region comparable to that of compound [$\mathbf{Si_7}$-$\mathbf{M_{33}}$], albeit that the new WAXS reflection was less pronounced. In contrast, additional peaks appeared at low q, located at $\sqrt{3}q^*$, $\sqrt{7}q^*$, $\sqrt{12}q^*$, and $\sqrt{13}q^*$. The reflection at $\sqrt{36}q^*$ disappeared, and the position of the primary scattering reflection remained unchanged. A similar change was found for BCO [$\mathbf{Si_{15}}$-$\mathbf{M_{33}}$], but the reflections above the OOT were broader. Interestingly, this BCO did not reveal the formation of a new WAXS reflection, but only the loss of the low-temperature reflection. Finally, formation of a disordered state was found for both BCOs at higher temperatures. Again, the transitions were fully reversible and occurred at temperatures that matched with the values found in the DSC measurements. The MAXS scattering reflections with the aforementioned peak location ratios are typically associated with the presence of microphase-segregated domains of hexagonally packed cylinders. Based on the volume fractions of the methylene block in [$\mathbf{Si_{11}}$-$\mathbf{M_{33}}$] (f_M = 0.40) and [$\mathbf{Si_{15}}$-$\mathbf{M_{33}}$] (f_M = 0.33), the formation of such structures can be expected if the crystalline interactions within the *o*M

block are weakened (*i.e.*, not sufficient to enforce a lamellar organization of the microphase-segregated system). We propose that the observed changes in the *o*M crystal structure at elevated temperatures are an indication of such weakening, and hence related to the alteration of the BCO morphology.

5.3.4 Variable temperature X-ray scattering for tri-BCOs

At room temperature, the ABA-type tri-BCO [$\mathbf{Si_7}$-$\mathbf{M_{66}}$-$\mathbf{Si_7}$] gave a scattering pattern that contained very sharp reflections at q^*, $\sqrt{9}q^*$, and $\sqrt{16}q^*$ as well as a weak reflection at $\sqrt{4}q^*$, pointing to a microphase-separated, lamellar structure (Figure 5–5A). Additionally, a narrow siloxane reflection, and alkane 110 and 200 reflections were found, nearly identical to those in the WAXS region of di-BCO [$\mathbf{Si_7}$-$\mathbf{M_{33}}$]. Intriguingly, the calculated domain spacing of the tri-BCO (d_{LAM} = 5.9 nm) was very close to the value for [$\mathbf{Si_7}$-$\mathbf{M_{33}}$] (d_{LAM} = 5.8 nm), despite the fact that the MW and *o*M block length were both doubled. Upon increasing the temperature, the scattering profiles remained nearly unchanged up to 70 °C, above which all reflections faded away with the formation of an isotropic phase. No morphological changes could be assigned to the (weak) thermal transition found with DSC at T = 46.6.

BAB-type tri-BCO [$\mathbf{M_{33}}$-$\mathbf{Si_{16}}$-$\mathbf{M_{33}}$] also showed equally spaced reflections at q^*, $\sqrt{4}q^*$, $\sqrt{9}q^*$, $\sqrt{16}q^*$ and $\sqrt{25}q^*$, related to a lamellar structure with d_{LAM} = 5.9 nm (Figure 5–5B). However, at room temperature, an extra peak at lower q ($q = q_2^*$, in gray) was found, which could not be identified with this domain spacing. Moreover, the q_2^* reflection was accompanied by very weak reflections $\sqrt{4}q_2^*$, $\sqrt{9}q_2^*$, $\sqrt{16}q_2^*$ (also indicated in gray). The reflection at $\sqrt{9}q_2^*$ resided partially under the $\sqrt{4}q^*$ peak. The spacing related to this second set of reflections was 8.6 nm. With increasing temperature, q_2^* and associated reflections shifted to higher q-values, resulting in better visibility of the $\sqrt{9}q_2^*$ reflection (see the gray arrow indicating the position of the $\sqrt{9}q_2^*$ peak at 40 °C in Figure 5–5B). All q_2^* reflections disappeared at 37°C, which was close to T_{OOT} = 34.9 found with DSC. The other reflections remained unchanged up to 47 °C, in agreement with T_m = 47.8 °C. The WAXS signals showed similar changes with temperature as those of di-BCO [$\mathbf{Si_7}$-$\mathbf{M_{33}}$], with transition temperatures matching T_{OOT} and T_m. Only the siloxane reflection band at q = 8.6 nm^{-1} was more broadened in the BAB-type tri-BCO.

Finally, scattering profiles for BCO [$\mathbf{M_{22}}$-$\mathbf{Si_{16}}$-$\mathbf{M_{44}}$], with unequal *o*M block distribution, can be found in Figure 5–5C. Again, q^*, $\sqrt{4}q^*$, $\sqrt{9}q^*$, $\sqrt{16}q^*$, and $\sqrt{49}q^*$ reflections revealed a lamellar organization at 17 °C. The peaks were slightly broadened compared to those of the other BCOs. Additional reflections in the WAXS region equaled those of [$\mathbf{M_{33}}$-$\mathbf{Si_{16}}$-$\mathbf{M_{33}}$] at room temperature. Remarkably, BCO [$\mathbf{M_{22}}$-$\mathbf{Si_{16}}$-$\mathbf{M_{44}}$] gave d_{LAM} = 12.0 nm, which is double the domain spacing of [$\mathbf{M_{33}}$-$\mathbf{Si_{16}}$-$\mathbf{M_{33}}$], [$\mathbf{Si_7}$-$\mathbf{M_{66}}$-$\mathbf{Si_7}$], or [$\mathbf{Si_7}$-$\mathbf{M_{33}}$]. Increasing the temperature

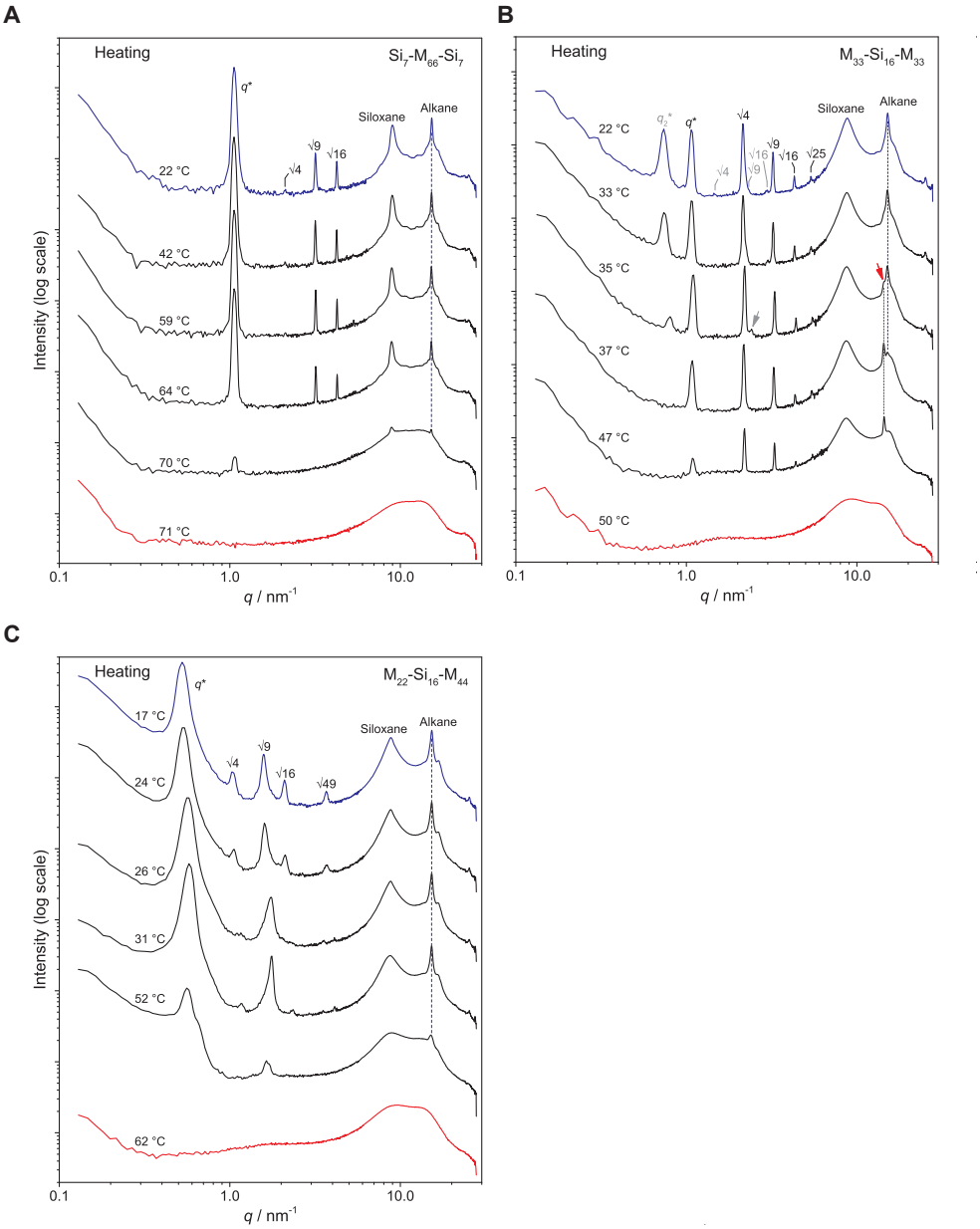

Figure 5–5. Reduced variable temperature transmission-SAXS data for [**Si$_7$-M$_{66}$-Si$_7$**] (**A**), [**M$_{33}$-Si$_{16}$-M$_{33}$**] (**B**), and [**M$_{22}$-Si$_{16}$-M$_{44}$**] (**C**). The data are shifted vertically for clarity. Lowest and highest temperature data are plotted in blue and red, respectively. A selection of (higher-order) Bragg reflections of the crystalline phase below the OOT is indicated is indicated as q/q^* values (in black). Reflections for a second lamellar packing in BCO [**M$_{33}$-Si$_{16}$-M$_{33}$**] are provided in gray. The blue and red, vertical, dashed lines follow the most intense alkane reflection in the WAXS region.

led to a slight increase of q^* and the appearance of a shoulder to the right side of the principal scattering peak when the temperature approached T_m. However, we assume that the system remained microphase-segregated in a lamellar morphology of which the domain spacing never became smaller than 11.2 nm. Also, no abrupt peak shift or appearance of new reflections was found in the WAXS regime. Thus, we expect little changes in the molecular arrangement of the alkane fragments in the *o*M block. As was the case for BCO [**Si$_7$-M$_{66}$-Si$_7$**], this matches with the very low and broad 'OOT' that was observed with DSC. Above 52 °C, all scattering reflections were lost, and the material became disordered.

5.4 Identification of the molecular organization

In the previous sections, we described the observed BCOs microphase separation on a mesoscopic level in which we identified the type of the microstructure as well as the location of the thermal transitions. Based on these observations and additional estimations using physical properties of the individual BCO components, we here rationalize the molecular organization within the individual domains of the microphase-segregated BCOs. For this, we first elucidate the location and orientation of individual molecules within the microphase-segregated domains of the di-BCOs (Section 5.4.1). In Section 5.4.2 we then correlate the effect of molecular architecture (*i.e.*, the differences between di- and tri-BCOs) to the self-assembly characteristics.

5.4.1 Molecular organization in di-BCOs

Pure tritriacontane ($C_{33}H_{68}$) crystallizes into a lamellar structure, with a lamellar domain spacing of 4.4 nm (see Table 5–1, entry 9 and literature values).[31] Based on the WAXS reflections, we concluded that the individual lamellae consist of alkane molecules packed in an orthorhombic sub-unit cell with cell dimensions: a = 7.42 Å, b = 4.95 Å, and c = 2.55 Å. This sub-unit cell is often observed for alkanes, and effectively holds two methylene residues of two *o*M chains (4 methylene residues in total). The molecular long-axis of the *o*M chains is aligned parallel to the c-axis of this elementary cell.[22] Since the length of the c-axis equals the length of two methylene residues of the alkane backbone, we can estimate a total length of 33 / 2 × 0.255 nm = 4.2 nm for the molecular long-axis of tritriacontane. This value corresponds very well to the lamellar domain spacing that we observed with SAXS, and confirms the presence of alkane molecules in an all-trans conformation, oriented (nearly) perpendicular to the lamellar domains. The lamellar organization of the alkane chains in tritriacontane is pictured schematically in Figure 5–6A. Because of the projection on a 2-D plane, we removed all details concerning the orthorhombic alkane packing.

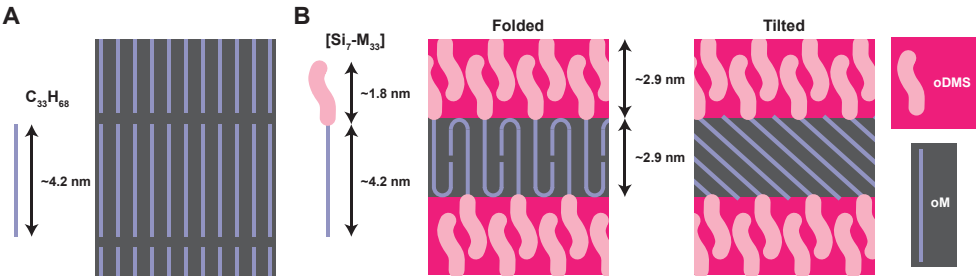

Figure 5–6. Schematic 2-D projections of: (**A**) Lamellar organization of tritriacontane crystals; (**B**) Envisioned molecular packing modes for BCO [**Si_7-M_{33}**] that comply with the measured lamellar domain spacings at room temperature. Gray = *o*M, pink = *o*DMS.

All di-BCOs are microphase-segregated into a lamellar structure below the order–order transition temperature (T_{OOT}). The tendency to form a lamellar organization regardless of the *o*M volume fraction is linked to the propensity of the *o*M chains to crystallize. Indeed, WAXS measurements indicated alkane packing in the same orthorhombic sub-unit cell as was found for the pure alkane.

BCO [**Si_7-M_{33}**], with nearly symmetric composition (f_M = 0.51), showed a full lamellar domain spacing d_{LAM} = 5.8 nm (Table 5–1, entry 1). Here, we assume that the alternating lamellar domains consist of 100% *o*DMS and 100% crystalline *o*M, respectively. When considering the dimensions of the individual blocks, we calculated a maximum molecular length of 1.8 nm for the Si_7 block based on the fully extended conformation of the molecular structure. Additionally, the *o*M chain has an extended chain length of 4.2 nm, equal to that of the pure alkane (see Figure 5–6B). Although these values approximately add up to the measured total domain spacing of 5.8 nm, the similar volume fractions of the two blocks dictate that the thicknesses of the individual *o*DMS and *o*M domains both should be around $\frac{1}{2}d_{LAM}$ = 2.9 nm. As a result, the alkane block cannot adopt a fully stretched conformation perpendicular to the *o*DMS–*o*M interface. Rather, the *o*M long-axis has to either fold once[44] or tilt with respect to the normal of the interdomain planes,[39] as shown in Figure 5–6B. In the first case, the methyl endgroups of the *o*M block will be positioned in the middle of the lamellar domain. In the tilted configuration the alkane chains are probably interdigitated, so that each methyl endgroup will be located close to the *o*DMS domain that does not contain the *o*DMS fragment that is part of the same molecule. In both cases, the *o*DMS domain consists of nearly stretched *o*DMS chains. Important to recognize is that the molecular length of the *o*DMS chains is significantly shorter than the thickness of the *o*DMS lamellae. Consequently, the chain-ends of the siloxane block will reside predominantly in the middle

of the *o*DMS domain (*i.e.*, a siloxane chain cannot 'bridge' between two consecutive *o*M lamellae).

With the (scattering) data that are currently available, it is not possible to discriminate between the folded or tilted packing modes. Typically, the folding of normal alkanes is not observed for chains shorter than 150 methylene residues,[45] suggesting that the much shorter *o*M chains of the BCO should adopt the unfolded, tilted organization. However, we already showed that covalently attached *o*DMS blocks have a considerable effect on packing mode of crystalline *i*-*o*LA. Therefore, we deliberately choose to display both orientations here and in the remainder of this discussion.

Assuming that the *o*M chains adopt either a folded or tilted structure, this also compensates for the larger diameter of the *o*DMS chain compared to *o*M: the *o*DMS block occupies more space perpendicular to the molecular long-axis than the *o*M block. In other words, *o*DMS is a 'thick' chain, and *o*M a 'thin' chain. This follows from their respective molecular structures, in which the $(-O-Si-)_x$ backbone is surrounded by relatively bulky methyl groups, whereas the all-carbon backbone in *o*M only has directly bound hydrogen atoms. Consequently, the density of chains protruding the *o*DMS–*o*M domain boundary is limited by the diameter of the *o*DMS chain. Nevertheless, the density of *o*M chains perpendicular to its molecular long-axis remains fixed because of the crystalline nature of this block, and exceeds the limit set by the bulky *o*DMS chains. To reduce the number of methylene groups at the domain boundary that are directly attached to an *o*DMS block—and hence the *o*DMS density—to acceptable values, the alkane either has to fold or tilt, as pictured in Figure 5–6B. In the 2-D representation of the molecular orientation, an induced fold results in three neighboring, parallel oriented alkane chain fragments for each *o*DMS–*o*M transition at both sides of the *o*M domain, whereas tilting (and interdigitation) gives two neighboring alkane chain fragments for each connected *o*DMS block.[vi]

A similar molecular ordering is expected for the compositionally asymmetrical ($f_M \neq 0.5$) BCOs [$\mathbf{Si_{11}}$-$\mathbf{M_{33}}$] and [$\mathbf{Si_{15}}$-$\mathbf{M_{33}}$]. Because of the unequal block volumes, the lamellar *o*DMS domain will be thicker than that in [$\mathbf{Si_7}$-$\mathbf{M_{33}}$]. If we calculate the thickness of the *o*M domain for [$\mathbf{Si_{11}}$-$\mathbf{M_{33}}$] and [$\mathbf{Si_{15}}$-$\mathbf{M_{33}}$] by multiplying the *o*M volume fraction with d_{LAM}, a value of 2.7 nm is found in both cases. Although these values are slightly smaller than the estimated *o*M lamellar thickness of 2.9 nm in [$\mathbf{Si_7}$-$\mathbf{M_{33}}$], we assume that the molecular organization depicted

[vi] The tilt induces a larger spacing between the alkane chains at the domain interface, hence the number of required neighboring alkane fragments for each interfacial connection with an *o*DMS chain is reduced.

in Figure 5–6B still holds.[vii] Finally, [**Si$_{15}$-M$_{69}$**] (d_{LAM} = 11.2 nm) and [**Si$_{23}$-M$_{69}$**] (d_{LAM} = 12.5 nm)—synthetically the closest accessible BCOs that were twice the size of [**Si$_7$-M$_{33}$**] and [**Si$_{11}$-M$_{33}$**]—give structures that are by approximation two times the size of the low-MW analogues. To summarize, *o*DMS–*o*M diblock BCOs adopt lamellar microphase-segregated structures below T_{OOT}, in which the alkane chains adopt either a tilted or folded orientation.

Above T_{OOT}, all three di-BCOs reveal a transformation in the crystal structure of the *o*M block. In BCOs [**Si$_7$-M$_{33}$**] and [**Si$_{11}$-M$_{33}$**], this results in a new scattering peak in the WAXS regions of the scattering profiles. In [**Si$_{15}$-M$_{33}$**], only a disappearance of the original scattering reflections is observed. Simultaneously, a small, discontinuous decrease in the lamellar thickness of [**Si$_7$-M$_{33}$**] was found, whereas both [**Si$_{11}$-M$_{33}$**] and [**Si$_{15}$-M$_{33}$**] transformed into a hexagonally packed assembly of 'cylindrical' structures. As already mentioned in the previous section, we propose that the observed changes in the *o*M crystal structure reduces the net strength of the van der Waals interactions that act between the *o*M blocks. Since the *o*DMS chains are conformationally completely locked in the lamellar structure, it is reasonable that a change in the BCO morphology that reduces the very high entropic strain occurs at higher temperatures in the di-BCOs with the longer *o*DMS blocks. Nonetheless, the *o*M domains remain highly crystalline, evidenced by the high ΔH_{fus}. Consequently, we picture that during the OOT, the *o*M lamellae will fragment into long, pseudo-1-D assemblies with a small, rectangular- or rhomboid-shaped cross section, which form a hexagonally packed array in a continuous *o*DMS matrix.

5.4.2 Architectural dependence in BCO self-assembly

In this section we compare the different types of BCO architectures (di-BCO and tri-BCO) with one another. Like the di-BCOs, all tri-BCOs formed lamellar structures around room temperature. However, we found an intriguing dependency of the lamellar domain spacing not only on the length of the crystalline *o*M fragments but also on the BCO architecture (AB-, ABA-, BAB- or B_1AB_2-type). For example, domain spacings varied by a factor of two for BCOs with (nearly) equal *o*M block length and f_M (*viz.* [**Si$_{15}$-M$_{69}$**] and [**Si$_7$-M$_{66}$-Si$_7$**]). On the other hand, similar domain spacings were found for BCOs with that differed significantly in MW ([**Si$_7$-M$_{33}$**] and [**M$_{33}$-Si$_{16}$-M$_{33}$**]). In this section, we try to include the effect of BCO architecture in the molecular organization model.

[vii] The calculated value of 2.7 or 2.9 nm greatly depends on a large number of assumptions, and likely has a maximum accuracy of ±0.1 nm.

First, BCOs [**Si$_7$-M$_{33}$**], [**Si$_{15}$-M$_{69}$**] and [**Si$_7$-M$_{66}$-Si$_7$**] are compared. Structurally, these molecules are related to each other in the triangular fashion that is depicted in Figure 5–7A. Starting from [**Si$_7$-M$_{33}$**], BCO [**Si$_{15}$-M$_{69}$**] can be seen as the approximate result of doubling the number of repeat units of both blocks. Next, [**Si$_7$-M$_{66}$-Si$_7$**] is obtained if half of the siloxane block in [**Si$_{15}$-M$_{69}$**] is transferred to the opposite side of the *o*M chain. Alternatively, dimerization of [**Si$_7$-M$_{33}$**] by connecting the methyl endgroups also gives [**Si$_7$-M$_{66}$-Si$_7$**].[viii] In terms of self-assembly, all three BCOs form a lamellar structure. BCOs [**Si$_7$-M$_{33}$**] and [**Si$_7$-M$_{66}$-Si$_7$**] have nearly the same domain spacing ($d_{LAM} \approx 5.8$ nm), whereas a larger domain spacing ($d_{LAM} = 11.2$) is found for BCO [**Si$_{15}$-M$_{69}$**].

If we apply the argumentation from Section 5.4.1 to elucidate the molecular organization in BCO [**Si$_{15}$-M$_{69}$**], it follows that a similar alkane organization is expected as for [**Si$_7$-M$_{33}$**]: folded or tilted. The size of both blocks in [**Si$_{15}$-M$_{69}$**] is twice that of those in [**Si$_7$-M$_{33}$**]. Consequently, the lamellar thicknesses of both blocks are multiplied by a factor of two. This is indeed corroborated by the SAXS measurements and schematically shown in the two cartoons to the left of the arrows in Figure 5–7B and C. Essentially, the density of chains protruding the *o*DMS–*o*M domain boundary in these cartoons is equal to that in [**Si$_7$-M$_{33}$**]. Again, three neighboring, parallel oriented alkane chain fragments are present near the domain boundary for each *o*DMS–*o*M transition if the alkanes adopt a folded state. If tilted, two neighboring alkane chain fragments are present for each connected *o*DMS block.

Finding the molecular organization of tri-BCO [**Si$_7$-M$_{66}$-Si$_7$**] is not trivial. Nevertheless, we can start from the proposed models for di-BCO [**Si$_{15}$-M$_{69}$**] and apply the partial displacement of the siloxane block as shown in Figure 5–7A. However, this leads to packing problems for both the folded or tilted molecular organization, as depicted in Figure 5–7B and C. In the folded structure (Figure 5–7B), the methyl endgroup of [**Si$_{15}$-M$_{69}$**]—to which half of the siloxane block will hypothetically be transferred—is located in the middle of the very densely packed alkane domain. Obviously, it is impossible for the siloxane block to be present at that location. Alternatively, if the *o*M chains are tilted (Figure 5–7C), a too high density of *o*DMS is obtained close to the domain boundary after translocation of the *o*DMS block. Besides, the density of *o*DMS residues in the middle of the *o*DMS domain will practically be zero because of the limited siloxane block length of approximately 1.8 nm. As such, the sketched molecular packing is very unlikely to exist.

[viii] These are all fictive transformations and not practically feasible.

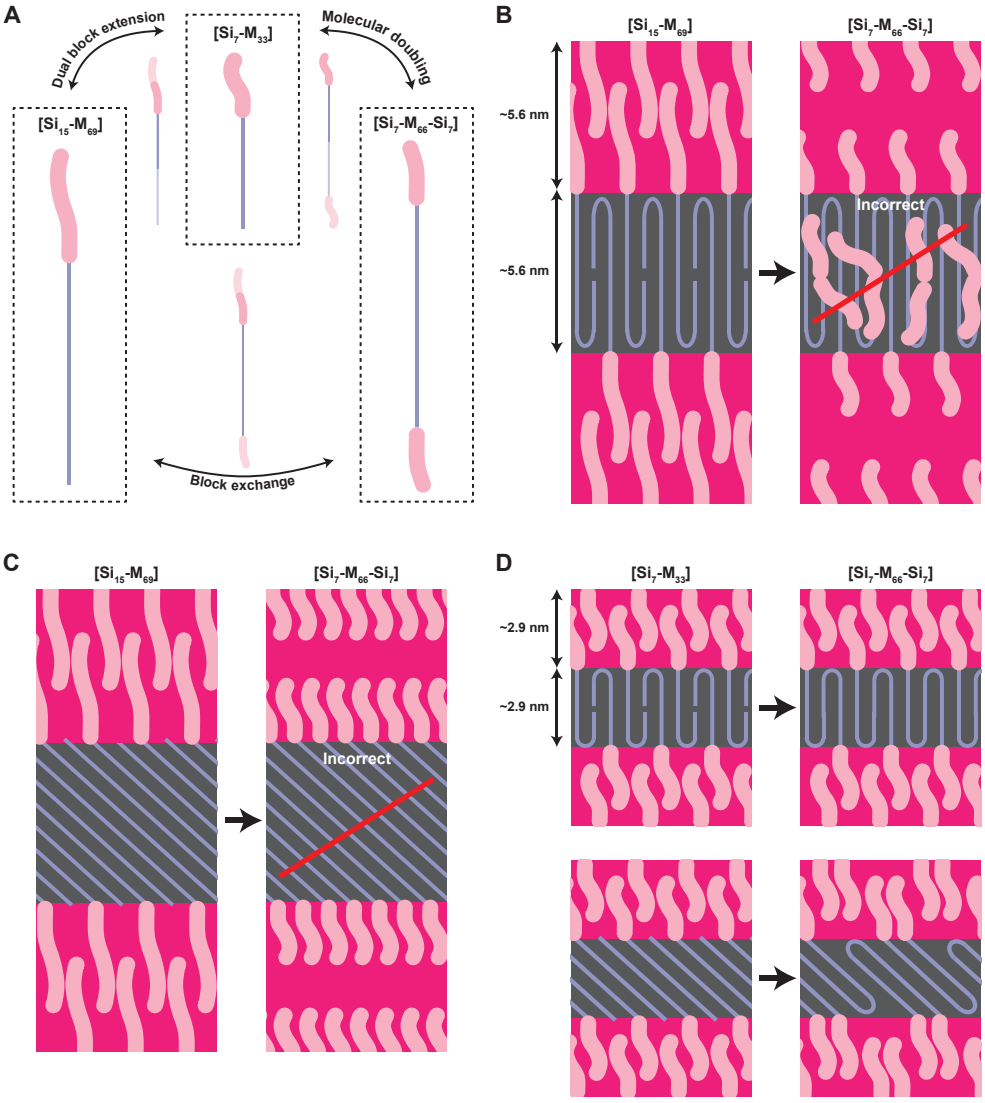

Figure 5–7. (**A**) Structural differences between [**Si**$_7$-**M**$_{33}$], [**Si**$_{15}$-**M**$_{69}$] and [**Si**$_7$-**M**$_{66}$-**Si**$_7$]; (**B–D**) Schematic 2-D projections of: (**B**) Lamellar organization of [**Si**$_{15}$-**M**$_{69}$] with folded *o*M chains and improbable packing of [**Si**$_7$-**M**$_{66}$-**Si**$_7$] after partial *o*DMS displacement; (**C**) Lamellar organization of [**Si**$_{15}$-**M**$_{69}$] with tilted *o*M chains and improbable packing of [**Si**$_7$-**M**$_{66}$-**Si**$_7$] after partial *o*DMS displacement; (**D**) Envisioned molecular packing modes for BCO [**Si**$_7$-**M**$_{33}$] and [**Si**$_7$-**M**$_{66}$-**Si**$_7$] in folded and tilted orientation. Gray = *o*M, pink = *o*DMS.

A more probable organization is shown in Figure 5–7D. Starting from the folded structure of di-BCO [**Si$_7$-M$_{33}$**], tri-BCO [**Si$_7$-M$_{66}$-Si$_7$**] is obtained by covalent linking of two methyl endgroups. The result is a twice folded *o*M chain with *o*DMS fragments connected at both sides of the *o*M block. No further molecular reorganization is required in this simplified cartoon, and the *o*DMS density close to the interlamellar domain remains unchanged. In a second possible structure, the long *o*M chain of [**Si$_7$-M$_{66}$-Si$_7$**] is folded once, and located in the *o*M blocks in a tilted configuration. Consequently, both *o*DMS fragments of each BCO molecule reside in the same *o*DMS domain. Although the distribution of *o*DMS–*o*M links looks more distorted in the 2-D image, no change of the *o*DMS density near the domain interface is required, and, more importantly, a more uniform arrangement of links in possible in three dimensions.[ix] Indeed, the proposed organization is in full agreement with the matching domain spacings of di-BCO [**Si$_7$-M$_{33}$**] and tri-BCO [**Si$_7$-M$_{66}$-Si$_7$**].

For the remaining tri-BCOs, [**M$_{33}$-Si$_{16}$-M$_{33}$**] and [**M$_{22}$-Si$_{16}$-M$_{44}$**], the molecular organization is less clear. The domain spacing of [**M$_{33}$-Si$_{16}$-M$_{33}$**] (d_{LAM} = 5.9 nm) is practically equal to that of [**Si$_7$-M$_{33}$**] (d_{LAM} = 5.8 nm). Hence, optional packing modes are similar to that of [**Si$_7$-M$_{33}$**], the only difference being that the siloxane endgroups of two [**Si$_7$-M$_{33}$**] molecules are covalently bound to form the tri-BCO (see Figure 5–8A).[x] However, this does not directly

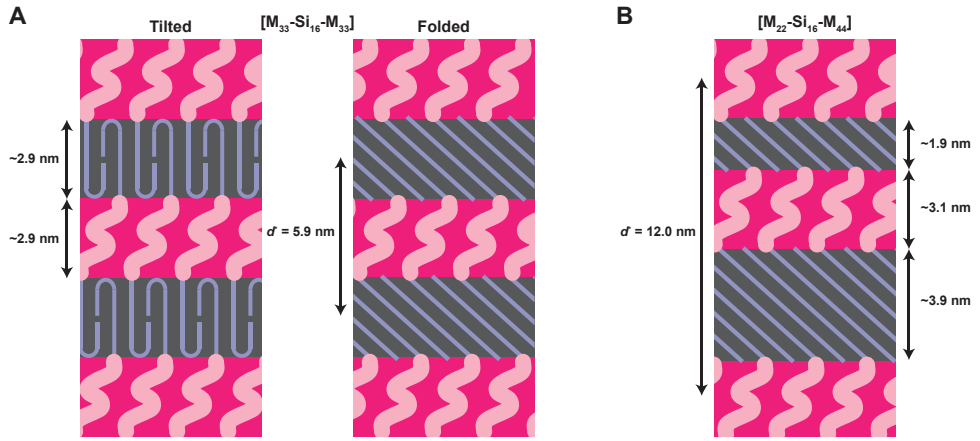

Figure 5–8 (**A**) Schematic 2-D projections of: (**A**) Lamellar organization of [**M$_{33}$-Si$_{16}$-M$_{33}$**] with folded or tilted *o*M chains; (**B**) Lamellar organization of [**M$_{22}$-Si$_{16}$-M$_{44}$**] with tilted *o*M chains. For both BCOs, the domain spacings and estimated block thicknesses are indicated. Gray = *o*M, pink = *o*DMS.

[ix] Also a non-folded structure is theoretically possible (not shown). Here, the tilt angle of the alkane chains with respect to the normal of the interdomain planes is even larger.

[x] Also, the siloxane can fold back. As a result, both M$_{33}$ blocks of one BCO molecule will reside in the same *o*M domain. No significant changes in domain spacing are expected for this alternative packing.

explain the second set of lamellar reflections observed during the SAXS measurements below T_{OOT}. The appearance of these scattering reflections seems related to the simultaneously observed change in in the alkane packing (evidenced by repositioning of the alkane reflection in the WAXS region). Consequently, we assume that the additional reflections are not caused by a co-existing, second lamellar phase, but the result of a change in the unit cell dimensions (or even space group). Apparently, this does not affect the primary lamellar spacing (d^*), but might change the overall symmetry of the system, allowing the second set of peaks to appear. Still, additional measurements are required to exactly determine the corresponding unit cell.

[$\mathbf{M_{22}}$-$\mathbf{Si_{16}}$-$\mathbf{M_{44}}$] formed lamellae with a total domain spacing of 12.0 nm. For this material, we initially envisioned that the two *o*M chains either can co-crystallize or self-sort. The first option would result in a simple alternation of *o*DMS and *o*M lamellae (similar to those in [$\mathbf{M_{33}}$-$\mathbf{Si_{16}}$-$\mathbf{M_{33}}$]), of which the latter contained both M_{22} and M_{44} chains. However, a calculation shows that the measured domain spacing of 12 nm is too large for a simple structure of alternating lamellae. Since the methylene volume fraction of this material is 0.48, a thickness for the *o*DMS domain of 6.2 nm can be calculated. However, the stretched chain length of Si_{16} is only 4–4.5 nm at maximum, restricting the *o*DMS domain to form the required layer thickness. Therefore, we propose an alternative, more complicated repeating structure of alternating M_{22} and M_{44} domains, separated by Si_{16} regions (*e.g.*, –*o*DMS_{16}–*o*M_{22}–*o*DMS_{16}–*o*M_{44}–; see Figure 5–8B). Here, two separate *o*DMS domains are present within the repeating structure, each containing *o*DMS chains with 16 repeat units. Hence, the combined *o*DMS domain thickness of 6.2 nm is (probably) shared equally by both *o*DMS subdomains in the proposed organization. Equivalently, each *o*DMS lamella measures a thickness of only 3.1 nm. The orientation of the *o*M chains in the M_{22} and M_{44} domains can either be tilted or folded, in full analogy to the symmetrical tri-BCO [$\mathbf{M_{33}}$-$\mathbf{Si_{16}}$-$\mathbf{M_{33}}$] or di-BCO [$\mathbf{Si_7}$-$\mathbf{M_{33}}$] (in Figure 5–8B, only the tilted structure is shown). We also consider the possibility that only the longer M_{44} domain is crystalline. The low melting point of docosane (T_m = 43 °C), absence of a two crystallization transitions in the DSC, and relatively low ΔH_{fus} (108.0 kJ (mol BCO)$^{-1}$) makes it probable that the M_{22} block is amorphous (or even partially mixed with the *o*DMS domains). Nonetheless, this would not significantly change the domain spacing.

5.5 Conclusions

We explored the self-assembly behavior and impact of crystallinity in uniform block co-oligomers comprised of oligodimethylsiloxane and oligomethylene blocks. Oligomethylenes containing up to 69 backbone carbon atoms were prepared in an iterative manner, employing

the Wittig reaction as a key reaction step. As a result, most *o*M blocks contained one or multiple internal double bonds, which hindered crystallization and ensured good solubility of the materials during synthesis, purification and characterization of the intermediate compounds. Thus, all methylene blocks could be ligated with *o*DMS hydrides of different lengths, leading to novel di- and triblock copolymer architectures of predetermined MW and composition, which lacked any form of dispersity. The transformation from an oily liquid to a brittle, flaky solid after hydrogenation of the unsaturated *o*M blocks confirmed the presence of strong London dispersion forces between the *o*M chains. Nevertheless, clear solubility differences between the *o*DMS–*o*M BCOs and pure tritriacontane revealed a diminished *o*M crystal integrity if connected to *o*DMS.

X-ray scattering experiments at or slightly below room temperature showed that all *o*DMS–*o*M conjugates microphase separated into lamellar structures, consisting of amorphous *o*DMS and crystalline *o*M domains. Exceptionally uniform microphase-segregated domains were found, as well as one of the smallest domain spacings ever reported (d_{LAM} = 5.8 nm). Overall, the combination of small features sizes and structural perfection is unique for this type of oligomeric/polymeric systems.

Upon heating, most BCOs showed a slight change in the *o*M crystal structure, followed by a melting transition. These transitions were captured by DSC, confirming the high crystallinity of the *o*M block. Above T_m, all BCOs directly transitioned into a disordered melt, in contrast to most of the *o*DMS–*o*LLA and *o*DMS–*o*DLA BCOs that were studied in the previous chapter. Accordingly, we conclude that the microphase separation process in these low-MW BCOs is initially driven by the crystallization of the alkanes. Although short- to intermediate-length alkanes typically give a lamellar type organization, also hexagonally packed, cylinder-like *o*M aggregates were found for compositionally asymmetric BCOs [$\mathbf{Si_{11}}$-$\mathbf{M_{33}}$] and [$\mathbf{Si_{15}}$-$\mathbf{M_{33}}$] in a temperature window below T_m. This indicated that the crystalline interactions within the *o*M domain were insufficiently strong at those temperatures to disrupt the (mainly) entropy driven formation of a non-lamellar structure in these systems.

By studying both di- and triblock configurations, we were able to link the observed domain sizes with molecular organization within the blocks. The discrete nature of the molecules allows to propose the organization of chains at molecular resolution, highlighting the balance between block volumes, block length and the density of interblock links at the domain boundary.

5.6 Experimental

5.6.1 Materials and methods

All chemicals were purchased from commercial sources and used without further purification. The syntheses of discrete-length Me-Si_7-H **14a**, Me-Si_{11}-H **14b**, Me-Si_{15}-H **14c**, Me-Si_{23}-H **14e**, H-Si_{16}-H **18g**, HO-Si_8-OH **17g**, and chlorosilane **11** are described in Chapter 2. Dry solvents were obtained with an MBRAUN Solvent Purification System (MB-SPS). Toluene was dried over 4Å molecular sieves before use. Oven-dried glassware (120 °C) was used for all reactions carried out under argon atmosphere. Reactions were followed by thin-layer chromatography (TLC) using 60-F254 silica gel plates from Merck and visualized by UV light at 254 nm and/or cerium molybdate (CeMo) staining. Automated column chromatography was conducted on a Grace Reveleris X2 Flash Chromatography System using Reveleris Silica Flash Cartridges. Elution gradients are specified in column volumes (CVs).

NMR spectra were recorded on Varian Mercury Vx 400 MHz, Varian 400MR 400 MHz, Bruker 400 MHz Ultrashield (400 MHz for ^{1}H NMR), and/or Varian Inova 500 MHz (500 MHz for ^{1}H NMR) spectrometers. Deuterated solvents used are indicated in each case. Chemical shifts (δ) are expressed in ppm and are referred to the residual peak of the solvent. Peak multiplicity is abbreviated as s: singlet; d: doublet; t: triplet; dt: doublet of triplets; ddt: doublet of doublets of triplets; td: triplet of doublets; tt: triplet of triplets; q: quartet; ABq: AB quartet; dq: doublet of quartets; qd: quartet of doublets; sept: septet; m: multiplet; bs: broad singlet. **Matrix assisted laser desorption/ionization time-of-flight** (MALDI-TOF) mass spectra were obtained on a PerSeptive Biosystems Voyager DE-PRO spectrometer using α-cyano-4-hydroxycinnamic acid (CHCA) or *trans*-2-[3-(4-*tert*-butylphenyl)-2-methyl-2-propenylidene]-malononitrile (DCTB) as matrix. **Gas chromatography-mass spectrometry** (GC-MS) measurements were conducted on a Shimadzu GC-17A gas chromatograph with a Shimadzu AOC-20i auto injector, Shimadzu GCMS-QP5000 gas chromatograph mass spectrometer and Phenomenex Zebron ZB-35 column (l = 30 meters, ID = 0.25 mm, film thickness = 0.25 μm). **Size exclusion chromatography** (SEC) measurements were conducted on a Shimadzu Prominence-i LC-2030C 3D with a Shimadzu RID-20A Refractive index detector, using an eluent flow of 1 mL min^{-1} (THF or $CHCl_3$). The molecular weight is determined based on narrow dispersity polystyrene standards purchased from Polymer Source Inc. **Differential scanning calorimetry** (DSC) data were collected on a DSC Q2000 from TA instruments, calibrated with an indium standard. The samples (4–8 mg) were weighed directly into aluminum pans and hermetically sealed. The samples were initially heated to 180 °C and then subjected to two cooling/heating cycles, typically from −50 °C to 180 °C with a rate of 10 °C min^{-1}. The data that are presented, represent the second heating/cooling cycle unless stated otherwise. Bulk **small-angle X-ray scattering** (SAXS) was performed on an instrument from Ganesha Lab. The flight tube and sample holder are all under vacuum in a single housing, with a GeniX-Cu ultra-low divergence X-ray generator. The source produces X-rays with a wavelength (λ) of 0.154 nm and a flux of 1×10^8 ph s^{-1}. Samples were stuck to Kapton tape, or put inside 1 mm diameter glass capillaries and annealed by heating above the (expected) melting point and slow (0.5 °C min^{-1}) cooling to room temperature. For room temperature measurements, the samples were positioned directly in the beamline. Variable temperature measurements (VT-SAXS) were performed using a Linkam heating stage. Samples were equilibrated at each temperature for 5 minutes prior to measuring and a heating/cooling rate of 5 °C min^{-1} was used in between the measurements. Scattered X-rays were captured on a 2-dimensional Pilatus 300K detector with 487 × 619 pixel resolution. Samples were measured in MAXS mode for 1200 seconds and WAXS mode for 300 seconds. The sample-to-detector distance was 0.084 m (WAXS mode) or 0.431 m (MAXS mode). The instrument was calibrated with diffraction patterns from silver behenate. The raw data files were calibrated and reduced to 1-D data with the SAXSGui software provided by JJ X-

Ray Systems ApS. MAXS and WAXS regions were merged into a single data file using the SAXSutilities software package provided by Michael Sztucki.

5.6.2 Synthetic procedures

*General method **A** for Wittig reaction between aldehyde and phosphonium salt*.

Phosphonium salt (*e.g.*, compound **67**, 1.03 mmol, 1.1 eq) was dissolved in dry THF (5 mL) in a 25 mL two-necked round-bottom flask under argon, and the mixture was cooled in ice water. KO*t*Bu (1 M in THF, 1.08 mmol, 1.15 eq) was added dropwise, resulting in a color change from light yellow to bright yellow, dark orange, red, or brown. After stirring for 15 minutes, a solution of aldehyde (*e.g.*, **46**, 0.936 mmol, 1 eq) in THF (5 mL) was added. Within 5 minutes, a white precipitate formed and the color changed to light orange or light brown. Stirring was continued for 10 minutes at 0 °C and then for 2–24 hours at room temperature. A typical work-up procedure involved concentrating the reaction mixture in *vacuo*, followed by suspending the remaining dark colored oil in heptane (15 mL). The suspension was then filtered through Celite, the residue was washed with heptane (3 × 10 mL), and the combined filtrates were concentrated in *vacuo*. This gave the crude product as a light brown oil.

*General method **B** for the Karstedt reaction between siloxane hydrides and terminal alkenes.*

Terminal alkene (*e.g.*, alkene **69**, 0.184 mmol, 1 eq) and Si_x hydride (*e.g.*, **14**, 0.184 mmol, 1 eq) were dissolved in dry DCM (1 mL) in a 10 mL Schlenk tube under argon atmosphere. Karstedt catalyst (1% Pt solution in xylenes, 1 drop) was added, and the mixture stirred for 30–60 min at room temperature. TLC (CeMo staining) and ^{1}H NMR were used to check for completion of the reaction. Then, the reaction mixture was concentrated in *vacuo*, giving the crude product.

*General method **C** for the synthesis of saturated BCOs* [$\mathbf{Si_x}$-$\mathbf{M_z}$].

Unsaturated BCO (*e.g.*, BCO **73a**, 0.089 mmol, 1 eq) was dissolved in EtOAc (4 mL) in a 50 mL round-bottom flask. Pd/C (10 w% Pd, 8.9 µmol Pd, 0.1 eq) was added and the flask was purged with hydrogen and stirred at room temperature or elevated temperatures (reactions at elevated temperatures were conducted with a reflux set-up). After 3 hours, the mixture was filtered through Celite, and the residue rinsed with EtOAc (3 × 5 mL). The combined filtrates were concentrated in *vacuo*, giving the pure product.

Synthesis of 11-bromo-1-undecanal (**39**).

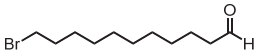

A solution of 11-bromoundecanol **38** (8.00 g, 31.8 mmol, 1 eq), TEMPO (530 mg, 3.39 mmol, 0.11 eq), and tetrabutylammonium chloride (TBAC, 750 mg, 2.70 mmol, 0.08 eq) in DCM (200 mL) was stirred in a 1 L round-bottom flask under argon. A solution of $NaHCO_3$ (13.37 g, 0.159 mol, 5 eq) and K_2CO_3 (2.23 g, 16.1 mmol, 0.5 eq) in water (300 mL) was added, and the biphasic mixture was vigorously stirred at room temperature. *N*-Chlorosuccinimide (6.0 g, 44.9 mmol, 1.4 eq) was added to the emulsion as a solid, and the mixture was stirred 24 hours at room temperature. Afterward, the mixture was transferred to a separatory funnel and washed with water (2 × 200 mL) and brine (200 mL). The orange colored organic layer was dried with $MgSO_4$, and the solvent was removed in *vacuo*. The remaining crude product (dark orange liquid; 8.15 g) was purified by automated column chromatography using heptane/chloroform (gradient 100/0 to 40/60) as eluent. The pure material was obtained as a white solid (6.75 g, 85 %). ^{1}H NMR (400 MHz, $CDCl_3$): δ = 9.76 (t, ^3J = 1.9 Hz, 1H, CH_2-C<u>H</u>O), 3.41 (t, ^3J = 6.8 Hz, 2H, Br-C<u>H</u>$_2$-CH_2), 2.42 (td, ^3J = 7.4 Hz, ^3J = 1.9 Hz, 2H, CH_2-C<u>H</u>$_2$-CHO), 1.85 (tt, ^3J = 7.4 Hz, ^3J = 6.9 Hz, 2H, CH_2-C<u>H</u>$_2$-CH_2-Br), 1.67–1.58 (m, 2H, CH_2-C<u>H</u>$_2$-CH_2-CHO), 1.46–1.38 (m, 2H, C<u>H</u>$_2$), 1.36–1.25 ppm (m, 10H, C<u>H</u>$_2$); ^{13}C NMR (100 MHz, $CDCl_3$): δ = 202.99, 44.04, 34.14, 32.95, 29.47, 29.42, 29.27, 28.85, 28.28, 22.20 ppm.

Synthesis of 11-bromo-1,1-dimethoxyundecane (**40**).

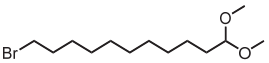

To a well stirred solution of bromoaldehyde **39** (15.91 g, 63.8 mmol, 1 eq) in methanol (100 mL). *p*-Toluene sulfonic acid monohydrate (TsOH·H_2O, 80 mg, 0.42 mmol, 0.007 eq) and trimethyl orthoformate (4.85 g, 5.0 ml, 45.7 mmol, 0.72 eq) were added. The mixture was stirred for 6 hours at room temperature, followed by the addition of NaOH solution (1 M, 100 mL) (the mixture heated up slightly). After stirring for an additional 30 minutes at room temperature, the contents were transferred to a separatory funnel and extracted with toluene (2 × 200 mL). The combined toluene fractions were concentrated in *vacuo*. Remaining water was removed by co-evaporation with toluene (100 mL), giving the pure product as a white solid (16.0 g, 85%). ^{1}H NMR (400 MHz, $CDCl_3$): δ = 4.36 (t, ^3J = 5.8 Hz, 1H, CH_2-C<u>H</u>(OCH_3)$_2$), 3.40 (t, ^3J = 6.9 Hz, 2H, Br-C<u>H</u>$_2$-CH_2), 3.31 (s, 6H, CH_2-CH(OC<u>H</u>$_3$)$_2$), 1.85 (tt, ^3J = 7.1 Hz, ^3J = 7.1 Hz, 2H, CH_2-C<u>H</u>$_2$-CH_2-Br), 1.59 (td, ^3J = 7.6 Hz, ^3J = 5.8 Hz, 2H, CH_2-C<u>H</u>$_2$-CH(OCH_3)$_2$), 1.46–1.37 (m, 2H, C<u>H</u>$_2$), 1.37–1.23 ppm (m, 12H, C<u>H</u>$_2$); ^{13}C NMR (100 MHz, $CDCl_3$): δ = 104.70, 52.73, 34.18, 32.98, 32.64, 29.64, 29.59, 29.56, 29.54, 28.89, 28.31, 24.73 ppm.

Synthesis of 2-(10-bromodecyl)-1,3-dioxolane (**41**).

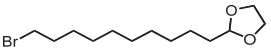

A mixture of bromo dimethyl acetal **40** (15.9 g, 53.9 mmol, 1 eq), ethylene glycol (6.68 g, 6.0 ml, 108 mmol, 2 eq), *p*-toluene sulfonic acid monohydrate (TsOH·H_2O, 160 mg, 0.84 mmol, 0.016 eq), and toluene (50 mL) was heated to 95 °C in a 250 mL round-bottom flask. The flask was continuously purged with nitrogen gas to remove the methanol that was liberated during the reaction. After 3.5 hours, total conversion to the ethylene acetal was confirmed by ^{1}H NMR of a basified sample. The mixture was cooled down to room temperature, transferred to a beaker with K_2CO_3 solution (10 w%, 100 mL) and stirred for 15 minutes. The contents of the beaker were then transferred to a separatory funnel and extracted with toluene (100 mL). The organic layer was washed with water (100 mL) and brine (200 mL). Removal of the solvent gave the title compound as a white solid (13.95 g, 88%). ^{1}H NMR (400 MHz, $CDCl_3$): δ = 4.84 (t, ^3J = 4.8 Hz, 1H, CH_2-C<u>H</u>(-O-CH_2-CH_2-O-)), 4.01–3.91 (m, 2H, CH_2-CH(-O-C<u>H</u>$_2$-C<u>H</u>$_2$-O-)), 3.89–3.80 (m, 2H, CH_2-CH(-O-C<u>H</u>$_2$-C<u>H</u>$_2$-O-)), 3.40 (t, ^3J = 6.9 Hz, 2H, CH_2-C<u>H</u>$_2$-Br), 1.91–1.80 (m, 2H, CH_2-C<u>H</u>$_2$-CH_2-Br), 1.69–1.61 (m, 2H, CH_2-C<u>H</u>$_2$-CH(-O-CH_2-CH_2-O-)), 1.48–1.24 ppm (m, 14H, C<u>H</u>$_2$); ^{13}C NMR (100 MHz, $CDCl_3$): δ = 104.84, 64.98, 34.19, 34.06, 32.99, 29.66, 29.62, 29.53, 28.89, 28.32, 24.22 ppm.

Synthesis of (10-(1,3-dioxolan-2-yl)decyl)triphenylphosphonium bromide (**42**).

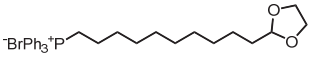

Bromo ethylene acetal **41** (13.85 g, 47.2 mmol, 1 eq) was co-evaporated with dry toluene (100 mL) to remove any residual water. Next, dry acetonitrile (20 mL), 2,2-dimethyl-1,3-dioxolane (2.78 g, 3.0 mL, 27.2 mmol, 0.58 eq) and triphenylphosphine (18.1 g, 69 mmol, 1.5 eq) were added. The mixture was stirred under reflux for 24 hours under argon. Next, the mixture was concentrated in *vacuo*. Ethyl acetate (300 mL) was added to the remaining viscous oil, and the mixture was stirred for 30 minutes. The solvent was then decanted, fresh ethyl acetate (200 mL was added), and the residue was again stirred for 30 minutes. Finally, the mixture was filtered over a Büchner filter and the residue washed with ethyl acetate (2 × 50 mL). The product was dried in vacuum at 40 °C, resulting in a white solid (20.84 g, 79%). ^{1}H NMR (400 MHz, $CDCl_3$): δ = 7.80–7.70 (m, 9H, Ar-<u>H</u>), 7.68–7.60 (m, 6H, Ar-<u>H</u>), 4.74 (t, ^3J = 4.8 Hz, 1H, CH_2-C<u>H</u>(-O-CH_2-CH_2-O-)), 3.93–3.71 (m, 4H, CH_2-CH(-O-C<u>H</u>$_2$-C<u>H</u>$_2$-O-)), 3.69–3.57 (m, 2H, CH_2-C<u>H</u>$_2$-P), 1.60–1.48 (m, 2H, CH_2-C<u>H</u>$_2$-CH(-O-CH_2-CH_2-O-)), 1.34–1.05 ppm (m, 16H, C<u>H</u>$_2$); ^{13}C NMR (100 MHz, $CDCl_3$): δ = 135.10, 135.07, 133.86, 133.76, 130.65, 130.52, 118.98, 118.13, 104.77, 64.92, 33.98, 30.58, 30.42,

29.80, 29.56, 29.51, 29.45, 29.30, 29.22, 24.15, 23.15, 22.79, 22.74, 22.66 ppm; ^{31}P NMR (162 MHz, $CDCl_3$): δ = 24.17 ppm; MS (MALDI-TOF): m/z calcd for $C_{31}H_{40}BrPO_2$–Br^-: 475.28 $[M-Br]^+$; found: 475.30.

Synthesis of 2-(21-bromohenicos-10-en-1-yl)-1,3-dioxolane (**43**).

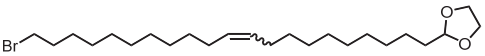

Phosphonium salt **42** (2.58 g, 4.6 mmol, 1.03 eq) and 11-bromoundecanal **39** (1.12 g, 4.5 mmol, 1 eq) were coupled using general method **A**. The crude product was obtained as a dark yellow oil and further purified by automated column chromatography using heptane/EtOAc (gradient 100/0 to 90/10) as eluent. The pure product was obtained as a colorless oil (1.18 g, 58%). ^{1}H NMR (400 MHz, $CDCl_3$): δ = 5.41–5.29 (m, 2H, CH_2-C<u>H</u>=C<u>H</u>-CH_2), 4.84 (t, ^3J = 4.9 Hz, 1H, CH_2-C<u>H</u>(-O-CH_2-CH_2-O-)), 4.02–3.91 (m, 2H, CH_2-CH(-O-C<u>H</u>$_2$-C<u>H</u>$_2$-O-)), 3.91–3.79 (m, 2H, CH_2-CH(-O-C<u>H</u>$_2$-C<u>H</u>$_2$-O-)), 3.40 (t, ^3J = 6.9 Hz, 2H, CH_2-C<u>H</u>$_2$-Br), 2.06–1.93 (m, 4H, C<u>H</u>$_2$-CH=CH-C<u>H</u>$_2$), 1.85 (tt, ^3J = 7.0 Hz, ^3J = 7.0 Hz, 2H, CH_2-C<u>H</u>$_2$-CH_2-Br), 1.70–1.61 (m, 2H, CH_2-C<u>H</u>$_2$-CH(-O-CH_2-CH_2-O-)), 1.47–1.21 ppm (m, 28H, C<u>H</u>$_2$); ^{13}C NMR (100 MHz, $CDCl_3$): δ = 130.52, 130.46, 130.06, 130.00, 104.86, 64.98, 34.19, 34.08, 33.00, 32.75, 29.92, 29.91, 29.71, 29.70, 29.68, 29.66, 29.65, 29.58, 29.45, 29.43, 29.30, 28.93, 28.34, 27.37, 27.35, 24.25 ppm.

Synthesis of (21-(1,3-dioxolan-2-yl)henicos-11-en-1-yl)triphenylphosphonium bromide (**44**).

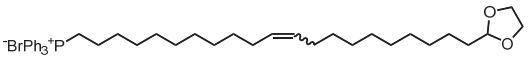

A mixture of bromoacetal **43** (7.0 g, 15.7 mmol, 1 eq), 2,2-dimethyl-1,3-dioxolane (1.39 g, 1.5 ml, 13.6 mmol, 0.87 eq), and triphenylphosphine (11 g, 41.9 mmol, 2.7 eq), and acetonitrile (12 mL) was stirred under reflux for 24 hours in a 100 mL round-bottom flask. Full conversion to the phosphonium salt was confirmed by ^{1}H NMR. The mixture was concentrated in *vacuo*, and the remaining crude product was dissolved in ethyl acetate (70 mL). The solution was added dropwise to well-stirred hexane (700 mL), resulting in precipitation of the product. The supernatant was decanted, and the remaining product was stirred with fresh hexane (250 mL) for 30 minutes. The mixture was filtered, and the residue was washed with hexane (3 × 50 mL). The remaining pure product (white solid) was dried in *vacuo* at 40 °C (8.85 g, 80%). ^{1}H NMR (400 MHz, $CDCl_3$): δ = 7.91–7.65 (m, 15H, Ar-<u>H</u>), 5.39–5.27 (m, 2H, CH_2-C<u>H</u>=C<u>H</u>-CH_2), 4.83 (t, ^3J = 4.8 Hz, 1H, CH_2-C<u>H</u>(-O-CH_2-CH_2-O-)), 3.99–3.79 (m, 6H, CH_2-CH(-O-C<u>H</u>$_2$-C<u>H</u>$_2$-O-) and CH_2-C<u>H</u>$_2$-P), 2.03–1.91 (m, 4H, C<u>H</u>$_2$-CH=CH-C<u>H</u>$_2$), 1.67–1.55 (m, 2H, CH_2-C<u>H</u>$_2$-CH(-O-CH_2-CH_2-O-)), 1.45–1.14 ppm (m, 30H, C<u>H</u>$_2$); ^{13}C NMR (100 MHz, $CDCl_3$): δ = 135.07, 135.04, 133.90, 133.80, 130.63, 130.51, 130.00, 129.97, 119.05, 118.20, 104.82, 64.95, 34.04, 30.62, 30.46, 29.89, 29.77, 29.68, 29.66, 29.64, 29.61, 29.41, 29.39, 29.31, 29.28, 27.34, 24.22, 23.16, 22.82, 22.78, 22.67 ppm; ^{31}P NMR (162 MHz, $CDCl_3$): δ = 24.56 ppm; MS (MALDI-TOF): m/z calcd for $C_{42}H_{60}BrO_2P$–Br^-: 627.43 $[M-Br]^+$; found: 627.49.

Synthesis of docosanal (M_{22} aldehyde) (**46**).

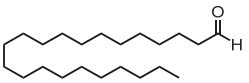

Alcohol **45** (20.5 g, 62.9 mmol, 1 eq), (2,2,6,6-tetramethylpiperidin-1-yl)oxyl (TEMPO, 0.98 g, 6.29 mmol, 0.1 eq), and tetrabutylammonium chloride (TBAC, 1.75 g, 6.29 mmol, 0.1 eq) were transferred to a 2 L round-bottom flask. DCM (300 mL) was added, and the resulting orange/pink suspension was stirred at room temperature (under argon atmosphere to prevent possible over-oxidation). A solution of $NaHCO_3$ (26.4 g, 314 mmol, 5 eq) and K_2CO_3 (4.35 g, 31.4 mmol, 0.5 eq) in water (350 mL, conc. ~1 M and ~0.1 M resp.) was added and the biphasic mixture stirred at high speed (~1000 rpm). *N*-Chlorosuccinimide (10.1 g, 75.5 mmol, 1.2 eq) was added as a solid and stirring of the suspension/emulsion was continued for 20 h at room temperature (most of the solids dissolved over time). Next, the mixture was transferred to a separation funnel, the organic layer was removed and the aq. layer extracted

with DCM (2 × 200 mL). The combined organic layers were washed with water (200 mL) and brine (100 mL), dried with $MgSO_4$ and concentrated in *vacuo*, resulting in a light yellow oil. The crude product was purified by automated column chromatography using heptane/DCM (isocratic 60/40) as eluent. Pure aldehyde **46** was obtained as a white solid (17.6 g, 86%). ^{1}H NMR (400 MHz, $CDCl_3$): δ = 9.76 (t, ^3J = 1.9 Hz, 1H, C<u>H</u>O), 2.41 (td, ^3J = 7.4 Hz, ^3J = 1.9 Hz, 2H, CHO-C<u>H</u>$_2$-CH$_2$), 1.63 (tt, ^3J = 6.6 Hz, ^3J = 6.6 Hz, 2H, CHO-CH$_2$-C<u>H</u>$_2$-CH$_2$), 1.36–1.20 (m, 36H, C<u>H</u>$_2$), 0.88 ppm (t, ^3J = 6.6 Hz, 3H, C<u>H</u>$_3$); ^{13}C NMR (100 MHz, $CDCl_3$): δ = 203.09, 44.08, 32.08, 29.86, 29.82, 29.80, 29.74, 29.59, 29.52, 29.33, 22.85, 22.25, 14.27 ppm; GC-MS (EI, oven 80–330 °C): t = 7.81 min.

Synthesis of 2-(dotriaconta-10,21-dien-1-yl)-1,3-dioxolane (M_{33} ethylene acetal) (**48**).

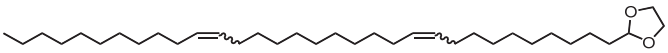

Phosphonium salt **44** (1.979 g, 2.796 mmol, 1.1 eq) was dissolved in dry THF (6 mL) in a 25 mL 2-necked round-bottom flask under argon, and the light yellow solution was cooled in ice water. The mixture was stirred, and KO*t*Bu (1M in THF, 3.050 mmol, 1.20 eq) was added dropwise, resulting in a dark orange-red solution. After 15 minutes, a solution of undecanal **47** (0.433 g, 2.542 mmol, 1 eq) in THF (0.5 mL) was added dropwise. The mixture changed color from red to light orange and a white precipitate was formed. The mixture was stirred for an additional hour at room temperature. ^{1}H NMR showed full consumption of the aldehyde. The reaction mixture was poured out in heptane (60 mL) and stirred for 1 hour. The white precipitate (PPh_3O) was filtered off over a Büchner funnel, and the residue was washed with additional heptane (30 mL). The slightly turbid, combined filtrates were washed with acetonitrile (50 mL), and the heptane layer was concentrated in *vacuo*. The crude product was purified by automated column chromatography using heptane/EtOAc (gradient 100/0 to 90/10) as eluent. Pure aldehyde acetal **48** was obtained as a colorless oil (1.065 g, 73%). ^{1}H NMR (400 MHz, $CDCl_3$): δ = 5.40–5.29 (m, 4H, CH$_2$-C<u>H</u>=C<u>H</u>-CH$_2$), 4.84 (t, ^3J = 4.8 Hz, 1H, C<u>H</u>(-OCH$_2$CH$_2$O-)), 4.01–3.79 (m, 4H, CH(-OC<u>H</u>$_2$C<u>H</u>$_2$O-)), 2.10–1.91 (m, 8H, C<u>H</u>$_2$-CH=CH-C<u>H</u>$_2$), 1.71–1.60 (m, 2H, C<u>H</u>$_2$-CH(-OCH$_2$CH$_2$O-)), 1.49–1.17 (m, 44H, C<u>H</u>$_2$), 0.88 ppm (t, ^3J = 6.8 Hz, 3H, C<u>H</u>$_3$); ^{13}C NMR (100 MHz, $CDCl_3$): δ = 130.49, 130.03, 104.86, 64.97, 34.09, 32.77, 32.08, 32.04, 29.93, 29.82, 29.80, 29.78, 29.72, 29.71, 29.69, 29.67, 29.52, 29.48, 29.46, 29.33, 27.37, 24.26, 22.85, 14.27 ppm.

Synthesis of 1,1-diethoxytritriaconta-11,22-diene (M_{33} diethyl acetal) (**49**).

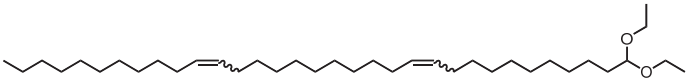

M_{33} ethylene acetal **48** (557 mg, 1.07 mmol, 1 eq) was suspended in ethanol (150 mL) in a 500 mL round-bottom flask. *p*-Toluene sulfonic acid monohydrate ($TsOH{\cdot}H_2O$, 13 mg, 0.075 mmol, 0.07 eq) was added as solid, and the mixture was heated to reflux (all material was dissolved at elevated temperatures). After 1 hour, nearly all ethylene acetal was converted (checked with TLC (hept/EtOAc 90/10; CeMo staining). The reaction mixture was cooled down to room temperature, resulting in partial precipitation of the product. Powdered KOH (~10 mg, 0.14 eq) was added to quench the TsOH, and the mixture was concentrated in *vacuo*. The crude material was dissolved in heptane (40 mL), and resulting slightly turbid solution was washed with water (2 × 25 mL). The clear organic layer was dried with $MgSO_4$ and concentrated in *vacuo*. The crude product was obtained as a colorless oil (576 mg, 97%) and was pure enough for further deprotection. ^{1}H NMR (400 MHz, $CDCl_3$): δ = 5.39–5.29 (m, 4H, CH$_2$-C<u>H</u>=C<u>H</u>-CH$_2$), 4.47 (t, ^3J = 5.7 Hz, 1H, CH$_2$-C<u>H</u>(-O-CH$_2$-CH$_3$)$_2$), 3.64 (dq, ^2J = 9.4 Hz, ^3J = 7.2 Hz, 4H, CH(-OC<u>H</u>$_2$CH$_3$)$_2$), 3.49 (dq, ^2J = 9.4 Hz, ^3J = 7.2 Hz, 4H, CH(-OC<u>H</u>$_2$CH$_3$)$_2$), 2.07–1.93 (m, 8H, C<u>H</u>$_2$-CH=CH-C<u>H</u>$_2$), 1.61 (dt, ^3J = 8.7 Hz, ^3J = 6.2 Hz, 2H, C<u>H</u>$_2$-CH(-OCH$_2$CH$_3$)$_2$), 1.38–1.23 (m, 44H, C<u>H</u>$_2$), 1.20 (t, ^3J = 6.9 Hz, 6H, O-CH$_2$-C<u>H</u>$_3$), 0.88 ppm (t, ^3J = 7.2 Hz, 3H, CH$_2$-C<u>H</u>$_3$); ^{13}C NMR (100 MHz, CDCl3): δ = 130.03, 103.13, 60.96, 33.77, 32.08, 39.94–29.48, 27.37, 24.93, 22.85, 15.51, 14.23 ppm.

Synthesis of tritriaconta-11,22-dienal (M_{33} aldehyde) (**50**).

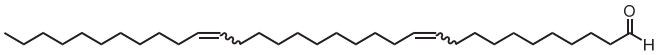

M_{33} diethyl acetal **49** (518 mg, 0.998 mmol, 1 eq) was dissolved in acetone (150 mL) in a 500 mL round-bottom flask. The solution was purged with argon to remove oxygen. *p*-Toluene sulfonic acid monohydrate ($TsOH{\cdot}H_2O$, 9 mg, 0.050 mmol, 0.05 eq) was added as a solid, and the mixture was stirred at room temperature under argon. After 3 hours, formation of the product was observed with TLC (hept/EtOAc; CeMo staining). The reaction was quenched with 10% Na_2CO_3 soln. (20 mL), and the resulting solution extracted with heptane (3 × 30 mL). The organic layer was washed with water (30 mL) and dried with $MgSO_4$. The solvent was removed in *vacuo*, giving deprotected product as a colorless oil (450 mg, 95%). ^{1}H NMR confirmed the complete absence of starting material. The product was stored under N_2 in the fridge. ^{1}H NMR (400 MHz, $CDCl_3$): δ = 9.77 (t, ^3J = 1.9 Hz, 1H, CH_2-C<u>H</u>O), 5.40–5.30 (m, 4H, CH_2-C<u>H</u>=C<u>H</u>-CH_2), 2.42 (dt, ^3J = 5.5 Hz, ^3J = 1.9 Hz, 2H, C<u>H</u>$_2$-CHO), 2.07–1.93 (m, 8H, C<u>H</u>$_2$-CH=CH-C<u>H</u>$_2$), 1.63 (tt, ^3J = 7.2 Hz, ^3J = 7.2 Hz, 2H, CH_2-C<u>H</u>$_2$-CH_2-CHO), 1.93–1.19 (m, 42H, C<u>H</u>$_2$), 0.88 ppm (t, ^3J = 6.7 Hz, 3H, CH_2-C<u>H</u>$_3$); ^{13}C NMR (100 MHz, CDCl3): δ = 203.06, 130.09, 130.07, 130.03, 129.98, 44.08, 32.08, 30.94–29.33, 27.37, 27.36, 24.85, 22.24, 14.35 ppm.

Synthesis of 2-(tritetraconta-10,21-dien-1-yl)-1,3-dioxolane (M_{44} ethylene acetal) (**51**).

Phosphonium salt **44** (7.0 g, 9.89 mmol, 1.03 eq) and docosanal **46** (3.0 g, 9.62 mmol, 1 eq) were coupled using general method **A**. The crude product was obtained as a dark yellow oil and further purified by automated column chromatography using heptane/EtOAc (gradient 100/0 to 98/2) as eluent. The pure product was obtained as a white solid (3.97 g, 60%). ^{1}H NMR (400 MHz, $CDCl_3$): δ = 5.44–5.26 (m, 4H, CH_2-C<u>H</u>=C<u>H</u>-CH_2), 4.84 (t, ^3J = 4.8 Hz, 1H, CH_2-C<u>H</u>(-O-CH_2-CH_2-O-)), 4.02–3.79 (m, 4H, CH_2-CH(-O-C<u>H</u>$_2$-C<u>H</u>$_2$-O-)), 2.06–1.93 (m, 8H, C<u>H</u>$_2$-CH=CH-C<u>H</u>$_2$), 1.69–1.61 (m, 2H, CH_2-C<u>H</u>$_2$-CH(-O-CH_2-CH_2-O-)), 1.45–1.20 (m, 66H, C<u>H</u>$_2$), 0.88 ppm (t, ^3J = 6.9 Hz, 3H, C<u>H</u>$_3$); ^{13}C NMR (100 MHz, $CDCl_3$): δ = 130.50, 130.05, 130.04, 104.87, 64.98, 34.09, 32.77, 32.09, 29.94, 29.86, 29.82, 29.79, 29.73, 29.71, 29.69, 29.67, 29.53, 29.49, 29.46, 29.34, 27.38, 24.26, 22.86, 14.28 ppm.

Synthesis of 1,1-diethoxytetratetraconta-11,22-diene (M_{44} diethyl acetal) (**52**).

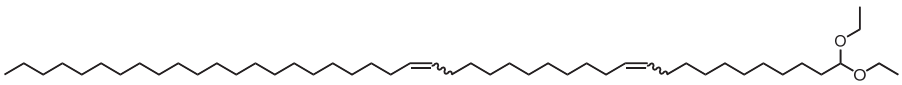

M_{44} ethylene acetal **51** (3.71 g, 5.51 mmol, 1 eq) was suspended in ethanol (500 mL) in a 1 L round-bottom flask. *p*-Toluene sulfonic acid monohydrate ($TsOH{\cdot}H_2O$, 55 mg, 0.32 mmol, 0.06 eq) was added as solid, and the mixture was heated to reflux (all material was dissolved at elevated temperatures). After 1.5 hour, all ethylene acetal was converted (checked with TLC (hept/EtOAc 90/10; CeMo staining). The reaction mixture was cooled down to room temperature, resulting in partial precipitation of the product. Powdered KOH (~145 mg, 0.47 eq) was added to quench the TsOH, and the mixture was concentrated in *vacuo*. The crude material was dissolved in heptane (200 mL), and resulting slightly turbid solution was washed with water (2 × 200 mL). The clear organic layer was dried with $MgSO_4$ and concentrated in *vacuo*. The crude product was obtained as a white solid (3.40 g, 88%) and pure enough for further deprotection. ^{1}H NMR (400 MHz, $CDCl_3$): δ = 5.41–5.28 (m, 4H, CH_2-C<u>H</u>=C<u>H</u>-CH_2), 4.47 (t, ^3J = 5.8 Hz, 1H, CH_2-C<u>H</u>(-O-CH_2-CH_3)$_2$), 3.64 (dq, ^2J = 9.5 Hz, ^3J = 7.1 Hz, 2H, CH(-O-C<u>H</u>$_2$-CH_3)$_2$), 3.49 (dq, ^2J = 9.5 Hz, ^3J = 7.1 Hz, 2H, CH(-O-C<u>H</u>$_2$-CH_3)$_2$), 2.06–1.93 (m, 8H, C<u>H</u>$_2$-CH=CH-C<u>H</u>$_2$), 1.63–1.57 (m, 2H, CH_2-C<u>H</u>$_2$-CH(-O-CH_2-CH_3)$_2$), 1.41–1.23 (m, 66H, C<u>H</u>$_2$), 1.20 (t, ^3J = 7.1 Hz, 6H, CH(-O-CH_2-C<u>H</u>$_3$)$_2$), 0.88 ppm (t, ^3J = 6.9 Hz, 3H, C<u>H</u>$_3$);

Synthesis of tetratetraconta-11,22-dienal (M_{44} aldehyde) (**53**).

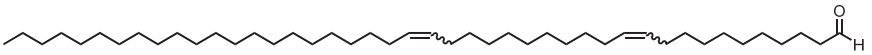

M_{44} diethyl acetal **52** (1.85 g, 2.63 mmol, 1 eq) was dissolved in a mixture of acetone (100 mL) and chloroform (100 mL) in a 500 mL round-bottom flask. The solution was purged with argon to remove oxygen. *p*-Toluene sulfonic acid monohydrate ($TsOH{\cdot}H_2O$, 48 mg, 0.28 mmol, 0.11 eq) was added as a solid, and the mixture was stirred at room temperature under argon. After 3 hours, formation of the product was observed with TLC (hept/EtOAc; CeMo staining). The reaction was quenched with 10% Na_2CO_3 soln. (90 mL), and the resulting solution extracted with heptane (3 × 70 mL). The organic layer was washed with water (60 mL) and dried with $MgSO_4$. The solvent was removed in *vacuo*, giving deprotected product as a white solid (1.65 g, quant.). ^{1}H NMR confirmed the complete absence of starting material. The product was stored under N_2 in the fridge. ^{1}H NMR (400 MHz, $CDCl_3$): δ = 9.76 (t, ^3J = 1.9 Hz, 1H, CH_2-C<u>H</u>O), 5.41–5.29 (m, 4H, CH_2-C<u>H</u>=C<u>H</u>-CH_2), 2.42 (td, ^3J = 7.4 Hz, ^3J = 1.9 Hz, 2H, CH_2-C<u>H</u>$_2$-CHO), 2.09–1.92 (m, 8H, C<u>H</u>$_2$-CH=CH-C<u>H</u>$_2$), 1.63 (tt, ^3J = 7.3 Hz, ^3J = 7.3 Hz, 2H, CH_2-C<u>H</u>$_2$-CH_2-CHO), 1.40–1.17 (m, 64H, C<u>H</u>$_2$), 0.88 ppm (t, ^3J = 6.9 Hz, 3H, C<u>H</u>$_3$); ^{13}C NMR (100 MHz, $CDCl_3$): δ = 203.04, 130.09, 130.06, 130.02, 129.97, 44.08, 32.77, 32.09, 29.94, 29.91, 29.87, 29.83, 29.79, 29.73, 29.63, 29.56, 29.53, 29.49, 29.43, 29.33, 27.38, 27.36, 22.86, 22.25, 14.28 ppm.

Synthesis of 2-(pentahexaconta-10,21,32,43-tetraen-1-yl)-1,3-dioxolane (M_{66} ethylene acetal) (**54**).

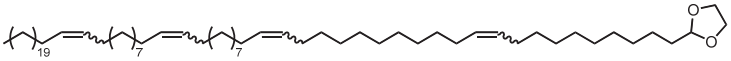

Phosphonium salt **44** (1.10 g, 1.55 mmol, 1.14 eq) and M_{44} aldehyde **53** (0.86 g, 1.36 mmol, 1 eq) were coupled using general method **A**. The crude product was obtained as a dark yellow oil and further purified by automated column chromatography using heptane/EtOAc (gradient 100/0 to 98/2) as eluent. The pure product was obtained as a white solid (870 g, 65%). ^{1}H NMR (400 MHz, $CDCl_3$): δ = 5.40–5.28 (m, 8H, CH_2-C<u>H</u>=C<u>H</u>-CH_2), 4.84 (t, ^3J = 4.9 Hz, 1H, CH_2-C<u>H</u>(-O-CH_2-CH_2-O-)), 4.01–3.80 (m, 4H, CH_2-CH(-O-C<u>H</u>$_2$-C<u>H</u>$_2$-O-)), 2.08–1.92 (m, 16H, C<u>H</u>$_2$-CH=CH-C<u>H</u>$_2$), 1.70–1.60 (m, 2H, CH_2-C<u>H</u>$_2$-CH(-O-CH_2-CH_2-O-)), 1.47–1.20 (m, 94H, C<u>H</u>$_2$), 0.88 ppm (t, ^3J = 6.7 Hz, 3H, C<u>H</u>$_3$); ^{13}C NMR (100 MHz, $CDCl_3$): δ = 130.50, 130.04, 104.87, 64.98, 34.09, 32.78, 32.09, 29.94, 29.87, 29.83, 29.79, 29.73, 29.69, 29.67, 29.53, 29.49, 29.47, 29.35, 27.38, 24.26, 22.86, 14.28 ppm.

Synthesis of 1,1-diethoxyhexahexaconta-11,22,33,44-tetraene (M_{66} diethyl acetal) (**55**).

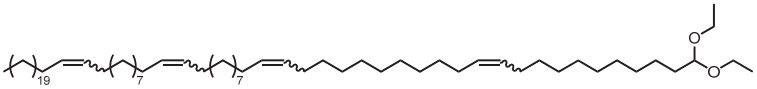

M_{66} ethylene acetal **54** was (310 mg, 0.317 mmol, 1 eq) was suspended in a mixture of ethanol (35 mL, ~2000 eq) and chloroform (10 mL) in a 100 mL round-bottom flask. *p*-Toluene sulfonic acid monohydrate ($TsOH{\cdot}H_2O$, 3 mg, 0.016 mmol, 0.05 eq) was added as a solid, and the mixture was heated to reflux (all material was dissolved at elevated temperatures). After 2 hours, nearly all ethylene acetal was converted (checked with TLC (hept/EtOAc 90/10; CeMo staining). The reaction mixture was cooled down to room temperature, resulting in partial precipitation of the product. Powdered KOH (~4 mg, 0.20 eq) was added to quench the TsOH, and the mixture was concentrated in *vacuo*. The crude material was dissolved in heptane (30 mL), and resulting slightly turbid solution was washed with water (2 × 20 mL). The clear organic layer was dried with $MgSO_4$ and concentrated in *vacuo*. The crude product was obtained as a colorless oil (332 mg, quant.) and was pure enough for further deprotection. ^{1}H NMR (400 MHz, $CDCl_3$): δ = 5.40–5.30 (m, 8H, CH_2-C<u>H</u>=C<u>H</u>-CH_2), 4.48 (t, ^3J = 5.8 Hz, 1H, C<u>H</u>(-OCH_2CH_3)$_2$), 3.64 (dq, ^2J = 9.4 Hz, ^3J = 7.1 Hz, 2H, CH(-OC<u>H</u>$_2$$CH_3$)$_2$), 3.49 (dq, ^2J = 9.4 Hz, ^3J = 7.1 Hz, 2H, CH(-OC<u>H</u>$_2$$CH_3$)$_2$), 2.05–1.93 (m, 16H, C<u>H</u>$_2$-CH=CH-C<u>H</u>$_2$), 1.64–1.56 (m, 2H, C<u>H</u>$_2$-CH(-OCH_2CH_3)$_2$), 1.38–1.23 (m, 94H, C<u>H</u>$_2$), 1.20 (t, ^3J = 7.1 Hz, 6H, C<u>H</u>$_3$-CH_2-O), 0.88 ppm (t, ^3J = 6.8 Hz, 3H, C<u>H</u>$_3$-CH_2-CH_2); ^{13}C NMR (100 MHz, $CDCl_3$): δ = 130.49,

130.03, 103.13, 60.94, 33.77, 32.78, 32.09, 29.95, 29.87, 29.83, 29.79, 29.74, 29.70, 29.67, 29.53, 29.49, 29.35, 27.38, 24.94, 22.86, 15.52, 14.27 ppm; MS (MALDI-TOF): *m/z* calcd for $C_{70}H_{134}O_2$+Na^+: 1030.03 $[M+Na]^+$; found: 1030.17.

Synthesis of hexahexaconta-11,22,33,44-tetraenal (M_{66} aldehyde) (**56**).

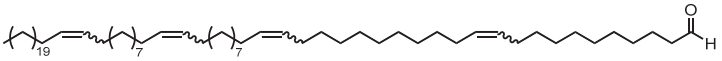

M_{66} diethyl acetal **55** (320 mg, 0.318 mmol, 1 eq) was dissolved in a mixture of chloroform (5 mL) and acetone (5 mL) in a 25 mL round-bottom flask. The solution was purged with argon to remove oxygen. *p*-Toluene sulfonic acid monohydrate ($TsOH{\cdot}H_2O$, 3 mg, 0.016 mmol, 0.05 eq) was added as solid, and the mixture was stirred at room temperature under argon. After 2 hours, formation of the product was observed with TLC (hept/EtOAc; CeMo staining). The reaction was quenched with 10% Na_2CO_3 soln. (20 mL), and the resulting solution extracted with heptane (20 mL). The organic layer was washed with water (10 mL) and dried with $MgSO_4$. The solvent was removed in *vacuo*, giving partially deprotected product (320 mg). ^{1}H NMR revealed the presence of ~5 % starting material. The above procedure was repeated, giving the title compound (286 mg, 96%) as a colorless oil (the material solidified upon cooling to 0 °C). ^{1}H NMR confirmed the complete absence of starting material. The product was stored under N_2 in the fridge. ^{1}H NMR (400 MHz, $CDCl_3$): δ = 9.76 (t, ^3J = 1.8 Hz, 1H, CH_2-C<u>H</u>O), 5.41–5.29 (m, 8H, CH_2-C<u>H</u>=C<u>H</u>-CH_2), 2.41 (td, ^3J = 7.4 Hz, ^3J = 1.9 Hz, 2H, CH_2-C<u>H</u>$_2$-CHO), 2.02 (td, ^3J = 6.7 Hz, ^3J = 6.5 Hz, 16H, CH_2-C<u>H</u>$_2$-CH=CH-C<u>H</u>$_2$-CH_2), 1.63 (tt, ^3J = 7.3 Hz, ^3J = 7.3 Hz, 2H, CH_2-C<u>H</u>$_2$-CH_2-CHO), 1.41–1.18 (m, 92H, C<u>H</u>$_2$), 0.89 ppm (t, ^3J = 6.9 Hz, 3H, C<u>H</u>$_3$); ^{13}C NMR (100 MHz, $CDCl_3$): δ = 202.56, 130.46, 130.03, 130.00, 129.98, 129.91, 44.07, 32.80, 32.13, 32.07, 29.96, 29.91, 29.87, 29.83, 29.77, 29.66, 29.59, 29.57, 29.55, 29.51, 29.45, 29.38, 29.36, 29.22, 27.39, 27.37, 22.87, 22.26, 14.25 ppm; MS (MALDI-TOF): *m/z* calcd for $C_{66}H_{124}O^+$: 932.97 M^+; found: 932.99.

Synthesis of dodecanedial (**58**).

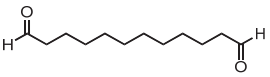

Dodecanediol (5.18 g, 25.6 mmol, 1 eq), tetrabutylammonium chloride (758 mg, 6.92 mmol, 0.27 eq), and (2,2,6,6-tetramethylpiperidin-1-yl)oxyl (TEMPO, 610 mg, 3.90 mmol, 0.15 eq) were added to DCM (200 mL) in a 1L round-bottom flask. A solution of $NaHCO_3$ (21.6 g, 257 mmol), K_2CO_3 (3.61 g, 26.1 mmol) in water (320 mL) was added, and the mixture vigorously stirred to get two intimately mixed layers (under argon atmosphere to prevent possible over-oxidation). *N*-Chlorosuccinimide (9.45 g, 70.8, 2.8 eq) was added as a solid and stirring of the suspension/emulsion was continued for 20 h at room temperature. After 20 hours, a ^{1}H NMR sample taken from the DCM layer confirmed complete conversion of the alcohol functionality. The DCM layer was washed with water (2 × 200 mL) and brine (300 mL). The organic layer was dried with MgSO4 and concentrated in *vacuo*, giving the crude product as a red oil (6.04 g). The materials was stirred in hot heptane (30 mL), cooled down to −20 °C in a freezer, and the supernatant was removed from the formed crystals with a Pasteur pipette. This procedure was repeated three times. The residue was subjected to automated column chromatography using heptane/chloroform (gradient 80/20 to 0/100) as eluent. Pure dodecanedial was obtained as a white solid (2.30 g, 45%). ^{1}H NMR (400 MHz, $CDCl_3$): δ = 9.76 (t, ^3J = 1.9 Hz, 2H, CH_2-C<u>H</u>O), 2.41 (td, ^3J = 7.3 Hz, ^3J = 1.9 Hz, 4H, CH_2-C<u>H</u>$_2$-CHO), 1.67–1.57 (m, 4H, CH_2-C<u>H</u>$_2$-CH_2-CHO), 1.36–1.22 ppm (m, 12H, C<u>H</u>$_2$); ^{13}C NMR (100 MHz, $CDCl_3$): δ = 203.04, 44.03, 29.43, 29.25, 22.18 ppm.

Synthesis of 2,2'-(tetrapentaconta-10,21,33,44-tetraene-1,54-diyl)bis(1,3-dioxolane) (M_{56} bis(ethylene acetal) (**59**).

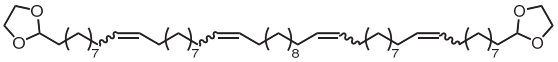

Phosphonium salt **44** (2.33 g, 3.29 mmol, 2.2 eq) and dodecanedial **58** (296 mg, 1.50 mmol, 1 eq) were coupled using general method **A**. After filtration, the heptane layer 100 mL) was washed with acetonitrile (6 × 50 mL). The heptane was removed in *vacuo*, giving the product as a white solid (1.032 g, 77%). No further purification was necessary. ^{1}H NMR (400 MHz, $CDCl_3$): δ = 5.41–5.29 (m, 8H, CH_2-C<u>H</u>=C<u>H</u>-CH_2), 4,48 (t, ^3J = 4,8 Hz, 2H, CH_2-C<u>H</u>(-O-CH_2-CH_2-O-)), 4.02–3.79 (m, 8H, CH_2-CH(-O-C<u>H</u>$_2$-C<u>H</u>$_2$-O-)), 2.07–1.93 (m, 16H, C<u>H</u>$_2$-CH=CH-C<u>H</u>$_2$), 1.70–1.61 (m, 4H, CH_2-C<u>H</u>$_2$-CH(-O-CH_2-CH_2-O-)), 1.46–1.21 ppm (m, 72H, C<u>H</u>$_2$); ^{13}C NMR (100 MHz, $CDCl_3$): δ = 130.50, 130.04, 104.87, 64.98, 34.09, 32.78, 29.94, 29.82, 29.79, 29.73, 29.72, 29.69, 29.67, 29.49, 29.46, 29.35, 27.38, 24.26 ppm.

Synthesis of 1,1,56,56-tetraethoxyhexapentaconta-11,22,34,45-tetraene (M_{56} bis(diethyl acetal)) (**60**).

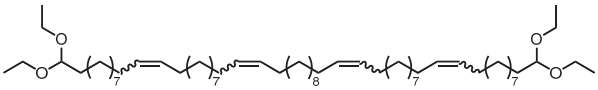

M_{56} bis(ethylene acetal) **59** (550 mg, 0.614 mmol, 1 eq) was suspended in a mixture of ethanol (80 mL, ~2000 eq) and chloroform (10 mL) in a 250 mL round-bottom flask. *p*-Toluene sulfonic acid monohydrate ($TsOH{\cdot}H_2O$, 12 mg, 0.061 mmol, 0.1 eq) was added as a solid, and the mixture was heated to reflux (all material was dissolved at elevated temperatures). After 2 hours, nearly all ethylene acetal was converted (checked with TLC (hept/EtOAc 90/10; CeMo staining). The reaction mixture was cooled down to room temperature, resulting in partial precipitation of the product. Powdered KOH (~4 mg, 0.20 eq) was added to quench the TsOH, and the mixture was concentrated in *vacuo*. The crude material was dissolved in DCM (20 mL), and resulting solution was washed with water (2 × 15 mL). The organic layer was dried with $MgSO_4$ and concentrated in *vacuo*. The crude product was obtained as a colorless oil (548 mg, 93%) and pure enough for further deprotection. ^{1}H NMR (400 MHz, $CDCl_3$): δ = 5.41–5.28 (m, 8H, CH_2-C<u>H</u>=C<u>H</u>-CH_2), 4.47 (t, ^3J = 5.8 Hz, 2H, C<u>H</u>(O-CH_2-CH_3)$_2$), 3.63 (dq, ^2J = 9.4, ^3J = 7.0 Hz, 4H, CH(O-C<u>H</u>$_2$-CH_3)$_2$), 3.49 (dq, ^2J = 9.4, ^3J = 7.1 Hz, 4H, CH(O-C<u>H</u>$_2$-CH_3)$_2$), 2.07–1.93 (m, 16H, C<u>H</u>$_2$-CH=CH-C<u>H</u>$_2$), 1.63–1.57 (m, 4H, C<u>H</u>$_2$-CH(-OCH_2CH_3)$_2$), 1.38–1.23 (m, 76H, C<u>H</u>$_2$), 1.20 ppm (t, ^3J = 7.0 Hz, 12H); ^{13}C NMR (100 MHz, $CDCl_3$): δ = 130.50, 130.04, 103.13, 60.95, 33.77, 32.78, 29.94, 29.82, 29.79, 29.73, 29.72, 29.70, 29.66, 29.49, 29.47, 27.38, 24.93, 15.52 ppm; MS (MALDI-TOF): *m/z* calcd for $C_{64}H_{122}O_4$+Na^+: 977.92 $[M+Na]^+$; found: 977.93.

Synthesis of hexapentaconta-11,22,34,45-tetraenedial (M_{56} bisaldehyde) (**61**).

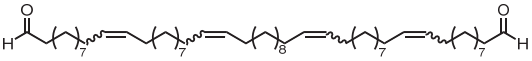

M_{56} bis(diethyl acetal) **60** (538 mg, 0.563 mmol, 1 eq) was dissolved in a mixture of DCM (8 mL) and acetone (8 mL) in a 50 mL round-bottom flask. The solution was purged with argon to remove oxygen. *p*-Toluene sulfonic acid monohydrate ($TsOH{\cdot}H_2O$, 5 mg, 0.03 mmol, 0.05 eq) was added as a solid, and the mixture was stirred at room temperature under argon. After 1 hour, formation of the product was observed with TLC (hept/EtOAc; CeMo staining). The reaction was quenched with 10% Na_2CO_3 soln. (15 mL), and the resulting solution extracted with heptane (20 mL). The organic layer was washed with water (10 mL) and dried with $MgSO_4$. The solvent was removed in *vacuo*, giving partially deprotected product (457 mg). ^{1}H NMR revealed the presence of ~15 % starting material. The above procedure was repeated, giving the title compound (451 mg, 99%) as a colorless oil. ^{1}H NMR confirmed the complete absence of starting material. The product was stored under N_2 in the fridge. ^{1}H NMR (400 MHz,

$CDCl_3$): δ = 9.74 (t, ^3J = 1.9 Hz, 2H, CH_2-C<u>H</u>O), 5.39–5.27 (m, 8H, CH_2-C<u>H</u>=C<u>H</u>-CH_2), 2.39 (td, ^3J = 7.4 Hz, ^3J = 1.9 Hz, 4H, C<u>H</u>$_2$-CHO), 2.08–1.91 and 1.65–1.55 (m, 16H, C<u>H</u>$_2$-CH=CH-C<u>H</u>$_2$), 1.38–1.18 ppm (m, 72H, C<u>H</u>$_2$); ^{13}C NMR (100 MHz, $CDCl_3$): δ = 202.71, 130.46, 130.42, 130.40, 130.35, 129.98, 129.95, 129.93, 129.88, 44.00, 32.72, 32.70, 29.89, 29.85, 29.77, 29.74, 29.68, 29.58, 29.54, 29.51, 29.47, 29.43, 29.37, 29.29, 29.28, 27.32, 27.30, 22.19 ppm; MS (MALDI-TOF): *m/z* calcd for $C_{56}H_{102}O_2$+Na^+: 829.78 $[M+Na]^+$; found: 829.79.

Synthesis of allyltriphenylphosphonium bromide (**65**).

Triphenylphosphine (1.094 g, 4.171 mmol, 1 eq) was dissolved in acetonitrile (10 mL) in a 50 mL round-bottom flask. Allyl bromide (0.505 g, 4.171 mmol, 1 eq) was added, and the resulting clear solution was stirred under reflux. After 45 min, a white crystalline precipitate had formed. The reaction mixture was cooled down to room temperature and diethyl ether (20 mL) was added. The mixture was stirred for 5 min at, resulting in further precipitation of the product. Afterward, the precipitate was allowed to settle, and the top layer of liquid was decanted. Additional diethyl ether (10 mL) was added, and the above described decantation procedure was repeated 2 more times. The remaining solid was dried in *vacuo*, resulting in the pure as white, fine crystals (1.339 g, 84%). ^{1}H NMR (400 MHz, $CDCl_3$): δ = 7.87–7.74 (m, 9H, Ar-<u>H</u>), 7.70–7.64 (m, 6H, Ar-<u>H</u>), 5.69 (dddt, ^3J = 16.5 Hz, ^3J = 9.6 Hz, ^3J = 6.9 Hz, $^3J_{P,H}$ = 5.0 Hz, 1H, CH_2=C<u>H</u>-CH_2-P), 5.57 (ddt, ^3J = 16.9 Hz, ^3J = 5.2 Hz, ^3J = 1.2 Hz, 1H, C<u>H</u>$_2$=CH-CH_2 (cis)), 5.36 (ddt, ^3J = 9.6 Hz, ^3J = 5.2 Hz, ^3J = 1.1 Hz, 1H, C<u>H</u>$_2$=CH-CH_2 (trans)), 4.78 ppm (dd, $^3J_{P,H}$ = 15.4 Hz, ^3J = 6.9 Hz, 2H, CH-C<u>H</u>$_2$-P); ^{13}C NMR (100 MHz, $CDCl_3$): δ = 139.00, 134.98, 134.95, 133.53, 133.43, 130.49, 130.36, 118.54, 117.69, 113.98, 33.59, 30.37, 30.21, 29.16, 29.01, 28.97, 28.85, 28.68, 22.92, 22.49, 22.45, 22.43 ppm; ^{31}P NMR (162 MHz, $CDCl_3$): δ = 24.11 ppm; MS (MALDI-TOF): *m/z* calcd for $C_{21}H_{20}$BrP−Br^-: 303.13 $[M-Br]^-$; found: 303.21.

Synthesis of pent-4-en-1-yltriphenylphosphonium bromide (**66**).

Triphenylphosphine (1.848 g, 7.046 mmol, 1.05 eq) and 5-bromopent-1-ene **63** (1.000 g, 6.710 mmol, 1 eq) were dissolved in acetonitrile (10 mL). The solution heated to reflux and stirred for 2 hours, resulting in the precipitation of the product. The mixture was then allowed to cool down to room temperature, most of the acetonitrile was removed in *vacuo*, and diethyl ether (40 mL) was added. The resulting suspension was stirred for 5 min at room temperature. Afterward, the precipitate was allowed to settle, and the top layer of liquid was decanted. Additional diethyl ether (15 mL) was added, and the above described decantation procedure was repeated 2 more times. The remaining solid was dried in *vacuo*, giving the pure product as white, fine crystals (2.327 g, 84%). ^{1}H NMR (400 MHz, $CDCl_3$): δ = 7.89–7.75 (m, 9H, Ar-<u>H</u>), 7.72–7.66 (m, 6H, Ar-H), 5.70 (ddt, ^3J = 17.0 Hz, ^3J = 10.2 Hz, ^3J = 6.7 Hz, 1H, CH_2=C<u>H</u>-CH_2), 5.07–4.96 (m, 2H, C<u>H</u>$_2$=CH-CH_2), 3.92–3.83 (m, 2H, C<u>H</u>$_2$-P), 2.47–2.40 (m, 2H, CH_2=CH_2-CH_2-C<u>H</u>$_2$), 1.79–1.67 ppm (m, 2H, CH_2=CH_2-C<u>H</u>$_2$); ^{13}C NMR (100 MHz, $CDCl_3$): δ = 136.56, 135.12, 135.09, 133.91, 133.81, 130.67, 130.54, 118.96, 118.11, 117.00, 33.98, 33.81, 22.41, 22.08, 22.04, 21.91 ppm; ^{31}P NMR (162 MHz, $CDCl_3$): δ = 24.66 ppm; MS (MALDI-TOF): *m/z* calcd for $C_{23}H_{24}$BrP−Br^-: 331.16 $[M-Br]^+$; found: 331.20.

Synthesis of undec-10-en-1-yltriphenylphosphonium bromide (**67**).

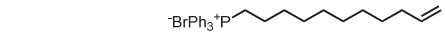

Alkene bromide (**64** (1.04 g, 4.45 mmol, 1 eq) and triphenylphosphine (1.40 g, 5.34 mmol, 1.2 eq) were suspended in acetonitrile (4 mL) in a 25 mL round-bottom flask with condenser. The mixture was heated to reflux, resulting in a light brown, clear solution. After 24 h, the mixture was cooled to room temperature, and transferred to a separation funnel. More acetonitrile (8 mL) was added and the solution washed with heptane (6 × 20 mL). The acetonitrile layer was then concentrated in *vacuo* giving the title compound as a light brown, very thick oil (2.02 g, 92%). The material is hygroscopic, and drying in high vacuum at 40 °C prior to further use is advised. ^{1}H NMR (400 MHz, $CDCl_3$): δ = 7.78–7.68 (m, 9H, Ar-<u>H</u>), 7.66–7.58 (m, 6H, Ar-<u>H</u>), 5.67 (ddt, ^3J = 17 Hz, ^3J = 10.1 Hz, ^2J = 6.7 Hz,

1H, CH_2=C<u>H</u>-CH_2), 4.85 (ddt, ^3J = 17 Hz, ^2J = 2 Hz, ^4J = 1.6 Hz, 1H, C<u>H</u>$_2$=CH-CH_2 (*cis*)), 4.79 (ddt, ^3J = 10.1 Hz, ^2J = 2 Hz, ^4J = 1.2 Hz, 1H, C<u>H</u>$_2$=CH-CH_2 (*trans*)), 3.64–3.54 (m, 2H, C<u>H</u>$_2$-P), 1.93–1.85 (m, 2H, CH_2=CH-C<u>H</u>$_2$), 1.58–1.46 (m, 4H, C<u>H</u>$_2$), 1.26–1.05 ppm (m, 10H, C<u>H</u>$_2$); ^{13}C NMR (100 MHz, $CDCl_3$): δ = 139.00, 134.98, 134.95, 133.53, 133.43, 130.49, 130.36, 118.54, 117.69, 113.98, 33.59, 30.37, 30.21, 29.16, 29.01, 28.97, 28.85, 28.68, 22.92, 22.49, 22.45, 22.43 ppm; ^{31}P NMR (162 MHz, $CDCl_3$): δ = 24.20 ppm.

Synthesis of docosa-1,11-diene (M_{22} alkene) (**68**).

Phosphonium salt **67** (610 mg, 1.23 mmol, 1.1 eq) and undecanal **47** (191 mg, 1.12 mmol, 1 eq) were coupled using general method **A**. The crude product was obtained as a dark yellow oil and further purified by automated column chromatography using heptane (100%, isocratic) as eluent. The pure product was obtained as a colorless oil (120 mg, 32%). ^{1}H NMR (400 MHz, $CDCl_3$): δ = 5.81 (ddt, ^3J = 16.9 Hz, ^3J = 10.2 Hz, ^3J = 6.7 Hz, 1H, CH_2-C<u>H</u>=CH_2), 5.40–5.31 (m, 2H, CH_2-C<u>H</u>=C<u>H</u>-CH_2), 4.99 (ddt, ^3J = 16.9 Hz, ^2J = 1.9 Hz, ^4J = 1.8 Hz, 1H, CH_2-CH=C<u>H</u>$_2$), 4.93 (ddt, ^3J = 10.2 Hz, ^2J = 1.9 Hz, ^4J = 0.9 Hz, 1H, CH_2-CH=C<u>H</u>$_2$), 2.08–1.93 (m, 6H, C<u>H</u>$_2$-CH=CH-C<u>H</u>$_2$ and C<u>H</u>$_2$-CH=CH_2), 1.43–1.19 (m, 28H, C<u>H</u>$_2$), 0.88 ppm (t, ^3J = 6.7 Hz, 3H, CH_2-C<u>H</u>$_3$); ^{13}C NMR (100 MHz, CDCl3): δ = 139.40, 130.06, 114.24, 33.98, 32.09, 29.94, 29.93, 29.87, 29.83, 29.73, 29.66, 29.64, 29.53, 29.49, 29.46, 29.31, 29.11, 27.37, 22.86, 14.28 ppm; GC-MS (EI, oven 80–300 °C): t = 3.63 min.

Synthesis of tritriaconta-1,11-diene (M_{33} alkene) (**69**).

Phosphonium salt **67** (690 mg, 1.27 mmol, 1.1 eq) and docosanal **46** (690 mg, 1.39 mmol, 1 eq) were coupled using general method **A**. The crude product was obtained as a light brown oil and further purified by automated column chromatography using heptane (100%, isocratic) as eluent. The pure product was obtained as a colorless oil (379 mg, 62%). ^{1}H NMR (400 MHz, $CDCl_3$): δ = 5.82 (ddt, ^3J = 17.0 Hz, ^3J = 10.2 Hz, ^3J = 6.7 Hz, 1H, CH_2=C<u>H</u>-CH_2), 5.44–5.31 (m, 2H, CH_2-C<u>H</u>=C<u>H</u>-CH_2), 5.00 (ddt, ^3J = 17.0 Hz, ^2J = 2.0 Hz, ^4J = 1.6 Hz, 1H, C<u>H</u>$_2$=CH-CH_2 (*cis*)), 4.94 (ddt, ^3J = 10.2 Hz, ^2J = 2.0 Hz, ^4J = 1.2 Hz, 1H, C<u>H</u>$_2$=CH-CH_2 (*trans*)), 2.09–1.94 (m, 6H, C<u>H</u>$_2$-CH=CH-C<u>H</u>$_2$, CH_2=CH-C<u>H</u>$_2$), 1.44–1.22 (m, 50H, C<u>H</u>$_2$), 0.89 ppm (t, ^3J = 6.7 Hz, 3H, C<u>H</u>$_3$); ^{13}C NMR (100 MHz, $CDCl_3$): δ = 139.34, 130.54, 130.48, 130.07, 130.01, 114.25, 34.01, 32.80, 32.13, 29.97, 29.96, 29.91, 29.87, 29.78, 29.70, 29.69, 29.57, 29.52, 29.49, 29.38, 29.35, 29.14, 27.39, 22.89, 14.29 ppm; GC-MS (EI, oven 80–300 °C): t = 6.88 min.

Synthesis of tritriacontane ($C_{33}H_{68}$).

M_{33} alkene **69** (58 mg, 0.125 mmol, 1 eq) was dissolved in EtOAc (4 mL) in a 25 mL round-bottom flask. Pd/C (10 w% Pd, 15 mg, 12.5 µmol Pd, 0.1 eq) was added and the flask was purged with hydrogen and stirred at room temperature. After 3 hours, the mixture was filtered through Celite, and the residue rinsed with EtOAc (3 × 5 mL). The combined filtrates were concentrated in *vacuo*, giving the pure product as a white solid (56 mg, 89%). ^{1}H NMR (400 MHz, $CDCl_3$): δ = 1.32–1.21 (m, 62H, C<u>H</u>$_2$), 0.88 ppm (t, ^3J = 6.7 Hz, 6H, C<u>H</u>$_3$); ^{13}C NMR (100 MHz, $CDCl_3$): δ = 32.02, 29.79, 29.45, 22.78, 14.18 ppm.

Synthesis of tetratetraconta-1,11,22,33-tetraene (M_{44} alkene) (**70**).

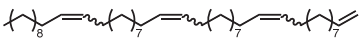

Phosphonium salt **67** (446 mg, 0.93 mmol, 1.1 eq) and M_{33} aldehyde **50** (401 mg, 0.85 mmol, 1 eq) were coupled using general method **A**. The crude product was obtained as a light brown oil and further purified by automated column chromatography using heptane/EtOAc (gradient 100/0 to 95/5) as eluent. The pure product was obtained as a colorless oil (146 mg, 28%). ^{1}H NMR (400 MHz, $CDCl_3$): δ = 5.81 (ddt, ^3J = 16.9 Hz, ^3J = 10.1 Hz, ^3J = 6.6 Hz, 1H, CH_2=C<u>H</u>-CH_2), 5.40–5.29 (m, 6H, CH_2-C<u>H</u>=C<u>H</u>-CH_2), 5.03–4.90 (m, 2H, C<u>H</u>$_2$=CH-CH_2), 2.08–1.93 (m, 14H,

C<u>H</u>$_2$-CH=CH-C<u>H</u>$_2$ and CH$_2$=CH-C<u>H</u>$_2$), 1.41–1.20 (m, 56H, C<u>H</u>$_2$), 0.88 ppm (t, ^3J = 6.7 Hz, 3H, CH$_2$-C<u>H</u>$_3$); ^{13}C NMR (100 MHz, CDCl$_3$): δ = 139.38, 130.05, 130.03, 114.24, 33.98, 32.77, 32.09, 29.94, 29.92, 29.83, 29.81, 29.79, 29.73, 29.66, 29.64, 29.52, 29.49, 29.46, 29.31, 29.11, 27.58, 27.38, 22.86, 14.28 ppm.

Synthesis of nonahexaconta-1,3,14,25,36,47-hexaene (M_{69} alkene) (**71**).

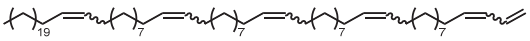

Phosphonium salt **65** (111 mg, 0.289 mmol, 1.05 eq) and M_{44} aldehyde **53** (257 mg, 0.275 mmol, 1 eq) were coupled using general method **A**. The waxy, orange residue was purified by automated column chromatography, using heptane as eluent, giving the pure product as a colorless oil (120 mg, 46%). ^{1}H NMR (400 MHz, CDCl$_3$): δ = 6.65 (ddd, ^3J = 16.9 Hz, ^3J = 11.2 Hz, ^3J = 10.1 Hz, ~0.5H, CH$_2$=C<u>H</u>-CH=CH-CH$_2$ (*cis*)), 6.31 (ddd, ^3J = 16.9 Hz, ^3J = 10.2 Hz, ~0.5H, CH$_2$=C<u>H</u>-CH=CH-CH$_2$ (*trans*)), 6.10–5.96 (m, 1H, CH$_2$=CH-C<u>H</u>=CH-CH$_2$), 5.71 (dt, ^3J = 14.6 Hz, ^3J = 7.0 Hz, ~0.5H, CH$_2$=CH-CH=C<u>H</u>-CH$_2$ (*trans*)), 5.46 (dt, ^3J = 11.1 Hz, ^3J = 7.8 Hz, ~0.5H, CH$_2$=CH-CH=C<u>H</u>-CH$_2$ (*cis*)), 5.41–5.30 (m, 8H, CH$_2$-C<u>H</u>=C<u>H</u>-CH$_2$), 5.18 (dd, ^3J = 16.9 Hz, ^3J = 2.0 Hz, 1H, C<u>H</u>$_2$=CH-CH=CH-CH$_2$ (*cis*,*cis*)), 5,09 (dd, ^3J = 11,2 Hz, ^3J = 2.0 Hz, 1H, C<u>H</u>$_2$=CH-CH=CH-CH$_2$ (*cis*,*trans*)), 5,08 (dd, ^3J = 16,9 Hz, ^3J = 1.7 Hz, 1H, C<u>H</u>$_2$=CH-CH=CH-CH$_2$ (*trans*,*cis*)), 4,95 (dd, ^3J = 11,2 Hz, ^3J = 1,7 Hz, 1H, C<u>H</u>$_2$=CH-CH=CH-CH$_2$ (*trans*,*trans*)), 2.23–2.04 (m, 2H, C<u>H</u>$_2$-CH=CH-C<u>H</u>$_2$), 2.06–1.95 (m, 108H, C<u>H</u>$_2$), 0,89 ppm (t , ^3J = 6,9 Hz, 3H, C<u>H</u>$_3$); ^{13}C NMR (100 MHz, CDCl$_3$): δ = 137.51, 135.70, 133.16, 132.49, 131.02, 130.49, 130.04, 130.02, 129.28, 116.77, 114.67, 32.79, 32.74, 32.11, 29.96, 29.89, 29.85, 29.81, 29.80, 29.76, 29.72, 29.68, 29.55, 29.51, 29.48, 29.42, 29.40, 29.38, 29.37, 27.91, 27.39, 22.87, 14.28 ppm.

Synthesis of hexahexaconta-1,5,16,27,38,49,60,65-octaene (M_{66} bisalkene) (**72**).

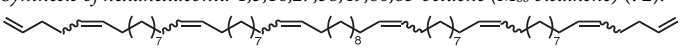

Phosphonium salt **66** (291 mg, 0.708 mmol, 2.2 eq) and M_{56} bisaldehyde **61** (260 mg, 0.322 mmol, 1 eq) were coupled using general method **A** (0.740 mmol, 2.3 eq of KO*t*Bu were used). The waxy, orange residue was purified by automated column chromatography, using heptane as eluent, giving the pure product as a colorless oil (212 mg, 72%). ^{1}H NMR (400 MHz, CDCl$_3$): δ = 5.83 (ddt, ^3J = 16.7 Hz, ^3J = 10.3 Hz, ^3J = 6.3 Hz, 2H, CH$_2$=C<u>H</u>-CH$_2$), 5.44–5.30 (m, 12H, CH$_2$-C<u>H</u>=C<u>H</u>-CH$_2$), 5.06–4.93 (m, 4H, C<u>H</u>$_2$=CH-CH$_2$), 2.18–1.92 (m, 28H, C<u>H</u>$_2$-CH=CH-C<u>H</u>$_2$ and CH$_2$=CH-C<u>H</u>$_2$), 2.37–1.22 ppm (m, 72H, C<u>H</u>$_2$); ^{13}C NMR (100 MHz, CDCl$_3$): δ = 138.68, 130.63, 130.51, 130.04, 128.97, 114.67, 77.48, 77.16, 76.84, 34.04, 32.77, 32.04, 29.94, 29.87, 29.82, 29.78, 29.73, 29.72, 29.49, 29.47, 29.18, 27.42, 27.38, 26.83 ppm;

Synthesis of [**Si$_7$-M$_{11}$=M$_{22}$**] (**73a**).

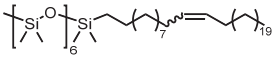

Alkene **69** (85 mg, 0.184 mmol, 1 eq) and Si$_7$ hydride **14a** (96 mg, 0.184 mmol, 1 eq) were coupled using general method **B**. The crude material was purified by automated column chromatography using heptane/chloroform (gradient 100/0 to 95/5 in 10 CV) as eluent. The pure title compound was obtained as a colorless oil (107 mg, 59%). ^{1}H NMR (400 MHz, CDCl$_3$): δ = 5.41–5.31 (m, 2H, CH$_2$-C<u>H</u>=C<u>H</u>-CH$_2$), 2.07–1.94 (m, 4H, C<u>H</u>$_2$-CH=CH-C<u>H</u>$_2$), 1.38–1.20 (m, 54H, C<u>H</u>$_2$), 0.89 (t, ^3J = 6.8 Hz, 3H, C<u>H</u>$_3$-CH$_2$), 0.57–0.51 (m, 2H, C<u>H</u>$_2$-Si), 0.10 (s, 9H, Si(C<u>H</u>$_3$)$_3$), 0.09 (s, 6H, Si(C<u>H</u>$_3$)$_2$), 0.08 (s, 6H, Si(C<u>H</u>$_3$)$_2$), 0.08 (s, 6H, Si(C<u>H</u>$_3$)$_2$), 0.07 (s, 6H, Si(C<u>H</u>$_3$)$_2$), 0.06 (s, 6H, Si(C<u>H</u>$_3$)$_2$), 0.06 ppm (s, 6H, Si(C<u>H</u>$_3$)$_2$); ^{13}C NMR (100 MHz, CDCl$_3$): δ = 130.52, 130.06, 33.68, 32.82, 32.13, 30.00, 29.98, 29.91, 29.87, 29.84, 29.79, 29.77, 29.74, 29.62, 29.57, 29.55, 29.52, 29.40, 29.38, 27.42, 27.41, 23.43, 22.89, 18.47, 14.30, 1.96, 1.35, 1.32, 1.24, 0.37 ppm; MS (MALDI-TOF): m/z calcd for $C_{48}H_{110}O_6Si_7$+Na$^+$: 1001.66 [M+Na]$^+$; found: 1001.65.

Synthesis of [**Qg$_{//}$+K$_{//}$; K$_{00}$**] (**51`**).

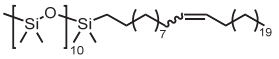

Alkene **47** (72 mg, 0.156 mmol, 1 eq) and Si$_{11}$ hydride **/2`** (127 mg, 0.156 mmol, 1 eq) were coupled using general method **@**. The crude material was purified by automated column chromatography using heptane/chloroform (100/0 for 3 CV, then gradient 100/0 to 95/5 in 10 CV) as eluent. The pure title compound was obtained as a colorless oil (122 mg, 61%). ^{1}H NMR (400 MHz, $CDCl_3$): δ = 5.41–5.33 (m, 2H, CH_2-C$\underline{H}$=C$\underline{H}$-CH_2), 2.08–1.93 (m, 4H, C$\underline{H}_2$-CH=CH-C$\underline{H}_2$), 1.39–1.20 (m, 54H, C$\underline{H}_2$), 0.89 (t, ^3J = 6.7 Hz, 3H, C$\underline{H}_3$-CH_2), 0.57–0.51 (m, 2H, C$\underline{H}_2$-Si), 0.10 (s, 9H, Si(C$\underline{H}_3$)$_3$), 0.09 (s, 6H, Si(C$\underline{H}_3$)$_2$), 0.08 (s, 6H, Si(C$\underline{H}_3$)$_2$), 0.08 (s, 6H, Si(C$\underline{H}_3$)$_2$), 0.07 (s, 6H, Si(C$\underline{H}_3$)$_2$), 0.06 (s, 6H, Si(C$\underline{H}_3$)$_2$), 0.06 ppm (s, 6H, Si(C$\underline{H}_3$)$_2$); ^{13}C NMR (100 MHz, $CDCl_3$): δ = 130.53, 130.06, 33.69, 32.83, 32.14, 32.10, 30.00, 29.99, 29.92, 29.87, 29.85, 29.80, 29.78, 29.63, 29.58, 29.55, 29.53, 29.41, 29.39, 27.43, 27.41, 23.44, 22.90, 18.47, 14.30, 1.96, 1.35, 1.32, 1.24, 0.37 ppm; MS (MALDI-TOF): *m/z* calcd for $C_{56}H_{134}O_{10}Si_{11}+Na^+$: 1297.734 $[M+Na]^+$; found: 1297.75.

Synthesis of [**Qg$_{/3}$+K$_{//}$; K$_{00}$**] (**51a**).

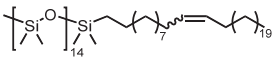

Alkene **47** (97 mg, 0.210 mmol, 1 eq) and Si$_{15}$ hydride **/2a** (234 mg, 0.210 mmol, 1 eq) were coupled using general method **@**. The crude material was purified by automated column chromatography using heptane/chloroform (100/0 for 5 CV, then gradient 100/0 to 96/4 in 10 CV) as eluent. The pure title compound was obtained as a colorless oil (269 mg, 81%). ^{1}H NMR (400 MHz, $CDCl_3$): δ = 5.40–5.32 (m, 2H, CH_2-C$\underline{H}$=C$\underline{H}$-CH_2), 2.06–1.93 (m, 4H, C$\underline{H}_2$-CH=CH-C$\underline{H}_2$), 1.37–1.21 (m, 54H, C$\underline{H}_2$), 0.88 (t, ^3J = 6.8 Hz, 3H, C$\underline{H}_3$), 0.56–0.50 (m, 2H, C$\underline{H}_2$-Si), 0.12–0.02 ppm (m, 93H, Si(C$\underline{H}_3$)$_2$); ^{13}C NMR (100 MHz, $CDCl_3$): δ = 130.51, 130.05, 33.65, 32.79, 32.10, 32.05, 29.97, 29.95, 29.87, 29.83, 29.81, 29.76, 29.74, 29.60, 29.53, 29.52, 29.49, 29.35, 29.19, 27.39, 27.38, 23.40, 22.86, 18.44, 14.28, 1.94, 1.58, 1.33, 1.30, 1.21, 0.84, 0.35 ppm; MS (MALDI-TOF): *m/z* calcd for $C_{64}H_{158}O_{14}Si_{15}+Na^+$: 1593.81 $[M+Na]^+$; found: 1593.83.

Synthesis of [**Qg$_5$+K$_{11}$**].

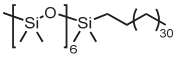

Unsaturated BCO **51_** (87 mg, 0.089 mmol, 1 eq) was hydrogenated at room temperature according to general method **A**. The product was obtained as a semi-transparent, white wax (88 mg, quant.). ^{1}H NMR (400 MHz, $CDCl_3$): δ = 1.36–1.20 (m, 62H, C$\underline{H}_2$), 0.89 (t, ^3J = 6.8 Hz, 3H, C$\underline{H}_3$-CH_2), 0.57–0.50 (m, 2H, C$\underline{H}_2$-Si), 0.10 (s, 9H, Si(C$\underline{H}_3$)$_3$), 0.09 (s, 6H, Si(C$\underline{H}_3$)$_2$), 0.08 (s, 6H, Si(C$\underline{H}_3$)$_2$), 0.08 (s, 6H, Si(C$\underline{H}_3$)$_2$), 0.07 (s, 6H, Si(C$\underline{H}_3$)$_2$), 0.06 (s, 6H, Si(C$\underline{H}_3$)$_2$), 0.05 ppm (s, 6H, Si(C$\underline{H}_3$)$_2$); ^{13}C NMR (100 MHz, $CDCl_3$): δ = 33.67, 32.13, 29.90, 29.84, 29.62, 29.57, 23.42, 22.89, 18.46, 14.30, 2.26, 1.96, 1.35, 1.32, 1.24, 0.37 ppm; MS (MALDI-TOF): m/z calcd for $C_{48}H_{112}O_6Si_7+Na^+$: 1003.67 $[M+Na]^+$; found: 1003.68.

Synthesis of [**Qg$_{//}$+K$_{11}$**].

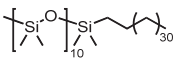

Unsaturated BCO **51`** (99 mg, 0.078 mmol, 1 eq) was hydrogenated at room temperature according to general method **A**. The product was obtained as a semi-transparent, white wax (93 mg, 94%). ^{1}H NMR (400 MHz, $CDCl_3$): δ = 1.36–1.19 (m, 62H, C$\underline{H}_2$), 0.89 (t, ^3J = 6,8 Hz, 3H, C$\underline{H}_3$-CH_2), 0.56–0.51 (m, 2H, C$\underline{H}_2$-Si), 0.10 (s, 9H, Si(C$\underline{H}_3$)$_3$), 0.08 (s, 30H, Si(C$\underline{H}_3$)$_2$), 0.08 (s, 6H, Si(C$\underline{H}_3$)$_2$), 0.08 (s, 6H, Si(C$\underline{H}_3$)$_2$), 0.07 (s, 6H, Si(C$\underline{H}_3$)$_2$), 0.06 (s, 6H, Si(C$\underline{H}_3$)$_2$), 0.05 ppm (s, 6H, Si(C$\underline{H}_3$)$_2$); ^{13}C NMR (100 MHz, $CDCl_3$): δ = 33.67, 32.13, 29.94–29.90, 29.86, 29.84, 29.62, 29.56,

23.42, 22.89, 18.46, 14.30, 1.96, 1.35, 1.32, 1.23, 0.37.ppm; MS (MALDI-TOF): *m/z* calcd for $C_{56}H_{136}O_{10}Si_{11}+Na^+$: 1299.75 $[M+Na]^+$; found: 1299.75.

Synthesis of [**Si$_{15}$-M$_{33}$**].

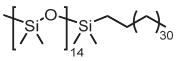

Unsaturated BCO **73c** (130 mg, 0.082 mmol, 1 eq) was hydrogenated at room temperature according to general method **C**. The product was obtained as a semi-transparent, white wax (119 mg, 92%). ^{1}H NMR (400 MHz, $CDCl_3$): δ = 1.35–1.21 (m, 62H, C$\underline{H}_2$), 0.89 (t, ^3J = 6.7 Hz, 3H, C$\underline{H}_3$-CH$_2$), 0.57–0.51 (m, 2H, C$\underline{H}_2$-Si), 0.12–0.02 ppm (m, 93H, Si(C$\underline{H}_3$)$_2$); ^{13}C NMR (100 MHz, $CDCl_3$): δ = 33.67, 32.13, 29.95–29.85, 29.62, 29.56, 23.42, 22.89, 18.46, 14.30, 1.96, 1.59 (^{29}Si satellite), 1.35, 1.31, 1.22, 0.85 (^{29}Si satellite) ppm; MS (MALDI-TOF): *m/z* calcd for $C_{64}H_{160}O_{14}Si_{15}+Na^+$: 1595.83 $[M+Na]^+$; found: 1595.83.

Synthesis of [**Si$_{15}$-M$_3$=M$_{11}$=M$_{11}$=M$_{11}$=M$_{22}$**] (**74c**).

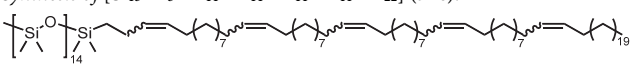

Alkene **71** (40 mg, 0.042 mmol, 1.05 eq) and Si$_{15}$ hydride **14c** (44 mg, 0.040 mmol, 1 eq) were coupled using general method **B**. The crude material was purified by automated column chromatography using heptane/chloroform (gradient 100/0 to 94/6 in 10 CV) as eluent. The pure title compound was obtained as a colorless oil (47 mg, 57%). ^{1}H NMR (400 MHz, $CDCl_3$): δ = 5.46–5.15 (m, 10H, CH$_2$-C$\underline{H}$=C$\underline{H}$-CH$_2$), 2.09–1.92 (m, 20H, C$\underline{H}_2$-CH=CH-C$\underline{H}_2$), 1.45–1.11 (m, 94H, C$\underline{H}_2$), 0.89 (t, ^3J = 6.9 Hz, 3H, CH$_3$), 0.65–0.57 (m, 2H, CH$_2$-C$\underline{H}_2$-Si(CH$_3$)$_2$), 0.13 to −0.02 ppm (m, 93H, Si(C$\underline{H}_3$)$_2$); ^{13}C NMR (100 MHz, $CDCl_3$): δ = 130.51, 130.06, 130.04, 33.17, 32.79, 32.11, 32.06, 29.96, 29.88, 29.84, 29.81, 29.77, 29.75, 29.72, 29.54, 29.53, 29.50, 29.37, 29.20, 27.40, 22.87, 18.37, 14.28, 1.95, 1.58, 1.34, 1.30, 1.21, 0.84, 0.41 ppm; MS (MALDI-TOF): m/z calcd for $C_{110}H_{222}O_{14}Si_{15}+Na^+$: 2090.31 $[M+Na]^+$; found: 2090.34.

Synthesis of [**Si$_{23}$-M$_3$=M$_{11}$=M$_{11}$=M$_{11}$=M$_{22}$**] (**74e**).

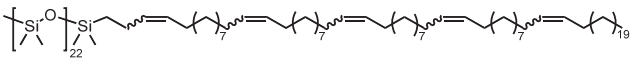

Alkene **71** (21 mg, 0.022 mmol, 1.05 eq) and Si$_{23}$ hydride **14e** (36 mg, 0.21 mmol, 1 eq) were coupled using general method **B**. The crude material was purified by automated column chromatography using heptane/chloroform (gradient 100/0 to 94/6 in 10 CV) as eluent. The pure title compound was obtained as a colorless oil (39 mg, 69%). ^{1}H NMR (400 MHz, $CDCl_3$): δ = 5.45–5.15 (m, 10H, CH$_2$-C$\underline{H}$=C$\underline{H}$-CH$_2$), 2.10–1.92 (m, 20H, C$\underline{H}_2$-CH=CH-C$\underline{H}_2$), 1.48–1.10 (m, 94H, C$\underline{H}_2$), 0.88 (t, ^3J = 6.9 Hz, 3H, C$\underline{H}_3$), 0.65–0.57 (m, 2H, CH$_2$-C$\underline{H}_2$-Si(CH$_3$)$_2$), 0.14 to −0.02 ppm (m, 141H, Si(C$\underline{H}_3$)$_2$); ^{13}C NMR (100 MHz, $CDCl_3$): δ = 130.51, 130.07, 130.04, 33.17, 32.79, 32.10, 32.06, 29.96, 29.88, 29.84, 29.80, 29.77, 29.75, 29.71, 29.54, 29.50, 29.36, 27.39, 22.86, 14.28, 1.94, 1.57, 1.33, 1.30, 1.20, 0.83, 0.45 ppm; MS (MALDI-TOF): m/z calcd for $C_{116}H_{270}O_{22}Si_{23}+Na^+$: 2682.46 $[M+Na]^+$; found: 2682.51.

Synthesis of [**Si$_{15}$-M$_{69}$**].

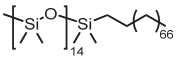

Unsaturated BCO **73c** (47 mg, 0.047 mmol, 1 eq) was hydrogenated at 60 °C according to general method **C**. After completion of the reaction (3 h), the solvent was removed in *vacuo* and the residue dissolved in chloroform, and the resulting black suspension was filtered hot (~45 °C) through Celite. The Celite was rinsed with warm chloroform (3 × 5 mL). The combined filtrates were concentrated in *vacuo*, giving the pure product as a white, waxy solid (47 mg, 99%). ^{1}H NMR (400 MHz, $CDCl_3$): δ = 1.35–1.13 (m, 134H, C$\underline{H}_2$), 0.88 (m, ^3J = 6.9 Hz, 3H, C$\underline{H}_3$), 0.64–0.57 (m, 2H, CH$_2$-C$\underline{H}_2$-Si(CH$_3$)$_2$), 0.11–0.01 ppm (m, 93H, Si(C$\underline{H}_3$)$_2$); ^{13}C NMR (100 MHz, $CDCl_3$): δ = 32.09, 29.87,

29.53, 22.86, 14.28, 1.94, 1.57, 1.33, 1.30, 1.21, 0.84, 0.47 ppm; MS (MALDI-TOF): m/z calcd for $C_{11}H_{232}O_{14}Si_{15}+Na^+$: 2100.39 $[M+Na]^+$; found: 2100.39.

Synthesis of [**Qg$_{01}$+K$_{47}$**].

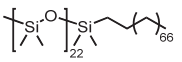

Unsaturated BCO **52c** (39 mg, 0.015 mmol, 1 eq) was hydrogenated at 60 °C according to general method **A**. After completion of the reaction (3 h), the solvent was removed in *vacuo* and the residue dissolved in chloroform, and the resulting black suspension was filtered through Celite. The Celite was rinsed with chloroform (3 × 5 mL). The combined filtrates were concentrated in *vacuo*, giving the pure product as a white, waxy solid (21 mg, 54%). ^{1}H NMR (400 MHz, $CDCl_3$): δ = 1.37–1.12 (m, 134H, C$\underline{H}_2$), 0.88 (m, ^3J = 6.9 Hz, 3H, C$\underline{H}_3$), 0.65–0.57 (m, 2H, CH_2-C$\underline{H}_2$-Si$(CH_3)_2$), 0.12 to −0.01 ppm (m, 141H, Si(C$\underline{H}_3)_2$); MS (MALDI-TOF): m/z calcd for $C_{116}H_{280}O_{22}Si_{23}+Na^+$: 2692.54 $[M+Na]^+$; found: 2692.52.

Synthesis of [**Qg$_5$+K$_3$; K$_{//}$; K$_{//}$; K$_{/0}$; K$_{//}$; K$_{//}$; K$_3$+Qg$_5$**] (**53**).

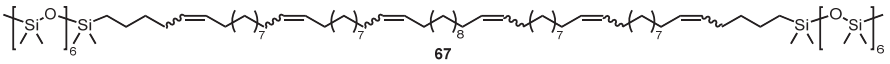

67

Alkene **50** (97 mg, 0.106 mmol, 1 eq) and Si$_7$ hydride **/2_** (116 mg, 0.223 mmol, 2.1 eq) were coupled using general method **@**. The crude material was first purified by automated column chromatography using heptane/EtOAc (gradient 100/0 to 95/5 in 10 CV) as eluent. The purest fractions were combined and further purified by automated column chromatography using heptane/chloroform (gradient 95/5 to 85/15 in 10 CV) as eluent The pure title compound was obtained as a colorless oil (120 mg, 58%). ^{1}H NMR (400 MHz, $CDCl_3$): δ = 5.41–5.32 (m, 12H, CH_2-C$\underline{H}$=C$\underline{H}$-CH_2), 2.05–1.92 (m, 24H, C$\underline{H}_2$-CH=CH-C$\underline{H}_2$), 1.39–1.23 (m, 80H, C$\underline{H}_2$), 0.57–0.50 (m, 4H, CH_2-C$\underline{H}_2$-Si$(CH_3)_2$), 0.11–0.02 ppm (m, 90H, Si(C$\underline{H}_3)_2$); ^{13}C NMR (100 MHz, $CDCl_3$): δ = 130.50, 130.04, 33.67, 32.78, 29.95, 29.84, 29.73, 29.50, 29.36, 27.38, 27.16, 23.10, 18.34, 1.95, 1.34, 1.31, 1.23, 0.36 ppm; MS (MALDI-TOF): *m/z* calcd for $C_{96}H_{210}O_{12}Si_{14}+Na^+$: 1970.25 $[M+Na]^+$; found: 1970.38.

Synthesis of [**Qg$_5$+K$_{44}$+Qg$_5$**].

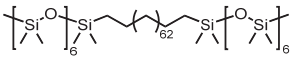

Unsaturated BCO **53** (87 mg, 0.045 mmol, 1 eq) was hydrogenated at 70 °C according to general method **A**. The product was obtained as a flaky, white solid (67 mg, 77%). ^{1}H NMR (400 MHz, $CDCl_3$): δ = 1.35–1.21 (m, 128H, C$\underline{H}_2$), 0.57–0.50 (m, 4H, CH_2-C$\underline{H}_2$-Si$(CH_3)_2$), 0.11–0.03 ppm (m, 90H, Si(C$\underline{H}_3)_2$); ^{13}C NMR (100 MHz, $CDCl_3$): δ = 33.64, 29.87, 29.59, 23.39, 18.43, 1.95, 1.34, 1.31, 1.23, 0.35 ppm; MS (MALDI-TOF): *m/z* calcd for $C_{96}H_{222}O_{12}Si_{14}+Na^+$: 1982.34 $[M+Na]^+$; found: 1982.44.

Synthesis of [**K$_{00}$; K$_{//}$+Qg$_{/4}$+K$_{//}$; K$_{00}$**] (**54**).

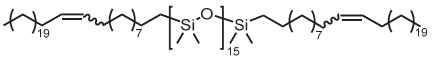

Alkene **47** (220 mg, 0.48 mmol, 2.2 eq) and H-Si$_{16}$-H **/6e** (272 mg, 1.23 mmol, 1 eq) were coupled using general method **@**. The crude material was purified by automated column chromatography using heptane/chloroform (gradient 100/0 to 95/5 in 10 CV) as eluent. The pure title compound was obtained as a colorless oil (345 mg, 35%). ^{1}H NMR (400 MHz, $CDCl_3$): δ = 5.36 (dt, ^3J = 14.4 Hz, ^3J = 4.8 Hz, 4H, CH_2-C$\underline{H}$=C$\underline{H}$-CH_2), 2.05–1.93 (m, 8H, C$\underline{H}_2$-CH=CH-C$\underline{H}_2$), 1.38–1.20 (m, 104H, C$\underline{H}_2$), 0.88 (t, ^3J = 6.4 Hz, 6H, C$\underline{H}_3$),

0.57–0.50 (m, 4H, CH_2-C$\underline{H}_2$-Si$(CH_3)_2$), 0.12–0.02 ppm (m, 96H, Si$(CH_3)_2$); ^{13}C NMR (100 MHz, CDCl3): δ = 130.04, 32.09, 29.86, 29.82, 29.52, 22.85, 18.43, 14.28, 1.33, 1.20, 0.35 ppm; MS (MALDI-TOF): *m/z* calcd for $C_{98}H_{226}O_{15}Si_{16}+Na^+$: 2114.31 $[M+Na]^+$; found: 2114.40.

Synthesis of [**M$_{33}$-Si$_{16}$-M$_{33}$**].

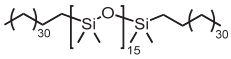

Unsaturated BCO **76** (204 mg, 0.097 mmol, 1 eq) was hydrogenated at room temperature according to general method **C**. After full conversion of the double bonds, the crude reaction mixture was not filtered, but the solvent was removed in a stream of nitrogen. The black-gray residue was suspended in heptane and directly purified by automated column chromatography using heptane/EtOAc (gradient 99/1 to 95/5 in 10 CV) as eluent. The product was obtained as a colorless oil (202 mg, 97%). ^{1}H NMR (400 MHz, $CDCl_3$): δ = 1.34–1.20 (m, 124H, C$\underline{H}_2$), 0.88 (t, ^{3}J = 6.7 Hz, 6H, CH_2-C$\underline{H}_3$), 0.57–0.51 (m, 4H, CH_2-CH_2-Si$(CH_3)_2$), 0.11–0.03 ppm (m, 96H, Si$(CH_3)_2$); ^{13}C NMR (100 MHz, $CDCl_3$): δ = 33.66, 32.09, 29.86, 29.82, 29.52, 23.39, 22.85, 18.43, 14.28, 1.33, 1.20, 0.35 ppm; MS (MALDI-TOF): *m/z* calcd for $C_{98}H_{230}O_{15}Si_{16}$+$Na^+$: 2118.34 [M+Na]$^+$; found: 2118.39.

Synthesis of HO-Si$_{12}$-H (**80**).

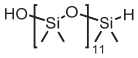

Silanol HO-Si$_8$-OH **17g** (1.071 g, 1.752 mmol, 1 eq) was dissolved in dry toluene (10 mL) in a 100 mL round-bottom flask under argon. Dry pyridine (~0.20 mL, ~ 2.5 mmol, 1.4 eq) was added, and the solution was cooled in an icebath. Chlorosilane **11** (0.556 g, 1.752 mmol, 1 eq) was dissolved in dry toluene (3 mL) and added dropwise (over a period of 10 min) to the cooled silanol solution. During the addition, a white suspension was formed. After the addition, the mixture was stirred for 3 h at room temperature. Afterward, the reaction mixture was diluted with toluene (50 mL) and washed with water (3 × 20 mL) to remove the white precipitate of pyridinium chloride. The organic layers was dried with $MgSO_4$, and the solvent was removed in *vacuo*. The remaining crude product was purified by automated column chromatography using heptane/DCM (gradient 100/0 to 20/80 in 10 CV) as eluent. The pure title compound was obtained as a colorless oil (692 mg, 44%). SEC ($CHCl_3$, RI) confirmed the absence of byproduct H-Si$_{16}$-H. ^{1}H NMR (400 MHz, $CDCl_3$): δ = 4.7 (h, ^{3}J = 2.7 Hz, 1H, Si$(CH_3)_2$-H), 2.24 (s, 1H, Si$(CH_3)_2$-OH), 0.20–0.17 (m, 6H, Si$(CH_3)_2$-H), 0.15–0.13 (m, 6H, Si$(CH_3)_2$-OH), 0.11–0.05 (m, 60H, Si$(CH_3)_2$); ^{13}C NMR (100 MHz, $CDCl_3$): δ = 1.21, 1.18, 1.15, 1.01, 0.84, 0.47 ppm;

Synthesis of HO-Si$_{12}$-M$_{11}$-M$_{11}$=M$_{11}$=M$_{11}$ (**81**).

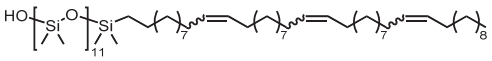

Alkene **70** (110 mg, 0.180 mmol, 1.1 eq) and HO-Si$_{12}$-H **80** (146 mg, 0.164 mmol, 1 eq) were coupled using general method **B**. The crude material (a dark brown oil) was purified by automated column chromatography using heptane/EtOAc (gradient 100/0 to 90/10 in 10 CV) as eluent. The pure title compound was obtained as a colorless oil (203 mg, 75%). ^{1}H NMR (400 MHz, $CDCl_3$): δ = 5.41–5.30 (m, 6H, CH_2-C$\underline{H}$=C$\underline{H}$-CH_2), 2.26 (s, 1H, Si$(CH_3)_2$-O$\underline{H}$), 2.08–1.93 (m, 12H, C$\underline{H}_2$-CH=CH-C$\underline{H}_2$), 1.40–1.20 (m, 60H, C$\underline{H}_2$), 0.88 (t, ^{3}J = 6.6 Hz, 3H, C$\underline{H}_3$), 0.57–0.50 (m, 2H, CH_2-C$\underline{H}_2$-Si$(CH_3)_2$), 0.14 (s, 6H, Si$(C\underline{H}_3)_2$-OH), 0.12–0.04 ppm (m, 66H, Si$(C\underline{H}_3)_2$); ^{13}C NMR (100 MHz, $CDCl_3$): δ = 130.51, 130.06, 130.04, 33.66, 32.79, 32.10, 29.98, 29.95, 29.88, 29.84, 29.82, 29.80, 29.78, 29.74, 29.60, 29.54, 29.50, 29.35, 27.40, 27.39, 23.41, 22.87, 18.44, 14.29, 1.59 (^{29}Si satellite), 1.34, 1.22, 1.15, 0.84 (^{29}Si satellite) , 0.48, 0.35 ppm; MS (MALDI-TOF): *m/z* calcd for $C_{68}H_{156}O_{12}Si_{12}$+$Na^+$: 1523.873 [M+Na]$^+$; found: 1523.92.

Synthesis of H-Si$_{16}$-M$_{11}$=M$_{11}$=M$_{11}$=M$_{11}$ (**82**).

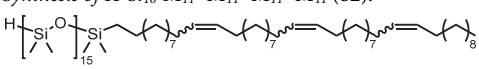

Chlorosilane **11** (47 mg, 0.150 mmol, 1.5 eq) and dry pyridine (13 mg, 0.170 mmol, 1.7 eq) were dissolved in dry toluene (0.5 mL) in a 10 mL Schlenk tube under argon. The mixture was cooled in ice water, and a solution of silanol **81** (150 mg, 0.100 mmol, 1 eq) in dry toluene (0.5 mL) was added dropwise, resulting in the formation of a

white precipitate. Stirring was continued at room temperature. After 2.5 h, the reaction mixture was diluted with toluene (5 mL) and washed with water (3 × 3 mL). The slightly turbid toluene layer was dried with $MgSO_4$, and the solvent was removed in *vacuo*. The remaining light yellow oil was dissolved in heptane (4 mL) in a 50 mL round-bottom flask and washed with acetonitrile (4 × 2 mL) to remove low-MW siloxanes (the acetonitrile was carefully removed with a glass pipette). The heptane layer was concentrated in *vacuo*. The remaining crude product was purified by automated column chromatography using heptane/DCM (gradient 100/0 to 20/80 in 10 CV) as eluent. The pure title compound was obtained as a colorless oil (142 mg, 80%). ^{1}H NMR (400 MHz, $CDCl_3$): δ = 5.45–5.30 (m, 6H, CH_2-C<u>H</u>=C<u>H</u>-CH_2), 4.72 (h, ^3J = 2.8 Hz, 1H, Si(CH_3)$_2$-<u>H</u>), 2.11–1.91 (m, 12H, C<u>H</u>$_2$-CH=CH-C<u>H</u>$_2$), 1.46–1.19 (m, 60H, C<u>H</u>$_2$), 0.89 (t, ^3J = 6.7 Hz, 3H, C<u>H</u>$_3$), 0.58–0.51 (m, 2H, CH_2-C<u>H</u>$_2$-Si(CH_3)$_2$), 0.21–0.18 (m, 6H, Si(C<u>H</u>$_3$)$_2$-H), 0.12–0.04 ppm (m, 90H, Si(C<u>H</u>$_3$)$_2$); ^{13}C NMR (100 MHz, $CDCl_3$): δ = 130.53, 130.07, 130.05, 33.68, 32.81, 32.13, 32.09, 30.00, 29.98, 29.91, 29.89, 29.87, 29.84, 29.80, 29.77, 29.74, 29.70, 29.63, 29.57, 29.55, 29.52, 29.42, 29.38, 27.43, 27.41, 23.43, 22.89, 18.47, 14.30, 1.59 (^{29}Si satellite), 1.35, 1.22, 1.19, 1.02, 0.86, 0.37 ppm; MS (MALDI-TOF): *m/z* calcd for $C_{76}H_{180}O_{15}Si_{16}$+$Na^+$: 1803.953 [M+Na]$^+$; found: 1803.95.

Synthesis of M_{11}=M_{11}-Si_{16}-M_{11}=M_{11}=M_{11}=M_{11} (**77**).

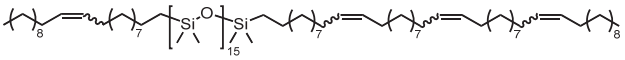

Alkene **68** (22 mg, 0.072 mmol, 1.2 eq) and silyl hydride H-Si_{16}-M_{11}=M_{11}=M_{11}=M_{11} **82** (107 mg, 0.060 mmol, 1 eq) were coupled using general method **B**. The crude material (a dark brown oil) was purified by automated column chromatography using heptane/DCM (gradient 100/0 to 80/20 in 10 CV) as eluent. The pure title compound was obtained as a colorless oil (34 mg, 27%). ^{1}H NMR (400 MHz, $CDCl_3$): δ = 5.44–5.28 (m, 8H, CH_2-C<u>H</u>=C<u>H</u>-CH_2), 2.06–1.92 (m, 16H, C<u>H</u>$_2$-CH=CH-C<u>H</u>$_2$), 1.38–1.21 (m, 92H, C<u>H</u>$_2$), 0.88 (t, ^3J = 6.6 Hz, 6H, C<u>H</u>$_3$), 0.57–0.49 (m, 4H, CH_2-C<u>H</u>$_2$-Si(CH_3)$_2$), 0.11–0.02 ppm (m, 96H, Si(C<u>H</u>$_3$)$_2$); ^{13}C NMR (100 MHz, $CDCl_3$): δ = 130.51, 130.05, 33.65, 32.78, 32.09, 29.96, 29.95, 29.87, 29.83, 29.81, 29.76, 29.73, 29.70, 29.67, 29.59, 29.53, 29.49, 29.39, 29.35, 27.38, 23.40, 22.86, 18.44, 14.28, 1.58 (^{29}Si satellite), 1.33, 1.21, 0.84 (^{29}Si satellite), 0.35 ppm; MS (MALDI-TOF): *m/z* calcd for $C_{98}H_{222}O_{15}Si_{16}^+Na^+$: 2110.2817 [M+Na]$^+$; found: 2110.3.

Synthesis of [**M_{22}-Si_{16}-M_{44}**].

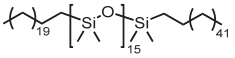

Unsaturated BCO **77** (34 mg, 0.0163 mmol, 1 eq) was hydrogenated at 60 °C according to general method **C**. After full conversion of the double bonds, the crude reaction mixture was not filtered, but the solvent was removed in a stream of nitrogen. The black-gray residue was suspended in heptane and directly purified by automated column chromatography using heptane/EtOAc (gradient 100/0 to 90/10 in 10 CV) as eluent. The product was obtained as a white solid (30 mg, 88%). ^{1}H NMR (400 MHz, $CDCl_3$): δ = 1.34–1.21 (m, 124H, C<u>H</u>$_2$), 0.88 (t, ^3J = 6.7 Hz, 6H, C<u>H</u>$_3$), 0.56–0.50 (m, 4H, CH_2-C<u>H</u>$_2$-Si(CH_3)$_2$), 0.11–0.02 ppm (m, 96H, Si(C<u>H</u>$_3$)$_2$); ^{13}C NMR (100 MHz, $CDCl_3$): δ = 33.64, 32.09, 29.87, 29.59, 29.53, 23.39, 22.86, 18.43, 14.28, 1.58 (^{29}Si satellite), 1.33, 1.21, 0.83 (^{29}Si satellite), 0.35 ppm; MS (MALDI-TOF): *m/z* calcd for $C_{98}H_{230}O_{15}Si_{16}$+$Na^+$: 2118.3443 [M+Na]$^+$; found: 2118.35;

5.7 References

(1) Jeong, G.; Yu, D. M.; Mapas, J. K. D.; Sun, Z.; Rzayev, J.; Russell, T. P. *Macromolecules* **2017**, *50*, 7148.

(2) Kwak, J.; Mishra, A. K.; Lee, J.; Lee, K. S.; Choi, C.; Maiti, S.; Kim, M.; Kim, J. K. *Macromolecules* **2017**, *50*, 6813.

(3) Nowak, S. R.; Hwang, W.; Sita, L. R. *J. Am. Chem. Soc.* **2017**, *139*, 5281.

(4) Oschmann, B.; Lawrence, J.; Schulze, M. W.; Ren, J. M.; Anastasaki, A.; Luo, Y.; Nothling, M. D.; Pester, C. W.; Delaney, K. T.; Connal, L. A.; McGrath, A. J.; Clark, P. G.; Bates, C. M.; Hawker, C. J. *ACS Macro Lett.* **2017**, *6*, 668.

(5) Carter, M. C. D.; Jennings, J.; Speetjens, F. W.; Lynn, D. M.; Mahanthappa, M. K. *Macromolecules* **2016**, *49*, 6268.

(6) Goodby, J. W.; Davis, E. J.; Mandle, R. J.; Cowling, S. J.; Goodby, J. W.; Davis, E. J.; Mandle, R. J.; Cowling, S. J. In *Handbook of Liquid Crystals*; Wiley-VCH Verlag GmbH & Co. KGaA: Weinheim, Germany, 2014; pp. 1–30.

(7) Tschierske, C. *J. Mater. Chem.* **1998**, *8*, 1485.

(8) Kato, T. *Science* **2002**, *295*, 2414.

(9) Nickmans, K.; Murphy, J. N.; de Waal, B.; Leclère, P.; Doise, J.; Gronheid, R.; Broer, D. J.; Schenning, A. P. H. J. *Adv. Mater.* **2016**, *28*, 10068.

(10) Zha, R. H.; de Waal, B. F. M.; Lutz, M.; Teunissen, A. J. P.; Meijer, E. W. *J. Am. Chem. Soc.* **2016**, *138*, 5693.

(11) Berrocal, J. A.; Zha, R. H.; de Waal, B. F. M.; Lugger, J. A. M.; Lutz, M.; Meijer, E. W. *ACS Nano* **2017**, *11*, 3733.

(12) Kim, H.-J.; Kim, T.; Lee, M. *Acc. Chem. Res.* **2011**, *44*, 72.

(13) Meisburger, S. P.; Thomas, W. C.; Watkins, M. B.; Ando, N. *Chem. Rev.* **2017**, *117*, 7615.

(14) DiMarzio, E. A.; Guttman, C. M.; Hoffman, J. D. *Macromolecules* **1980**, *13*, 1194.

(15) Flory, P. J. *J. Am. Chem. Soc.* **1962**, *84*, 2857.

(16) Vilgis, T.; Halperin, A. *Macromolecules* **1991**, *24*, 2090.

(17) Mandelkern, L. *Acc. Chem. Res.* **1990**, *23*, 380.

(18) Fritzsching, K. J.; Mao, K.; Schmidt-Rohr, K. *Macromolecules* **2017**, *50*, 1521.

(19) Pulst, M.; Schneemann, C.; Ruda, P.; Golitsyn, Y.; Grefe, A.-K.; Stühn, B.; Busse, K.; Reichert, D.; Kressler, J. *ACS Macro Lett.* **2017**, 1207.

(20) Piringer, O.-G.; Baner, A. L. *Plastic packaging : interactions with food and pharmaceuticals*; Wiley-VCH, 2008.

(21) Wutz, C.; Tanner, M. J.; Brookhart, M.; Samulski, E. T. *Macromolecules* **2017**, *50*, 9066.

(22) Mnyukh, Y. V. *J. Struct. Chem.* **1960**, *1*, 346.

(23) Karstedt, B. D. Platinum complexes of unsaturated siloxanes and platinum containing organopolysiloxanes. US3775452, 1973.

(24) Bidd, I.; Kelly, D. J.; Ottley, P. M.; Paynter, O. I.; Simmonds, D. J.; Whiting, M. C. *J. Chem. Soc. Perkin Trans. 1* **1983**, 1369.

(25) Igner, E.; Paynter, O. I.; Simmonds, D. J.; Whiting, M. C. *J. Chem. Soc. Perkin Trans. 1* **1987**, 2447.

(26) Bidd, I.; Holdup, D. W.; Whiting, M. C. *J. Chem. Soc. Perkin Trans. 1* **1987**, 2455.

(27) Adegoke, E. A.; Ephraim-Bassey, H.; Kelly, D. J.; Whiting, M. C. *J. Chem. Soc. Perkin Trans. 1* **1987**, 2465.

(28) Einhorn, J.; Einhorn, C.; Ratajczak, F.; Pierre, J.-L. *J. Org. Chem.* **1996**, *61*, 7452.

(29) Nicolaou, K. C.; Härter, M. W.; Gunzner, J. L.; Nadin, A. *European J. Org. Chem.* **1997**, *1997*, 1283.

(30) Markó, I. E.; Stérin, S.; Buisine, O.; Mignani, G.; Branlard, P.; Tinant, B.; Declercq, J.-P. *Science* **2002**, *298*, 204.

(31) Strobl, G.; Ewen, B.; Fischer, E. W.; Piesczek, W. *J. Chem. Phys.* **1974**, *61*, 5250.

(32) Asinger, F. *Paraffins : Chemistry and Technology*; First edit.; Pergamon Press, 1968.

(33) He, W.-N.; Xu, J.-T. *Prog. Polym. Sci.* **2012**, *37*, 1350.

(34) Nandan, B.; Hsu, J.-Y.; Chen, H.-L. *J. Macromol. Sci. Part C Polym. Rev.* **2006**, *46*, 143.

(35) Ungar, G. *J. Phys. Chem.* **1983**, *87*, 689.

(36) Sirota, E.; Singer, D. *J. Chem. Phys.* **1994**, *101*, 10873.
(37) Wentzel, N.; Milner, S. T. *J. Chem. Phys.* **2010**, *132*, 44901.
(38) Lynd, N. A.; Hamilton, B. D.; Hillmyer, M. A. *J. Polym. Sci. Part B Polym. Phys.* **2007**, *45*, 3386.
(39) Swales, T. G. E.; Domszy, R. C.; Beddoes, R. L.; Price, C.; Booth, C. *J. Polym. Sci. Polym. Phys. Ed.* **1985**, *23*, 1585.
(40) Hashimoto, T.; Tanaka, H.; Hasegawa, H. *Macromolecules* **1985**, *18*, 1864.
(41) Muller, A. *Proc. R. Soc. A Math. Phys. Eng. Sci.* **1928**, *120*, 437.
(42) Smith, A. E. *J. Chem. Phys.* **1953**, *21*, 2229.
(43) Milner, S. T. *J. Polym. Sci. Part B Polym. Phys.* **1994**, *32*, 2743.
(44) Yeates, S. G.; Booth, C. *Eur. Polym. J.* **1985**, *21*, 217.
(45) Ungar, G.; Stejny, J.; Keller, A.; Bidd, I.; Whiting, M. C. *Science* **1985**, *229*, 386.

♦ Epilogue ♦

Picture Perfect Polymers:
A New Design Feature?

"So, if you've ever made a block copolymer with a broad molecular weight distribution, don't throw it away. Send it to me instead."

—Marc A. Hillmyer, 2007.[1]

Picture Perfect Polymers

The question 'What is the effect of molecular uniformity on block co-polymer (BCP) self-assembly?' remained an important trigger for all the research described in this thesis. Will the elimination of every remaining bit of dispersity alter or improve BCP phase behavior, and, if so, do these new self-assembly characteristics counterbalance the increased synthetic effort to generate the materials?

We showed that robust synthetic strategies and strict purity control of the intermediate compounds allows the fabrication of oligomeric blocks of diverse molecular make-up. Oligodimethylsiloxane (*o*DMS), oligolactic acid (*o*LA), and oligomethylene (*o*M), as well as their derived block co-oligomers (BCOs) could be obtained and were studied in detail, despite the great synthetic endeavor initially required to start exploring this intriguing field of discrete-length (co-)oligomers. Admittedly, the current purification protocols make kilogram-scale synthesis of the materials still challenging, but are most certainly not as limiting as many solid-phase strategies and also do not require improvement at this stage of research. Moreover, the obtained molecular weights of up to 6.9 kDa show that, albeit laborious, producing discrete-length compounds of considerable molecular weight—truly deserving the label 'polymer'—certainly is achievable.

In our view, block-copolymer self-assembly is well-understood on a mesoscale level. That is, the unified behavior of a large number of almost equal molecules, of which the average properties dictate the outcome of microphase segregation. Nevertheless, we would like to stress the importance of molecular details and the effect of non-uniformity, primarily in the case of low-MW BCPs or BCOs. Microphase separation of *o*DMS–*o*LA BCOs clearly is affected by dispersity. Part of the observed differences indeed confirmed predictions by earlier (theoretical) studies (see Chapter 3 for more details), but others—such as the improved organization and long-range order in microphase-segregated, uniform BCOs—were unprecedented observations. The study by Hawker and coworkers[2] and, later, Mahanthappa and coworkers[3] on other types of discrete and disperse BCOs further revealed the unpredictable behavior high χ–low N block copolymers that constitute different backbone types, which further accentuates the abovementioned impact of the exact molecular make-up of the self-assembling system. Obviously, in the limit of $N \rightarrow 1$, an exact

molecular understanding of BCP aggregation principles is key and calls for further research on perfectly defined materials.

If we amalgamate additional interactions (*e.g.*, those leading to crystalline properties) with BCO systems, chimera-type molecules are obtained that further diffuse the invisible boundary between small, self-assembling molecules and long, linear polymers. The two types of semicrystalline BCOs described in this thesis incorporated very simple crystalline blocks, comprised of enantiopure lactic acid or methylene residues (*i.e.*, molecules of which the crystallinity solely originated from a large number of weak (induced) dipole–dipole interactions). Totally unexpectedly, most of these materials microphase-separated into lamellar morphologies that were much more organized than those seen for conventional (semicrystalline) BCPs. We found that molecular perfection is of paramount importance for obtaining such high level of organization: incorporation of a disperse, crystalline block completely disrupted the ordered lamellar aggregates.

At first, we were puzzled by some of the apparent differences between the microphase segregation characteristics of semicrystalline *o*DMS–*o*LLA (Chapter 4) and *o*DMS–*o*M (Chapter 5). However, in hindsight, it seems that both self-assembly processes remain governed by very similar basic rules (for example, the restriction on the maximum block-link density). Here, the precise occupation of space by each molecular entity can no longer be ignored, in contrast to what is usually seen in descriptions of the phase-segregated state of 'traditional' block copolymers.

Although a conclusive image of the exact molecular organization within microphase-separated, low-MW (semicrystalline) BCOs does not exist yet, we propose that discrete-length materials offer a new platform that allows a very systematic exploration and better understanding of many (new) (multi)block copolymer designs. In a sense, we may argue that a part of polymer science should slowly evolve back to the traditional organic chemistry it once departed from. Even more important, we are convinced that the same strategy can be applied to generate new insights into related research fields, involving liquid crystalline materials or brush type polymers. We hope that the findings provided in this thesis point out the many similarities in molecular self-assembly, and offer alternative viewpoints to design new, functional materials.[4]

From an application aspect, it must be accepted that traditional, disperse oligomers or polymers will remain superior to the discrete materials in terms of ease of synthesis. For that reason, we questioned whether additional work for making the discrete materials is worth the effort. However, the answer to that question is way less trivial than the question itself. The

short answer: it depends. We clearly showed that uniform block copolymers provide otherwise inaccessible self-assembly characteristics. And likely, this is not restricted to only block co-oligomers. However, the usefulness of these unique characteristics totally depends on the intended application of the material. In fact, in some cases, dispersity might even be a prerequisite for obtaining the desired material properties.[5,6] In a sense, this is similar to selective use of either disperse or discrete (polymeric) materials for particular functions by Nature. Now, all we have to do is to decide when to use which one.

References

(1) Hillmyer, M. A. *J. Polym. Sci. Part B Polym. Phys.* **2007**, *45*, 3249.

(2) Oschmann, B.; Lawrence, J.; Schulze, M. W.; Ren, J. M.; Anastasaki, A.; Luo, Y.; Nothling, M. D.; Pester, C. W.; Delaney, K. T.; Connal, L. A.; McGrath, A. J.; Clark, P. G.; Bates, C. M.; Hawker, C. J. *ACS Macro Lett.* **2017**, *6*, 668.

(3) Schmitt, A. K.; Mahanthappa, M. K. *Macromolecules* **2017**, *50*, 6779.

(4) Bates, C. M.; Bates, F. S. *Macromolecules* **2017**, *50*, 3.

(5) Pernot, H.; Baumert, M.; Court, F.; Leibler, L. *Nat. Mater.* **2002**, *1*, 54.

(6) Register, R. A. *Nature* **2012**, *483*, 167.

♦ Summary ♦

The Art of Perfection: On the Self-Assembly of Discrete Block Co-Oligomers

Block copolymer (BCP) self-assembly is a proven method to generate well-ordered, nanoscale morphologies by exploiting the propensity of the large, blocky molecules to microphase segregate. Modern polymerization techniques and sophisticated post-modification reactions allow the fabrication of practically any desired BCP design, offering tailor-made self-assembly characteristics. Nevertheless, a major and inevitable shortcoming of these synthetic protocols is that they introduce chain-length and composition variation between the different molecules in the material—dispersity, $Đ$, in short.

An additional trend in BCP research is the use of polymer backbones with lengths that slowly become indistinguishable from those of traditional organic molecules. Still, the discrepancy between these systems in terms of dispersity raises the intriguing question how molecular uniformity influences BCP self-assembly. In this thesis, the synthesis and self-assembly characteristics of various types of discrete-length, low-MW block copolymers, *i.e.*, block co-oligomers (BCOs), is described. This allows a unique comparison of the microphase segregation of discrete and disperse materials, leading to a better understanding of the influential range of dispersity and new insights on how to improve BCO self-assembly.

In **Chapter 1** we provide an overview of the limited number of synthetic protocols that have been developed for the generation of uniform ($Đ = 1$) polymers containing more than 20 repeat units. Additionally, we discuss the most important principles of block copolymer microphase separation and the recent quest for block-copolymers that exhibit extremely small feature sizes. To better understand the self-assembly of polymer-like molecules at the molecular level, our aim is to create and explore the properties of perfectly defined, low-MW block co-oligomers.

The development of iterative synthetic protocols for uniform oligodimethylsiloxane (*o*DMS) and oligolactic acid (*o*LA) is described in **Chapter 2**. The robustness of the synthetic strategy permits the multi-gram fabrication of discrete-length blocks containing up to 59 siloxane repeat units or 64 lactic acid repeat units. Ligation of these blocks gives two libraries of BCOs, with molar masses up to 6.9 kDa and ultra-low molar mass dispersities ($Đ \leq 1.00002$). The two sets of BCOs can be categorized as fully amorphous and semicrystalline.

The incompatibility of the *o*DMS and *o*LA blocks made the final coupling more demanding as the block length increases.

In **Chapter 3**, we study the properties of a series of fully amorphous, discrete-length *o*DMS–*o*LA block co-oligomers. With various analytical techniques, microphase segregation into classical BCP morphologies (cylindrical, gyroid, and lamellar) with exceptionally small feature sizes (down to 3.5 nm) is observed. When comparing the discrete-length materials with disperse analogues, we find that an increase in the dispersity of these BCOs results in: 1) an increase of the *stability* of the microphase-segregated state, 2) a decrease of the overall *degree of ordering*, and 3) an increase of the *domain spacing*.

The set of uniform *o*DMS–*o*LA BCOs with an isotactic oligolactic acid (*i*-*o*LA) block is examined in **Chapter 4**. We show that the crystalline nature of the *i*-*o*LA domain is preserved after ligation with amorphous *o*DMS, resulting in lamellar microphase-segregated structures. For a select number of BCOs an unprecedented uniformity in the domain spacing is found, resulting from the correct balance of crystallization kinetics and molecular pre-organization provided by the discrete nature of the materials. Additionally, we discover the devastating effect of chain length dispersity in the crystalline block on the microphase segregation process, which can be explained with an intuitive molecular organization model.

Chapter 5 deals with a new class of discrete-length block co-oligomers comprising oligodimethylsiloxane (*o*DMS) and oligomethylene (*o*M). Uniform *o*M blocks containing up to 69 backbone carbons are accessed with an iterative, Wittig reaction based strategy. This is followed by ligation with *o*DMS hydrides of various lengths. Crystallization of the alkane chains results in crystallization-driven microphase separation of the *o*DMS–*o*M conjugates into lamellar structures with extremely small domain spacings. The use of different BCO architectures enabled us to propose a detailed view of the molecular organization within the microphase segregated domains, highlighting the close relation between the exact molecular structure and self-assembly characteristics.

As postulated in the **Epilogue**, polymer science should partially evolve back to the traditional organic chemistry it once departed from. We showed the largely overlooked impact of molecular uniformity in low-MW BCP systems and the usefulness of such discrete-length materials as a tool to very systematically explore the self-assembly behavior of block copolymers, offering alternative viewpoints to design new, functional materials.

♦ Curriculum Vitae ♦

Bas van Genabeek werd geboren op 11 juli 1990 te 's-Hertogenbosch. In 2008 rondde hij zijn VWO opleiding af aan het Gymnasium Beekvliet in Sint-Michielsgestel. Hierna startte hij met de bacheloropleiding Scheikundige Technologie en een aansluitende minor in Biomedische Technologie, beiden aan de Technische Universiteit Eindhoven (TU/e). Tijdens zijn studie deed hij onder andere onderzoek aan aceton sensoren op basis van vloeibare kristallen in de onderzoeksgroep van prof. dr. R.P. Sijbesma en de invloed van peptide modificaties op het bindingsgedrag met androgeen en estrogeen kernreceptoren onder de supervisie van prof. dr. ir. L. Brunsveld. De bachelorstudie werd cum laude afgesloten en verder beloond met de KHMW Jong Talent Aanmoedigingsprijs en de Sixma Organische Chemie Prijs. De vervolg masteropleiding Chemical Engineering, eveneens aan de TU/e, werd afgerond met een bedrijfsstage bij Syncom in Groningen en onderzoek aan watertolerante organocatalysatoren gebaseerd op supramoleculaire motieven in de onderzoeksgroep van prof. dr. E.W. Meijer. In 2014 ontving Bas de prijs voor de beste master thesis in Chemical Engineering and Chemistry van de TU/e en de Unilever Research Prize voor de beste master thesis. Na het behalen van zijn ingenieurstitel (cum laude) startte hij in 2014 met zijn promotieonderzoek in de capaciteitsgroep Macromoleculaire en Organische Chemie en het Instituut voor Complexe Moleculaire Systemen aan de TU/e, onder begeleiding van prof. dr. E.W. Meijer en dr. ir. A.R.A. Palmans. Dit onderzoek omvatte de synthese en bestudering van het faseschеidingsgedrag van blokcopolymeren zonder ketenlengtedistributie, waarvan de belangrijkste resultaten staan beschreven in dit proefschrift. Tijdens zijn promotie ontving Bas een drietal prijzen voor beste lezingen: Dutch Polymer Days Plenary Lecture Award, Best Oral Presentation op de Emerging Polymer Technologies Summit in Melbourne (2nd place) en de LANXESS Talent Award (DWI / RWTH Aachen).

Bas van Genabeek was born on July 11th, 1990 in 's-Hertogenbosch, the Netherlands. In 2008, he completed his secondary education at Gymnasium Beekvliet in Sint-Michielsgestel. Afterward, he obtained his B. Sc. degree (*cum laude*) in Chemical Engineering at the Eindhoven University of Technology (TU/e), including a minor in Biomedical Engineering. During his bachelor studies, he developed liquid crystal based acetone sensors using cholesteric liquid crystals in the research group of prof. dr. R.P. Sijbesma and studied the

influence of peptide modifications on the binding affinity with androgen and estrogen receptors, supervised by prof. dr. ir. L. Brunsveld. Also, he was awarded the KHMW Jong Talent Aanmoedigingsprijs and Sixma Organic Chemistry Prize. During his master studies in Chemical Engineering (TU/e), he worked as an intern at Syncom in Groningen and designed hydrogen-bonding based supramolecular systems for efficient organocatalysis in water in the research group of prof. dr. E.W. Meijer. In 2014, Bas was awarded a prize for the best master thesis in Chemical Engineering and Chemistry at the TU/e and the Unilever Research Prize for the best master thesis. Having obtained his M. Sc. degree (*cum laude*) in 2014, he started his PhD research in the laboratory of Macromolecular and Organic Chemistry and the Institute for Complex Molecular Systems at the TU/e, under supervision of prof. dr. E.W. Meijer and dr. ir. A.R.A. Palmans. This work focused on the synthesis and study of the phase behavior of block copolymers with no chain length distribution, of which the most important results are described in this thesis. During his PdD research, Bas was awarded three best lecture awards: the Dutch Polymer Days Plenary Lecture Award, Best Oral Presentation at the Emerging Polymer Technologies Summit in Melbourne (2nd place) and the LANXESS Talent Award (DWI / RWTH Aachen).

♦ List of Publications ♦

A Modular Approach to Introduce Function into Single-Chain Polymeric Nanoparticles. E. Huerta; B. van Genabeek; P. J. M. Stals; E. W. Meijer; A. R. A. Palmans. *Macromol. Rapid Commun.* **2014**, *35*, 1320.

Triggering Activity of Catalytic Rod-Like Supramolecular Polymers. E. Huerta; B. van Genabeek; B. A. G. Lamers; M. M. E. Koenigs; E. W. Meijer; A. R. A. Palmans. *Chem. - A Eur. J.* **2015**, *21*, 3682.

Synthesis and Self-Assembly of Discrete Dimethylsiloxane-Lactic Acid Diblock Co-oligomers: The Dononacontamer and Its Shorter Homologues. B. van Genabeek; B. F. M. de Waal; M. M. J. Gosens; L. M. Pitet; A. R. A. Palmans; E. W. Meijer. *J. Am. Chem. Soc.* **2016**, *138*, 4210.

Dispersity under Scrutiny: Phase Behavior Differences between Disperse and Discrete Low Molecular Weight Block Co-Oligomers. B. van Genabeek; B. F. M. de Waal; B. Ligt; A. R. A. Palmans; E. W. Meijer. *ACS Macro Lett.* **2017**, 674.

Amplifying (Im)perfection: The Impact of Crystallinity in Discrete and Disperse Block Co-oligomers. B. van Genabeek; B. A. G. Lamers; B. F. M. de Waal; M. H. C. van Son; A. R. A. Palmans; E. W. Meijer. *J. Am. Chem. Soc.* **2017**, *139*, 14869.

♦ Conference Contributions ♦

Poster: CHemistry As INovating Science (CHAINS 2014), Veldhoven (Netherlands).

Poster: ICMS Outreach Symposium (2015), Eindhoven (Netherlands).

Lecture: Stratingh Institute 2015 Workweek, Eindhoven (Netherlands).

Poster: CHemistry As INovating Science (CHAINS 2015), Veldhoven (Netherlands).

Lecture: CHemistry As INovating Science (CHAINS 2015), Veldhoven (Netherlands).

Poster: CHemistry As INovating Science (CHAINS 2016), Veldhoven (Netherlands).

Lecture (+ award): Dutch Polymer Days (DPD 2016), Lunteren (Netherlands).

Lecture (+ award): Emerging Polymer Technologies Summit (EPTS 2016), Melbourne (Australia).

Lecture: ICMS Scattering Workshop (2016), Eindhoven (Netherlands).

Lecture: Clariant company visit (2017), Frankfurt am Main (Germany).

Lecture (+ award): DWI / RWTH Aachen Summer School (2017), Aachen (Germany).

♦ Dankwoord ♦

In zekere zin is het wel grappig dat de komende pagina's voor velen waarschijnlijk de eerste en enige van dit proefschrift zijn die ze lezen, terwijl het tegelijkertijd voor mij juist staat voor een afronding van een volle vier jaar werk (en de opvulling van heel wat pagina's voorafgaand aan deze). Desondanks dient de volgende tekst eenzelfde functie: een dankwoord aan iedereen die op welke wijze dan ook heeft bijdragen aan dit werk of mij heeft ondersteund bij de totstandkoming ervan.

Pap, mam, Marloes, Gijs, opa, oma, oma en de rest van de familie: waarschijnlijk zijn jullie het beste voorbeeld van onvoorwaardelijke steun aan iemand, niet voor wat hij doet, maar puur omdat hij het doet. Ik beloof dat ik ergens dit jaar (het is nu 2018) probeer om jullie eindelijk duidelijk te maken wat ik precies heb gedaan (en waarom).

Binnen de SMO/MST familie wisten velen vanzelfsprekend wel waar ik mee bezig was, maar dat maakt mijn dank voor hun ondersteuning niet minder groot. Bert, als promotor heb jij mij de kans geboden om de afgelopen 4 jaar deel te mogen uitmaken van een fantastische vakgroep met een uiterst divers karakter. De vele adviezen die je had voor mij, zowel op wetenschappelijk als persoonlijk vlak, hebben veel vorm gegeven aan zowel mijn onderzoek als mijn eigen individu. Daarnaast spreek ik graag mijn enorme waardering uit voor de vele kansen, mogelijkheden en vrijheid die je me geboden hebt, waardoor ik mijzelf steeds verder heb kunnen ontwikkelen.

Anja, voordat je mijn copromotor werd, kenden wij elkaar al. Eerst via het Spinoza instituut, waar ik mijn eerste BTAs in elkaar heb geknutseld, en later natuurlijk dankzij jouw begeleiding tijdens mijn afstuderen. Het vele corrigeerwerk van al mijn teksten zal niet altijd je favoriete werk geweest zijn, maar heeft mij wel enorm veel geholpen. Het feit dat je kantoortje maar 2 deuren bij de mijne vandaag lag, droeg waarschijnlijk flink bij aan de ononderbroken klachtenregen die je soms van mij over je heen kreeg. Toch wist je er op een of andere manier altijd wel een positieve twist aan wist te geven (of je ging mee klagen, dat kon ook). Inderdaad was je erkenning dat het antieke CIS-PRO chemicaliën beheer systeem totaal niet meer functioneerde een goed excuus voor mij om mijn programmeer-skills verder te ontwikkelen. Ook onze nauwe samenwerking voor het vak Macro-Organische Chemie en het organisch practicum was soms een welkome afleiding van het promotie-onderzoek zelf.

I am very grateful to prof. Craig Hawker for taking part in my Doctorate Committee and coming to Eindhoven for the defense ceremony. Ook bedank ik graag prof. René Janssen,

prof. Dick Broer, prof. Rint Sijbesma en dr. Hans Heuts voor hun deelname aan mijn promotiecommissie en het aanwezig zijn bij mijn verdediging.

Brigitte; collega, oud-studente, paranimf en labmaatje. Ik zie jou nog bezig zijn tijdens het practicum in de tijd dat ik zelf afstudeerder was. Volgens mij is in dat jaar de halve glaswerkvoorraad op het practicumlab vernieuwd. Maar zonder dollen, ik was heel blij dat je zowel je BEP en afstuderen onder mijn begeleiding wilde uitvoeren. Je hebt hier fantastische resultaten bereikt, en het is dan ook meer dan terecht dat je na je afstuderen als promovendus terecht kon bij MST. Veel succes met het hele promotiegebeuren, de borrels die je weer nieuw leven in hebt geblazen en het onder controle houden alle gebeurtenissen op lab 4.

Gijs, als jaargenoot van mijn bachelor- en masterstudie ken ik jou al wat langer, maar met name tijdens ons nagenoeg gelijktijdig afstuderen zijn we meer met elkaar gaan optrekken. Ik blijf ontzag houden voor jouw vermogen om jezelf volledig onzichtbaar te maken voor mensen die dingen waar je geen zin in hebt van je gedaan willen krijgen (vooral omdat ik daar zelf wat minder bedreven in ben). Jouw droge humor wordt ook zeer gewaardeerd tijdens ons jaarlijks wintersporttripje, net als de regelmatige keren dat je semi-ongecontroleerd met je gezicht vol de sneeuw in duikt. Vanzelfsprekend ook bedankt dat jij mijn andere paranimf wil zijn tijdens mijn verdediging, hoewel ik daar later wellicht nog op terug moet komen.

Bas de Waal, als iemand behoort tot de onmisbare mensen die nodig waren bij het totstandkomen van al het werk beschreven in dit proefschrift, dan ben jij het wel. Als het geen tientallen verbindingen zijn die jij hebt gemaakt dan zijn het er honderen, stuk voor stuk broodnodig om de uiteindelijke moleculen te maken waar het mij om ging. De afgelopen 4 jaar, maar zeker ook daarvoor, hebben we talloze keren discussies gevoerd over van alles en nog wat en regelmatig gefoeterd op iedereen die minder liefde voor de Biotage en Grace machines had dan wijzelf. Mocht je ooit nog van plan zijn een spin-off bedrijfje te beginnen dat monodisperse siloxanen produceert, bel dan even.

Jolanda, vaak word jij bedankt voor de vele moleculen die je maakt voor anderen. Ik wil je daarentegen juist bedanken voor alle zaken die jij ook nog even tussen de synthesetaken door regelt. Veiligheidschecks, het practicum en het georganiseerd houden van het chemicaliën magazijn. Die periode rond Kerst dat we samen meer dan duizend barcode labels op oude potjes hebben staan plakken met Skyradio op de achtergrond zal ik niet snel vergeten.

Graag bedank ik ook alle mensen die hebben geholpen met belangrijke metingen: Ralf Bovee, Xianwen Lou, Joost van Dongen, Henk Janssen, Timo Sciarone en Anne Spoelstra. Ralf Bovee, in het bijzonder bedankt voor het meten van de vele MALDI-TOF spectra van mijn verbindingen. Marco Hendrix, zonder jou was het SAXS apparaat waarschijnlijk nog vaker buiten gebruik. Dank voor het draaiende houden van de hele bende.

Henk Eding, ik durf niet te schatten hoeveel uren ik koffie heb gedronken op de vroege ochtend samen met Bardo, Jeroen en jou, maar waarschijnlijk zijn het er veel te veel. Desondanks kan ik geen betere start van de dag bedenken.

Martina, Carla en Margot, zoals al regelmatig gezegd door Bert: zonder jullie was MST geen MST. Enorm bedankt voor het regelen van alles waar niemand anders zin in had en vooral het enthousiasme waarmee jullie dat doen. Margot, als MST-mama en werk-psychiater heb je me de laatste 2 jaar tegen beter weten in proberen te veranderen in een beter mens. Ik weet niet of je ooit aan een ander gevraagd hebt of dat gelukt is (ik denk zelf van wel), maar misschien is het toch handig om voor komend jaar alvast wat nieuwe sessies in te plannen.

Hans, thanks voor de talloze bestelling die je voor mij gedaan hebt en de vele dozen silica die je naar lab 4 hebt gesjouwd. Ik hoop dat de omschakeling naar onze nieuwe ChemDatabase het leven voor jou ook wat makkelijker heeft gemaakt.

Peter, veel mensen kunnen voorbeeld nemen aan het plezier waarmee jij je werk doet, waarmee jij er elke dag weer voor zorgde dat onze verdieping netjes en schoon bleef.

Het begeleiden en onderwijzen van studenten vond ik (meestal) een van de leukste dingen om te doen. Tijdens het verzorgen van de werkcolleges voor het vak Macro-Organische Chemie en het voorbespreken tijdens het practicum kon ik veel van mijn enthousiasme voor het vakgebied kwijt. Daarnaast was de samenwerking met bachelor- en masterstudenten Brigitte, Mark, Jan, Martin, Bianca, Lisette en Wouter heel productief en leerzaam (hopelijk voor beide partijen).

Dank aan de Supramolecular Polymers & Materials subgroep, de subgroep voorzitters, lab-, kantoor- en anderzijds betrokken groepsgenoten voor alle gezelligheid en (non-)productieve discussies: José, Brigitte, Andreas, Beatrice, Chidambar, Katja, Ghislaine, Elisabeth, Anindita, Ronald, Gijs, Mathijs, Simone, Sjors, Helen, Rachel, Louis, Bram, Anneloes, Marcin, Andreas, Nic, Lafayette, Nathan, Daan, Eveline, Robin, Ilja, Jody en Tim.

Sandra, mijn favoriete sinus, hoeveel pakjes post-its werk jij in 1 jaar weg? Fijn dat je altijd kopjes thee en knuffels kwam brengen als ik moest schrijven. Jouw haast oneindige geheugen voor data blijft me verbazen. Stuur me zo nu en dan maar een reminder voor een etentje.

Patty, Vic, Eline, Eric, Maartje, Eric, Laura, Thijs en Gijs. Alle wintersporttrips, wie-is-de-mol-weekenden, BBQ's, oudejaarsvieringen en late avonden in 't Paultje waren de perfecte afleiding na de vele lange dagen in Helix. Rickardo, Olga, Lara en alle ISIS-groep 4 schaatsmatties, het samen sporten was een belangrijk moment van ontspanning voor mij. Evi, thanks voor alle steun tijdens de eerste jaren van mijn promotie. Nicolette, jij bent waarschijnlijk de enige met wie ik over alle rare sprongen van Frits & Flip kan praten. Farah, de enige goede reden om over die verschrikkelijke A50 naar Nijmegen te rijden was jij. Laura, als ik ooit nog een goede arts nodig heb, wil jij dat dan zijn?

Erika, in korte tijd ben jij een heel speciaal persoon geworden voor mij. Misschien dat je wel nog een enkele keer naar een bemiddelingspraatje van Margot moet als ik weer eens niet snap hoe vrouwen werken, maar daarbuiten hoop ik vooral dat je voor alle andere praatjes je toevlucht zoekt bij mij. Veel succes met het afronden van je studie.

Liefs,

Bas